

Aaron Micallef
Sebastian Krastel
Alessandra Savini *Editors*

Submarine Geomorphology

Springer Geology

The book series Springer Geology comprises a broad portfolio of scientific books, aiming at researchers, students, and everyone interested in geology. The series includes peer-reviewed monographs, edited volumes, textbooks, and conference proceedings. It covers the entire research area of geology including, but not limited to, economic geology, mineral resources, historical geology, quantitative geology, structural geology, geomorphology, paleontology, and sedimentology.

More information about this series at <http://www.springer.com/series/10172>

Aaron Micallef · Sebastian Krastel
Alessandra Savini
Editors

Submarine Geomorphology



Springer

Editors

Aaron Micallef

Marine Geology & Seafloor Surveying
Group, Department of Geosciences,
Faculty of Science
University of Malta
Msida
Malta

Alessandra Savini

Department of Earth and Environmental
Sciences
Università degli Studi Milano Bicocca
Milan
Italy

Sebastian Krastel

Institute of Geosciences
Christian-Albrechts-Universität zu Kiel
Kiel, Schleswig-Holstein
Germany

ISSN 2197-9545

Springer Geology

ISBN 978-3-319-57851-4

DOI 10.1007/978-3-319-57852-1

ISSN 2197-9553 (electronic)

ISBN 978-3-319-57852-1 (eBook)

Library of Congress Control Number: 2017940240

© Springer International Publishing AG 2018, corrected publication 2018

This work is subject to copyright. All rights are reserved by the Publisher, whether the whole or part of the material is concerned, specifically the rights of translation, reprinting, reuse of illustrations, recitation, broadcasting, reproduction on microfilms or in any other physical way, and transmission or information storage and retrieval, electronic adaptation, computer software, or by similar or dissimilar methodology now known or hereafter developed.

The use of general descriptive names, registered names, trademarks, service marks, etc. in this publication does not imply, even in the absence of a specific statement, that such names are exempt from the relevant protective laws and regulations and therefore free for general use.

The publisher, the authors and the editors are safe to assume that the advice and information in this book are believed to be true and accurate at the date of publication. Neither the publisher nor the authors or the editors give a warranty, express or implied, with respect to the material contained herein or for any errors or omissions that may have been made. The publisher remains neutral with regard to jurisdictional claims in published maps and institutional affiliations.

Printed on acid-free paper

This Springer imprint is published by Springer Nature

The registered company is Springer International Publishing AG

The registered company address is: Gewerbestrasse 11, 6330 Cham, Switzerland

*To
Christian Berndt
Lucienne Bonnici
Denys Brunsden
Cesare Corselli
Andrew Goudie
Douglas Masson
Paolo Orrù
Giuseppe Verdicchio
Heather Viles
For your support and guidance.*

Foreword

The role of the International Association of Geomorphologists is to support innovative research in the field of geomorphology and the young researchers involved in such subjects. Seafloors of oceans are the last unexplored part of our planet. Technological progress has made the exploration of such environments increasingly accurate. Geomorphology is one of the key disciplines involved in this exploration.

This is why the Submarine Geomorphology working group was set up during the 8th International Conference on Geomorphology of the International Association of Geomorphologists, which took place in Paris in August 2013. The objectives of this working group are to establish submarine geomorphology as a field of research, disseminate its concepts and techniques among earth scientists and professionals, and encourage students to develop skills and knowledge in this field. This book is a first, important step towards achieving these objectives. Involving more than 60 academics and practitioners worldwide, this book provides a detailed review of the state of the art of the study of submarine landforms and processes, extending from shallow coastal environments to deep abyssal plains. It also presents the principal methods used to investigate submarine landscapes, and the key research questions that need to be addressed in the near future. I believe this book constitutes a valuable tool for students and professionals alike to achieve a thorough understanding of a rapidly evolving, and increasingly significant, field of geomorphology.

A fascinating book to read!

Eric Fouache
President of the International Association of Geomorphologists
Paris-Sorbonne University Abu Dhabi
Abu Dhabi, United Arab Emirates

*The original version of the book was revised:
For detailed information please see Erratum.
The erratum to the book is available at
https://doi.org/10.1007/978-3-319-57852-1_28*

Acknowledgements

We acknowledge the support of the International Association of Geomorphologists, Marie Curie Career Integration Grant PCIG13-GA-2013-618149 (SCARP) under the 7th European Community Framework Programme and ERC Starting Grant no 677898 (MARCAN) under the European Union's Horizon 2020 research and innovation programme.

We are indebted to the following colleagues for reviewing chapters in this book: Grigorii Akhmanov, Donna Blackman, Denys Brunsden, Andrea Fildani, Tim Freudenthal, Andrew Green, Veerle Huvenne, Tim Le Bas, Alice Lefebvre, David Mosher, Cesar Ranero, David van Rooij, William Ryan, Alessandro Tibaldi, Brian Todd, and Wilhelm Weinrebe.

We also thank Felix Gross and Daniel Cuñarro Otero for their assistance in the preparation of this book.

Contents

Introduction	1
Aaron Micallef, Sebastian Krastel and Alessandra Savini	

Part I Data and Methods in Submarine Geomorphology

Sidescan Sonar	13
Ingo Klaucke	
Multibeam Echosounders	25
John E. Hughes Clarke	
Reflection and Refraction Seismic Methods	43
Gareth J. Crutchley and Heidrun Kopp	
Quantitative Analyses of Morphological Data	63
Philippe Blondel	
Seafloor Sediment and Rock Sampling	75
Aggeliki Georgioupolou	
ROVs and AUVs	93
Veerle A.I. Huvenne, Katleen Robert, Leigh Marsh, Claudio Lo Iacono, Tim Le Bas and Russell B. Wynn	

Part II Submarine Landforms and Processes

Origin and Geomorphic Characteristics of Ocean Basins	111
Peter T. Harris and Miles Macmillan-Lawler	
Drivers of Seafloor Geomorphic Change	135
Angelo Camerlenghi	
Shallow Coastal Landforms	161
Fantina Madricardo and Federica Rizzetto	

Continental Shelf Landforms	185
Ruth Durán and Jorge Guillén	
Submarine Glacial Landforms	207
Christine L. Batchelor, Julian A. Dowdeswell and Dag Ottesen	
Submarine Landslides	235
Joshu Mountjoy and Aaron Micallef	
Submarine Canyons and Gullies	251
David Amblas, Silvia Ceramicola, Thomas P. Gerber, Miquel Canals, Francesco L. Chiocci, Julian A. Dowdeswell, Peter T. Harris, Veerle A.I. Huvenne, Steven Y.J. Lai, Galderic Lastras, Claudio Lo Iacono, Aaron Micallef, Joshu J. Mountjoy, Charles K. Paull, Pere Puig and Anna Sanchez-Vidal	
Submarine Fans and Their Channels, Levees, and Lobes	273
Mark E. Deptuck and Zoltán Sylvester	
Contourite Drifts and Associated Bedforms	301
Ibimina Esentia, Dorrik Stow and Zeinab Smillie	
Volcanic Islands and Seamounts	333
Daniele Casalbore	
Mid-ocean Ridges	349
Neil C. Mitchell	
Cold Seep Systems	367
Silvia Ceramicola, Stéphanie Dupré, Luis Somoza and John Woodside	
Abyssal Hills and Abyssal Plains	389
Marie-Helene Cormier and Heather Sloan	
Oceanic Trenches	409
Jacob Geersen, David Voelker and Jan H. Behrmann	
Cold-Water Carbonate Bioconstructions	425
Claudio Lo Iacono, Alessandra Savini and Daniela Basso	
Part III Applied Submarine Geomorphology	
Applied Geomorphology and Geohazard Assessment for Deepwater Development	459
Roger Moore, Geoff Davis and Oliver Dabson	
Seabed Mining	481
Anne Peukert, Sven Petersen, Jens Greinert and François Charlot	
Fishing Activities	503
Ferdinand K.J. Oberle, Pere Puig and Jacobo Martín	

National Programmes: Geomorphological Mapping at Multiple Scales for Multiple Purposes	535
Terje Thorsnes, Lilja R. Bjarnadóttir, Alexandra Jarna, Nicole Baeten, Gill Scott, Janine Guinan, Xavier Monteys, Dayton Dove, Sophie Green, Joana Gafeira and Alan Stevenson	

Part IV Conclusion

Conclusion	555
Aaron Micallef, Sebastian Krastel and Alessandra Savini	
Erratum to: Submarine Geomorphology	E1
Aaron Micallef, Sebastian Krastel and Alessandra Savini	

Introduction

Aaron Micallef, Sebastian Krastel and Alessandra Savini

1 Our Blue Planet

Extending from the coastline to the deepest oceans, the submarine realm constitutes more than the 70% of our planet. The ocean comprises 1334 million cubic kilometres (320 million cubic miles) of seawater, comprising 97% of Earth's available water and covering 361 million square kilometres (139 million square miles) of seafloor (Costello et al. 2015; Trujillo and Thurman 2016). The vast majority of this seafloor cannot be directly observed by humans. Technological progress, particularly during the last century, has resulted in an explosion of knowledge on the marine realm that has radically transformed our view of the ocean and our planet in general.

The ocean is today a less remote and more fascinating place than it was 70 years ago. However, it still represents a frontier for research and resource exploitation. We have better maps of the surfaces of Mars, Venus and Earth's Moon than of our seafloor. Most of the ocean floor is mapped at a spatial resolution of only a few kilometres (Smith and Sandwell 1997), which means that the majority of the fine-scale submarine landforms are still uncharted. Surveying such landscapes is

A. Micallef (✉)

Marine Geology & Seafloor Surveying, Department of Geosciences,
University of Malta, Msida 2080, MSD, Malta
e-mail: aaron.micallef@um.edu.mt

S. Krastel

Institute of Geosciences, Christian-Albrechts-Universität zu Kiel,
Otto-Hahn-Platz 1, 24118 Kiel, Germany

A. Savini

Department of Earth and Environmental Sciences, Universita' degli Studi
di Milano Bicocca, Piazza della Scienza 4, 20126 Milan, Italy

both expensive and time consuming; it has been estimated that it would take approximately 125 years to chart all ocean basins using the latest swath-mapping tools (Sandwell et al. 2002).

2 Submarine Geomorphology

Geomorphology is the study (-logy, from $\lambda\omega\gamma\sigma\zeta$) of the forms (-morpho-, from $\mu\omega\rho\varphi\eta$) of the Earth (geo-, from $\gamma\eta$). Geomorphologists describe and classify the Earth's surface to investigate the complex interaction between form and process, and to unravel the evolution of landforms and landscapes through space and time.

Submarine geomorphology is the study of landforms and processes in the submarine domain. The ocean hosts a tremendous variety of forms that reflect the action of a range of tectonic, sedimentary, oceanographic and biological processes at multiple spatio-temporal scales (Fig. 1). The aim of this book is to present the state-of-the-art in the standard data and methods used in submarine geomorphology (Part 1), to introduce the most significant submarine landforms and the processes that form them (Part 2), and to highlight the applied value of submarine geomorphology to industry and ocean governance based on selected examples (Part 3). This book is written for anybody with an interest in submarine geomorphology, although it is primarily aimed for undergraduate and graduate students, and professionals with limited training in marine geosciences. Our hope is that this book will encourage an interaction with terrestrial geomorphologists as well as scientists from other disciplines that results in significant advances in submarine geomorphology.

The investigation of the form, processes and evolution of submarine landscapes has strong basic and applied value, and it is becoming a priority for many academic and research institutions, government authorities and industries globally. The seafloor is a vast reservoir of renewable and non-renewable resources, which include marine ecosystems, fisheries, hydrocarbons, freshwater, aggregates, deep sea minerals and blue energy, among others. Industries that exploit these resources are increasingly moving offshore and deeper as the shallow and more accessible resources become depleted. Sound knowledge of seafloor geomorphology is key to maritime spatial planning, the designation of marine protected areas, the construction and operation of offshore infrastructure, and the implementation of environmental monitoring programmes. Seafloor processes constitute a geohazard to key offshore infrastructure and coastal communities. The seafloor is also an important archive of global change (e.g. climate, ocean circulation, sea level).

The International Association of Geomorphologists has recognised the increasing significance of submarine geomorphology by setting up the Submarine Geomorphology working group in August 2013. This group joins other initiatives, such as S4SLIDE (Assessing Geohazards, Environmental Implications and

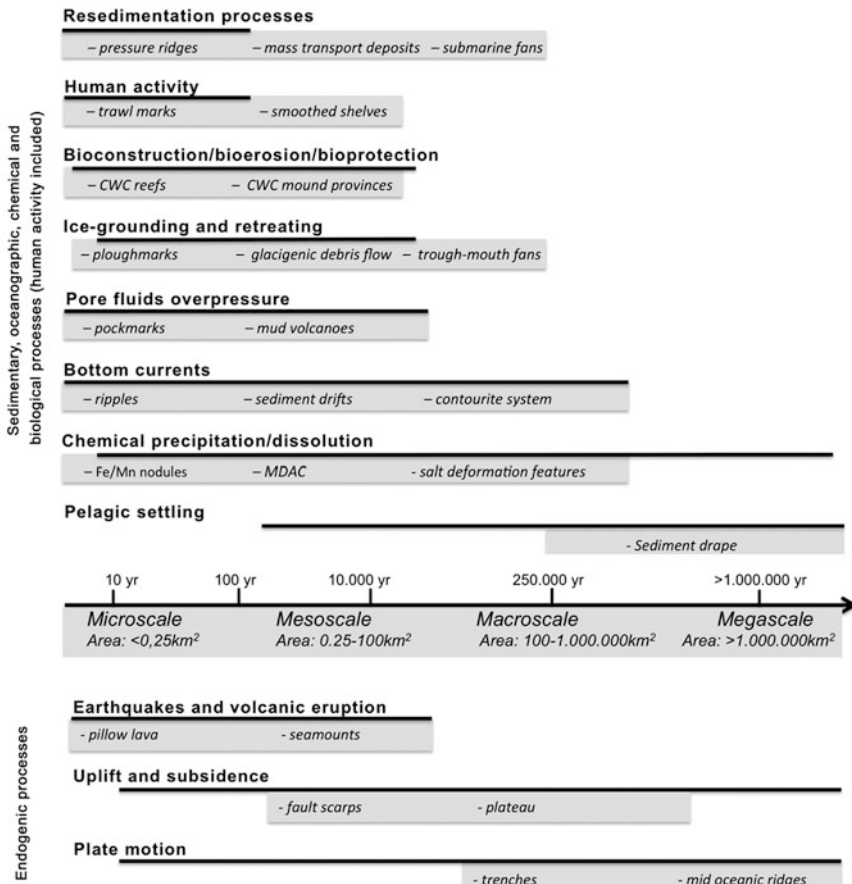


Fig. 1 A list of the main drivers of seafloor geomorphic changes in submarine environments (see Chapter “Drivers of Seafloor Geomorphic Change”) and examples of resulting landforms at different spatial and temporal scales. The *black line* associated to each process refers to the temporal scale (see the *black arrow* for reference values), indicating the process lifespan required to create representative landforms. The *grey boxes* include an example of representative landforms for each spatial scale (see the *grey box* under the *black arrow* for reference values) (CWC = Cold-Water Corals; MDAC = Methane Derived Authigenic Carbonates)

Economic Significance of Subaqueous Landslides across the World’s Continental Margins; funded by IGCP-640), and INCISE (International Network for submarine Canyon Investigation and Scientific Exchange), in bringing together scientists, students and professionals working on various aspects of submarine geomorphology, and to stimulate discussions with geoscientists from related fields of research.

3 History of Submarine Geomorphology

Submarine geomorphology is a relatively young scientific discipline. This is largely a result of the difficulties inherent to the investigation of the ocean floor. Submarine geomorphology has relied heavily on ‘remote sensing’ of the ocean floor, primarily through the use of acoustic waves. Developments in submarine geomorphology have therefore been closely linked to developments in geophysics.

The first pioneers to measure the depth of the ocean did so using plumb lines. A time consuming and inaccurate method, this involved a weight attached to cable that was lowered to the seafloor while the ship was stationary. The length of the cable was used to estimate the depth of the ocean floor. The first known attempt to measure ocean depth in this manner was by Ferdinand Magellan in the central Pacific around 1500 AD, but his attempt failed because the plumb line he used was too short. Lt. Matthew Fontaine Maury published the first deep-sea bathymetric map based on measurements with plumbs in 1855 (Fig. 2). This map covers the North Atlantic Ocean and is based on sparse soundings. Maury included a bathymetric profile between Mexico and NW-Africa along an area with a relatively high density of soundings. This profile showed numerous important morphological features, such as

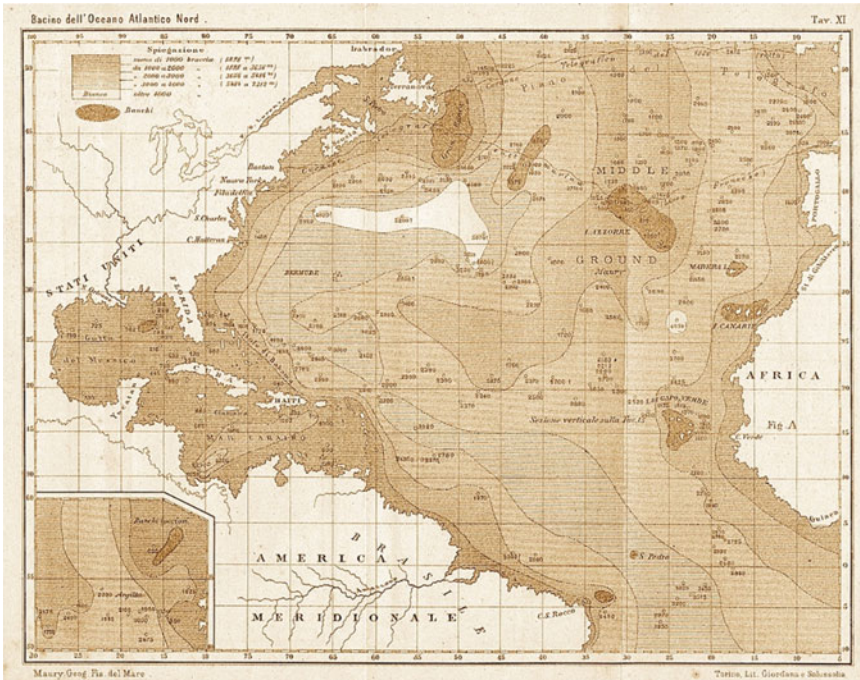


Fig. 2 Maury’s map of the North Atlantic, Italian edition from 1877. The map content is identical to that of the original edition published in 1855. (Reprinted from Sound images of the ocean, Wille 2005, with permission from Springer.)

the Mid-Atlantic Ridge and the first indications of typical continental margin and abyssal plain morphologies. Another 100 years had to pass before these features could be understood in the frame of the theory of plate tectonics.

The first great oceanographic expeditions also took place in the second half of the 19th century. The Challenger Expedition, for example, circumnavigated the globe from 1872–1876 and made nearly 500 deep soundings using a lead weight attached to a hemp rope. During this time, several attempts were made to mechanise depth soundings and make them less time consuming and expensive. This was partly driven by the need to lay down the first transatlantic cables. One technique was developed by William Thomson and consisted of a motorised drum of piano wire with a lead and a dial. Another instrument was the gravity-measuring bathometer developed by Siemens (1876), but it failed to achieve the accuracy of plumb lines and was never routinely used.

In view of the lack of detailed morphological maps of the ocean, scientists in the late 19th century joined forces to study the ocean floor systematically. During the 7th International Geographic Congress in Berlin in 1899, a proposal was made to develop an international agreement on nomenclature and systematic terminology for sub-oceanic relief features. In response to this proposal, a commission was formed and charged with the preparation of a bathymetric map of the oceans. In 1903, His Serene Highness Prince Albert I of Monaco offered to organise and finance the production of a map series named ‘*la Carte générale bathymétrique des océans*’ (the General Bathymetric Chart of the Oceans, GEBCO) (Carpine-Lancré et al. 2003). This was the origin of GEBCO, which nowadays operates under the joint auspices of the International Hydrographic Organization (IHO) and the Intergovernmental Oceanographic Commission (IOC) of UNESCO. GEBCO today offers a 30 arc minute grid (ca. 1 km), which is an important reference map for the morphology of the world’s oceans.

A milestone in the investigation of submarine geomorphology was the development of ocean echo sounders in the early 20th century. These instruments allowed measuring water depth from moving vessels by means of acoustic waves. The invention of echo sounders happened independently at two places (Wille 2005). The Canadian engineer Reginald A. Fessenden started the development of an acoustic echo ranging device in Boston in 1912. German physicist Alexander Behm built his first echo sounder in Kiel in 1913. Both workers were stimulated by the loss of the Titanic after a collision with an iceberg in 1912. The main aim of both developments was the detection of icebergs and obstacles with acoustic waves. Alexander Behm failed with his approach to detect icebergs with horizontal sound propagation, but vertical soundings allowed very precise measurements of water depth. Several ships were equipped with echo sounders soon afterwards. A first echo sounding line crossing the Atlantic Ocean was collected on the USS Stewart in 1922 using an acoustic echo sounder devised by Dr Harvey Hayes, a U.S. Navy scientist. The German Meteor Expedition (1925–1927) systematically surveyed the South Atlantic Ocean by crossing it 13 times between 20° north and 55° south using echo sounding equipment and other oceanographic tools. In total, they collected about 67,000 soundings along lines spaced at 600 km. This expedition showed for the first time

that ocean floors have irregularities as great as suberial landscapes. The continuity of the Mid-Atlantic Ridge was proven beyond doubt during this expedition. Sediment coring during this cruise also led to the first estimates of sedimentation rates in the deep ocean. The first operational multibeam sounding system was installed on the USNS Compass Island (Glenn 1970). For the first time, detailed bathymetric maps of the ocean floor became available, which revolutionised our understanding of seafloor morphology and seafloor processes (see Chapter “[Multibeam Echosounders](#)”).

The first marine seismic measurements were conducted in 1938 (Ewing and Vine 1938). Ewing was one of the pioneers in the development of seismic reflection and refraction systems for the exploration of ocean basins. Early measurements were done from stationary vessels with explosives as source. Early marine seismic measurements imaged thick sedimentary successions on the continental shelves, which quickly drew the attention of the hydrocarbon industry.

Major technical achievements in the investigation of the oceans were made during World War II, mainly in relation to the detection and safe navigation of submarines. Some of the engineers moved to academic institutions and private companies after the end of the war, thus making the newly developed techniques available to civil society. An important step for the investigation of submarine geomorphology was the invention of sidescan sonars, which permitted the acquisition of seafloor images at significantly high resolutions (see Chapter “[Sidescan Sonar](#)”). The Geological Long-Range Inclined Asdic GLORIA came in service in the late 1960s, and it was used to map large portions of the seafloor, including the entire Exclusive Economic Zone of the continental United States. These and other surveys significantly contributed to the improved morphological analysis of continental margins and other seafloor features such as Mid-Ocean Ridges (Laughton 1981).

The increasing availability and quality of seafloor maps led to pioneering work on various aspects of submarine geomorphology. Francis Parker Shepard, an American sedimentologist, became well known for his work on the origin of continental margins and submarine canyons (especially along the US continental shelves and slopes), as well as the first global statistical study of seafloor morphology. Jaques Bourcart carried out similar work offshore France, particularly in the Mediterranean Sea. The global hypothesis for ocean margin morphology was developed by a meteorologist—Alfred Wegener—whose hypothesis of continental drift is now an integral part of seafloor spreading and plate tectonics. The theory of seafloor spreading was consolidated by the work on flat-topped seamounts (guyots) by Harry H. Hess, and the mapping carried out by Bruce C. Heezen and Marie Tharp.¹ The famous seafloor map published by Heezen and Tharp in 1977 is a

¹In the early years of their cooperation, Bruce C. Heezen used to collect the data aboard the research vessels while Marie Tharp drew the maps, as women were excluded from seagoing activities at that time. It was only in 1965 that Marie Tharp was able to join a data collection expedition. As quoted in “The Floor of the Sea” by William Wertenbaker (1974), Bruce Heezen related the following story concerning the realisation that a rift valley existed in the middle of the Mid-Atlantic Ridge: “Marie’s job for me was to decide what a structure was... In three of the transatlantic profiles she noticed an unmistakable notch in the Mid-Atlantic Ridge, and she



Fig. 3 The Bruce Heezen-Marie Tharp world ocean floor map, painted by Heinrich Berann. *Photograph Library of Congress*

masterpiece that illustrates all the major morphological elements of plate tectonics (Fig. 3). This map is surprisingly accurate even in areas where no data were available at that time. Heezen's work is extremely diverse—it extended to all parts of the world and covered both broad and fine scale submarine geomorphology. Reported in more than 300 publications, Heezen's work has left an indelible mark on submarine geomorphology.

A milestone in marine geosciences was the initiation of the Deep Sea Drilling Program (DSDP) in 1966 using the Drilling Vessel Glomar Challenger (Chapter “[Seafloor Sediment and Rock Sampling](#)”). Ocean drilling is not a direct method for investigating submarine geomorphology, but the analysis of rock and sediment sampling contributes to the understanding of the processes shaping the seafloor. DSDP was followed by the Ocean Drilling Program (ODP, 1983–2003), the Integrated Ocean Drilling Program (IODP, 2003–2013), and the ongoing International Ocean Discovery Program (IODP, since 2013). All of these programs are truly international and multidisciplinary endeavors that significantly contribute to the understanding of the ocean floor and planet Earth in general.

(Footnote 1 continued)

decided they were a continuous rift valley and told me. I discounted it as girl talk and didn't believe it for a year". "Marie was the grand dame of ocean exploration," said Bill Ryan, Doherty Senior Scholar at Lamont-Doherty and a long-time colleague of Tharp's. "She didn't just make maps; she understood how the Earth works".

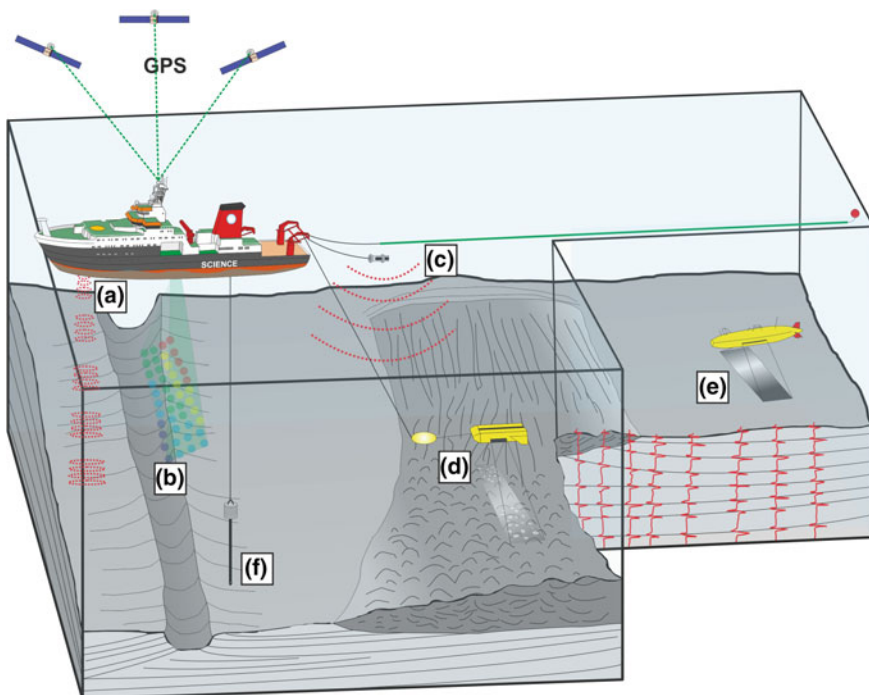


Fig. 4 Typical setup for a submarine geomorphological survey. (a) Sub-bottom profiler, (b) multibeam echosounder, (c) reflection seismic system, (d) sidescan sonar, (e) autonomous underwater vehicle, (f) sediment sampling (gravity corer)

Several technological advances in the last few decades have allowed investigating submarine geomorphology in increasing detail. Major advances include the use of underwater vehicles (see Chapter “[ROVs and AUVs](#)”), the accurate navigation of surface vessels and underwater vehicles, and improved resolution and penetration of acoustic imaging tools. As a result, modern submarine geomorphic investigations are based on a wide range of techniques (Fig. 4). The main strength of these techniques is that they provide an insight into both the exterior and interior structures of submarine landforms. The first part of this book presents the most commonly used techniques for data collection in submarine geomorphology.

References

- Carpine-Lancré J, Fisher F, Harper B, Hunter P, Jones M, Kerr A, Laughton A, Ritchie S, Scott D, Whitmarsh M (2003) The history of GEBCO 1903–2003, the 100-year story of the general bathymetric chart of the oceans. GITC bv, Lemmer, Netherlands

- Costello MJ, Smith M, Fraczek W (2015) Correction to surface area and the seabed area, volume, depth, slope, and topographic variation for the world's seas, oceans, and countries. *Environ Sci Technol* 49:7071–7072
- Ewing M, Vine A (1938) Deep-sea measurements without wires or cables. *EOS* 19(1):248–251
- Glenn MF (1970) Introducing an operational multi-beam array sonar. *Int Hydrogr Rev* 47(1): 35–39
- Laughton AS (1981) The first decade of GLORIA. *J Geophys Res* 86(B12):11511–11534
- Sandwell DT, Gille ST, Smith WHF (eds) (2002) Bathymetry from Space: Oceanography, Geophysics, and Climate, Geoscience Professional Services, Bethesda, Maryland, June 2002, 24 pp
- Siemens CW (1876) On determining the depth of the sea without the use of the sounding-line, and on an attraction-meter. *Proc R Soc Lond* 24:317–321
- Smith WHF, Sandwell DT (1997) Global sea floor topography from satellite altimetry and ship depth soundings. *Science* 277:1956–1962
- Trujillo AP, Thurman HV (2016) Essential of oceanography, 12th edn. Prentice Hall
- Wille PC (2005) Sound images of the ocean. Springer, Berlin

Part I

**Data and Methods in Submarine
Geomorphology**

Sidescan Sonar

Ingo Klaucke

Abstract Sidescan sonar allows obtaining an acoustic image of the seafloor at high resolution, wide swath and relatively low cost. For that purpose the backscattered signal of an acoustic pulse sent out sideways from an instrument carrier is registered. At low incident angles small-scale relief is well imaged and the length of shadows allows calculation of the height of seafloor features but sidescan sonar is particularly useful in mapping compositional differences of the seafloor. Sidescan sonar images are, however, mostly uncalibrated and need some form of ground-truthing for meaningful geological interpretation. Interferometric sidescan sonar systems now also provide bathymetric information together with backscatter strength.

1 History of Sonar

The acronym Sonar stands for SOund NAVigation and Ranging and was coined during WW II in analogy to Radar or Radio detection and ranging. The use of sound for the detection of obstacles such as icebergs or submarines, however, dates back to developments made in the aftermath of the sinking of RMS Titanic and WW I (Hackmann 1985). The Canadian engineer Reginald Fessenden and independently Alexander Behm in Germany developed the first working echosounders (Wille 2005). In an echosounder piezoelectric elements transform an electrical pulse into an acoustic signal and vice versa. Behm in particular intended his sonar for the detection of icebergs, which did not work out because of too many reflections from surface waves. His invention, however, quickly turned out to be useful for measuring the depth of the seafloor.

The first experiences with side-scan sonar were carried out by Hagemann (1958) but his work for the US Navy was kept secret and only published in 1980. Based on Hagemann's work, a first side-looking sonar (called the Shadow Graph) was built

I. Klaucke (✉)

GEOMAR Helmholtz Centre for Ocean Research Kiel, Kiel, Germany
e-mail: iklaucke@geomar.de

by a company specialised in military equipment (Westinghouse) in the early 1960s (MIT Museum 2016). At the same period in Great Britain sound was also used for imaging the seafloor (Chesterman et al. 1958) and soon later a first sidescan sonar was built for the National Institute of Oceanography (Tucker and Stubbs 1961), which is now part of the National Oceanography Centre Southampton. Additional experiments with side-looking sonar were carried out by Harold Edgerton, an electrical engineer at MIT who had become famous for using stroboscope flash lighting in photography in order to make fast moving processes visible. Building on this experience, he used sound to “image” the seafloor with repeating acoustic pulses and via his company EG&G worked on several projects for the US Navy (MIT Museum 2016). Very quickly, sidescan sonar proved to be a valuable tool for the systematic investigation of the seafloor and the generation of seafloor image mosaics (Clay et al. 1964) showing much hitherto unknown details (Belderson et al. 1972). The earliest commercial sidescan sonar systems were used for marine archaeological purposes, in particular the search for sunken ships (Bass 1968; Rosencrantz et al. 1972). At the end of the 1960s the evolution of sidescan sonar to that point culminated in the construction of the Geological Long-Range Inclined Asdic GLORIA (Rusby 1970; Somers et al. 1978), which was capable of achieving up to 60 km wide swaths by using a 6.5 kHz signal. From 1984 onwards the US Geological Survey started mapping the entire Economic Exclusive Zone of the continental United States. The resulting mosaics were the first systematic inventory of major areas of the seafloor (EEZ-Scan 84 Scientific Staff 1986; EEZ-Scan 85 Scientific Staff 1987; EEZ-Scan 87 Scientific Staff 1991) and spawned a wealth of scientific discoveries (Garder et al. 1996 and references therein). Further information can also be found at the USGS web page <http://coastalmap.marine.usgs.gov/gloria/>. Similar long-range, 6.5–12 kHz systems (SeaMARC-II, Hawaii MR-1) and mid-range, 30–35 kHz (SeaMARC-I, TOBI) sidescan sonar systems were developed in the late 1970s and early 1980s for different research institutes, but the instruments were also used commercially (Kosalos and Chayes 1983; Huggett and Millard 1992).

Sidescan sonar then underwent a phase of quiet evolution and constant improvements rather than evolutionary steps. This evolution was driven by commercial manufacturers and included the use of digital rather than analogue recording of the data, the use of increasingly higher frequencies for shallow water applications, and the use of frequency-modulated (chirp) signals that allow a better signal-to-noise ratio and less power consumption than the traditional pulse. The next major step in the development of sidescan sonar was the more widespread use of interferometric sonar systems that use two or more parallel receiver arrays that allow calculating bathymetry from phase differences of the signal received by the different receivers (Blackinton et al. 1983). These interferometric sidescan sonars originally achieved swath widths of up to 7 times the towing altitude and less resolution than multibeam systems (de Moustier 1988), but advances in signal processing now allow modern systems calculating interferometric bathymetry over the entire swath, i.e. up to 15 times the towing altitude.

To obtain high-resolution imagery along-track either the pulse repetition rate is high or the speed of the system travelling through the water must be decreased. In addition the along-track beam angle must be low. A high pulse repetition rate will restrict the distance the pulse can travel, therefore be usually used with higher sonar frequencies. The high sonar frequencies however have strong signal attenuation and consequently a limited range. The beam angle, on the other hand, is a function of the length of the transducer, as long transducer arrays produce a narrower beam. The length of transducers, however, is limited by the length of the towfish. More recently the development of synthetic aperture sonar allowed major improvements in the along-track resolution of sidescan sonar systems. These new systems have a high pulse repetition rate and allow calculation of a large synthetic transducer length. This technique requires very high precision in towfish position and altitude. The synthetic aperture sonar has been recently combined with a parametric signal that has been used for quite some time in sediment echosounding (see Chapter “[Reflection and Refraction Seismic Methods](#)” for more information) in order to derive sidescan sonar imagery from both parametric and the primary signals (Zakharina and Dybedal [2007](#)).

2 Principles of Sidescan Sonar

In sidescan sonar systems an acoustic pulse with a narrow opening angle in the along-track and wide opening angle in the across-track direction is emitted sideways from either a vessel, a towed body or an autonomous vehicle (Fig. 1). Upon reaching an interface with sufficient acoustic impedance contrast, such as the seafloor, most of the acoustic energy will be reflected away from the instrument. At the same time multi-directional scattering will occur at the interface and some of the scattered energy will be scattered back to the instrument. This backscattered energy carries the information that is used in sidescan sonar imaging. As for all sonar systems this can be described by the active sonar formula:

$$\text{BS} = \text{SL} - 2\text{TL} + \text{TS}$$

where BS is the backscatter strength, SL the source level, TL the transmission loss and TS the target strength.

The backscatter strength depends on a number of factors including the angle of incidence, the roughness of the seafloor and the scattering behaviour of the material at the seafloor. However, depending on the frequency of the acoustic signal, not all acoustic energy will be reflected and scattered but some portion will also be refracted into the sediments and scattered at deeper interfaces (Fig. 1) resulting in volume backscatter to be registered. This effect increases with decreasing sonar frequency.

The resolution of the sonar system is determined by the pulse length and sampling frequency for the across-track resolution (Fig. 2), and by the beam angle and

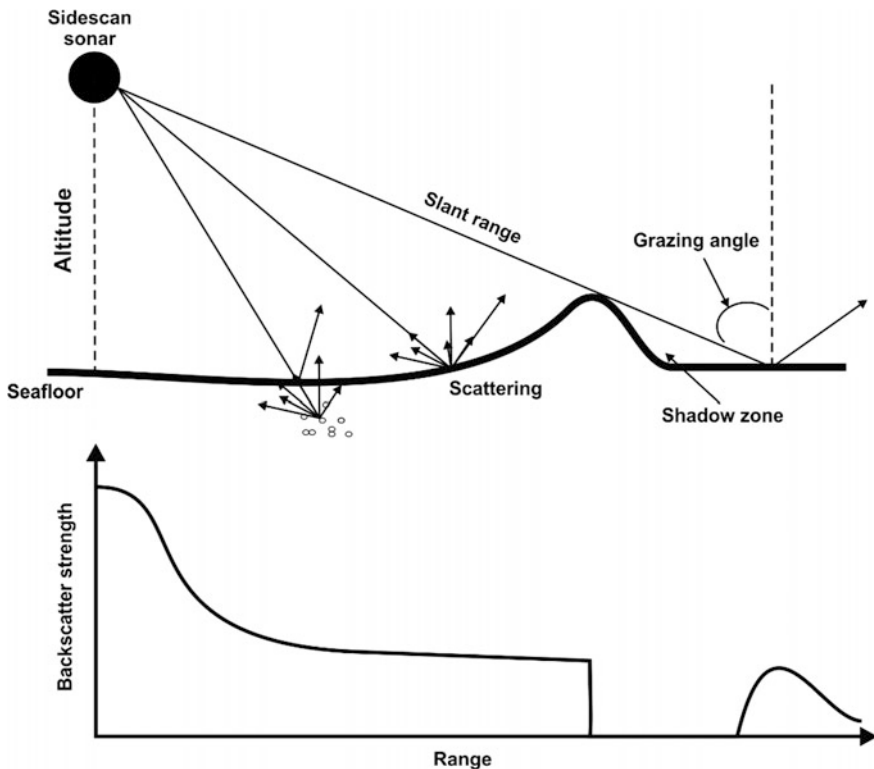


Fig. 1 Principles of sidescan sonar and definition of terms used in the text. Backscatter strength is high with near vertical incidence and produces no return in the shadow zone

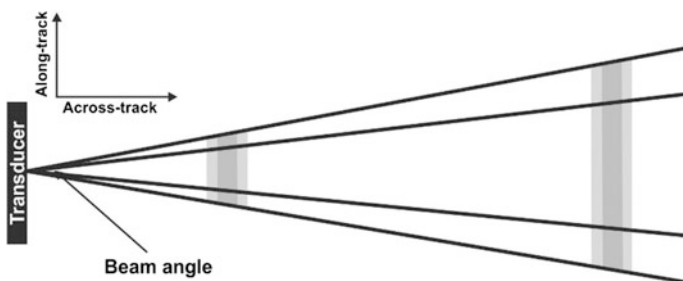


Fig. 2 Across-track and along-track resolution in digital sidescan sonar. Higher frequency or wider bandwidth result in better across-track resolution (dark grey vs. light grey). A smaller beam angle improves along-track resolution. In conventional, non-digital systems, the far range across-track resolution would be worse than the near-range resolution because of the increasing footprint size of the acoustic signal

survey speed for the along-track resolution. The across-track resolution of analogue systems is given by:

$$X = \frac{cL}{2 \cos \theta} = \frac{c}{2B}$$

where L is the pulse length of the transmitted pulse, θ is the grazing angle, c is the speed of sound in water, and B is the bandwidth. The resolution of digital systems, on the other hand, is determined by the sampling frequency of the A/D converter. The along-track resolution is the width of the beam on the ground or the distance travelled by the transducer during the reception interval, whichever is less. The width of the beam on the ground is given by:

$$Y = R\varphi$$

where R is the range and φ is the beam angle in radians. The along-track resolution consequently decreases with increasing range and the along-track resolution is generally much lower than the across-track resolution.

3 State of the Art

Long-range sidescan sonar systems such as GLORIA or the Hawaii MR-1 system have become obsolete by the continuous development of full ocean depth multi-beam bathymetry systems (see Chapter “[Multibeam Echosounders](#)”). Mid-range, deep-towed systems such as SeaMarc-I, TOBI or the Russian MAK-I system have been retired as well, leaving just a few deep-towed systems working in the 75–120 kHz range on the market. Such systems provide up to 1500 m wide swaths and depending on survey speed allow processing the data with roughly 1 m pixel size. In the past, they were commonly installed on a neutrally-buoyant towfish but increasingly more systems are now used on autonomous underwater vehicles (AUV). The majority of sidescan sonar systems on the market, however, are small, portable, high-frequency systems for use in relatively shallow water, i.e. on the continental shelves and upper slope areas. These systems operate with signal frequencies in excess of 200 kHz with some systems now exceeding 1 MHz. This choice of frequencies and depth ratings closely reflects the main usage of sidescan sonar, which includes marine archaeology, submarine cable and pipeline inspection, obstacle recognition and search and rescue operations, mine detection, marine habitat mapping, and marine geological and fisheries applications.

Raw sidescan sonar data are commonly displayed as a water-fall image during data acquisition. However, a certain number of data processing steps have to be applied in order to derive georeferenced sidescan sonar mosaics of the seafloor. The effects of these processing steps should be known by the interpreter, as they may induce or enhance artefacts and distortions. Sidescan sonar instruments record the

acoustic amplitude at the receiver versus time. Historically the received signals were recorded on electro-static paper and high backscatter intensities corresponding to high electrical currents would burn the paper dark. Nowadays, with digital processing of the data, both positive (high backscatter is white and shadows are black) and negative representation of the backscatter data are possible. Verifying the display convention is therefore required before interpretation.

Typical waterfall displays show no signal returns as the acoustic energy travels through the water column, followed by a strong signal including specular reflection from the seafloor beneath the instrument, being the closest reflecting object. As time increases, signals returning from further and further away give a complete swath of backscatter returns for the single ping. The received signal decreases in amplitude for increasing range due to the transmission losses in the water (Fig. 3). A time-varying gain (TVG) function is generally applied in order to highlight backscatter changes at far range. The raw sidescan sonar data are displayed as backscatter intensity versus time or sample number, which is the slant range and

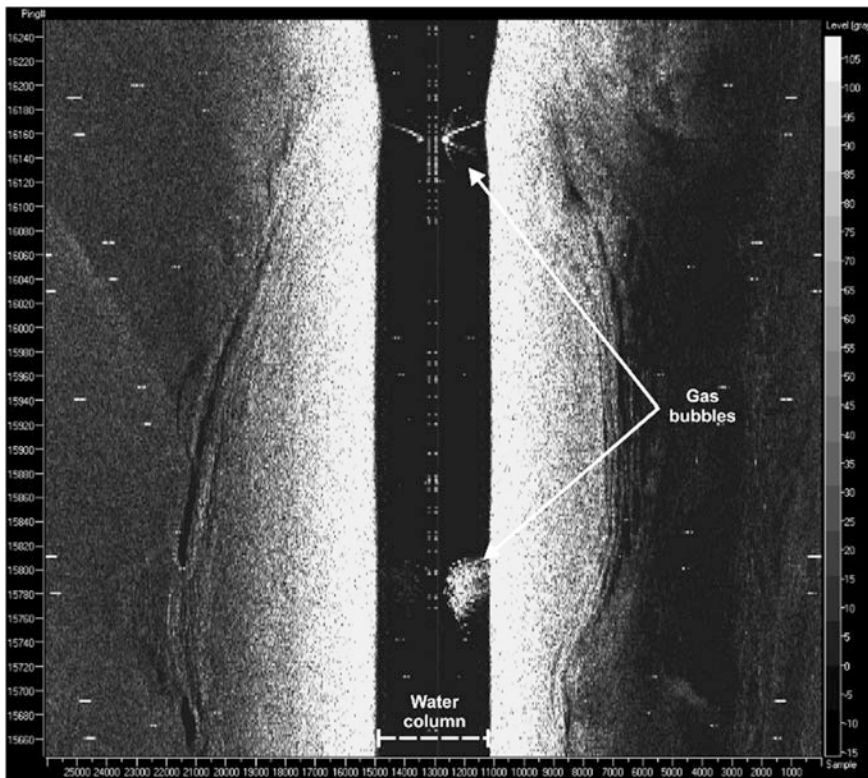


Fig. 3 Unprocessed sidescan sonar record during acquisition. Weak or no backscatter is displayed as *dark grey* or *black* whereas strong backscatter is shown as *white*. The *central black stripe* corresponds to lack of returns from the water column

corresponds to the distance between the transducer and the seafloor (Fig. 1). Knowing the altitude of the receiver over the seafloor, the ground range D can be calculated using:

$$D = \sqrt{R^2 - h^2}$$

where R is the slant-range distance and h the altitude of the instrument above the seafloor. This equation assumes a flat seafloor, but can induce distortion if this assumption is significantly invalid. Many sidescan sonar acquisition packages allow online display of the slant-to-ground-range correction, but this also cuts out the water column data that can contain valuable information such as fish schools, gas bubbles (Fig. 3), or nepheloid layers. Once the slant-to-ground-range correction has been applied, navigation, heading and attitude information are combined with the backscatter intensity values in order to correctly position the latter on a geographic map (Fig. 4). For this purpose, precise positioning is crucial, but the resolution of

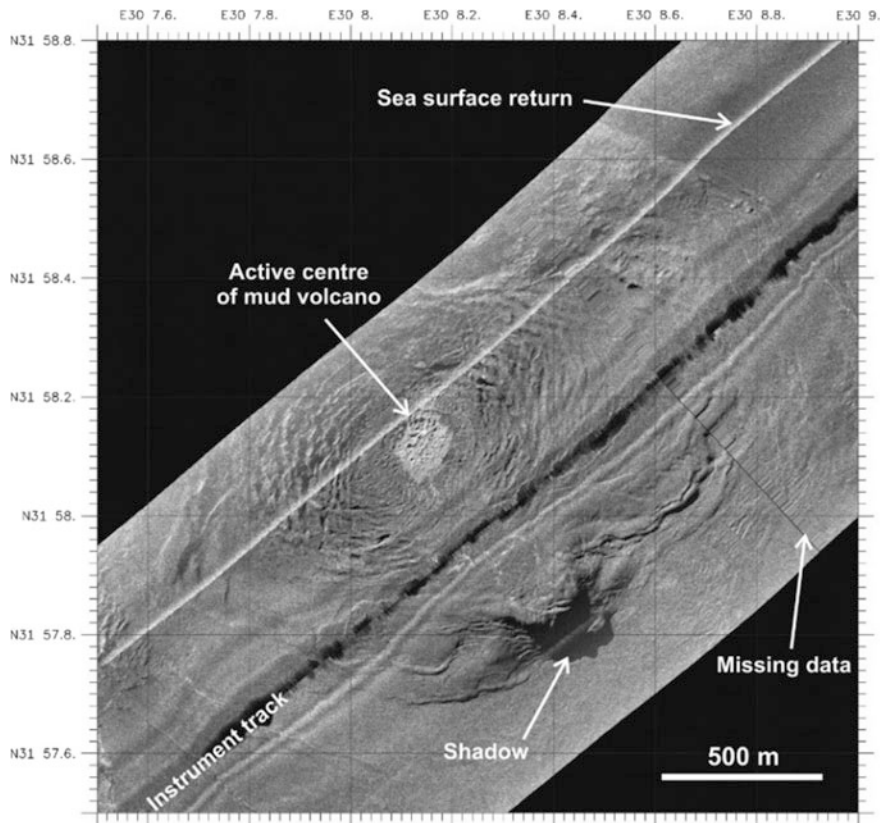


Fig. 4 Geo-referenced sidescan sonar image of a submarine mud volcano showing different backscatter intensities on the seafloor and relief in form of shadows. High backscatter is *white*

sidescan sonar images, which can be smaller than 10 cm, frequently exceeds the navigational precision. In addition, physically correct positioning of each sidescan sonar pixel on the ground generally leads to blurred images that are difficult to interpret. For this reason, sidescan sonar images are based on smoothed track, heading and attitude values that induce a certain degree of distortion and inaccurate positioning. Precise positioning, however, becomes crucial for synthetic aperture sonars. Most sidescan sonar systems are positioned using a layback method, where the length and azimuth of the towing cable is combined with the ship's position. More precise positioning requires the use of a range finder, transponders on the seafloor (long baseline system), an inertial navigation system, an ultra-short baseline system (for deep-towed sonars), or a combination of these systems.

The interpretation of sidescan sonar images still relies on the experience of the user, as calibrated sidescan sonar images relating specific backscatter intensities to well-defined lithologies are generally not available. Although standard sidescan sonar systems do not provide bathymetry, relief can be deduced from sidescan sonar images using the length of shadows and the altitude of the instrument above the seafloor (Fig. 4). In addition, lateral incidence at the far range highlights even small scale relief. The real benefit of sidescan sonar, however, is the distinction of areas of different seafloor roughness that is directly related to lithological differences. In that way sandy deposits, for instance, can be distinguished from muddy environments even if no difference in relief is involved. Different software packages are available to aid the user in establishing different backscatter classes that ultimately require "ground-truthing" in order to derive a meaningful geological interpretation.

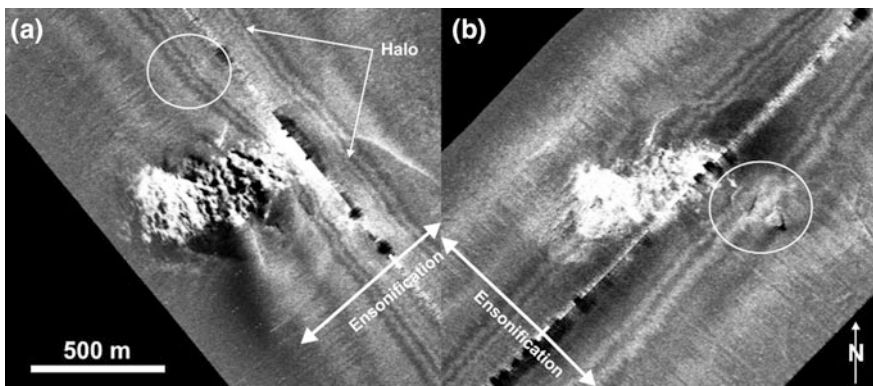


Fig. 5 Sidescan sonar image of Mound 12 offshore Costa Rica (modified after Klaucke et al. 2008) showing the effect of ensonification direction on the imaging of NW-SE trending structures. **a** Survey track parallel to the structures. **b** Survey track perpendicular to the structures. Note Alternating bands of high and low backscatter intensity (*the halo*) parallel to the nadir are the effect of side lobes during the beamforming of the sonar signal. Wiggly returns (white circle in picture **a**) indicate roll of the tow-fish that was not corrected for. Also note that features in the nadir region are poorly imaged (white circle in picture **b** and invisible in picture **a**)

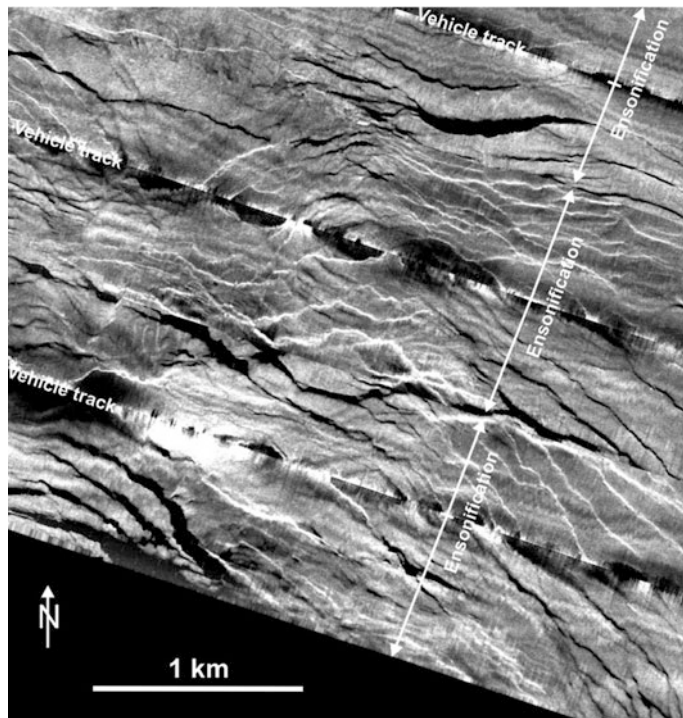


Fig. 6 Mosaic of sidescan sonar images showing fault scarps. Note that depending on ensonification direction the fault scarp changes from high backscatter (white) to shadows (black). Most fault scarps are dipping to the SW

Guidelines for the interpretation of sidescan sonar images have been published previously (Belderson et al. 1972; Johnson and Helferty 1990). For geomorphological interpretations, particular attention must be paid to the direction of ensonification. Linear structures are generally well imaged along tracks that are parallel to the alignment orientation (i.e. ensonification is perpendicular to the alignments), but may be subdued or invisible on tracks that are perpendicular to the structures (Fig. 5). In addition, features that are close to the nadir (vehicle track) are only poorly imaged. Sidescan sonar survey lines are consequently best planned at a 45° angle to elongated structures and at some distance to smaller targets in order to ensure lateral ensonification. Finally, attention must be paid to adjacent sonar images composing a mosaic. Features showing high backscatter intensity on one track (or one channel) may show low backscatter intensity on the adjacent track (channel) due to different directions of ensonification (Fig. 6).

4 Strengths and Weaknesses

Compared to other acoustic systems used for mapping the seafloor such as multibeam bathymetry systems (see Chapter “[Multibeam Echosounders](#)”), sidescan sonar systems are relatively cheap and simple to use. Time-consuming calibration procedures are not necessary nor are expensive additional sensors such as high-precision motion and heading sensors, although basic motion information can help in data processing. In addition, sidescan sonar provides high-resolution seafloor images over comparably large swath widths. Finally, sidescan sonar allows imaging very small-scale relief (in particular at high grazing angles) and provides important indications for the nature and composition of the seafloor. Among the drawbacks of sidescan sonar systems is the fact that the vast majority is used on towed or autonomous underwater vehicles resulting in difficulties to provide accurate navigational data. Some users find it difficult to interpret backscatter data that are generally uncalibrated and frequently show alternating angles of ensonification across the swath (Fig. 6). The latter can be overcome by a survey design using more than 50% overlap between adjoining swaths. This survey design has the advantage of producing two images with different “illumination” but almost doubles survey time. The biggest drawback, however, for many users is the absence of bathymetric information from standard sidescan sonar systems. Interferometric sidescan sonar overcomes this problem and provides a cost-effective tool for quick bathymetric and seafloor backscatter imagery surveys of the seafloor, as these systems are still cheaper than multibeam systems and cover wider swaths. Survey parameters such as towing altitude and choice of pulse length are well-tuned for either bathymetry or seafloor backscatter imagery.

5 Future Developments

Sidescan sonar systems are still widely used in mine detection, submarine pipeline inspection and marine archaeology. It is easy to predict that current developments such as synthetic aperture sonar and parametric synthetic aperture sonar will become more widely available even though these systems are significantly more expensive than traditional systems and require improvement in the navigation accuracy of the towfish and/or AUV. In terms of frequencies used for sidescan sonar, the end of the range appears to be reached. Physics effectively limits the use of even higher frequencies, because attenuation becomes too strong and in consequence the range becomes too small. Additional progress will likely come from improvements in signal processing and a better use of multi-frequency sonar capabilities. The use of colour to represent the different sonar frequencies allows representing more of the information content of the data and appears to be promising (Tamsett et al. 2016). At present, this is limited to multi-frequency instruments, but in the future it might be possible to use the chirp signal for such an

approach. Another field that is likely to develop in the future is the use of multi-platform sonars that are installed on an entire swarm of AUVs that communicate with each other. In this way, specific targets on the seafloor are illuminated from several different grazing angles and even different frequencies, which may significantly improve our capacities to characterise the seafloor at any given location.

Acknowledgements Tim Le Bas is thanked for the critical reading of an earlier version of this chapter.

References

- Bass GF (1968) New tool for undersea archaeology. *Nat Geogr* 134:403–423
- Belderson RH, Kenyon NH, Stride AH, Stubbs AR (1972) Sonographs of the sea floor. A picture atlas. Elsevier, Amsterdam
- Blackinton JG, Hussong DM, Kososalos JG (1983) First results from a combination of side-scan and seafloor mapping system (SeaMARC II). *Proc Offshore Technol Conf OTC* 4478:307–314
- Chesterman WD, Clynick PR, Stride AH (1958) An acoustic aid to sea bed survey. *Acustica* 8:185–290
- Clay CS, Ess J, Weisman I (1964) Lateral echo sounding of the ocean bottom on the continental rise. *J Geophys Res* 69:3823–3835
- De Moustier C (1988) State of the art in swath bathymetry survey systems. *Int Hydro Rev* LXV: 25–54
- EEZ-Scan 84 Scientific Staff (1986) Atlas of the U.S. Exclusive Economic Zone, Western Conterminous United States: U.S. Geological Survey Miscellaneous Investigations Series I-1792, scale 1:500,000, 152 pp
- EEZ-Scan 85 Scientific Staff (1987) Atlas of the U. S. Exclusive Economic Zone, Gulf of Mexico and Eastern Caribbean Areas: U. S. Geological Survey Miscellaneous Investigations I-1864-A, scale 1:500,00, 104 pp
- EEZ-Scan 87 Scientific Staff (1991) Atlas of the U. S. exclusive economic zone Atlantic continental margin: U. S. Geological Survey Miscellaneous Investigations Series I-2054, 174 pp
- Gardner JV, Field ME, Twichell DC (eds) (1996) Geology of the United States Seafloor: the view from GLORIA. Cambridge University Press, Cambridge, p 371
- Hackmann WD (1985) Seek and strike: sonar, anti-submarine warfare and the Royal Navy, 1914–54. Stationery Office Books, London, p 522
- Hagemann J (1958) Facsimile recording of sonic values of the ocean bottom. US Patent 4197591A. <http://www.google.com/patents/US4197591>. Accessed on 28 Apr 2016
- Huggett QJ, Millard NW (1992) Towed ocean bottom instrument TOBI: a new deep-towed platform for side-scan sonar and other geophysical surveys. *Offshore Technol Conf*. doi:[10.4043/6849-MS](https://doi.org/10.4043/6849-MS)
- Johnson HP, Helferty M (1990) The geological interpretation of sidescan sonar. *Rev Geophys* 28:357–380
- Klaucke I, Masson DG, Petersen CJ, Weinrebe W, Ranero CR (2008) Multifrequency geoacoustic imaging of fluid escape structures offshore Costa Rica: implications for the quantification of seep processes. *G-cubed* 9:Q04010. doi:[10.1029/2007gc001708](https://doi.org/10.1029/2007gc001708)
- Kosalos JG, Chayes D (1983) A portable system for ocean bottom imaging and charting. *OCEANS'83 proceedings*, pp 619–656
- MIT museum. <http://web.mit.edu/museum/exhibitions/klein-side-scan-sonar.html>. Accessed 26 Jul 2016

- Rosencrantz DM, Klein M, Edgerton HE (1972) The use of sonar. In: Underwater archeology: a nascent discipline, Paris, pp 257–270
- Rusby S (1970) A long-range sidescan sonar for use in the deep sea (G.L.O.R.I.A. project). Int Hydrogr Rev 47:25–39
- Somers ML, Carson RM, Revie JA, Edge RH, Barrows BJ, Andrews AG (1978) GLORIA II—an improved long range sidescan sonar. In: Proceedings of the Institute of Electrical Engineering on Offshore Instrumentation and Communications, Oceanology International Technical Session J BPS Publications, London pp 16–24
- Tamsett D, McIlveny J, Watts A (2016) Colour sonar: multi-frequency sidescan sonar images of the seabed in the inner sound of the Pentland Firth, Scotland. *J Mar Sci Eng* 4:26. doi:[10.3390/jmse4010026](https://doi.org/10.3390/jmse4010026)
- Tucker MJ, Stubbs AR (1961) A narrow-beam echo-ranger for fishery and geological investigations. *Brit J Appl Phys* 12:103–110
- Wille PC (2005) Sound images of the ocean in research and monitoring. Springer, Heidelberg, p 471
- Zakharina M, Dybedal J (2007) The parametric sidescan sonar instrument and synthetic aperture sonar processing. In: Blondel P, Caiti A (eds) Buried waste in the seabed: acoustic imaging and biotoxicity (results from the European SITAR project). Springer, Heidelberg, pp 13–18

Multibeam Echosounders

John E. Hughes Clarke

Abstract Multibeam echosounders have revolutionized our ability to resolve seabed geomorphology and regionally define its substrate. Using a fan of narrow acoustic beams, the slant ranges, angles and returned backscattered intensity can be employed to define the seabed elevation and infer the substrate. A corridor of data with a width proportional to the projected angular sector is acquired along a vehicle track. Before interpreting the resulting geomorphology, however, it is critical to understand the practical resolution and accuracy limitations that result from a particular system configuration. The spatial resolution of the data depend on a combination of the pulse bandwidth, the projected beam widths and their resulting spacing and stabilization. For a given configuration, the single biggest factor controlling the resulting resolution is the altitude of the platform. For surface mounted systems this results in degrading definition of morphology with depth. As multibeam systems improve, there is the potential to monitor temporal changes in submarine geomorphology. To do so, however, each survey has be positioned to a standard finer than the expected change. The total propagated uncertainty in the location of the resolved topography is a combination of the uncertainty in the position and orientation sensors and their integration as well as the bottom detection algorithm and sound speed field. When interpreting apparent change, it is critical to comprehend the realistic achievable accuracies.

1 Introduction

1.1 *Review and History*

Multibeam sonar systems have become ubiquitous with underway marine geological operations. They have now been available to the scientific community for

J.E. Hughes Clarke (✉)
Center for Coastal and Ocean Mapping,
University of New Hampshire, Durham, NH, USA
e-mail: jhc@ccom.unh.edu

almost four decades. The first operational system was developed for the US Navy in 1964 (Glenn 1970) and by 1977 the first declassified version was available for scientific submarine geomorphological studies (Farr 1980). Since that time, the academic fleets have progressively adopted hull mounted multibeam systems as a standard tool and their use has revolutionized our understanding of seafloor processes.

All these early systems were developed for deeper water using frequencies ranging from 12–30 kHz. The first really shallow water multibeam (500–1000 kHz), was developed in 1984 for offshore oil and gas infrastructure support (Hammerstad et al. 1985). Since that time these shorter range systems have increasingly been adopted to define coastal and shelf submarine geomorphology (Hughes Clarke et al. 1996).

The original driving force behind the development of multibeam sonar arose from military requirements to navigate submarines and ballistic missiles over ocean basins using inertial sensors. Bathymetric terrain matching allowed submarines to update their position without surfacing. Deflections of the gravity vector due to large scale seabed relief such as seamounts were a significant source of error for inertial navigation. The technology was rapidly adopted to support the laying of both military and commercial deep sea cables. As an incidental byproduct of the surveying, it became apparent that there was much to be learnt about seabed morphology at lengths scales above a few hundred metres. This length scale reflected the resolvable topography at those depths and matched the best capable offshore navigational accuracy of the time (transit satellites and single point GPS).

The incentive to develop these systems in continental shelf depths was driven by the increasing exploitation of offshore oil and gas fields. At shorter ranges, features could now be resolved down to wavelengths less than 10 m. As such it placed increasing demands on navigational accuracy. Near coastal navigation systems such as Decca and Loran were not adequate, but as Differential GPS was developed this became feasible. Over the past two decades, the parallel improvements in positioning and sonar technology have continued to drive down the positioning uncertainty and minimum resolvable dimensions. This has opened up new applications in submarine geomorphology.

1.2 *Current Uses in Submarine Geomorphology*

As the early systems were all developed for oceanic depths, the immediate benefit was primarily for deep ocean morphology ranging from mid ocean ridge fabric to continental margin mass wasting. The great advantage over single beam sounding was that the observer could now examine a three dimensional surface rather than interpolate between sparse two dimensional profiles. This allows the discrimination of lineaments in azimuth, something that previously had not been possible without

subjective extrapolation. With a 3D surface, the directional roughness spectrum could now be directly measured (Fox and Hayes 1985). At the same time it became apparent that geomorphic interpretation had to be tempered by knowledge of the limitations inherent in the multibeam systems themselves (de Moustier and Kleinrock 1986).

For the first 20 years of use, given the paucity of preceding data, the main aim was to define the current state of the seafloor. Beginning in the early 90's as survey density increased, interest arose in the ability to resolve seabed change.

The first example of this for change detection was Fox et al. (1992). They were able to recognize the localized expression of 50 m depth changes (in 2000 m of water) due to fresh lava flows. The lateral extent of the flows were several hundred metres, allowing identification even with the poor positioning confidence of the time.

2 Physical/Technical Principles of the Method

2.1 Imaging Geometry

A multibeam sonar consists of a pair of orthogonally mounted linear acoustic arrays. The transmitter (Tx) is usually oriented along the fore-aft axis of the bottom of the vessel whereas the receiver (Rx) is mounted athwartship. The system may be broken into its transmit geometry and reception geometry (Fig. 1). The initial description herein reflects a single sector multibeam.

On transmission, a corridor across track is illuminated with a beam that is narrow in the fore-aft direction. Using the receiver, multiple channels are simultaneously formed from beams which are spaced at different across-track steering elevations (Fig. 1c). When the illumination pattern on the seafloor is matched with the reception pattern, a series of small beam footprints are formed. Within each of those footprints, a slant range to the seabed can be estimated and the backscattered intensity at that point can be measured. Using the imaging geometry (azimuth and depression angle of the beam) and correcting for the refracted ray path, a depth at each footprint can be estimated. And if the received intensity is corrected for geometry (ensonified area and range) and radiometry (source level and beam patterns), an estimate of the bottom backscatter strength may be derived (de Moustier 1986) which is strongly correlated with the seabed composition (see also Chapter “[Sidescan Sonar](#)”).

A bathymetric and bottom backscatter map can thus be collated by combining these data collected along a swath on either side of the ship’s track (Fig. 2). As the swath is defined by an angular sector, the swath width usually grows linearly with depth. Similarly, as the solution density reflects the projection of beams spaced at different angles across the swath, the achievable resolution of the system will also degrade linearly with depth.

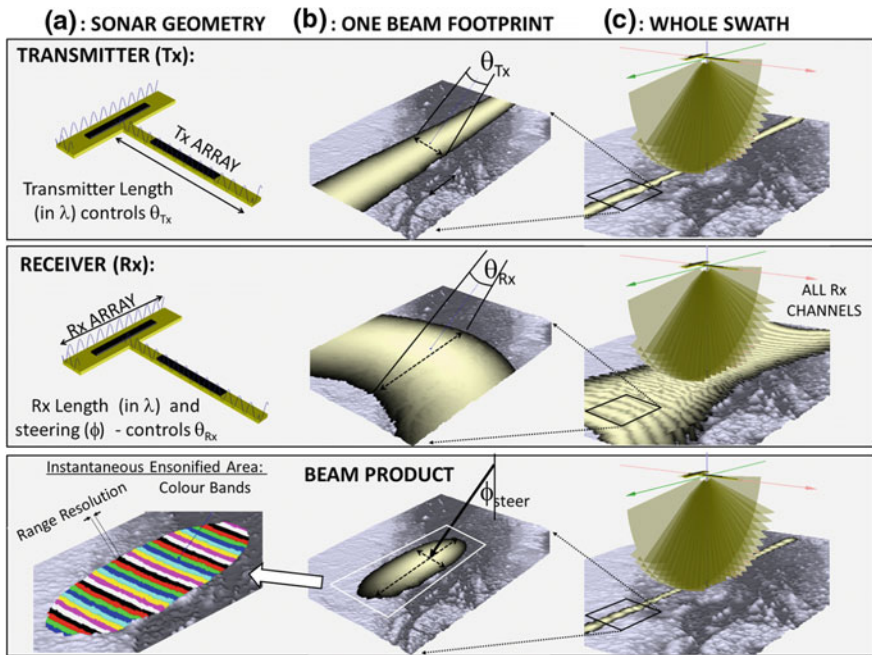


Fig. 1 Combination of the transmitter (Tx) and multiple receiver (Rx) beam footprints to generate multiple narrow beams across track. Illustrating the projection of the two narrow axes of the Tx and Rx beams to form a single elliptical footprint product

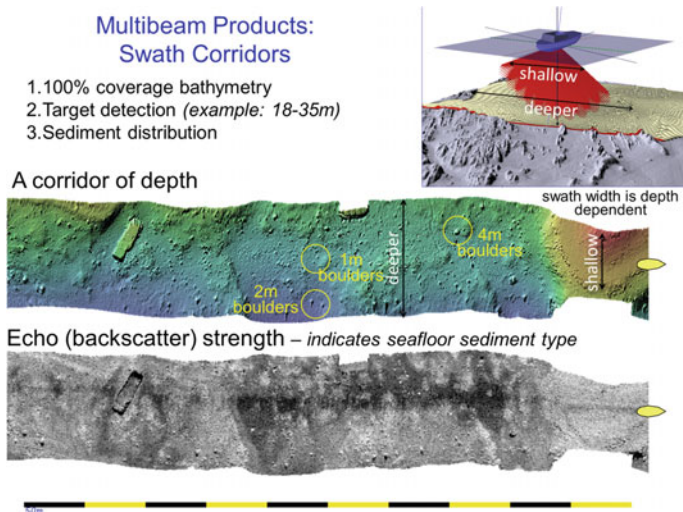


Fig. 2 Acquiring a corridor of multibeam bathymetry and backscatter over varying depth terrain

2.2 Range Performance

As multibeams are most commonly used from the surface, the required range performance will vary from full ocean to coastal depths. Depending on the depth in the area of interest, the sonar frequency choice needs to be optimized. Range performance of a system is based on maintaining sufficient signal to noise ratio (SNR). The range dependent component of this has both a geometric component (spherical spreading) which is frequency independent and a path length attenuation component which is strongly frequency dependent (Francois and Garrison 1982). As a result lower frequencies, which have lower attenuation coefficients, are utilized in deeper water.

The total achievable range is dependent on the source level, the frequency dependent attenuation coefficient, the scattering properties of the seafloor, the length of the pulse utilized and the background noise levels. Most sonars operate at their maximum source level and thus the only operator-controlled variable is the pulse length. As the pulse length controls the ensonified area (colour bands in Fig. 1 lower left), as a sonar system goes deeper, the pulse length is usually increased to maximize the signal to noise.

The net result of all these factors is that a performance envelope plot (Fig. 3) can be generated that predicts the useable depth and swath width coverage that can be achieved for a given sonar frequency. Note that the swath width initially grows linearly with depth until the outer most beam bottom detections drop below the usable SNR. Beyond that depth, the advertised maximum angular sector of the sonar can no longer be obtained and the total swath width in metres generally slowly shrinks with depth. Those bottom detections close to the SNR limit will exhibit higher range uncertainty.

Given a specific sonar configuration, the environmental factors that affect range performance are noise conditions and seafloor geology. Plots like Fig. 3 usually provide a family of curves depending on seabed type (gravel, sand, mud) and assume a specific noise level. While there are environmental factors that control noise in the ocean, one of the largest factors is vessel self-generated noise. One particular factor is flow noise and engine/propeller noise. Both of these usually increase with speed. The net result is, to achieve the intended swath width, the vessel can rarely steam at its full transit speed. Slowing down provides notably improved data quality. The geomorphologist should thus temper their desire to increase coverage by using higher speeds.

An ideal choice of multibeam is one in which the SNR threshold has not been reached at the outer edge of the desired swath. At the lowest frequencies commonly used (~ 12 kHz), this is not limiting until about 2–3000 m depth. If a wide range of depths need to be covered, however, the frequency most suitable for the deeper end of the depth range will not have the best range resolution in shallower depths. We thus have to consider the tradeoff between range performance and range resolution.

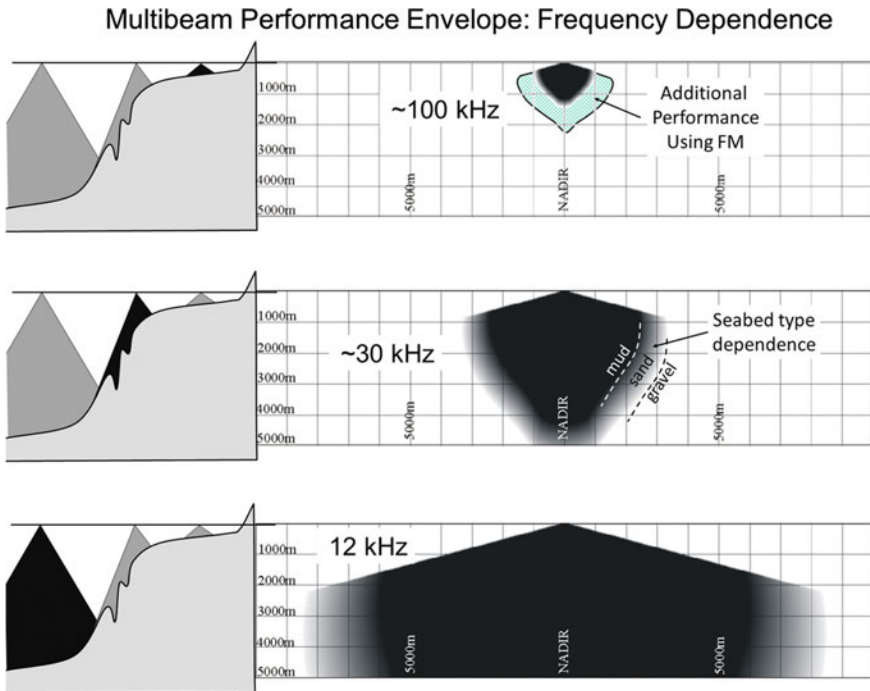


Fig. 3 Performance envelope of typical shelf, slope and rise multibeam systems

2.3 Range Resolution

The ability to discriminate targets in range (time) is a product of the bandwidth of the transmitted pulse. For a simple continuous wave (CW) pulse in which the carrier frequency is not varied, the effective range resolution corresponds closely to the pulse length. In this case the bandwidth of the pulse is approximately the reciprocal of the time duration of the pulse length. The shortest pulses that most sonars can generate are about 10 wavelengths long (equivalent to having a bandwidth of 1/10 of the centre frequency). Thus low frequency sonars usually have poorer range resolution. For example a deep water 12 kHz sonar typically has a best range resolution of 1–2 m. For this reason, as a survey moves into shallow water, and the range performance is no longer needed, higher frequency sonars are preferred.

Since ~2005 frequency modulated (FM) pulses have been introduced that maintain high bandwidth even with longer pulses. This has meant that the higher frequency systems can now be used in deeper water (see 100 kHz FM example in Fig. 3). As a result even higher frequency coastal sonars (200–400 kHz) are now being used on the shelf and 30 kHz systems are being used to full ocean depth.

As Fig. 3 indicates, there is a natural progression from the continental shelf to the full ocean depths of switching between multibeams of progressively lower centre frequencies as the tradeoff between range resolution and range performance is optimized. The next system component to consider is the angular resolution.

2.4 Angular Resolution

The angular resolution is a combination of the achievable beam width and the potential to discriminate angles within a single beam. The width of an unsteered sonar beam is approximately inversely proportional to the number of wavelength along the length of the linear arrays. For example a 1° beam (with reasonable sidelobe suppression) requires about 60–70 wavelengths. Thus a typical deep water 1° 12 kHz multibeam has a transmitter that is about 8 m long. A 30 kHz system requires about 3.5 m and a 100 kHz system needs only 1 m.

Larger arrays are both more expensive and require more available space on the bottom of the hull. Thus many multibeam systems come in a choice of array sizes depending on the surveyors need for angular resolution. Figure 4 illustrates the effect of varying beam width on the definition of a seabed target (in this case an object that subtends $\sim 0.75^\circ$ at that depth).

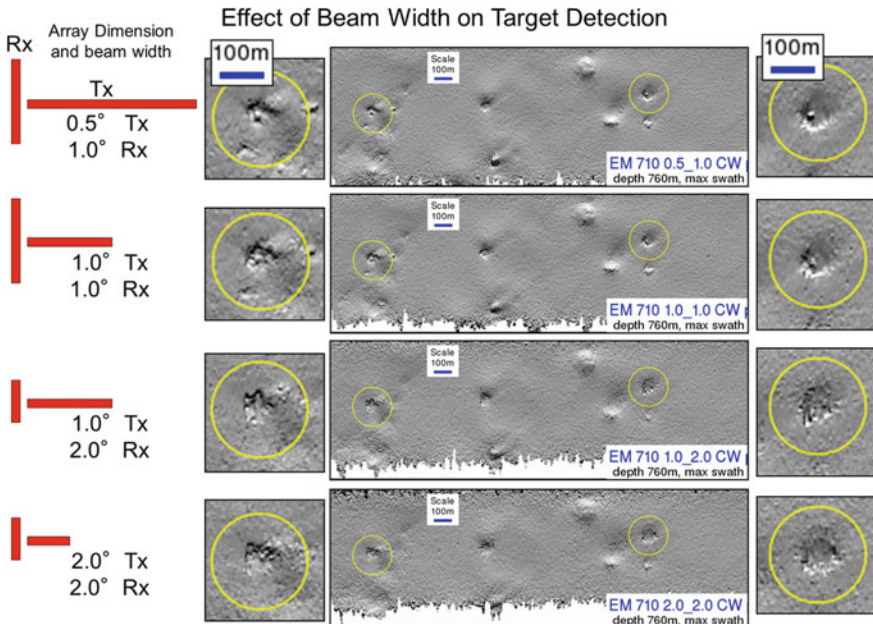


Fig. 4 Varying resolution as a function of beam width. Scour depression around targets in 760 m of water. 100 m wide, 5 m deep depressions in which a ~ 10 m wide target is centred. In each pass the utilized length of the transmitter and receiver arrays is altered to illustrate the effect of projected along and across track beam width on the target definition

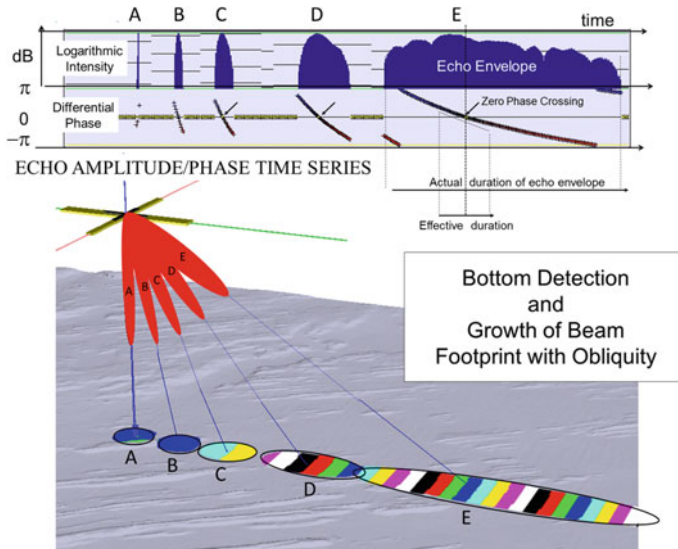


Fig. 5 Cartoon illustrating 5 representative steered beams with their projected beam footprints and corresponding echo amplitude and phase time series. Beams A and B would favour amplitude detection whereas beams C, D and E would favour phase detection

The simple relationship described above only applies to an unsteered beam. As the beam is steered its width grows inversely with the cosine of the steering angle. Thus, for example, beams steered at 60° are twice as wide. As most multibeam receivers are mounted horizontally that means that the beam width fattens away from nadir. Combined with the fact that the slant range to the seafloor is greater at oblique angles, and the beam subtends an oblique angle on the seabed, it can be appreciated that the across-track beam footprint (Figs. 1 and 5) grows rapidly toward the edge of the swath.

2.5 Bottom Detection

Given a specific range resolution and angular resolution, the multibeam needs to estimate the slant range within each projected beam footprint. A variety of methods are employed depending on the grazing angle of the beam.

Beams that are oriented close to normal incidence generally employ an amplitude detection method based on finding the centre of the echo envelope (indicated in Fig. 5). This results in an estimate of an average depth over an area the size of the whole beam footprint (defined by the projected across and along track beam widths, Fig. 1b). At lower grazing angles, the projected beam footprint rapidly becomes very large resulting in poor amplitude detection results. In this case split-aperture

methods based on differential phase are preferred (Pohner and Lunde 1990). These provide an estimate of the depth over an area that now has an effective across track dimension much narrower than the physical across track beam size (Fig. 5). This is because it is based on the ability to discern the point of zero phase crossing (Fig. 5) rather than the actual duration of the echo envelope. In this way, across track morphologic resolution can be maintained. A detailed review of bottom detection algorithms is provided in de Moustier (1993).

2.6 Sounding Density

To describe a certain minimum spatial wavelength on the seafloor, depth solutions have to be at least spaced at less than half that dimension (the Nyquist criteria). Additionally the effective projected beam footprint should not exceed that same half wavelength criteria in order that relief at that scale not be filtered out.

Even if these conditions are met, however, as each beam range solution has uncertainty, the minimum amplitude of that desired seafloor roughness will be overprinted by the pseudo random bottom detection noise. To alleviate this it helps to overlap the individual bottom detection footprints to get multiple redundant observations. Under these conditions, spatial averaging of the solutions by gridding will suppress the uncorrelated sounding noise but preserve the resolvable relief, thereby providing a better view of the short wavelength seabed morphology.

The amount of overlap between beam footprints depends on the along and across track beam spacing. The across track spacing is generally controlled by the desired swath sector. As the multibeam has a finite number of beam forming channels, the wider the requested sector, the less the noise suppression. In addition to the speed of the vessel, the along track spacing depends on the acoustic travel time to the outermost beams and back. Thus again the wider the swath angular sector the less the noise suppression.

Thus by bringing in the angular sector, both the across and along track beam overlap can be increased. This will markedly improve the definition of the seabed targets. Figure 6 illustrates a pair of small volcanic edifices which are imaged by the same sonar varying both the incidence angle and the swath sector. As can be seen, by selecting narrow sectors, the definition of the relief on the edifice improves.

3 Integrated Sensors

The sonar system can only provide range and angle discrimination within a coordinate system oriented relative to the two arrays. That is only of value when integrated with the 3D position of the sonar, its orientation and any subsequent modification of the beam vector in the heterogeneous ocean medium.

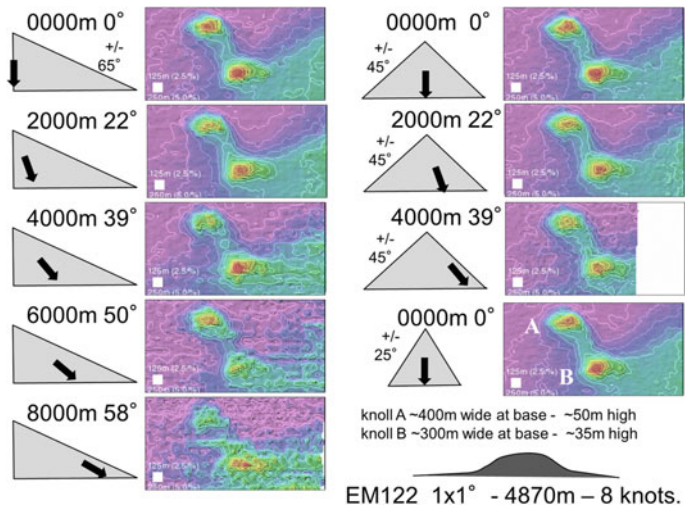


Fig. 6 Varying resolution as a function of angular sector and incidence angle. The same sonar is used with $\pm 65^\circ$, $\pm 45^\circ$ and $\pm 25^\circ$ sectors. The same pair of knolls are viewed using each sector width and from a range of incidence angles. A 125 m cube is illustrated for scale (2.5% of depth) and the contours are at 5 m intervals. Note particularly the presence of a secondary peak on the southern knoll

The detailed calculations to perform this integration are beyond the scope of this chapter. The curious geomorphologist should, however, be aware of the steps involved as imperfections in these steps will impact the resulting topographic surface producing both static biases as well as periodic undulations. These false deviations will degrade the morphology thereby obscuring the real relief. Additionally, if repetitive surveying is the aim, these biases and false oscillations will become embedded in the apparent seabed change map obscuring the signature of real sedimentary processes (Hughes Clarke 2012).

3.1 Vessel Reference Frame

In order to relate ancillary position and orientation measurements to a sonar, all of the position, orientation and sonar sensors needs to be located and oriented within a common vessel reference frame (VRF, Fig. 7a), which is fixed within the vessel and centred on a reference point (RP). Additionally, the relative timing (latency) between sensor outputs must be established.

Errors in the offset vectors are most critical in shallow water as they represent a significant percentage of the total range to the seabed. Angular errors are equally important irrespective of depth as the distortion of the resulting beam vector (Fig. 7b) produces a depth error that is a fixed percentage of the slant range.

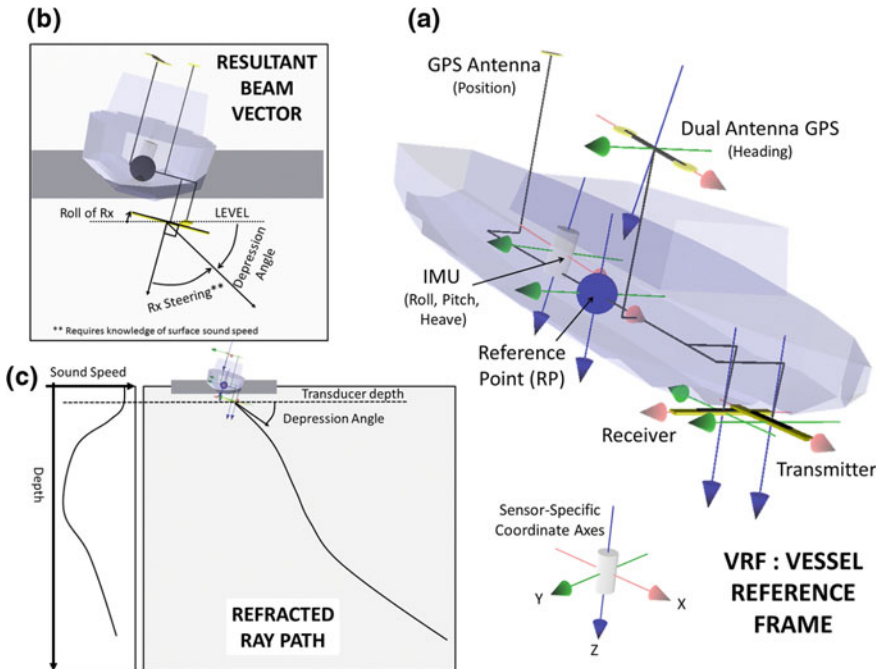


Fig. 7 Integration steps. **a** Vessel reference frame, showing sensor offsets and alignments. **b** Resultant beam vector, **c** Refracted ray path

Standardized field calibration procedures [the Patch Test (Godin 1998)] are used to estimate the sensor to sensor angular misalignments and time latency. Failure to constrain these errors will result in biases in the geomorphology and impact estimates of seabed change.

3.2 Orientation

The orientation, measured by the inertial measurement unit (IMU) is used in two steps. First, the orientation is required to account for the rotation of the lever arm between positioning source and sonar (Fig. 7a). This is a combination of (1): the instantaneous orientation of the IMU at transmit time and receive time and (2): the mount angle of the IMU with respect to the VRF. Once the sonar location is known, the next step requiring orientation is to calculate the beam vector from the sonar in both azimuth and depression angle relative to the local level (Fig. 7b). This is a combination of all of (1) the instantaneous orientation of the VRF at transmit time and receive time (2) the mounting angles of the Tx and Rx in the VRF and (3) the sonar-relative beam vector.

Orientation angle accuracy is now feasible within 0.02° (1σ). Of greater concern is usually the accuracy with which the IMU, Tx and Rx mount angles in the VRF are known. These can result in systematic biases in the resulting swath.

Given the rapid rate of change of orientation, any time latency in the motion output relative to the sonar clock will result in periodic distortions of the resulting swath (“wobbles”, Hughes Clarke 2003). Both the static biases and the periodic errors will distort the morphology and overprint the apparent seabed change.

3.3 Horizontal Positioning

With the arrival of the GPS constellation, and now other satellite constellations (e.g.: GLONASS), surface platform positioning confidence at the antenna location can range from a few metres (Differential GPS) to a few decimeters (Precise Point Positioning) to a few centimetres (Kinematic GPS).

Legacy multibeam data acquired prior to 1990 may have used transit satellite positioning with a horizontal uncertainty in the 200+ m range. Data acquired using single point GPS prior to 2004 would have been degraded by Selective Availability which limits the positioning to ~ 50 m. Given the size of a beam footprint in the deep ocean, such errors can be tolerated when examining morphology at those depths.

For continental shelf surveys, however, which only really started in the 1990s, little useful data would have been acquired that was not at least Differential GPS and thus positioning within 2 m could be reliably achieved.

For more recent precise inshore multibeam surveys, in which the beam footprint is less than a metre, correspondingly higher antenna positioning accuracy would be required. To take full advantage of that level of accuracy, the VRF and its instantaneous orientation are essential to determine the unique trajectories of the sonar sensors (Fig. 8a).

3.4 Vertical Positioning

The sonar-relative depth provided by the multibeam has the vertical trajectory of the sonar embedded into it (Fig. 8b). In order to assign a meaningful depth, a vertical datum needs to be defined against which that sonar-relative elevation is referenced. Common options include mean sea level (MSL), the Geoid, Chart Datum, and the Ellipsoid. The first three are water level based and thus will be described together. The fourth datum is hard to practically realize but, as will be explained has significant advantages in reproducibility.

To reduce to the chosen datum requires a measure of the instantaneous relative offset of the sonar. That offset can be broken down into different motion periods. At the highest frequencies, the sonar is moving up and down with motions around the

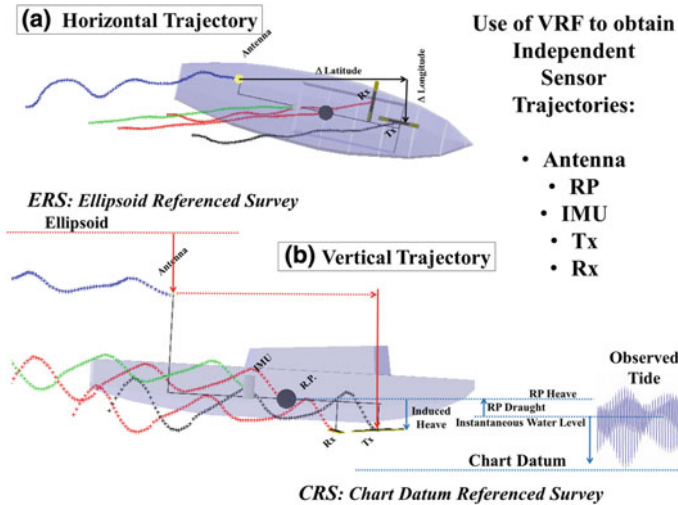


Fig. 8 Illustration of the use of the VRF to calculate the unique (a) horizontal and (b) vertical trajectories for each of the sensors in the ship. The two alternate vertical referencing strategies (*ellipsoid* or *chart-datum*) are shown

ocean wave spectrum. This can be captured using accelerometer-based heave sensing. Care must be taken to account for additional high frequency motion due to lever arm effects between the point at which the heave is reported (usually the RP) and the sonar (the induced heave).

For all the water level datums, once the short period motion is removed, the offset between the RP and the wave free water surface (the RP draught) needs to be estimated (CRS: Fig. 8b). This has both static and dynamic effects resulting from vessel loading and speed through the water. The remaining step is to measure the height of the wave free surface relative to the datum. This long period signal is dominated by tidal frequencies. As the amplitude and phase of the tide varies spatially this can be the single largest source of error for water level based vertical referencing.

An alternate to water level based referencing is to use the coordinate system that GPS is inherently measured in. The horizontal positioning is already WGS84 referenced, but an antenna height relative to that ellipsoid is also available (ERS: Fig. 8b). The offset between the geoid or mean sea-level from the ellipsoid varies, however by over a 100 m globally. Thus that offset needs to be measured separately (if required). If, however, the aim of the survey is seabed change, then if both surveys are ellipsoid referenced, they can be compared directly and all the imperfections in heave, draught and tide measurement are avoided completely.

3.5 Sound Speed

The final step in the integration is to account for the refracted ray path of the beam vector through the heterogeneous sound speed structure in the ocean (Fig. 7c). The sound speed is controlled by the temperature and salinity structure which varies due to oceanographic forcing. To correct for refraction, a vertical profile of the sound speed must be obtained which usually involves stopping the vessel. The challenge facing the surveyor is to decide how frequent that should be as it represents time lost toward expanding the coverage. To address this, the operator should be cognisant of the likely spatial and temporal variability in the local oceanography.

The application of sound speed involves two steps. Firstly, the array-relative beam steering requires knowledge of the speed of sound at the transducer face. Ideally there is a probe permanently mounted beside the transducers to update this continuously. This dictates the sonar relative beam vectors that are used in Sect. 3.2 to arrive at the local-level relative beam vector (Fig. 7b). The second step involves accounting for the refracted path as that ray vector leaves (and returns to) the transducer through a medium in which sound speed is known to be variable (Fig. 7c).

Imperfections in the sound speed reduction result in a depth error that grows non-linearly with across track distance. For the first step, this depth error is time varying as the vessel rolls and thus results in periodic outer swath oscillations (Hughes Clarke 2003). The second step results in a systematic bias with the across track profile either curved upward or downward (commonly referred to as “smiles and frowns”). Both of these effects degrade the resulting geomorphology.

4 State of the Art Tools

Position and orientation sensors have become increasingly reliable and accurate as well as affordable. To meet that improved positioning capability, higher resolutions are always in demand. For the sonar systems, the most common improvement has been narrower beams (culminating in the typical 0.5° – 1.0° beam widths seen today), more beam forming channels, and better bottom detection algorithms.

Given all of that, the remaining limitations in sonar resolution are mainly dictated by sounding density. Two principal factors limit even and high density sounding solutions: yaw perturbations and speed limitations. Both these can be solved if the older single transmit sector is broken down into multiple sub-sectors across track which can be independently steered (Fig. 9 left). This allows active yaw stabilization which ensures that yaw perturbations of the vessel no longer result in gaps in seafloor coverage. As an extension of this concept if those sectors are duplicated fore-aft (dual swath), one can generate more than one across track profile in a single ping cycle allowing doubling of the along track data density with resulting improved resolution (Fig. 9).

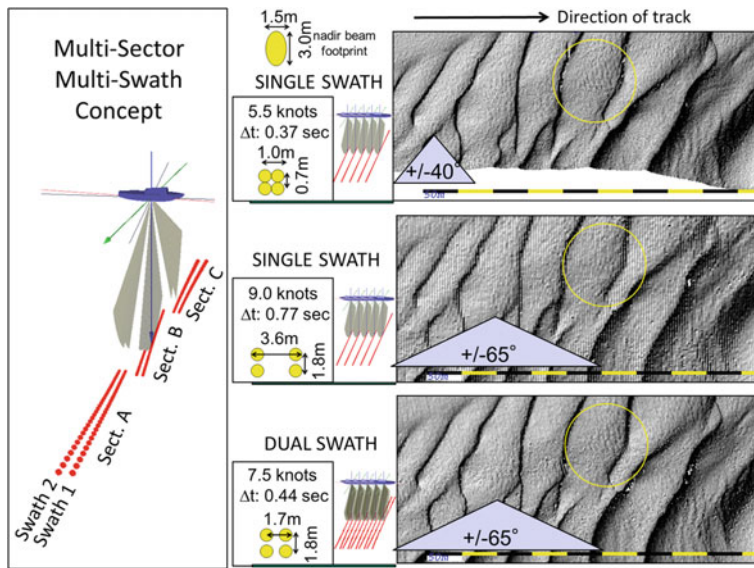


Fig. 9 Resolution and coverage benefits of dual swath. Three passes are compared over the same seafloor with ~25 cm high, 8 m long dunes (*circled*) developed on the back of larger dunes in 170 m of water. With single swath, the features are lost using a standard $\pm 65^\circ$ sector. To see them either requires pulling in the swath to less than half the width, or adding the second swath

State of the art multibeam echosounders nowadays also feature the “water column imaging” technique which adds the ability to detect features in the water column, such as bubble streams. While this is a direct indicator of seafloor processes, it is not strictly submarine geomorphology, and thus is not included in this chapter.

5 Strength and Weaknesses of the Method for Investigating Submarine Geomorphology

All the aspects explained above should aid the geomorphologist in predicting the minimum resolvable dimensions and with what confidence they can be positioned. This will impact the design of the multibeam survey which is always a compromise between desired resolution and areal extent. Thus the first thing to decide upon is the intent behind the survey. Specifically what is the smallest dimension of feature that needs to be resolved to address the geomorphic analysis, and what (if any) scale of change are you expecting?

Modern surface-mounted multibeam systems permit resolution down to a minimum horizontal wavelength of ~2% of altitude. Each step higher in resolution requires bringing the sonar closer to the seabed. If the required altitude is less than

the depth, then submerged vehicles have to be utilized. A submerged vehicle does not enjoy the advantages of continuous satellite position updates. The relative impact of additional position uncertainty due to submergence will be discussed in Chapter “[ROVs and AUVs](#)”. In short, the gain in resolution has to be balanced against the potential loss in accuracy.

Assuming the only option is a surface vessel, there are tradeoffs that can be made in order to balance coverage and resolution/accuracy. Given the slow and fixed speed of a survey vessel, the rate of areal coverage is mainly dependent on the angular sector employed. A wider sector allows greater coverage but there are a number of compromises in achieved resolution and accuracy.

For a given angular sector, the projected beam grows nonlinearly with obliquity which results in both larger footprints and associated higher bottom detection noise. Similarly, integration errors generally grow with increased obliquity. And with wider sectors, the across track beam spacing is wider and the along track beam spacing is sparser both of which result in less footprint to footprint overlap. All of these conspire to decrease the noise suppression and hence the effective resolution.

If the intent of the survey is to monitor changes in the resolved morphology through successive surveys, then accuracy will be critical. As discussed (in Sect. 3.3), the total propagated uncertainty reflects the choice of positioning and orientation sensors, their integration, the bottom detection and the refracted ray imperfections. For accuracy, it is primarily the systematic biases due to poor lever arms, imperfect mount angles, tidal errors and incorrect water column that dominate the accuracy. Again many of these contributions compound toward the edges of the swath.

In summary, while it may be attractive to cover more ground with a wider angular sector, the quality of the data, both in resolution and accuracy can be compromised. Narrower angular sectors provide both better along and across track data density as well as higher accuracy in bottom detection registration.

6 Conclusions

Multibeam echosounders are one of the most effective ways of resolving and locating seabed geomorphology. A submarine geomorphologist would ideally like both sufficient resolution to identify the signature of active land forming processes, as well as sufficient areal extent to understand the lateral variability in that signature. For a given sonar configuration, however, the resolution is predominantly a function of projected range which, for a surface mounted system, decays with depth. At the same time though, for a fixed angular sector, areal coverage can grow with depth. This benefit should be weighed against the option of constraining the angular sector to help maintain higher sounding density. Proper interpretation of the resulting resolved morphology relies on understanding how these factors can impact the achieved resolution.

The total achievable accuracy, from which you can start to estimate seabed change, is primarily a product of the integration of sensors comprising horizontal and vertical positioning, orientation and sound speed. The uncertainty in all of these can be minimized through proper calibration of alignments, offsets and latencies, as well as frequent sound speed updates and realistic choice of swath width. Understanding what realistic scale of resolvable change is achievable is critical when interpreting apparent geomorphic change.

References

- De Moustier C, Kleinrock MC (1986) Bathymetric artifacts in sea beam data: how to recognize them, what causes them. *J Geophys Res* 91(B3):3407–3424
- De Moustier C (1986) Beyond bathymetry: mapping acoustic backscattering from the deep sea floor with Sea Beam. *JASA* 79(2):316–331
- De Moustier C (1993) Signal processing for swath bathymetry and concurrent seafloor acoustic imaging. In: Moura and Louttit (eds) *Acoustic signal processing for ocean exploration*, pp 329–354
- Farr HK (1980) Multibeam bathymetric sonar: sea beam and hydrochart. *Mar Geodesy* 4(2): 77–93. doi:[10.1080/15210608009379375](https://doi.org/10.1080/15210608009379375)
- Fox CG, Hayes DE (1985) Quantitative methods for analyzing the roughness of the seafloor. *Rev Geophys* 23:1–48. doi:[10.1029/RG023i001p00001](https://doi.org/10.1029/RG023i001p00001)
- Fox CG, Chadwick WW Jr, Embley RW (1992) Detection of changes in ridge-crest morphology using repeated multibeam sonar surveys. *J Geophys Res* 92(B7):11149–11162
- Francois RE, Garrison GR (1982) Sound absorption based on ocean measurements: part I: pure water and magnesium sulfate contributions. *JASA* 72:896–907
- Glenn MF (1970) Introducing an operational multi-beam array sonar. *Int Hydrogr Rev* 47(1): 35–39
- Godin A (1998) The calibration of shallow water multibeam echo-sounding systems, M Eng. Report, Department of Geodesy and Geomatics Engineering Technical Report No. 190, University of New Brunswick, Fredericton, New Brunswick, Canada, 182 pp
- Hammerstad E, Lovik A, Minde S, Krane L, Steinset M (1985) Field performance of the benigraph high-resolution multibeam seafloor mapping system. *IEEE OCEANS'85*, pp 682–685. doi:[10.1109/OCEANS.1985.1160138](https://doi.org/10.1109/OCEANS.1985.1160138)
- Hughes Clarke JE (2003) Dynamic motion residuals in swath sonar data: ironing out the creases. *Int Hydrogr Rev* 4(1):6–23
- Hughes Clarke JE (2012) Optimal use of multibeam technology in the study of shelf morphodynamics. IAS Special Publication # 44. *Sediments, Morphology and Sedimentary Processes on Continental Shelves*, pp 1–28
- Hughes Clarke JE, Mayer LA, Wells DE (1996) Shallow-water imaging multibeam sonars: a new tool for investigating seafloor processes in the coastal zone and on the continental shelf. *Mar Geophys Res* 18:607–629
- Pohner F, Lunde EB (1990) Hydrographic applications of interferometric signal processing: proc. FIG XIX congress, commission 4, Helsinki

Reflection and Refraction Seismic Methods

Gareth J. Crutchley and Heidrun Kopp

Abstract Seismic reflection and refraction methods are routinely used to illuminate sub-seafloor geological relationships, thereby providing a means to investigate a wide range of Earth processes that influence submarine geomorphology. Since the birth of seismic methods for exploration of ore bodies and petroleum in the early part of the 20th century, progressive technological advancements have ensured that the seismic method remains a fundamental geophysical tool in both the oil and gas industry and scientific research. For both marine seismic reflection and refraction methods, the primary principles are based around the notion of sending artificially-generated sound waves downward into the Earth and recording the energy that returns to recording instruments (receivers). In the case of seismic reflection, the down-going wavefield reflects off geological boundaries characterized by density and velocity contrasts before being recorded by an array of receivers. In seismic refraction experiments, the notion is to record energy that has been refracted at multiple geological boundaries before, ultimately, being refracted at a critical angle and then returning to receivers on the seafloor. Survey designs for both methods are many and varied, ranging from relatively simple two-dimensional surveys, to multi-azimuth three-dimensional surveys that illuminate the subsurface from different directions. Although the state of the art in seismic methods is continually evolving, this chapter gives some examples of modern and developing trends that are relevant to investigations into submarine geomorphology. Examples include high-resolution 3D seismic imaging, high-frequency sub-bottom profiling, waveform inversion and deep-towed seismic acquisition. The strength of the seismic reflection method lies in its ability to gain insight into structural and stratigraphic relationships beneath the seafloor, as well as in investigating fluid flow processes. The refraction method, on the other hand, is often used as the tool of choice for crustal-scale investigations into deeply-rooted geological processes that

G.J. Crutchley (✉)

GNS Science—Te Pū Ao, 1 Fairway Drive, Lower Hutt 5011, New Zealand
e-mail: g.crutchley@gns.cri.nz

H. Kopp

GEOMAR Helmholtz Centre for Ocean Research Kiel, Kiel, Germany
e-mail: hkopp@geomar.de

shape the seafloor, such as plate tectonics and volcanism. As with all scientific methods, seismic methods are most powerful when combined with complementary geophysical, geological or geochemical methods to address a common Earth science question.

1 History of Seismic Methods

The marine seismic method involves the generation and recording of sound waves that reflect and refract as they interact with geological boundaries beneath the seafloor. The methods can therefore be divided into *reflection* and *refraction* seismic methods. A brief history of these methods is given here; a more thorough discussion can be found in Sheriff and Geldart (1995) and references therein.

Seismic waves reflected and refracted from geological boundaries were first noticed on recordings of waves produced by earthquakes. The use of controlled-source (i.e. not earthquake source) seismology to explore subsurface geology grew mainly out of commercial endeavors, in particular petroleum exploration. In 1924, the seismic refraction method was used by the company Seismos (founded by the German mine surveyor Ludger Mintrop) to make what is generally believed to be the first seismic hydrocarbon discovery.

The Canadian Reginald Fessender was the first to propose the use of seismic reflections for finding ore bodies, in a U.S. patent he submitted in 1914. In 1919, the American geophysicist John Clarence Karcher applied for patents in reflection seismology and later co-founded a geological engineering company that conducted field tests in Oklahoma. In 1925, Karcher and Everette Lee DeGolyer formed a company called Geophysical Research Corporation (GRC) and acquired Fessenden's patent. A few years later, one of the exploration parties working under GRC used the reflection method to find a geological structure that was drilled in 1928 to produce oil—the first successful application of the method for petroleum production. By 1930, the reflection method had begun to take over from the refraction method as the standard for oil and gas exploration.

A major advancement in seismic methods was made in the 1950s, with W. Harry Mayne's invention of common mid-point (CMP) stacking, which dramatically improved signal to noise ratios in the data. The principle of CMP stacking is introduced later in this chapter. The arrival of digital technology in the 1960s represented a revolution for seismic methods, as seismic data collection, storage and processing were all optimized. Another revolution, in the late 1960s and early 1970s, was the advent of three-dimensional (3D) seismic acquisition and processing; until that time, seismic surveys had been designed as two-dimensional (2D) profiles. Today, 3D surveying is the norm in the oil and gas industry, and is also widely adopted for academic research. However, 2D reflection and refraction surveys are still widely carried out for both regional and small-scale geological investigations, particularly in academic research.

2 Physical Principles

2.1 Basic Principles of the Seismic Reflection Method

The general principle of the seismic reflection method is that artificially-generated compressional seismic waves (known as *P-waves*) travel downward into the Earth, where they reflect off geological boundaries and then travel back to the surface to be recorded. In the marine environment, the seismic waves are usually generated behind a vessel from a controlled seismic source towed just below the sea surface (Fig. 1a). Reflected energy from these waves is recorded by receivers that are towed behind the source in a single cable or multiple cables. The recorded data are referred to as a shot record. By collecting lots of shot records at different locations, a seismic dataset is generated that is then processed to generate seismic images that reveal the nature of subsurface geology, including features like lithological boundaries, unconformities and faults (Fig. 1b). The vertical axes of seismic images are usually given in two-way travel time (s), rather than depth (m), since the reflections are recorded as the time it takes for the waves to travel from the source, down to the reflector, and back up to the receiver array. If the sub-surface seismic velocities can be adequately approximated, it is often appropriate to use these velocities to convert the sections from two-way time to depth, making them more intuitive for geological interpretation.

The first strong reflection in a marine seismic survey comes from the seafloor,¹ where there is a contrast in the physical properties of the water column above and the seafloor sediment below (Fig. 1b). This physical property contrast is known as an *acoustic impedance contrast*; each medium has its own acoustic impedance (Z), which is the product of the medium's inherent P-wave velocity (V_p) and density (ρ). The greater the acoustic impedance contrast, the more reflective is an interface between two layers. This reflectivity is represented by the *reflection coefficient* 'RC', which is defined at the interface between two layers as the ratio of the difference in the layers' acoustic impedance to the sum of the layers' acoustic impedance (Fig. 1c). The seafloor typically creates clear, well-defined seismic reflections due to the pronounced density contrast between water and sediment. Many other reflections (some strong, some weak) are also recorded after the seafloor, due to velocity and density contrasts inherent in sub-seafloor sequences of stratified sediments and underlying bedrock (e.g. Fig. 1b).

The depth to which one can 'see' seismic reflections beneath the seafloor depends on the penetration of the seismic signal, which is a function of the energy of the source and the physical nature of the geological media through which it travels. For example, layer boundaries with high reflection coefficients, such as a

¹It should be noted that seismic reflections can also be imaged above (i.e. before) the seafloor: Seismic oceanography is a relatively modern discipline that involves imaging stratification within the ocean (Holbrook et al. 2003).

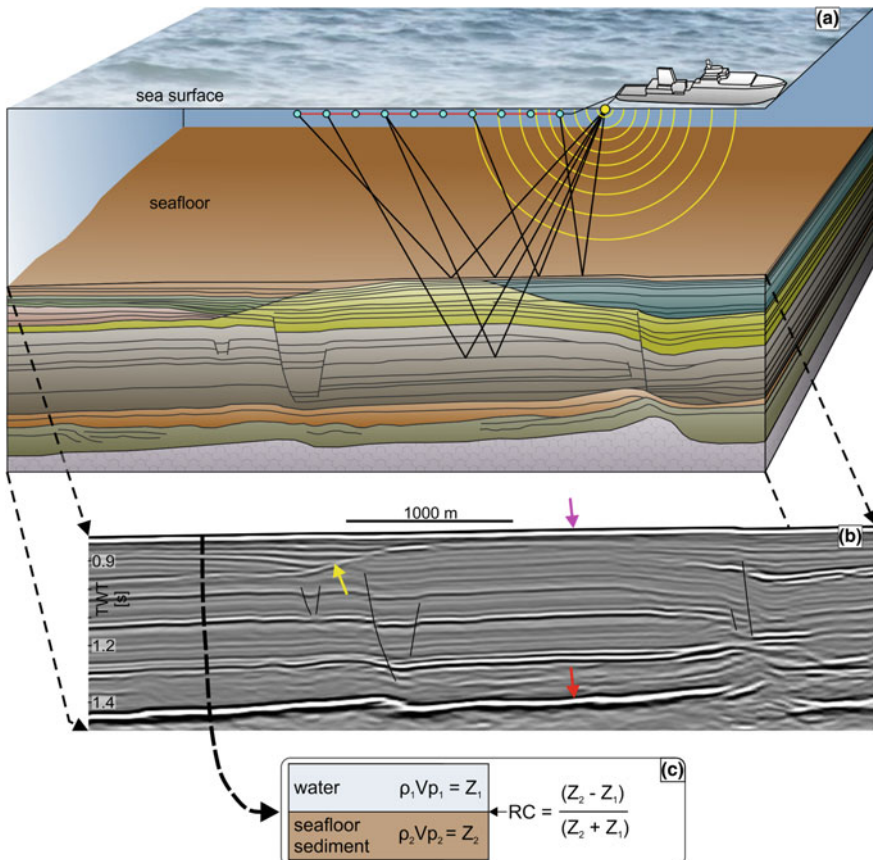


Fig. 1 **a** Schematic illustration of the seismic reflection method. Yellow dot behind the vessel is the seismic source. Yellow arcs represent propagation of seismic wave energy through the water column. Black lines are selected seismic ray paths that reflect off the seafloor and sub-seafloor layer boundaries. Cyan dots are sound receivers towed within a cable (red line) behind the vessel. **b** Example seismic image from the Chatham Rise, offshore New Zealand (data processed by Geotrace 2010). Purple arrow seafloor reflection; yellow arrow unconformity; red arrow strong reflection from bedrock; black lines faults. **c** The reflection coefficient (RC) of a geological interface is defined by the acoustic impedance (Z) of the layers above and below the interface

boundary between soft sediments and hard bedrock (Fig. 1b), will reflect much of the seismic energy and transmit only a small amount to greater depths.

The recoverable vertical resolution of reflections in a survey is a function of the frequency of the source. A general rule of thumb is that reflectors spaced vertically more than $\frac{1}{4}$ of a wavelength apart will be distinguishable (Sheriff and Geldart 1995). Thus, higher frequencies, which result in shorter wavelengths for a given seismic velocity (i.e. $v = f\lambda$), result in higher vertical seismic resolution. The seismic image in Fig. 1b has a dominant frequency of ~ 40 Hz, which means that

just beneath the seafloor, where seismic velocities are approximately 1500 ms^{-1} or slightly higher, the maximum vertical resolution is $\sim 10 \text{ m}$. Higher-frequency sources such as *Boomer* systems that operate at $\sim 1 \text{ kHz}$ can deliver vertical resolutions of less than 1 m (e.g. Müller et al. 2002).

2.2 Basic Principles of the Seismic Refraction Method

In contrast to the reflection seismic approach, refraction studies in academia are most commonly used to investigate large scale layering of the lithosphere's crust and mantle. Subsequent to data acquisition and processing, refraction studies involve forward and/or inverse data modeling to gain information on layer thickness and velocity.

The same basic physical principles of the seismic reflection method also apply to the seismic refraction method, where artificially-generated seismic waves propagate into the Earth and spread out as hemispherical wave fronts (Fig. 2a). The concept of a *ray path*, which trends perpendicular to the wave front, is used to describe the subsurface propagation of a wave. The wave returns to the surface by refraction at subsurface interfaces, which are characterized by an acoustic impedance contrast. The seismic signal is recorded by receivers that are placed on the seafloor at distances from the source that may reach ten times the depth of seismic energy penetration, which depending on the source and physical properties and heterogeneity of the subsurface, may be up to 30–40 km. Each receiver collects a *record section* of all shots fired along the profile. The horizontal axes of record sections usually display the shot's offset from the receiver, resulting in negative and positive offsets around the central zero offset where the receiver is located. The vertical axes are usually given in reduced time, i.e. travel time minus distance divided by a pre-selected velocity value (e.g. 8000 ms^{-1}), resulting in a data display where refraction arrivals with a P-wave velocity corresponding to the pre-selected velocity value will be horizontal in the travel-time diagram.

When seismic waves encounter a positive impedance contrast at a lithological contact between two rock types, the incident ray will be reflected (see Sect. 2.1) as well as transmitted into the lower medium. A transmitted wave through the lower medium is termed a diving wave. The angle of transmission (t) is related to the angle of incidence (i) through the compressional velocity ratio between the upper and lower medium (i.e. v_1/v_2) following Snell's law (Fig. 2a—inset). When the angle of incidence reaches the *critical angle* i_c , the angle of transmission is 90°. The critical angle is defined by the inverse sine of v_1/v_2 . The critically refracted wave then travels along the velocity interface at the velocity of the lower medium (i.e. v_2) and is continually refracting energy back into the upper medium at an exit angle equal to i_c . The resulting wave front is called a *head wave*, which provides constraints on the velocity boundary depth, like the Moho depth for example. It should be noted that an increase of seismic velocity with depth is a pre-requisite for a critically refracted wave. A velocity inversion will not generate a critical refraction

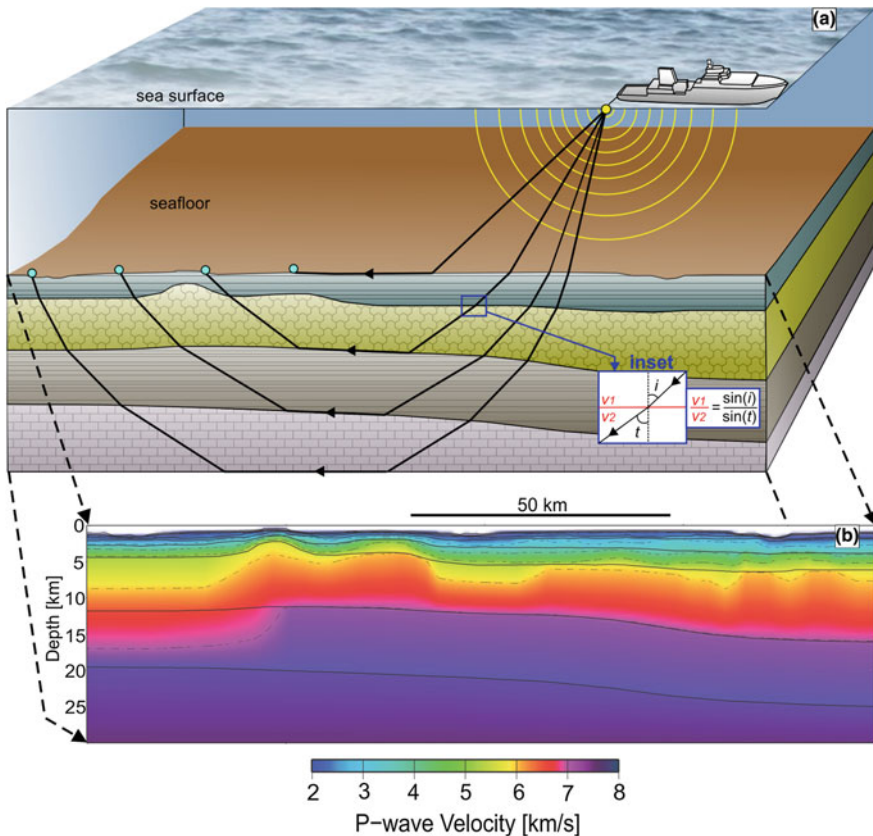


Fig. 2 **a** Schematic illustration of the seismic refraction method. Yellow dot behind the vessel is the seismic source. Yellow arcs represent propagation of seismic wave energy through the water column. Black lines are selected seismic ray paths that are critically refracted at the seafloor and sub-seafloor layer boundaries. Cyan dots are sound receivers on the seafloor. **a** (inset) Enlargement of raypaths at a layer boundary, where ' v_1 ' and ' v_2 ' are the velocities of the upper and lower layers, respectively, and ' i ' and ' t ' are the incidence and transmission angles, respectively. **b** Example seismic velocity profile after modeling. This velocity profile comes from an area near the Java forearc basin

and hence information from this ‘hidden’ layer is not recorded as the refracted rays are bent towards the normal (e.g. Banerjee and Gupta 1975).

In marine refraction studies, shots from a controlled seismic source are generated at equidistant intervals, which are commonly larger than shot intervals in reflection studies on account of the longer ray paths required for refracted arrivals. Hence, data acquisition for reflection and refraction seismic studies usually cannot be conducted simultaneously, but must be performed independently (Kopp et al. 2002). Due to the wide-angle geometry of refracted waves, acoustic wave generation by a controlled source should be extended to offsets beyond the seafloor

receiver transect in order to capture the entire wave field. The vertical resolution of seismic refraction studies is about 10–20% of the depth, while the lateral resolution is about half the receiver spacing on the seafloor. An example velocity model derived from a seismic refraction survey is given in Fig. 2b.

3 Survey Design and Processing

3.1 Seismic Reflection Surveys

3.1.1 Types of Marine Seismic Reflection Surveys

Marine seismic reflection surveys can be designed to produce 2D seismic sections (like the section in Fig. 1b) or 3D seismic volumes. For 3D data, the recent advent of *multi-azimuth* and *wide-azimuth* surveys has improved subsurface imaging in challenging geological environments, like beneath salt structures (Michell et al. 2006). 3D surveys that are repeated over time are known as 4D surveys, since they incorporate the extra dimension of time. Such surveys are used, for example, to monitor the progress of a reservoir during production (Fayemendy et al. 2012), or the sequestration of CO₂ into the subsurface (Chadwick et al. 2009). In this section, we provide a brief summary of fundamentals of acquisition and processing of seismic reflection data.

3.1.2 The Seismic Source

By far the most commonly used marine seismic source is the airgun, which, in essence, is a chamber of compressed air that is rapidly released into the water column as a bubble to generate an acoustic pulse (Parkes and Hatton 1986). A common type of airgun used in academic seismic reflection surveys is the *GI Airgun*, or *Mini GI Airgun*, where ‘GI’ stands for generator–injector. The principle is that the gun first fires compressed air from the primary chamber (generator) to produce the primary pulse, and then moments later fires from a secondary chamber (injector) to inject a pulse of air into the bubble near its maximum expansion. This second pulse dampens undesirable secondary energy produced during expansion and collapse of the bubble.

A range of other marine seismic sources exist, including implosive sources such as *water guns* and *Boomer* systems, and *sparker* systems that generate a source upon discharge of a large capacitor between two electrodes. Boomers and sparkers, for example, are commonly used for very high-resolution imaging of shallow sub-seafloor targets.

Marine vibrator-type sources are currently being developed in order to minimize the impact of seismic surveying on marine mammals (Pramik 2013). These sources, however, are still in a prototype phase.

3.1.3 Receiver Arrays

The receivers used to record the reflected energy in marine seismic experiments are called *hydrophones*, which are towed behind a vessel in cables called *streamers*. The hydrophones detect and measure pressure fluctuations in the water caused by the reflected sound waves.

In a 2D survey, a single streamer is towed behind the vessel (Fig. 1a). For oil and gas exploration, streamers are often as long as ~ 10 km to provide a large range of source-receiver offsets that are useful for multiple attenuation and seismic inversion—processes routinely carried out when exploring for oil and gas. Academic surveys often use much shorter streamers.

Receiver arrays used for 3D surveys are based on the principle of towing multiple streamers parallel to each other. In this way, multiple, closely-spaced subsurface lines can be acquired by a single sail line. 3D receiver arrays take on many different shapes and sizes, ranging from those designed to cover relatively small areas at high-resolution (e.g. array widths of ~ 100 m—Petersen et al. 2010) to large industry projects² where arrays can be more than 1 km across.

3.1.4 Recording Parameters

The amount and resolution of data recorded for both 2D and 3D seismic surveys depends on a range of recording parameters. These include the spacing between successive shots, the recording duration for each shot, and the sample rate during recording—i.e. how often a sample of the wavefield is recorded (e.g. every 2 ms). High-resolution surveys typically have relatively close spacing between shots, high sampling rates and short record lengths, while lower-resolution, deep-penetration surveys have sparser shot spacing and longer record lengths. Along with the selection of a source type and receiver array, these parameters need to be carefully considered during the design phase of a survey to ensure that the subsurface targets will be adequately imaged.

3.1.5 Basic Processing Steps

Seismic processing methodologies can be highly-specialized and variable, depending on the desired output product from the data. Methods are also constantly evolving to improve imaging and inversion for physical properties. Here, we give a succinct summary of some fundamental steps involved in conventional

²In 2013, the geoscience company CGG released a press statement claiming the largest man-made moving object on Earth—a 3D receiver array with an acquisition footprint of 13.44 km^2 . This was achieved by towing eight 12 km-long streamers in parallel, with 160 m spacing between the streamers.

image-based processing. Readers seeking more information on processing techniques are directed toward Yilmaz (2001) and Robertsson et al. (2015).

Deconvolution and filtering are early stage processes that are used to improve the temporal resolution and signal-to-noise ratio of seismic data. These processes are usually applied to the raw field data of each shot in the survey.

Geometry processing and CMP stacking involves defining all locations of shots and receivers in a survey, and assigning common midpoints (CMPs) between shot-receiver pairs. CMPs are geographic locations in the subsurface that will have been sampled numerous times by different shot-receiver pairs (Fig. 3). The shot-domain data (as collected in the field) can then be re-sorted into CMP gathers that have samples of the reflected seismic wavefield from different shots and receivers that originate from approximately the same geographic location. Using an understanding of sub-surface velocities, traces within a CMP gather are then stacked together to create just one representative vertical trace for a given location. Many CMP traces plotted next to each other produce a stacked seismic section.

Seismic migration, typically the last major stage in a conventional reflection processing workflow, is the process of moving dipping reflections to their true sub-surface locations and collapsing diffractions (Yilmaz 2001). The result is a sub-surface image like that shown in Fig. 1b. In modern seismic processing, migration routines are commonly carried out prior to stacking, either in the time domain, or, in the case of pronounced lateral velocity variations, in the depth domain. The image in Fig. 1b was generated by pre-stack time migration.

3.2 Seismic Refraction Surveys

3.2.1 Acquisition Geometries

Analogous to seismic reflection surveys, marine refraction studies may be conducted in a 2D or 3D geometry using receivers placed on the seafloor. 4D surveys are repeated recordings to monitor subsurface changes in space and time. 2D surveys are commonly laid out normal to the geological structure of interest, whereas 3D studies result in a data cube or volume (e.g. Westbrook et al. 2008). This geometry is also used in multi-azimuth surveys, where the azimuth is the angle between the shot line and the direction to a given receiver on the seafloor. Multi- to full-azimuth acquisition layouts hence ‘illuminate’ the subsurface target from different angles. The subsurface geology, including the geometry of lithological boundaries, is not directly obvious from the record sections of the individual receivers and is only evident after ray-tracing to iteratively account for all travel time arrivals and velocities.

3.2.2 Receiver Types

Conventional refraction surveys use four-component *ocean bottom seismometers* (4C OBS), combining one vertical and two horizontal geophones that are oriented orthogonal to each other and a pressure sensor (hydrophone) (Fig. 4). In addition to

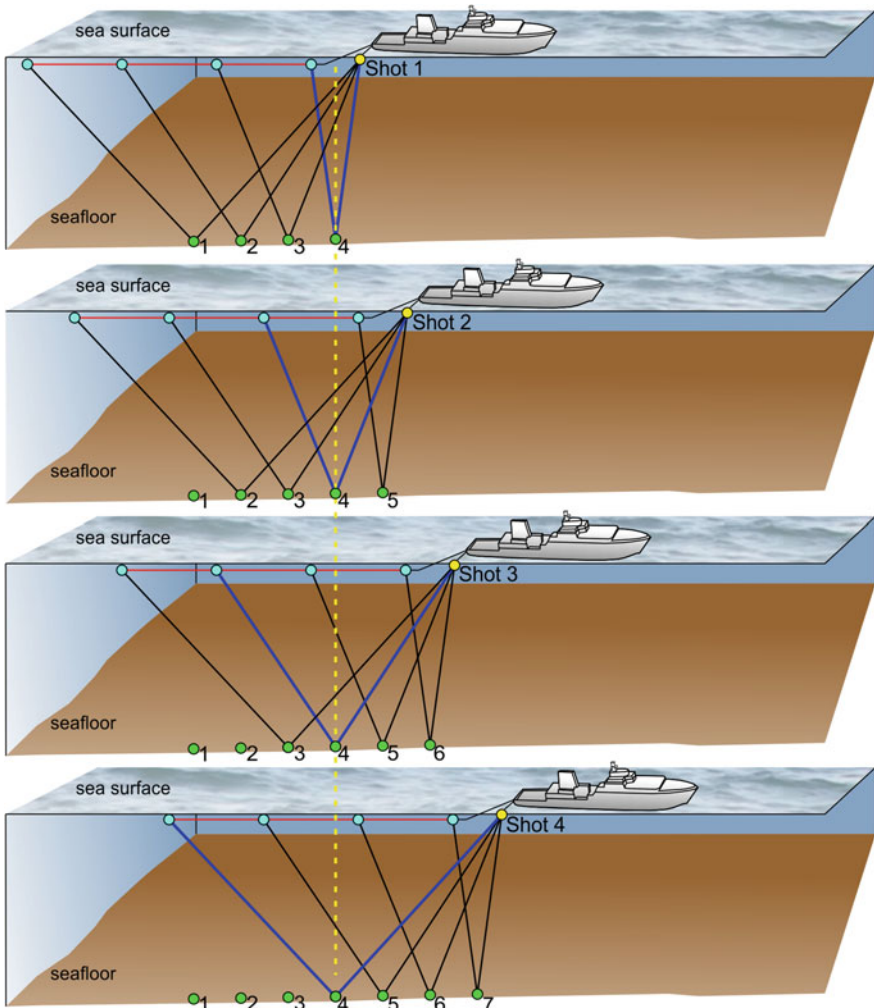


Fig. 3 Schematic illustration of combining different source-receiver pairs into a single CMP gather. Four successive shots are shown from *top* to *bottom* (Shots 1–4—yellow dots). For each shot, reflected energy is recorded in the four hydrophones (cyan dots). CMPs are the numbered green dots on the seafloor. The *broken yellow line* highlights CMP 4, which is sampled by each of the four shots over a range of source-receiver offsets (i.e. the *blue lines* showing ray paths.)

compressional P-waves, four-component receivers also record shear waves (S-waves), which present a significant motivation for recording data on the seabed. *Ocean bottom hydrophones* (OBH) only carry a pressure sensor. Both receiver types are usually deployed in a free-fall mode from a vessel. They carry a release unit to clear the anchor upon receiving an acoustic release signal. A flotation brings the instrument back up to the surface, where it will be recovered. Where higher

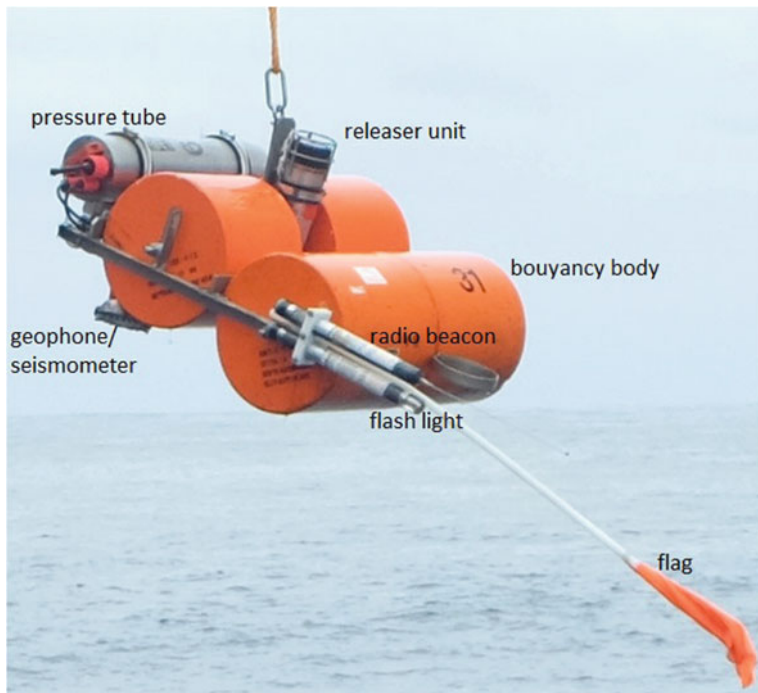


Fig. 4 Ocean bottom seismometer (OBS) designed by GEOMAR, Germany. During deployment to the seafloor the entire system rests horizontally on the anchor frame. The instrument is attached to the anchor with a release transponder. Communication with the instrument over ranges of 4–5 nautical miles ($\sim 8\text{--}9$ km) for release and range is possible through a transducer hydrophone. After releasing its anchor weight of approximately 60 kg, the instrument turns 90° into the vertical and ascends to the surface with the floatation on top

precision deployment locations are required, e.g. in areas with dense offshore infrastructure, autonomous *ocean bottom nodes* (OBN) are deployed and subsequently recovered with the use of remotely operated vehicles (ROV). *Ocean bottom cables* (OBC) contain numerous four-component sensors and are laid on the seafloor by a cable vessel. Alternatively, an OBC may be permanently deployed or buried in the ocean bottom to monitor temporal changes—a method known as life of field seismic acquisition.

3.2.3 Basic Processing Scheme

Standard processing of OBS data includes *clock drift correction* if differences between the long-term stabilization of the internal clock and the sample frequency clock occur. Additionally, within a given sample period, fewer or more samples than required can be recorded, e.g. 99 samples instead of 100, which needs to be corrected.

Drifting of the OBS in the water column during deployment may cause instrument positions to be mislocated by up to several hundred meters, leading to data asymmetry and incorrect travel time information in the record section. *Instrument re-location* is carried out using the water wave arrival and exact shot geometry.

Subsequently, a standard signal processing scheme will include a *time-gated deconvolution* to remove predictable bubble reverberations and obtain a clean signal without disturbing interference of multiple and primary phases. A deconvolution will improve the temporal resolution of the seismic data by compressing the basic seismic wavelet. The recorded wavelet has many components, including the source signature, recording filter, and hydrophone/geophone response. Ideally, the deconvolution should compress the wavelet components to leave only the subsurface reflectivity in the seismic trace. As the amplitude spectra of seismic traces vary with time and offset, the deconvolution must be able to follow these variations and hence is time-gated. In a further step, a *time and offset-variant frequency filter* accounts for frequency changes caused by signal attenuation. The filter's passband continuously shifts towards lower frequencies as offset and record time increase.

3.2.4 Forward and Inverse Modeling

Modeling of seismic refraction data includes the identification and picking of the various phases recorded. The data picks then are used as input to forward and inverse modeling approaches. Often, both approaches are used alternately to supplement each other. The idea of forward modeling is to solve the equation of motion for seismic waves. Rays travel through the geological model and the corresponding synthetic travel times are compared with the recorded seismic data. If the fit is within an acceptable level of accuracy, the model is a reasonable representation of the subsurface. If the travel time misfit is too large, the model is altered and new synthetic travel times are computed. This process continues iteratively until the misfit between calculated and real travel times matches the requirements.

In contrast, the inverse approach calculates the velocity-depth model from the acquired travel-time data, based on the linearized relationship between the travel time data and the velocity structure $Gm = d$, where 'm' is the unknown slowness vector (model), 'd' is the travel time vector (data) and 'G' is a matrix whose rows contain path lengths through each model element (grid) for a given ray path. Commonly the forward model provides the input model to the inversion. The determined model differences between forward and inverted velocity models are updated and refined in the forward model. The updated forward model then provides a new input model to the inverse step. The advantage of this procedure is the full control and stepwise adjustment of the model structures, which are built in the forward model.

4 State of the Art Tools and Methods

4.1 Overview

Seismic methods are continually evolving, often with much of the impetus coming from the oil and gas industry investing in new technologies to find oil and gas. In this section, we give a brief overview of a selection of state of the art tools and techniques that are applicable to submarine geomorphological investigations. What we present is just a selection of many important areas of reflection and refraction seismic methods, which are providing better illumination of challenging targets and allowing more constrained velocity models to be generated from seismic data.

4.2 Parametric Single-Beam Echo-Sounding

Acoustic imaging at the high end of vertical resolution is valuable for understanding fine detail of the most geologically recent processes that have influenced submarine geomorphology. Parametric single-beam echo-sounders are ship-mounted instruments that generate two, slightly different, high frequency signals (e.g. 36–39 kHz and 41–44 kHz, for the Kongsberg TOPAS PS40 system). The interference of these two high frequency signals in the water column results in a lower frequency signal (e.g. 2–8 kHz for the TOPAS PS40 system) with a narrow beam width that produces very high resolution images of the shallow sub-surface (e.g. more than 75 m penetration at a vertical resolution of ~ 15 cm in ideal cases—[Vardy et al. 2012](#)). Modern systems like this can produce very detailed images of sub-surface stratigraphy, structure and fluid flow processes.

4.3 Deep-Towed Seismic Acquisition

Much higher lateral resolution in marine seismic data can be achieved by towing the hydrophones close to the seafloor, rather than just beneath the sea surface (e.g. [Breitzke and Bialas 2003](#); [He et al. 2002](#); [Marsset et al. 2014](#)). Recent advancements in the field of deep-towed seismic acquisition have been driven by the development of a seismic source that is capable of operating effectively and consistently at variable water depths—that is, operating independent of hydrostatic pressure. The French marine research institute IFREMER has used such a deep-towed source with a single-channel receiver ([Leon et al. 2009](#)) and more recently with a deep-towed multi-channel streamer ([Marsset et al. 2014](#)). A major challenge with this technology is obtaining the very accurate positioning of the source and the hydrophones that is required for optimal imaging. [Marsset et al. \(2014\)](#) used a source with a frequency bandwidth of 220–1050 Hz, together with a

streamer comprising 52 channels spaced 2 meters apart. In order to be able to accurately predict the shape of the streamer at depth in the water column, each hydrophone was equipped with sensors to monitor changes in pitch, roll and heading during acquisition. Their dataset, acquired in the Western Mediterranean Sea, provided excellent high-resolution imaging of mass transport deposits amid turbidite and hemipelagic sedimentary successions.

4.4 High-Resolution 3D Seismic Imaging

High-resolution 3D images of the sub-seafloor are very powerful for studies of submarine geomorphology because they enable sedimentary and tectonic processes to be unraveled at a high level of detail. Technology that is at the state of the art in this space is the P-Cable seismic system, which was initially developed in Norway in 2001 and patented shortly thereafter (Planke and Berndt 2003). The system is based on multiple (up to 24) relatively short streamers (typically 25–100 m in length) towed close to each other (~ 10 m apart) behind the vessel. Dense receiver spacing within each of the closely-spaced streamers results in very high spatial resolution. Figure 5 shows an example of P-Cable seismic data from offshore Costa Rica that images paleo-channel systems. The horizontal resolution of these data is ~ 6 m and the dominant frequency is ~ 100 Hz. 3D surveying with even higher resolution systems (e.g. a 1.5–13 kHz chirp transducer array; Gutowski et al. 2008) can deliver vertical and spatial resolutions at the decimeter scale.

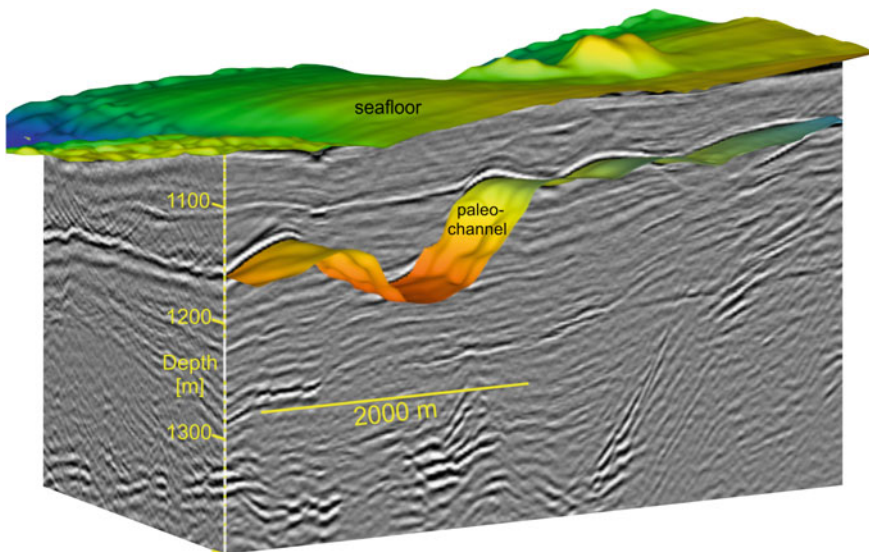


Fig. 5 3D view of high-resolution, depth-migrated P-Cable seismic data from offshore Costa Rica (data processed by Crutchley et al. 2014). Colored horizons are the seafloor and a paleo-channel

4.5 *Broadband Imaging*

A significant issue inherent in seismic acquisition comes from the *free surface ghost*—a phenomenon caused by the downward reflection of the upward travelling wavefield at the sea surface due to the fact that both source and receiver are towed beneath the sea surface. The result of the free surface ghost is both constructive and destructive interference of the seismic signal over the natural bandwidth of the source. The nature of the interference depends primarily on the depth of the receivers beneath the sea surface, and can result in major loss of energy at certain (desirable) frequencies. Towing the receiver array (i.e. streamers) at relatively shallow depths will compromise the ability to recover low frequencies, whereas towing at relatively deep depths will compromise high frequencies.

In recent years there has been a strong focus on extending the bandwidth of seismic frequencies recovered during acquisition—i.e. efforts have been made to design methods that reduce the ghost effect described above. One such method is the over-under deghosting method, where streamers are deployed as vertically aligned pairs at two different tow depths (Hill et al. 2006; Sonneland et al. 1986). In this method, the tow depths can be set such that the compromised parts of the frequency spectrum in one streamer are compensated for by the other, and vice versa. Combining the frequency spectra from both streamers in the under-over pair results in a broader frequency bandwidth with, in particular, greater recorded amplitudes at low frequencies. Using deeper tow depths than conventional acquisition also decreases the noise due to wave motion. Such deghosting methods can yield dramatic improvements in seismic imaging. For more information on this topic, the reader is referred to Robertsson et al. (2015) and references therein.

4.6 *Mirror Imaging of OBS Data*

The wavefield recorded by a seafloor receiver is composed of primary reflections, which travel up from the interface to the seafloor (up-going), as well as receiver ghosts or sea surface multiples. The latter represent an additional reflection off the sea surface, which acts as a ‘mirror’ (Fig. 6). The signal then travels back down from the sea surface to the seafloor (down-going). OBS surveys using only primary signals yield notoriously poor illumination for interfaces beneath the seabed that are shallower than the station interval (Grion et al. 2007). Illumination is improved by mirror imaging, where the multiple signals are also used (e.g. Dash et al. 2009). Depending on the water depth, the shot point grid laterally extends far beyond the receiver grid. Hence the mirror signal yields a much broader subsurface illumination than the primary signal. Mirror imaging consequently provides highly improved coverage and imaging of shallow structural elements. The receiver datum for mirror imaging is shifted to a level twice the water depth to account for the additional ray path of the multiple through the water column. The method is applied

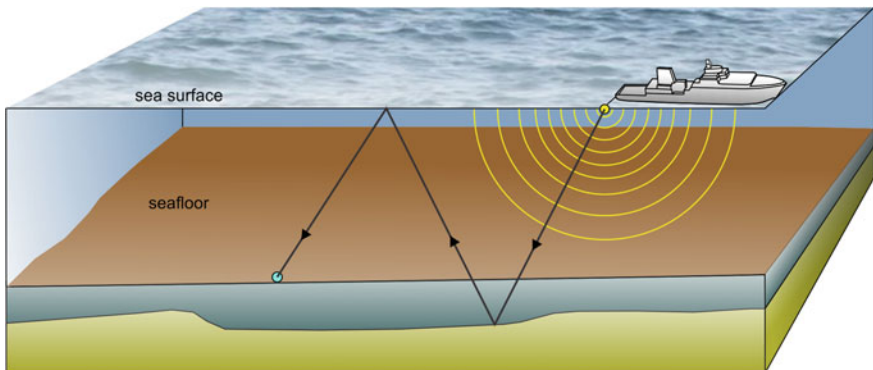


Fig. 6 The concept of mirror imaging in OBS data acquisition (modified after Grion et al. 2007). The sea surface acts as a mirror for primary reflections, which ultimately allows for better imaging of the shallow sub-surface

for coarsely spaced seafloor receivers and in studies targeting shallow subsurface structure.

4.7 Joint Inversion of Refraction and Reflection Data

The incorporation of reflection seismic streamer data in the modeling process is beneficial to coincident refraction studies to include a priori structural information on lithological boundaries. Seismic tomography has proven successful to determine the velocity-depth structure in conjunction with subsurface reflectors and faults (e.g. Korenaga et al. 2000). This approach is based on the simultaneous inversion of refracted and reflected phases with floating reflectors. The method employs a hybrid ray tracing scheme combining the *graph method* with further refinements utilizing ray bending with the *conjugate gradient* method (the reader is referred to Korenaga et al. 2000 for a more detailed discussion). Smoothing and damping constraints regularize the iterative inversion. The velocity model is defined as an irregular grid hung from the seafloor reflection. From the coincident MCS seismic data, the well resolved upper (sedimentary) portions may be included as a priori structure into the starting model and fixed during the iterations using spatially variable velocity damping. To make use of secondary arrivals and different reflections, a *layer stripping* approach is utilized and subsequently the velocity model is built from top to bottom (e.g. Planert et al. 2010). This approach further involves the use of spatially variable velocity damping for the upper layers, e.g., when restricting the picks to the lower layers, and the incorporation of velocity jumps into the input models at primary features such as the basement, plate boundary and the crust-mantle boundary (Moho).

4.8 3D Full-Waveform Inversion of Wide-Angle, Multi-azimuth Data

Full waveform inversion (FWI) is a method widely used in the petroleum sector, and for academic research, to produce high-resolution velocity models of the sub-surface. Such velocity models can make it possible to identify lithology types and pore fluid compositions that might otherwise not be discernable from seismic reflection imaging alone. Recent studies have highlighted the strength of FWI to produce detailed P-wave velocity models if surveys are acquired to record wide-angle, multi-azimuth refractions (Morgan et al. 2013). By testing recoverable resolutions for synthetic seismic data, Morgan et al. (2013) discuss how such surveys, with an array of ocean bottom receivers, can resolve deep structures in the crust better than any other geophysical technique. Future developments in this area could significantly improve our ability to investigate deep-seated geological processes like arc volcanism, for example, that have distinct submarine geomorphological manifestations.

5 Strengths and Weaknesses

The clear strength of seismic methods in submarine geomorphology is the ability to illuminate the sub-surface over large areas, either by acquiring a number of 2D seismic profiles or by acquiring 3D datasets. Other geophysical tools like multi-beam echo-sounders and sidescan sonar systems (Chapters “[Sidescan Sonar](#)” and “[Multibeam Echosounders](#)”, respectively) efficiently deliver remarkably high-resolution images of the seafloor, but do not image sub-seafloor geology. Thus, seismic reflection and refraction methods are routinely used to investigate the deeper processes that shape the seafloor.

In comparing reflection and refraction methods, it is clear that the seismic reflection method is the tool of choice for producing high-resolution images of buried strata and structures. 3D seismic reflection methods, in particular, can deliver imagery that allows us to examine past geomorphological expressions, such as meandering channel systems and mass transport deposits (e.g. Kolla et al. 2007). On the other hand, seismic refraction experiments have their strength in developing large-scale velocity models that are consistently used to explore deep, crustal processes, like subduction, seafloor spreading, and arc volcanism (e.g. Kopp et al. 2011). In terms of low-cost academic surveys, high-resolution 2D seismic reflection profiles are generally simpler to acquire, process and interpret than crustal-scale 2D seismic refraction profiles. The latter require greater source volumes, longer source-receiver offsets, as well as the deployment and recovery of instruments on the seafloor.

When compared to other data acquisition methods used in submarine geomorphology, seismic methods are probably best considered as a tool that provides the

‘bigger picture’ context for a given geomorphological investigation. In this sense, they are similar to electric and electromagnetic methods that are also used to remotely sense the sub-surface. The strength of seismic methods is not in delivering detailed seafloor characteristics; that is best investigated with higher-resolution side-scan sonar imaging (Chapter “[Sidescan Sonar](#)”) and targeted seabed sampling (Chapter “[Seafloor Sediment and Rock Sampling](#)”). Indeed, direct sampling methods are the only way to confirm lithological interpretations that are made from remotely-sensed data. Seismic methods are most powerful when combined with other geo-scientific methods. For example, the integration of high-resolution seismic data and shallow sediment samples often vastly improves the understanding of submarine slope failure processes that dramatically change seafloor morphology (e.g. Vardy et al. 2012). In another example, the combination of controlled-source electromagnetic data with seismic data can help to identify and characterize sub-seafloor fluid flow processes that also often manifest themselves at the seafloor (Goswami et al. 2015).

Acknowledgements We are grateful to the editors of this book for their invitation to write this chapter, and to Sebastian Krastel in particular for his review of the text. We also thank Joerg Bialas and Sebastian Krastel for their permission to present the seismic data shown in Fig. 5.

References

- Banerjee B, Gupta SK (1975) Hidden layer problem in seismic refraction work. *Geophys Pros* 23:642–652
- Breitzke M, Bialas J (2003) A deep-towed multichannel seismic streamer for very high-resolution surveys in full ocean depth. *First Break* 21:59–65
- Chadwick RA, Noy D, Arts R, Eiken O (2009) Latest time-lapse seismic data from Sleipner yield new insights into CO₂ plume development. *Energy Procedia* 1:2103–2110
- Crutchley GJ, Klaeschen D, Planert L, Bialas J, Berndt C, Papenberg C, Hensen C, Hornbach M, Krastel S, Brueckmann W (2014) The impact of fluid advection on gas hydrate stability: Investigations at sites of methane seepage offshore Costa Rica. *Earth Planet Sci Lett* 401:95–109
- Dash R, Spence G, Hyndman R, Grion S, Wang Y, Ronen S (2009) Wide-area imaging from OBS multiples. *Geophysics* 74:Q41–Q47
- Fayemendy C, Espedal PI, Andersen L, Lygren M (2012) Time-lapse seismic surveying: a multi-disciplinary tool for reservoir management on Snorre. *First Break* 30:49–55
- Geotrace (2010) Pegasus, bounty trough, great South Basin and Shake processing report. Ministry of EconomicDevelopment New Zealand, Unpublished petroleum report PR4279
- Goswami BK, Weitemeyer KA, Minshull TA, Sinha MC, Westbrook GK, Chabert A, Henstock TJ, Ker S (2015) A joint electromagnetic and seismic study of an active pockmark within the hydrate stability field at the Vestnesa Ridge, West Svalbard margin. *J Geophys Res* 120:6797–6822
- Grion S, Exley R, Manin M, Miao X-G, Pica A, Wang Y, Granger P-Y, Ronen S (2007) Mirror imaging of OBS data. *First Break* 25:37–42
- Gutowski M, Bull JM, Dix JK, Henstock TJ, Hogarth P, Hiller T, Leighton TG, White PR (2008) 3D high-resolution acoustic imaging of the sub-seabed. *Appl Acoust* 69:262–271

- He T, Spence G, Wood W, Riedel M, Hyndman R (2002) Imaging a hydrate-related cold vent offshore Vancouver Island from deep-towed multichannel seismic data. *Geophysics* 74:B23–B26
- Hill D, Combee L, Bacon J (2006) Over/under acquisition and data processing: the next quantum leap in seismic technology? *First Break* 24:81–96
- Holbrook WS, Páramo P, Pearse S, Schmitt RW (2003) Thermohaline fine structure in an oceanographic front from seismic reflection profiling. *Science* 301:821–824
- Kolla V, Posamentier HW, Wood LJ (2007) Deep-water and fluvial sinuous channels—Characteristics, similarities and dissimilarities, and modes of formation. *Mar Petrol Geol* 24:388–405
- Kopp H, Klaeschen D, Flueh ER, Bialas J, Reichert C (2002) Crustal structure of the Java margin from seismic wide-angle and multichannel reflection data. *J Geophys Res* 107:ETG 1-1–ETG 1-24
- Kopp H, Weinzierl W, Becel A, Charvis P, Evain M, Flueh ER, Gailler A, Galve A, Hirn A, Kandilarov A, Klaeschen D, Laigle M, Papenberg C, Planert L, Roux E (2011) Deep structure of the central Lesser Antilles Island Arc: relevance for the formation of continental crust. *Earth Planet Sci Lett* 304:121–134
- Korenaga J, Holbrook WS, Kent GM, Kelemen PB, Detrick RS, Larsen H-C, Hopper JR, Dahl-Jensen T (2000) Crustal structure of the Southeast Greenland margin from joint refraction and reflection seismic tomography. *J Geophys Res* 105:21591–21614
- Leon P, Ker S, Marsset B, LeGall Y, Voisset M (2009) SYSIF a new seismic tool for near bottom very high resolution profiling in deep water. In: Proceedings of the OCEANS 2009 Europe Conference, v. Bremen, 11–14 May
- Marsset B, Menut E, Ker S, Thomas Y, Regnault J-P, Leon P, Martinossi H, Artzner L, Chenot, Dentrecolas S, Spyckalski B, Mellier G, Sultan N (2014) Deep-towed high resolution multichannel seismic imaging. *Deep Sea Res I* 93:83–90
- Michell S, Shoshtaishvili E, Chergotis D, Sharp J, Etgen J (2006) Wide azimuth streamer imaging of Mad Dog; Have we solved the subsalt imaging problem? In: Proceedings 2006 SEG annual meeting 2006, Society of Exploration Geophysicists
- Morgan J, Warner M, Bell R, Ashley J, Barnes D, Little R, Roele K, Jones C (2013) Next-generation seismic experiments: wide-angle, multi-azimuth, three-dimensional, full-waveform inversion. *Geophys J Int* 195:1657–1678
- Müller C, Milkereit B, Bohlen T, Theilen F (2002) Towards high-resolution 3D marine seismic surveying using Boomer sources. *Geophys Prosp* 50:517–526
- Parkes G, Hatton L (1986) The marine seismic source. Springer Science & Business Media, Dordrecht 114 pp
- Petersen CJ, Bünz S, Hustoft S, Mienert J, Klaeschen D (2010) High-resolution P-Cable 3D seismic imaging of gas chimney structures in gas hydrated sediments of an Arctic sediment drift. *Mar Petrol Geol* 27:1981–1994
- Planert L, Kopp H, Lueschen E, Mueller C, Flueh ER, Shulgin A, Djajadihardja Y, Krabbenhoft A (2010) Lower plate structure and upper plate deformational segmentation at the Sunda-Banda arc transition. *Indonesia J Geophys Res* 115:B08107. doi:[10.1029/2009JB006713](https://doi.org/10.1029/2009JB006713)
- Planke S, Berndt C (2003) Anordning for seismikkmalning. Norwegian Patent no. 317652 (UK Pat. No. GB 2401684; US Pat No. US7,221,620 B2)
- Pramik B (2013) Marine vibroseis: shaking up the industry. *First Break* 31:67–72
- Robertsson JOA, Laws RM, Kragh JE (2015) Tools and techniques: marine seismic methods. In: Schubert G, Slater L, and Bercovici D (eds) *Treatise on geophysics. resources in near-surface earth*, vol 11. Elsevier, Amsterdam
- Sheriff RE, Geldart LP (1995) *Exploration seismology*. Cambridge University Press, Cambridge, 592 pp
- Sonneland L, Berg L, Eidsvig P, Haugen A, Fotland B, Vestby I (1986) 2D deghosting using vertical receiver arrays. 56th Annual International Meeting, SEG, Expanded Abstracts, pp 516–519

- Vardy ME, L'Heureux J-S, Vanneste M, Longva O, Steiner A, Forsberg CF, Haflidason H, Brendryen J (2012) Multidisciplinary investigation of a shallow near-shore landslide, Finneidfjord, Norway. *Near Surf Geophys* pp 267–277
- Westbrook GK, Chand S, Rossi G, Long C, Bünz S, Camerlenghi A, Carcione JM, Dean S, Foucher J-P, Flueh E, Gei D, Haacke RR, Madrussani G, Mienert J, Minshull TA, Nouzé H, Peacock S, Reston TJ, Vanneste M, Zillmer M (2008) Estimation of gas hydrate concentration from multi-component seismic data at sites on the continental margins of NW Svalbard and the Storegga region of Norway. *Mar Petrol Geol* 25(8):744–758. ISSN: 0264-8172. <https://doi.org/10.1016/j.marpgeo.2008.02.003>
- Yilmaz O (2001) Seismic data analysis: processing, inversion, and interpretation of seismic data, Society of Exploration Geophysicists, Tulsa

Quantitative Analyses of Morphological Data

Philippe Blondel

Abstract Submarine morphologies are complex and analysed based on shapes, dimensions and internal variations. They are also analysed based on their surroundings. This chapter starts by comparing the sensors providing this information: most of them are based on remote sensing (acoustic/electromagnetic). They produce Digital Terrain Models (DTMs), corresponding to regularly sampled (and/or interpolated) grids. Illustrated with regular examples, the chapter shows the basic measurements used to describe and compare morphologic data, their variations with multi-scale approaches (e.g. Fourier space, fractals) and how this can be used to identify trends and patterns. Geographic Information Systems and the emerging applications of Artificial Intelligence and data mining are also presented.

1 Mapping Submarine Morphologies

Geological structures on the seabed or below are analysed based on their shapes, their dimensions and their internal variations. They are also compared to their general surroundings, to provide more context and refine their interpretation. For example, sand ripples are recognised as elongate structures with relatively small heights, occurring in groups of generally similar characteristics and situated in shallow waters susceptible to wave action. Variations in their directions, their relative dimensions and their sedimentary composition might provide additional information on their emplacement and evolution with time. Volcanic edifices will generally present circular or sub-circular shapes, with clear variations in topography associated with dome emplacement and additional cones; individual lava flows will give information about eruption stages, their types and their relative chronologies. But where does this morphologic information come from?

The previous chapters have presented a variety of techniques, most of them based on remote sensing: sidescan sonar (Chapter “[Sidescan Sonar](#)”), multibeam

P. Blondel (✉)
Department of Physics, University of Bath, Bath, UK
e-mail: P.Blondel@bath.ac.uk

echo sounder (Chapter “[Multibeam Echosounders](#)”), and seismics (Chapter “[Reflection and Refraction Seismic Methods](#)”). The following chapters will present direct physical sampling (Chapter “[Seafloor Sediment and Rock Sampling](#)”) and localised surveys with bespoke subsea platforms (Chapter “[ROVs and AUVs](#)”), although the former might not always measure morphology directly. Other approaches worthy of mention are the emerging uses of airborne lidar (e.g. Vrbancich, in Blondel 2012), airborne or spaceborne synthetic-aperture radar (e.g. Marghany, also in Blondel 2012), and subsea stereo-photogrammetry (Pouliquen et al. 2002, see also Chapter “[ROVs and AUVs](#)”). This multiplicity of tools is highlighted by Lecours et al. (2016), who review the different applications and advocate combining sensors and data sources as much as possible [the related discussion paper by Mitchell (2016) offers helpful comments too].

This chapter will assume a reasonably accurate Digital Terrain Model (DTM) has been created, with a final resolution commensurate with the processes of interest. This DTM will most likely have been created by acoustic remote sensing. Because of their large swath coverage and increasing resolutions, multibeam echosounders are often and rightly considered the tools of choice to measure morphology (as shown in Chapter “[Multibeam Echosounders](#)”). Ideally, their measurements have been processed to international standards, e.g. the International Hydrographic Organisation (IHO) standards S-44 for hydrographic surveys (https://www.ihodata.org/standards/S-44_5E.pdf). Primarily intended for navigation, their accuracy means this standard is still fully relevant to geomorphologists. De facto standards are also recommended for processing multibeam backscatter (Lurton and Lamarche 2015, and references therein), as it provides other information about topography. To a lesser extent, sidescan sonars can provide comparable information, either by design (interferometric sonars), by operation (multi-angle operation) or through additional processing (for example deriving heights and shapes of protruding objects imaged at grazing angles, although this is strongly limited by the grazing angles used, see also Chapter “[Sidescan Sonar](#)”).

The interactions of acoustic waves with the seabed are complex and presented in multiple textbooks (e.g. Blondel 2009; Lurton 2010). The first contributor to acoustic reflectivity is the slope of the surface being imaged (Fig. 1a). Because of the size of the sonar footprint at this location, the actual depth will vary between the centre of the footprint (average) and its edges (minimum and maximum values). Depending on how acoustic returns are processed, the depth returned to the user might be any value within the full range (ideally the median or the mean). The acoustic reflectivity will be also extremely sensitive to the micro-scale roughness of the seabed, at scales comparable to the imaging wavelength (for a 150 kHz sonar, this would be roughly 1 cm). Because of the wavelengths used to quantify seabed morphologies, this is generally less of an issue. The third and smallest contributor to acoustic reflectivity will in fact become the second largest contributor to depth accuracies: depending on seabed type and imaging frequencies, the sonar waves might travel within the immediate sub-seabed, and acoustic returns might come from deeper than expected. This is seen with dual-frequency systems: Blondel and Pouliquen (2004) show for example how 100-kHz maps show returns from the top

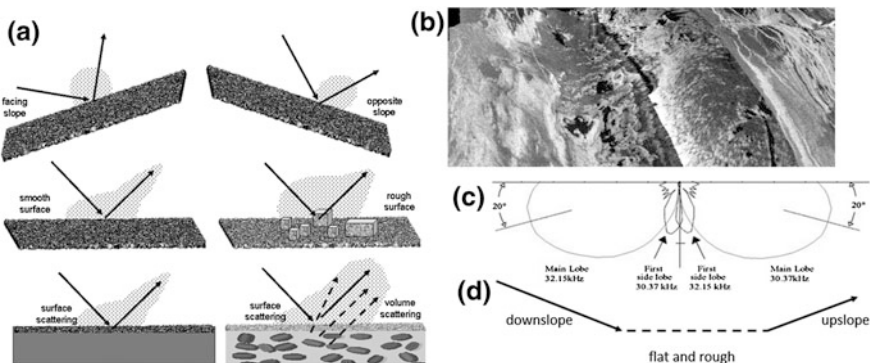


Fig. 1 **a** The scattering of waves (acoustic or electromagnetic) from a complex surface will be affected by its orientation, how rough it is (relative to the imaging wavelength) and how deep below the surface waves can penetrate and scatter; **b** this typical image of a mid-ocean ridge combines sidescan sonar imagery and multibeam bathymetry; **c** its interpretation needs to take into account the beam pattern of the imaging sonar(s); **d** the slopes facing toward or away from the sonar also need to be considered. Figure modified after Blondel (2009)

of underwater vegetation, whereas simultaneous 384-kHz measurements show slightly deeper returns from the seabed itself. In extreme cases, e.g. with low-frequency sonars such as GLORIA (6.5 kHz), it is possible to detect structures well below a thick mud cover (Moore et al. 1989). Care should therefore always be taken when using sonar measurements, and it is necessary to check whether the acoustic waves can actually show returns from deeper in the seabed than expected.

2 Quantitative Structures, Shapes and Their Variations

Seabed morphology is inherently complex, both at regional and local scales. Figure 2 shows idealised landforms in a sedimentary environment. Other landforms not represented here would include volcanic constructs (from lava flows to small cones or large domes), large faults and landslides (potentially with different debris slides), hydrothermal areas (with small and large edifices, deposits and small fissures), and any seabed affected by marine life (e.g. vegetation, burrowing) or human activities (from shipwrecks to cables or caissons). Readers interested in how these other structures look like when imaged with sonars are invited to read the “Handbook of Sidescan Sonar” (Blondel 2009), which provides many examples from around the world. The key points here are how these different generic shapes can be detected, quantified and analysed.

At a regional scale, the seabed is best characterised by its regular sloping topography, best revealed by comparison of along-slope profiles. Local variations are visible, for example, the canyon in the middle of the sketch (Fig. 2). Two-dimensional

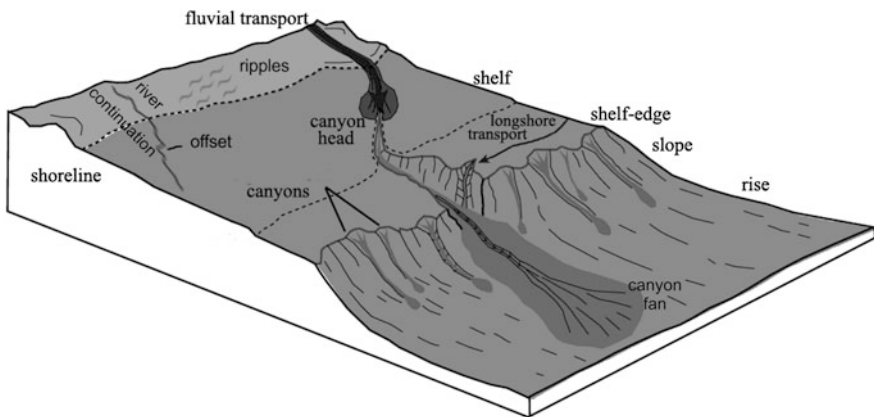


Fig. 2 Typical sedimentary shore, showing a variety of morphologic structures. Baseline figure from Obelcz et al. (2014) with permission from Elsevier

analyses of the shelf edges and slopes would reveal more about the dynamic sedimentary regimes, in particular along-shore transport of sediments. Finer-scale analyses (in 2-D) would reveal the presence of sand ripples in the shallow waters exposed to wave action, and 3-D analyses might show differences in their formation and evolution. Small structures like underwater prolongation of rivers (top left) might also show offsets, indicative of tectonic activity. Larger structures, like the canyon fan (bottom right) would need quantifying in 2-D and 3-D to show variations in sediment supplies and links to the geology (and morphology) of deeper waters.

Practically speaking, this means the geomorphologist needs to analyse 2-D profiles and 3-D sections of parts of the DTM. In the case of a submarine canyon (Fig. 3, left), cross-sections taken at regular intervals can reveal canyon evolution and depth variations, steep slopes and potential asymmetry, and variations in sediment deposits in the canyon and on its banks. Repeat surveys can be used to measure steepening of the slopes, or further changes, which might lead to geo-hazards. Figure 3 (top right) shows a portion of the Mid-Atlantic Ridge, with high-resolution data near the ridge axis and lower-resolution bathymetry away from the active part of the ridge. Cross-sections (Fig. 3, bottom right) will reveal different processes depending on the scale at which these measurements are made, highlighting the need for high resolution. Lecours et al. (2016) recommend “extending the analysis beyond the basic 3×3 neighbourhood [...] as it facilitates the identification of spatial scales” relevant to specific processes. This multi-scale analysis should be a necessity, and not just a recommendation, as it is the only way to enable meaningful comparisons between datasets measured with different sensors.

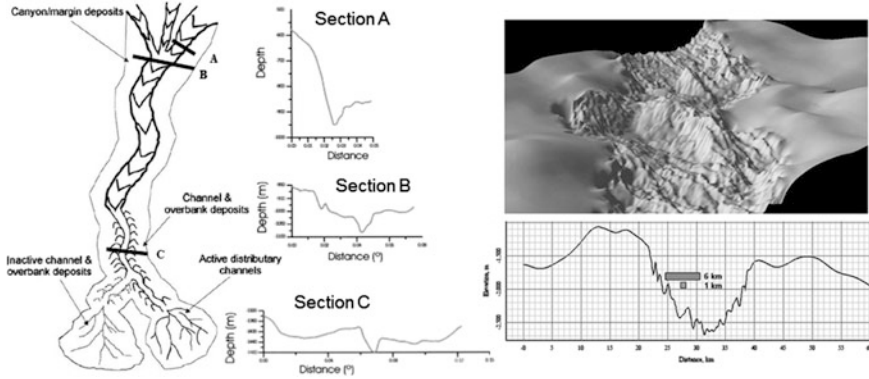


Fig. 3 Left successive analyses of bathymetric profiles across a submarine canyon reveal its evolution, with steep, unconsolidated slopes (*Section A*) and several levels of deposits (*Sections B and C*). Modified after Gómez Sichi et al. (2005). Right Bathymetry from the Mid-Atlantic Ridge (from the R2K database) is compiled with high resolution near the ridge axis and lower resolution data away from the main segments (*top*). Bathymetric profiles will reveal different information based on their resolution (*bottom*). Modified after Blondel (2009)

3 Geostatistics to Geographical Information Systems

3.1 Basic Measurements

A bathymetric profile across a surface of interest can be expressed as a collection of points, with depths $z(i)$, measured at N points regularly spaced (and denoted with index i , varying from 1 to N). The first parameter of interest will be the average depth $\langle z \rangle$:

$$\langle z \rangle = \frac{1}{N} \sum_{i=1}^N z(i) \quad (1)$$

If choosing a reference depth z_0 , the average height $\langle h \rangle$ will be calculated with reference to the relative depths $z(i) - z_0$, giving rise to a similar equation:

$$\langle h \rangle = \frac{1}{N} \sum_{i=1}^N (z(i) - z_0) \quad (2)$$

For a portion of the map, assumed square for simplicity (i.e. N points along one direction and N points along the orthogonal direction), the average depth is then expressed as:

$$\langle z \rangle = \frac{1}{N^2} \sum_{i=1}^N \sum_{j=1}^N z_{i,j} \quad (3)$$

The next equations will follow the same assumption of a square sampling, justified if the original measurements have been processed with square gridding (which is the case in most software now) or interpolated to the same resolution along both axes. Changing to non-square samples is mathematically straightforward, replacing N with M where needed. All subsequent equations can also be adapted simply to profiles along a single direction (using only one summation, for example).

The average height or depth does not account for small-scale variations, which can be very important in describing the surface (e.g. for talus deposits or for lava flows). From an acoustic point of view, the roughness will also be indicative of the likely scattering processes (cf. Blondel 2009). The average roughness, also called rms roughness, is traditionally calculated as:

$$z_0 = \sqrt{\frac{1}{N^2 - 1} \sum_{i=1}^N \sum_{j=1}^N (z_{i,j} - \langle z \rangle)^2} \quad (4)$$

This roughness can be biased if the underlying surface is on a slope, and it is often recommended to measure the rms tilt over a range Δx :

$$s_0 = \sqrt{\frac{\langle (z(x) - z(x + \Delta x))^2 \rangle}{\Delta x}} \quad (5)$$

This tilt can be used to remove the underlying surface from the measurements, if it is regular enough or known well enough. This operation is often known as de-trending, and it requires accurate assessment of what the background surface is like, or should be like, to avoid biasing the final results.

Local slopes are also of interest, as they can be used to delineate features. The slope gradient is defined as the maximum rate of elevation change, and it can be calculated over different ranges (in some datasets, using the maximum resolution available can indeed add noise and it is then necessary to apply simple low-pass filters, for example 3×3 moving averages). In its simplest form, the slope gradient is defined as:

$$\text{gradient} = \text{atan} \left(\left(\frac{\partial z}{\partial x} \right)^2 + \left(\frac{\partial z}{\partial y} \right)^2 \right) \quad (6)$$

Variations in slope gradients over large areas can be used to distinguish terrains based on their statistical differences, and not on any qualitative interpretations.

Micallef et al. (2012) use, for example, the cumulative frequency distribution of slope gradients to identify points of inflection. This allows the quantitative separation of morphological units such as flat zones, sloping zones, crests, depressions and breaks of slopes. Shaw and Smith (1990) quantify the spatial correlation of these variations with auto-covariance functions to distinguish very different types of heterogeneous terrains.

A tool now frequently used by marine geomorphologists (e.g. Verfaillie et al. 2007) is the Bathymetry Position Index (BPI). Implemented in common software like ArcGIS™, the BPI algorithm measures height differences between a focal point and the average calculated over surrounding cells within a user-defined shape (which can therefore be square, but can also be restricted to a specific morphological feature like a canyon or depression). By definition, negative BPIs correspond to local depressions and positive BPIs to crests.

The BPI can be used in conjunction with the topographic ruggedness index (TRI), introduced by Riley et al. (1999). The TRI measures the square root of the average of squared height differences between a centre point and the closest measurements (i.e. 8 measurements for a square grid).

More complex equations can quantify other parameters of interest, like the profile curvature, which represents the maximum change in slope gradients between adjacent cells in a chosen neighbourhood. It is used for example to identify convex and concave breaks of slope (i.e. faults, fissures and steep escarpments). It is defined by Micallef et al. (2012) by looking at derivatives of the height z over orthogonal directions x and y (over at least 3 consecutive points, but any range can be considered):

$$\text{Curvature} = - \frac{\left(\frac{\partial z}{\partial x} \right)^2 \times \frac{\partial^2 z}{\partial x^2} + 2 \times \frac{\partial z}{\partial x} \times \frac{\partial z}{\partial y} \times \frac{\partial^2 z}{\partial x \partial y} + \left(\frac{\partial z}{\partial y} \right)^2 \frac{\partial^2 z}{\partial y^2}}{\left(\left(\frac{\partial z}{\partial x} \right)^2 + \left(\frac{\partial z}{\partial y} \right)^2 \right) \left(1 + \left(\frac{\partial z}{\partial x} \right)^2 + \left(\frac{\partial z}{\partial y} \right)^2 \right)^{\frac{3}{2}}} \quad (7)$$

Once identified on the maps, for example through image processing or geostatistics, some morpho-geological units can be quantified with other parameters, like their lengths, widths, areas or volumes (if knowing where the base of the unit is likely to be). For submarine canyons and other similar features, it is often interesting to calculate the sinuosity index SI , defined as the ratio of the length along the structure to the straight distance between its extremities (Euclidean distance). In terrestrial geomorphology (e.g. Mueller 1968), these values are traditionally interpreted as “almost straight” ($SI < 1.05$), “winding” ($1.05 \leq SI < 1.25$), “twisty” ($1.25 \leq SI < 1.50$) and “meandering” ($SI > 1.50$). For closed structures, other parameters of interest will be the overall shape, which can be characterised with tools like the Hough transform or by measures of similarity with expected shapes (circles, ellipses, etc.). More information can be derived from combining different measurements (e.g. principal axes of several structures, lengths, widths, slope histograms), as shown in Shaw and Smith (1987), inter alia.

3.2 Variations with Spatial Scales

If regular enough, i.e. occurring at specific spatial intervals (or wavelengths), morphogeological variations show a range of spatial frequencies (not to be confused with the imaging frequency). This is best measured using simple Fourier transforms, whose values are calculated at different spatial frequencies f :

$$F(f) = \int_{-\infty}^{+\infty} z(x)e^{-i2\pi f x} dx \quad (8)$$

From a mathematical point of view, the integral sign is used to denote summation over samples as close as possible to each other, and over as large a range as possible ($-\infty$ and $+\infty$). In practice, the use of finite ranges of integration will limit the frequencies measurable.

Power spectral densities $W(f)$ are a good way to check which frequencies are predominant:

$$W(f) = \frac{1}{L} \left(\text{Re}(F(f))^2 + \text{Im}(F(f))^2 \right) \quad (9)$$

For example, sand ripples with a spacing X will have much higher power in the spatial frequency $1/X$. Ripple systems with different heights, different widths and different distances will show in the Fourier spectra with different spatial frequencies (along each direction chosen), and this might be used to highlight overlain ripple fields, or assess how they degrade with currents or wave action. Other types of decompositions, e.g. with wavelet transforms, are available; they will not be presented here, but their use should always keep in mind how much physical reality can be represented with specific mathematical functions.

The role of scale is important, as it is conditioned by the data acquisition (resolution of the mapping sensor and small-scale accuracy), by the processing (quality of the interpolation and gridding schemes used) and by the physical processes themselves. The Nyquist theorem states that measurements should cover at least twice the frequency to analyse. A topographic process changing every 2 m would need measuring at least every 1 m to get an accurate representation of its variability. And the number of measurements is commensurate with the parameter to derive. For example, if using a bathymetry dataset with 10-m resolution, calculating the local slope uses 3 points, i.e. distances of 30 m. Mean slopes need to average over 3 values or more, i.e. distances close to 100 m (calculating local slopes every 10 m would bias the measurements, as neighbouring points will include similar bathymetry values).

Sometimes, measurements made over particular spatial scales will be very different if done over different scales. This was first formalised by Mandelbrot (1967), who described how the size of complex lengths/surfaces will increase as the

measuring unit decreases. This can be plotted as a logarithmic function, indicative of the fractal dimension D (in this case, the slope of the function equates $D - 1$). This started the research into fractals, also known as self-affine or fractional Brownian statistics (more detailed information is available at: <http://www.math.yale.edu/mandelbrot/>).

Variations of heights with the horizontal measurement scale L follow power laws and can for example be used to derive a scaling constant C_H and a quantity H (known as the Hurst exponent and in the range 0–1):

$$\langle h \rangle = C_H \times \left(\frac{L}{L_0} \right)^H \quad (10)$$

C_H is the rms height when $L = L_0$, and the fractal dimension is directly related to the Hurst exponent:

$$\begin{cases} D = 2 - H & (\text{for a profile}) \\ D = 3 - H & (\text{for a surface}) \end{cases} \quad (11)$$

In the case of radar remote sensing of planetary surfaces, these parameters can be used to easily distinguish between lava flows, such as smooth pahoehoe ($H = 0.63$, $C_H = 0.05$), rough pahoehoe ($H = 0.48$ and $C_H = 0.16$) and a'a ($H = 0.26$, $C_H = 0.24$) (Campbell 2011). Fractal dimensions can therefore be considered a measure of roughness, at least in this case.

Fractals are very useful to describe scale-independent processes, i.e. processes which will produce the same results at small and large scales. In some cases, the processes are more complex and cannot be described with a single fractal dimension consistent at all scales (multifractals) (e.g. Iijasz-Vasquez et al. 1992). The mathematics can rapidly become complex and thus will not be treated here. Interested readers can find more in books and articles by Benoit Mandelbrot, who founded this field, and look at applications to seabed morphologies in Mareschal (1989), Malinverno (1989) and Goff et al. (1993).

3.3 Finding Trends and Patterns

There are many other measures than those presented in the previous two sub-sections. All should be related to physically meaningful descriptions of the seabed and of morphological structures. Some metrics, e.g. lengths, widths, directions, can be directly associated to geological processes, for example the evolution of a submarine canyon. Other metrics might be more difficult to interpret, and this is where data can be usefully compared to expected distributions.

Simple bathymetric profiles, for example, can be interpreted as the combination of a background profile, associated to the regional slope, systematic deviations, associated to local processes, and random or pseudo-random smaller deviations.

Auto-regressive (AR) models and auto-regressive moving-average (ARMA) derivations can be used to unravel the local and regional contributions (see Box et al. 2015 for examples in a variety of domains). More deterministic approaches have been followed, for example matching existing profiles to spline functions and relating each base function to a specific geological process.

Surface analyses have similarly aimed at separating the stochastic part of the seafloor morphology from more local (and/or random) processes. Goff and Jordan (1989) used the covariance of bathymetry to study abyssal hill formation in different regions, taking great care to remove the effects of data acquisition and resolution. Mitchell (1996) designed a technique to automatically fit paraboloid shapes to bathymetry, and used this approach to interpret transport processes at continental slopes (Mitchell and Huthnance 2007). The field of pattern-matching is vast, and these are only two examples, selected because they are perfect demonstrations of how to match theoretical patterns to existing data, within the constraints of how it was acquired, and how to derive meaningful interpretations of geomorphological processes.

Geographic Information Systems (GIS) combine datasets and measurements in geo-located and inter-comparable databases. They allow direct query of specific characteristics (e.g. “can sediment flow from this canyon affect this area down-slope?”, “how far are hydrothermal vents from small-scale fissures?”). Many examples are currently available on the market, and to cite but one, ArcGISTM seems rather prevalent at the moment, with new tools specifically built for the geomorphological community (e.g. Rigol-Sanchez et al. 2015; Kelner et al. 2016). Other techniques, such as multivariate analyses (e.g. Husson et al. 2009), neural networks (e.g. Mallat 2016), or Artificial Intelligence (e.g. Gvishiani and Dubois 2002) aim to extend this guided approach by exploring how subsets of the data might relate to each other. Used in many other data-rich fields, the new discipline of data mining is likely to revolutionise submarine morphometry (e.g. Wan et al. 2010; Planella Gonzalez et al. 2013). One *caveat* is that market leaders, and any GIS for that matter, should always clearly present the rationale behind the calculations, avoiding a “black box” approach where numbers lose their meaning by not being testable or not matching a physical meaning. This is often why some communities rely on programming languages like Matlab or R (e.g. Husson et al. 2009) to keep this important open-source aspect.

4 Conclusions

Modern sensors can map the seabed at spatial resolutions varying from a kilometre (for the oldest generation) to sub-metre (for most systems available now), with depth accuracies generally below a metre. The resulting datasets are extremely large and they can provide important information on the morphology of the seabed, on the formation and evolution of different structures, and how they are affected with time (for example when doing repeat surveys). It is therefore important to quantify

accurately the different morphologies and to be able to relate them to geologically meaningful processes.

This chapter introduced some of the key metrics for morphology, selected on the basis of simplicity and demonstrated applicability to remote sensing (acoustic or electromagnetic). From simple profiles to surfaces and volumes, these measurements aim at quantifying the underlying processes. How accurate they are depends on how good the measurements are, and how well their potential limitations are understood (imaging accuracy, combination of different resolutions, role of volume scattering vs. surface scattering). The use of multiple resolutions is highlighted as it can provide important information when geological processes are superposed in space. The development of Geographic Information Systems offers very useful tools to the interpreters, provided the mathematical details of the different metrics are well understood, traceable and comparable. Applications of data mining and Artificial Intelligence to submarine morphology are appearing and also proving very attractive.

References

- Blondel P (ed) (2012) Bathymetry and its applications. In Tech. Open Access: <http://www.intechopen.com/books/show/title/bathymetry-and-its-applications>. doi:[10.5772/2132](https://doi.org/10.5772/2132)
- Blondel P, Pouliquen E (2004) Acoustic textures and detection of shipwreck cargo—example of a Roman ship near Elba, Italy. In: Akal T, Ballard RD, Bass GD (eds) Proceedings of first internal congress on the application of recent advances in underwater detection and survey techniques to underwater archaeology, pp 135–142
- Blondel P (2009) Handbook of sidescan sonar. Springer, Berlin
- Box G, Jenkins GM, Reinsel GC (2015) Time series analysis: forecasting and control, 4th edn. Prentice-Hall, Englewood Cliffs
- Campbell BA (2011) Radar remote sensing of planetary surfaces. Cambridge University Press, Cambridge
- François H, Lê S, Pagès J (2009) Exploratory multivariate analysis by example using R. CRC-Press, London
- Goff JA, Jordan TH (1989) Stochastic modelling of seafloor morphology: resolution of topographic parameters by sea beam data. IEEE J Oceanic Eng 14(4):326–337
- Goff JA, Malinverno A, Fornari DJ, Cochran JR (1993) Abyssal hill segmentation: quantitative analysis of the East Pacific rise flanks 7°S–9°S. J Geophys Res 98(B8):13851–13862
- Gómez Sichi O, Blondel Ph, Gracia E, Dañobeitia JJ (2005) Quantitative textural analyses of TOBI sonar imagery along the Almería Canyon (Almería Margin, Alborán Sea, SE Spain). In: Hodgson DM, Flint SS (eds) Submarine slope systems: processes and products, vol 244. Geological Society Special Publication, London, pp 141–154
- Gvishiani A, Dubois JO (2002) Artificial intelligence and dynamic systems for geophysical applications. Springer, Berlin
- Iijasz-Vasquez EJ, Rodriguez-Iturbe I, Bras RL (1992) On the multifractal characterization of river basins. Geomorphology 5(3):297–310
- Kelner M, Migeon S, Tric E, Couboulex F, Dano A, Lebourg T, Taboada A (2016) Frequency and triggering of small-scale submarine landslides on decadal timescales: analysis of 4D bathymetric data from the continental slope offshore Nice (France). Mar Geol 379:281–297
- Lecours V, Dolan MFJ, Micallef A, Lucieer VL (2016) A review of marine geomorphometry, the quantitative study of the seafloor. Hydrol Earth Syst Sci 20:3207–3244

- Lurton X (2010) An introduction to underwater acoustics—principles and applications. Springer, Heidelberg
- Lurton X, Lamarche G (eds) (2015) Backscatter measurements by seafloor-mapping sonars. Guidelines and recommendations. <http://geohab.org/wp-content/uploads/2014/05/BSWG-REPORT-MAY2015.pdf>. Accessed 24 Oct 2016
- Malinverno A (1989) Segmentation of topographic profiles of the seafloor based on a self-affine model. *IEEE J Oceanic Eng* 14(4):348–359
- Mallat S (2016) Understanding deep convolutional networks. *Phil Trans R Soc A* 374:20150203. doi:[10.1098/rsta.2015.0203](https://doi.org/10.1098/rsta.2015.0203)
- Mandelbrot BB (1967) How long is the coast of Britain? Stat self-similarity and fractional dimension. *Science* 156(3775):636
- Mareschal J-C (1989) Fractal reconstruction of sea-floor topography. *Pure Appl Geophys* 151:197–210
- Micallef A, Le Bas TP, Huvenne VA, Blondel P, Hühnerbach V, Deidun A (2012) A multi-method approach for benthic habitat mapping of shallow coastal areas with high-resolution multibeam data. *Cont Shelf Res* 39–40:14–26
- Mitchell NC (1996) Processing and analysis of Simrad multibeam sonar data. *Mar Geophys Res* 18:729–739
- Mitchell N (2016) Interactive comment on “Characterising the ocean frontier: a review of marine and coastal geomorphometry” by Lecours V et al. *Hydrol Earth Syst Sci Discuss*. doi:[10.5194/hess-2016-73-RC1](https://doi.org/10.5194/hess-2016-73-RC1)
- Mitchell NC, Huthnance JM (2007) Comparing the smooth, parabolic shapes of interfluves in continental slopes to predictions of diffusion transport models. *Mar Geol* 236:189–208
- Mueller J (1968) An introduction to the hydraulic and topographic sinuosity indexes (1). *Ann Assoc Am Geogr* 58(2):371–385
- Moore JG, Clague DA, Holcomb RT, Lipman PW, Normark WR, Torresan ME (1989) Prodigious submarine landslides on the Hawaiian Ridge. *J Geophys Res* 94(B12):17465–17484
- Obelcz J, Brothers D, Chaytor J, ten Brink U, Ross SW, Brooke S (2014) Geomorphic characterization of four shelf-sourced submarine canyons along the U.S. Mid-Atlantic continental margin. *Deep Sea Res II* 104:106–119
- Planella Gonzalez LF, Gomez Pivel MA, Alcoba Ruiz DD (2013) Improving bathymetric images exploration: a data mining approach. *Comput Geosci* 54:142–147
- Pouliquen E, Blondel P, Canepa G, Hollett R (2002) Multi-sensor analysis of the seabed in shallow-water areas: overview of the MAPLE-2001 experiment. In: Proceedings of sixth European conference on underwater acoustics ECUA-2002, Gdańsk, Poland, pp 167–175
- Rigol-Sánchez JP, Stuart N, Pulido-Bosch A (2015) ArcGeomorphometry: a toolbox for geomorphometric characterisation of DEMs in the ArcGIS environment. *Comput Geosci* 85:155–163
- Riley SJ, DeGloria SD, Elliot R (1999) A terrain ruggedness index that quantifies topographic heterogeneity. *Intermt J Sci* 5(1–4):23–27
- Shaw PR, Smith DK (1990) Robust description of statistically heterogeneous seafloor topography through its slope distribution. *J Geophys Res* 95(B6):8705–8722
- Shaw PR, Smith DK (1987) Statistical methods for describing seafloor topography. *Geophys Res Lett* 14:1061–1064
- Verfaillie E, Doornenbal P, Mitchell AJ, White J, Van Lancker V (2007) The bathymetric position index (BPI) as a support tool for habitat mapping. Worked example for the MESH Final Guidance, 14 pp. ([http://www.emodnet-seabedhabitats.eu/PDF/GMHM4_Bathymetric_position_index_\(BPI\).pdf](http://www.emodnet-seabedhabitats.eu/PDF/GMHM4_Bathymetric_position_index_(BPI).pdf)). Last accessed 06 Feb 2017
- Wan S, Lei TC, Chou TY (2010) A novel data mining technique of analysis and classification for landslide problem. *Nat Hazards* 52:211. doi:[10.1007/s11069-009-9366-3](https://doi.org/10.1007/s11069-009-9366-3)

Seafloor Sediment and Rock Sampling

Aggeliki Georgioupolou

Abstract There are a variety of methodologies to obtain seafloor sediment and rock samples, and deciding which one to use depends on the scientific question being addressed, the type of seafloor material being targeted, what the vessel can support and finally the cost. Nowadays, any type of seafloor can be sampled, no matter how soft or hard or inhospitable and technological advances, largely driven by the hydrocarbon industry, continuously allow us to go deeper and deeper into the sub-seafloor and, by definition, into geological time.

1 Introduction

Marine sediments record the Earth's history, its climate, the ocean currents, the ocean productivity, sea level changes, sea temperature changes, tectonic movements, environmental changes, evolution and ecology among other parameters. Therefore, it has always been important to be able to collect sediment cores as they offer us a window through geological time. The longer the sediment sample the longer the time record we can study. Nonetheless, not all research vessels can support long and heavy corers whose operation is more costly financially and timewise. There are many sampling devices each with advantages and disadvantages and it is important to choose the appropriate device depending on the research question. For example, there is no need to use a giant piston corer if the research question relates with the sediment-water interface. Users must always be aware of the research vessel capabilities, its cranes, winches and wires.

It is important to note that seafloor sampling and site selection need to be supported and guided by an acoustic pre-site survey, such as seafloor backscatter imaging (Chapter “[Sidescan Sonar](#)”), bathymetric surveying (Chapter “[Multibeam](#)

A. Georgioupolou (✉)

UCD School of Earth Sciences, University College Dublin, Dublin, Ireland
e-mail: aggie.georg@ucd.ie

A. Georgioupolou

UCD Earth Institute, University College Dublin, Dublin, Ireland

Echosounders") and high-resolution seismic profiling (Chapter “[Reflection and Refraction Seismic Methods](#)”), in order to decide on the best location for coring, both for optimum sample retrieval but also for the safety of the instrument. It is also crucial to be aware that coring tends to oversample the top 10–15 m by about 30–35% (Széréméta et al. 2004).

2 Surface Sediment Sampling

2.1 Dredging

Dredging is a technique that has not changed much over the years. It is used to collect loose rocks that sit on the seafloor in order to understand the distribution and genetic processes of hard rocks that shape the seafloor morphology. Dredging uses a chain-link mesh bag with a metal-jawed opening, about 1 m wide, that gets dragged along the seafloor and collects the loose rocks in the bag. The dredge is lowered to the seafloor by a steel wire cable whose length needs to be significantly longer than the water depth to allow for the dragging on the seafloor operation. An anchor chain provides the necessary weight to keep the equipment on the seafloor during dredging.

2.2 Box Corer

This corer has been developed to take a 50–60 cm² seafloor sample, down to a depth of 45–60 cm below the seafloor, depending on the set up. The corer consists of a gimballed sample box and spade assembly (Fig. 1), originally designed by Reineck (1963). Some box corers operate with one spade, others with two, but on the same principle. The sample box is covered by two flaps that remain open while the corer is descending, allowing the water to flow freely through. During descent the spade(s) is kept with a lock mechanism on the side of the sample box.

The corer is lowered to the seafloor at a controlled speed until its frame rests on the seafloor. The sample box then sinks into the sediment under its own weight. As soon as the corer is pulled by its wire, a mechanism releases the spade that swings below the sample box, sealing the sediment in. At the same time the spring-loaded flaps above the sample box shut to prevent the sediment being disturbed during recovery. This technique is favoured when the seafloor is soft and when the seafloor surface needs to be retrieved undisturbed, however the penetration is shallow.

2.3 Grab Sampler

The grab sampler consists of two quadrant shaped jaws, a clamshell bucket, made of stainless steel mounted onto a frame (Fig. 2). Lead weights can be attached to the

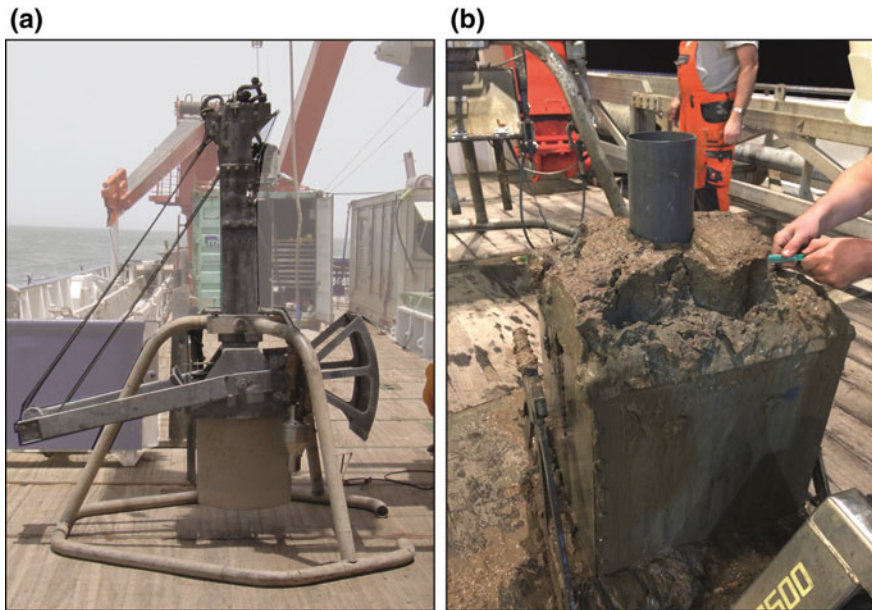


Fig. 1 **a** Set up of box corer, ready for deployment onboard RV Maria S. Merian and **b** subsampling with core liners of a full box corer

frame to allow the sampler better penetration depending on the sediment type. The grab sampler is lowered to the seafloor with the jaws open. A trigger mechanism releases the jaws when the sampler comes in contact with the seafloor. As soon as retrieval begins, the pull triggers the jaws to close and retrieve the sediment. This is one of the easiest sediment sampling techniques but it also causes the most disturbance. For this reason it is commonly used to retrieve rock samples, e.g. from volcanic environments.

2.4 ROV Push Cores

The operation and practices of Remotely Operated Vehicles is addressed in Chapter “[ROVs and AUVs](#)”. Here we are only mentioning the ability to collect short push cores from carefully selected areas in real time as they are being imaged by video. Short cores, up to 30 cm in length can be pushed by the ROV arm into the seafloor (Fig. 3). The core is then retrieved and pushed into a rubber-ended lid to ensure maximum retrieval of sediment. There are certain disadvantages in using this technique, the corer is very short and a lot of material may be lost while securing the core onto the rubber-ended lid when the sediments are soft and particularly unconsolidated. The advantage is that this technique is ideal for ground-truthing bathymetry and



Fig. 2 Grab sampler being deployed from RV *Urania*

backscatter data very fast and efficiently as the sampling location is selected by video and it can be clearly seen how representative of the extended area the sample is.

3 Shallow Sediment Coring

3.1 Gravity Corer

Gravity corers are usually chosen to collect cohesive soft sediments; therefore, this method is extensively used on the continental slope and in deeper basins. Thin sands encased in cohesive muddier sediments can also be retrieved with this method and so it is also often used on the continental shelf, albeit these cores may be shorter due to the friction generated by the sands on the corer lining. Its name demonstrates its mode of operation, lead weights attached to the top of the corer are used to lower it to the seafloor and drive it through (Fig. 4). The weight varies between 100 to 1000 kg but can sometimes exceed two tons; therefore, a powerful winch and wire are required to lower it to the seafloor. The corer is also fitted with stabilising fins to ensure that the corer penetrates the seabed in a straight line.

Most commonly a 6 or 9 m set up is used, although multiple steel core barrels can be used to make the corer longer. Usually it is not recommended to exceed 15 m because of the weight that may cause the corer to buckle when it comes in contact with the seafloor. The barrel is fitted with a sharpened replaceable carbon

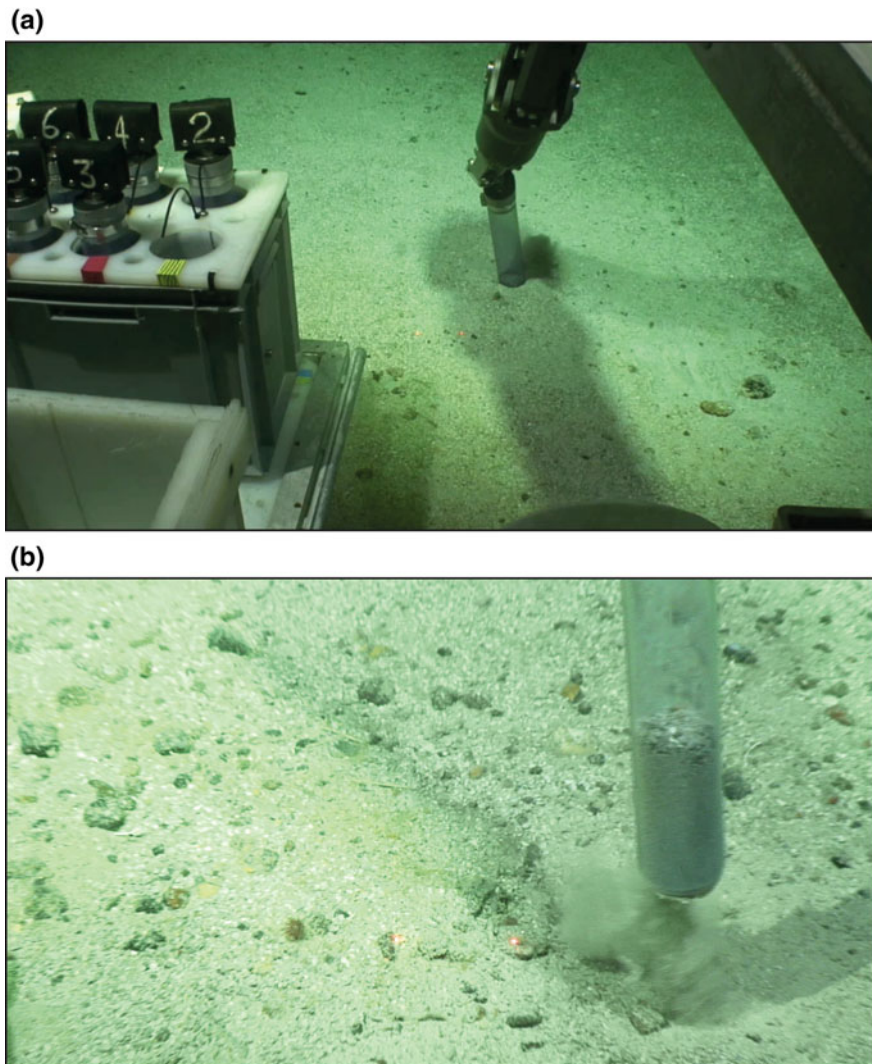


Fig. 3 **a** The ROV Holland I of the Irish Marine Institute sampling with push cores and **b** retrieving sediment. Note that the distance between the *small red laser dots* is 10 cm

steel core cutter to ensure minimal disturbance as the corer penetrates the seafloor. Sample loss on retrieval is minimised by a core catcher fitted inside the end of the barrel.

This method's advantage is that there is little cost associated with it, it is simple, easy to use and requires little maintenance. However, it may cause compression to the sediments, especially near the top and in particular if the sediments are soft, due to the large weight on the top.

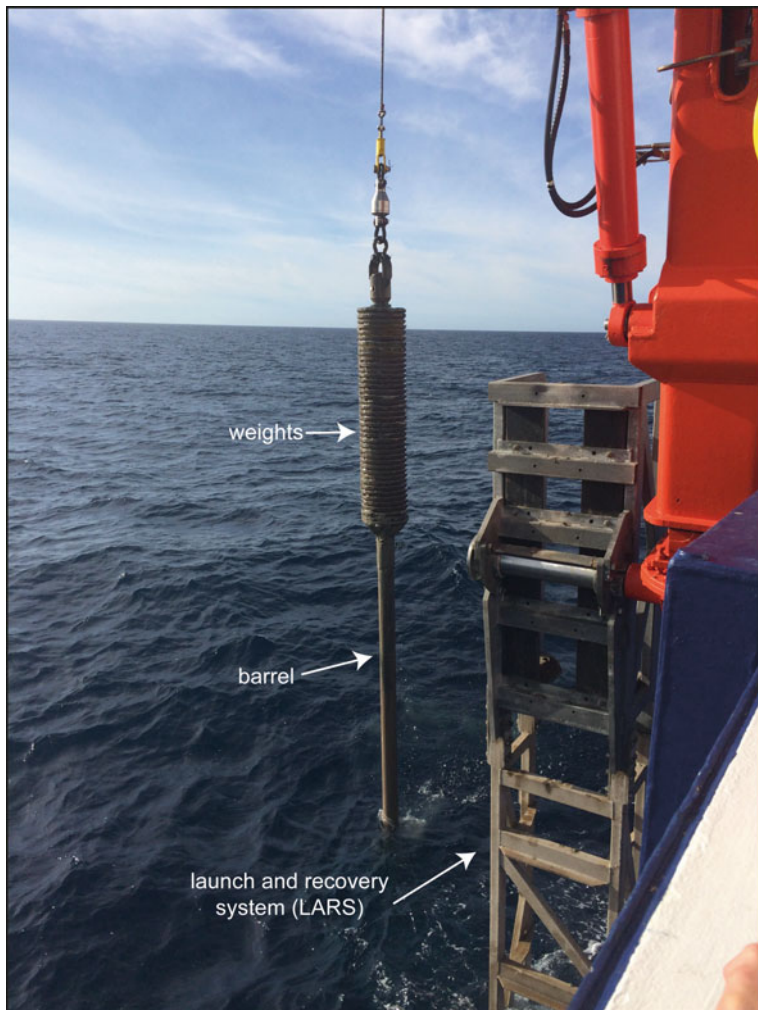


Fig. 4 Deployment of a gravity corer from RV Maria S. Merian. The corer has just been manoeuvred out of the launch and recovery system (*LARS*)

3.2 *Piston Corer*

The piston corer was invented in 1947 by Professor Borje Kullenberg (Kullenberg 1947) to allow the Swedish Deep Sea Expedition to take long (up to 24 m) samples of sediment from beneath the seafloor. Nowadays, together with the Gravity Corer, it is one of the more common shallow sediment sampling methods. The length can be adjusted by adding more barrels. The total barrel length is usually up to 24 m, but can be longer.

The piston corer consists of a tight-fitting piston inside the core barrel. The system requires a triggering mechanism, which will allow it to freefall from several meters above the seafloor. The role of the triggering device is usually performed by a short (1 m) gravity core, which is commonly called the trigger weight core. The trigger weight core hangs from a release arm (pelican) several meters below the base of the piston corer (Fig. 5). Several meters of wire are coiled between the pelican and the piston corer. Upon impact of the trigger weight core with the seafloor the triggering device releases the coiled wire and activates the free fall (Fig. 5). The piston corer uses its freefall kinetic energy and own weight to drive the core barrel into the seabed. As the barrel penetrates the seabed, the piston action reduces the effect of internal wall friction thus increasing seabed penetration and thereby permits the collection of long, relatively undisturbed sediment samples. A special valve may exist in the piston to allow the operator to select the maximum under-pressure required to prevent the PVC core liner from imploding. The length of the wire coiled in the pelican depends on the type of sediment being sampled, the water depth and the length of corer being used. Ideally the length of the wire is calculated so that the piston begins to move up the core barrel just ahead of the sediment. If it moves faster or slower it will cause sediment disturbance.

The length of sediment recovered depends on the nature of the sediment being sampled. Generally soft sediments such as muds and clays are easier to penetrate, while water-saturated sands and foraminiferal oozes less so. When different types of sediments alternate, as is often the case in abyssal plains, the length of core recovery depends on the relative thicknesses of the “difficult” layers.

3.3 Kasten Corer

A kasten corer is a variation of the standard gravity coring. It was designed by Kögler (1963). The steel barrels are square-shaped, made of sheet metal, either 15 or 30 cm², with a square core catcher attached to the nose of the barrel. No liner is used. A cutter section fitted to the end of the sample tube has two spring loaded flaps, which close when the Corer is withdrawn from the sediment. The sample tube is designed to be split to gain access to the sample. Square plastic boxes (usually up to 1 m long) must be pushed into the sediment to subsample the corer. Kasten corers are designed to retrieve large volumes of sediment. This is why this method is particularly favoured where specific target components are known to occur in low amounts, e.g. biogenic material. The maximum length for kasten cores is 15 m.

3.4 Vibrocoring

The vibrocoring has a vibrating mechanism, the vibrohead, which operates with hydraulic, pneumatic, mechanical or electrical power from an external source. The

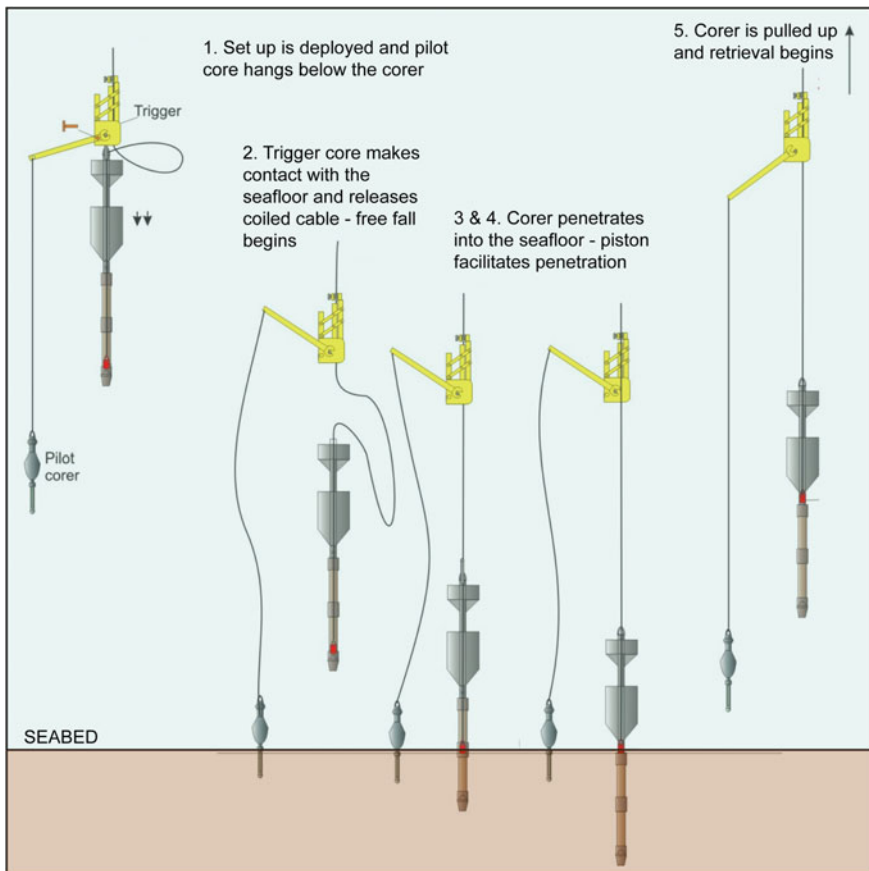


Fig. 5 Steps in the deployment and operation of a piston corer from the set up through to triggering and retrieval (modified from GEO Marine Survey Systems b.v.)

power source stays on the ship and the corer, which is often fixed to a rig that can firmly rest on the seabed (Fig. 6), is lowered to the seafloor while still being connected through cables with the power generator on the ship. The core barrel is driven into the sediment by the force of gravity, enhanced by the vibration energy. The vibration reduces friction and facilitates core penetration into the substrate. When the corer has penetrated fully into the sediment, the vibration is switched off and the barrel pulled and retrieved, with the core catcher at the nose of the barrel preventing the sediment from being lost.

Vibrocoring is the preferred technique when dealing with unconsolidated, heterogeneous sediments, such as compact sands and stiff clays or even unconsolidated chalk, but if the vibration force is high enough it is able to sample consolidated sediments too. It is also effective with glacial shelf sediments. However, due to the need for power connection the water depth to which this corer

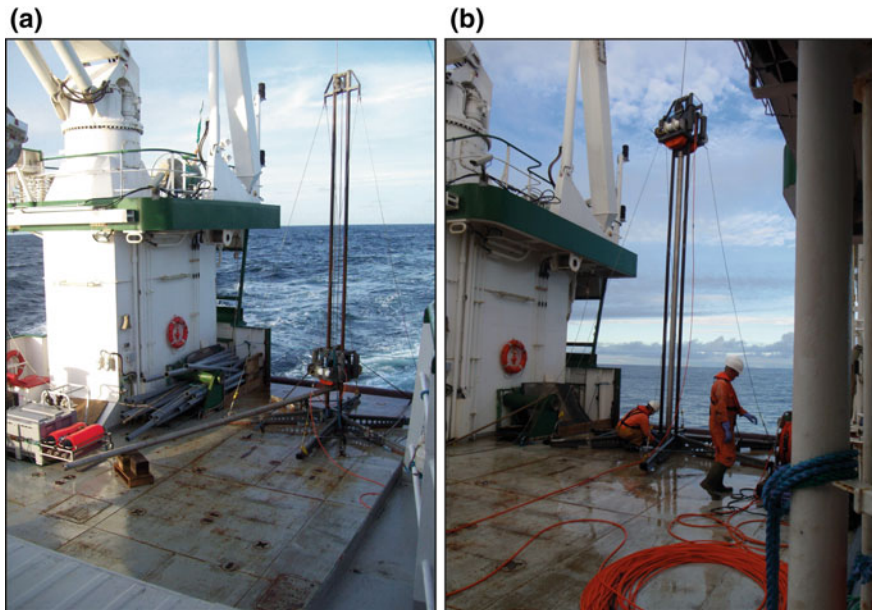


Fig. 6 **a** Vibrocorer on the deck of RV Celtic Explorer and **b** being prepared for deployment. In the foreground of **b** the umbilical cable can be clearly seen

can be used is often limited. Disturbance to the sediment due to the vibration is limited to the few millimetres adjacent to the tube and the surface sediment that may be stirred up by the corer as it penetrates, but the centre of the core is usually intact.

3.5 Multi-corer and Mega Corer

When multiple samples are needed from the same location, a multi-corer or a mega corer are the most time-efficient ways to retrieve them. Multiple plastic tubes are fixed to a tubular frame with a sampling head attached to it by a hydraulic damper (Fig. 7). Lead weights attached to the head allows for regulation of the depth of samples taken. The corer is slowly lowered until it rests on the seafloor. The core tubes penetrate the sediment under the force of gravity but at a controlled rate regulated by the hydraulic damper and the lead weight on the head. A series of spring-loaded arms swing under the tubes to seal the sediment in and plug the top of the tubes to prevent disturbance when the corer is pulled for retrieval (like the hammer spade in the box corer).

This method is preferred when multiple samples are needed from the same site but also when the sediment-water interface needs to be sampled as this is the most efficient method of retrieving it.



Fig. 7 Megacorer set up with nine sampling tubes has just been retrieved on RRS James Cook

3.6 Giant Piston Corer and the CALYPSO Corer

The Giant piston corer was designed by Hollister et al. (1973) to obtain long piston cores from large water depths (5000 m). The length that can be achieved is usually 30–40 m. The device is not much different to the conventional piston corer with only a few modifications to its diameter (14 cm outside, 11.5 cm inner diameter), larger weights (up to 6 tons) and, most notably, a parachute to control the speed of penetration and avoid over-penetrating and compressing the sediments.

The CALYPSO piston corer, is a giant piston corer that was developed onboard R/V Marion Dufresne and is used to collect even longer cores, up to 75 m in length at full ocean depth. The corer is deployed using a specially made wire that prevents it from rotating and is weightless in the water (Aramid cable). It can be triggered using either a counter weight similar to the trigger weight core as described above for the conventional piston corer or by using a programmable acoustic release, both of which enable the corer to freefall.

4 Seafloor Drilling

Most seafloor shaping processes last for long periods, in the order of thousands to millions of years, whether volcanic or sedimentary. Marine geomorphologists ideally prefer to have access to a longer record in order to understand the present-day seafloor morphology and to that vein techniques that drill into the seafloor and generate longer and continuous records of samples are commonly pursued. However, seafloor drilling is a technologically demanding, difficult and expensive activity and therefore not easily employed. The oil and gas industry operations produce samples that are ideal for use in marine geomorphology and frequently this data is made available to researchers. Correspondingly, the International Ocean Discovery Programme (IODP) provides similar datasets, but the actual operation takes many years of planning. There are other seafloor drills, such as the FUGRO seafloor drill and the MARUM MeBo, that have shallower sub-seafloor reach but that are more flexible and mobile than the oil and gas industry or the IODP and consequently easier to use. Below are descriptions of the operations of these three types of drilling techniques. Other seafloor drills are available but not described here as they operate at similar principles.

4.1 Oil and Gas Industry Operations

Offshore drilling has had to adapt to considerably challenging environments of variable water depths ranging from relatively shallow water on the continental shelf to deep water slopes and ultra-deep water basins. This has resulted in the development of three main types of drilling rigs, each one appropriate for different water depths and specific local conditions (geology, weather). Based on operation those three types are Jack-up rigs, semi-submersibles and drillships.

Jack-up rigs are the most commonly used worldwide. They operate in shallow water depths, up to 150 m, and preferably on a firm seafloor. The rig is floated into position and three or four legs are lowered and penetrate the seafloor for stability. Jack-ups are self-elevating and stand clear of the highwater level. In deeper water depths (up to 500 m) or unstable seafloor a semi-submersible rig is used, which is a mobile and floating rig, with a platform on a submerged framework kept buoyant with ballasted columns and watertight pontoons that sit about 20 m below the water surface and below fairweather wave base, providing some relative stability. Mooring lines anchored to the seafloor and dynamic positioning keep the rig in position. In fact dynamic positioning can in some cases completely replace anchored moorings. Finally, for deeper water locations, drillships have been constructed, which could be used in water depths in excess of 3500 m. These can work in any water depth apart from very shallow water. They are ship-shaped and this allows them total mobility and can be mobilised globally to even the remotest areas. However, they are particularly affected by weather conditions. Other rig types

include drill barges, tender-assist rigs, compliant towers, platform rigs and Spar rigs. The deepest floating rig is the Perdido Spar in the Gulf of Mexico at a water depth of about 2450 m operated by Shell Oil.

When discoveries are made temporary exploratory wells reveal shows and serve also to assess the quality of the hydrocarbon before proceeding to the drilling of a production well. Exploratory wells that find oil or gas where neither has been found before are called wild cats. If a well strikes oil or gas it is called discovery well. Step-out or appraisal wells are drilled either to determine the limits of a field following discovery or to explore for other reservoirs in the vicinity of known fields. When a well is unsuccessful in finding oil or gas it is called a dry well.

The most common drilling technique is rotary drilling where a drill bit is screwed to the end of a drill string, which is made of a set of drill pipes (about 9 m long each). The drill bit attached to the drill string is lowered through the water until it reaches the seafloor. A hole is commenced, or spudded, with the rotary steel-toothed or diamond-studded bit. Cooling, cleaning and pressure stabilisation is achieved by using a drilling fluid, which is pumped through the drill pipe and out through the drill bit and back up the hole to the mud pits on the drilling rig, before it gets recirculated. The drilling fluid may be a mixture of sea water, clay such as barite and bentonite, and other chemicals. The initial hole is usually 36 in. in diameter. Each time the bit drills the equivalent of one pipe length, drilling stops for another joint of pipe to be added to the drill string (making a connection). The hole needs to be cased to prevent collapse or caving. Casing is achieved by cementing a steel pipe to the rock wall of the hole. A smaller diameter hole can then be drilled from the base of the first hole, which will also be cased by cementing steel pipes to the hole walls but also the larger diameter hole above it and so on. The hole keeps getting lengthened this way with ever narrower diameter. Wireline logging is performed before the casing is cemented to the walls. Sitting on the seafloor and connected to the top of the hole is the “blow-out preventer” (BOP), which consists of a series of pipes and valves to prevent the sudden rush of fluid or gas to the seafloor in case overpressurised oil or gas are unexpectedly encountered.

Other drilling methods include percussion drilling which involves crushing the rock by raising and dropping a heavy chisel bit, rotary percussion drilling which is a combination method that uses a rotary drill that also pounds into the rocks, sonic (vibratory) drilling which uses a sonic drill that generates high frequency resonant vibrations that cause magnification of the amplitude of the drill bit and fluidisation of particles, and directional drilling which is rotary drilling but directed along a curved path as the hole deepens. For further information, the reader is directed to more dedicated books and publications, such as Tanaka et al. (2005), Devold (2009), Offshore Operations Subgroup (2011) and a plethora of websites (e.g. <http://www.petroleumonline.com/> and <http://www.slb.com/services/drilling.aspx>).

4.2 International Ocean Discovery Program

Benefiting from the technology developed by the oil and gas industry, and particularly dynamic positioning which can keep vessels on target in strong currents, scientific deep sea drilling became possible. Originally called the Deep Sea Drilling Project (DSDP), it started in 1966, using the Drilling Vessel *Glomar Challenger*. In 1985 it became the Ocean Drilling Program (ODP) when the *Glomar Challenger* was decommissioned and replaced by the *JOIDES Resolution*. The Integrated Ocean Drilling Program (IODP) continued using a refurbished *JOIDES Resolution* and the Japanese Deep Sea Drilling Vessel *Chikyu* (Japanese for Planet Earth). In addition, a third component, so called Mission Specific Platforms, were added for settings, where none of the above mentioned drill ships can operate (e.g., ice-covered regions and very shallow water conditions) (Fig. 8). As of 2013 the Integrated Ocean Drilling Program continues under the new collaboration of the International Ocean Discovery Program (IODP) (Fig. 9).

IODP uses multiple drilling platforms to access different sub-seafloor environments during research expeditions. Their website is a very valuable source of information and details on the tools and techniques they use (<http://iodp.tamu.edu/tools/index.html>). The *JOIDES Resolution* has riser-less drilling technology, which uses seawater as the primary drilling fluid, pumped into the drillpipe. The role of the seawater is to cool and clean the drill bit as well as deliver cuttings out of the hole to a cone on the vessel. On the other hand, *Chikyu* operates with riser technology. It uses an outer casing that surrounds the drill pipe, which provides return circulation of engineered drilling fluid maintaining the pressure in the hole at an equilibrium. At the same time cuttings are removed and the drill hole is cleaned allowing for deeper drilling. A blowout preventer (BOP) protects from overpressure build-up. A tall metal drilling rig allows to conduct rotary drilling with the Rotary Core Barrel, which is the oldest and most basic technique and is used to retrieve medium to hard lithified sediments and crystalline rock cores.



Fig. 8 IODP uses multiple drilling platforms, but most commonly **a** the riser-less *JOIDES Resolution*, image taken from <http://iodp.tamu.edu>, Photo Credit William Crawford, IODP-JRSO **b** the riser vessel *Chikyu*, photo courtesy of JAMSTEC; CC BY-NC 4.0, **c** Mission-Specific Platforms chosen for the specific conditions of the expedition; pictured here is the ice breaker *Vidar Viking* from the Arctic Coring Expedition (ACEX), 2004 (photo Martin Jakobsson © ECORD/IODP)

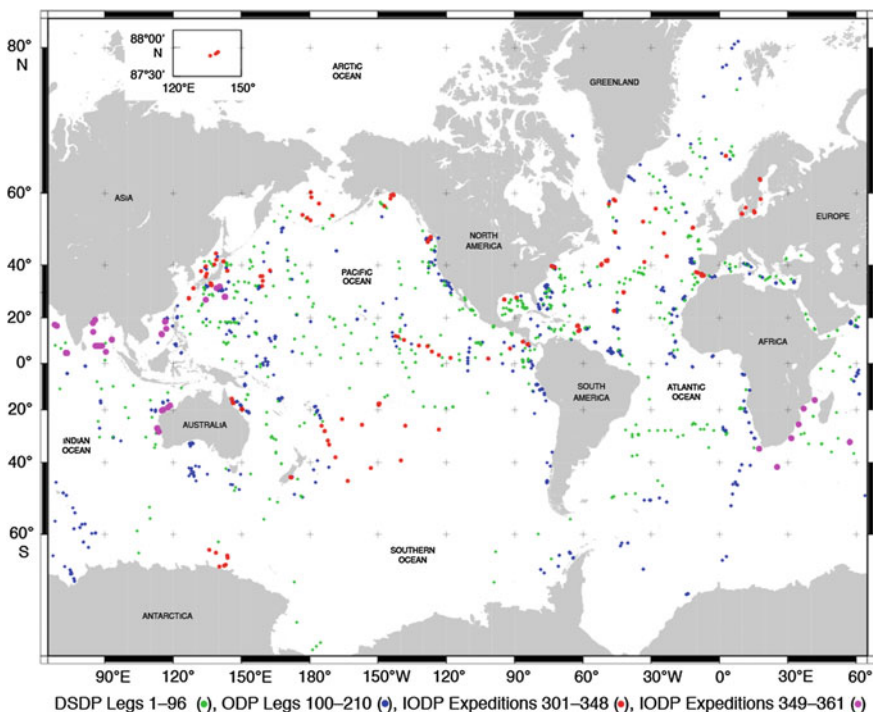


Fig. 9 Global map of the distribution of boreholes from all four phases of the international marine research drilling programme, legs 1–369. Map taken from <https://iodp.tamu.edu/scienceops/maps.html>

Other coring techniques include the Hydraulic Piston Corer (HPC) and the Advanced Piston Corer (APC), which are push-type, no rotation involved and use hydraulic actuated piston coring (<http://iodp.tamu.edu/tools/index.html>). This technique is ideal for climate and palaeoceanographic studies as it retrieves the least disturbed sediments but on the downside, it is limited to the upper 200 m. The Half-Length APC (HLAPC) is a shorter version of the APC and is used to recover high-quality, high-resolution cores from short intervals of soft sediments between harder layers, such as oozes, between chert layers. For the recovery of deeper but more consolidated sediments the Extended Core Barrel (XCB) can be used. It is usually deployed when the sediments are too stiff for the piston corer but too soft for the RCB. It is interchangeable with the HPC and APC, depending on the sediments encountered. The operation of the XCB uses rotation of the drill string to advance the hole while the cutting shoe trims the sample.

IODP holes can be re-entered at a later stage with technologies such as the Free-Fall Funnel (FFF) and the Reentry Cone and Casing (RECC), the latter being a permanent seafloor installation. The RECC allows multiple visits to the same hole deepening it or installing permanent/long-term downhole measuring and sampling.

Apart from the core retrieval, downhole logging typically takes place in an IODP hole, which includes standard wireline logging (i.e. porosity, litho-density, natural gamma ray, enhanced digital telemetry, resistivity imaging, magnetic susceptibility, sonic imaging, microscanning, inclinometry and borehole seismic) and downhole memory measurements (temperature of rocks and sediments, pressure in soft sediments, magnetic orientation, etc.). Downhole logging can either be performed after drilling, lowering the logging tools through the open hole, which is the conventional method, or while drilling (Logging While Drilling—LWD), allowing real time data feedback. The latter is preferred when hole conditions are expected to be unsuitable for conventional wireline logging.

4.3 Seafloor Drill Rigs

Access to IODP vessels is limited and requires many years of planning, while other drill ships are expensive. An intermediate coring technique, bridging the gap between IODP and the standard coring tools described above, are seafloor drill rigs. There is a variety of seafloor drills operational in the world, used commercially and academically. A seafloor drill is lowered onto the seafloor from a purpose-built research vessel on an umbilical cable that provides control, communications, power and hoist capability. It may have a single core barrel that can drill to a depth of 5 m or may be equipped with a drill-pipe magazine that can take multiple barrels which allows to drill to greater depths by attaching extension pipes to the drill string (Freudenthal and Wefer 2013).

Commercial seafloor drills include the Fugro Seafloor Drill that can retrieve samples up to 150 m below the seafloor at water depths up to 4000 m, the Portable Remotely Operated Drill (PROD) that can operate at waterdepths of 3000 m and retrieve more than 130 m of core and the Underwater Seafloor Drilling Rig (USDR) that has no water depth limit of operation (Sheshtawy 2007), amongst many others.

The British Geological Survey (BGS) rockdrill can retrieve up to 50 m of core at water depths up to 3000 m, which originally could only retrieve 5 m when it was initially conceived in 1982 (Wilson 2006). Development was and still is continuous with updates in software, camera, cable and connectors technologies, but also in progressing from a single barrel to a multi-barrel operation (Wilson 2006). BGS also operate an orientated rockdrill, which can be deployed at 4500 m water depth and which allows for cores to be orientated with reference to a compass heading and thus it is used in palaeomagnetic analysis (Wilson 2006).

MeBo (Meeresborden-Bohrgerät) (Fig. 10a) was developed by Marum, the Centre for Marine Environmental Sciences of the University of Bremen, Germany (Freudenthal and Wefer 2006, 2007, 2013) and can drill cores up to 80 m deep in unconsolidated sediments and in hard rocks at water depths up to 2000 m. The drill rig is powered by four hydraulic pumps. MeBo combines rotary and push operation; the drill head is mounted on a guide that moves up and down that generates a maximum push force of 4 tons. Seawater is pumped through the drill string to cool

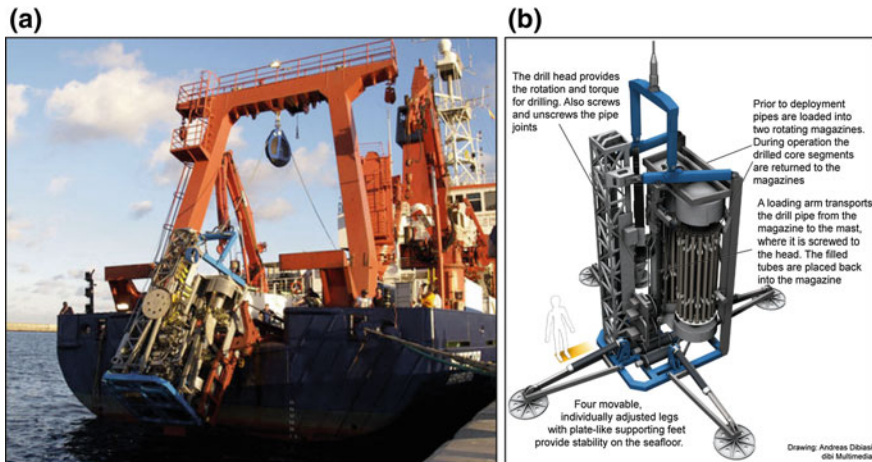


Fig. 10 **a** Deployment of MeBo from RV Meteor and **b** schematic of MeBo parts and operation

and clean the drill bit from cuttings. Barrels are taken off the magazine and threaded to the drill head as drilling progresses (Fig. 10b). Every three meters of sampling the barrel gets stored together with the drilled core in the magazine and the next empty barrel is lowered to the drill hole and attached to the drill head, a 3 m rod is added and drilling continues.

The MeBo 200 is the latest development of this tool. It can recover cores up to 200 m length.

5 Core Handling

Users need to be aware that improper handling or faults in the design of the coring device may result in severely disturbed and unrepresentative samples. The most common and most severe problems that may arise are (1) loss of surface sediment (the seafloor), (2) redistribution and resuspension of enclosed sediment (running along the core liner), and (3) repenetration (bounce of the device after penetrating partially and then repenetrating in same location) (Blomqvist 1991). Other problems may arise from compaction of layers and shortening, particularly towards the base of the core, or extension and sediment stretching near the top of the core (Skinner and McCave 2003; Széréméta et al. 2004).

When cores are retrieved on deck they are labelled and cut into 1–1.5 m sections to make transportation and handing easier. Soft sediment cores are stored in fridges kept at 4 °C temperature, simulating deep sea temperatures, in order to maintain their moisture and chemistry. To analyse the sediment, cores are split into two halves, one is labelled “Working” and is used for sampling and the other is labelled “Archive” (Fig. 11) and is kept intact for posterity.



Fig. 11 Split piston core, way up towards the *top left corner*. One half will be archived and the other half will be used for logging and sampling

Multiple analyses can then be performed on the working half, starting with non-destructive methods, such as physical properties logging (Multi-Sensor Core Logger) and elemental composition scanning (ITRAX) (e.g. Georgioupolou et al. 2012). Destructive methods that require subsampling need to be performed last and modestly so as not to oversample the core.

References

- Blomqvist S (1991) Quantitative sampling of soft-bottom sediments: problems and solutions. *Mar Ecol Prog Ser* 72:295–304
- Devold H (2009) Oil and gas production handbook: an introduction to oil and gas production. ABB ATAP Oil and Gas, Oslo, pp 116
- Freudenthal T, Wefer G (2006) The sea-floor drill rig “MeBo”: robotic retrieval of marine sediment cores. *Pages News* 14(1):10
- Freudenthal T, Wefer G (2007) Scientific drilling with the sea floor drill rig MeBo. *Sci Dril* 5: 63–66
- Freudenthal T, Wefer G (2013) Drilling cores on the sea floor with the remote-controlled sea floor drilling rig MeBo. *Geosci Instr Meth Data Syst* 2:329–337
- Georgioupolou A, Benetti S, Shannon PM, Haughton PDW, McCarron S (2012) Gravity flow deposits in the deep Rockall Trough, Northeast Atlantic. In: Yamada Y, Kawamura K,

- Ikehara K, Ogawa Y, Mosher D, Chaytor J, Strasser M (eds) Advances in natural and technological hazards research, submarine mass movements and their consequences, 4th edn. Springer, pp 695–707
- Hollister CD, Silva AJ, Driscoll A (1973) A giant piston-corer. *Ocean Eng* 2:159–168
- Kögler F-C (1963) Das kastenlot. *Meyniana* 13:1–7
- Kullenberg B (1947) The piston core sampler. *Svenska Hydrografiske-Biologiska Kommissionens skrifter, Tredje Serien: Hydrografi*, Band 1, Hafte 2, p 46
- Offshore Operations Subgroup of the Operations & Environment Task Group (2011) Subsea drilling, well operations and completions. paper #2–11, Working Document of the NPC North American Resource Development Study, p 45
- Reineck HE (1963) Der Kastengreifer. *Natur und Museum.* vol 93. pp 102–108
- Skinner LC, McCave IN (2003) Analysis and modelling of gravity- and piston coring based on soil mechanics. *Mar Geol* 199:181–2004
- Széréméta N, Bassinot F, Balut Y, Labeyrie L, Pagel M (2004) Oversampling of sedimentary series collected by giant piston corer: evidence and corrections based on 3.5-kHz chirp profiles. *Paleoceanography* 19:PA1005
- Sheshtawy A (2007) Underwater seafloor drilling rig. american association of drilling engineers national technical conference and exhibition, Texas, AADE-07-NTCE-30, 10–12 Apr 2007
- Tanaka S, Okada Y, Ichikawa Y (2005) Offshore drilling and production equipment, in civil engineering. In: Kiyoshi Horikawa, Qizhong Guo (eds) in encyclopedia of life support systems (EOLSS). Developed under the Auspices of the UNESCO, Eolss Publishers, Oxford, UK, (<http://www.eolss.net>)
- Wilson M (2006) Drilling at sea. *Earthwise Br Geol Surv* 23:32–33

ROVs and AUVs

**Veerle A.I. Huvenne, Kathleen Robert, Leigh Marsh,
Claudio Lo Iacono, Tim Le Bas and Russell B. Wynn**

Abstract The most significant breakthroughs in science are often made as a result of technological developments and innovation. A new capacity to gather more data, measure more precisely or make entirely new observations generally leads to new insights and fundamental understanding. The future of ocean research and exploration therefore lies in robotics: marine robotic systems can be deployed at depths and in environments that are out of direct reach for humans, they can work around the clock, and they can be autonomous, freeing up time and money for other activities. To advance the field of submarine geomorphology, the two types of robots that currently make the biggest difference are Remotely Operated Vehicles (ROVs) and Autonomous Underwater Vehicles (AUVs). Other autonomous or robotic systems are available for marine research (e.g. gliders, autonomous surface vehicles, benthic crawlers etc.), but their application for geomorphological studies is less extensive. This chapter gives an overview of the main characteristics of ROVs and AUVs, their advantages and disadvantages, and their main applications for geomorphological research. In comparison to the other geomorphological methods discussed in this book, however, it has to be made clear that ROVs and AUVs are not so much methods per se, instead they are platforms from which existing and new approaches can be applied.

V.A.I. Huvenne (✉) · K. Robert · L. Marsh · C. Lo Iacono · T. Le Bas · R.B. Wynn
National Oceanography Centre, University of Southampton
Waterfront Campus, Southampton, UK
e-mail: vaih@noc.ac.uk

L. Marsh
Ocean and Earth Science, National Oceanography Centre,
University of Southampton, Southampton, UK

1 Method Descriptions

1.1 Remotely Operated Vehicles

Remotely Operated Vehicles (ROVs) are tethered robotic devices used for exploration, inspection and the execution of specific tasks under water. A typical ROV (Fig. 1) consists of a sturdy frame, a floatation unit to provide buoyancy (generally, ROVs are marginally positively buoyant), a number of thrusters to enable manoeuvrability in three dimensions, and a tether which connects the system to the host ship. The tether can also be connected to a Tether Management System (TMS): a separate non-buoyant unit that is lowered with the ROV on an armoured cable from the ship, and dampens the effect of the ship's motions on the ROV.

Initially, ROVs were developed in the 1960s for military use (recovery operations, mine clearing, etc.), and were named CURV: “Cable-controlled Underwater Recovery Vehicles” (Christ and Wernli 2007; Ridao et al. 2007). The technology was introduced into the industrial domain in the late 1970s and 1980s, to enable operations beyond depths that could be reached by divers. Nowadays they are mainly used by the Oil and Gas sector, but they are also deployed for scientific research and salvage operations.

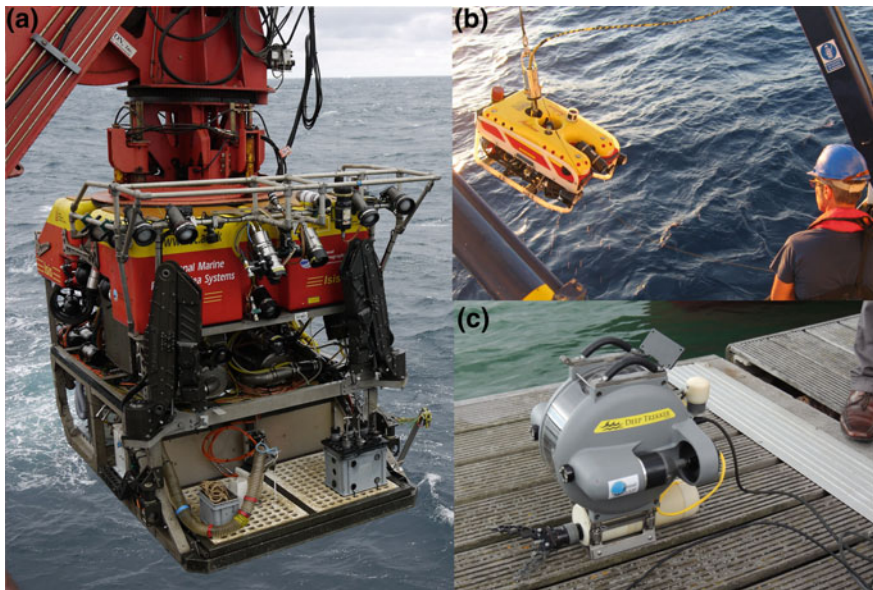


Fig. 1 Types of ROV used for seafloor studies: the scientific working class ROV *Isis* from the National Oceanography Centre, UK (a photo by L. Marsh), the *Falcon* inspection class ROV from Plymouth University (b photo by V. Huvenne) and the *Deep Trekker* mini-ROV from the NOC (c photo by Tim Le Bas, NOC)

Based on the size of the frame, the operational requirements and the vehicle's depth rating, an ROV can be equipped with a range of sensors, instruments and tools. In the most basic configuration, an ROV will carry one or more video cameras, of which the data is transferred to the on-board operator in real time. In addition, there may be one or two manipulator arms with various levels of functionality, and a 'basket' or storage device to store samples or tools. In more advanced configurations, other sensors or equipment can be integrated into the system, ranging from small CTDs, optical sensors or chemical sensors to HD cameras, sector scanning sonars, multibeam echosounders and suction samplers.

ROVs come in a wide range of capabilities (Marine Technology Society 2015; Kernow Marine Explorations Global Limited 2016). Apart from their depth-rating, ROVs are typically classified according to their size: work-class ROVs are large and powerful vehicles (up to 2 m high and 4 m long), that can be used for complex operations and can carry several instruments or a large volume of samples. In most cases they are equipped with two 5- or 7-function manipulator arms. Within the scientific domain, some of the best-known examples include the *Jason* ROV from the Woods Hole Oceanographic Institution (WHOI), the *Isis* ROV from the National Oceanography Centre (NOC), and the ROV *Victor* from the Institut Français de Recherche pour l'Exploitation de la Mer (IFREMER), which can all operate down to 6000 m water depth (e.g. Yoerger et al. 2000; Rigaud 2007; Marsh et al. 2013). Inspection or observation class ROVs are smaller (metre-size), often have only one manipulator arm, and are mainly used for video surveys. Although more compact than the work-class vehicles, they still have sufficient power to work in full marine conditions, in some cases down to 3000 or 4000 m water depth. Besides video surveying, they can often carry out a number of other tasks (Pacunski et al. 2008). Eyeball class ROVs (also known as mini- and micro-ROVs) are even smaller. They can often be packed in a single suitcase, and can be deployed by a single person. They are specifically built for inspection work, generally in relatively calm and shallow waters (<200 m). Assembly kits are now available online that allow users to build their own mini-ROV (e.g. OpenROV 2016).

1.2 Autonomous Underwater Vehicles

Autonomous Underwater Vehicles (AUVs) are unmanned, un-tethered robot submarines that operate fully independently to carry out pre-programmed operations and surveys (Griffiths 2003). AUV endurance typically ranges from a few hours to several days, although rapid technological developments are now bringing long-range operations within the possibilities, with endurances stretching to weeks or even months (Hobson et al. 2012; Furlong et al. 2012). Operational depths range from a few hundred metres for the smaller vehicles (Griffiths 2003; Wynn et al. 2014) to full ocean depth for the larger models (>6000 m; Huvenne et al. 2009).

AUVs are typically categorised as either "cruising" or "hovering" vehicles (Fig. 2). Cruising, or survey AUVs are generally torpedo-shaped and driven by a

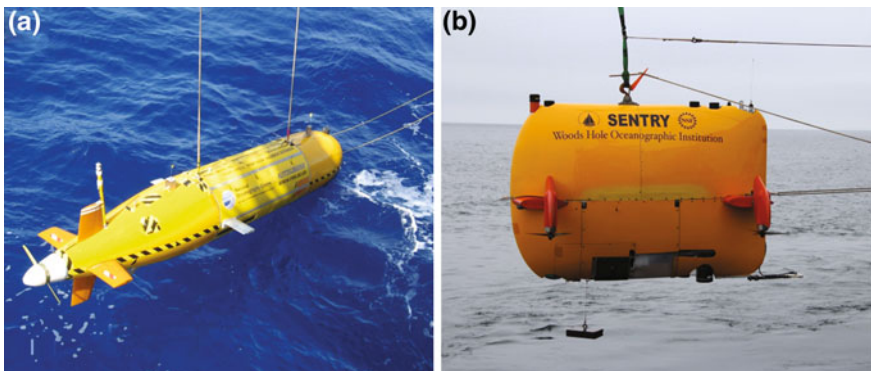


Fig. 2 Examples of AUV types: the torpedo-shaped survey AUV *Autosub6000* from the National Oceanography Centre UK (**a** photo by V. Huvenne), and the hovering AUV *Sentry* from WHOI (**b** photo by Oscar Pizarro, Australian Centre for Field Robotics, University of Sydney)

single propeller. They move at speeds up to 2 m/s, and are optimised to cover large distances along pre-designed tracks (Wynn et al. 2014). They form the main type of AUVs used in the commercial world, while some of the most prominent scientific examples include the *Autosub* series from the NOC, the *AsterX* and *IdefX* from IFREMER and the *Dorado* series from MBARI (Rigaud 2007; Caress et al. 2008; McPhail 2009). Hovering AUVs, on the other hand, have several propellers/thrusters, which allow them to move in any direction and provide them with a high manoeuvrability, much like an ROV. They are designed for precision operations, slow motion surveys (e.g. seabed photography) and work in distinctly 3-dimensional terrains, such as around hydrothermal vents or coral reefs. Among the best-known scientific examples of hovering AUVs are *ABE* and *Sentry* from WHOI (e.g. Yoerger et al. 1998; Wagner et al. 2013).

Similar to ROVs, depending on their depth rating and size, AUVs can be equipped with a range of sensors (CTDs, ADCPs, chemical sensors, photo cameras, sonars, magnetometers, gravimeters etc.) (e.g. Caress et al. 2008; Connelly et al. 2012; Sumner et al. 2013; Williams et al. 2010; Yoerger et al. 1998). However, the lack of tether, and hence of direct power input, limits the sensor power consumption and duration of activity. In addition, AUVs are currently not yet equipped for extensive seabed or faunal sampling, although sampling of the water column has been achieved (Pennington et al. 2016). Overall, AUVs are more suited for survey operations, acquiring sensor data along smooth, pre-programmed tracklines, while ROVs are optimal for high-resolution, highly detailed and interactive work, including HD video surveying and sampling. An extensive review of the use and capabilities of AUVs for geological research was recently published by Wynn et al. (2014).

Over the last 5 years, a number of ‘hybrid underwater vehicles’ have been developed, combining advantages of ROVs and AUVs (Bowen et al. 2013). Undoubtedly the most famous example was the *Nereus* H-ROV, engineered by WHOI, which unfortunately was lost at sea in 2014 in the Kermadec Trench

(Cressey 2014). Using a single optical fibre as tether, the dual-purpose vehicle could be used as an interactive ROV, enabling sampling operations, while it could equally operate as a hovering AUV, without tether. However, as the single fibre only provided data transfer capacity, the power limitations for the vehicle and its scientific payload still remained.

1.3 *Using Robotic Vehicles to Study Seafloor Geomorphology*

Nested surveys: The availability of underwater vehicles such as ROVs and AUVs has revolutionised our understanding of seafloor morphology and processes. Their free-diving capability means that the activity of seafloor mapping is no longer restricted to measurements carried out from the sea surface, or from towed vehicles. Using AUVs or ROVs, high-frequency sonars can be operated with high precision close to the seafloor, offering the opportunity to create maps of any required resolution. In principle, the altitude of the echosounder above the seabed can be freely chosen (within the limitations of the instruments used), and therefore, through simple geometry, also the resolution of the resulting map. The increased detail achieved in this way provides insights that previously were impossible to obtain. The trade-off for this extra resolution is generally a reduction in the area that can be mapped within a certain timeframe, as a reduction in altitude of the sonar or optical sensor above the seabed results in a reduction in coverage of single swaths or images. Furthermore, AUVs, and certainly ROVs, travel at a slower speed than surface vessels, and therefore can cover less ground. Hence, underwater vehicles are generally used to complement ship-board mapping activities, rather than replacing them. Operations are often planned in a nested scheme: target areas identified on conventional ship-borne multibeam bathymetry maps are surveyed by a cruising AUV equipped with a multibeam or sidescan sonar system (see Chapters “Sidescan Sonar” and “Multibeam Echosounders”). To achieve the highest level of detail, ROV-based multibeam or photogrammetry techniques are then applied to specific features of interest (see below).

Navigation: One of the biggest challenges when using underwater robotic vehicles for high-resolution seafloor mapping is to obtain precise and accurate positioning information. Recording datasets with a spatial resolution in the order of 10 cm is a lost effort if the relative positional accuracy of the vehicle between consecutive depth measurements is not at least an order of magnitude more precise. Navigation for ROVs and AUVs is generally based on a combination of acoustic techniques. As a result of spherical spreading and attenuation of the signal in the water, those become less accurate in deeper water and over larger distances. When high-accuracy maps are required and sufficient time and funds are available, a long base-line (LBL) transponder network can be installed on the seafloor, to enable high-precision triangulation of the vehicle position (Milne 1983). However,

the time-investment required for such a set-up, especially in deep water, can be extensive. In most cases, ROV positioning is based on ultra-short base-line (USBL) navigation from the host ship (Christ and Wernli 2007). Once close to the seafloor, ROV systems can also use dead-reckoning based on an inertial navigation system and a Doppler Velocity Log (DVL, Kinsey and Whitcomb 2004). This provides a better relative positioning, but may be subject to a cumulative error or ‘drift’ that gradually builds up over longer distances. Regularly re-setting the inertial navigation with reference to the USBL positioning is recommended. AUVs use the same dead-reckoning technology, but are generally only positioned with the help of the ship’s USBL at the start (and sometimes end) of their mission if they operate fully independently from the host ship. To increase accuracy of the mission start position, specific techniques can be applied (e.g. “range-only navigation”, see McPhail and Pebody 2009).

Further corrections to the vehicle navigation can be applied through feature matching algorithms on overlapping sections of the seafloor mapping data. This can be carried out manually in post-processing, or increasingly in real-time using SLAM algorithms (Simultaneous Localisation and Mapping, e.g. Barkby et al. 2009). SLAM can be described as the process whereby the system continuously builds up a database of landmarks and features of the environment in which it is moving, and simultaneously correlates this database with its current observations to determine its location (West and Syrmos 2006). Similar approaches can be used to integrate new seafloor surveys with existing seafloor data, either from previous shipboard surveys, or from previous AUV or ROV missions.

2 Different Applications of ROVs and AUVs for Geomorphological Studies

2.1 *High-Resolution Multibeam Bathymetry*

By far the most common use of marine robotic vehicles for geomorphological studies is for the acquisition of high-resolution multibeam echosounder data. ROV- and AUV-based surveys can create spectacular digital terrain models that illustrate a wide range of smaller-scale processes which are traditionally overlooked in studies based on shipboard bathymetry alone. One of the most pertinent examples is the illustration of large deep-sea scours in the outflow channels of submarine canyons (Fig. 3)—features that are normally not resolved by shipboard multibeam maps, but that provide an important insight in the occurrence of sediment gravity flows and their erosive strength (e.g. Caress et al. 2008; Huvenne et al. 2009; Macdonald et al. 2011). Apart from scours and erosive features, AUV- and ROV-based multibeam maps of submarine canyons also reveal bedform morphologies and their evolution (e.g. Paull et al. 2013; Tubau et al. 2015), the location of local cliffs and outcrops (e.g. Masson et al. 2011) and detailed gully systems (e.g. Rona et al. 2015).

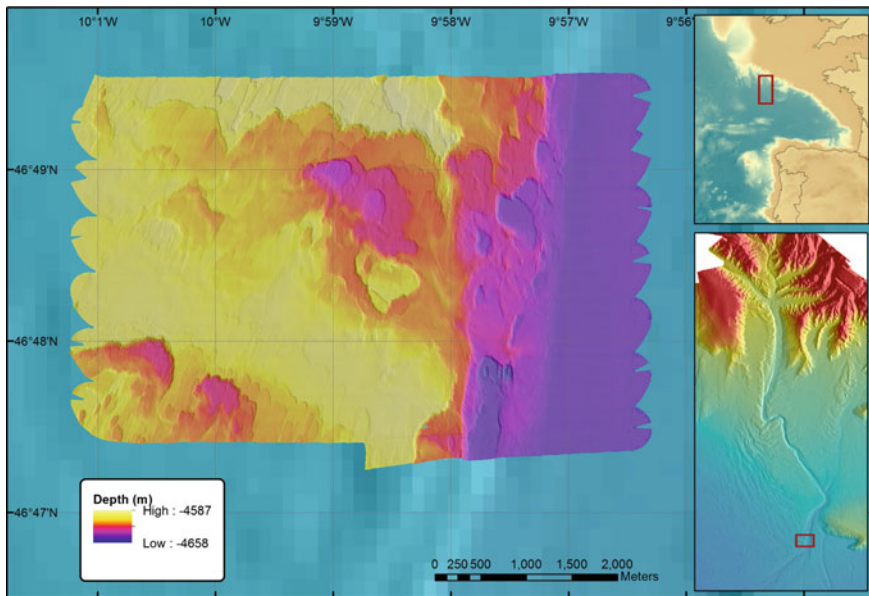


Fig. 3 High-resolution multibeam bathymetry acquired by the AUV *Autosub6000* at ca. 4600 m water depth on the margin of the Whittard Canyon outflow channel in the Bay of Biscay, illustrating large scours which cannot be mapped with traditional shipboard multibeam systems (*lower right inset*). Modified after MacDonald et al. (2011)

A similar revolution in the interpretation of deep-sea geomorphology has been achieved through the ROV- and AUV-mapping of landslide scars (e.g. Lee and George 2004), hydrothermal vents and mid-ocean ridges (e.g. Yoerger et al. 2000; Rogers et al. 2012), mud volcanoes (e.g. Jerosch et al. 2007; Dupré et al. 2008) and cold-water coral mounds (e.g. Huvenne et al. 2005; Grasmueck et al. 2006), for example.

2.2 True 3-Dimensional Morphology

In addition to bringing instruments as close to the seafloor as necessary, robotic technology has created new opportunities to develop unusual sensor configurations. By mounting sonar systems in a sideway or even upward-directed orientation, the true 3-dimensional morphology of underwater terrains can be mapped: something that can never be achieved with a traditional downward-facing set-up. Yoerger et al. (2000) carried out pioneering work when they deployed a forward-looking pencil beam scanning sonar on the *Jason* ROV to create 3D digital models of hydrothermal vents on the Juan de Fuca Ridge. Similarly, Gary et al. (2008) used an array of 54 single narrow-beam sonars on the DEPTHX AUV, to obtain the

complete morphology of submerged caves. Expanding the approach to multibeam sonars to achieve higher data density, Wadhams et al. (2006) mounted an upward-facing EM2000 multibeam system on the Autosub II AUV to develop detailed maps of the underside of icebergs and sea ice. Huvenne et al. (2011) placed an SM2000 multibeam system in a forward-looking position on the front of the Isis ROV and moved the ROV sideways in order to map the geological fabric and biological habitat of vertical and overhanging cliffs in a submarine canyon. They also applied the same approach to map the intricate morphology of submarine landslide headwall scarps (Fig. 4; Huvenne et al. 2016).

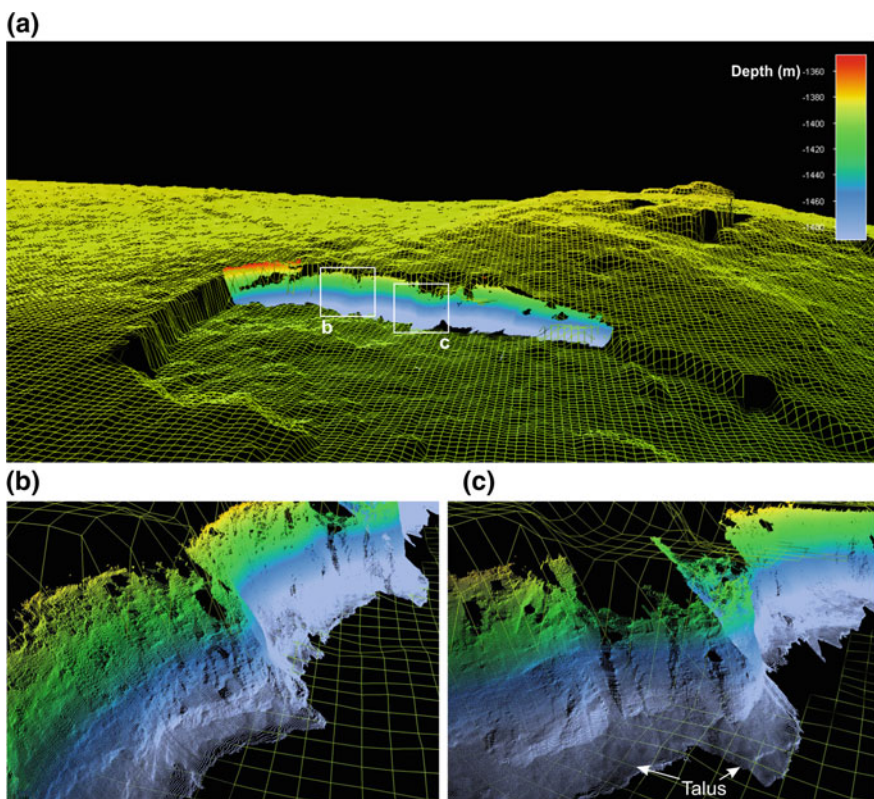


Fig. 4 Application of ROV-based forward mapping of *vertical* substrates: submarine landslide headwall scarp at ca. 1400 m water depth on SW Rockall Bank. ROV bathymetry nested in the shipboard bathymetric grid (a), and details of the headwall scarp represented as point clouds (b, c), illustrating individual blocks protruding from the headwall scarp, and *vertical* cliffs fringed by talus. Modified after Huvenne et al. (2016)

2.3 Sidescan and Synthetic Aperture Sonar

While multibeam bathymetry naturally forms the primary source of information for seafloor geomorphology studies, in certain cases the use of sidescan or synthetic aperture sonars mounted on ROVs or AUVs may be a better choice. The low grazing angle used by the latter acoustic systems allows identification of subtle changes in the terrain, such as those caused by pockmarks (e.g. Wagner et al. 2013) or small-scale bedforms (e.g. Wynn et al. 2014) that are not easily resolved by multibeam systems (see also Chapter “[Sidescan Sonar](#)”). In addition, the backscatter intensity of sidescan or synthetic aperture sonars, registered at higher resolution than what can be achieved with multibeam systems providing the same swath width, may reveal patterns that are either exclusively expressed or at least accentuated in the sediment type or seafloor roughness. The example in Fig. 5 shows a field of iceberg ploughmarks on Rockall Bank (NE Atlantic, see also Robert et al. 2014). Although these features do have a bathymetric expression at the seafloor, their pattern is enhanced in the backscatter response registered by the sidescan sonar system. The characteristic gravel ridges at either side of the ploughmarks create a high-intensity backscatter return, while the finer-grained sediments ponded in the troughs have a much lower backscatter. In addition, the high-resolution sidescan data (400 kHz) allow identification of individual cold-water coral colonies, based on their high backscatter signal and their acoustic shadow.

2.4 Photomosaicking and Photogrammetry

To reach the finest scale in the nested scheme of geomorphological observations, photographic and video techniques are generally used. However, as a result of the attenuation and backscatter of light in the marine environment, the extent of underwater scenes that can be imaged from an ROV or AUV at any single point in time is severely limited. To place individual visual observations within their direct spatial context, photo- and video mosaicking techniques have been developed, where composite images are created from a large number of overlapping individual pictures or frames (e.g. Pizarro and Singh 2003; Singh et al. 2007). Extensive image corrections need to be applied to compensate for backscatter, non-uniform illumination, colour balance and geometric distortions (Morris et al. 2014). Using common features in overlapping images, photographs or frames can then be tiled together and georeferenced to create large mosaics of extensive seafloor areas that cannot be imaged at once (e.g. Yoerger et al. 2000; Jerosch et al. 2007; Escartin et al. 2015). The method can equally be applied to image large vertical structures, such as hydrothermal vent chimneys that are several metres high (e.g. Marsh et al. 2013).

Where pairs of photographs are available that picture the same scene from slightly different points of view, techniques of photogrammetry can be used to

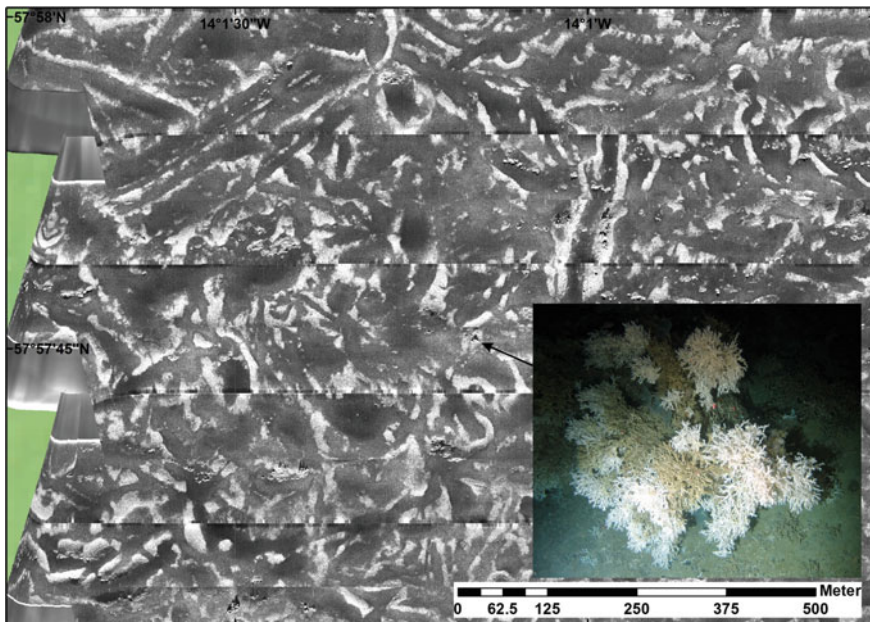


Fig. 5 High-resolution 400 kHz sidescan sonar mosaic collected with the *Autosub6000* AUV at ca. 200 m water depth on Rockall Bank, NE Atlantic. Iceberg ploughmarks are represented by the high backscatter gravel ridges (*light colours*) and low backscatter ponded sediments (*darker colours*). Cold-water coral colonies (as illustrated) can be recognised as small features on the gravel ridges. Modified after Robert et al. (2014)

interpret the 3D morphology of the scene in great detail (Fig. 6). This can be achieved either through the use of stereophotographic cameras, or by using consecutive photographs from a single moving camera that have sufficient overlap. Using the former approach, Ling et al. (2016) mapped the fine-scale morphology of coral reefs, identifying the key habitat for invasive urchins. It equally allowed for the quantification of reef rugosity, slope and aspect (Friedman et al. 2012). The second technique, also named “structure from motion”, has seen huge development over the last few years under the influence of the mobile phone market. The technique, however, is just as applicable to the marine environment, and can result in very detailed representations of the seafloor, that allow ‘virtual geological fieldwork’ (e.g. Kwasnitschka et al. 2013).

2.5 Laser Line Scan

In addition to the acoustic and optical techniques described above, a further technology has been developed that potentially can fill a resolution gap between

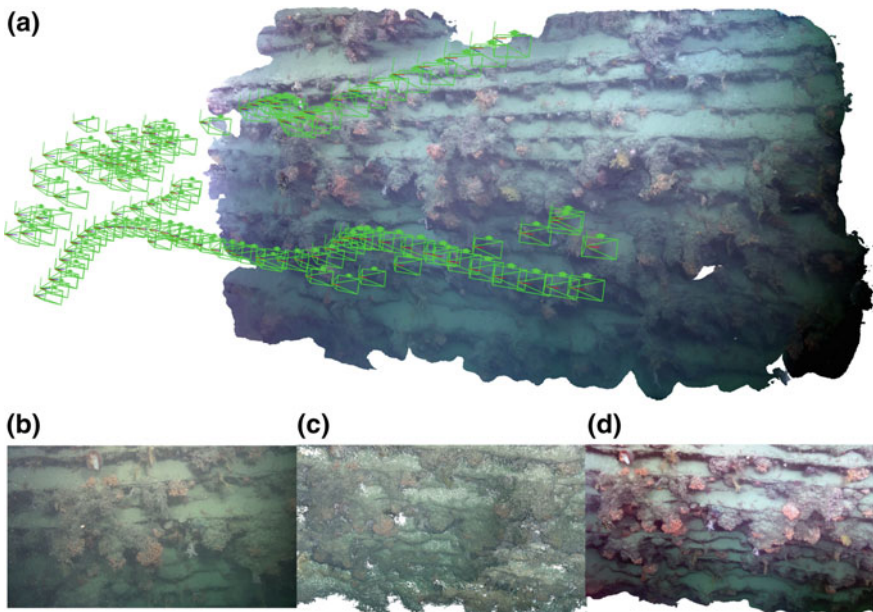


Fig. 6 Example of photogrammetry results. **a** 3D textured mesh reconstructed from HD video frames (position in green) acquired during an *Isis* ROV dive on a *vertical* cliff face in Whittard Canyon at ca. 1300 m depth, illustrating step-like features and overhanging coral framework. Steps involved in the reconstruction: **b** video frames, **c** generated point cloud and **d** zoom on a section of the resulting high resolution textured mesh

multibeam and sidescan sonar mapping on the one hand, and photogrammetry on the other hand. This technique is generally referred to as “Laser Line Scanning”, and can be used to image the seafloor (e.g. Carey et al. 2003) or to obtain 3D morphological reconstructions (e.g. Tetlow and Spours 1999). In both cases, a strip of seabed across the path of the robotic vehicle is illuminated, either by a sheet laser or by a scanning pencil laser. As the vehicle moves forward, the changing reflectivity and shape of the strip is recorded in a series of (stereo-)photographs, from which a seabed image or 3D reconstruction is created line by line. The method was developed to image man-made structures such as pipelines or mines (e.g. Tetlow and Spours 1999), but has also been applied to map archeological remains (e.g. Roman et al. 2010, 2012; Bruno et al. 2011) or the morphology of hydrothermal vents and benthic communities (e.g. Maki et al. 2011). Recent developments have also expanded the technique for the detection of diffuse seafloor venting (which would equally disturb the path of the laser beam; Smart et al. 2013). Because laser mapping works with narrower beam widths than acoustic approaches, it can potentially provide a finer resolution than most multibeam or sidescan systems (Roman et al. 2010, 2012). At the same time, the narrow light source in the laser pencil or sheet produces less backscattering in the water column, which means the approach is also applicable in fairly turbid waters, where photogrammetry methods

would fail (Bruno et al. 2011). A number of laser line scanning systems are now available on the market, although their use is still less common than multibeam, sidescan or photography.

3 Future Directions

Given the wide range of advantages offered by autonomous and robotic vehicles (cost savings for mapping and monitoring, improved resolution, ability to reach inaccessible places, ...), the rapid technological developments in the field, their increasing availability and the resulting reduction in cost, it is to be expected that the use of unmanned vehicles will only increase in the future. As they become more common, new applications and configurations will equally become mainstream. This may include new sensors, or engineering solutions for automated seafloor monitoring capabilities and repeat surveys, for example. However, by far the most promising development in the field is the increasing deployment of fleets of vehicles in coordinated operations. Combinations of AUVs and USVs (Unmanned Surface Vehicles) are currently being tested, for example the Innovate UK Autonomous Surface/Sub-surface Survey System (ASSS) project (Research Councils UK 2016), with one or more USVs providing continuous USBL navigation to the submarine AUVs, reducing navigation uncertainty or the need to follow the vehicles with a surface vessel. They will also enable the operator to continuously monitor the AUV position, data and performance from shore, via acoustic and satellite links with the USV. Equally, squads of vehicles may be deployed simultaneously to increase the area covered during single surveys, or to create nested observations of seafloor and water column characteristics in one single operation. Small-scale AUVs that can be rapidly deployed from USVs or manned/unmanned aerial vehicles will in the future provide the ability to rapidly respond to e.g. oil spills and/or map extensive areas of seabed at reduced cost. Finally, there are major developments underway in automated adaptive sampling, whereby AUVs can respond to environmental cues and adapt their survey pattern accordingly without human control, e.g. an AUV chemically detecting a signature of active hydrothermal venting could automatically adjust its mission to then map and image the targeted feature, without having to return to the surface. Thanks to these new multi-vehicle, and increasingly intelligent and adaptive operations, it can be expected that the volume of high-resolution seabed morphology data will increase rapidly in the near future, opening exciting opportunities for new insights in seafloor geomorphology.

Acknowledgements The authors would like to thank all captains, crews and scientific teams that have assisted with the collection of the different datasets discussed and presented. K. Robert and V. Huvenne are supported by the ERC Starting Grant CODEMAP (Grant no 258482), while the whole author team receives support from the NERC MAREMAP programme.

References

- Barkby S, Williams S, Pizarro O, Jakuba M (2009) An efficient approach to bathymetric SLAM. In: The IEEE/RSJ international conference on intelligent robots and systems. St. Louis, USA, pp 219–224
- Bowen AD, Juakuba MV, Farr NE, Ware J, Taylor C, Gomez-Ibanez D, Machado CR, Pontbriand C (2013) An un-tethered ROV for routine access and intervention in the deep sea. In: Oceans 2013. IEEE, San Diego, p 7
- Bruno F, Bianco G, Muzzupappa M, Barone S, Razonale AV (2011) Experimentation of structured light and stereo vision for underwater 3D reconstruction. *ISPRS J Photogrammetry Remote Sens* 66:508–518. doi:[10.1016/j.isprsjprs.2011.02.009](https://doi.org/10.1016/j.isprsjprs.2011.02.009)
- Caress DW, Thomas H, Kirkwood WJ, McEwen R, Henthorn R, Clague DA, Paull CK, Paduan J, Maier K (2008) High-resolution multibeam, sidescan and subbottom surveys using the MBARI AUV D. Allan B. In: Reynolds JR, Greene HG (eds) Marine habitat mapping technology for Alaska. Alaska Sea Grant College Program, Fairbanks, pp 47–69
- Carey DA, Rhoads DC, Hecker B (2003) Use of laser line scan for assessment of response of benthic habitats and demersal fish to seafloor disturbance. *J Exp Mar Biol Ecol* 285–286: 435–452
- Christ RD, Wernli RL (2007) The ROV manual. A user guide for Remotely Operated Vehicles, Elsevier, Amsterdam
- Connelly DP, Copley JT, Murton BJ, Stansfield K, Tyler PA, German CR, Van Dover CL, Amon D, Furlong M, Grindlay N, Hayman N, Hühnerbach V, Judge M, Le Bas T, McPhail S, Meier A, Nakamura K, Nye V, Pebody M, Pedersen R, Plouviez S, Sands C, Searle RC, Stevenson P, Taws S, Wilcox S (2012) Hydrothermal vent fields and chemosynthetic biota on the world's deepest seafloor spreading centre. *Nature Commun* 3(620):1–9. doi:[10.1038/ncomms1636](https://doi.org/10.1038/ncomms1636)
- Cressey D (2014) Submersible loss hits research. *Nature* 509:408–409
- Dupre S, Buffet G, Mascle J, Foucher J-P, Gauger S, Boetius A, Marfia C, Team TAA, Team TQR, party TBs (2008) High-resolution mapping of large gas emitting mud volcanoes on the Egyptian continental margin (Nile Deep Sea Fan) by AUV surveys. *Mar Geophys Res* 29:275–290 doi:[10.1007/s11001-009-9063-3](https://doi.org/10.1007/s11001-009-9063-3)
- Escartin J, Barreye T, Cannat M, Garcia R, Gracias N, Deschamps A, Salocchi A, Sarradin P-M, Ballu V (2015) Hydrothermal activity along the slow-spreading Lucky Strike ridge segment (Mid-Atlantic Ridge): distribution, heatflux, and geological controls. *Earth Planet Sci Lett* 431:173–185. doi:[10.1016/j.epsl.2015.09.025](https://doi.org/10.1016/j.epsl.2015.09.025)
- Friedman A, Pizarro O, Williams SB, Johnson-Robertson M (2012) Multi-scale measures of rugosity, slope and aspect from benthic stereo image reconstructions. *PLoS ONE* 7(12): e50440. doi:[10.1371/journal.pone.0050440](https://doi.org/10.1371/journal.pone.0050440)
- Furlong M, Paxton D, Stevenson P, Pebody M, McPhail SD, Perrett J (2012) Autosub long range: a long range deep diving AUV for ocean monitoring. In: 2012 IEEE/OES Autonomous Underwater Vehicles. IEEE, Southampton, pp 1–7
- Gary M, Fairfield N, Stone WC, Wettergreen D, Kantor G, Sharp JM (2008) 3D Mapping and characterization of Sistema Zacatón from DEPTHX (DEep Phreatic Thermal eXplorer). In: Yuhr LB, Alexander EC, Beck BF (eds) Sinkholes and the Engineering and Environmental Impacts of Karst, vol 183. American Society of Civil Engineers, Tallahassee, Florida, US, pp 202–212
- Grasmueck M, Eberli GP, Viggiano DA, Correa T, Rathwell G, Luo J (2006) Autonomous Underwater Vehicle (AUV) mapping reveals coral mound distribution, morphology and oceanography in deep water of the Straits of Florida. *Geophys Res Lett* 33:L23616. doi:[10.1029/2006GL027734](https://doi.org/10.1029/2006GL027734)
- Griffiths G (2003) Technology and applications of Autonomous Underwater Vehicles. Taylor & Francis, London

- Hobson BW, Bellingham JG, Kieft R, McEwen R, Godin M, Zhang Y (2012) Tethys-class long range AUVs—extending the endurance of propeller-driven cruising AUVs from days to weeks. In: 2012 IEEE/OES Autonomous Underwater Vehicles (AUV). IEEE, Southampton, pp 1–8
- Huvenne VAI, Beyer A, de Haas H, Dekindt K, Henriet JP, Kozachenko M, Olu-Le Roy K, Wheeler AJ, The TOBI/Pelagia 197 and CARACOLE Cruise Participants (2005) The seabed appearance of different coral bank provinces in the Porcupine Seabight, NE Atlantic: results from sidescan sonar and ROV seabed mapping. In: Freiwald A, Roberts JM (eds) Cold-water corals and ecosystems. Springer, Heidelberg, pp 535–569
- Huvenne VAI, McPhail SD, Wynn RB, Furlong M, Stevenson P (2009) Mapping giant scours in the deep ocean. *EOS* 90(32):274–275
- Huvenne VAI, Tyler PA, Masson DG, Fisher EH, Hauton C, Hühnerbach V, Le Bas TP, Wolff GA (2011) A picture on the wall: innovative mapping reveals cold-water coral refuge in submarine canyon. *PLoS ONE* 6(12):e28755. doi:[10.1371/journal.pone.0028755](https://doi.org/10.1371/journal.pone.0028755)
- Huvenne VAI, Georgioupolou A, Chaumillon L, Lo Iacono C, Wynn RB (2016) Novel method to map the morphology of submarine landslide headwall scarps using remotely operated vehicles. In: Lamarche G, Mountjoy J, Bull S, Hubble T, Krastel S, Lane E, Micallef A, Moscardelli L, Mueller C, Pecher I, Woelz S (eds) Submarine mass movements and their consequences, 7th international symposium, vol 41. Springer, Heidelberg, pp 135–144
- Jerosch K, Lüdtke A, Schlüter M, Ioannidis GT (2007) Automatic content-based analysis of georeferenced image data: detection of Beggiatoa mats in seafloor mosaics from the Håkon Mosby mud volcano. *Comput Geosci* 33(2):202–218
- Kernow Marine Explorations Global Limited (2016) What are ROV's. <http://www.kmexgroup.com/whatr-are-rov.html>. Accessed 2 Aug 2016
- Kinsey JC, Whitcomb LL (2004) Preliminary field experience with the DVLNAV integrated navigation system for oceanographic submersibles. *Control Eng Pract* 12:1541–1549. doi: [10.1016/j.conengprac.2003.12.010](https://doi.org/10.1016/j.conengprac.2003.12.010)
- Kwasnitschka T, Hansteen TH, Devey CW, Kutterolf S (2013) Doing fieldwork on the seafloor: photogrammetric techniques to yield 3D visual models from ROV video. *Comput Geosci* 52:218–226. doi:[10.1016/j.cageo.2012.10.008](https://doi.org/10.1016/j.cageo.2012.10.008)
- Lee Y-DE, George RY (2004) High-resolution geological AUV survey results across a portion of the eastern Sigsbee Escarpment. *AAPG Bull* 88(6):747–764. doi:[10.1306/01260404011](https://doi.org/10.1306/01260404011)
- Ling SD, Mahon I, Marzloff P, Pizarro O, Johnson CR, Williams SB (2016) Stereo-imaging AUV detects trends in sea urchin abundance on deep overgrazed reefs. *Limnol Oceanogr Methods* 17:293–304. doi:[10.1002/lom3.10089](https://doi.org/10.1002/lom3.10089)
- Macdonald HA, Wynn RB, Huvenne VAI, Peakall J, Masson DG, Weaver PPE, McPhail SD (2011) New insights into the morphology, fill, and remarkable longevity (>0.2 m.y.) of modern deep-water erosional scours along the northeast Atlantic margin. *Geosphere* 7(4):845–867. doi:[10.1130/GES00611.1](https://doi.org/10.1130/GES00611.1)
- Maki T, Kume A, Ura T (2011) Volumetric mapping of tubeworm colonies in Kagoshima Bay through autonomous robotic surveys. *Deep Sea Res I* 58:757–767. doi:[10.1016/j.dsr.2011.05.006](https://doi.org/10.1016/j.dsr.2011.05.006)
- Marine Technology Society (2015) ROV categories—summary. http://www.rov.org/rov_categories.cfm. Accessed 2 Aug 2016
- Marsh L, Copley JT, Huvenne VAI, Tyler PA, the ISIS ROV Facility (2013) Getting the bigger picture: using precision remotely operated vehicle (ROV) videography to acquire high-definition mosaic images of newly discovered hydrothermal vents in the Southern Ocean. *Deep Sea Res II* 92:124–135. doi:[10.1016/j.dsr2.2013.02.007](https://doi.org/10.1016/j.dsr2.2013.02.007)
- Masson DG, Huvenne VAI, de Stigter HC, Arzola RG, Le Bas TP (2011) Sedimentary processes in the middle Nazaré Canyon: the importance of small-scale heterogeneity in defining the large-scale canyon environment. *Deep Sea Res II* 58:2369–2387. doi:[10.1016/j.dsr2.2011.04.003](https://doi.org/10.1016/j.dsr2.2011.04.003)
- McPhail S (2009) Autosub6000: a deep diving long range AUV. *J Bionic Eng* 6(55–62). doi:[10.1016/S1672-6529\(08\)60095-5](https://doi.org/10.1016/S1672-6529(08)60095-5)

- McPhail S, Pebody M (2009) Range-only positioning of a deep-diving Autonomous Underwater Vehicle from a surface ship. *IEEE J Oceanic Eng* 34(4):669–677. doi:[10.1109/JOE.2009.2030223](https://doi.org/10.1109/JOE.2009.2030223)
- Milne PH (1983) Underwater acoustic positioning systems. Gulf Publishing Company, Houston, 284pp
- Morris KJ, Bett BJ, Durden JM, Huvenne VAI, Milligan R, Jones DOB, McPhail S, Robert K, Bailey DM, Ruhl HA (2014) A new method for ecological surveying of the abyss using Autonomous Underwater Vehicle photography. *Limnol Oceanogr Methods* 12:795–809. doi:[10.4319/lom.201.12.795](https://doi.org/10.4319/lom.201.12.795)
- OpenROV (2016) www.openrov.com. Accessed 2 Nov 2016
- Pacunski RE, Paisson WA, Greene HG, Gunderson D (2008) Conducting visual surveys with a small ROV in shallow water. In: Reynolds JR, Greene HG (eds) Marine habitat mapping technology for Alaska. Alaska Sea Grant College Program, Fairbanks, pp 109–128
- Paull CK, Caress DW, Lundsten E, Gwiadza R, Anderson K, McGann M, Conrad J, Edwards B, Sumner EJ (2013) Anatomy of the La Jolla submarine canyon system; offshore southern California. *Mar Geol* 335:16–34. doi:[10.1016/j.margeo.2012.10.003](https://doi.org/10.1016/j.margeo.2012.10.003)
- Pennington JT, Blum M, Chavez FP (2016) Seawater sampling by an Autonomous Underwater Vehicle: “Gulper” sample validation for nitrate, chlorophyll, phytoplankton, and primary production. *Limnol Oceanogr Methods* 14:14–23. doi:[10.1002/lomc.310065](https://doi.org/10.1002/lomc.310065)
- Pizarro O, Singh H (2003) Toward large-area mosaicing for underwater scientific applications. *IEEE J Oceanic Eng* 28(4):651–672. doi:[10.1109/JOE.2003.819154](https://doi.org/10.1109/JOE.2003.819154)
- Research Councils UK (2016) Autonomous Surface/sub-surface survey system. <http://gtr.rcuk.ac.uk/projects?ref=102304>. Accessed 04 Nov 2016
- Ridao P, Carreras M, Hernandez E, Palomeras N (2007) Underwater telerobotics for collaborative research. In: Ferre Mea (ed) Advances in telerobotics, vol 31. Springer, Heidelberg, pp 347–359
- Rigaud (2007) Innovation and operation with robotized underwater systems. *J Field Rob* 24(6):449–459. doi:[10.1002/rob.20195](https://doi.org/10.1002/rob.20195)
- Robert K, Jones DAB, Huvenne VAI (2014) Megafaunal distribution and biodiversity in a heterogeneous landscape: the iceberg-scoured Rockall Bank, NE Atlantic. *Marine Ecology Progress Series*, pp 67–88. doi:[10.3354/meps10677](https://doi.org/10.3354/meps10677)
- Rogers AD, Tyler PA, Connolly DP, Copley JT, James R, Larter RD, Linse K, Mills RA, Naveira Garabato A, Pancost RD, Pearce DA, Polunin NVC, German CR, Shank T, Boersch-Supan PH, Alker BJ, Aquilina A, Bennett SA, Clarke A, Dinley RJ, Graham AGC, Green DRH, Hawkes JA, Hepburn L, Hilario A, Huvenne VAI, Marsh L, Ramirez-Llodra E, Reid WDK, Roterman CN, Sweeting CJ, Thatje S, Zwirglmaier K (2012) The discovery of new deep-sea hydrothermal vent communities in the southern Ocean and implications for biogeography. *PLoS Biol* 10(1):e1001234. doi:[10.1371/journal.pbio.1001234](https://doi.org/10.1371/journal.pbio.1001234)
- Roman C, Inglis G, Rutter J (2010) Application of structured light imaging for high resolution mapping of underwater archeological sites. In: Oceans 2010 IEEE. Sydney, 24–27 May, pp 1–9
- Roman C, Inglis G, Vaughn I, Smart C, Dansereau D, Bongiorno D, Johnson-Robertson M, Bryson M (2012) New tools and methods for precision seafloor mapping. *Oceanography* 25(1, supplement):42–45
- Rona P, Guida V, Scranton M, Gong D, Macelloni L, Pierdomenico M, Diercks A-R, Asper V, Haag S (2015) Hudson submarine canyon head offshore New York and New Jersey: a physical and geochemical investigation. *Deep Sea Res II* 121:213–232. doi:[10.1016/j.dsr2.2015.07.019](https://doi.org/10.1016/j.dsr2.2015.07.019)
- Singh H, Roman C, Pizarro O, Eustice R, Can A (2007) Towards high-resolution imaging from underwater vehicles. *Int J Robot Res* 26(1):55–74. doi:[10.1177/0278364907074473](https://doi.org/10.1177/0278364907074473)
- Smart CJ, Roman C, Carey SN (2013) Detection of diffuse seafloor venting using structured light imaging. *Geochem Geophys Geosyst* 14(11):4743–4757. doi:[10.1002/ggge.20280](https://doi.org/10.1002/ggge.20280)
- Sumner EJ, Peakall J, Parsons DR, Wynn RB, Darby SE, Dorrell RM, McPhail SD, Perrett J, Webb A, White D (2013) First direct measurements of hydraulic jumps in an active submarine density current. *Geophys Res Lett* 40:5904–5908. doi:[10.1002/2013GL057862](https://doi.org/10.1002/2013GL057862)

- Tetlow S, Spours J (1999) Three-dimensional measurement of underwater work sites using structured laser light. *Meas Sci Technol* 10:1162–1167
- Tubau X, Paull CK, Lastras G, Caress DW, Canals M, Lundsten E, Anderson K, Gwiazda R, Amblas D (2015) Submarine canyons of Santa Monica Bay, Southern California: variability in morphology and sedimentary processes. *Mar Geol* 365:61–79. doi:[10.1016/j.margeo.2015.04.004](https://doi.org/10.1016/j.margeo.2015.04.004)
- Wadhams P, Wilkinson JP, McPhail SD (2006) A new view of the underside of Arctic sea ice. *Geophys Res Lett* 33:L04501. doi:[10.1029/2005GL025131](https://doi.org/10.1029/2005GL025131)
- Wagner JKS, McEntee MH, Brothers LL, German CR, Kaiser CL, Yoerger DR, Van Dover CL (2013) Cold-seep habitat mapping: high-resolution spatial characterisation of the blake ridge diapir seep field. *Deep Sea Res II* 92:183–188. doi:[10.1016/j.dsret.2013.02.008](https://doi.org/10.1016/j.dsret.2013.02.008)
- West ME, Syrmos VL (2006) Navigation of an Autonomous Underwater Vehicle (AUV) using robust SLAM. In: The 2006 IEEE conference on control applications. Munich, Germany, pp 1801–1806
- Williams SB, Pizarro O, Webster JM, Beaman RJ, Mahon I, Johnson-Robertson M, Bridge TCI (2010) Autonomous Underwater Vehicle-assisted surveying of drowned reefs on the shelf edge of the Great Barrier Reef. *Aust J Field Rob* 27(5):675–697. doi:[10.1002/rob.20356](https://doi.org/10.1002/rob.20356)
- Wynn RB, Huvenne VAI, Le Bas TP, Murton BJ, Connally DP, Bett BJ, Ruhl HA, Morris KJ, Peakall J, Parsons DR, Sumner EJ, Darby SE, Dorrell RM, Hunt JE (2014) Autonomous Underwater Vehicles (AUVs): their past, presence and future contributions to the advancement of marine geoscience. *Mar Geol* 352:451–468. doi:[10.1016/j.margeo.2014.03.012](https://doi.org/10.1016/j.margeo.2014.03.012)
- Yoerger DR, Bradley AM, Walden BB, Singh H, Bachmayer R (1998) Surveying a subsea lava flow using the Autonomous Benthic Explorer (ABE). *Int J Syst Sci* 29(10):1031–1044. doi:[10.1080/0020772980829596](https://doi.org/10.1080/0020772980829596)
- Yoerger DR, Kelley DS, Delaney JR (2000) Fine-scale three-dimensional mapping of a deep-sea hydrothermal vent site using the Jason ROV system. *Int J Robot Res* 19(11):1000–1014

Part II

Submarine Landforms and Processes

Origin and Geomorphic Characteristics of Ocean Basins

Peter T. Harris and Miles Macmillan-Lawler

Abstract The results of a multivariate classification of ocean basins is presented, based on an existing digital global map of seafloor features that are related to major phases of evolution, namely young, mature, declining and terminal evolutionary stages. “Young” basins are characterised by the absence of ocean trenches, young ocean crust (<8 MA), large areas of continental slope, thick sediments, and large percentage area of mid-ocean ridge rift valley (above 1.7%). “Mature” ocean basins are characterised by relatively thick sediment deposits (mean of 940 m), large percentage areas of continental rise (mean of 19.8%) and large areas of submarine fans (mean of 4.3%). The area of ocean trench is relatively small in all “mature” ocean basins, ranging from 0 to 0.3%. A defining geomorphic feature of the “declining” category is that around 1% of their area is trench. “Declining” ocean basins contain the highest concentration of seamounts (3.5–5 seamounts per 100,000 km²), which is more than double the mean value (1.4 seamounts per 100,000 km²) that occurs for the “mature” category with the next highest concentration. The “terminal” category of ocean basins is characterised by the greatest mean sediment thickness (4311 m) and greatest percentage area of submarine fans (7.2%) of any ocean basin. Bottom water occurring within 33 major bathymetric basins (located within the broader ocean basins) is found to exhibit a spatial relationship to near-bottom dissolved oxygen (DO) concentrations. Gradients of decreasing DO concentration suggests bottom water pathways within basins and between adjacent basins of similar (or greater) depth.

1 Introduction

Studies of seafloor geomorphology have expanded in recent years with the advent of new technologies and new methods that have revealed the true shape of the ocean floor, which lies otherwise hidden beneath kilometres of ocean (Hillier et al.

P.T. Harris (✉) · M. Macmillan-Lawler
GRID-Arendal, Postboks 183, 4836 Arendal, Norway
e-mail: Peter.Harris@grida.no

2008). These methods include new swath sonar seafloor mapping technologies (see Chapters “[Sidescan Sonar](#)”, “[Multibeam Echosounders](#)” and “[Quantitative Analyses of Morphological Data](#)” of this volume), but also new global compilations of digital bathymetry compiled from sonar and satellite altimetry data (Smith and Sandwell 1997; Becker et al. 2009). Such global compilations of bathymetric data permit global assessments of different categories of seafloor geomorphic features, examples being seamounts (Wessel 2001; Hillier and Watts 2007; Yesson et al. 2011), trenches (Jamieson et al. 2010) and submarine canyons (Harris and Whiteway 2011), but also integrated assessments of global seafloor geomorphology (Harris et al. 2014). From such compilations it is now possible, for the first time, to examine global patterns of categories of seafloor features mapped digitally, individually or as assemblages, using quantitative and statistical methods and to relate them to the formative processes. It is, indeed, the dawning of a new era in the study of the geomorphology of the oceans (Hillier et al. 2008).

This chapter contributes to previous global studies of ocean geomorphology to examine the evolution of ocean basins, from their youth through their old age and demise, in terms of the geomorphic characteristics that define them at each evolutionary stage. A second, related topic is the control that seafloor geomorphology exerts on the circulation of bottom water within and between ocean basins. The purpose of this work is to reveal interlinkages between geomorphic form and process, through the examination of basin evolution and water circulation at a global spatial scale.

1.1 Definition of Terms—Ocean Basins and Bathymetric Basins

The earth’s ocean basins are comprised of all the seafloor features that are apart from the continents; they comprise that part of the earth’s surface that is composed primarily of basaltic, ocean crust, in contrast with the mainly granitic, continental crust forming the continents. The transition from basaltic, ocean crust, to granitic, continental crust occurs within the continental slope. If the boundary of ocean basins is taken as the continental shelf-break, then the continental slope is also included within ocean basins (i.e. only the continental shelf is excluded). In this broad definition, ocean basins cover approximately 329,640,970 km² or about 65% of the earth’s surface.¹ They contain all of the mid-ocean ridges, abyssal hills and mountains, abyssal plains, seamounts, troughs, trenches, plateaus, slope-incising

¹Although the oceans are commonly stated as covering 72% of the earth, this figure includes the (submerged) continental shelves, which are geologically extensions of the continents and not part of the ocean basins. Continental shelves cover an area of 32,242,540 km² or 8.91% of the oceans (Harris et al. 2014).

submarine canyons, fans, continental rise and the numerous other features found in the deep ocean.

There are, furthermore, smaller bathymetric basins nested within the more broadly defined ocean basins. According to the International Hydrographic Organization, a bathymetric basin is “a depression, in the sea floor, more or less equidimensional in plan and of variable extent” (IHO 2008). The largest bathymetric basins of the major oceans are nominally bounded by the foot of slope and by the mid-ocean spreading ridges (Wright and Rothery 1998; Gille et al. 2004). Bathymetric basins can be mapped based on the identification of the most shoal, closed, bathymetric contours, examined regionally for the major ocean basins and shelf seas. In addition, numerous smaller basins of the bathyal and hadal zones, located outside of the major ocean basin areas, occur, identified by their most shoal, closed, bathymetric contours. Tracking the flow of dense, bottom water formed in the oceans is linked to the spatial distribution of bathymetric basins, because such dense water is transported into basins by gravity. At abyssal depths, using this approach, Harris et al. (2014) distinguished between 33 major bathymetric basins having a mean size of 3.8 million km², 1917 large bathymetric basins (>800 km²), and 4520 small bathymetric basins (<800 km²). A further 1507 bathymetric basins were mapped, perched on the continental slope.

Bathymetric (geomorphic) basins are not to be confused with sedimentary basins studied by geologists and stratigraphers. Sedimentary basins are regions commonly located along continental margins where long-term subsidence creates accommodation space for infilling by sediments. They do not necessarily exhibit the surface expression of a “bathymetric basin” as defined above.

Bathymetric basins (depressions) perched on the continental shelf and slope, are not the main subject of this chapter. Shelf-perched basins are most common on glaciated continental margins where glacial erosion has excavated a trough on the continental shelf. Tectonic rifting, volcanism, gas escape and other processes may also give rise to the formation of localised depressions and small basins perched on the continental shelf and slope.

1.2 *Tectonic Origin of Ocean Basins*

Ocean basins are ultimately the product of rifting of ocean crust, seafloor spreading followed by subduction and destruction of ocean crust (Hess 1962), giving rise to the so-called Wilson Cycle (Wilson 1966; Fig. 1). The Wilson Cycle is initiated where upwelling of mantle magma causes a rifting of continental crust; the great rift valley of east Africa is an example (Baker et al. 1972). The rift opens and becomes flooded with seawater, forming a new arm of the ocean. The Red Sea and Gulf of California are examples (Table 1). Next comes the establishment of mid-ocean spreading ridges, seafloor spreading and the formation of ocean crust at which stage the ocean basin has reached a mature stage (e.g. the North and South Atlantic Oceans). This is followed by the formation of subduction zones and ocean trench

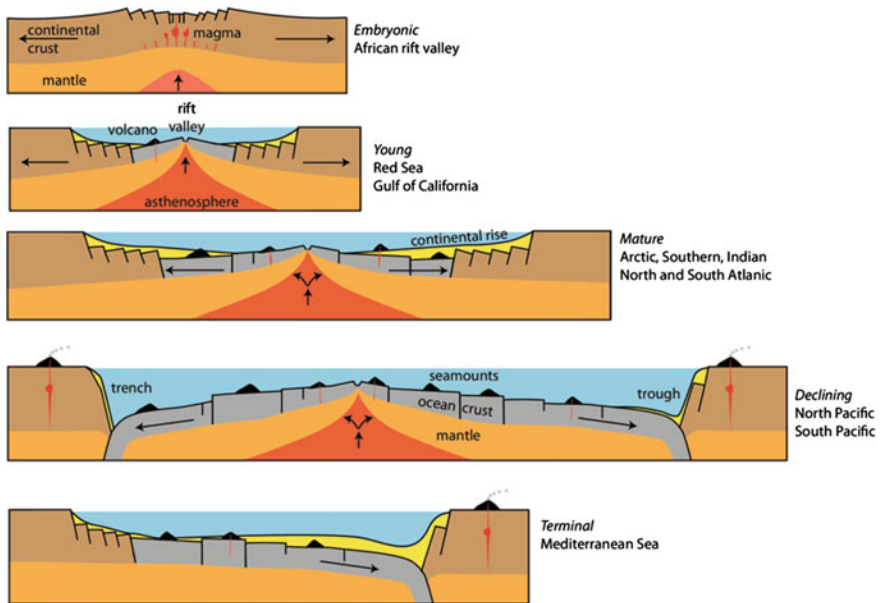


Fig. 1 Wilson Cycle (Wilson 1966) of ocean basin evolution

Table 1 Evolution of ocean basins (Wilson Cycle), from rifting to terminal phase (adapted from Wright and Rothery 1998)

Stage	Examples	Dominant tectonic motions	Characteristic geomorphic features
1. Embryonic	East African rift valleys	Crustal extension and uplift	Rift valleys
2. Young	Red Sea	Subsidence and spreading	Narrow seas with parallel coasts and central depression
3. Mature	Atlantic Ocean	Spreading	Ocean basin with active mid-ocean ridge
4. Declining	Pacific Ocean	Spreading and subduction (active margins)	Ocean basin with active mid-ocean ridge; island arcs; trenches along most margins
5. Terminal	Mediterranean Sea	Subduction and uplift	Young mountains

systems, whereby the basin enters a declining phase (e.g. the North and South Pacific Oceans). Eventually the rate at which ocean crust is destroyed in subduction zones exceeds the rate at which it is formed at spreading ridges. The basin thus becomes dominated by the subduction process and shrinks in area. Finally it enters its terminal phase, an example being the Mediterranean Sea (Table 1).

The applicability of the Wilson Cycle model for understanding the evolution of ocean basins has been documented in the geologic record with regards to the

formation, growth and demise of the Tethys Ocean (Ricou 1996; Stow 2010). This ocean basin is thought to have been initiated prior to the Permian and became a mature basin as a “C” shaped indentation along the eastern, equatorial coast of Pangea during the Late Permian (260 MA). Tethys transformed from a mature ocean basin into a declining basin during the Cretaceous, at which time it occupied a space between the continents of Gondwana and Laurasia. As tectonic forces moved the continental plates over geologic time, the Tethys Ocean became squeezed into a seaway confined between Africa and Eurasia by the Eocene. It ceased to exist as an ocean by around 6 MA and it is now in its final, terminal phase, represented by the Mediterranean Sea.

1.3 Multiple Origins of Bathymetric Ocean Basins

Declining and mature ocean basins (Table 1) have an asymmetric bathymetric profile with their deepest parts adjacent to continents (with declining basins containing trenches or troughs) gently shoaling towards the mid-ocean spreading ridge. Hence the bathymetric ocean basins commonly have the mid-ocean spreading ridges as one of their boundaries and continental landmasses as the other. Such basins have been termed *thalassogens* by Pushcharovsky (2006).

After ocean crust is formed at mid-ocean spreading ridges, it is transported laterally away from the spreading ridge where it gradually cools and subsides. It has been shown (e.g. Hillier and Watts 2005) that the rate of subsidence generally adheres to the infinite half-space model between change in seafloor depth Δh (km) and the age of ocean crust t (MA), given as:

$$\Delta h = C(t)^{1/2}, \quad (1)$$

where C is an empirically defined coefficient (m), given as 307 by Hillier and Watts (2005) for $t < 80$ MA. The infinite half-space model holds true for ocean crust flanking the mid-ocean spreading ridges, but it is not universal because factors other than ageing and cooling play a role in ocean crust subsidence. Such factors include volcanism, tectonic rifting, isostasy, etc. and these may cause lateral variations in the rate of subsidence and hence result in the formation of localised bathymetric basins (Hillier and Watts 2005; Pushcharovsky 2006). Consequently, there are different types of bathymetric basins. Two examples are those that are formed by raised ocean crust associated with chains of volcanos, which have been termed *intermontane* basins, and those formed by tectonic rifting and fracturing of ocean crust, which have been termed *interfault* basins (Pushcharovsky 2006).

An example of an *intermontane* bathymetric basin is the Kamehameha Basin in the central Pacific. This basin is formed as a seafloor depression surrounded by zones of numerous seamounts and ridge complexes on its southern and western

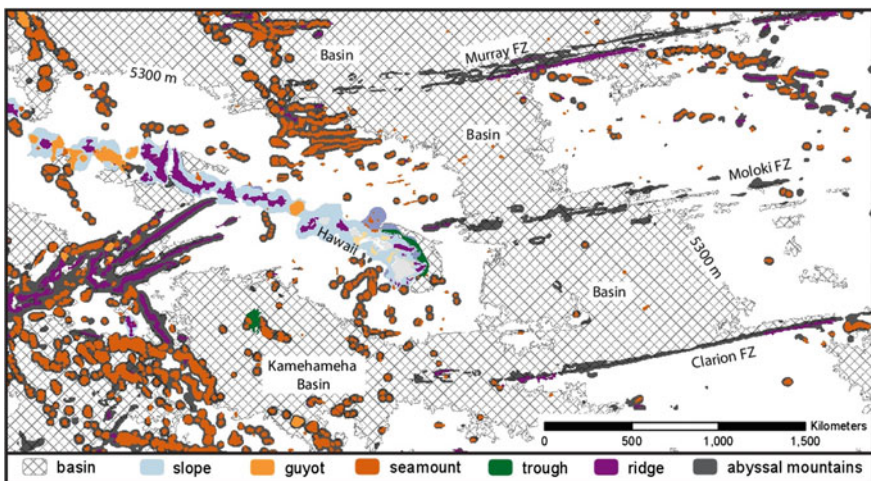


Fig. 2 Map of selected seafloor geomorphic features from the global seafloor features map; see Harris et al. (2014) for definitions of features and methods used to map them

margins with the Hawaiian archipelago forming the northern and eastern boundaries (Fig. 2). The Kamehameha Basin is delimited by the 5300 m depth contour and it is connected to other basins located further east (Fig. 2).

Examples of *interfault* basins are those located between the major fracture zones of the northeast Pacific (i.e. the Clipperton, Clarion, Moloki, Murray and Mendocino Fracture Zones). These bathymetric basins are also delimited by the 5300 m depth contour, which is clearly deflected along the Clarion, Moloki and Murray fracture zones (Fig. 2) by their positive relief. The basin complex is partially confined by the fracture zones along their northern and southern margins, although the regional basin complex is interconnected (at a depth of 5300 m).

1.4 Aims of This Study

The tectonic processes governing the evolution of ocean basins (Wilson Cycle) give rise to different assemblages of geomorphic features as they pass through the different stages of evolution (i.e. from embryonic to terminal stages; Table 1). These features include rift valleys, spreading ridges and ocean trenches, but it is apparent that other processes, specifically volcanism and sedimentation, play a role in basin evolution. These processes, in turn, influence the nature of geomorphic features that characterise ocean basins at different stages of their evolution. Although we have a broad conceptual model on the stages of ocean basin evolution (Fig. 1), a

quantitative assessment of geomorphic features that characterise ocean basins at different stages of their evolution has not previously been completed. Here, we analyse a recently published geomorphic features map of the global ocean (Harris et al. 2014) in order to fill this knowledge gap. The aim of this study is to identify and document changes in the composition of geomorphic features that characterise the earth's ocean basins as they evolve from embryonic to terminal stages of evolution according to the Wilson Cycle.

2 Methods

Our analysis includes a classification of ocean basins using hierarchical clustering in the R statistical package. The first step in our analysis was to divide the oceans into areas consistent with the evolutionary processes described above (Table 1) and based on the IHO Sea Area definitions.² Hence the ocean areas considered are: Red Sea; Gulf of California; Arctic Ocean; Southern Ocean; Indian Ocean; South Atlantic Ocean; North Atlantic Ocean; South Pacific Ocean; North Pacific Ocean; and the Mediterranean Sea (Fig. 3). For the purpose of this analysis the shelf regions and their associated features were removed and only those features occurring on the continental slope and at abyssal to hadal depths were considered.

The next step was to define input data to be used in the clustering analysis. We used geomorphic feature statistics based on the mapped surface areas of geomorphic features reported by Harris et al. (2014), who describe the methods used to map 29 seafloor feature types in the global ocean. Only those features that occur seaward of the shelf break were used in the present study, resulting in the inclusion of 24 of the 29 feature categories mapped by Harris et al. (2014). All 24 features were examined for correlations with ocean age (mean and maximum) and trench area using the 'cor' function in the R statistical package. The following variables were used: % (percentage area of) continental slope; % abyssal plains; % hadal area; % bathymetric basin; % submarine fan; % seamount; % ridge; % rift valley; % continental rise; and % spreading ridge.

In addition to geomorphic feature statistics, we used the global sediment thickness map of Divins (2003), the average rate of seafloor spreading and age of ocean crust calculated using digital isochrones of Muller et al. (1997) to derive an average spreading rate, age-range and mean age for each ocean basin.

Clustering was carried out using the 'hclust' hierarchical clustering algorithm in the R statistical package based on the mean values for the geomorphic features and other basin values defined above (Table 2).

²VLIZ (2005). IHO Sea Areas. Available online at <http://www.marineregions.org/>. Consulted on 2016-04-04.

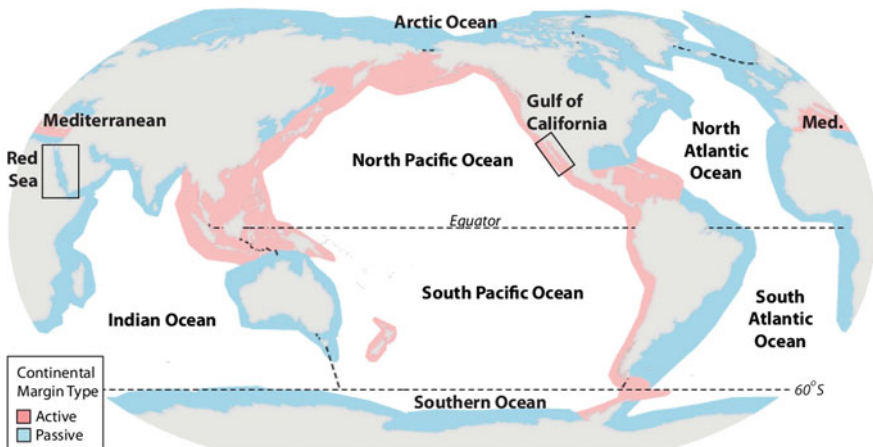


Fig. 3 Ocean basins used in the analysis; the areas of passive and active continental margins are indicated

3 Results

Clustering using the input date listed in Table 2 placed each of the 10 defined ocean areas into four separate categories (young; mature; declining; terminal; Figs. 1 and 4). The young category includes the Gulf of California and the Red Sea (Fig. 5). These relatively small ocean areas are characterised by the absence of ocean trenches and hadal depth ocean floor, young ocean crust (<8 MA), comparatively large areas of continental slope (33–75% slope for the Gulf of California and the Red Sea, respectively), thick sediments, small areas of abyssal plains and a relatively large percent area of mid-ocean ridge rift valley (above 1.7%). The area of submarine canyons in all ocean basins (Table 3) is correlated with the area of slope ($r = 0.80$), and therefore the area of canyons is also relatively greater in young ocean basins.

The mature category includes 5 major oceans (Fig. 4), listed here in order of increasing percentage area of ocean trench: Arctic (Fig. 6a); Southern; Indian; South Atlantic and North Atlantic (Fig. 6b). The area of ocean trench is relatively small in all mature ocean basins compared with declining and terminal basins, ranging from 0 to 0.3% (Table 2). The mean age of ocean crust in these basins is 65 MA and the mean maximum age is 160 MA. These are comparable values to the two declining ocean basins but much greater than the young basins and much younger than the terminal Mediterranean Sea. The mature ocean basins have a mean mid-ocean ridge spreading rate of 28.6 mm/year, which is comparable to the approximate spreading rates reported for the young ocean basins but only about half the speed of the two declining ocean basins (which average 58 mm/year). From a

Table 2 Statistics on variables used in clustering ocean basins into one of the four evolutionary categories

Stage	Ocean basin name	Trench (%)	Age mean (MA)	Age max (MA)	Sediment thickness (m)	Spreading rate mm/year	Slope (%)	Abyssal plains (%)	Hadial (%)	Bathymetric basin (%)	Fan (%)	Seamount (%)	Seamounts per 10 ⁵ km ²	Ridge (%)	Rift valley (%)	Rise (%)	Spreading ridge (%)
Young	Red sea	0	0	0	1248	10	33.3	11.5	0	96.5	0	0	0	4.5	0	0	0.5
	Gulf of California	0	1	8	357	43	74.9	3.6	0	16.7	0.9	0.5	0.9	0	1.7	0	0.5
Mature	Arctic Ocean	0	69	159	854	31	14.6	33	0	46.4	2.4	0.1	0.123	1.9	0.5	14.5	4
	Southern Ocean	0.04	70	160	984	27	3.5	48.6	0.01	54.2	6.6	0.9	1.24	1.8	0.1	38.1	1.9
Declining	Indian Ocean	0.2	55	159	703	40	6.1	32.5	0.4	48.7	6.5	1.4	1.56	2.5	0.2	9.3	2.3
	South Atlantic Ocean	0.2	57	139	722	26	4.1	26.1	0.5	46.7	2.3	2.1	2.46	2.8	0.3	16.2	3
Terminal	North Atlantic Ocean	0.3	74	180	1442	19	9.2	27.4	0.8	45.1	3.5	1.4	1.74	2.6	0.3	20.9	1.8
	South Pacific Ocean	0.9	47	152	229	58	3.8	26.8	0.5	46.5	0.03	2.8	3.49	3	0.2	0.7	2.2
	North Pacific Ocean	1.1	79	175	386	57	6.2	32.9	3	44.6	0.3	4.1	4.95	3.7	0.1	1.3	1.1
	Med. Sea	0.6	186	278	4311	29	39.2	26.5	0	69.7	7.2	0.3	0.827	1.1	0	16.6	0

Data on mean crustal age and spreading rates are from Müller et al. (1997). Sediment thickness data are taken from Divins (2003) and Backman et al. (2004). Data on geomorphic features are from Harris et al. (2014).

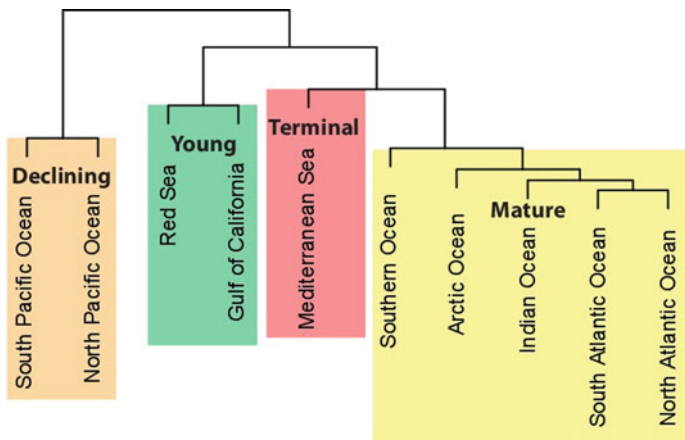


Fig. 4 Results of cluster analysis derived using the ‘*hclust*’ hierarchical clustering algorithm in the R statistical package based on the mean values for the geomorphic features (listed in Table 2)

geomorphic feature perspective, the mature ocean basins are characterised by relatively large percentage areas of continental rise (mean of 19.8%) and submarine fans (mean of 4.3%), which is consistent with the relatively thick sediments deposited in these basins (mean thickness of 940 m).

The declining category includes 2 major oceans (the North and South Pacific; Fig. 7) which together cover 169,056,690 km² equal to 47% of the global ocean. A defining geomorphic feature of the declining category is that around 1% of their area is trench. This is more than twice the area of trenches contained in the other categories. Another characteristic is the rapid mid-ocean ridge mean spreading rate of 57–58 mm/year. The thin nature of sediment deposits (mean thickness of about 300 m) is also a characteristic of the declining category, which is consistent with its relatively small percentage areas of continental rise (about 1%) and submarine fans (0.03–0.3%). Finally, the declining ocean basins contain the highest concentration of seamounts (3.5–5 seamounts per 100,000 km²), which is more than double the mean value (1.4 seamounts per 100,000 km²) that occurs for the mature category with the next highest concentration.

The terminal category of ocean basins is represented only by the Mediterranean Sea (Fig. 8). It is characterised by the greatest mean and maximum ages of ocean crust (186 and 278 MA, respectively) which is more than twice the ages of the mature and declining categories. The terminal category is also characterised by the greatest mean sediment thickness (4311 m) and greatest percentage area of submarine fans (7.2%) of any ocean basin.

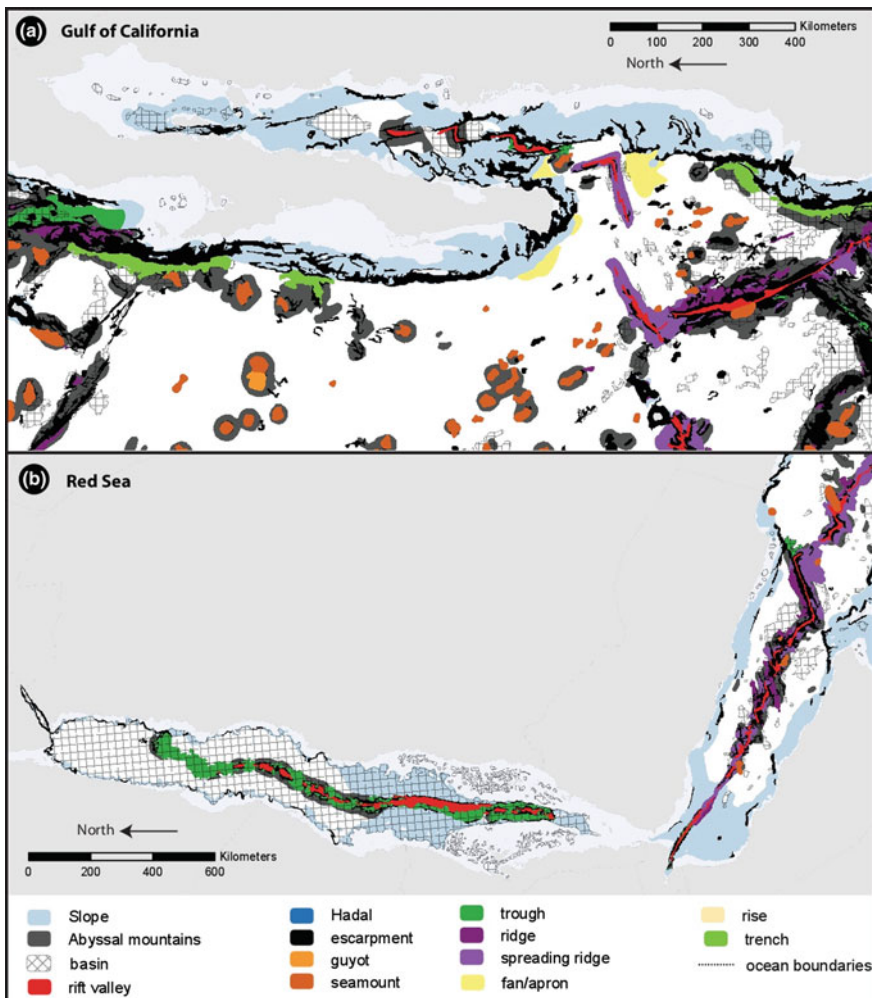


Fig. 5 Maps of selected geomorphic features from the global seafloor features map of Harris et al. (2014), illustrating examples of young ocean basins: **a** Gulf of California; and **b** the Red Sea

4 Discussion

4.1 Key Drivers of Basin Evolution

Based on the review presented above, it is apparent that the fundamental, main drivers of basin geomorphic evolution are tectonism, volcanism and sedimentation. Tectonism is the process which gives rise to the basin in the first instance and which governs its progress through the evolutionary Wilson Cycle, culminating in its ultimate destruction via subduction (Fig. 1). A principle geomorphic expression of

Table 3 Statistics on variables not used in clustering ocean basins into one of the four evolutionary categories

Stage	Ocean basin name	Trough (%)	Abyssal (%)	Escarpments (%)	Canyons (%)	Plateaus (%)	Abyssal hills (%)	Abyssal Mts (%)	Terraces (%)	Active margin (%)
Young	Red Sea	20	66.7	7.2	1.30	0	42.2	1.3	12	0
	Gulf of California	2.4	25.1	17.9	8.80	0	14.4	7.2	2.7	(100)
Mature	Arctic Ocean	0.7	85.4	3.3	5.70	19	35.8	16.5	3.6	0
	Southern Ocean	0.5	96.5	3.7	3.10	2.6	38	9.9	0.2	16
Declining	Indian Ocean	0.5	93.5	4.8	1.10	7.1	44.9	16.2	1.2	36
	South Atlantic Ocean	0.4	95.3	5.0	0.80	3.1	50.8	18.3	0.7	2
Terminal	North Atlantic Ocean	0.8	90	7.3	2.00	4.3	44	18.6	0.9	37
	South Pacific Ocean	0.8	90.8	8.5	1.10	2.4	39.2	18.7	0.4	84
Terminal	North Pacific Ocean	1.3	95.8	6.6	0.80	8.1	52.1	16.9	0.2	96
	Med. Sea	2.8	60.8	10.5	7.00	0	26.5	7.7	2.2	76

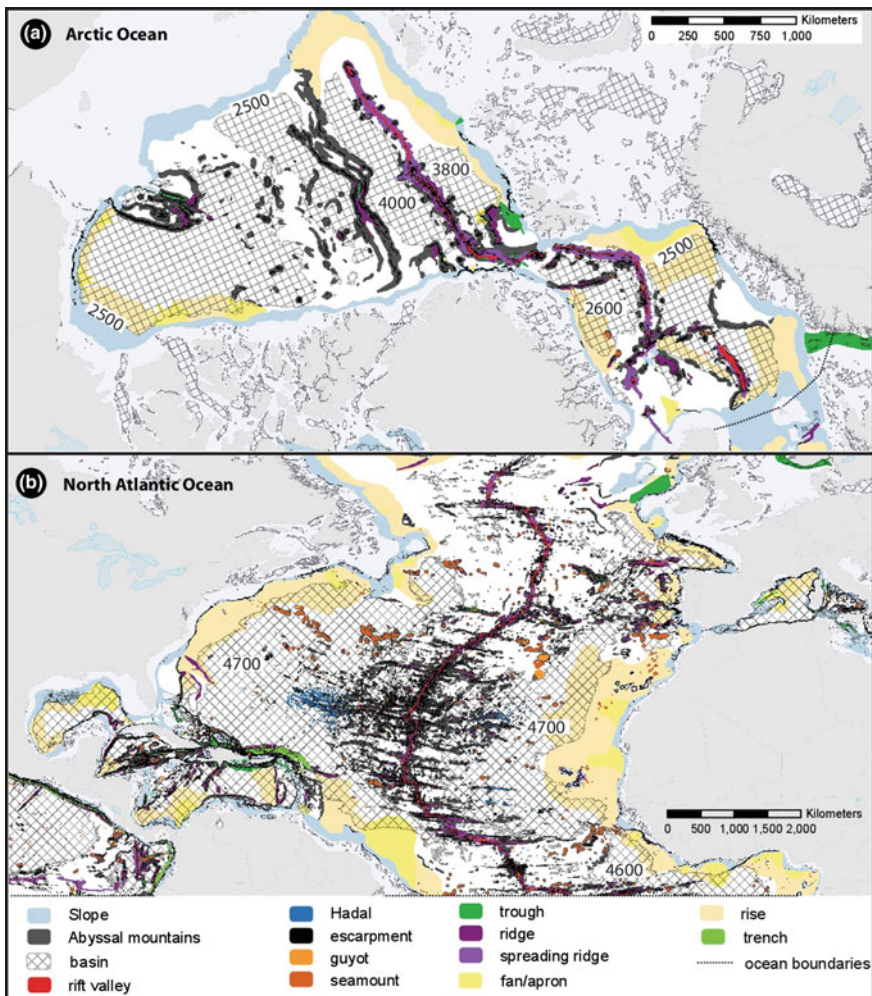


Fig. 6 Maps of selected geomorphic features from the global seafloor features map of Harris et al. (2014), illustrating examples of mature ocean basins: **a** Arctic Ocean; and **b** North Atlantic Ocean. The Arctic Ocean is the youngest of the “mature” ocean basins, relatively small in size and characterised by the absence of trenches, its large areas of slope and large areas of submarine canyons. In contrast the North Atlantic exhibits some trench areas (the Puerto Rico Trench) along its small length of active margin

tectonism that characterises ocean basins as they progress through the Wilson Cycle is the percentage area of deep ocean trench, reflecting the subduction of oceanic crust (Table 2) along active margins (Table 3; Fig. 3). Trench area is correlated with the area of troughs in mature and declining ocean basins ($r = 0.81$). This is explained by the fact that troughs are sometimes trenches that have been partially infilled with sediment. In mature and declining ocean basins, the percentage area of

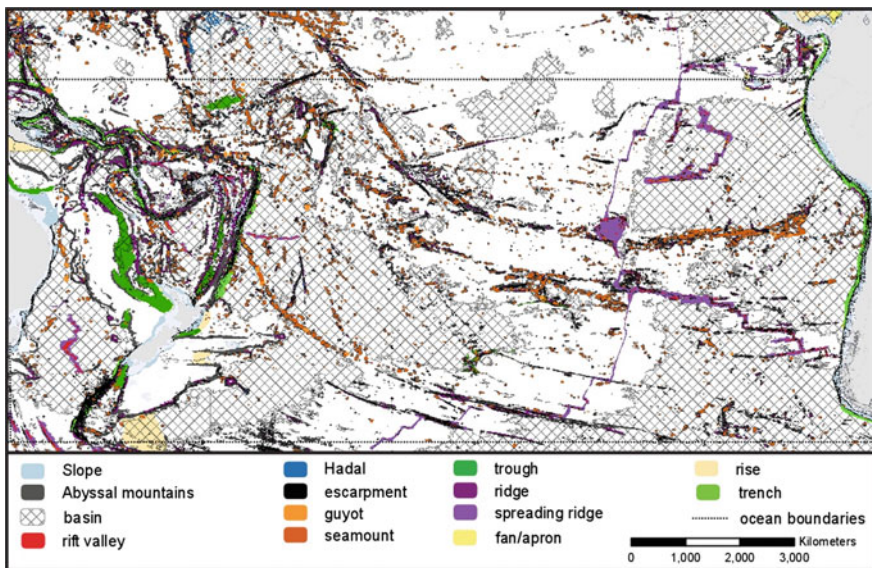


Fig. 7 Map of selected geomorphic features from the global seafloor features map of Harris et al. (2014), illustrating the “declining” South Pacific Ocean basin. A defining geomorphic feature of the “declining” category is that around 1% of their area is trench, which is more than twice the area of trenches contained in the other categories. “Declining” ocean basins contain the highest concentration of seamounts (3.5–5 seamounts per 100,000 km²), which is more than double the mean value (1.4 seamounts per 100,000 km²) that occurs for the “mature” category with the next highest concentration

the steepest ocean floor (represented by escarpments) is positively correlated with trenches ($r = 0.77$) and steep-sided features such as ridges ($r = 0.72$) and seamounts ($r = 0.69$). Thus, as the ocean basin evolves from a mature phase and enters a declining phase, the percentage areas of trenches, troughs, ridges, seamounts and escarpments reaches a peak.

By contrast, the percentage area of the continental slope is inversely related to the occurrence of subduction zones along active margins. The percentage area of slope attains its maximum in the youthful and terminal stages of basin evolution. Slope area is also associated with the relative volume of sediment deposited in basins having passive margins, as discussed below.

The geomorphic expression of volcanism is manifest as the occurrence of mid-ocean spreading ridges, their associated rift valleys and seamounts. Young ocean basins are characterised by large percentage areas of rift valley (1.7 and 4.5% of the basin area for the Gulf of California and Red Sea, respectively) whereas mature ocean basins have the highest percentage area of spreading ridges (1.8–4% of basin area; Table 2). Seamounts are formed mainly along spreading ridges, proximal to the rift valley and located over the thinnest ocean crust (Wright and Rothery 1998; see also Chapters “Mid-Ocean Ridges” and “Cold Seep Systems” in

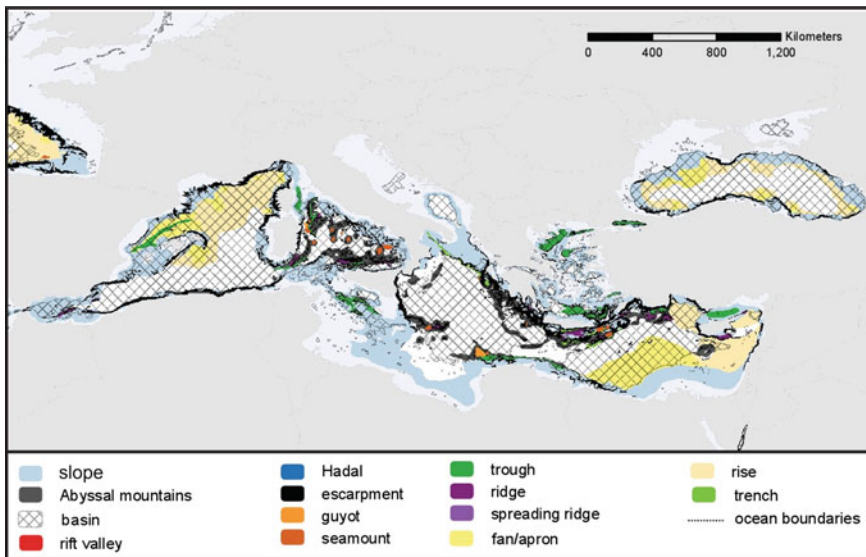


Fig. 8 Map of selected geomorphic features from the global seafloor features map of Harris et al. (2014), illustrating the “terminal” Mediterranean Sea basin. “Terminal” basins are characterized by the greatest mean sediment thickness (4311 m) and greatest percentage area of submarine fans (7.2%) of any ocean basin

this volume); seamounts appear to reach a maximum concentration (measured as seamounts per 100,000 km² of ocean basin) in declining ocean basins; possible explanations for this trend are discussed below.

Sedimentation also has a strong influence over the geomorphology of ocean basins at different stages of their evolution. In the youthful stage of basin evolution, sediments are transported into the basin forming thick deposits along the margins. In the Red Sea, sediments have a mean thickness of over 1200 m (Table 2), comprised of a Cenozoic evaporite succession laid-down during periods when the basin was episodically flooded and then cut-off from the adjacent ocean (Wright and Rothery 1998). Sediments extend across the full width of the basin and are reported from recent multibeam sonar surveys to be locally slumping into the central rift valley, forming bridges that separate deeper, isolated segments of the rift valley complex (Augustin et al. 2014). The same process of bridge formation by sediment slumping into the Mariana Trench has been described by Gardner and Armstrong (2011). This pattern of isolated segments of rift valley separated by bridges is detectable in maps of both the Gulf of California and the Red Sea (Fig. 5).

Mature ocean basins also contain thick sediment deposits along their (mainly) passive continental margins that attain mean thicknesses of between 700 to over 1400 m (Table 2). The geomorphic expression of these thick sediment deposits are large areas of continental rise (9–38% of basin area), large areas of submarine fans (2.3–6.6% of basin area) and a more subdued terrain, manifested as relatively small

areas of escarpment (generally less than 7% of basin area). In their analysis of the geomorphology of passive continental margins, O’Grady et al. (2000) reported that gently sloped margins tend to occur in regions with high sediment input, whereas higher gradient margins tend to have lower sediment input, which is consistent with the present interpretation of margin geomorphology.

When a basin enters its declining phase, the basin margins become dominated by a semi-continuous trench-trough system, created through the process of tectonic subduction of oceanic crust beneath continental crust. The trenches and troughs capture terrigenous sediments entering the basin sourced from the land, trapping them within the narrow subduction zone and inhibiting deposition seaward of the trench-trough system inside the basin. The result is that sediment deposits within declining ocean basins are very thin, attaining mean thicknesses of only 229 and 386 m in the South and North Pacific basins, respectively.

The transition from the mature to the declining evolutionary phase of ocean basins coincides with the basin margins changing from tectonically passive margins to active margins (Fig. 3). Another geomorphic signature of this transition from passive to active margins is the change in overall submarine canyon geomorphology (see Chap. 15 in this volume). Harris and Whiteway (2011) found that active continental margins contain 15% more canyons than passive margins and the canyons are steeper, shorter, more dendritic and more closely spaced on active than on passive continental margins. It was also found that river-associated, shelf-incising canyons are more numerous on active continental margins than on passive margins and that the occurrence of shelf-incising canyons is associated with the overall rate of sediment input (Harris and Whiteway 2011).

At locations where the rate of sediment influx into the trench-trough system exceeds the rate at which crust is subducted into the earth’s mantle (i.e. where sediment influx rates are very high and/or where the rate of subduction is very slow) submarine fans and the development of a continental rise may occur along active plate margins. Such a pattern is manifest along the Pacific coast of California where the Pacific plate engages with the North American plate (Fig. 9); the boundary changes from mainly strike-slip between the Mendocino and Murray fracture zones to more complex movements that include partial subduction north of the Mendocino and south of the Murray fracture zones (Nicholson et al. 1994). In the mostly strike-slip region located between the Mendocino and Murray fracture zones, the absence of a trench-trough system has allowed sediments to be deposited along the margin to form a prograding continental rise, which is confined to the region between the two fracture zones (Fig. 9). To the south of the Murray fracture zone, offshore of southern California and Mexico, the plate motion is more complex and involves partial subduction as expressed geomorphologically by a very narrow continental slope, the occurrence of troughs adjacent to the foot of slope with a complex ridge and swale terrain further offshore (Fig. 9). To the north of the Mendocino fracture zone and offshore of the states of Washington and Oregon, the Cascadia (thrust-faulted) margin exhibits only localised submarine fan complexes (Nitinat and Astoria Fans; Atwater et al. 2014) and a continental rise has not developed (Fig. 9).

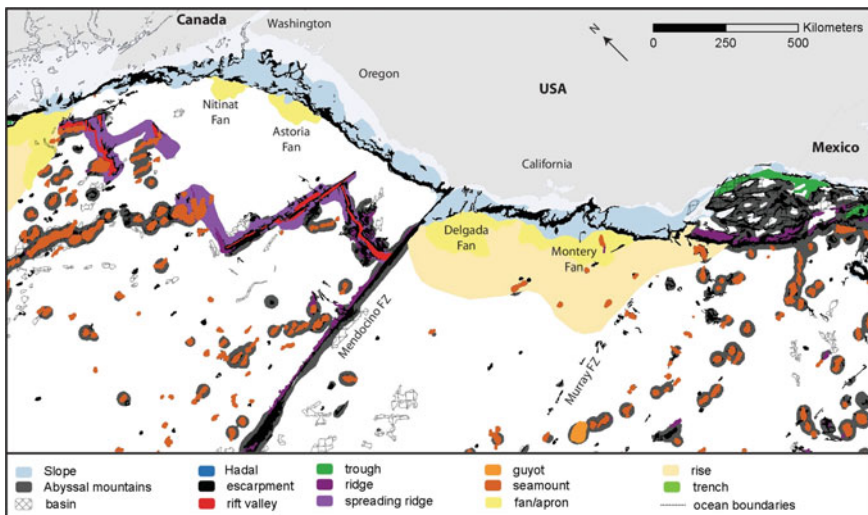


Fig. 9 Map of selected geomorphic features from the global seafloor features map of Harris et al. (2014), illustrating the relationship between the occurrence of continental rise with fracture zones along the western continental margin of California. Continental rise is developed between the Mendocino and Murray fracture zones (FZ) but does not occur to the north or south of this location; see text for explanation. The locations of submarine fans mentioned in the text are indicated

The Mediterranean Sea is the only example of the terminal phase of the Wilson Cycle and in this case the rate of sediment influx into the trench-trough system exceeds the rate at which ocean crust is subducted. This basin exhibits the greatest mean sediment thickness of any basin (mean thickness of 4311 m; Table 2).

4.2 Seamount Frequency of Occurrence and Sediment Thickness

An interesting pattern of seamount distribution in the oceans is their greater frequency of occurrence in declining ocean basins, compared with mature basins (e.g. Yesson et al. 2011; Table 2). Possible explanations for the differences in the spatial distribution pattern of seamounts across and between oceans could be possibly related to volcanic processes, such as temporal variability in the rate of volcanic eruptions along spreading ridges (Hillier and Watts 2007) or to differential burial of seamounts (Wright and Rothery 1998).

As noted above, the deposits of sediments in declining ocean basins are thin and patchy because land-derived sediments are intercepted and trapped by trench and trough systems located over the subduction zones of active continental margins. In contrast, the passive (trench-free) margins of mature ocean basins exhibit thick

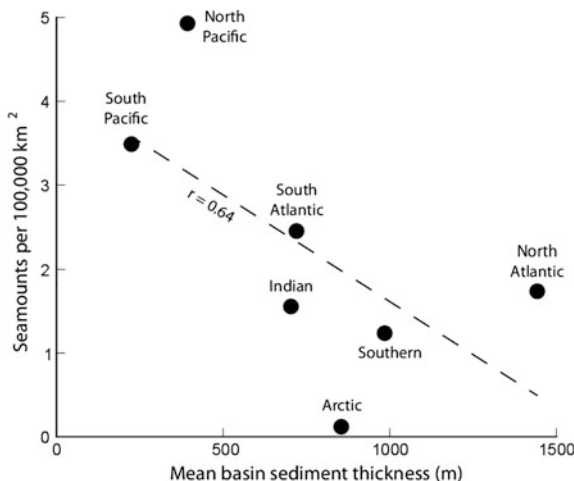


Fig. 10 Plot of mean seamount concentration (seamounts per $100,000 \text{ km}^2$) versus mean sediment thickness in mature and declining ocean basins. The linear correlation coefficient (r) is indicated. Fig. 11 Bathymetric basins of the North and South Atlantic and Indian Oceans with near-bottom dissolved oxygen (DO) concentration from the NOAA Ocean Atlas (2005). Major basins defined by closed bathymetric contours (from the GSFM database; Harris et al. 2014), in which the *numbers* indicate depths of major ocean basins based on the most shallow, closed, bathymetric contour that defines the basin outline. *Arrows* indicate gradients of decreasing DO concentration within basins and between adjacent basins that are descending or approximately ($\pm 100 \text{ m}$) equal in depth. The *arrows* and DO indicate southward flow of North Atlantic Deep Water (NADW) formed in the Norwegian and Labrador Seas and the northward flow of Antarctic Bottom Water (AABW) formed in the Weddell Sea and along the East Antarctic continental shelf. The depths illustrate how shallow basins adjacent to Antarctica at 4500 m feed into basins of the South Atlantic (at 4500 m) and finally into the deepest basins located in the northwest Pacific (at 5300 m)

sediments. It appears that seamounts are more common in the Pacific (declining basins) than in mature (Atlantic-type) ocean basins simply because Pacific seamounts are not buried in as much sediment and therefore have greater vertical expression than seamounts found in mature (more sediment-filled) ocean basins (Wright and Rothery 1998). In fact, among mature and declining ocean basins there is a trend for seamount concentration to decrease with increasing mean sediment thickness (Fig. 10).

To test the hypothesis that seamount abundance is a function of depth of sediment burial, we conducted an experiment using the available sediment thickness and seamount elevation data in the North and South Atlantic and the North and South Pacific Oceans. We note that the average sediment depth for the Atlantic is 1082 m (1442 m in North Atlantic and 772 m in South Atlantic), whereas the average sediment depth in the Pacific is 308 m (386 m in North Pacific and 229 in South Pacific). Thus the difference is on average 774 m. Recalling that the definition of seamounts used in this study specifies a minimum elevation of 1000 m above the level of surrounding seafloor and that the elevation of seamounts is

recorded in our database, we can adjust the number of apparent seamounts in different ocean areas by subtraction of elevation data. Subtracting 774 m from the elevations of seamounts in the South and North Pacific (both declining ocean basins) yields 2.0 and 3.1 seamounts per 100,000 km² for the South and North Pacific, respectively and subtracting 1000 m yields 1.6 and 2.7 seamounts per 100,000 km², respectively. The latter values (1.6 and 2.7 seamounts per 100,000 km²) are not significantly different from those of the North and South Atlantic (2.1 and 2.5 seamounts per 100,000 km², respectively).

4.3 Geomorphology and Global Bottom Water Circulation

Seafloor geomorphic features exert control over the flow of water within and between ocean basins. This occurs through bathymetric steering, the deflection of flow around obstacles and the constriction of flow through narrow choke points and over sills (Whitehead 1998; Gille et al. 2004). Here we focus on the flow of water between the 33 major bathymetric basins and pathways of flow that could be influenced (or in some cases actually determined) by their depth and configuration.

The formation of cold, dense water that occupies the abyssal layer of the global ocean occurs in the polar regions of the earth and it is driven by two major processes: (1) the cooling of Gulf Stream waters around Iceland to form North Atlantic Deep Water; and (2) the formation of bottom water by sea ice formation and brine rejection (Ivanov et al. 2004; Rintoul 2007). North Atlantic Deep Water (NADW) is formed as cold surface waters during the winter in the Greenland and Norwegian Seas. This water sinks to fill the basin north of a ridge spanning the distance from Greenland to Scotland (Whitehead 1998; Ivanov et al. 2004).

The coldest bottom water, Antarctic Bottom Water (AABW), is created in winter on the continental shelf of Antarctica by sea ice formation. It is about -1 °C and it fills basins in the Southern Ocean adjacent to Antarctica (Rintoul 2007). As dense AABW water flows into a bathymetric basin, the basin eventually becomes filled and overflows, driven by gravity. The descent of bottom water flowing from one basin into another (deeper) basin becomes focused at sills and bathymetric choke points. Sills are “a sea floor barrier of relatively shallow depth restricting water movement between basins” (IHO 2008). Thus every basin has a sill, over which fluid would escape if the basin were filled to overflowing. This leads to the consideration of bathymetric basins and their sills as factors controlling the flow of bottom water within and between ocean basins (see also Whitehead 1998).

Sills can be a biogeographic barrier for species located in deep basins on either side. The basin environments are vastly different from the shallow water depths, high current energy, and warmer water temperature of the sill environment. The Strait of Gibraltar is a type-case for geomorphic sills. Here, ocean circulation is characterized by a two-layer system: an eastward-directed, Atlantic water inflow at the surface and a deep westward outflow of saline Mediterranean water. The two different water layers have a variable interface depth of around 100 m and the Strait

of Gibraltar sill depth is located at a depth of around 200 m. De Mol et al. (2012) document reef-forming cold-water coral deposits up to 40 m in thickness in the deepest part of the Strait of Gibraltar between 180 and 330 m water depth, which have developed to exploit the unique oceanographic conditions. Coral buildups on the tops of north-south orientated rocky crests (i.e. oriented transverse to the direction of flow) are the most common form in the Strait of Gibraltar.

Another critical aspect of bottom water is that it is the source of oxygen for all benthic animals inhabiting the deep ocean environment, a property that could be affected by anthropogenic climate change (Long et al. 2016). As AABW and NADW sink into the deep ocean basins and move away from the poles they are gradually depleted of dissolved oxygen through the respiration of benthic fauna and oxidation of minerals and organic matter. Thus the concentration of dissolved oxygen in deep bottom waters is a conservative tracer that we can use to track pathways of bottom water dispersal in the abyssal ocean.

In order to examine the flow of water between bathymetric basins, we have plotted the near-bottom dissolved oxygen (DO) concentration from the NOAA Ocean Atlas (2005) and overlaid the major bathymetric basins defined by closed bathymetric contours from the GSFM database (Harris et al. 2014). The results (Figs. 11 and 12) illustrate how the bathymetric basins coincide remarkably well

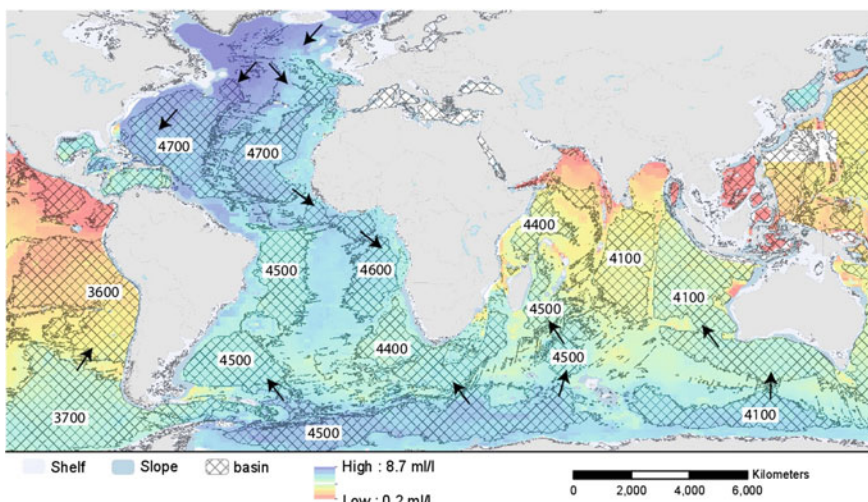


Fig. 11 Bathymetric basins of the Southern, Indian and North and South Atlantic Oceans with near-bottom dissolved oxygen (DO) concentration from the NOAA Ocean Atlas (2005). Major basins defined by closed bathymetric contours (from the GSFM database; Harris et al. 2014), in which the numbers indicate depths of major ocean basins based on the most shallow, closed, bathymetric contour that defines the basin outline. Arrows indicate gradients of decreasing DO concentration within basins and between adjacent basins that are descending or approximately (± 100 m) equal in depth. The arrows and DO indicate southward flow of North Atlantic Deep Water (NADW) formed in the North Atlantic and Arctic Oceans, and northward flow of Antarctic Bottom Water (AABW) formed in the Weddell Sea and along the East Antarctic continental shelf

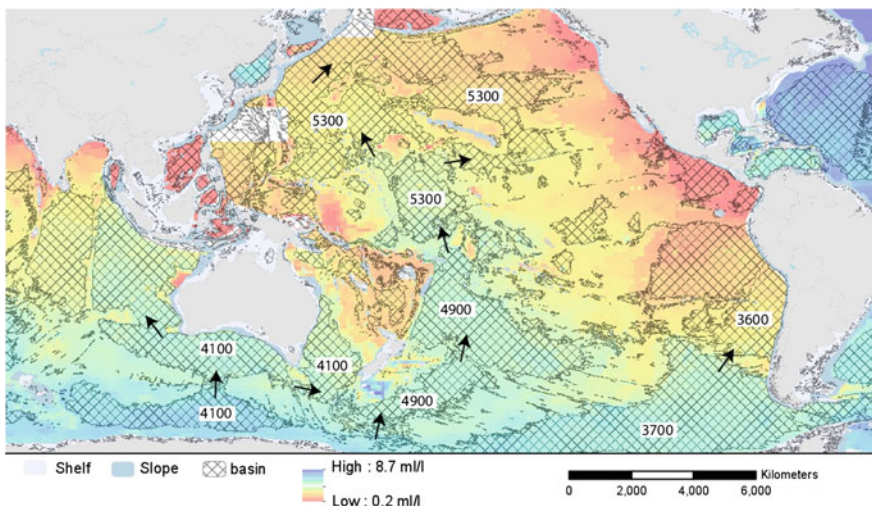


Fig. 12 Bathymetric basins of the Southern and North and South Pacific Oceans with near-bottom dissolved oxygen (*DO*) concentration from the NOAA Ocean Atlas (2005). Major basins defined by closed bathymetric contours (from the GSFM database; Harris et al. 2014), in which the numbers indicate depths of major ocean basins based on the most shallow, closed, bathymetric contour that defines the basin outline. Arrows indicate gradients of decreasing *DO* concentration within basins and between adjacent basins that are descending or approximately (± 100 m) equal in depth. The arrows and *DO* indicate northward flow of Antarctic Bottom Water (AABW) formed in the Ross Sea and along the East Antarctic continental shelf. The depths illustrate how shallow basins adjacent to Antarctica at 3700 and 4100 m feed into deeper basins of the central South Pacific (at 4900 m) and finally into the deepest basins located in the northwest Pacific (at 5300 m)

with discrete areas having like values of *DO*. Arrows shown on Figs. 11 and 12 indicate gradients of decreasing *DO* concentration within basins and between adjacent basins that are descending or approximately (± 100 m) equal in depth.

As NADW sinks into the North Atlantic it flows southwards into the (4900 m) deep basins located to the east and west of the mid-Atlantic ridge (Fig. 11). These bottom currents are consistent with the pattern inferred by Schmitz and McCartney (1993). The gradient in *DO* suggests a pattern of southward flow between basins located on the eastern side of the mid-Atlantic ridge as far south as the Gulf of Guinea (West Africa).

The dispersal of AABW water from the basin at 4500 m depth located adjacent to the Weddell Sea of Antarctica appears to flow into basins at a similar depth located adjacent to eastern South America (Argentine Basin) and also into the Indian Ocean basin adjacent to Madagascar (Fig. 11). This pattern is consistent with bottom flows suggested by Tchernia (1980). Bottom waters become depleted of *DO* with increasing distance northward into the Indian Ocean, reaching minima in the Bay of Bengal and in the Arabian Sea (Fig. 11).

The dispersal of AABW from the basin at 4100 m depth located adjacent to East Antarctica appears to flow into a basin at a similar depth adjacent to the southern

and western margins of Australia. Bottom waters become depleted of DO with increasing distance northward in this 4100 m basin, that extends northwards into the eastern Indian Ocean. The two basins at 4100 m depth located in the eastern Indian Ocean are divided by the 90 East Ridge, with the western basin being clearly more depleted of DO than the eastern basin (Fig. 11).

The dispersal of AABW water from the basin at 3700 m depth located adjacent to East Antarctica appears to involve the northward flow of water into a series of basins of increasing depth moving northwards from basins adjacent to New Zealand and into the western North Pacific Ocean (Fig. 12). This pattern is also consistent with bottom flows suggested by Tchernia (1980). As the water ages it becomes warmer and is depleted of oxygen along this pathway, reaching a minimum in the basins of the western North Pacific. At this point, at the end of the global ocean conveyor (Broecker 1991), it contains less than 1 ml/l dissolved oxygen.

5 Conclusions

The present study has shown how the evolution of the earth's ocean basins via the Wilson Cycle give rise to stages of geomorphological development that can be quantified using available digital datasets. Basins, formed initially by tectonic rifting of continental plates, evolve and are modified by volcanism and sedimentation processes. Young basins such as the Gulf of California and the Red Sea are characterized by the absence of ocean trenches, young ocean crust (<8 MA), comparatively large areas of continental slope, thick sediments, and a relatively large percent area of mid-ocean ridge rift valley (above 1.7%). Mature ocean basins are characterized by relatively large percentage areas of continental rise (mean of 19.8%) and submarine fans (mean of 4.3%), which is consistent with the relatively thick sediments deposited in these basins (mean thickness of 940 m). The area of ocean trench is relatively small in all mature ocean basins compared with declining and terminal basins, ranging from 0 to 0.3% (Table 2). A defining geomorphic feature of the declining category is that around 1% of their area is trench, which is more than twice the area of trenches contained in the other categories. Declining ocean basins contain the highest concentration of seamounts (3.5–5 seamounts per 100,000 km²), which is more than double the mean value (1.4 seamounts per 100,000 km²) that occurs for the mature category with the next highest concentration. The terminal category of ocean basins is represented only by the Mediterranean Sea. It is characterised by the greatest mean sediment thickness (4311 m) and greatest percentage area of submarine fans (7.2%) of any ocean basin.

Sedimentation is reduced in declining ocean basins by virtue of trenches and troughs that capture terrigenous sediments entering the basin, trapping them within the narrow subduction zone and inhibiting deposition seaward of the trench-trough system inside the basin. Consequently, sediment deposits within declining ocean basins are very thin, with mean thicknesses of 229 and 386 m in the South and North Pacific basins, respectively. The thin nature of sediment deposits in declining

ocean basins explains their greater apparent concentration of seamounts; seamounts are not buried in as much sediment in declining ocean basins and therefore have greater vertical expression than seamounts found in mature (more sediment-filled) ocean basins.

Areas having similar near-bottom dissolved oxygen (DO) concentrations derived from the NOAA Ocean Atlas (2005) coincide very well with major bathymetric basins defined by closed bathymetric contours from the GSFM database (Harris et al. 2014). Examination of gradients of decreasing DO concentration within basins and between adjacent basins suggests pathways of bottom water flow that are generally consistent with previously published assessments of bottom currents.

Acknowledgements The work described in this paper was produced with financial support from GRID-Arendal.

References

- Atwater BF, Carson B, Griggs GB, Johnson HP, Salmi MS (2014) Rethinking turbidite paleoseismology along the Cascadia subduction zone. *Geology* 42:827–830
- Augustin N, Devey CW, van der Zwan FM, Feldens P, Tominaga M, Bantan RA, Kwasnitschka T (2014) The rifting to spreading transition in the Red Sea. *Earth Planet Sci Lett* 395:217–230
- Backman J, Jakobsson M, Løvlie R, Polyak L, Febo LA (2004) Is the central Arctic Ocean a sediment starved basin? *Quat Sci Rev* 23:1435–1454
- Baker BH, Mohr PA, Williams LAJ (1972) Geology of the eastern rift system of Africa. *Geol Soc Am Spec Pap* 136:1–68
- Becker JJ, Sandwell DT, Smith WHF, Braud J, Binder B, Depner J, Fabre D, Factor J, Ingalls S, Kim SH, Ladner R, Marks K, Nelson S, Pharaoh A, Trimmer R, Von Rosenberg J, Wallace G, Weatherall P (2009) Global bathymetry and elevation data at 30 arc seconds resolution: SRTM30_PLUS. *Mar Geodesy* 32:355–371
- Broecker WS (1991) The great ocean conveyor. *Oceanography* 4:79–89
- De Mol B, Amblas D, Alvarez G, Busquets P, Calafat A, Canals M, Duran R, Lavoie C, Acosta J, Muñoz A (2012) Cold-water coral distribution in an erosional environment: the strait of gibraltar gateway. In: Harris PT, Baker EK (eds) *Seafloor geomorphology as benthic habitat: GeoHAB atlas of seafloor geomorphic features and benthic habitats*. Elsevier, Amsterdam, pp 636–643
- Divins DL (2003) Thickness of sedimentary cover in the Eastern Pacific Ocean. In: Uditsev GB (ed) *International geological atlas of the Pacific Ocean*. Intergovernmental Oceanographic Commission, Moscow, St Petersburg, pp 120–130
- Gardner JV, Armstrong AA (2011) The Mariana trench: a new view based on multibeam echo sounding. American Geophysical Union, Fall Meeting 2011. American Geophysical Union, San Francisco
- Gille ST, Metzger EJ, Tokmakian R (2004) Seafloor topography and ocean circulation. *Oceanography* 17:47–54
- Harris PT, Whiteway T (2011) Global distribution of large submarine canyons: geomorphic differences between active and passive continental margins. *Mar Geol* 285:69–86
- Harris PT, MacMillan-Lawler M, Rupp J, Baker EK (2014) *Geomorphology of the oceans*. Mar Geol 352:4–24
- Hess HH (1962) History of ocean basins. In: Engel AEJ, James HL, Leonard BF (eds) *Petrologic studies: a volume in honor of A. F. Buddington*. Geological Society of America, New York, pp 599–620

- Hillier JK, Watts AB (2005) Relationship between depth and age in the North Pacific Ocean. *J Geophys Res* 110:405
- Hillier JK, Watts AB (2007) Global distribution of seamounts from ship-track bathymetry data. *Geophys Res Lett* 34:13
- Hillier JK, Tilmann F, Hovius N (2008) Submarine geomorphology: new views on an ‘unseen’ landscape. *Basin Res* 20:467–472
- IHO (2008) Standardization of undersea feature names: guidelines, proposal, form, terminology, 4th edn. International Hydrographic Organisation and Intergovernmental Oceanographic Commission, Monaco, p 32
- Ivanov VV, Shapiro GI, Huthnance JM, Aleynik DL, Golovin PN (2004) Cascades of dense water around the world ocean. *Prog Oceanogr* 60:47–98
- Jamieson AJ, Fujii T, Mayor DJ, Solan M, Priede IG (2010) Hadal trenches: the ecology of the deepest places on Earth. *Trends Ecol Evol* 25:190–197
- Long MC, Deutsch C, Ito T (2016) Finding forced trends in oceanic oxygen. *Global Biogeochem Cycles* 30:381–397
- Muller RD, Roest WR, Royer JY, Gahagan LM, Sclater JG (1997) Digital isochrons of the world’s ocean floor. *J Geophys Res* 102:3211–3214
- Nicholson C, Sorlien CC, Atwater T, Crowell JC, Luyendyk BP (1994) Microplate capture, rotation of the western transverse ranges, and initiation of the San Andreas transform as a low-angle fault system. *Geology* 22:491–495
- O’Grady DB, Syvitski JPM, Pratson LF, Sarg JF (2000) Categorizing the morphologic variability of siliciclastic passive continental margins. *Geology* 28:207–210. <http://elpub.wdcb.ru/journals/rjes/v06/tje04146/tje04146.htm>
- Pushcharovsky YM (2006) Tectonic types of the Pacific abyssal basins. *Geotectonics* 40:345–356
- Ricou L-E (1996) The plate tectonic history of the past Tethys Ocean. In: Nairn AEM, Ricou L-E, Vrielynck B, Dercourt J (eds) *The Tethys Ocean*. Springer, Boston, pp 3–70
- Rintoul SR (2007) Rapid freshening of Antarctic bottom water formed in the Indian and Pacific Oceans. *Geophys Res Lett* 34:6. doi:[10.1029/2006GL028550](https://doi.org/10.1029/2006GL028550)
- Schmitz WJ, McCartney MS (1993) On the north Atlantic circulation. *Rev Geophys* 31:29–49
- Smith WH, Sandwell DT (1997) Global sea floor topography from satellite altimetry and ship depth soundings. *Science* 277:1956–1962
- Stow DAV (2010) *Vanished ocean: how Tethys reshaped the world*. Oxford University Press, 300 pp
- Tchemia P (1980) Descriptive regional oceanography. Pergamon Marine Series, Oxford
- Wessel P (2001) Global distribution of seamounts inferred from gridded Geosat/ERS-1 altimetry. *J Geophys Res* 106:19431–19441
- Whitehead JA (1998) Topographic control of oceanic flows in deep passages and straits. *Rev Geophys* 36:423–440
- Wilson JT (1966) Did the Atlantic close and then reopen? *Nature* 211:676–681
- NOAA (2005) World ocean atlas data. Available from: http://www.nodc.noaa.gov/OC5/WOA05/pr_woa05.html
- Wright J, Rothery DA (1998) *The ocean basins: their structure and evolution*, 2nd edn. Elsevier Ltd., Open University, Milton Keynes, UK
- Yesson C, Clark MR, Taylor ML, Rogers AD (2011) The global distribution of seamounts based on 30 arc seconds bathymetry data. *Deep Sea Res Part I* 58:442–453

Drivers of Seafloor Geomorphic Change

Angelo Camerlenghi

Abstract Oceanic basins are shaped by a variety of natural drivers that impact the seafloor morphology at different scales, spanning from hundreds of kilometres for plate motions to decimetres for bio-constructions by benthic organisms. In the post-industrial period of the oceanic basin history, anthropic activity on the seabed has started to provide an additional morphologic imprint. Because oceanic basins are sinks for sediments produced on land, the majority of the seafloor morphology is produced by forces acting on sediments, resulting in sediment accumulation, transport, erosion and deformation. Plate tectonics forces are reflected dramatically in the morphology of areas of the oceans where the sedimentary cover is thin, or even absent, along the mid ocean ridges, and fracture zones. Chemical reactions in the oceanic subsurface induce mineral precipitation, dissolution or transformation that may also indirectly impact the seafloor.

1 Introduction

Oceanic basins are formed by tectonic forces that produce the break-up of pre-existing continents and the sinking of the newly formed denser oceanic lithosphere into the mantle (Fig. 1). They become the primary sink of sediments produced on land by the alteration and erosion of mountain belts and transported to the oceans by rivers. In addition, oceanic basins are the sink of biogenic sediments produced by the accumulation at the seafloor of the mineral remains of marine living organisms, and host the accumulation of chemical precipitates (mainly evaporitic rocks).

A. Camerlenghi (✉)

National Institute of Oceanography and Applied Geophysics - OGS,
Borgo Grotta Gigante, 42/C, 34010 Sgonico, Trieste, Italy
e-mail: acamerlenghi@inogs.it

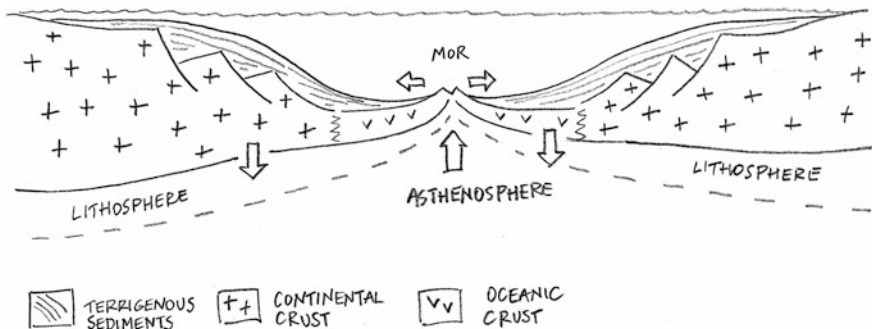


Fig. 1 Drivers for the large-scale morphological evolution of oceanic basins. After an initial thermal uplift due to the asthenospheric plumes breaking through the continental lithosphere (not displayed in the figure), it is cooling that determines the sinking of the newly formed oceanic crust. In parallel, the lava eruption at the mid-ocean ridge (*MOR*) exerts lateral push that drives the widening of the ocean. The ocean floor formed with this process is dominated by volcanic processes and transform faults near the *MOR* (see Fig. 2). These morphologies are rapidly buried by terrigenous sediment accumulation near the ocean margins

If an ocean basin had no sediment in it, the morphologies of tectonic processes would be entirely exposed at the surface. A similar situation happens, for example, on Mars, where we can observe the morphology of an ancient plate tectonic system at the surface of the planet.

However, the tectonic landscape produced throughout the lifetime of an ocean basin is attenuated by the burial of sediments that fill and drape in various ways the oceanic floor. Continuing tectonic movements deforming not only the crystalline basement of the oceans but also the sedimentary cover, together with the transfer of sediments from the continents to the oceanic basins give rise to an extraordinary variety of submarine landforms reflecting both tectonic and sedimentary processes.

Gravity also plays a fundamental role in shaping the bottom of the oceans when, as a consequence of tectonic forces and/or sediment load, the equilibrium between acting and resisting forces is broken and portions of ocean basin margins collapse or creep downslope. The pressure, temperature, and chemical gradients induced by tectonic and sedimentary processes also trigger fluid flow within both sedimentary sequences and crystalline rocks that induce fluid and solid mass transfer to the seafloor with a significant imprint on its morphology.

The interaction between oceanic circulation and the sedimentary cover generates distinct, though often subdued morphologies especially in the deep sea and on continental margins.

Finally, the cryosphere significantly affects the morphology of continental shelves and, indirectly, the continental slopes, in polar regions, where ice streams are grounded on the seafloor primarily during periods of glacial maxima.

2 Plate Tectonics—Continental Break-up and Fate of the Oceanic Lithosphere at Convergent Plate Boundaries

2.1 Oceanic Spreading Centres

The continental break-up that initiates the formation of oceanic ridges and seafloor spreading occurs in crystalline rocks with mechanisms of brittle deformation near the Earth surface. The continental crust is uplifted by the underlying mantle plume, stretched, thinned and ultimately the continental plate breaks-up into smaller fragments and an oceanic basin develops by spreading at the two sides of an axial volcanic ridge (Mid-Ocean Ridge—MOR). The volcanic centres located at the ridge axes and at volcanic hot spots emit molten rocks at the seafloor, giving rise to various types of submarine lava flows. However, it is deformation resulting from shear stress that produces the most impacting oceanic morphologies of brittle deformation at divergent oceanic plate boundaries (Fig. 2). As these plate boundaries typically lie in the open ocean, away from the source of river sediment discharge, their morphological imprint on the seafloor is clearly recognised in the bathymetry even if the crystalline basement is draped by thin veneers of marine sediments. We can say, therefore, that in open ocean the main driver for the ocean floor morphology is tectonic deformation in the crystalline basement.

More information on the above is available in Chapter “[Origin and Geomorphic Characteristics of Ocean Basins](#)”.

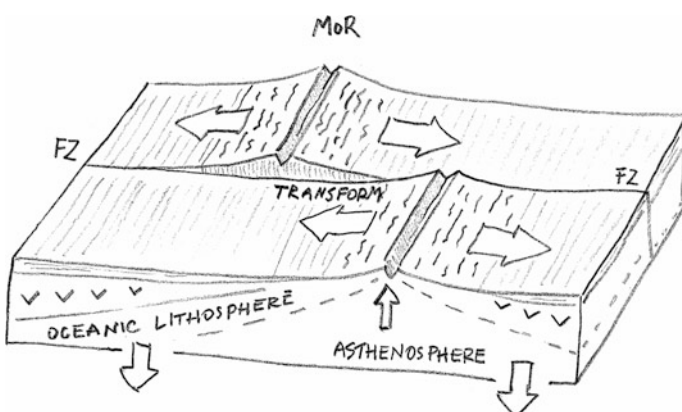


Fig. 2 The mid-ocean ridges (*MOR*) are typically offset by transform faults systems (when the spreading direction at the two sides of the fault is in opposite direction), that evolve laterally to fracture zones (*FZ*). The alteration of upper mantle peridotites determines important density contrasts between the rocks at the two sides of the transform faults that in turn drive spectacular vertical movements

2.2 *Transform Faults and Fracture Zones*

Mid-ocean ridges are offset by large fractures that interrupt their lateral continuity. At the two sides of a transform fault are two different oceanic plates moving in opposite direction, while at the two sides of a fracture zone the plate is the same and moves in the same direction (Fig. 2). In both cases these fractures and faults host among the most spectacular submarine landscapes, with very large offsets of the seafloor (hundreds of metres) and very steep slopes produced by the vertical motion induced by alteration of the deeply rooted crystalline rocks once they come in contact with seawater.

2.3 *Subduction Zones*

Where plate boundaries are convergent (i.e. at lithospheric subduction zones), tectonic forces affect not only the crystalline basements of the converging plates, but also a thick pile of sediments accumulated along the continental margin of the overriding plate, to form the fore-arc basin and the accretionary prism (where this occurs) (Fig. 3). These sediments are deformed mostly with a ductile behaviour to form folds, and with a brittle behaviour to form thrust faults and ramps, with a striking influence on the seafloor morphology. We can say, therefore, that along active continental margins the main driver for the ocean floor morphology is tectonic deformation in the accretionary prism where sediment accretion prevails, and complex basement/sediment/rock deformation where tectonic erosion prevails.

More information on the above is available in Chapter “[Oceanic Trenches](#)”.

2.4 *Volcanic Islands*

Although the vast majority of submarine volcanoes occurs along the MOR, there are many other volcanoes in other geological environments (Fig. 4). If not reaching the sea surface, submarine volcanoes originate ‘seamounts’ and when their summit is close to the sea surface in tropical regions they become colonised by living organisms forming atolls. The sinking lithosphere on which these volcanoes are located, or a fast global sea level rise may cause the atoll to drown, generating a guyot. Such volcanoes are generally formed as ‘hot spots’, which are surface expression of mantle plumes that cause melting of the lithosphere and generation of volcanoes. Other volcanoes are generated on the seafloor in back-arc basins when subducting lithosphere is molten below oceanic crust.

More information on the above is available in Chapter “[Volcanic Islands and Seamounts](#)”.

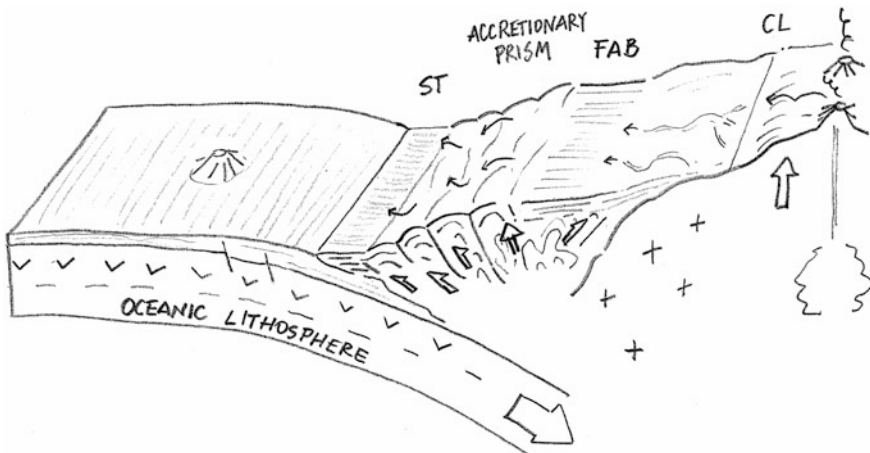


Fig. 3 At convergent margins, the oceanic crust and lithosphere formed by the processes described in Figs. 1 and 2 subducts under the continental lithosphere of the ocean margin. Typically, the sediments of the subducting plate are scraped off their original position forming an accretionary prism. The deepest part of the seafloor in front of the prism is called subduction trench (*ST*) and is filled by the terrigenous sediments derived from the adjacent land masses. These sediments, carried by turbidity currents, generally form a sedimentary basin between the margin and the accretionary prism, called fore-arc basin (*FAB*). *CL* identifies the coast line. The accretionary prism grows by uplifting as a consequence of the development of thrust faults. Coastal ranges dominated by volcanic processes characterize the adjacent landmasses. The subduction of a rough seafloor with volcanic seamounts (see Fig. 4) may determine tectonic erosion of the margin (including the previously formed accretionary prism)

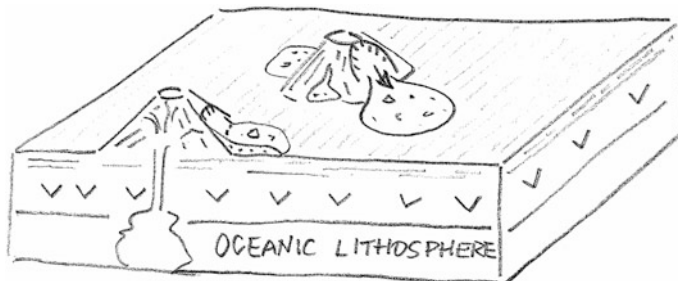


Fig. 4 Volcanic processes dominate the morphology of ocean floor, especially in the Pacific and Indian oceans. Volcanoes may emerge to form volcanic islands, remain submerged, or sink progressively through time as consequence of the sinking of the oceanic lithosphere, or subaerial erosion. The flanks of volcanic island experience catastrophic collapse driven by gravity, leaving on the seafloor impressive morphologies reflecting sediment mass transport and deposition

3 Sediment Types

There is a large variety of sediment types that settle at the seafloor in oceanic basins. Below is a simple classification based on sediment composition.

3.1 Terrigenous Sediments (Also: Lithogenous)

These sediments are made of rock fragments eroded from land and transported to the oceans by water in rivers (e.g., river-transported sediment), wind (through a process called *aeolian transport*, e.g., windblown dust), and ice (e.g., ice-rafter rocks).

Terrigenous sediments reach the seafloor under the action of gravity, both via settling of grains (also after flocculation of small clay particles) through the water column, and via turbidity currents. The latter convey, through a process of mass-transport, large quantities of sediment grains in seawater-sediment suspension generated mostly by seafloor collapse. Gravity may also generate the mass-transport of high density debris-flows or sediment-rock blocks.

Depending on the mean size of the grains, terrigenous sediments can be further classified as:

Gravels	(2 – 64 mm)
Sands	(63 µm – 2 mm)
Silts	(2 – 63 µm)
Clays	(<2 µm)

Clays are primarily composed of the following hydrate aluminosilicate minerals (phyllosilicates): kaolinite, chlorite, illite, and montmorillonite.

Besides their terrigenous origins, abyssal clays can also be generated by dissolution of calcareous plankton and benthos (red clays, or pelagic clays) below the Carbonate Compensation Depth (CCD) in the open ocean.

3.2 Biogenic Sediments (Also: Biogenous)

These are composed of mineral remains of dead organisms, like macroscopic shells, bones, teeth and microscopic tiny shells, or tests, which settle through the water column.

Calcium carbonate (CaCO_3) biogenous sediments are composed of mineral remains of coccolithophores (algae), foraminifera (protozoans), and pteropods (planktonic gastropods made of aragonite, a more soluble variety of calcite).

Silica (SiO_2 or $\text{SiO}_2 \cdot n\text{H}_2\text{O}$) biogenic sediments are composed of diatoms (algae) and radiolarians (protozoans).

3.3 Authigenic Sediments (Also: Hydrogenous)

These are mineral precipitates formed on the seafloor or within the sediments. They comprise manganese nodules, phosphates (beneath areas in surface ocean of very high biological productivity), carbonates (aragonite and calcite), metal sulphides (associated with hydrothermal vents), and evaporites (minerals precipitates as a consequence of evaporation of seawater).

3.4 Volcanogenic Sediments

Volcanogenic sediments are made of the products of volcanic eruptions, both as fragments of erupted lava fallen through the water column (ashes, lapilli, and larger blocks), and as underwater lava flows.

3.5 Cosmogenous Sediments

These are made of particles fallen on the seafloor from the outer space.

3.6 Plastics

For the sake of completeness, plastic debris (>5 mm size) and microplastics (<5 mm size)—of which primary microplastics are deliberately manufactured while secondary microplastics are break-down products of larger debris—can be nowadays be easily found both within very recent sediments (microplastics) and on the seafloor (plastics). Most plastics derive from land-based sources (household and industrial waste, wastewater, fishing, aquaculture, shipping, tourist activities, etc.).

4 Gravity—Density Currents, Slope Instability and Mass Transport Deposits

4.1 *The Ocean as a Sediment Sink*

Because oceans are the areas of the planet with the lowest topographic relief, any sediment produced on land by erosion and chemical weathering is transported by rivers and released into the oceans. The latter can thus be seen as the global sink of sediments produced on land. The distribution of land-derived sediments in the oceans is focussed at the mouths of the major river systems on passive margins, where the tectonic subsidence following the continental rifting process allows for the accumulation of huge sedimentary sequences (Fig. 1).

Marine sediments settle at the bottom of the oceans at very low rates. In the open ocean, an average accumulation rate is in the order of a few centimetres per thousand of years. In such a way, the compaction of sediments occurs without development of excess pore water pressure, and the resistance of the sediments to shear stress is maximum. Nevertheless, the angle of repose of marine sediments is very low, in the range of a few degrees. This is because the normal granular soil angle of repose in dry conditions (34° in sands), is reduced by the lower submerged weight of the grains, the presence of a clay matrix, and the low bulk density (due to a high water content) of the sediments. The angle of the world's continental slopes generated by the settlement of sediment transported by rivers is around 4° . Steeper slopes can form only through erosion of indurated sediments or rocks, or deposition of over-consolidated material such as subglacially-generated debris-flow deposits on glaciated margins (see Sect. 5). Locally, the rate of sediment deposition can be orders of magnitude larger than in the open ocean. This is on river deltas and pro-deltas, at the mouth of glacial troughs in polar margins, and during certain chemical precipitation (evaporites).

4.2 *Density Currents, Erosion, Transport and Deposition*

Sediment particles suspended in the water column, whether they are biogenic or terrigenous clays, settle on the seafloor driven by gravity, draping its topography. These sediments do not alter the underlying morphology, and eventually they only smoothen ocean floor topography by attenuating topographic relief.

However, the vast majority of terrigenous sediments is transferred from river mouths to abyssal plains via density currents, also driven by gravity (Fig. 5).

These currents, also called “turbidity currents”, are avalanches of sediments re-suspended following a slope failure, or developing from the settlement of sediment suspension from surges of sediment-laden waters from rivers or glaciers,

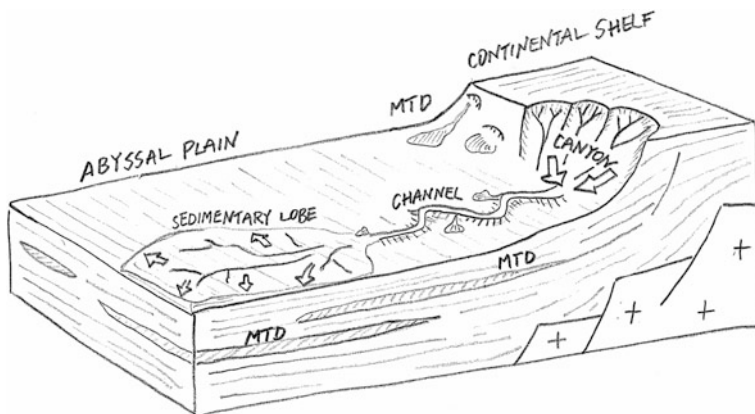


Fig. 5 Ocean passive margins (rifted margins) experience the highest sediment accumulation, enabled by large land-derived sediment flux and deposition favoured by the accommodation space created by the subsidence of the underlying lithosphere. The total sediment thickness overlying the crust may reach 20 km. The seafloor morphology of these margin is dominated by sediment dynamics. Deep sea channels, bounded by levées, convey the terrigenous sediments from the continental shelf to the abyssal plain via turbidity currents. The continental slope is incised by canyons systems where erosional processes dominate. At the mouth of the channels, when the energy of the sediment flux decreases, deposition occurs in large, subdued sedimentary lobes. Failure of the slope, caused by a combination of resisting forces that decrease the strength of the sediments and acting forces that increase the stress on the sediments (such as increased sedimentation, earthquake shaking) determines the deposition of mass transport deposits (*MTD*) that characterize slope and even abyssal plains. This sediment dynamics characterise primarily low-latitude (non-glacial) ocean margins

forming hyper-pycnal flows. The characteristic of these flows is that the density of the flowing suspension is slightly larger than that of the fluid they move through (seawater), so friction does not play a major role within the body of the flow. These flows can attain very high velocities on the continental slope (tens of metres per second), have a high erosional power, and cause the settlement of particles in deposits that are known as “turbidites”. The repeated occurrence of turbidity currents contributes to the formation of preferred flow paths on the continental slope, such as “canyons”, which attain very steep slopes on their margins (tens of degrees) through a dendritic pattern of sediment transfer. At the mouth of canyons on the lower continental slope, where the flow often undergoes a hydraulic jump, the flow decreases in velocity and normally becomes channelised in a “deep-sea channels”. Deep sea channels can be considered as ‘underwater rivers’, and often exhibit a meandering shape. The overspill of turbid water at the side of deep sea channels generates sedimentary banks of fine-grained particles, called “levées”, until the remaining finest particles settle at the mouth of the channel forming a low-relief sedimentary lobe. The sedimentary complex formed by lateral migration of

channels throughout the history of a sedimentary basin forms a “deep sea fan”. Fans consist of huge sedimentary sequences, the largest of which, located off the mouth of the Gange and Indus rivers in the Indian Ocean, attain thousands of kilometres in length and several kilometres in thickness. Their underwater morphology is visible at planetary scale.

More information on the above is available in Chapters “[Submarine Canyons and Gullies](#)” and “[Submarine Fans and Their Channels, Levees, and Lobes](#)”.

4.3 Submarine Slope Instability and Mass-Transport Deposits

A submarine slope is stable until the ratio between acting forces and resisting forces is more than or equal to 1. Acting forces include the static load of the sediment (variable as the slope angle evolves), sedimentary load (during extreme sedimentary events), tectonic load (evolving through time as fold and thrusts), cyclic loads produced by ground shaking (earthquakes), and the load from waves such as storm and tsunami waves. Resisting forces include the internal friction between grains, cohesion, and cementation resulting from diagenesis (chemical precipitation on sediment grains after their settlement). Resisting forces largely depend on the pore pressure regime of the sedimentary sequence. Pore pressure exceeding the hydrostatic pressure exerts a force on the grains resulting in a decrease of the strength. In granular and un-cemented sediments, the resistance of the sediment is null and the sediment become fluidised when the pore pressure equals the lithostatic pressure. A process of increasing pore water pressure (like rapid sedimentation, rapid tectonic load, production of pore water through smectite dehydration and smectite-illite transformation, or change of gypsum to anhydrite), gas formation and migration in the pore space, or increasing load on the aquifer when connected to land, may reduce the ratio between acting and resisting force and make a submarine slope prone to failure. An external event, such as an earthquake, can trigger the slope instability and the sediment mass movement downslope, driven by gravity.

If failed sediments do not disaggregate completely into turbidity currents, sediment mass movement occurs in a variety of modes, giving rise to a variety of deposits. Classification and nomenclature are not standardised. In Fig. 6 we make reference to the classification of gravity-induced deposits published by Moscardelli and Wood (2007). All the resulting deposits bear morphological significance on the seafloor. Characteristic diagnostic characters are also found in seismic reflection profiles, often used in association with bathymetry, to characterize these deposits.

More information on the above is available in Chapter “[Submarine Landslides](#)”.

GRAVITY INDUCED DEPOSITS		Genetic Classification Transport Mechanism	Descriptive Classification Sedimentary Structures	Seismically Recognizable Features (Moscardelli et al., 2006; this work)
Mass Transport Complex	Slide		Shear failure along discrete shear planes with little or no internal deformation or rotation	Essentially undeformed, continuous bedding
	Slump		Shear failure accompanied by rotation along discrete shear surfaces with various degrees of internal deformation	Compressional ridges, imbricate slides, irregular upper bedding contacts, duplex structures, tension faults, joints, slickensides, grooves, rotational blocks
	Debris Flow		Shear distributed throughout the sediment mass. Strength is principally from cohesion due to clay content. Additional matrix support may come from buoyancy. Plastic rheology and laminar state.	Matrix supported, random fabric, clast size variable, matrix variable. Rip ups, rafts, inverse grading and flow structures possible.
Turbidity Current	Turbidite		Supported by fluid turbulence (newtonian rheology)	Mega rafted and/or detached blocks, irregular upper bedding contacts, lateral pinch-out geometries, oriented ridges and scour. Low-amplitude, semitransparent chaotic reflections.
			Normal size grading, sharp basal contacts, gradational upper contacts.	Lobate features Laterally continuous

Fig. 6 Classification of gravity-induced deposits (from Moscardelli and Wood 2007, John Wiley & Sons Ltd; Blackwell Publishing Ltd.)

5 Ice–Ice Bull-Dozing Effect from Land to the Sea on Polar Continental Margins

5.1 Ice Streams

Ice streams are ‘rivers of ice’. The continental ice that makes up ice sheets flows towards the ice sheet edges both onshore and offshore. The speed of the ice generally increases from the interior to the external parts of the ice sheet as the ice sheet becomes thinner. Due to a control exerted by the topography of the ice sheet and the topography of the substratum, the ice flow focuses in fast-moving “ice streams”, where maximum velocities can be of the order of a few kilometres per year. The thickness of the ice stream is such that it grounds on the seabed in offshore areas. During glacial maxima, the ice streams are commonly grounded at the continental shelf edge, so that the entire continental shelf is subject to erosion and transport of sediments below the ice (Fig. 7).

Because the ice streams advance periodically on polar continental shelves in response to changing climate, the erosion and transport of sediment is often called “bull-dozing effect”.

The sediment is delivered at the continental shelf break onto the continental slope facing the mouth of the glacial trough where the ice streams flow. The resulting sedimentary apron is called “trough-mouth fan (TMF)” and represents the major offshore depo-center in a glacially-influenced continental margin. Because the orbitally-driven climate change is cyclic (Milankovic cycles), and each cycle is composed by a longer gradual cooling phase, a short-lived cold peak (glacial maximum), followed by a very rapid warming (deglaciation) and, finally, a

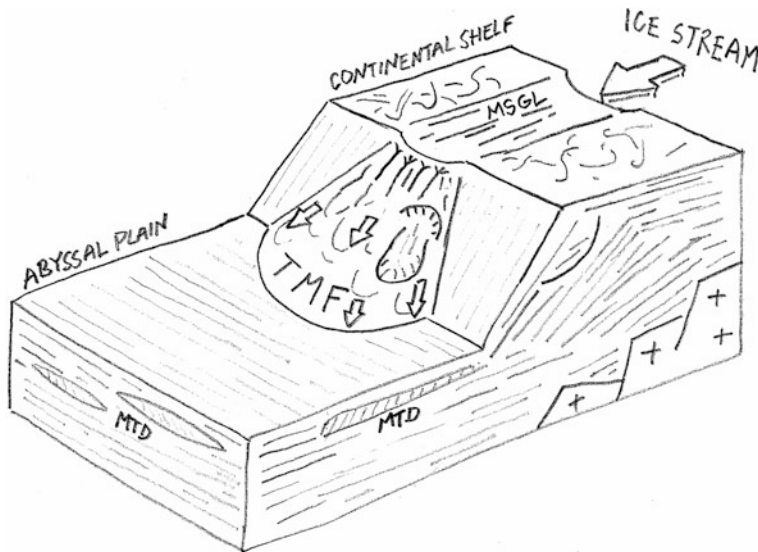


Fig. 7 The mechanisms that determine the morphology of ocean seafloor in polar areas (mostly passive) differ substantially from low latitude ones. The main driver for sediment transport from the continent to the ocean margin here is an ice stream, which is the fast flowing part of an ice sheet. An ice stream may be considered a ‘river of ice’. Ice streams erode deeply the land masses and the continental shelves, as the ice thickness allows for grounding of the ice below sea level, excavating glacial troughs, bound by higher relief banks covered by slow-moving, or still, ice. The ice streaming leaves impressive mega scale glacial ideations (*MSGL*) on the sea floor of glacial troughs. The eroded sediments are transported at the base of the ice stream and are released at the grounding line, where ice detaches from the seafloor. During periods of glacial maxima this line typically coincides with the continental shelf break. The sediments, over-consolidated by the weight of the ice and mixed during sub-glacial transport, is transferred down the continental slope via the formation of dense debris flows, whose stack forms a trough-mouth fan (*TMF*). The massive sediment input concentrated in short glacial maxima periods obliterates the previous slope morphology and does not allow for the formation of deep sea canyons. Hyper-pycnal flows of sediment laden melt waters typically incises short-lived gullies on the upper slope. The episodic mode of sediment accumulation on the continental slope, where the sub-glacially derived debris flows are deposited on water rich interglacial glaci-marine sediments, or de-glacial plumes, favours the gravitational collapse of the margin, with the formation of very large submarine landslides and mass transport deposits (*MTD*)

relatively short warm (interglacial). The sediment transported to the grounding line by an advancing ice stream is thus kept on the continental shelf until the grounding line reaches the shelf break during the glacial maximum. It is only at this stage that sediments are delivered directly to the upper continental slope, producing stacks of “glacigenic debris flow deposits”. Sedimentation rate during these short periods can be extremely high, in the order of 10 m per thousand of years.

At the onset of the deglaciation phase that follows a glacial maximum the melting of the ice produces a huge basal melt-water flow that transports fine grained sediments to the water column, where the coarsest fraction (silts and sands) sinks to

the seafloor forming hyper-pycnal flows, while the finest fraction (clays) settles through flocculation. The resulting pairs of coarse and fine sediments form laminated deposits called “plumites” on the upper continental slope. They are usually covered by slow sedimentation of hemipelagic sediments during the interglacial period.

TMFs are therefore composed by alternations of glacially derived debris-flow deposits (accumulated during glacial maxima) and plumites/hemiplagites (accumulated during deglaciations and interglacials). The periodic and rapid accumulation of glacially derived debris flow deposits prevents the development of submarine canyons on TMFs.

5.2 *Ice Grounding at the Continental Shelf Edge*

The shear stress exerted by the ice streams flowing grounded on the continental shelves, combined with the weight of the ice on the seabed, produce a remoulding of the underlying sediment to form layers of “till”, unsorted structure-less sediment, made of a fine grained matrix that incorporates poorly rounded clasts of very variable size and composition. Tills are typically over-consolidated sediments, meaning that the maximum stress that they have experienced is higher than the stress they experience in situ. Consequently, their water content and porosity are low compared to normally consolidated marine sediments, and their resistance to shear is high.

An important consequence of the mechanisms of sediment erosion and transport on glacial margins is that the water depth in high-latitude continental shelves is deeper (the shelf edge can be 300–500 m deep) than on low-latitude ones, where the maximum depth of about 120 m is controlled solely by the eustatic sea-level change. In addition, the erosional forces of ice-streams can excavate the seafloor, producing continental shelf troughs with water depths exceeding 1000 m on the inner shelf (this is particularly common on the Antarctic margins). The distinctive morphological evidence of ice streaming is represented by Mega-Scale Glacial Lineations (MSGL).

Finally, due to the gradual thinning of the grounded ice, the basal forces decrease from the inner to the outer continental shelves, so that often the inner shelves are carved in hard rock basement (the sediments are entirely removed by basal erosion), while sediment deposition (till layers) occurs on the outer shelves. Such change in the composition of the substratum is nicely reflected in the seabed morphology.

5.3 *Ice Retreating During Deglaciations*

The retreat of the grounded ice streams from continental shelves during the de-glaciation that follows the ice maxima occurs in steps. This is because the

grounding of the ice depends on the balance between the buoyancy forces exerted by the increasing sea level and the decreasing weight of the ice, becoming thinner as melting continues. The ice streams remain grounded on a certain line until they are lifted off the seafloor; the grounding line then retreats instantaneously to a different line landwards that is established by the existing topography. Such grounding line retreats can be of tens of kilometres. Each lift-off phase produces the release of mega-icebergs that carve the seafloor in large water depths on the outer continental shelves.

The prolonged permanence of the grounding line in a given location produces the delivery of sediments at the grounding line also during ice stream retreat. Such deposits are named “Grounding Zone Wedges (GZW)” and are composed of a mix of tills (on the inner part, formed below the ices) and debris flow deposits and melt-water plume deposits (on the outer part).

More information on the above is available in Chapter “[Submarine Glacial Landforms](#)”.

6 Compaction Disequilibrium—Pore Fluids Overpressure in Marine Sedimentary Sequences

The accumulation on the seafloor of sediment grains settling from the water column leaves water-filled voids between particles that become incorporated in the sedimentary structure below the seafloor. The volumetric percentage of voids (porosity) can be as high as 70–80% in the uppermost few centimetres of an open marine sedimentary sequence and rapidly decreases with depth below the seafloor, with an exponential law that depends on the compressibility of the bulk sediment. The process of porosity reduction by expulsion of pore fluids is called “consolidation” or “compaction” and is driven by the gravity forces induced by the weight of the overlying sediment acting on the grains in a given position of the sedimentary sequence. In a normally-consolidated sedimentary sequence, the submerged weight of the grains (lithostatic stress) is sustained by the underlying grains because the pore fluids have partly migrated out of the pore space to accommodate compaction. The pore fluid pressure therefore is hydrostatic, and the sedimentary sequence is said to be in compaction equilibrium (Fig. 8).

However, compaction disequilibrium is a common situation in marine sedimentary sequences, at any depth below the seafloor, and occurs when pore fluid pressure is above hydrostatic. This occurs when the pore fluids cannot migrate out of the pores and the lithostatic stress acts not only on the rigid skeleton of the sediment (the grains) but also on the pore fluids. If the pore fluid pressure equals the lithostatic stress, the sediments are in a critical situation in which the resistance to shear is null (the grains ‘float’ in the pore fluids) and the sediments tend to flow as a fluid. The flow of fluidised sediments in many cases is upwards, along pre-existing

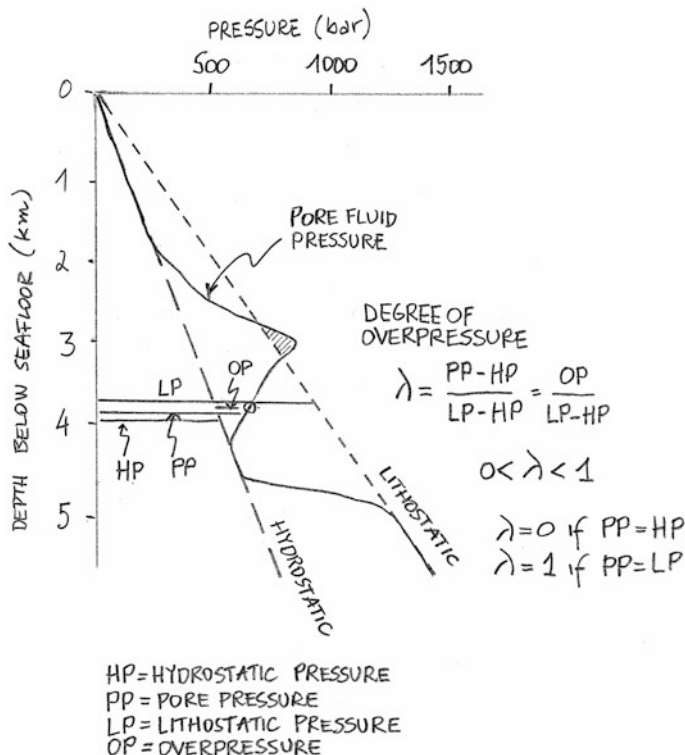


Fig. 8 Diagram that describes the process of compaction disequilibrium, the main driver for fluid and mass transport from the sedimentary sequence to the seafloor in the form of mud diapirism, mud volcanism, and fluid venting in general. The pore fluid pressure in a normally consolidating sequence equals the hydrostatic pressure. If the permeability of the sediment does not allow for fluid drainage during the increasing lithostatic weight that accompanies burial, or if the fluid volume in the pores increases due to diagenetic or catagenetic reactions, an overpressure develops (pressure in excess of the hydrostatic one), and compactions disequilibrium occurs. In compaction disequilibrium conditions, the effective shear strength of the sediment is decreased until it is reduced to zero when the pore fluid pressure equals (or exceeds) the lithostatic pressure. In such conditions, the sediment behaves as a fluid and flows along fractures (at times induced by hydro-fracturing of the surrounding sediments and rocks) mostly upwards, until a mixture of sediment, water, and gases erupts on the seafloor

fractures or faults, or along newly formed fractures caused by a process called “hydro-fracturing”.

Compaction disequilibrium is favoured by low permeability and high compressibility of the sediment, and is driven by the following factors.

Stress-related factors. These are important when the sedimentation rate is high (low permeability, high compressibility clays develop excess pore fluid pressure with sedimentation rates exceeding 1 mm per year), or there is a rapidly increasing tectonically induced load (e.g. thrusts emplacement at the front of accretionary prisms).

Pore fluid volumetric increase. These factors are important in the case of aquathermal expansion of pore fluids due to extreme temperatures, mineral transformation (illite de-hydration, illite-smectite transformation, gypsum dehydration to anhydrite), and hydrocarbon generation (especially in near surface area biogenic methane generation and natural gas hydrate dissociation).

Pore fluid movement. These factors are relevant in the case of natural osmosis across semi-permeable membranes, increased hydraulic head from aquifers charged on land (in near shore areas), and hydrocarbon buoyancy.

The manifestations of fluid migration in marine sedimentary sequences are mud volcanoes and diapirs, gas chimneys, pockmarks, fluid vents in general, and bottom simulating reflectors in seismic profiles, produced by the acoustic impedance contrast between overlying gas-hydrate-bearing sediments, and underlying free gas in the pore space.

More information on the above is available in Chapter “[Cold Seep Systems](#)”.

7 Oceanic Circulation, Waves and Tides, and Sea Level Change

7.1 Bottom Currents

Water masses in the oceans move as a consequence of density differences induced by changes of temperature and salinity (“thermo-haline circulation”), and the stress induced by winds (“wind-driven circulation”). When moving, water masses are subject to the Coriolis force, resulting from the Earth rotation, which deflects any moving object (including water masses) on the Earth to the right in the northern hemisphere, and to the left in the southern hemisphere.

Water masses displacement under these forces occurs at any water depth, and includes “bottom waters” (those waters that are in contact with the seabed). Bottom currents are defined as any ‘persistent’ water current near the sea-floor, generally with a net flow in the along-slope direction. From this definition it is obvious that turbidity currents, which also move along the seabed, driven by gravity, are not bottom currents because they result from episodic, though very powerful, events.

Bottom waters move preferentially along-slope, with varying velocities, typically in the order of a few centimetres to decimetres per second, and are pushed by the Coriolis force against the eastern ocean margins in the northern hemisphere, and along the western ocean margins in the southern hemisphere (Fig. 9).

Oceanic water masses moving along the seabed carry in suspension sediment particles captured from the vertical settling through the water column and from the suspensions produced by turbidity currents. If velocity at the seabed is sufficiently high, bottom currents can inhibit settling or even re-suspend previously settled

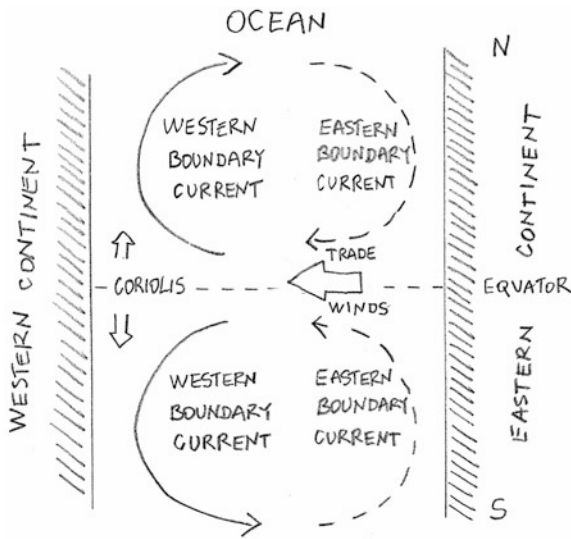


Fig. 9 In a highly simplified way, oceans (except for the Arctic and the Southern Oceans) can be described as a water mass bound by continents to the east and west. The trade winds are easterly winds (blowing from the East) in the tropics that trigger surface oceanic currents towards the western current. The Coriolis effect (push to the right in the northern hemisphere, and to the left in the southern hemisphere) drives a general surface circulation system with intensified currents on the western boundary of the oceans, and a less intense, return current on the eastern boundary. The Gulf Stream is formed in this way. The water movement is transferred down to about 1000 m water depth and interacts with the upper slope of the ocean margins. Bottom currents may erode, transport and deposit sediments, mostly fine grained, to form sedimentary deposits called Sediment Drifts. Coupled with the wind-driven oceanic circulation is the thermo-haline circulation, driven by water density contrasts between the polar areas and the lower latitudes, with a mainly latitudinal spread and an extension to the deepest levels of the oceanic water masses

particles, causing a net removal of sedimentary layers. When the flow velocity decreases, the suspended particles settle again at the seafloor to form mounded or sheeted sedimentary deposits called “sediment drifts”. They are typically very large sediment bodies (hundreds of kilometres in horizontal dimension) generally composed of fine-grained particles and elongated against continental margins, from which they are separated by a moat. Sediments deposited, or significantly affected, by bottom currents are called ‘contourites’ (bottom currents following the slope contour are also called contour currents).

More information on the above is available in Chapter “[Contourite Drifts and Associated Bedforms](#)”.

7.2 Waves and Tides

The motion of oceanic water masses interacts with the seabed also in shallow coastal areas. Such interaction produces very characteristic seabed morphologies and sedimentary structures that permit the identification of the sedimentary environment in the fossil marine sedimentary record.

Waves are generated by wind stress on sea surface. Water particles are moved orbitally, with decreasing energy with depth. Waves transport energy across the oceans, but they do not transport water. When the orbital motion of water particles within waves interacts with the seafloor, complex mechanisms of water transport are generated, producing erosion, transport and deposition in loose beach sediments, and hydraulic action, abrasion, attrition, and even solution on steep hard-rock cliffs.

Tides are generated by the gravitational pull of the moon and the sun. In shallow water they generate tidal currents that control the shape and extent of river deltas and the topographic profile of sandy beaches. Tides induce processes of solution, suspension, saltation and traction at the sediment-water interface.

More information on the above is available in Chapter “[Shallow Coastal Landforms](#)”.

7.3 Sea Level Change

Sea level is controlled by the gravity field of the Earth acting on the oceanic water masses. The volume of the oceanic waters varies throughout the geological time, primarily as a consequence of:

- Volume of the ocean basins
- Mass of the water filling the ocean basins
- Volume of the water filling the ocean basins

Changes in sea level occur over a broad range of temporal and spatial scales. Regional sea level changes can occur as a consequence of local temperature and salinity anomalies in the water masses, water mass circulation, and regional atmospheric pressure anomalies. The changing distribution of continents and oceanic basins produces changes in the mean sea level at the scale of millions of years. For the purpose of the impact on seabed morphology, a good assumption is to consider the two factors universally considered as the drivers of global sea level (GSL) change: the exchange of water between continents and oceans, and the temperature of the oceanic water masses.

Orbitally-driven climatic change results in cyclic alternation of glacial and interglacial periods that in the last one million years have alternated with a period of 100,000 years. Before, glacial-interglacial cyclicity had a period of approximately 40,000 years. Such climatic cycles produce a periodic change in ice sheets and

glaciers volume and a corresponding global sea level change. At the present day (an interglacial period) ice sheets and glaciers trap in the solid state $33.2 \times 10^6 \text{ km}^3$ of water ($2 \times 10^5 \text{ km}^3$ of which in glaciers), while the total volume of the oceans is $1.3 \times 10^9 \text{ km}^3$. The two largest ice sheets of today are in Antarctica and Greenland (80 and 8% respectively of the global fresh water reservoir). During the last glacial maximum (approximately 20,000 years before present) the global sea level was approximately 120 m lower than today. This was not only the result of the transfer of mass of water from the ocean to the continents in the form of snow and ice, but also of the density change of the oceanic water masses induced by a lower temperature of the upper layer of the ocean (700 m). As a term of comparison, the observed sea level rise from 1993 to 2003 (2.4 mm/year) can be explained by a 50% contribution from thermal expansion of seawater, and 50% contribution from ice sheets and glacier water mass transfer from continents to the ocean.

The varying sea level, at the scale of thousands of years, has a profound impact on seabed morphology on the continental margins, the most obvious of which is the location of the continental shelf break on low latitude (non-glacial) continental margins, which is controlled by the global sea level oscillations. The rising and lowering of the sea level also leaves an important imprint on the morphology of continental shelves from the edge to the shoreline.

8 Chemical Precipitation/Dissolution and Bioconstructions

As a mixture of organic and inorganic compounds in a salty aqueous solution, marine sediments represent a reactive environment in which chemical reactions occur from the very early stages after particle deposition. The changes (mostly chemical) that affect marine sediments after their deposition are identified with the term “diagenesis”. “Early diagenesis” identifies the changes in marine sediments that occur in the upper few hundred meters where temperature is relatively low ($<\sim 150^\circ\text{C}$), and porosity is high enough to preserve the necessary quantity of water to participate in the reactions. Besides compaction, already described in Sect. 6, early diagenesis includes biological processes produced by burrowing organisms, precipitation of new minerals, transformation and dissolution of existing minerals, and degradation of organic matter by micro-organisms. Mineral transformation and hydrocarbon generation have already been mentioned among the factors that drive fluid migration within sedimentary sequences.

In this section we introduce two mechanisms of chemical precipitation that generate processes that affect seabed morphology: “authigenesis”, which refers to processes by which minerals form within sediments, and salt precipitation on the seafloor from “evaporation” of seawater.

8.1 Methane-Derived Carbonate Precipitation

The most common authigenic minerals are carbonates that precipitate at the interface between the sulphate-reduction zone (above) and the methane-bearing zone (below). Such interface is called Sulphate-Methane Transition Zone (SMTZ) and can occur from a few centimetres below the seabed to several tens of metres below.

The origin of methane at shallow subsurface depth in marine sediments is two-fold:

In situ biogenic methane. Bacteria living within the sediments oxidise the residual organic matter trapped in the pore space in aerobic conditions (respiration using free oxygen from the pore waters). In case of abundance of organic matter and high sedimentation rate in fine grained (low permeability) sediments, bacteria begin to extract the oxygen from nitrates, manganese oxides, iron oxides, and, finally, the sulphate ion (SO_4^{2-}) dissolved in the pore water. This occurs after all oxygen from the pore spaces has been used. If all the available sulphates are used, the remaining organic matter is metabolised via fermentation by methano-genic bacteria, and biogenic methane is produced *in situ*.

Upward migration of deep-sourced methane. Methane produced by maturation of organic matter to generate hydrocarbons (oil and alkane gases)—a process called catagenesis—produces methane that migrates upwards through faults and fractures.

In the majority of deep water oceanic environments, such methane is present within shallow sediments in the solid, hydrated form.

At the SMTZ, microbial activity is commonly associated with the anaerobic oxidation of methane (AOM), which is carried out by syntrophic associations between sulfate-reducing bacteria and methane-oxidising archaea. Methane-trophic archaea oxidise methane anaerobically via sulphate reduction, releasing CO_2 in the pore water, with production of bi-carbonate ion (HCO_3^-) that induces oversaturation of the pore water with respect to calcite and other carbonate minerals. Calcite therefore precipitates to form nodules, crusts, and even chimneys surrounding methane escape conduits. Relict carbonate mounds and chimneys are often associated to mud volcanoes, pockmarks, and fluid venting zones, affecting intensively the seafloor morphology, and often providing a hard substratum in soft seabed for deep coral communities to grow.

8.2 Weathering at Hydrothermal Vents

Mostly in volcanic areas, along the mid-ocean ridges and around submarine volcanoes in general, a huge hydrothermal water circulation system is established in the subsurface as a consequence of the temperature difference between the near-surface magmas, or newly solidified rocks, and the bottom oceanic waters. A peculiar characteristic of the rocks near volcanic centres is their high degree of

fracturing, consequent of contraction during cooling. Seawater can circulate through these fractures. The water at depth is heated to temperatures exceeding 350 °C and moves upwards driven by buoyancy forming a plume of rapidly ascending hot waters that are discharged at the seafloor in the oceanic water column. The sites of hot water discharge are called “hydrothermal vents”. In turn, cold bottom water is driven from the seafloor down to balance the ascending water flow (Fig. 10).

There are different chemical reactions between seawater and rocks within these convective cells: During the descent of cold seawater through the permeable increasingly warmer basaltic rocks, the fluids lose almost entirely the magnesium, calcium, and sulphate ions through the precipitation of Mg hydroxides in clays (olivine and interstitial glass in the basalts are replaced by smectite clay minerals) and anhydrite (CaSO_4). The water composition changes further at the bottom of the convective cell, where temperatures are highest. During the ascent, the waters reach quickly, without important heat loss, the cold temperature at the seafloor and release large amounts of metals forming crusts of poly-metallic sulfide deposits (particularly pyrite (FeS) and chalcopyrite (CuFeS_2)). The encrustations around the vent site form distinctive “chimneys”, or smokers (high temperature “black smokers” and low temperature “white smokers”). The mineral particles suspended in the water, gradually settle and further promote mineral exchange, removing phosphate, arsenic and vanadium from the seawater. Such extreme environments (characterised by high pressure, very high temperature, and reactive chemical environment), are sites of very active deep sea ecosystems. The mineral precipitation and the benthic communities determine a peculiar morphology of the seabed. Poly-metallic

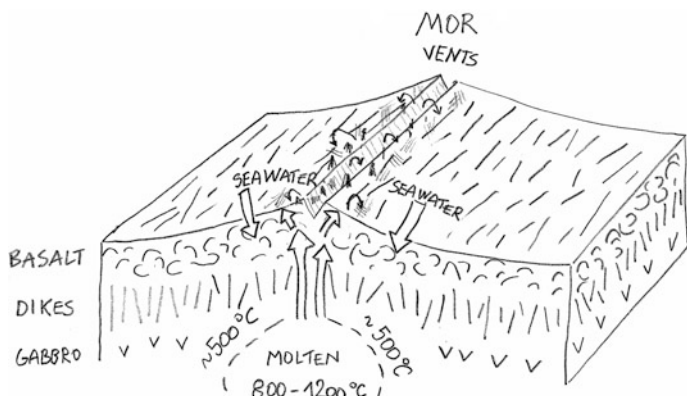


Fig. 10 Around mid-ocean ridges (MOR) the heat produced at shallow depth by the rising mantle induces a vigorous convective underground water circulation that implies rock-water mineral exchanges both in the down-going and up-going waters. Hot ion-enriched water venting at the seafloor release poly-metallic sulphides that accumulate massively at or near the surface. Such deposits are the target of the nascent industry of deep sea mining

sulphides, together with Fe–Mn nodules, constitute a potential resource of strategic minerals that the mining industry (deep sea mining) is considering for economic purposes.

8.3 Salt Deformation

Sea water evaporation to a level that alters significantly the concentration of dissolved ions induces salt precipitation. This occurs when an oceanic basins suffer from a reduced water exchange with the global ocean, and evaporation exceeds the influx of water from rivers and precipitation. As an example, the Mediterranean Sea of today needs a constant inflow of marine water from the Atlantic Ocean through the Gibraltar Strait to compensate for an excess in evaporation.

Gateways that control the water exchange in enclosed basins form during the early phases of the development of an ocean, during the rifting of a continent, or in the final stage of an ocean, when, due to oceanic lithosphere consumption at subduction zones, a relict oceanic basin becomes nearly entirely surrounded by landmasses.

With the present-day composition of seawater, evaporation produces a sequence of mineral precipitation: Calcite first (CaCO_3), followed by gypsum (CaSO_4), halite (NaCl), and at last, various chlorides and potassium sulphates. In evaporitic sequences formed by gradual inflow of seawater and river water in a sedimentary basin, the dominant salt is often halite, which can attain thickness of hundreds of metres and at times a few kilometres. Halite has a peculiar property of being a low-density mineral (2160 kg m^{-3}) that reacts in a ductile way to geological stress. Salt may rise diapirically when buried by higher density formations, and, most importantly, spreads laterally and vertically when undergoing a differential stress (differential load from sediment accumulation), or glides along an inclined substratum under the gravity force.

Salt structures often breach the seafloor, or deform the shallow sediments with a dramatic impact on the seabed landscape.

8.4 Submarine Karst

In certain areas of the world's continental margins, low-temperature soluble rocks outcrop at the seafloor. These are primarily carbonate rocks, but evaporites (halite and gypsum primarily) must also be considered.

Oceanic waters are normally saturated or supersaturated with respect to calcium carbonate (CaCO_3). A certain water depth exists below which seawater is undersaturated. This depth is called Calcite Compensation Depth (CCD) and varies from about 4000–5000 m in the low latitude oceans. In polar areas and in upwelling zones, the CCD can be shallower. However, there is a possibility that calcium

carbonate can dissolve in supersaturated seawater, well above the CCD. This occurs when two fluids with different salinities combine as a consequence of the non-linearity of the CaCO_3 saturation curve in water. Rock dissolution structures such as sink-holes and dolines can therefore form underwater where fresh water flows mixes with seawater in coastal zones or along ocean margins. The process of submarine karst in carbonate rocks may be so widespread to control the morphology of underwater escarpments worldwide.

Contrary to calcium carbonate (whose origin is mostly non-evaporitic), evaporitic minerals like halite and gypsum are soluble in seawater. Evaporitic formations are normally separated from the seawater by thick layers of deep sea muds and sands. However, salt deformation may bring halite and gypsum in contact with seawater and dissolution occurs. The most spectacular evidence of submarine karst in evaporitic rocks are in the Eastern Mediterranean, where a number of submarine brine lakes have formed collecting the dense brines into rimmed seafloor depressions in which salt recrystallisation from the brines often occurs. Salt dissolution in the subsurface is postulated to occur also as a consequence of the downward flow of seawater triggered by the osmotic properties of marine sediments covering salt deposits.

8.5 *Benthic Organisms*

There are many different species of benthic marine organisms. These include animals or plants that live on, in, or attached to the sea floor. The size of benthic animals (zoobenthos) varies considerably. Microbenthos is composed of organisms smaller than 0.1 mm in size, such as bacteria, diatoms, ciliates, amoeba, flagellates, foraminifera, or bacteria. Organisms between 0.1 and 1 mm in size compose the meiobenthos, and include nematodes, foraminifers, copepods and ostracods. Larger organisms compose the macrobenthos, including polychaete worms, bivalves, echinoderms, sea anemones, corals, sponges, sea squirts, and larger crustaceans. Among plants, diatoms are microscopic organisms, while seaweeds are macroscopic organisms.

Colonies of such organisms, or entire ecosystems based on benthic organisms, may impact on seafloor morphology and habitats. With the term “bioconstructions”, reference is made to durable elevated biogenic structures formed by the aggregation and accumulation of their hard (calcareous) skeletons.

The largest morphological imprint on the sea floor is produced by coral colonies (deep water and shallow water coral reefs), and *Posidonia oceanica* meadows in shallow waters. In addition, the ecosystems living around cold and hot hydrothermal vents may support associations of benthic organisms (tube worms, various bivalves, also of very large dimensions) that may become important from the morphological point of view. Deep water coral reefs are often associated to methane seeps, but the link between deep corals and methane seeps depends on the

presence of a hard substratum made of authigenic carbonates (needed by the corals for fixing their skeleton to the sea floor) rather than to a primary source of food.

More information on the above is available in Chapter “[Cold-Water Carbonate Bioconstructions](#)”.

9 Human Activity

Human activity on the seafloor is capable of affecting its morphology at a local scale. The use of the seafloor for economic activities is rapidly increasing, also in the deep sea, in spite of the persisting deficit of knowledge of the marine environment. The primary use of the seafloor is related to the exploitation of mineral resources (mainly hydrocarbons), communications, and fishing. The hydrocarbon industry has moved operations from the continental shelves to the slopes, and the use of seabed installations for hydrocarbon extraction is becoming common. Furthermore, pipelines with diameters varying from about 75 cm to 1.8 m are laid on the seafloor, in which they may only partially sink, and therefore they impact the morphology in a way that is detectable in high-resolution surveys. The trenching of pipelines is operated close to the landfalls for protection from wave erosion, currents, and fishing. Communication cables are smaller in size (a few centimetres in diameter), and they have a lower morphological impact. In shallow water the largest impact is produced by bottom trawling. This is an industrial fishing method where a large net with heavy weights kept open by the use of heavy ‘doors’ at the sides, is dragged on the seafloor in water depth as deep as 2000 m, collecting in the net anything is encountered on or near the sea floor. The width of the trawl can be several tens of metres.

More information on the above is available in Chapters “[Applied Geomorphology and Geohazard Assessment for Deepwater Development](#)”, “[Seabed Mining](#)” and “[Fishing Activities](#)”.

Suggested Reading

Section 2

Cox A, Hart RB (1986) Plate tectonics: how it works. Wiley-Blackwell

Section 3

Sengupta SM (2012) Introduction to sedimentology. CBS Publisher

Section 4

- Moscardelli L, Wood L (2007) New classification system for mass transport complexes in offshore Trinidad. *Basin Res* 201:73–98
- Shipp RC, Weimer P, Posamentier HW (2011) Mass-transport deposits in deepwater settings. SEPM Special Publication 96, Tulsa, Oklahoma
- Weimer P, Link MH (2013) Seismic facies and sedimentary processes of submarine fans and turbidite systems. Springer Science & Business Media

Section 5

- Hambrey MJ, Christoffersen P, Glasser NF et al (2007) Glacial sedimentary processes and products. IAS Special Publication 39, Wiley

Section 6

- Judd A, Hovland M (2009) Seabed fluid flow: the impact on geology, biology and the marine environment. Cambridge University Press

Section 7

- Rebesco M, Camerlenghi A (2008) Contourites. Development in Sedimentology Series 60, Elsevier, Amsterdam

Section 8

- Burdige DJ (2006) Geochemistry of marine sediments. Princeton University Press
- Dean WE (2014) Marine evaporites. In: Harff J, Meschede M, Petersen S, Thiede J (eds) Encyclopedia of marine geosciences. Springer, pp 1–10
- Fleury P, Bakalowicz M, de Marsily G (2007) Submarine springs and coastal karst aquifers: a review. *J Hydrol* 339:79–92
- Harris PT, Baker EK (2011) Seafloor geomorphology as benthic habitat: GeoHAB atlas of seafloor geomorphic features and benthic habitats, 1st edn. Elsevier
- Tivey MK (1991) Hydrothermal vent systems. *Oceanus* 34:68–74

Section 9

- National Research Council (1989) Our seabed frontier: challenges and choices. Report of the committee on existing and potential uses of the seafloor, Division on Engineering and Physical Sciences; Commission on Engineering and Technical Systems. National Academic Press

Shallow Coastal Landforms

Fantina Madricardo and Federica Rizzetto

Abstract Shallow coastal landforms are often highly dynamic environments due to natural and anthropogenic pressure. The action of waves, tidal currents, rivers inputs, sea-level rise, climate, geology and coastal engineering shapes their morphology at different temporal and spatial scales. The recent technological development of the multibeam echosounder, LiDAR and satellite systems now permits the mapping of shallow coastal landforms at very high resolution, even for depths shallower than 10 m, providing improved understanding of these morphological features. In this chapter, we provide a review of the main shallow coastal submarine landforms and of the newest methods to map them and measure their changes over time.

1 Introduction

Shallow coastal submarine landforms, commonly defined as bedforms, are submerged morphological features that can be found on the seafloor in nearshore waters. They have a large spectrum of sizes and shapes and are the result of a combination of different forcing factors and processes, such as sea-level history, geological characteristics of the coast, river inputs, waves and tides. These processes determine ‘the adjustment of topography and fluid dynamics involving sediment transport’ (Wright and Thom 1977). Cowell and Thom (1994) group them into four overlapping classes defined on the basis of the different spatial and temporal scales involved in the coastal evolution and landform formation: instantaneous, event, engineering and geological time scales (Fig. 1a). The instantaneous time scales involve the evolution of morphology, such as the migration of dunes

F. Madricardo (✉) · F. Rizzetto
ISMAR-CNR, Arsenale—Tesa 104, Castello 2737/F, 30122 Venezia, Italy
e-mail: fantina.madricardo@ismar.cnr.it

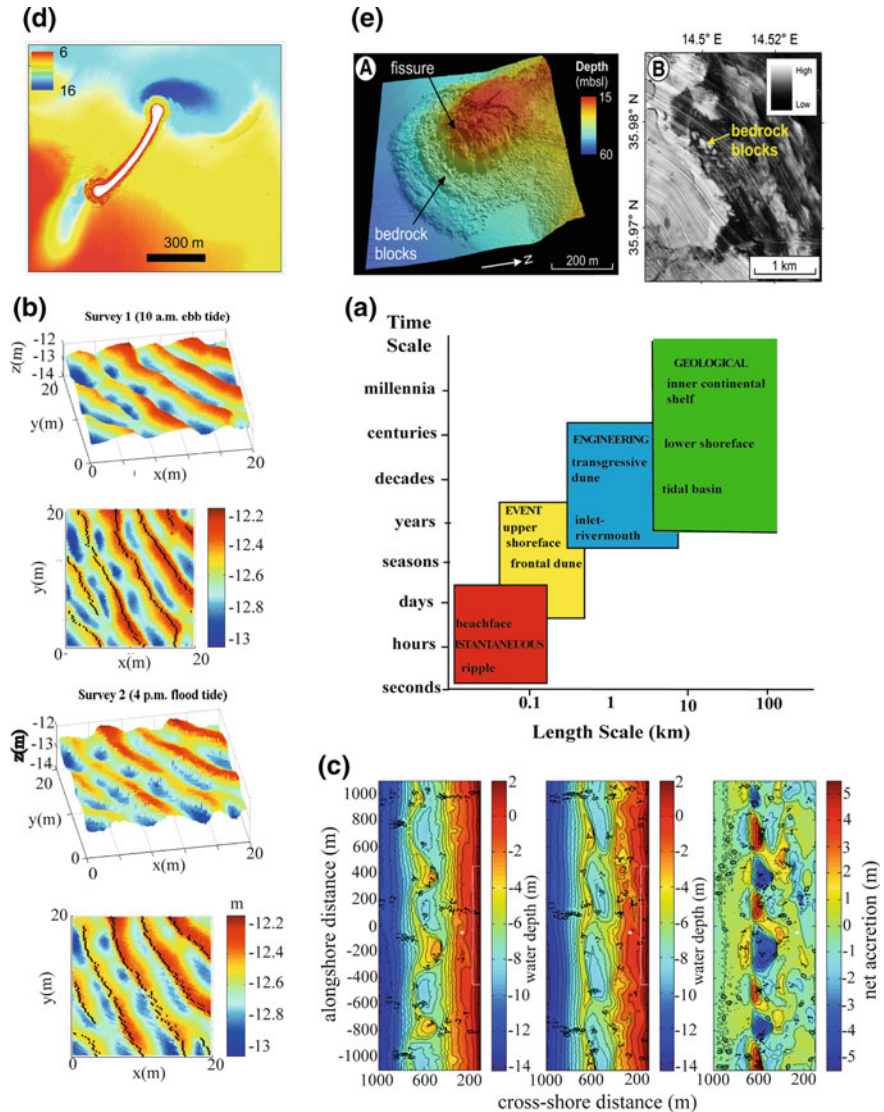


(Fig. 1b), or the onshore migration of an intertidal bar over a single tidal cycle. The event time scales include changes over time spans from individual/tide events to seasons. An example is illustrated in Fig. 1c where the morphological changes of a beach shoreface resulting from a cluster of storms are illustrated; in the right panel, the net morphological change shows erosion and deposition areas as a consequence of the storm sequence. The engineering time scales are time scales of years or centuries and include changes such as migration of tidal inlets and the build-up of sediments in beaches, or direct consequences of engineering interventions.

◀Fig. 1 **a** Definition of spatial and temporal scales involved in coastal evolution (modified from Cowell and Thom 1994). **b** Example of instantaneous time scale: change of orientation of dunes during a tidal cycle in the Lido Inlet of the Venice Lagoon, Italy (from Madricardo et al. 2015): passing from the Survey 1 to Survey 2 the dunes change orientation and the automatically picked position of the crests (*black points*) is shifted. **c** Example of event time scale: changes of a part of shoreface of the Truc Vert beach, located south of Bordeaux, France, due to storms. Panels show the topography and bathymetry as a function of alongshore and cross-shore position before (*left panel*) and after (*middle panel*) the storm cluster and the net morphological change over less than two months (Reprinted from Coco et al. 2014, with permission from Elsevier). **d** Example of engineering time scale: scours holes appeared after the construction of artificial breakwaters (shown in *white*) outside the Chioggia Inlet, Venice Lagoon, Italy within a time scale of about 8 years (from Fogarin 2015, data available in Madricardo et al. 2016). **e** Example of geological time scale: a 3-D bathymetric DTM of bedrock blocks located along the southern edge of Sikka l-Bajda reef close to the Island of Malta (Reprinted from Micallef et al. 2013, with permission from Elsevier)

An example of the latter is given in Fig. 1d): over a time span of ca 10 years, an artificial breakwater built in front of a tidal inlet induced erosion (and consequent development of large scour holes) at the edges of the hard anthropogenic structure and formation of a sand bank due to sediment redeposition close to one of the two scour holes. The geological time scales extend from decades to millennia, and are related to long term driving forces like sea-level changes, climate and tectonics. In Fig. 1e) we show the 3-D bathymetric Digital Terrain Model (DTM) of bedrocks blocks generated by lateral spreading along the edge of a reef (Micallef et al. 2013).

The first systematic classifications of shallow coastal landforms date back to the late 1960s (e.g. Allen 1968b, 1971b). At the same time, several flume experiments were carried out to understand the processes responsible for bedform creation and evolution (e.g. Guy et al. 1966). In the late 1970s, the development of sonographs enabled the observation of large bedforms in the continental shelf (see for example Flemming 1980) whereas extensive direct measurements were carried out in the intertidal zone (e.g. Darlymple et al. 1978).

Starting from the 1980s, the implementation of high-resolution swath bathymetry (e.g. Hughes-Clarke et al. 1996; Ferrini and Flood 2005; Duffy and Hughes-Clarke 2005; Ernstsen et al. 2006; Barnard et al. 2011; Micallef et al. 2012; Feldens et al. 2015) allowed three-dimensional mapping and spatial analysis of the small submarine landforms also in very shallow water. The instrumental performance of the underwater acoustic (e.g. interferometric or multibeam echosounder (MBES) systems) and Light Detection and Ranging (LiDAR) systems improved substantially in the 1990s with the advances in technologies such as the Global Positioning System (GPS), and Inertial Measuring Units (IMUs). These instruments provide a cloud of bathymetric points that can be interpolated into a DTM, reaching metric to sub-metric horizontal resolution (Axelsson 2010; Cossio et al. 2011; Pfenningbauer et al. 2011; Montereale-Gavazzi et al. 2016). Moreover, new LiDAR systems can combine terrestrial and bathymetric mapping and it is now possible to obtain detailed emerged and submerged surfaces in a single pass (Fernandez-Diaz et al.

Fig. 2 **a** Plot of mean flow velocity against median sediment size showing stability fields of bed phases (modified from Ashley 1990). **b** Image of sand ripples in a wave tank experiment with the green laser line used to extract the bed elevation profile and **c** the model flow field due to the action of the waves over the ripples (from Nienhuis et al. 2014). **d** Asymmetric ripple terminology (from Boggs 2006, fig. 4.12). **e** Medium dune field and relative 1-D profile (I) ($\lambda \sim 4.5$ m, $h \sim 0.3$ m) in the internal part of the Chioggia Inlet, Lagoon of Venice, Italy (modified from Fogarin 2015, data available in Madricardo et al. 2016). **f** Large dunes in the external part of the Chioggia Inlet, Lagoon of Venice, Italy and relative 1-D profile ($\lambda \sim 120$ m, $h \sim 2$ m) (modified from Fogarin 2015)

2014). The availability of high-resolution maps of shallow water seabed made it possible to characterise coastal submarine landforms and to study their dynamics.

Shallow coastal submarine landforms are best considered in two broad categories—depositional and erosional—each including a large variety of structures that we will describe below.

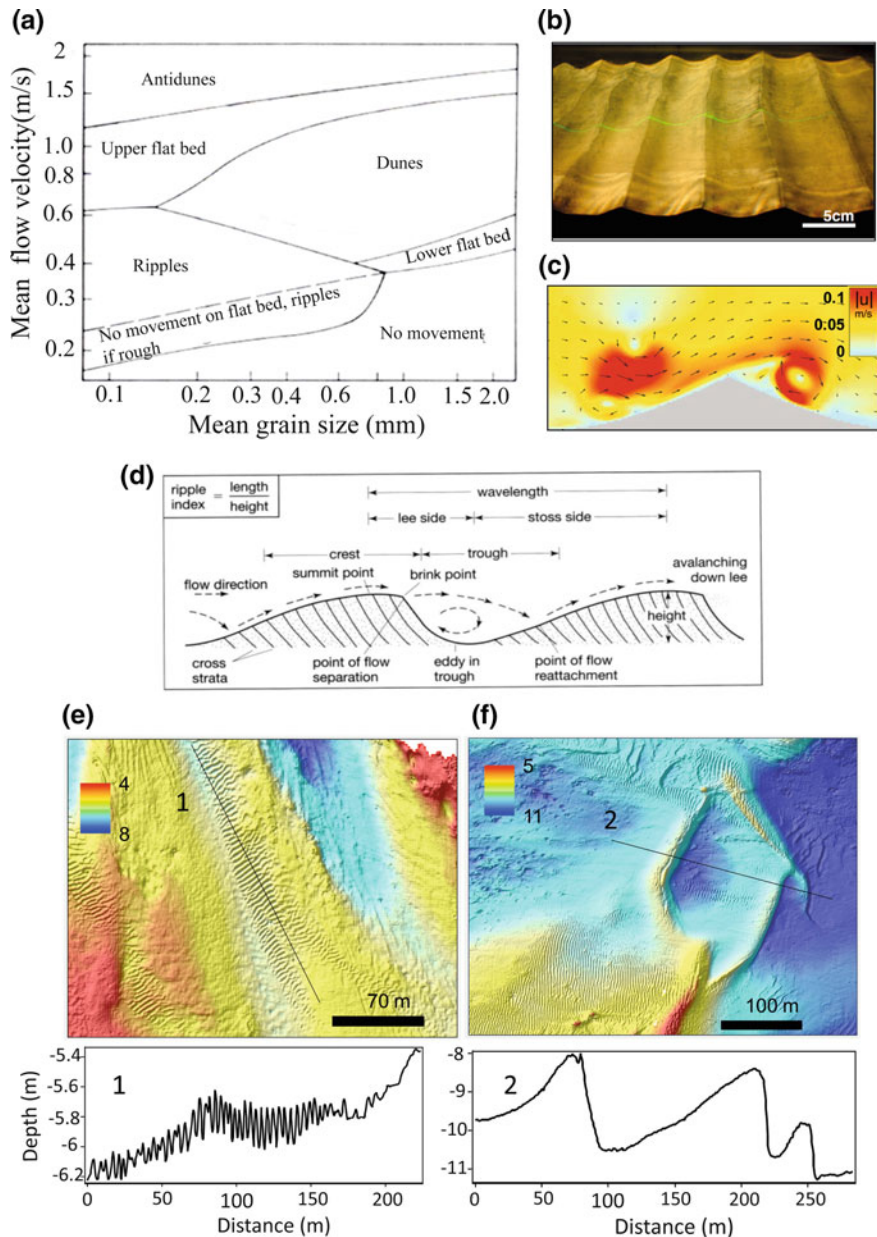
2 Depositional Shallow Coastal Landforms

Depositional shallow coastal landforms can be subdivided into three main categories depending on their orientation relative to the long-term resultant sediment-transport direction. Transverse bedforms and longitudinal bedforms have crestlines oriented roughly perpendicular and approximately parallel to the resultant transport direction, respectively. The maximum divergence from perfectly transverse or perfectly longitudinal is $\pm 15^\circ$; bedforms with intermediate trends (crestlines oriented between 15° and 75° from the vector) are considered to be oblique (Rubin and Hunter 1987; Reading 1996).

2.1 Ripples, Dunes, Sand Waves and Antidunes

Ripples, dunes, sand waves and antidunes are transverse bedforms, commonly present in rivers, tidal environments and continental shelves. The mechanism of their formation and migration is crucial to understand sediment transport and flux dynamics. The bedform type depends on current velocity and sediment grain size, with a transition from ripples to dunes to plane beds and antidunes with increasing flow velocity (Fig. 2a).

Transverse bedforms are classified by their main morphologic characteristics: height (H); crest-to-crest spacing or wavelength (λ); orientation ($^\circ$) and shape (Fig. 2d). There are many different names to describe the transverse bedforms. Here, we follow the classification scheme given by Ashley (1990), which separates them into two main groups: small-scale subaqueous bedforms or ripples (Fig. 2b, c)



and large-scale subaqueous bedforms or dunes (Fig. 2d, e). In general, ripples and dunes are identified as separate bedforms in most classification schemes (e.g. Ashley 1990 and references therein).

Sand ripples may be defined as periodic bedforms arranged transversely to the current and the spacing of which does not exceed 0.6 m (Ashley 1990). They seem to be limited to develop in sands of up to about 0.6 mm in diametre (Fig. 2a).

Ripples are the first bedforms forming when the water velocity exceeds the critical shear stress for motion; they are related to viscous forces in the steep velocity gradients adjacent to the bed and the sand grains (Yalin 1977). In Fig. 2c the results of a numerical simulation are shown for ripples generated by waves reproducing the flow separation and vortex development typical of their morphodynamics. Conventionally, ripples are seen as independent of water depth, although a new model presented by Bartholdy et al. (2015) seems to contradict this view. For their small dimensions, they are generally hard to detect in the field by swath bathymetry, but they have been observed by divers, photography or videos (e.g. Lyons et al. 2002; Voulgaris and Morin 2008) and with the help of very high-frequency scanning sonar systems (e.g. Skarke and Trembanis 2011).

Subaqueous dunes originate on a bed of sand or gravel and their formation depends in some way on turbulence in the whole depth of the flow (Yalin 1977). For descriptive purposes, they can be subdivided as small (0.6–5 m wavelength), medium (5–10 m), large (10–100 m), and very large (>100 m) (Ashley 1990). Unlike ripples, dune size is related to flow depth (i.e., mean dune length and mean height increase with mean flow depth). Their size and shape are also controlled by current speed and grain size (Flemming 1980; van Rijn 1982; Southard and Boguchwal 1990). The maximum height of the dunes is related to the wavelength by the following empirical relation $h_{\max} = 0.16 \lambda^{0.84}$ found by Flemming (2000).

In his review of river dunes, Best (2005) summarised the characteristics of a steady uniform unidirectional flow over asymmetric dunes. The flow has five major regions: (1) at the crest or at the brink point, flow separates and a recirculating eddy is formed, with reattachment occurring downstream of the trough; (2) above the separation zone, there is a shear layer, along which large-scale turbulence is generated in the form of Kelvin-Helmholtz instabilities, creating a wake zone that grows and dissipates downstream; (3) in the dune leeside there is a region of expanding flow; (4) a new internal boundary layer grows downstream of the point reattachment “as flow re-establishes itself and develops a more logarithmic velocity profile”; (5) over the dune crest maximum horizontal velocity occurs.

Owing to the unidirectional residual sediment transport, dunes are typically asymmetric also in active tidal environments, where they display a steeper lee face inclined in the direction of the net sediment movement; weakly asymmetric dunes can sometimes be found in areas of weak tidal asymmetry (Reynaud and Dalrymple 2012). Superposition of small dunes (also called secondary bedforms) over larger dunes (primary bedforms) occur very often (Barnard et al. 2011 and references therein). Secondary bedforms generally reverse their orientation with tidal flows (as is shown for example in Fig. 1b), whereas large primary bedforms keep their orientation and migrate with the residual current (Ernsten et al. 2006). Large dunes may also exhibit small structures that reflect the flow in the opposite (subordinate) direction (Longhitano et al. 2012). The speed of dune migration in the direction of residual transport increases with dune asymmetry, but decreases with dune size.

The precise repeated mapping of dune fields obtained with MBES permits an estimate of dune migration, which provides a quantification of bedload transport (e.g. Williams et al. 2003).

Very large dunes are defined as periodic morphological features with a crest to crest distance of hundreds of metres and amplitudes of a few metres (van Oyen et al. 2013). Very large dunes can migrate with rates of up to tens of metres per year (e.g. Besio et al. 2004; van Dijk and Kleinhans 2005).

Compound tidal dunes, formerly called sand waves by Allen (1980), are formed from a stacking of simple tidal dunes (Olariu et al. 2012). Their architecture, described by Dalrymple (1984), Dalrymple and Rhodes (1995), and Berné et al. (1993), is characterised by internal surfaces that dip in the same general direction as the dominant current, forming a forward-accretion structure (Olariu et al. 2012). Tidal sand waves are observed in many shallow continental shelves; they are characterised by sand abundance and dominated by tidal currents. Their occurrence has been intensively studied in the last two decades (see Besio et al. 2008 for a review).

Most studies have dealt with morphologies that are essentially two-dimensional and have no 3-D shape or curvature (with the exception of Venditti 2007; Maddux et al. 2003a, 2003b; Parsons et al. 2005; Omidyeganeh and Piomelli 2013, who investigated unidirectional flow over 3-D bedforms, and Fraccascia et al. 2016, who explained the orientation and migration of primary bedforms by means of residual currents simulation). However, two-dimentional bedforms are rare in nature (see for example the 3-D dunes in Fig. 2e, f). Three-dimensionality makes the flow considerably more complex, as compared to a 2-D counterpart. As already shown by Allen (1968b), the 3-D dunes can “generate both flow-parallel and spanwise vorticity, and complex convergence and divergence of flow” (Best 2005). Three-dimensionality can now be observed with high detail thanks to the development of remote sensing techniques (e.g. MBES), and the information on dune characteristics from field studies has increased substantially (e.g. Ferrini and Flood 2005; Duffy and Hughes-Clarke 2005, Ernstsen et al. 2006; Barnard et al. 2011; Feldens et al. 2015).

2.2 *Sand Ribbons, Sand Patches, Sand Banks*

Belderson et al. (1982) define three types of quasi-longitudinal depositional bedforms that develop more or less parallel to the tidal flow—sand ribbons, longitudinal sand patches and sand banks.

Sand ribbons are “longitudinal bodies of thinly spread sand that lie on, and are separated by, floors of shell or gravel” (Belderson et al. 1982). These bedforms are associated with strong currents (near-surface mean spring peak tidal or non-tidal currents of about 1 m/s). Some sand ribbons can develop due to the presence of an obstacle mark, but in general they are related to helical circulation—the presence of non-uniform bottom roughness between the sand ribbons and the adjacent coarser

strips gives rise to a non-uniform turbulence field that drives the secondary helical flow (McLean 1981).

Sand ribbons can be up to 15 km long and 200 m wide, and their length to width ratio generally exceeds 40:1. Their edges are fairly sharply defined and parallel or almost parallel. They are generally not very thick, varying from a few sand grains up to 1 m.

Longitudinal sand patches are similar to sand ribbons but they are found in areas of the world's continental shelves characterised by weak tidal currents (near surface or other currents less than 0.5 m/s). The longitudinal sand bank length to width ratio is much smaller than the one of sand ribbons; their edges are not regular and their orientations are non-parallel (Belderson et al. 1982). Their size and shape are variable and they tend to be thicker than sand ribbons, with a thickness that can reach up to 2–3 m.

Tidal sand banks are the largest bedforms of seas with strong tidal currents. They tend to occur in a wide range of water depths where there is abundant sand and where there is a hydrodynamic regime capable of transporting the sediment, e.g. in estuaries or open tidal seas, occurring either in groups or as a solitary near-coastal features in the lee of headlands, islands, submerged rock shoals and gaps in rock ridges.

The sand bank morphology is a result of non-linear interaction between tidal currents, sediment transport, and bed topography. In their review on sand banks, Dyer and Huntley (1999) propose the following classification of different types of sand banks in the light of their origin and development: *Type 1*: Open Shelf Ridges; *Type 2*: Estuary mouth with (A) Ridges (wide mouth) (B) Tidal deltas (narrow mouth), (i) Without recession (ebb tidal deltas), (ii) With recession (shoreface connected ridges); *Type 3*: Headland associated banks with (A) Banner Banks (non-recessional headland) (B) Alternating Ridges (recessional headland).

Open shelf linear ridges (*Type 1*) can be found in shallow tidal seas where currents exceeds 0.5 m/s. They can be up to 80 km long, average 13 km wide and are tens of metres high. They are oriented at a small oblique angle to the main flow direction and are asymmetrical, having slopes of around 6° on the steep side and less than 1° on their gentler side. Open shelf linear ridges gradually move in the direction of their steep face and appear to be in near equilibrium with the flow.

Linear ridges formed in mouths of wide estuaries (*Type 2A*), instead, are generally aligned with the flow direction, and migrate away from their steeper face.

Tidal deltas (*Type 2Bi*) are sand banks that form close to the mouth of narrow-mouthed estuaries and inlets as ebb and flood deltas. Tidal currents are strong only close to the mouth where waves are more dominant. When the coast is retreating, the ebb delta forms a primary source of sand to the nearshore region, which can become modified by storm flows into 'shoreface connected ridges' at angles to the coastline (*Type 2Bii*).

Headland associated banks can be created by tidal eddies as isolated banner banks (*Type 3A*), or as closely spaced ridges (*Type 3B*) when the headland is retreating. The latter can become isolated from the coast as it recedes. Coastal retreat and rising sea level can then cause the ridges to become moribund.

A number of models have been developed to explain the formation of the different types of sand banks. They are well described in Dyer and Huntley (1999), who grouped the existing theories as follows: (a) the theories that consider sand banks as a result of the response of sand to the action of hydrodynamics and that describe how secondary flows (e.g., helicoidal flows, headland eddies, long period waves) can produce convergence of sediment transport towards a sand bank crest; (b) the theories that consider the interaction of water and sand, using coupled hydrodynamic and morphodynamic models.

In particular, *type 3A* sand banks are related to residual currents and the eddies forming close to headlands. With the help of their morphodynamic model, Berthot and Pattiaratchi (2006) showed that *type 3A* sand banks form as a result of the reversing tidal flow creating asymmetry in the sediment transport on each side of the bank (see also Neill and Scourse 2009). The formation of *Type 1* sand banks, instead, was explained by Huthnance (1982a, 1982b) based upon a stability analysis that clarified why these types of sand banks have a certain inclination to the flow direction.

For the *Type 2A* and ebb tidal deltas (2Bi), the development of a generic model has so far been precluded by the dependence of the sand banks on the characteristics of the surrounding banks, coastlines and inlet.

3 Erosional Shallow Coastal Landforms

Erosional structures are negative relief features produced by the hydraulic action of the water flowing on the seabed, which removes sediments and creates scours. Variations in flow velocity in relation to the different conditions of the sea bottom (e.g., grain size and biological agents, which influence sediment cohesion, and the presence of obstacles that modify the local hydrodynamics) give rise to different morphological responses, and various kinds of erosional bedforms, from channels to small scours, are formed (Fig. 3).

Scours are localised erosional features produced over a sediment surface in a turbulent current. They can be due to flow separation around obstructions and consequent creation of local vortices that are strong enough to erode depressions at the base of the obstacles (Picard and High 1973; Reineck and Singh 1975; Nichols 2009). Erosion can also be produced by the abrasive action of grains suspended in eddies (Reineck and Singh 1975). On passive beds without obstructions, scours can result from the unequal distribution of water velocity across a channel cross-section or from semi-permanent vortices over point-bars produced by flow deflection in meanders (Picard and High 1973). On strong muddy surfaces, the characteristics of the scours depend on defects existing in the bed, the duration of the eroding process, and the flow properties. On weakly cohesive mud, instead, they are mainly due to the flow properties (Allen 1971a; Reineck and Singh 1975).

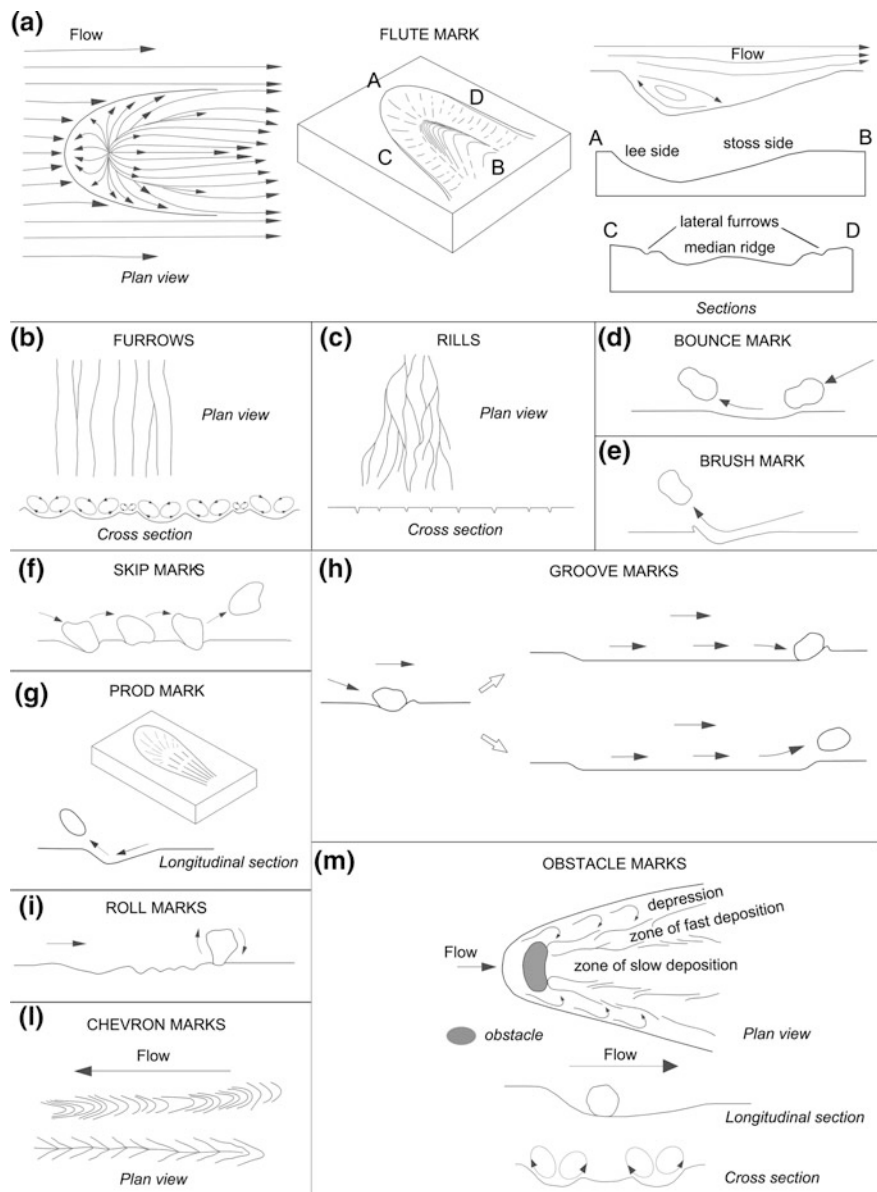


Fig. 3 Erosional shallow coastal landforms: **a** Flute mark (modified after Allen 1971a); **b** Furrows (modified after Allen 1975); **c** Rills; **d** Bounce mark (modified after Ricci Lucchi 1970); **e** Brush mark (modified after Ricci Lucchi 1970); **f** Skip marks (modified after Ricci Lucchi 1970); **g** Prod mark; **h** Groove marks (modified after Ricci Lucchi 1970); **i** Roll marks (modified after Ricci Lucchi 1970); **l** Chevron marks; **m** Obstacle marks (modified after Sengupta 1966)

In marine environments, erosional bedforms are mainly found in lagoons, tidal flats and wave-agitated near-shore areas (Picard and High 1973; Reineck and Singh 1975) or in proximity of anthropogenic structures.

3.1 Scours Produced by Vortex Flow: Flute Marks, Gutter Marks, and Furrows

Flutes are erosional bedforms formed in turbulent zones, on low-angled surfaces, by vortex erosion produced by eddies acting on the bed (Dzulynski and Walton 1965; Allen 1968a, 1968b, 1971a; Reineck and Singh 1975; Varkonyiv and Hargitai 2014). They may also be produced by pure fluid stress alone (Leeder 1982).

Flute marks may appear in a large variety of shapes and sizes (e.g., Rücklin 1938; Vassoevic 1953; Ten Haaf 1959; Dzulynski and Walton 1965; Allen 1971a, 1982a). However, the elongated parabolic shape, closed at the upstream end and with the long axis parallel to the direction of flow (Fig. 3a), is the most common; it is the result of flow separation from the lip of the initial depression and flow reattachment downstream (Leeder 1982).

Flute marks may be isolated and discontinuous or arranged in groups displaying different patterns. Scallop assemblage originates from a field of initially isolated flutes that begin to interfere owing to their enlargement (Allen 1971a, 1971b; Goodchild and Ford 1971; Ford and Williams 1989). If they join, they give rise to scallops characterised by crests transverse to the flow (Richardson and Carling 2005).

Gutter marks are large-scale longitudinal scour holes, characterised by a narrow shape, more elongated than a flute planform. In shallow sub-tidal environments, they are generated by water moving along horizontal unidirectional helicoidal paths on muddy sediments, mainly during storm events (Whitaker 1973; Aigner 1985; Browne and Myrow 1994; Amos et al. 2003).

Furrows are rectilinear longitudinal bedforms, elongated parallel to flow direction and separated by continuous ridges (Fig. 3b), which form in cohesive fine-grained sediments (Dzulynski and Walton 1965; Flood 1983; Dellapenna et al. 2001). They may be aligned over long distances or occasionally coalesce in a downstream direction (Dzulynski and Walton 1965).

Furrows that develop in carbonate-rich cohesive sediments are broad and have gently sloping walls. In muddy cohesive sediments, furrows tend to have steep walls and flat floors; they form where the seabed is swept by recurring, directionally stable, and episodically strong currents. The formation process initiates when a secondary circulation, characterised by a stream-wise helicoidal flow (Flood 1981, 1983), aligns coarse debris (e.g., as shells and branches) in ribbon-like bedforms.

As the debris moves along the seafloor, it abrades small longitudinal troughs into the mud (Flood 1983; Dellapenna et al. 2001). Under conditions of increasing flow, these streaks evolve into longitudinal, rectilinear furrows, which become sinuous as the flow increases. Further development may be controlled by the balance between sediment deposition and erosion (Flood 1983). Consequently, “narrow” furrows (width 1/5 to 1/15 of spacing) appear where deposition exceeds erosion, whereas “wide” furrows (width 1/2 of spacing) develop where erosion exceeds or equals deposition.

3.2 Other Erosional Bedforms Produced by Turbulent Flow: Channels and Rills

Once a scour is produced by turbulent water flow over a sediment surface, fluxes concentrate in it, thus increasing its size and favouring the formation of a channel (Fagherazzi and Sun 2004; Nichols 2009). The dimensions of channels are variable: depth and width may range from decimetres to metres, whereas their length ranges from metres to kilometres. Their large size usually distinguishes channels from other scour features, although the key criterion is that a channel confines the flow, whereas other scours do not (Nichols 2009).

Channels are common features in intertidal flats areas (Reineck and Singh 1975) and are the major geomorphological component of coastal marshes (Allen 2000). In fact, tidal fluxes produce elevated shear stresses at the marsh bottom that lead to erosion and local incision (Fagherazzi and Sun 2004). Channels are characterised by the presence of well-developed bars and other kinds of depositional and erosional bedforms (e.g., dunes, ripples, scours).

Rills are concentrated flow paths that create systems of small, arborescent furrows like river networks, but drain small amounts of water from intermittently exposed sediment surfaces (Allen 1982b) (Fig. 3c). Generally, they can be found in intertidal zones and beaches, where they are created by tidal flow and wave swash, respectively. In tidal channels, they are present on the top of most longitudinal and transverse bars, in both braided and dendritic systems (Picard and High 1973). In contrast, they are not common on point and lateral bars.

Trends of rills appear at large angles to the direction of stream flow. If two sets of rills are present, stream flow is in the direction of a line bisecting the smaller angle (Picard and High 1973).

Rills are only a few millimetres to some centimetres deep, whereas their length ranges from a few centimetres to 3–4 m (Picard and High 1973; Giménez et al. 2004).

3.3 *Erosional Bedforms Caused by Imprints of Objects: Bounce, Brush, Skip, Prod, Groove, Roll and Chevron Marks*

Tool marks are imprints produced on soft sediment surfaces by the impact, dragging, or rolling of large objects (tools), entrained in the flow and moved by a strong current over the seafloor. Reineck and Singh (1975) used the expression “moving tool marks” to distinguish this kind of markings from those produced by objects lying on the seafloor.

The different types of markings depend on the shape and the size of the tools, the mode of transportation, and the sedimentological characteristics of the surface (Reineck and Singh 1975). “Continuous marks” are elongated erosional bedforms produced by tools dragged on the bottom (groove, roll, and chevron marks), whereas “discontinuous marks” are short and distinct because they are the result of the repeated contact (saltation) of an object with the sea bottom (bounce, brush, skip, and prod marks) (Dzulynski and Sanders 1962; Dzulynski and Walton 1965) (Fig. 3d–g).

Groove marks are elongated, narrow, straight erosional bedforms produced by objects dragged along a cohesive mud bottom by the flow (currents or waves) (Fig. 3h). They may be flat-bottomed and tend to flare out downstream (Picard and High 1973). Tools characterised by irregular shapes produce groove marks varying in cross-section.

Similar features may be also created by rolling objects, but generally it is not possible to distinguish between the two (Reineck and Singh 1975). Roll marks are made by cylindrical or discoidal tools that roll over the bed with their axis of symmetry perpendicular to flow (Krejci-Graf 1932; Allen 1982b). As they remain in continuous contact with the surface, a continuous track is created (Fig. 3i). If the tool is moved across the seafloor by waves, the movement is punctuated by short-time breaks. Each new wave pushes the object farther, generally with a slight change in direction of movement and an irregular, but continuous, swinging course is produced (Reineck and Singh 1975).

Chevron marks are features made up of continuous open V-shaped or chevron-shaped marks, closing in the down-current direction and arranged to form puckers (Fig. 3l). They are produced by objects moving just above the surface of a viscous mud (Dunbar and Rodgers 1957; Dzulynski and Walton 1965). The eddying effect that develops behind the moving tool sucks the weak but cohesive sediment and rucks it into chevrons. As a result, the consistency of mud plays an important role in their formation (Dzulynski and Walton 1965). Reversed chevron marks with V forms closing in an up-current direction are also known (Reineck and Singh 1975).

If a falling tool approaches the sediment surface at a rather low angle and immediately bounces back into the current, a quasi symmetrical depression, termed bounce mark, is produced (Fig. 3d). This bedform is widest and deepest in the

middle and fades out gradually in both the up-current and down-current directions (Dzulynski and Walton 1965; Reineck and Singh 1975; Neuendorf et al. 2005).

A brush mark (Dzulynski and Slackza 1958) has a shape similar to the bounce mark (Fig. 3e), but with a slight crescentic ridge at one end that points downcurrent (Neuendorf et al. 2005). This ridge is formed by mud pushed up by and in front of the object as it slides along the bottom. Aligned brush marks, produced by object saltation, are called skip marks (Dzulynski and Slackza 1958) (Fig. 3f).

Prod marks are long, asymmetrical, semi-conical to triangular depressions (Reineck and Singh 1975), which differ from flute marks as they have sharply defined edges, small size, and typically parallel, non-flaring sides (Fig. 3g). Moreover, contrary to what is observed in flute marks, their steeper margin and deeper point are on their downstream end because prod marks are produced by an elongated object that first strikes the substrate at a high angle in a downcurrent-dipping attitude and is then lifted upwards again into the flow (Dzulynski and Walton 1965; Ricci Lucchi 1970; Allen 1982b). The upstream slope is gentle and often longitudinally striated, reflecting irregularities of the object surface (Allen 1982b). Their deep ends face in the same or in the opposite direction depending on whether they are produced by currents or waves, respectively.

3.4 Bedforms Produced by Objects Lying on the Seafloor: Obstacle Marks and Current Crescents

These bedforms are a combination of scours and sediment ridges. They are produced by the presence of resting passive objects on the seafloor, and are therefore also termed “stationary tool marks” (Reineck and Singh 1975).

Objects lying on the seabed in the way of a current tend to deflect the flow lines and to generate upstream erosion and downstream deposition (Picard and High 1973). In fact, the presence of an obstacle is responsible for the formation of secondary flows around the object and for the emergence of a turbulent horseshoe vortex system (Escauriaza and Sotiropoulos 2011). Increase of both velocity and bed shear stress occurs in front of and to the sides of the obstacle, triggering local erosion and preventing deposition (Karcz 1968; Allen 1982b). The eroded sediments are entrained by the fluid, transported in the horseshoe vortex system, and then deposited behind the object, where velocity gets smaller and bed shear stress reduces (Burkow and Griebel 2016). Consequently, sediment accumulates in the lee of the bedform and gives origin to a ridge tapering downcurrent. More than one ridge, alternating with grooves, may be formed behind the obstacles (Reineck and Sing 1975). With a large obstacle, strong turbulence is possible, resulting in scour on all sides (Picard and High 1973).

Obstacle marks may have different shapes and dimensions as a result of the complex interaction among flow dynamics, obstacle characteristics (size, shape and orientation), seabed material, and duration of the process (Fig. 3 m). Generally,

their size is controlled by the size of the object, and their geometry by the secondary flow patterns induced within the main current by the obstacles themselves (Karcz 1968).

Various types of obstacle marks have been described (e.g., Karcz 1968), but there is no generally accepted classification; Allen (1982b) identified three broad characteristics: (1) current crescents, (2) current shadows, and (3) scour-remnant ridges. Obstacle scours are commonly known as current crescents because they are lunate or horseshoe-shaped troughs (concave downstream). The arms of the crescent point downcurrent, embracing one or more flow-aligned sediment ridges. Their shape may be controlled by sediment characteristics, so that crescents in sands tend to be larger and more irregular than those developed in mud (Picard and High 1973). Current shadows may comprise a single ridge of sediment, a ridge bifurcating downstream or a group of parallel ridges (Allen 1982b). In these cases, furrows upstream or on the flanks must however be lacking. Scour-remnant ridges are generally simple ridges that result from differential erosion and gradually taper and lose height downcurrent in the lee of an obstacle (Allen 1965, 1982b).

4 Addressing Key Issues in Shallow Coastal Landform Evolution

The recent technological advances of seafloor mapping in shallow coastal areas allow not only the 3-D quantitative description of shallow coastal landforms but also the characterisation of their sedimentological properties, as we will see below. This quantitative assessment can be now used to answer the following fundamental questions: (i) How do shallow coastal landform change over time and what are the mechanisms driving these changes? (ii) How are bedforms related to benthic habitats? The understanding of these mechanisms, of natural or anthropogenic origin, is crucial for the management of coastal areas. These areas are generally very populated, of high economic interest and they are in continuous evolution even over short time scales.

To address these questions it would be important for the scientific community to adhere to this methodology:

- (1) Define and follow general protocols for the quantitative measurements of shallow coastal landform properties ensuring their objectivity and repeatability;
- (2) Estimate measurement errors in order to allow comparison with other studies;
- (3) Adopt a multidisciplinary approach integrating information from modelling and in situ observation.

4.1 Shallow Coastal Landform Changes: Geomorphometric Measurements

Following the example of modern land geomorphometry, shallow water coastal geomorphometry should focus on the extraction of metrics (coastal landform or bedform parametres) and spatial features (coastal landform objects) from digital bathymetry. Recently acquired large MBES or LiDAR datasets are extremely suitable for automatic and repeatable methods to extract bedform dimensions and assess their changes over time through repeated surveys.

The general modes of geomorphometric analysis first distinguished by Evans (1972) were applied recently to the submarine landscape by many authors (see Lecours et al. 2016 for a review). Pike et al. (2009) defined a land surface parameter as a descriptive measure of surface form (e.g. slope, aspect, topographic wetness index) and a land surface object as a discrete surface feature (e.g. watershed boundary, alluvial fan, drainage network). These concepts can be extended to coastal geomorphometry, where the calculation of the derivatives of the bathymetry (slope, aspect, roughness, etc.) define the parameters of coastal landforms. The taxonomy summarised in this chapter can help the classification of landforms as discrete features by applying different statistical approaches (e.g. Micallef et al. 2007; Lecours et al. 2016). Some of these methods were adapted from concepts conceived for satellite data such as the Benthic Terrain Modeller (Wright et al. 2005) and the Benthic Position Index (Erdey-Heydorn 2008), which has been widely used in recent studies (Ierodiaconu et al. 2011; Micallef et al. 2012). This type of analysis allows the definition of the limits of coastal landforms in a quantitative and repeatable way. It should be mentioned, though, that the creation of DTM can itself introduce errors that can propagate in the calculation of the DTM derivatives. These errors need to be quantitatively estimated also during bedform classification (Wilson 2012). This is particularly true when the geomorphometric analysis aims to assess morphological changes and to estimate volumes of eroded or deposited sediment (Schimel et al. 2015). Since bedload sediment transport in coastal areas is often related to dune migration, many efforts have recently been devoted to automatically detect dune dimension and migration rate from bathymetric profiles or more recently from DTMs. For example, Duffy and Hughes-Clarke (2005, 2012) adopted spatial cross-correlation techniques to track dunes from MBES data (using the slope of bathymetry), to estimate their migration rate and to assess the bedload transport related to due migration. Van Dijk et al. (2008) compared a geostatistical method and a method based on the Fourier decomposition of the bathymetry to separate superimposed bedforms (dunes over sandwaves) and automatically measure their morphodynamic parameters. Cazenave et al. (2013) developed a simple algorithm that applies the 2D Discrete Fourier Transform to the DTM to extract the dune dimensions from a 2D dune field. However, very little has been done for the automatic mapping and dimension extraction of other type of shallow coastal landforms from bathymetric data (apart from e.g. Lefebvre et al. 2011; Micallef et al. 2012; Kruss et al. 2014). Therefore,

further effort should be placed in this direction, as the knowledge of shallow coastal landforms dynamics and of their interaction with human-made structures or other interventions (e.g., breakwalls, harbour structures and dredging) are crucial in coastal zone management.

4.2 *Shallow Coastal Landforms and Sediments: A New Approach to Benthic Habitat Mapping*

MBES backscatter intensity is related to the type of sediment or substrata covering shallow coastal landforms. In the last decade, rapid progress has been made in terms of classification and interpretation of the backscatter angular response and the backscatter mosaics of the seabed that can be obtained from the MBES acquisition. The combined analysis of the bathymetric and backscatter MBES data and their derivatives can provide not only a solid base for benthic habitat mapping (Brown et al. 2011; Ierodiaconou et al. 2011; Hasan et al. 2014), but also become a new basis for the understanding of shallow coastal landforms and their evolution. In particular, the knowledge of sediment sorting in correspondence to a bedform can provide insight into sediment transport and the dynamical processes shaping it (e.g., van Oyen et al. 2013).

A large number of studies have been devoted to comparisons among different backscatter mosaics and angular response classification methods (i.e. angular response, pixel-, field and object-based image analyses) (e.g. Brown and Blondel 2009; Lucieer and Lucieer 2009; Brown et al. 2011; Ierodiaconou et al. 2011; Lucieer and Lamarche 2011; Parnum and Gravrilov 2011; Diesing et al. 2014; McGonigle and Collier 2014).

However, their application in very shallow waters is only very recent (e.g. De Falco et al. 2010; Micallef et al. 2012; Montereale Gavazzi et al. 2016). So far, only the pioneering work of Rattray et al. (2013) has evaluated changes of the seafloor habitats over time and space based on MBES data. In this regard, the definition of common protocols is essential for the extensive mapping of substrata and for monitoring and preservation of shallow water habitats and biodiversity.

Finally, particular attention needs to be devoted to the accuracy assessment related to seafloor classification (Diesing et al. 2014), following the example of remote sensing studies (Foody 2002, 2004, 2010).

5 Conclusions

Given that the world's shallow coastal areas are still mostly unexplored, the first step needed in the study of coastal morphodynamics is the definition of a common taxonomy of the main bedforms, highlighting the major dynamic processes

responsible for their shape and occurrence. Recent developments of MBES and LiDAR instruments in very shallow water coastal environments call for a new effort to define these submerged landforms and their properties. Very high-resolution mapping provides a novel understanding of the processes modifying the littoral zone at different temporal and spatial scales. However, in order to define the evolution of the shallow water coastal landforms, it is necessary to establish methods to quantitatively estimate their changes over time, following and extending on previous experience collected in the field of satellite remote sensing. In particular, there is a need to define workflows to automatically analyse the high-resolution data taking into account shallow water bathymetry and backscatter data, which have to be correlated with the relative errors and accuracy assessment of their classification. In this regard, the first steps have been taken, but there is still a need for a general and shared approach to the classification, the mapping and the monitoring over time of shallow coastal landforms.

References

- Aigner T (1985) Storm depositional systems: dynamic stratigraphy in modern and ancient shallow-marine sequences. Lecture Notes in Earth Sciences vol 3. Springer, Berlin, Heidelberg
- Allen JRL (1965) Scour marks in snow. *J Sed Petrol* 35(2):331–338
- Allen JRL (1968a) Flute marks and flute separation. *Nature* 219:602–604
- Allen JRL (1968b) Current ripples: their relation to patterns of water and sediment motion. Elsevier, New York
- Allen JRL (1971a) Transverse erosional marks of mud and rock: their physical basis and geological significance. *Sed Geol* 5:167–385
- Allen JRL (1971b) Bed forms due to mass transfer in turbulent flows: a kaleidoscope of phenomena. *J Fluid Mech* 49(1):49–63
- Allen JRL (1975) Development of flute-mark assemblages, 2. Evolution of trios of defects. *Sed Geol* 13:1–26
- Allen JRL (1980) Sand waves: a model of origin and internal structure. *Sed Geol* 26(4):281–328
- Allen JRL (ed) (1982a) Developments in sedimentology, sedimentary structures, their character and physical basis. Vol I. 30A. Elsevier Scientific Publishing Company, Amsterdam
- Allen JRL (ed) (1982b) Developments in sedimentology, sedimentary structures, their character and physical basis. Vol II. 30B. Elsevier Scientific Publishing Company, Amsterdam
- Allen JRL (2000) Morphodynamics of Holocene salt marshes: a review sketch from the Atlantic and Southern North Sea coasts of Europe. *Quat Sci Rev* 19:1155–1231
- Amos CL, Li MZ, Chiocci FL et al (2003) Origin of shore-normal channels from the shoreface of Sable Island. *Can J Geophys Res* 108(C3):3094
- Ashley GM (1990) Classification of large-scale subaqueous bedforms: a new look at an old problem—SEPM bedforms and bedding structures. *J Sedim Petrol* 60:160–172
- Axelsson A (2010) Rapid topographic and bathymetric reconnaissance using airborne LiDAR. In: Proceedings of SPIE—The International Society For Optical Engineering, vol 7835, Toulouse, France
- Barnard PL, Erikson LH, Kvitek RG (2011) Small-scale sediment transport patterns and bedform morphodynamics: new insights from high-resolution multibeam bathymetry. *Geo-Mar Lett* 31(4):227–236
- Bartholdy J, Ernstsen VB, Flemming BW, Winter C, Bartholomä A, Kroon A (2015) On the formation of current ripples. *Sci Rep* 5(1)

- Belderson RH, Johnson MA, Kenyon NH (1982) Bedforms. In: Stride (ed) Offshore tidal sands, 1st edn. Chapman and Hall, pp 27–57
- Berné S, Castaing P, Le Drezén E et al (1993) Morphology, internal structure, and reversal of asymmetry of large sub-tidal dunes in the entrance to Gironde Estuary (France). *J Sediment Res* 63:780–793
- Berthot A, Pattiarchi C (2006) Mechanisms for the formation of headland-associated linear sandbanks. *Cont Shelf Res* 26(8):987–1004
- Besio G, Blondeaux P, Brocchini M et al (2004) On the modeling of sand wave migration. *J Geophys Res Oceans* 109(C4)
- Besio G, Blondeaux P, Brocchini M et al (2008) The morphodynamics of tidal sand waves: a model overview. *Coast Eng* 55(7):657–670
- Best JL (2005) The fluid dynamics of river dunes: a review and some future research directions. *J Geophys Res Earth* 110(F4)
- Boggs S (2006) Principles of sedimentology and stratigraphy. Pearson Prentice Hall, Upper Saddle River, NJ
- Brown CJ, Blondel P (2009) Developments in the application of multibeam sonar backscatter for seafloor habitat mapping. *Appl Acoust* 70(10):1242–1247
- Brown CJ, Smith SJ, Lawton P et al (2011) Benthic habitat mapping: a review of progress towards improved understanding of the spatial ecology of the seafloor using acoustic techniques. *Estuar Coast Shelf Sci* 92(3):502–520
- Browne GH, Myrow PM (1994) Pot and gutter casts from the Chapel Island Formation, Southeast Newfoundland; discussion and reply. *J Sediment Res* 64(3a):706–709
- Burkow M, Griebel M (2016) A full three dimensional numerical simulation of the sediment transport and the scouring at a rectangular obstacle. *Comput Fluids* 125:1–10
- Cazenave PW, Dix JK, Lambkin DO et al (2013) A method for semi-automated objective quantification of linear bedforms from multi-scale digital elevation models. *Earth Surf Proc Land* 38(3):221–236
- Coco G, Senechal N, Rejas A et al (2014) Beach response to a sequence of extreme storms. *Geomorphology* 204:493–501
- Cossio T, Slatton KC et al (2011) Predicting small target detection performance of low-SNR airborne LiDAR. *IEEE J Sel Top Appl Earth Obs Remote Sens* 99:1–17
- Cowell PJ, Thom BG (1994) Morphodynamics of coastal evolution. Cambridge University Press, Cambridge
- Dalrymple RW, John Knight R, Lambiase JJ (1978) Bedforms and their hydraulic stability relationships in a tidal environment, Bay of Fundy, Canada. *Nature* 275 (5676):100–104
- Dalrymple RW (1984) The morphology of internal structure of sandwaves in the Bay of Fundy. *Sedimentology* 31:365–382
- Dalrymple RW, Rhodes RN (1995) Estuarine dunes and barforms, in geomorphology and sedimentology of estuaries. In: Perillo GM (ed) Developments in sedimentology. Elsevier, Amsterdam, pp 359–422
- De Falco G, Tonielli R, Di Martino G et al (2010) Relationships between multibeam backscatter, sediment grain size and Posidonia oceanica seagrass distribution. *Cont Shelf Res* 30(18):1941–1950
- Dellapenna TM, Kuehl SA, Pitts L (2001) Transient, longitudinal, sedimentary furrows in the York River Subestuary, Chesapeake Bay: furrow evolution and effects on seabed mixing and sediment transport. *Estuaries* 24(2):215–227
- Diesing M, Green SL, Stephens D et al (2014) Mapping seabed sediments: comparison of manual, geostatistical, object-based image analysis and machine learning approaches. *Cont Shelf Res* 84:107–111
- Duffy GP, Hughes-Clarke JE (2005) Application of spatial cross correlation to detection of migration of submarine sand dunes. *J Geophys Res* 110:F04S12
- Duffy GP, Hughes-Clarke JE (2012) Measurement of bedload transport in a coastal sea using repeat swath bathymetry surveys: assessing bedload formulae using sand dune migration.

- Sediments, morphology and sedimentary processes on continental shelves: advances in technologies, research and applications. International Association of Sedimentology, Wiley
- Dunbar CO, Rodgers J (1957) Principles of stratigraphy. Wiley, New York
- Dyer KR, Huntley DA (1999) The origin, classification and modelling of sand banks and ridges. *Cont Shelf Res* 19(10):1285–1330
- Dzulynski S, Sanders JE (1962) Current marks on firm mud bottoms. *Trans Connecticut Acad Arts Sci* 42:57–96
- Dzulynski S, Slaczka A (1958) Directional structures and sedimentation of the Krosno Beds (Carpathian flysch). *Ann Soc Geol Pologne* 16:205–259
- Dzulynski S, Walton EK (1965) Sedimentary features of flysch and greywackes. Developments in sedimentology, vol 7. Elsevier, Amsterdam
- Erdey-Heydorn MD (2008) An ArcGIS seabed characterization toolbox developed for investigating benthic habitats. *Mainer Geodesy* 31(4):318–358
- Ernstsén VB, Noormets R, Winter et al (2006) Quantification of dune dynamics during a tidal cycle in an inlet channel of the Danish Wadden Sea. *Geo Mar Lett* 26(3):151–163
- Escauriaza C, Sotiropoulos F (2011) Initial stages of erosion and bed form development in a turbulent flow around a cylindrical pier. *J Geophys Res* 116:F03007
- Evans IS (1972) General geomorphometry, derivatives of altitude, and descriptive statistics. *Spatial Analysis in Geomorphology*, pp 17–90
- Fagherazzi S, Sun T (2004) A stochastic model for the formation of channel networks in tidal marshes. *Geophys Res Lett* 31:L21503
- Feldens P, Diesing M, Schwarzer K et al (2015) Occurrence of flow parallel and flow transverse bedforms in Fehmarn Belt (SW Baltic Sea) related to the local palaeomorphology. *Geomorphology* 231:53–62
- Fernandez-Diaz JC, Glennie CL, Carter WE et al (2014) Early results of simultaneous terrain and shallow water bathymetry mapping using a single-wavelength airborne LiDAR sensor. *IEEE J Sel Top Appl Earth Obs Remote Sens* 99 7(2):623–635
- Ferrini VL, Flood RD (2005) A comparison of rippled scour depressions identified with multibeam sonar: evidence of sediment transport in inner shelf environments. *Cont Shelf Res* 25 (16):1979–1995
- Flemming BW (1980) Sand transport and bedform patterns on the continental shelf between Durban and Port Elizabeth (Southeast African continental margin). *Sed Geol* 26:179–205
- Flemming BW (2000) The role of grain size, water depth and flow velocity as scaling factors controlling the size of subaqueous dunes. In: *Marine sandwave dynamics, international workshop*, pp 23–24
- Fogarin S (2015) Mappatura dell'ambiente sedimentario della bocca tidale di Chioggia (Laguna di Venezia): backscatter acustico, morfologia del fondale e distribuzione dimensionale, dissertation, University of Ca' Foscari, Venice
- Flood RD (1981) Distribution, morphology, and origin of sedimentary furrows in cohesive sediments, Southampton Water. *Sedimentology* 28:511–529
- Flood RD (1983) Classification of sedimentary furrows and a model for furrow initiation and evolution. *Geol Soc Am Bull* 94(5):630–639
- Foody GM (2002) Status of land cover classification accuracy assessment. *Remote Sens Environ* 80(1):185–201
- Foody GM (2004) Thematic map comparison. *Photogram Eng Remote Sens* 70(5):627–633
- Foody GM (2010) Assessing the accuracy of land cover change with imperfect ground reference data. *Remote Sens Environ* 114(10):2271–2285
- Ford DC, Williams P (1989) Karst geomorphology and hydrology. Unwin Hyman, London, UK
- Fraccascia S, Winter C, Ernstsén VB et al (2016) Residual currents and bedform migration in a natural tidal inlet (Knudedyb, Danish Wadden Sea). *Geomorphology* 271:74–83
- Giménez R, Planchon O, Silvera N et al (2004) Longitudinal velocity patterns and bed morphology interaction in a rill. *Earth Surf Proc Land* 29:105–114
- Goodchild MF, Ford DC (1971) Analysis of scallop patterns under controlled conditions. *J Geol* 79(1):52–62

- Guy HP, Simons DB, Richardson EV (1966) Summary of alluvial channel data from flume experiments, 1956–61
- Hasan RC, Ierodiaconou D, Laurenson L, Schimel A (2014) Integrating multibeam backscatter angular response, mosaic and bathymetry data for benthic habitat mapping. *Plos one* 9(5): e97339
- Hughes-Clarke JE, Mayer LA et al (1996) Shallow-water imaging multibeam sonars: a new tool for investigating seafloor processes in the coastal zone and on the continental shelf. *Mar Geophys Res* 18(6):607–629
- Huthnance JM (1982a) On one mechanism forming linear sandbanks. *Estuar Coast Mar Sci* 14 (1982):19–99
- Huthnance JM (1982b) On the formation of sand banks of finite extent. *Estuar Coast Mar Sci* 15 (1982):277–299
- Ierodiaconou D, Monk J, Rattray A et al (2011) Comparison of automated classification techniques for predicting benthic biological communities using hydroacoustics and video observations. *Cont Shelf Res* 31(2):S28–S38
- Karcz I (1968) Fluvial obstacle marks from the wadis of the Negev (Southern Israel). *J Sediment Res* 38:1000–1012
- Krejci-Graf J (1932) Definition der Begriffe Marken, Spuren, Fahrten, Bauten, Hieroglyphen und Fucoiden. *Senckenbergiana* 14:19–39
- Kruss A, Madricardo F, Tegowski J et al (2014) A combined GIS-2DFFT multi-parameter analysis of very high resolution bathymetric data: a case study from the Venice Lagoon. In: 2nd International Conference and Exhibition on Underwater Acoustic (UA2014), Rhodes, Greece
- Lecours V, Dolan MFJ, Micallef A, Lucieer VL (2016) A review of marine geomorphometry, the quantitative study of the seafloor. *Hydrol Earth Syst Sci* 20:3207–3244
- Leeder MR (1982) Sedimentology: process and product. Allen & Unwin, London
- Lefebvre A, Ernstsen VB, Winter C (2011) Bedform characterization through 2D spectral analysis. *J Coastal Res* 64:781
- Longhitano SG, Mellere D, Steel RJ et al (2012) Tidal depositional systems in the rock record: a review and new insights. *Sed Geol* 279:2–22
- Lucieer V, Lamarche G (2011) Unsupervised fuzzy classification and object-based image analysis of multibeam data to map deep water substrates, Cook Strait, New Zealand. *Cont Shelf Res* 31:1236–1247
- Lucieer V, Lucieer A (2009) Fuzzy clustering for seafloor classification. *Mar Geol* 264(3):230–241
- Lyons AP, Fox WL, Hasiotis T et al (2002) Characterization of the two-dimensional roughness of wave-rippled sea floors using digital photogrammetry. *IEEE J Oceanic Eng* 27(3):515–524
- Maddux TB, Nelson JM, McLean SR (2003a) Turbulent flow over three-dimensional dunes: 1. Free surface and flow response. *J Geophys Res* 108(F1)
- Maddux TB, McLean SR, Nelson JM (2003b) Turbulent flow over three-dimensional dunes: 2. Fluid and bed stresses. *J Geophys Res* 108(F1):6010
- Madricardo F, Amos CL, De Pascalis F et al (2015) Sediment transport in a tidal inlet: the case of the Lido inlet, Venice Italy. In: Proceedings of ECSA 55: unbounded boundaries and shifting baselines: estuaries and coastal seas in a rapidly changing world, London 2015
- Madricardo F, Foglini F, Tricardi F (2016) Processed high-resolution ASCII: ESRI gridded bathymetry data (EM2040 and EM3002) from the Lagoon of Venice collected in 2013. *Integr Earth Data Appl (IEDA)*. <http://dx.doi.org/10.1594/IEDA/323605>. Accessed 23 Feb 2017
- McGonigle C, Collier J (2014) Interlinking backscatter, grain size and benthic community structure. *Estuar Coast Shelf Sci* 147:123–136
- McLean SR (1981) The role of non-uniform roughness in the formation of sand ribbons. *Dev Sedimentol* 32:49–74
- Micallef A, Berndt C, Masson DG et al (2007) A technique for the morphological characterization of submarine landscapes as exemplified by debris flows of the Storegga Slide. *J Geophys Res* 112:F02001
- Micallef A, Le Bas TP, Huvenne VA et al (2012) A multi-method approach for benthic habitat mapping of shallow coastal areas with high-resolution multibeam data. *Cont Shelf Res* 39:14–26

- Micallef A, Foglini F, Le Bas et al (2013) The submerged paleolandscape of the Maltese Islands: morphology, evolution and relation to quaternary environmental change. *Mar Geol* 335:129–147
- Montereale Gavazzi GM, Madricardo F, Janowski L et al (2016) Evaluation of seabed mapping methods for fine-scale classification of extremely shallow benthic habitats—Application to the Venice Lagoon, Italy. *Estuar Coast Shelf Sci* 170:45–60
- Neill SP, Scourse JD (2009) The formation of headland/island sandbanks. *Cont Shelf Res* 29 (18):2167–2177
- Neuendorf KKE, Mehl JP Jr, Jackson JA (eds) (2005) Glossary of geology, 5th edn. American Geological Institute, Alexandria
- Nichols G (2009) Sedimentology and stratigraphy, 2nd edn. Wiley, New York
- Nienhuis JH, Perron JT, Kao JC et al (2014) Wavelength selection and symmetry breaking in orbital wave ripples. *J Geophys Res Earth* 119(10):2239–2257
- Olariu C, Steel RJ, Dalrymple RW et al (2012) Tidal dunes versus tidal bars: The sedimentological and architectural characteristics of compound dunes in a tidal seaway, the lower Baronia Sandstone (Lower Eocene), Ager Basin, Spain. *Sed Geol* 279:134–155
- Omidyeganeh M, Piomelli U (2013) Large-eddy simulation of three-dimensional dunes in a steady, unidirectional flow. Part 2. Flow structures. *J Fluid Mech* 734:509–534
- Parnum IM, Gavrilov AN (2011) High-frequency multibeam echo-sounder measurements of seafloor backscatter in shallow water: part 1—data acquisition and processing. *Underwater Technol* 30(1):3–12
- Parsons DR, Best JL, Orfeo O et al (2005) Morphology and flow fields of three-dimensional dunes, Rio Paraná, Argentina: results from simultaneous multibeam echo sounding and acoustic Doppler current profiling. *J Geophys Res Earth* 110(F4)
- Pfenningbauer M, Ullrich A et al. (2011) High resolution hydrographic airborne laser scanner for surveying inland waters and shallow coastal zones. In: Proceedings SPIE 8037:80375
- Picard MD, High LR Jr (1973) Sedimentary structures of ephemeral streams. Developments in sedimentology vol 17. Elsevier, Amsterdam
- Pike RJ, Evans IS, Hengl T (2009) Geomorphometry: a brief guide. *Dev Soil Sci* 33:3–30
- Rattray A, Ierodiaconou D, Monk J et al (2013) Detecting patterns of change in benthic habitats by acoustic remote sensing. *Mar Ecol Prog Ser* 477:1–3
- Reading HG (ed) (1996) Sedimentary environments: processes, facies and stratigraphy, 3rd edn. Wiley-Blackwell, Oxford, pp 249–272
- Reineck HE, Singh IB (eds) (1975) Depositional sedimentary environments with reference to terrigenous clastics. Corrected reprint of the 1st edn. Springer, Berlin
- Reynaud JY, Dalrymple RW (2012) Shallow-marine tidal deposits. In: Davis S, Dalrymple RW (eds) Principles of tidal sedimentology. Springer, New York, pp 335–370
- Ricci Lucchi F (1970) Sedimentografia. Atlante fotografico delle strutture primarie dei sedimenti, Zanichelli, Bologna
- Richardson K, Carling PA (2005) A typology of sculpted forms in open bedrock channels. *Geol Soc Am Spec Pap* 392:108
- Rubin DM, Hunter RE (1987) Bedform alignment in directionally varying flows. *Science* 237 (4812):276–278
- Rücklin H (1938) Strömungsmarken im unteren Muschelkalk des Saarlandes. *Senckenbergiana* 20:94–114
- Schimel AC, Ierodiaconou D, Hulands L et al (2015) Accounting for uncertainty in volumes of seabed change measured with repeat multibeam sonar surveys. *Cont Shelf Res* 111:52–68
- Sengupta S (1966) Studies on orientation and imbrication of pebbles with respect to cross-stratification. *J Sedimentol Petrol* 36(2):362–369
- Skarke A, Trembanis AC (2011) Parametrization of bedform morphology and defect density with fingerprint analysis techniques. *Cont Shelf Res* 31(16):1688–1700
- Southard JB, Boguchwal LA (1990) Bed configurations in steady unidirectional water flows. Part 2. Synthesis of flume data. *J Sediment Res* 60(5)

- Ten Haaf E (1959) Graded beds of the Northern Apennines. Ph.D. dissertation, University of Groningen
- Várkonyi P, Hargitai H (2014) Scour marks. Encyclopedia of planetary landforms. Springer Science, Business Media, New York
- van Dijk TA, Kleinhans MG (2005) Processes controlling the dynamics of compound sand waves in the North Sea, Netherlands. *J Geophys Res Earth* 110(F4)
- van Dijk TA, Lindenbergh RC, Egberts PJ (2008) Separating bathymetric data representing multiscale rhythmic bed forms: a geostatistical and spectral method compared. *J Geophys Res Earth* 113(F4)
- van Oyen T, Blondeaux P, van den Eynde D (2013) Sediment sorting along tidal sand waves: a comparison between field observations and theoretical predictions. *Cont Shelf Res* 63:23–33
- van Rijn LC (1982) Prediction of bed forms, alluvial roughness and sediment transport. *Delft Hydraulics S* 487–11
- Vassoevic NB (1953) On some structures in the flysch (English summary). *Tr Lvovsk Geol Obscesto* 3:17–85
- Venditti JG (2007) Turbulent flow and drag over fixed two and three-dimensional dunes. *J Geophys Res Earth* 112(F4)
- Voulgaris G, Morin JP (2008) A long-term real time sea bed morphology evolution system in the South Atlantic Bight. In: IEEE/OES 9th working conference on current measurement technology, CMTC 2008, pp 71–79
- Whitaker JH McD (1973) ‘Gutter casts’, a new name for scour-and-fill structures: with examples from the Llandoverian of Ringerike and Malmoya, Southern Norway. *Nor Geol Tidsskr* 53:403–417
- Williams JJ, Bell PS, Thorne PD (2003) Field measurements of flow fields and sediment transport above mobile bed forms. *J Geophys Res Oceans* 108(C4):3109
- Wilson JP (2012) Digital terrain modeling. *Geomorphology* 137(1):107–121
- Wright LD, Thom BG (1977) Coastal depositional landforms: a morphodynamic approach. *Prog Phys Geogr* 1(3):412–459
- Wright DJ, Lundblad ER, Larkin EM et al (2005) NOAA Coastal Services Center, ArcGIS Benthic Terrain Modeler, version 1.0. Accessed April 2017
- Yalin MS (1977) Mechanics of sediment transport. Elsevier, New York

Continental Shelf Landforms

Ruth Durán and Jorge Guillén

Abstract Continental shelves comprise the zone adjacent to the continents, extending from the infralittoral to a marked change in slope known as the shelf break. The shelf break is located at a variable depth from 20 to 550 m, with a global average depth of 140 m. They develop in passive and active margins and can be dominated by different processes, which include tides, waves and currents. The present day geomorphology of the continental shelf comprises a wide variety of modern and relict features as a result of different controlling factors—geological structure, sea-level change, and sediment delivery and dispersal systems—acting at varying time scales. This chapter illustrates the most common landforms observed in siliciclastic continental shelves, with special attention to the processes that generate them. Landforms include consolidated bottoms, erosive morphologies, prograding landforms, bedforms, gas-related morphologies and anthropogenic features.

1 Introduction

Continental shelves represent the transitional zone between the subaerial landmass and the deep ocean, occupying an area of about 27 million km², which is equivalent to almost 9% of the surface area of the oceans (Harris et al. 2014). The continental shelf extends from the shoreface to a marked change in slope known as the shelf break. In a global context, the shelf break varies from 20 m in tropical continental shelves to 550 m in polar regions, with a global average of 140 m water depth. The shelf width typically ranges between 30 and 60 km, although it can vary significantly worldwide. For instance, it is drastically reduced in active margins or in areas where submarine canyons deeply incise the continental shelf such as La Jolla and Scripps canyons in California, whereas in other settings such as the Siberian continental shelf into the Arctic Ocean, the width can be up to 1210 km.

R. Durán (✉) · J. Guillén

Instituto de Ciencias del Mar, CSIC, Passeig Marítim de la Barceloneta,
37-49, 08003 Barcelona, Spain
e-mail: rduran@icm.csic.es

Continental shelves occur in passive and active margins and in all climate environments, showing distinctive geomorphic characteristics (Shepard 1963). Several classifications have been proposed for modern continental shelves according to different criteria: tectonic setting (active and passive) (Emery 1980), shelf morphology (narrow, wide, shallow, and deep shelves) (Inman and Nordstrom 1971), vertical relief (low-, medium- and high-relief shelves) (Harris et al. 2014), prevailing energy regime (wave- and storm, tidal-current, and oceanic current dominated (Swift 1972), or climatic classification, based on latitudinal variations (high-latitude or glacial shelves, tropical or carbonate shelves and middle-latitude or siliciclastic shelves) (Thompson 1961). In spite of the simplifications associated with the climatic classification, we use it for a descriptive overview of the continental shelves types because of their associated characteristic morphological features (Fig. 1).

Glacial continental shelves range from a few tens to several hundred kilometres in width (Dowdeswell et al. 2002). Although shelf sediment is commonly deposited during ice sheet advance and retreat over the continental shelf, some shelves such as the East Siberian shelf are mainly supplied with sediment by major rivers rather

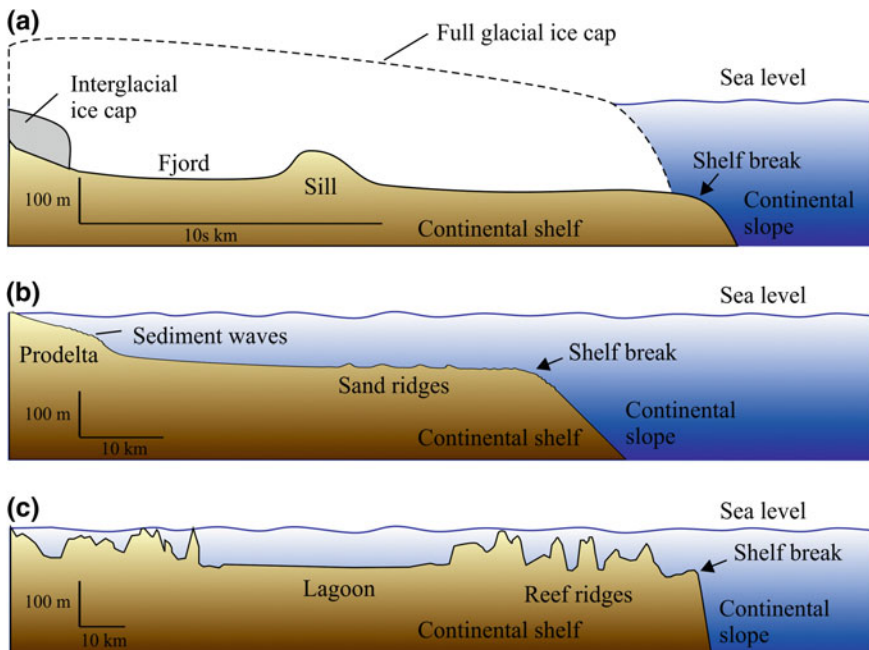


Fig. 1 Schematic representation of the three shelf types based on the climatic classification: **a** glacial shelf, **b** mid-latitude (siliciclastic) shelf, and **c** tropical (carbonate) shelf. Note that horizontal scale differs among the three shelf types. Synthesised from Dowdeswell et al. (2002), Durán et al. (2014) and Lewis (2001)

than from glacial delivery of debris (Dowdeswell et al. 2002). Glacial continental shelves are characterised by a rugged seafloor produced by subglacial processes and/or grounded icebergs. The most common landforms described in these shelves include mega-scale lineations, drumlins, ribbed moraines and crag-and-tails (e.g. Clark 1993; Ottesen and Dowdeswell 2006).

Mid-latitude or siliciclastic continental shelves can be dominated by a variety of processes, such as tides, storms or currents (Swift 1972). Terrigenous sediment supply to the shelf occurs mainly at river mouths with a very uneven geographical distribution; a few rivers in Asia supply about 70% of the total annual amount of terrigenous sediment input to the ocean by rivers (Milliman and Meade 1983). Across the shelf, sediment distribution consists largely of sands on the inner shelf, muds occupying the middle shelf and sand and gravel on the outer shelf (Emery 1952). Overall, inner-shelf sands and middle-shelf muds are currently being supplied from the continent. Away from the river mouths, however, the shelf is a sediment-starved environment in which sedimentation is dominated by the reworking of older sediment. Main landforms in these continental shelves include tidal scours, palaeo-river channels, modern and relict prograding sediment bodies and a wide variety of bedforms, such as sand banks, sand ridges, ribbons, sediment waves, subaqueous dunes and sorted bedforms.

Tropical or carbonate continental shelves have a very low gradient depositional slope (commonly less than 0.1°) from the shoreline or lagoon to a basin floor (Burchette and Wrigth 1992). Shelf sediment is commonly characterised by biogenic material instead of terrigenous sediment supplied by rivers. Typical examples of tropical continental shelves are Bahamas, Florida shelf or the Great Barrier Reef in Australia. Continental shelf landforms in these environments include spurs and grooves, terraces, reef ridges, pinnacles, platforms, carbonate-sand shoals and lagoons (Harris and Davies 1989; Lewis 2001; Duce et al. 2016).

This chapter focuses on mid-latitude shelves characterised by transport and deposition of siliciclastic sediment. Glacial and tropical continental shelf landforms are discussed in Chap 13 (Batchelor et al. 2018) and 23 (Lo Iacono et al. 2018).

2 Brief History of Research on Continental Shelf Landforms

The first studies on continental shelf morphology, sediment distribution patterns and material composition were carried out in the late 1950s, mostly focusing on the textural, mineralogical and biological aspects of sediment and diagenetic processes (e.g. Shepard and Moore 1955; Potter 1967; Emery 1968; Swift et al. 1971). In the late 1960s, the development of new instrumentation and techniques designed for marine use has advanced the knowledge of fluid and sedimentary processes on

continental shelves, allowing scientists to make short-term observations of some important dynamic and sedimentary parameters such as currents, suspended sediment concentration, settling velocity, near-bed bottom shear stress and flocculation (Sternberg et al. 1986). Following this approach, several studies involving simultaneous records at the boundary layer have improved the understanding of the mechanisms, pathways and rates of sediment movement (Evans and Collins 1975; Flemming 1978). Particular attention was paid to examining the mutual interactions between landforms and the processes acting on them (Wright and Thom 1977).

In the following years, some comprehensive classifications have been proposed for continental shelf bedforms based on the relation between bedforms and sediment input, flow velocity/bed shear stress and sediment-size (Belderson et al. 1982; Ashley 1990; Southard and Boguchwal 1990). Belderson et al. (1982) proposed a qualitative model that related the formation of different sedimentary features with the current strength and sand availability. Subsequent experimental studies revealed that a number of bedform states exist that are stable only between certain values of flow velocity/bed shear stress and sediment-size (Southard and Boguchwal 1990). These authors proposed a sequence of equilibrium bedform states as the flow velocity increases for a given sediment-size: lower stage plane bed, ripples, dunes, plane bed, and finally antidunes. In the same year, Ashley (1990) presented a new classification for large-scale flow-transverse sandy bedforms in fluvial and shallow marine environments.

With the introduction of high-resolution mapping systems in the 1990s, such as the multibeam echosounder, bathymetric LiDAR, underwater photography and video, new information has become available on seafloor characteristics allowing the characterisation of the present shelf seafloor at a high level of detail. The detailed geomorphic mapping of submerged continental margins provided the basis for mapping physical habitats (Kostylev et al. 2001), palaeolandscape reconstruction (Micallef et al. 2013), assessment of the anthropogenic impact on the seafloor (Puig et al. 2012) and discovery of potentially significant archaeological sites (Bailey and Flemming 2008).

Coupled with improvements on direct observations, in situ measurements and advances in numerical modelling of hydrodynamics, knowledge about processes that govern the morphodynamics of bedforms has also been significantly enhanced in recent years. At present, investigations into the origin, morphology and evolution of bedforms on the continental shelf involve several distinctive approaches along three main lines of research: (a) the morphology and sediment characterisation of bedforms (e.g. Amos and King 1984; Li and King 2007; Durán et al. 2015), (b) their formation and dynamics (e.g. McBride and Moslow 1991; Calvete et al. 2011; Simarro et al. 2015), and (c) their internal structure (Dalrymple and Hoogendoorn 1997; Goff et al. 2005).

3 Processes

The present day geomorphology of most continental shelves results from combinations of relict and modern features, reflecting a complex interplay among different controlling factors acting at varying time scales. The most relevant factors include the geological structure, sea-level change, sediment delivery and dispersal systems. The geological structure, acting at scales of thousands and millions of years, plays two main roles. It directly controls the overall configuration of the margin (width and slope, and the deep structure of the subsurface), thus determining the gross morphology of the continental shelf, and it indirectly controls the supply of sedimentary material to the marine environment and their composition by influencing the morphometry and lithology of the watersheds.

Continental shelves are sensitive to sea-level change. During the Quaternary, sea-level cycles were characterised by slow, stepped sea-level falls and abrupt sea-level rises with short-lived lowstands and highstands (Siddall et al. 2007). As a consequence, most of the shelf was exposed several times to subaerial processes. The most recent sea-level fall coincided with the Last Glacial Maximum (LGM) about 18,000 years ago, when sea-level fell about 120 m below the present-day sea-level (Fairbanks 1989; Hanebuth et al. 2000) and the coastline was located near the shelf edge. Since the end of the LGM, sea-level rose rapidly, forcing the landward migration of the shoreline and coastal environments and drowning the previously exposed landscape. The successive shoreline migrations across the shelf led to the formation of distinctive morphological features such as drowned barrier islands, beachrocks, prograding sediment bodies and sand ridges located in the mid-outer shelf, which are used as indicators of sea-level positions. The geomorphology of continental shelf drowned landscapes is therefore a valuable tool for better understanding the formation and evolution of ancient landscapes in relation to the youngest climatic-eustatic cycles (Cohen and Lobo 2013).

Sediment supply on mid-latitude continental shelves mainly depends on the hydrology of contributing rivers, which in turn is controlled by climate and drainage basin characteristics (Syvitski and Morehead 1999). In addition to natural factors, human interventions on the river course may also cause changes in the sediment yield. Once the sediment reaches the continental shelf it is dispersed by processes that act on a wide range of temporal scales (from seconds to hundreds of years) such as buoyant plumes, waves, tides, wind-induced and thermohaline currents, internal waves and sediment gravity flows (Nittrouer and Wright 1994) (Fig. 2). The across- and along-shelf sediment fluxes caused by the interplay of hydrodynamic processes determine the sediment distribution, the development or evolution of bedforms and the presence of sedimentary structures on the seafloor.

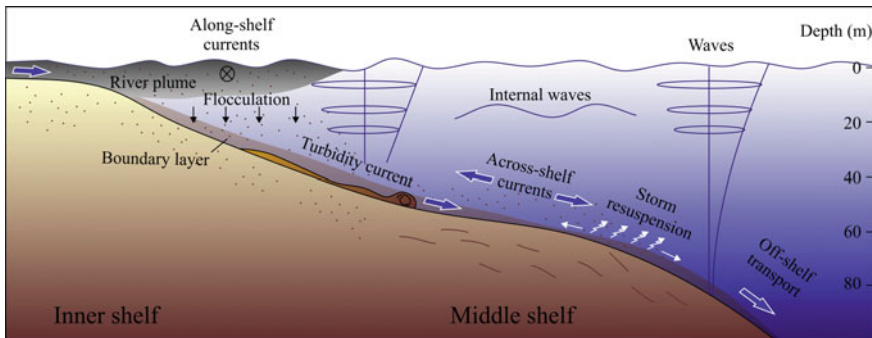


Fig. 2 Diagram showing main physical processes and sediment dispersal across the continental shelf. Redrawn from Geyer and Traykovski (2001)

4 Continental Shelf Landforms

Landforms on the continental shelf reflect the combined effect of geological structure, glacio-eustatic changes in sea-level and dominant sedimentary processes acting at different time-scales. The variety of identified morphologies is huge and some of them are referred to using different terms. Therefore, the following sections are far from an exhaustive inventory of landforms on continental shelves, but they aim to highlight the main categories and processes. Landforms are grouped as: (a) associated to consolidated bottoms, (b) erosive morphologies, (c) prograding landforms, (d) bedforms, (e) gas-related features, and (f) anthropogenic features.

4.1 Consolidated Bottoms

Two main types of landforms are described in this section: (a) bedrock outcrops on the seafloor, and (b) coastal sedimentary bodies that were cemented by intertidal processes or during low-stand periods.

In areas of low sediment input or dominated by erosional processes, underlying structure can be exposed at the seafloor resulting in a rough bathymetry with variable relief (Fig. 3). *Rocky outcrops* are a common feature in the continental shelf that can occupy large areas (Galparsoro et al. 2010; Micallef et al. 2013; Durán et al. 2014). Locally, *faults* affecting the basement can outcrop at the seafloor, resulting in high escarpments that can be up to 50 m high and have been described in several continental shelves (Liquete et al. 2007; Micallef et al. 2013).

Marine terraces are shore platforms formed by subaerial weathering during lowstand exposure and wave erosion that drove the coastline landward during subsequent sea-level rise (Anderson 1999; Pirazzoli 2005; Micallef et al. 2013). They consist of a flat to gently inclined surface that can locally terminate in a

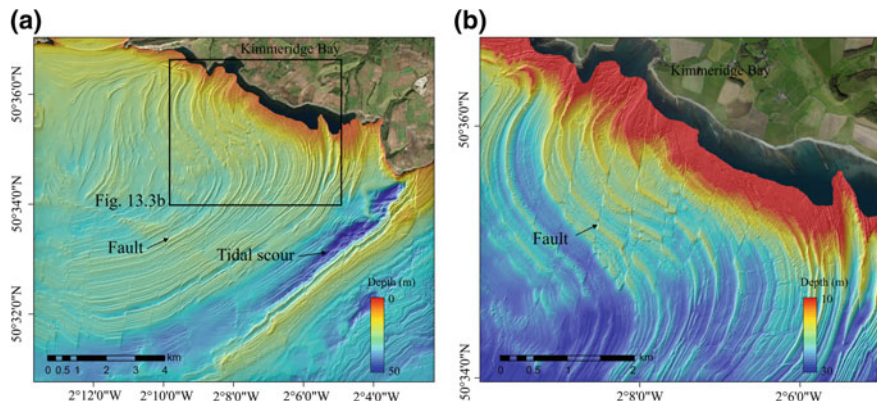


Fig. 3 **a** Shaded colour multibeam bathymetry of the Kimmeridge Clay in the English Channel coast, Dorset, England. Tidal currents excavate the soft mudstones resulting in large scours. **b** Close view showing extensional faults affecting the outcrops. Data courtesy of the Channel Coastal Observatory (www.channelcoast.org)

step-like morphology. The position of the marine terraces is controlled by eustacy and/or tectonics; thus they are considered as reliable sea-level indicators, recording periods of stationary (Bradley and Griggs 1976) or slow rates of sea-level (Collina-Girard 2002; Martínez-Martos et al. 2016).

Submerged barrier islands and *beachrocks* are examples of coastal sedimentary deposits that can be cemented through the precipitation of carbonate cements, mostly of high-Mg calcite and aragonite (Bricker 1971). Lithification usually takes place in the intertidal zone and may involve all sorts of sediment, such as sands and gravels of both clastic and biogenic origin (e.g. Russell 1963; Kelletat 2006). *Submerged barrier islands* are elongate morphologies that can reach tens of kilometres in length and several metres in height (Gardner et al. 2007). *Beachrocks* are sharp, convex structures that range from tens to centimetres to several metres in height, and 150 m to 10 km in length (Liquete et al. 2007). The location of these morphologies on the continental shelf, caused by subsidence or sea-level rise, is also considered a proxy for Quaternary sea-level and neotectonic displacements (Ramsay and Cooper 2002; Kelletat 2006).

4.2 Erosive Morphologies

Erosive morphologies on continental shelves are generated by strong bottom currents and exhibit a wide variety of shapes and dimensions. They include channels, scours (irregular shaped depressions), obstacle marks, large-scale lineations and furrows. The most common erosive features are the *palaeo-river channels*, which originate during periods of low sea-level when fluvial systems extended their limits

basinward, widening the exposed shelf and eroding the underlying strata (Harris et al. 2013). These channels show V-shaped cross-sections and can be linear or sinuous in plan view (Micallef et al. 2013).

Scours are erosional features that show a variety of shapes, sizes and configurations; from small (around 0.5 m deep) to large scale features up to 20–30 m deep (Shaw et al. 2012; Durán et al. 2014). They are frequently associated with the interaction of intense bottom currents with geomorphological restrictions such as straits, narrow openings between islands, coastal headlands or rocky outcrops. Where constricted, the flow is enhanced and turbulence from the strong currents scours the seafloor. An excellent example of large scours generated by strong bottom currents is the Minas Passage in the Bay of Fundy, Canada, where a large scour trough occupies an area of 240 km², incising 20–30 m into the seabed (Shaw et al. 2012) (Fig. 4).

At a smaller spatial scale, when a bottom current encounters an individual obstacle, such as scattered rocky outcrops, the flow is constricted and accelerated, which may result in erosion in front of the obstacles. Downstream from the obstacle, a shadow zone is generated where turbulence intensity slowly diminishes (Allen 1982). These features are named *obstacle marks*. Depending on the bottom currents intensity, obstacles may cause sediment deposition but also non-deposition or even sediment erosion at the downstream side of the obstacle generating crescent scour and comet marks (Werner and Newton 1975).

Finally, *large-scale lineations and furrows* represent flow-parallel bottom structures that develop under episodic, energetic and directionally stable bottom currents that generate helical motions within the benthic boundary layer (Dyer 1970; Flood 1983). Lineations can be up to several kilometres long with a negative relief of several metres (Lo Iacono et al. 2010; Durán et al. 2014). Furrows are also

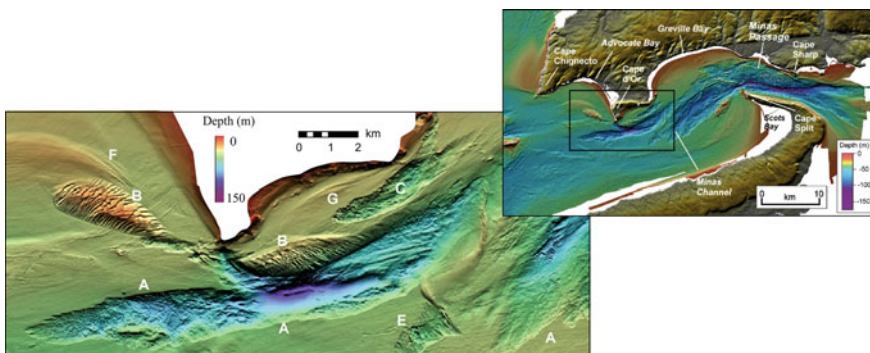


Fig. 4 Shaded colour bathymetric map of the Minas Passage in the Bay of Fundy, Canada. Inset map of the western part of the scour trough system shows different seafloor features such as: (A) the sharply-defined western edge of the principal trough; (B) a pair of banner banks; (C) a small scour trough; (E) transversely-aligned symmetrical dunes. (F) and (G) are shadow sand banks. (Reprinted from Shaw et al. 2012, with permission from Elsevier)

longitudinal bedforms that develop in fine-grained, cohesive sediment (Flood 1983). They consist of a series of parallel, regularly spaced grooves in the seafloor that can be 20 m wide and 2 m deep (Flood 1983).

4.3 Prograding Landforms

Along the inner shelf, modern deposits are organised in prograding sediment bodies that comprise prodeltas and infralittoral prograding wedges. When clastic sediment is delivered to the coast and inner shelf, it is reworked by marine processes forming a *delta* (Elliot 1986). Large deltas build huge submarine prograding sediment bodies that can extend tens of kilometres seaward. The main delta physiographic zones include the subaerial and the subaqueous delta plain, which comprises the delta front and the prodelta (Wright 1985) (Fig. 5). The morphology of a delta depends on the discharge regime, but also on the relative magnitudes of tides, waves and currents (Colleman 1975). Based on the dominant process, three main types of deltas are distinguished: river-dominated deltas such as the Mississippi River delta, wave-dominated deltas (e.g. the Nile River delta), and tide-dominated deltas such as the Amazon River delta (Galloway 1975).

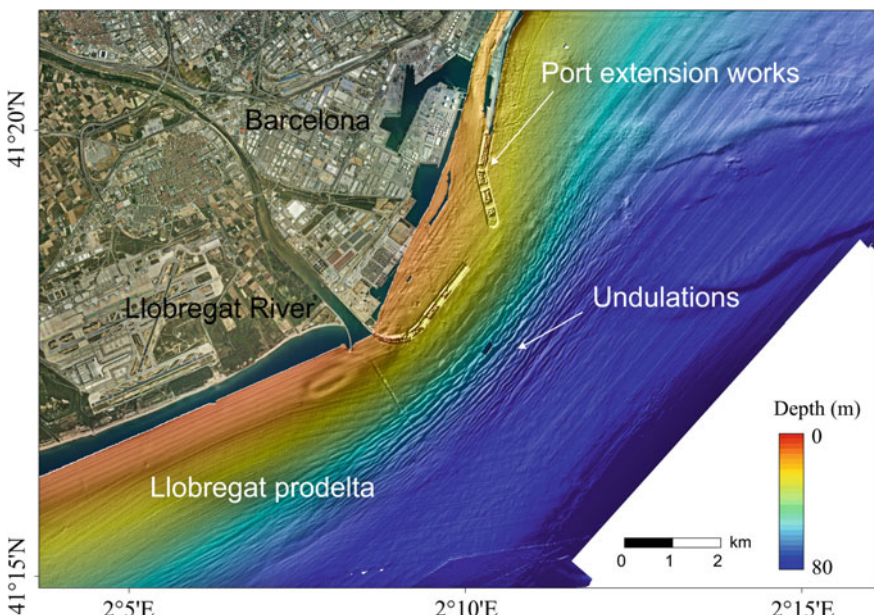


Fig. 5 Shaded colour multibeam bathymetry of the Llobregat prodelta in the Catalan continental shelf, NW Mediterranean Sea, showing undulated sedimentary features (from Urgeles et al. 2011 with permission of Springer)

The *infralittoral prograding wedge* (IPW) develops in the infralittoral environment but is not directly linked to a significant fluvial supply. It is generated by downwelling currents and associated seaward transport of sediment. The IPW extends from the supralittoral to the storm wave-base level, showing lateral continuities of tens of kilometres and thickness of several metres (Hernández-Molina et al. 2000). Across-shelf, it forms a low-angle slope (0.6° on average) that is bounded seaward by an abrupt increase in the slope gradient (about 2° on average) that extends to water depths of 40–50 m (Pickrill 1983). The main progradational development of modern IPWs has taken place during the Holocene sea-level highstand stabilisation (Hernández-Molina et al. 2000; Ercilla et al. 2010).

Large prograding sediment bodies have been also documented on the mid-outer shelf, and particularly at the shelf edge (Gardner et al. 2007; Liquete et al. 2007; Ercilla et al. 2010; Durán et al. 2013). Their location detached from the shoreline is related to the last sea-level rise. At times of slow rise, or stillstand, the shore position remained nearly constant allowing the development of prograding coastal deposits, which were drowned during subsequent episodes of rapid sea-level rise.

4.4 Bedforms

Bedforms are morphological features formed by the interaction between a flow and a sedimentary bed. They can be composed of gravel, sand or mud and of siliciclastic or carbonate sediment, displaying a wide range of spatial scales. This section focuses on different types of bedforms that are ubiquitous in continental shelves, with emphasis on their morphology, sediment characteristics, present-day activity and the processes that govern their formation and evolution.

Sand Banks, Sand Ridges and Sand Ribbons

Sand banks, sand ridges and sand ribbons are common features on many continental shelves. *Sand banks* are found on continental shelves where large amounts of sand are available from the local seabed or coastal erosion, and where strong currents are capable of moving the sediment (Dyer and Huntley 1989). Most sand banks appear to have been created during the post-glacial rise in sea-level, but they have been subsequently modified by changing currents and waves. A descriptive classification of sand banks was provided by Dyer and Huntley (1989) based on the morphology and main sediment transport pathways associated to each sand bank type; these include estuary mouth ridges, headland banner banks and open shelf ridges. Banner banks are located near headlands, islands or large rocks. They are separated from them by a channel and can be generated by unidirectional and bidirectional currents (Belderson et al. 1982; Kenyon and Cooper 2005). These bedforms are few kilometres in size and have an elongated pear-shaped form (Dyer and Huntley 1989). Sand banks are asymmetrical in cross-section, with the steeper leeward slope oblique to the direction of the flow and net sand transport.

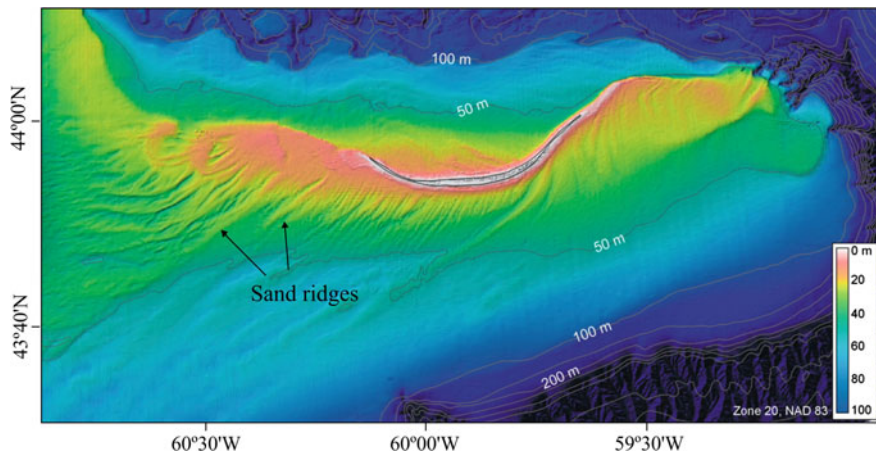


Fig. 6 Shaded colour multibeam bathymetry of Sable Island Bank, showing shoreface-connected and offshore sand ridges. (Reprinted from Li and King 2007, with permission from Elsevier)

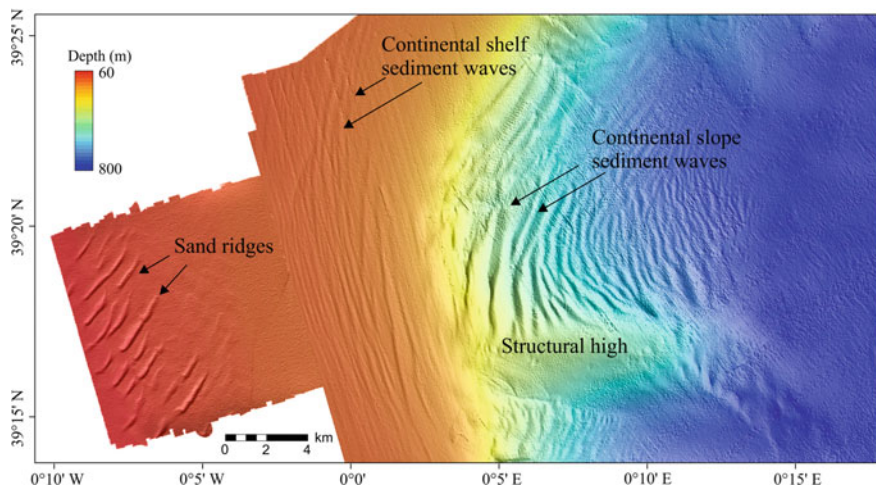


Fig. 7 Shaded colour multibeam bathymetry of the Gulf of Valencia (Western Mediterranean Sea) outer shelf and continental slope showing sand ridges in the middle shelf and sediment waves in the outer shelf and continental slope. Courtesy of M. Ribó

Sand ridges are a specific type of sand bank (Dyer and Huntley 1989), also referred to as large and very large subaqueous dunes when they are active bedforms (Ashley 1990). They are pervasive bedforms on many continental shelves worldwide (Figs. 6 and 7). In tidal-dominated settings, sand ridges show elevations up to 40 m with orientations that are primarily determined by the peak tidal direction (Dyer and Huntley 1989; Liu et al. 2007). Sand ridges in non-tidal continental

shelves, however, are smaller (up to 12 m high) and show an orientation oblique to the shoreline (Snedden et al. 2011). They show a linear, elongated shape and a predominantly asymmetric transverse profile, with steeper down-current flanks (Bassetti et al. 2006; Li and King 2007).

Sand ridges have been observed in the inner shelf but also in the middle and outer shelf at water depths greater than 40 m (Bassetti et al. 2006; Simarro et al. 2015). Sand ridges located in the middle and outer shelf are interpreted as formed in the shoreface environment through similar mechanisms to those proposed for shoreface-connected ridges, and subsequently detached from the shoreline during sea-level rise (Goff et al. 2005; Calvete et al. 2011; Nnafie et al. 2014).

Sand ribbons are flow-parallel bedforms that are much smaller than sand ridges; they are less than 200 m wide and 0.5 m high (Kenyon 1970; Amos and King 1984). They are characterised by thin, elongate bands of sand overlying a coarser lag sediment that is exposed between them (McLean 1981). They are interpreted as generated by longitudinal roll vortices or helical flow cells (McLean 1981; Amos and King 1984).

Sediment Waves

Sediment waves are large-scale (generally tens of metres to a few kilometres wavelength and several metres high) undulating, depositional bedforms that are generated beneath a current flowing at, or close to, the seafloor (Wynn et al. 2000). They consist of fine sediment (mud and silt dominated) and have been described in prodeltas (Mulder and Syvitski 1995; Trincardi and Normark 1988) (Fig. 5) as well as in the outer continental shelf (Ribó et al. 2016) (Fig. 7).

Prodeltaic sediment waves show variable sizes, with wavelengths of 20–400 m and maximum amplitudes of 4 m (Urgelés et al. 2011) (Fig. 5). They commonly have sinuous to rectilinear crests that are parallel to the bathymetric contours. Undulated sediment features on modern prodeltas have been initially interpreted as a result of sediment deformation and slope failure phenomena (Corregiari et al. 2001). However, subsequent studies suggest that the most likely mechanisms for the formation of these morphologies are related to processes in the bottom boundary layer, including sediment resuspension by internal waves (Puig et al. 2007), bottom currents (Urgeles et al. 2011) and hyperpycnal flows (Wheatcroft et al. 2006; Urgeles et al. 2011). Sediment waves have also been described in the outer shelf and upper slope showing wavelengths of several hundred metres and wave heights of up to several metres (Ribó et al. 2016). The main processes responsible for their formation include bottom currents (Lonsdale and Hollister 1979) and internal waves (Ribó et al. 2016); although in many cases multiple processes are involved (Faugères et al. 2002).

Subaqueous Dunes

Subaqueous dunes is the general term suggested by Ashley (1990) for sandy, dynamic, flow-transverse bedforms on shallow waters. The term *sand waves* is also used to describe the same type of bedforms, although they are mostly related to tidal currents (Amos and King 1984). These bedforms are ubiquitous on the continental shelf and exhibit a wide range of dimensions with heights ranging from centimetres

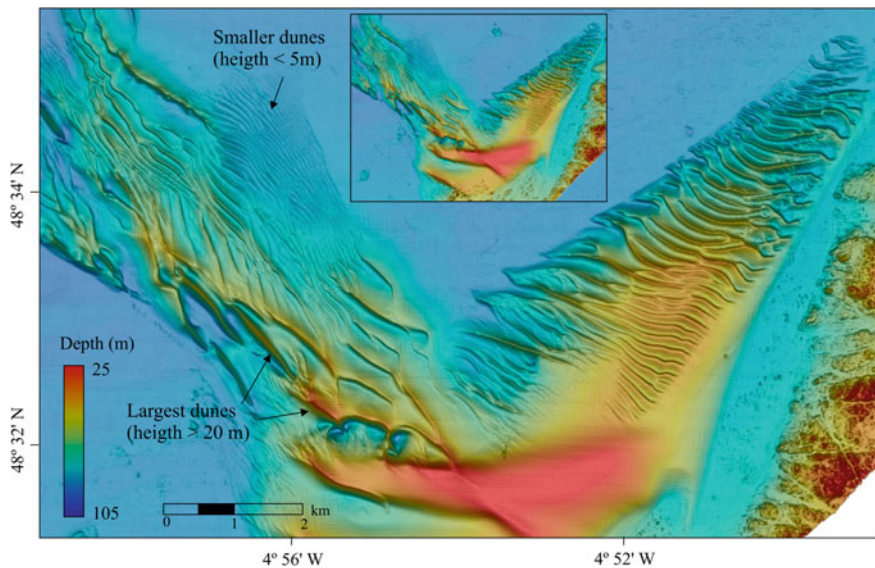


Fig. 8 Shaded colour multibeam bathymetry of the Banc du Four (Western Brittany, France). The morphology of the Banc du Four field is composed of large dunes exhibiting a great diversity of shapes and sizes developed in a deep (70–105 m depth) tidal-dominated environment. (Reprinted from Franzetti et al. 2013, with permission from Elsevier)

to 30 m, and spacing of up to 100 m (e.g. Bassetti et al. 2006; Franzetti et al. 2013) (Fig. 8). Dunes are classified based on primary descriptors of shape (2-D or 3-D) and size. Based on the wavelength (λ), Ashley (1990) classifies dunes as small (0.6–5 m), medium (5–10 m), large (10–100 m) and very large dunes ($\lambda > 100$ m). Another important morphology parameter is the dune height. Flemming (2000) provides evidence for the existence of an equilibrium geometrical relationship between wavelength and height, placing an upper limit in dune height.

Dunes may appear in extensive fields over broad sandy shelf areas or as secondary features superimposed over large-scale features, such as large and very large dunes or sand ridges (Lobo et al. 2000; Goff et al. 2005; Li and King 2007; Durán et al. 2017c). Forcing mechanisms able to induce dune formation on the continental shelf are related to tidal currents (Berné et al. 2002; Franzetti et al. 2013), wind-induced bottom currents (Cacchione et al. 1987; Guerrero et al. 2017) and water masses flowing under geostrophic conditions (Bassetti et al. 2006; Lo Iacono et al. 2010). Dunes can be stationary bedforms (Whitmeyer and FitzGerald 2008) or migrate at different rates (Ernstsen et al. 2006; Franzetti et al. 2013), providing valuable information on the local and regional current patterns and sediment transport. In non-tidal shelves, recent observations indicated that dunes migrate at very low rates (Durán et al. 2017c), but they migrate at rates of $1\text{--}17 \text{ m year}^{-1}$ in tidal settings (Le Bot et al. 2000; Schwab et al. 2014).

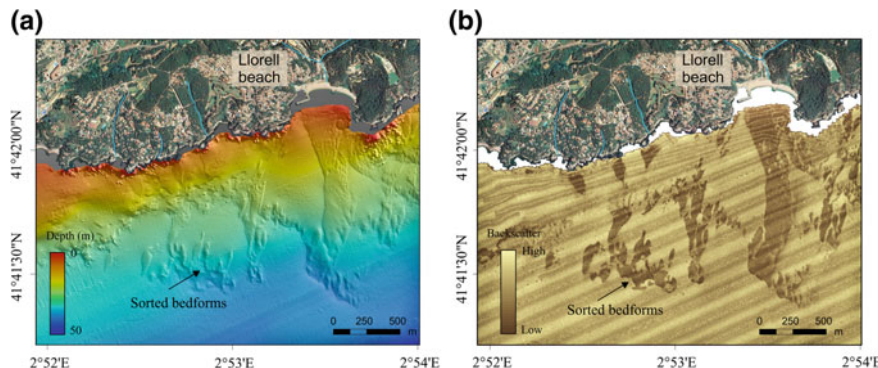


Fig. 9 **a** Shaded multibeam bathymetry and **b** backscatter imagery of the Catalan continental shelf (NW Mediterranean Sea) showing the morphology of sorted bedforms developed in the inner shelf (from Durán et al. 2017b, with permission of Springer)

Sorted Bedforms

Sorted bedforms are spatially extensive (m to km) features with subtle bathymetric relief (cm-m) present on many continental shelves. They are characterised by a sharply edged sequence of coarse-grained and fine-grained domains with little topographic relief (about 1 m) relative to the bedform spacing, which varies from metres to kilometres (Murray and Thieler 2004) (Fig. 9). They have been observed on a variety of continental shelves at water depths ranging from 10 to 90 m (e.g. Hume et al. 2003; Durán et al. 2017a, 2017b). Their formation has been related to a feedback between bed composition and sediment flux in a self-organised pattern (Murray and Thieler 2004; Coco et al. 2007). Several studies have shown that sorted bedforms tend to be ephemeral in shallow waters (down to 15–20 m) (Hume et al. 2003), while in deeper waters they are more persistent (Lo Iacono and Guillén 2008; De Falco et al. 2015).

4.5 Gas-Related Features

The presence of fluid escape features, such as seafloor *pockmarks*, was first introduced by King and MacLean (1970) over the Nova Scotian shelf. Pockmarks are seafloor depressions with steep sides and flat floors. In plan-view, they are usually circular, elliptical or elongated, and may be composite in shape (Fig. 10). Pockmarks are constrained to fine-grained substrates and show variable dimensions that can be up to 150 m wide, 200 m long, and 10 m deep (Andresen et al. 2008). Their shape, dimensions and spatial distribution depend on the capacity and composition of fluid reservoirs sourcing the venting fluids, type of the fluid escape,

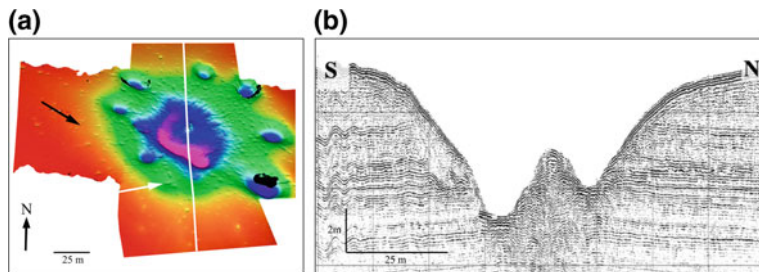


Fig. 10 **a** Perspective view of a shaded relief digital terrain model from a series of pockmarks in the Norwegian Trough. Black arrow points at a trawl-scar associated unit pockmark and white arrow points at a possible 'incipient' pockmark. White line indicates the location of the Sub-bottom profiler (SBP) record crossing the pockmark **(b)**. (Reprinted from Hovland et al. 2010, with permission from Elsevier)

sediment characteristics and configuration of underlying structures, water depth and morphology of the surrounding seafloor (Hovland and Judd 1988; Hovland et al. 2010).

4.6 Anthropogenic Features

The increasing anthropogenic activity on the continental shelf has a direct impact on the seabed. Most of the impacts are derived from bottom trawling, mineral exploitation, waste disposal and the increasing production of renewable energy. The direct physical effects of bottom trawling include scraping and ploughing of the seabed and sediment resuspension (Jones 1992; Palanques et al. 2001, 2014). Scars left by the trawl doors have a particularly strong signature on the seafloor, as evidenced by large depressions of 5–20 cm depth in sandy sediment (Krost et al. 1990). Furthermore, in areas of intense fishing, the reworking of the seafloor by trawling is so severe that it gradually modifies the shape of the submarine landscape over large spatial scales, smoothening the seabed (Fonteyne 2000; Puig et al. 2012).

The impacts of dredging activities on the seafloor, either for aggregate mining or dredging of navigation channels and harbours, entail modification of the seabed morphology and sediment dispersal during dredging and the subsequent disposal of the dredged material. As a consequence of these activities, large depressions form on the seafloor and massive sedimentation of fine sediment occurs in the dredged and disposal areas (Du Four and Van Lanker 2008; Durán et al. 2017a). Hard structures, such as pipelines on the seafloor or wind farms, can also modify sediment dynamics nearby the structures, resulting in large scours on the seafloor (Whitehouse 1998; Harris et al. 2010).

5 Key Research Questions and Future Directions

Continental shelves represent a vulnerable environment due to their extensive use for navigation, recreation, fishing and aquaculture, mineral exploration, waste disposal, and the production of renewable energy from waves, tidal currents and wind (Barrie and Conway 2014; Chiocci and Chivas 2016). Furthermore, continental shelves constitute archives of long-term environmental changes in the complex interaction among climate, sea level and sediment input (Gao and Collins 2014; Lobo and Ridente 2014). They, therefore, can be used to better understand how coastal regions have evolved in response to past sea-level changes in order to predict how they will respond to future climate change.

Over the past decades, great efforts have been made to better understand the geomorphology, seafloor characteristics and sediment transport processes on the continental shelf. However, despite the huge progress made in recent years, only a small fraction of the continental shelf is covered with high-resolution bathymetric data and several key research questions still remain to be addressed, which constitute the core of ongoing and future research. These include: (a) the evolution of continental shelves during the youngest climatic-eustatic cycles; (b) the sediment transport processes associated with the formation and dynamics of bedforms and the transfer of sediment from the continent to the deep sea; (c) the impact of exploitations activities on the continental shelf, such as dredging and sediment disposal, fishing activities, deployment of wind farms, wave power and tidal/current energy plants on the continental shelf landscape; (d) the accurate characterisation of seabed processes and landforms using permanent monitoring observatories and their integration in the marine spatial planning, particularly those associated to new uses of the marine environment such as wind farms, marine protected areas or aquaculture; and (e) the use of new accurately and fully geomorphic data mapping of continental shelves landscapes for understanding the evolutionary history of ancient landscapes and identifying potentially significant archaeological sites on the seabed.

In the last years, the characterisation of the geomorphic variability of continental shelves has seen significant evolution with innovations in seafloor mapping, especially through the advances in multibeam echosounding, laser-light detection and ranging (LiDAR), side scan sonar, ship-deployed remotely operated vehicles (ROVs), autonomous underwater vehicles (AUVs) and seismic sub-bottom profiling techniques. In association with these enhancements, improved and new methods of analysis and dating of sediment cores have provided better knowledge of the continental shelf landscape and its recent evolution during the last glacial-interglacial cycles. With the development in seafloor mapping, methods of bedform analysis are also progressing substantially to analyse high-resolution spatial data that allow quantifying bedform geometry and evolution (changes in shape and migration) and seafloor morphological changes. This, together with advances in the predictive ability of morphodynamic models and the integration of morphological, sedimentological and hydrodynamic data, contribute to advancing

the understanding of the formation, evolution and present-day dynamics of bed-forms and to assess the impact of human interventions on continental shelf morphology.

In addition to innovation in the approaches and methods, progress in the geomorphological research of continental shelves evolves thanks to knowledge transfer between different scientific disciplines and research areas. One of the most representative examples is the integration of seabed geomorphology and benthic habitats to support government spatial marine planning, management and decision making, and the designation of marine protected areas. Recently, several investigations have also paid attention to the potential of studying continental shelf morphology to update the submerged archaeological record and understand patterns of human settlement and dispersal (Bailey and Flemming 2008; Evans et al. 2014; Harff et al. 2016). This represents a new and multidisciplinary field for research where geomorphology will play a major role.

Acknowledgements This work is a contribution to the FORMED (CGL2012-33989) and ABIDES (CTM2015-65142-R) projects funded by the Spanish Ministry of Economy and Competitiveness. Our sincere appreciation goes to Marta Ribó for providing seafloor images.

References

- Allen JR (1982) Sedimentary structures: their character and physical basis. Development in Sedimentology, vol 1. Elsevier, Oxford
- Amos CL, King EL (1984) Bedforms of the Canadian eastern seaboard: a comparison with global occurrences. *Mar Geol* 57:167–208
- Anderson JB (1999) Antarctic marine geology. Cambridge University Press, Cambridge
- Andresen KJ, Huuse M, Clausen OR (2008) Morphology and distribution of Oligocene and Miocene pockmarks in the Danish North Sea—implications for bottom current activity and fluid migration. *Basin Res* 20(3):445–466
- Ashley GM (1990) Classification of large-scale subaqueous bedforms: a new look at an old problem. *J Sediment Res* 60:160–172
- Bailey G, Flemming N (2008) Archaeology of the continental shelf. *Quatern Sci Rev* 27:2153–2165
- Barrie JV, Conway KW (2014) Seabed characterization for the development of marine renewable energy on the Pacific margin of Canada. *Cont Shelf Res* 83:45–52
- Bassetti M, Jouet G, Dufois F et al (2006) Sand bodies at the shelf edge in the Gulf of Lions (Western Mediterranean): deglacial history and modern processes. *Marine Geol* 234:93–109
- Batchelor CL, Dowdeswell JA, Ottesen D (2018) Submarine Glacial Landforms. In: Micallef A, Krastel S, Savini A (eds) Submarine Geomorphology. Springer International Publishing
- Belderson RH, Johnson MA, Kenyon NH (1982) Bedforms. In: Stride AH (ed) Offshore tidal sands processes and deposits. Chapman and Hall, London, pp 27–57
- Berné S, Vagner P, Guichard F et al (2002) Pleistocene forced regressions and tidal sand ridges in the East China Sea. *Mar Geol* 188:293–315
- Bradley WC, Griggs GB (1976) Form, genesis, and deformation of central California wave-cut platforms. *Geol Soc Am Bull* 87(3):433
- Bricker OP (1971) Beachrock and intertidal cement. In: Bricker OP (ed) Carbonate cements. Johns Hopkins Press, Baltimore, pp 1–13
- Burchette TP, Wrigth VP (1992) Carbonate ramp depositional systems. *Sed Geol* 79:3–57

- Cacchione DA, Grant WD, Drake DE et al (1987) Storm-dominated bottom boundary layer dynamics on the northern California continental shelf: measurements and predictions. *J Geophys Res* 92:1817–1827
- Calvete D, Falqués A, de Swart HE et al (2011) Modelling the formation of shoreface-connected sand ridges on storm-dominated inner shelves. *J Fluid Mech* 441:169–193
- Chiocci F, Chivas AR (2016) An overview of the continental shelves of the world: their evolution during the last glacio-eustatic cycle. *Geol Soc Lond Mem* 41:1–5
- Clark CD (1993) Mega-scale glacial lineations and cross-cutting ice flow landforms. *Earth Surf Proc Land* 18:1–29
- Coco G, Murray B, Green MO (2007) Sorted bed forms as self-organized patterns: 1. Model development. *J Geophys Res* 112:F03015
- Coleman, J (1975) Deltas: processes of deposition and models for exploration (Continuing Education, Champaign, IL)
- Cohen KM, Lobo FJ (2013) Continental shelf drowned landscapes: submerged geomorphological and sedimentary record of the youngest cycles. *Geomorphology* 203:1–5
- Collina-Girard J (2002) Underwater mapping of Late quaternary submerged shorelines in the Western Mediterranean Sea and the Caribbean Sea. *Quatern Int* 92:63–72
- Correggiari A, Trincardi F, Langone L et al (2001) Styles of failure in late Holocene highstand prodelta wedges on the Adriatic shelf. *J Sediment Res* 71:218–236
- Dalrymple RW, Hoogendoorn EL (1997) Erosion and deposition on migrating shoreface-attached Ridges, Sable Island, Eastern Canada. *Geosci Can* 24:25–35
- De Falco G, Budillon F, Conforti A et al (2015) Sorted bedforms over transgressive deposits along the continental shelf of western Sardinia (Mediterranean Sea). *Mar Geol* 259:75–88
- Dowdeswell JA, Ó Cofaigh C, Taylor J et al (2002) On the architecture of high-latitude continental margins: the influence of ice-sheet and sea-ice processes in the Polar North Atlantic, vol 203. Geological Society, London, Special Publications, pp 33–54
- Du Four I, Van Lancker V (2008) Changes of sedimentological patterns and morphological features due to the disposal of dredge spoil and the regeneration after cessation of the disposal activities. *Mar Geol* 255:15–29
- Duce S, Vila-Concejo A, Hamylton SM et al (2016) A morphometric assessment and classification of coral reef spur and groove morphology. *Geomorphology* 265:68–83
- Durán R, Canals M, Lastras G et al (2013) Sediment dynamics and post-glacial evolution of the continental shelf around the Blanes submarine canyon head (NW Mediterranean). *Prog Oceanogr* 118:28–46
- Durán R, Canals M, Sanz JL et al (2014) Morphology and sediment dynamics of the northern Catalan continental shelf northwestern Mediterranean Sea. *Geomorphology* 204:1–20
- Durán R, Guillén J, Simarro G et al (2015) Sand ridges in the mid–outer shelf as potential sand borrows areas (NW Mediterranean). In: *Coastal sediments 2015*, World Scientific
- Durán R, Alonso B, Ercilla G et al (2017a) Dynamics of sorted bedforms on a shallow infralittoral prograding wedge influenced by dredging (El Masnou, NW Mediterranean). In: Guillén J, Acosta J, Chiocci F, Palanques A (eds) *Atlas of Mediterranean bedforms*, pp 135–141
- Durán R, Guillén J, Muñoz A (2017b) Sorted bedforms developed on Sandy deposits derived from small ephemeral steams (Catalan continental shelf). In: Guillén J, Acosta J, Chiocci F, Palanques A (eds) *Atlas of Mediterranean bedforms*, pp 127–133
- Durán R, Guillén J, Rivera J et al (2017c) Subaqueous dunes over sand ridges in the Murcia outer shelf. In: Guillén J, Acosta J, Chiocci F, Palanques A (eds) *Atlas of bedforms in the Western Mediterranean*, pp 187–192
- Dyer KR (1970) Linear erosional furrows in Southampton water. *Nature* 255:56–58
- Dyer KR, Huntley DA (1989) The origin, classification and modelling of sand banks and ridges. *Cont Shelf Res* 19:1285–1330
- Elliot T (1986) Deltas. In: Reading HG (ed) *Sedimentary environments and facies*. Blackwell Scientific Publications, Oxford, pp 113–154
- Emery KO (1952) Continental shelf sediments of southern California. *Geol Soc Am Bull* 63:1005–1108

- Emery KO (1968) Relict sediments on continental shelves of world. *Geol Soc Am Bull* 52:445–464
- Emery KO (1980) Continental margins—classification and petroleum prospects. *Geol Soc Am Bull* 64:297–315
- Ercilla G, Estrada F, Casa D et al (2010) The El Masnou infralittoral sedimentary environment (Barcelona province, NW Mediterranean Sea): morphology and Holocene seismic stratigraphy. *Scientia Mar* 74:179–196
- Ernstsen VB, Noormets R, Winter C et al (2006) Quantification of dune dynamics during a tidal cycle in an inlet channel of the Danish Wadden Sea. *Geo Marine Lett* 26:151–163
- Evans G, Collins BM (1975) The transportation and deposition of suspended sediment over the intertidal flats of the Wash. In: Hails J, Carr A (eds) *Nearshore sediment dynamics and sedimentation*. Wiley, Chichester, pp 273–306
- Evans A, Flemming N, Flatman J (2014) *Prehistoric archaeology of the continental shelf*. Springer, New York
- Fairbanks RG (1989) A 17,000-year glacio-eustatic sea-level record: influence of glacial melting rates on the Younger Dryas event and deep-ocean circulation. *Nature* 342:637–642
- Faugères J-C, Gonthier E, Mulder T et al (2002) Multi-process generated sediment waves on the Landes Plateau (Bay of Biscay, North Atlantic). *Mar Geol* 182:279–302
- Flemming BW (1978) Underwater sand dunes along the southeast African continental margin—observations and implications. *Mar Geol* 26:177–198
- Flemming BW (2000) The role of grain size, water depth and flow velocity as scaling factors controlling the size of subaqueous dunes. In: Trentesaux A, Garlan T (eds) *Mar Sandwave Dyn* 23:55–60
- Flood RD (1983) Classification of sedimentary furrows and a model for furrow initiation and evolution. *Geol Soc Am Bull* 94:630–639
- Fonteyne R (2000) Physical impacts of beam trawls on sea bed sediments. In: Kaiser MJ, de Groot SJ (eds) *Effects of fishing on non-target species and habitats. Biological, conservation and socio-economic issues*. Blackwell Science, Oxford, pp 15–36
- Franzetti M, Le Roy P, Delacourt C et al (2013) Giant dune morphologies and dynamics in a deep continental shelf environment: example of the banc du four (Western Brittany, France). *Mar Geol* 346:17–30
- Galloway WE (1975) Process framework for describing the morphological and stratigraphic evolution of deltaic depositional systems. In: Broussard ML (ed) *Deltas*. Houston Geological Society, Texas, pp 87–98
- Galparsoro I, Borja A, Legorburu I et al (2010) Morphological characteristics of the Basque continental shelf (Bay of Biscay, northern Spain); their implications for Integrated Coastal Zone Management. *Geomorphology* 118:314–329
- Gao S, Collins MB (2014) Holocene sedimentary systems on continental shelves. *Mar Geol* 352:268–294
- Gardner JV, Calder BR, Hughes Clarke JE et al (2007) Drowned shelf–edge deltas, barrier islands and related features along the outer continental shelf north of the head of De Soto Canyon, NE Gulf of Mexico. *Geomorphology* 89:370–390
- Geyer WR, Traykovski P (2001) Modeling of clinoforms created by wave/current supported gravity flows. Carl Friedrichs, Virginia Institute of Marine Science
- Goff JA, Jr Austin, Gulick S et al (2005) Recent and modern marine erosion on the New Jersey outer shelf. *Mar Geol* 216:275–296
- Guerrero Q, Guillén J, Durán R et al (2017) Contemporary subaqueous dune field development over and abandoned river mouth (Ebro Delta). In: Guillén J, Acosta J, Chiocci F, Palanques A (eds) *Atlas of Mediterranean bedforms*, pp 89–93
- Hanebuth T, Stattegger K, Groote PM (2000) Rapid Flooding of the Sunda Shelf: a late-glacial sea-level record. *Science* 288:1033–1035
- Harff J, Bailey GN, Lüth F (2016) Geology and archaeology: submerged landscapes of the continental shelf: an introduction, vol 411. Geological Society London, Special Publications, pp 1–8

- Harris PT, Davies PJ (1989) Submerged reefs and terraces on the shelf edge of the Great Barrier Reef, Australia—morphology, occurrence and implications for reef evolution. *Coral Reefs* 8:87–98
- Harris PT, Macmillan-Lawler M, Rupp J et al (2014) Geomorphology of the oceans. *Mar Geol* 352:4–24
- Harris MS, Sautter LR, Johnson KL et al (2013) Continental shelf landscapes of the southeastern United States since the last interglacial. *Geomorphology* 203:6–24
- Harris JM, Whitehouse RJS, Benson T (2010) The time evolution of scour around offshore structures. *Marit Eng* 163:3–17
- Hernández-Molina FJ, Fernández-Salas LM, Lobo F et al (2000) The infralittoral prograding wedge: a new large-scale progradational sedimentary body in shallow water environments. *Geo Mar Lett* 20:109–117
- Hovland M, Judd AG (1988) Seabed pockmarks and seepages. Impact on geology, biology and the marine environment. Graham & Trotman Ltd., London
- Hovland M, Heggland R, De Vries MH et al (2010) Unit-pockmarks and their potential significance for predicting fluid flow. *Marine Petroleum Geology* 27:1190–1199
- Hume TM, Trembanis AC, Hill A et al (2003) Spatially variable, temporally stable, sedimentary facies on an energetic inner shelf. *Coastal Sediments'03*. ASCE Press, Clearwater Beach, Florida
- Inman DL, Nordstrom CE (1971) On the tectonic and morphologic classification of coasts. *J Geol* 79:1–21
- Jones JB (1992) Environmental impact of trawling on the seabed: a review. *NZ J Mar Freshwat Res* 26:59–67
- Kelletat D (2006) Beachrock as sea-level indicator? Remarks from a geomorphological point of view. *J Coastal Res* 22:1555–1564
- Kenyon NH (1970) Sand ribbons of European tidal seas. *Mar Geol* 9:25–39
- Kenyon NH, Cooper B (2005) Sand banks, sand transport and offshore wind farms. Technical report by ABP Marine Environmental Research Ltd. (ABPmer)
- King LH, MacLean B (1970) Pockmarks on the Scotian Shelf. *Geol Soc Am Bull* 81:3141–3148
- Kostylev VE, Todd BJ, Fader GBJ et al (2001) Benthic habitat mapping on the Scotian Shelf based on multibeam bathymetry, surficial geology and sea floor photographs. *Mar Ecol Prog Ser* 219:121–137
- Krost P, Bernhard M, Werner F et al (1990) Otter trawl tracks in Kiel Bay (Western Baltic) mapped by side-scan sonar. *Meeresforschung* 32:344–353
- Le Bot S, Trentesaux A, Garlan T et al (2000) Influence des tempêtes sur la mobilité des dunes tidales dans le détroit du Pas-de-Calais. *Oceanol Acta* 23:129–141
- Lewis A (2001) Great Barrier Reef Depth and Elevation Model (GBRDEM). Technical Report 33, CRC Reef Research Centre, Townsville
- Li MZ, King EL (2007) Multibeam bathymetric investigations of the morphology of sand ridges and associated bedforms and their relation to storm processes, Sable Island Bank, Scotian Shelf. *Mar Geol* 243:200–228
- Liquete C, Canals M, Lastras G et al (2007) Long-term development and current status of the Barcelona continental shelf: A source-to-sink approach. *Cont Shelf Res* 27(1779–1800):9
- Liu Z, Berné S, Saitoc Y et al (2007) Internal architecture and mobility of tidal sand ridges in the East China Sea. *Cont Shelf Res* 27:1820–1834
- Lo Iacono C, Guillén J (2008) Environmental conditions for gravelly and pebbly dunes and sorted bedforms on a moderate-energy inner shelf (Marettimo Island, Italy, western Mediterranean). *Cont Shelf Res* 28:245–256
- Lo Iacono C, Guillén J, Puig P et al (2010) Large-scale bedforms along a tideless outer shelf setting in the western Mediterranean. *Cont Shelf Res* 30:1802–1813
- Lo Iacono C, Savini A, Basso D (2018) Cold-water carbonate bioconstructions. In: Micallef A, Krastel S, Savini A (eds) *Submarine Geomorphology*, Springer International Publishing

- Lobo FJ, Ridente D (2014) Stratigraphic architecture and spatio-temporal variability of high-frequency (Milankovitch) depositional cycles on modern continental margins: An overview. *Mar Geol* 352:215–247
- Lonsdale PF, Hollister C (1979) A near-bottom traverse of Rockall Trough: hydrographic and geologic inferences. *Oceanol Acta* 2:91–105
- Martinez-Martos M, Galindo-Zaldívar J, Lobo FJ et al (2016) Buried marine-cut terraces and submerged marine-built terraces: the Carchuna-Calahonda coastal area (southeast Iberian Peninsula). *Geomorphology* 264:29–40
- McBride RA, Moslow TF (1991) Origin, evolution, and distribution of shoreface sand ridges, Atlantic inner shelf, U.S.A. *Mar Geol* 97:57–85
- McLean S (1981) The role of non-uniform roughness in the formation of sand ribbons. *Mar Geol* 42:49–74
- Micallef A, Foglini F, Le Bas T et al (2013) The submerged paleolandscape of the Maltese Islands: Morphology, evolution and relation to Quaternary environmental change. *Mar Geol* 335:129–147
- Milliman JD, Meade RH (1983) World-wide delivery of river sediment to the oceans. *J Geol* 91:1–21
- Mulder T, Syvitski JPM (1995) Turbidity currents generated at river mouths during exceptional discharges to the world oceans. *J Geol* 103:285–299
- Murray AB, Thieler ER (2004) A new hypothesis and exploratory model for the formation of large-scale inner-shelf sediment sorting and “rippled scour depressions”. *Cont Shelf Res* 24:295–315
- Nittrouer CA, Wright LD (1994) Transport of particles across continental shelves. *Rev Geophys* 32:85–113
- Nnafei A, De Swart HE, Calvete D et al (2014) Effects of sea-level rise on the formation and drowning of shoreface-connected sand ridges, a model study. *Cont Shelf Res* 80:32–48
- Ottesen D, Dowdeswell JA (2006) Assemblages of submarine landforms produced by tidewater glaciers in Svalbard. *J Geophys Res* 111:F01016
- Palanques A, Guillén J, Puig P (2001) Impact of bottom trawling on water turbidity and muddy sediment of an unfished continental shelf. *Limnol Oceanogr* 46:1100–1110
- Palanques A, Puig P, Guillén J et al (2014) Effects of bottom trawling on the Ebro continental shelf sedimentary system (NW Mediterranean). *Cont Shelf Res* 72:83–98
- Pickrill RA (1983) Wave-built shelves on some low-energy coasts. *Mar Geol* 51:193–216
- Pirazzoli PA (2005) Marine terraces. In: Schwartz M (ed) *Encyclopedia of coastal science*. Springer, Berlin
- Potter PE (1967) Sand bodies and sedimentary environments; a review. *Geol Soc Am Bull* 51:337–365
- Puig P, Ogston AS, Guillén J et al (2007) Sediment transport processes from the topset to the foreset of a crenulated clinoform (Adriatic Sea). *Cont Shelf Res* 27:452–474
- Puig P, Canals M, Company JB et al (2012) Ploughing the deep sea floor. *Nature* 489:286–289
- Ramsay PJ, Cooper JAG (2002) Late quaternary sea-level change in South Africa. *Quatern Res* 57:82–90
- Ribó M, Puig P, Muñoz A et al (2016) Morphobathymetric analysis of the large fine-grained sediment waves over the Gulf of Valencia continental slope (NW Mediterranean). *Geomorphology* 253:22–37
- Russel RJ (1963) Beachrock. *J Trop Geogr* 17:24–27
- Schwab WC, Baldwin E, Denny JF et al (2014) Modification of the Quaternary stratigraphic framework of the inner-continental shelf by Holocene marine transgression: an example offshore of Fire Island, New York. *Mar Geol* 355:346–360
- Shaw J, Todd BJ, Li MZ et al (2012) Anatomy of the tidal scour system at Minas Passage, Bay of Fundy, Canada. *Mar Geol* 323:123–134
- Shepard FP (1963) Submarine geology, 2nd edn. Harper and Row, New York
- Shepard FP, Moore DG (1955) Central Texas coast sedimentation: characteristics of sedimentary environment, recent history, and diagenesis. *Bull AAPG* 39:1463–1593

- Siddall M, Chappell J, Potter EK (2007) Eustatic sea-level during past interglacials. In: Sirocko F, Claussen M, Goñi MFS, Litt T (eds) *The climate of past interglacials developments in quaternary sciences*. Elsevier, Amsterdam, pp 75–92
- Simarro G, Guillén J, Puig P et al (2015) Sediment dynamics over sand ridges on a tideless mid-outer continental shelf. *Mar Geol* 361:25–40
- Snedden JW, Tillman RW, Culver SJ (2011) Genesis and evolution of a mid-shelf, storm-built sand ridge, New Jersey continental shelf, U.S.A. *J Sediment Res* 81:534–552
- Southard JB, Boguchwal LA (1990) Bed configurations in steady unidirectional water flows, part 2. synthesis of flume data. *J Sediment Petrol* 60:658–679
- Sternberg RW, Johnson RV II, Cacchione DA et al (1986) An instrument system for monitoring and sampling suspended sediment in the benthic boundary layer. *Mar Geol* 71:187–199
- Swift DJP, Stanley DJ, Curran JR (1971) Relict sediments on continental shelves: a reconsideration. *J Geol* 79:322–346
- Swift DJP (1972) Implications of sediment dispersal from bottom current measurements; some specific problems in understanding bottom sediment distribution and dispersal on the continental shelf: a discussion of two papers. In: Swift DJP, Duane DB, Pilkey OH (eds) *Shelf sediment transport: process and pattern* Dowden, Hutchinson and Ross, Stroudsburg, Pennsylvania, pp 363–371
- Syvitski JPM, Morehead MD (1999) Estimating river-sediment discharge to the ocean: application to the Eel Margin, northern California. *Mar Geol* 154:13–28
- Thompson WC (1961) A genetic classification of continental shelves. *Proc Pacific Sci Congr* 12:30–39
- Trincardi F, Normark WR (1988) Sediment waves on the Tiber prodelta slope: interaction of deltaic sedimentation and currents along the shelf. *Geo Mar Lett* 8:149–157
- Urgeles R, Cattaneo A, Puig P et al (2011) A review of undulated sediment features on Mediterranean prodeltas: distinguishing sediment transport structures from sediment deformation. *Marine Geophys Res* 32:49–69
- Werner F, Newton RS (1975) The pattern of large-scale bedforms in the Langeland Belt (Baltic Sea). *Mar Geol* 19:25–59
- Wheatcroft RA, Stevens AW, Hunt LM et al (2006) The large-scale distribution and internal geometry of the fall 2000 Po river flood deposit: evidence from digital X-radiography. *Cont Shelf Res* 26:499–516
- Whitehouse RJS (1998) *Scour at marine structures: a manual for practical applications*. Thomas Telford, London
- Whitmeyer SJ, Fitzgerald DM (2008) Episodic dynamics of a sand wave field. *Mar Geol* 252: 24–37
- Wright LD (1985) River deltas. In: Davis AR (ed) *Coastal sedimentary environments*. Springer, New York, pp 1–76
- Wright LD, Thom BG (1977) Coastal depositional landforms: a morphodynamic approach. *Prog Phys Geogr* 1:412–459
- Wynn RB, Weaver PPE, Ercilla G et al (2000) Sedimentary processes in the Selvage sediment-wave field, NE Atlantic: new insights into the formation of sediment waves by turbidity currents. *Sedimentology* 47:1181–1197

Submarine Glacial Landforms

Christine L. Batchelor, Julian A. Dowdeswell and Dag Ottesen

Abstract The development of a range of geophysical imaging techniques, including multi-beam swath bathymetry and shallow-acoustic profiling, has enabled the identification and interpretation of submarine glacial landforms on and beneath the seafloor of formerly-glaciated continental margins. The analysis of these landforms provides information about past ice-sheet dynamic behaviour and the mechanisms by which sediment is eroded, transported and deposited by ice sheets. Submarine glacial landforms can be categorised into subglacial, ice-marginal and glacimarine features. The majority of subglacially produced landforms, including mega-scale glacial lineations and drumlins, are elongate features that are orientated parallel to the direction of former ice flow. In contrast, ice-marginal landforms, including moraines and grounding-zone wedges, are orientated transverse to the former ice-flow direction. Ice-marginal landforms reveal the positions of still-stands or minor re-advances in the grounding-zone during general ice-sheet retreat. Glacimarine landform associations include ploughmarks that are formed by the grounding of iceberg keels on the seafloor, and smooth basin-fill sediments produced by suspension settling of material derived from meltwater plumes. The typical distribution of glacial landforms on formerly glaciated continental margins is illustrated using the case study of the Norwegian continental shelf and slope. The locations of former fast-flowing ice streams are associated with deep cross-shelf troughs that contain elongate subglacial landforms. Major glacial-sedimentary depocentres or trough-mouth fans are typically present on the continental slope beyond trough mouths. In contrast, relatively shallow inter-ice stream banks on the continental shelf are characterised by transverse moraine ridges and widespread iceberg ploughmarks.

C.L. Batchelor (✉) · J.A. Dowdeswell
Scott Polar Research Institute, University of Cambridge,
Cambridge CB2 1ER, Cambridge, England, UK
e-mail: clb70@cam.ac.uk

D. Ottesen
Geological Survey of Norway, Postboks 6315 Sluppen, N-7491, Trondheim, Norway

1 Introduction

Ice sheets expanded across the continental shelf beyond mid- and high-latitude land masses on many occasions during the glacial-interglacial cycles of the Quaternary (e.g. Svendsen et al. 1999; Dyke et al. 2002). The advance and retreat of ice across these margins has resulted in the formation of distinctive assemblages of subglacial, ice-marginal and glacimarine landforms (Table 1). Whereas subaerial erosion and human activity have led to a fragmented record of glacial activity on land, glacial landforms are often well preserved in the marine environment, where they can be identified within deglaciated fjords and on the continental shelf and slope (e.g. Solheim et al. 1990; Shipp et al. 1999; Dowdeswell et al. 2002; Ottesen et al. 2005; Larter et al. 2012).

The interpretation of submarine glacial landforms has been made possible by the advent of geophysical imaging techniques. The morphology of the seafloor was initially investigated using single-beam echo sounders, which acquired a line of seafloor depth soundings beneath the ship (e.g. Damuth 1978). Technological improvements in the past few decades have facilitated the use of, first, side-scan sonar and then multi-beam echo sounders to map wide regions of the seafloor, whilst shallow-acoustic and 2-D seismic-reflection profiles enabled the initial recognition of older landforms on buried horizons. More recently, 3-D seismic reflection surveys have been used to interpret the submarine glacial landform record with high temporal and spatial resolution (e.g. Dowdeswell et al. 2006).

The analysis of submarine glacial landforms facilitates reconstructions of the configuration and dynamics of past glaciers and ice sheets. Understanding past rates of change is also important information against which to assess model predictions of future responses of the Greenland and Antarctic ice sheets to climatic change (Stokes et al. 2016). A key focus within ice-sheet reconstruction is the identification of the sites of former ice streams, which are relatively narrow corridors of fast-flowing ice set within slower-flowing regions of an ice sheet (Bentley 1987; Dowdeswell and Siegert 1999; Whillans et al. 2001). Ice streams respond dynamically to perturbations over short, sub-decadal, time-scales (e.g. Anandakrishnan and Alley 1997; Joughin et al. 2003) and also have the potential to force abrupt climatic change through the rapid delivery of ice and meltwater to the marine ice-sheet margin (e.g. MacAyeal 1993; Clark 1994).

Erosion of the continental shelf by fast-flowing ice streams has resulted in the formation of deep bathymetric depressions termed cross-shelf troughs, which are bordered by shallower banks (Vorren and Laberg 1997; Dowdeswell and Siegert 1999; Batchelor and Dowdeswell 2014). Cross-shelf troughs typically contain assemblages of glacial landforms that are indicative of fast, ice-streaming flow, including subglacially produced elongate and streamlined landforms and pervasively deformed till (e.g. Stokes and Clark 2001; Shipp et al. 1999; Ó Cofaigh et al. 2002; Dowdeswell et al. 2004a). Prograding sedimentary depocentres, known as trough-mouth fans, typically develop on the continental slope seaward of cross-shelf troughs that have experienced high rates of sediment delivery to the

Table 1 List of studies covering the environments and landforms discussed in this chapter

Environment	Landform	References
<u>Subglacial</u>	Mega-scale glacial lineations	Stokes and Clark (1999, 2002); Ó Cofaigh et al. (2002); Dowdeswell et al. (2004a); Ottesen et al. (2005, 2007)
	Flutes and drumlins	Shipp et al. (1999); Wellner et al. (2001); Ó Cofaigh et al. (2002)
	Crag-and-tails	Ottesen et al. (2005); Ó Cofaigh et al. (2013)
	Ice-moulded bedrock	Wellner et al. (2001); Dowdeswell et al. (2014)
	Hill-hole pairs	Sættem (1990); Ottesen et al. (2005); Dowdeswell et al. (2010)
	Crevasse-fill ridges	Solheim (1991); Boulton et al. (1996); Ottesen and Dowdeswell (2006), Ottesen et al. (2008)
	Tunnel valleys (glaciifluvial)	Ó Cofaigh (1996); Praeg (2003)
<u>Ice-marginal</u>	Eskers (glaciifluvial)	Ottesen and Dowdeswell (2006); Ottesen et al. (2008)
	Terminal and recessional moraine ridges	Powell (1983); Seramur et al. (1997); Vorren and Plassen (2002); Ottesen et al. (2005); Bradwell et al. (2008)
	Hummocky-terrain belts	Ottesen and Dowdeswell (2009); Elvenes and Dowdeswell (2016)
	Small retreat moraines	Boulton (1986); Shipp et al. (2002); Ottesen and Dowdeswell (2006); Todd et al. (2007)
	Grounding-zone wedges	Anderson (1997); Powell and Alley (1997); Ó Cofaigh et al. (2005); Dowdeswell and Fugelli (2012); Batchelor and Dowdeswell (2015)
	Ice-proximal fans	Powell (1990); Lønne (1995); Powell and Domack (1995); Dowdeswell et al. (2015)
	Ice-stream lateral shear-zone moraines	Stokes and Clark (2002); Ottesen et al. (2005, 2008)
<u>Glacimarine</u>	Ice-stream lateral marginal-moraines	Rydningen et al. (2013); Batchelor and Dowdeswell (2016)
	Trough-mouth fan	Vorren et al. (1988); King et al. (1996); Dowdeswell et al. (1998); Laberg et al. (2000)
<u>Marine</u>	Iceberg and sea-ice keel ploughmarks	Woodworth-Lynas et al. (1991); Dowdeswell et al. (1993); Mertz et al. (2008)
	Smooth basin-fill from meltwater plumes	Cowan and Powell (1990); Cai et al. (1997); Ó Cofaigh and Dowdeswell (2001)
Wave and current features	Howe and Pudsey (1999); Garçia et al. (2012)	
Mass movement events	Laberg and Vorren (1993); Vanneste et al. (2006); Piper et al. (2012)	

shelf edge over successive full-glacial periods (Dowdeswell et al. 1996; Elverhøi et al. 1998; Dowdeswell and Siegert 1999). The glacial landforms that are preserved on the intervening shallower banks are characteristic of slower-flowing ice (e.g. Ottesen and Dowdeswell 2009).

In this chapter, we describe the submarine glacial landforms that have been identified on mid- to high-latitude continental margins (Figs. 1, 2, 3, 4, 5 and Table 1). The typical distribution of these landforms within cross-shelf troughs and on shallower banks is illustrated using the example of the formerly-glaciated Norwegian margin (Figs. 6 and 7).

2 Landforms Produced in Different Glacial-Process Environments

2.1 Subglacial Landforms

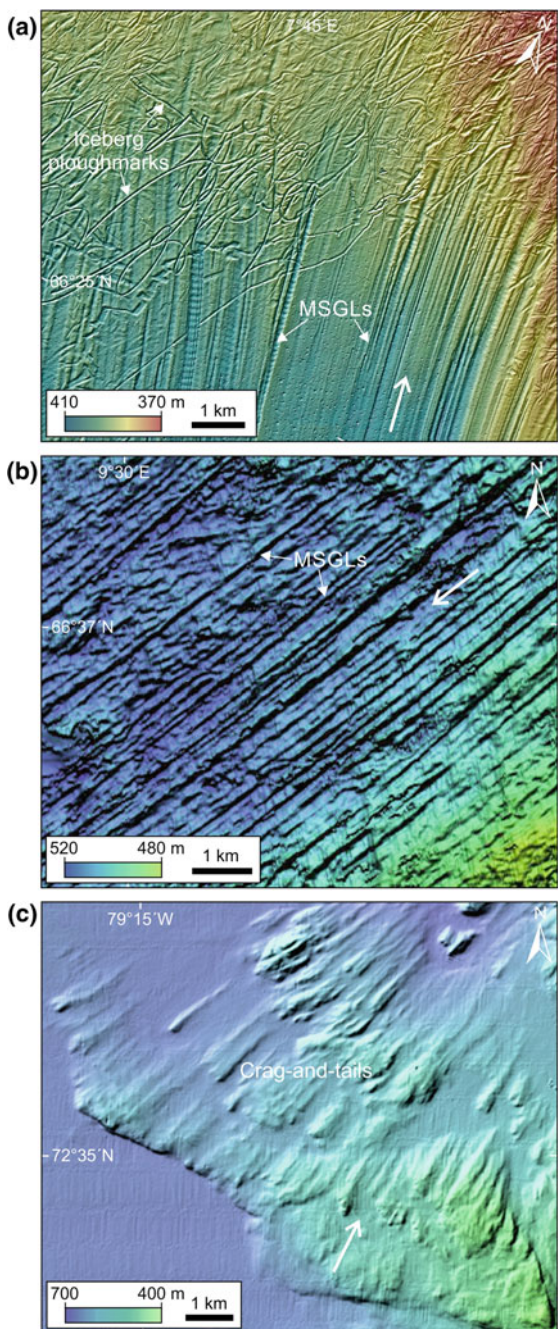
The majority of subglacially produced landforms, including mega-scale glacial lineations (MSGLs), flutes, drumlins, crag-and-tails and ice-moulded bedrock, are streamlined in the direction of ice flow (Fig. 1 and Table 1) and can therefore be used to infer former ice-flow patterns. Hill-hole pairs, crevasse-fill ridges and glacifluvial tunnel valleys and eskers (Fig. 2) are also formed subglacially.

2.1.1 Mega-Scale Glacial Lineations and Other Streamlined Subglacial Landforms

MSGLs (Fig. 1a, b) are elongate sedimentary ridges that have typical lengths of up to a few tens of kilometres, widths of a few hundred metres and amplitudes of a few metres (Stokes and Clark 2002). They have high elongation (length:width) ratios of greater than 10:1, and generally occur in groups of parallel to sub-parallel ridges that have regular spacing of a few hundred metres (Clark 1993; Stokes and Clark 2002; Spagnolo et al. 2014). MSGLs have been recognised on the seafloor of a number of formerly glaciated continental margins, where they are typically identified within cross-shelf troughs (Elverhøi et al. 1995; Shipp et al. 1999; Ó Cofaigh et al. 2002; Ottesen et al. 2005; Dowdeswell et al. 2014). Sub-bottom acoustic profiles (e.g. Fig. 5a) and sediment cores show that MSGLs are formed within an acoustically-transparent structureless diamict of low shear strength, which is interpreted as subglacial deformation till (e.g. Dowdeswell et al. 2004a).

The close association of MSGLs with cross-shelf troughs and areas of deformable sediment has led to these features being considered diagnostic of grounded, fast-flowing ice within ice streams (e.g. Stokes and Clark 2002; Dowdeswell et al. 2004a; Evans et al. 2005). This interpretation is supported by the identification of MSGLs forming beneath modern active ice streams in West Antarctica (King et al. 2009).

Fig. 1 Examples of subglacially produced streamlined submarine landforms. White arrows show former ice-flow directions. **a** Seafloor mega-scale glacial lineations (*MSGLs*) overprinted by iceberg ploughmarks on the Norwegian continental shelf. **b** MSGLs on a buried surface around 100 m deep on the mid-Norwegian margin (adapted from Dowdeswell et al. 2006). **c** Seafloor crag-and-tail features in Eclipse Sound, Baffin Island, Arctic Canada (adapted from Dowdeswell et al. 2016)



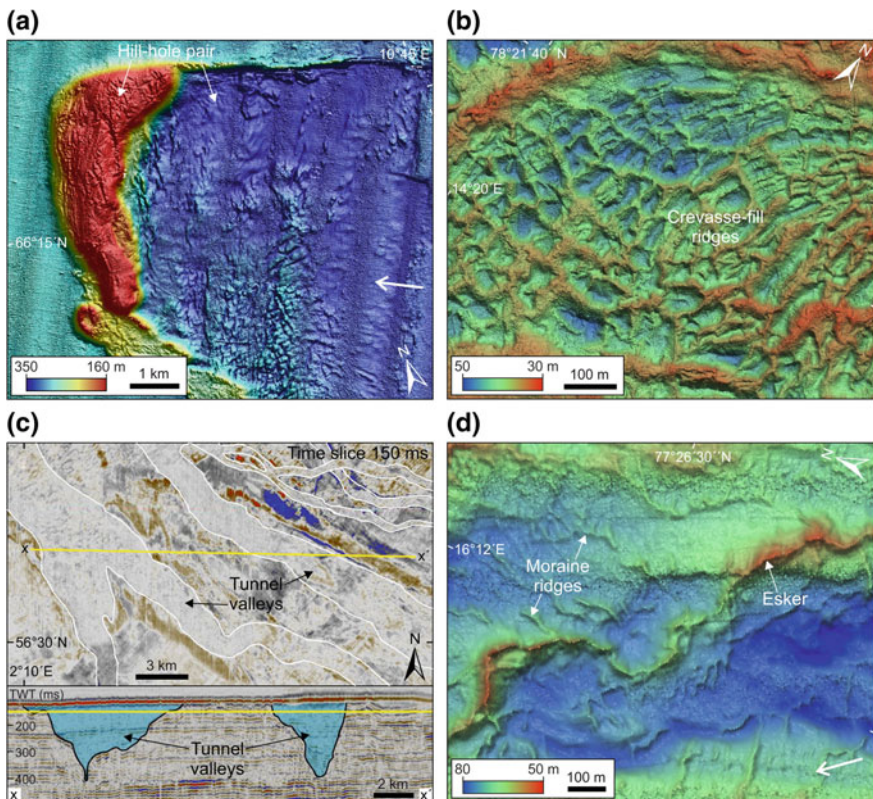


Fig. 2 Examples of subglacially produced, non-streamlined landforms. **a** Seafloor hill-hole pair on the Norwegian margin. **b** Crevasse-fill ridges on the seafloor of Borebukta, Isfjorden, Spitsbergen. **c** Upper time slice of 3D seismic-reflection data, showing a network of tunnel valleys in the North Sea. Lower seismic cross-profile of tunnel valleys in the North Sea. **d** Sinuous esker on the seafloor of Van Keulenfjorden, Spitsbergen

There is currently no consensus regarding the process by which MSGLs are formed. Some theories invoke a predominantly erosional mechanism, by which MSGLs are produced by the ploughing action of basal ice keels across a sedimentary substrate (Clark et al. 2003), whilst others advocate a constructional process involving downflow attenuation by pervasive subglacial sediment deformation (Boulton and Hindmarsh 1987; Clark 1993). The observation that MSGLs tend towards a relatively consistent spacing, size and shape has been interpreted as evidence that some type of instability, possibly involving a film of water at the ice-sediment interface, may be involved in their formation (Fowler 2010).

Although the majority of submarine MSGLs have been recognised on or close to the seafloor, the analysis of 3-D seismic-reflection data facilitates the identification of landforms, including MSGLs, on older surfaces that are buried within the

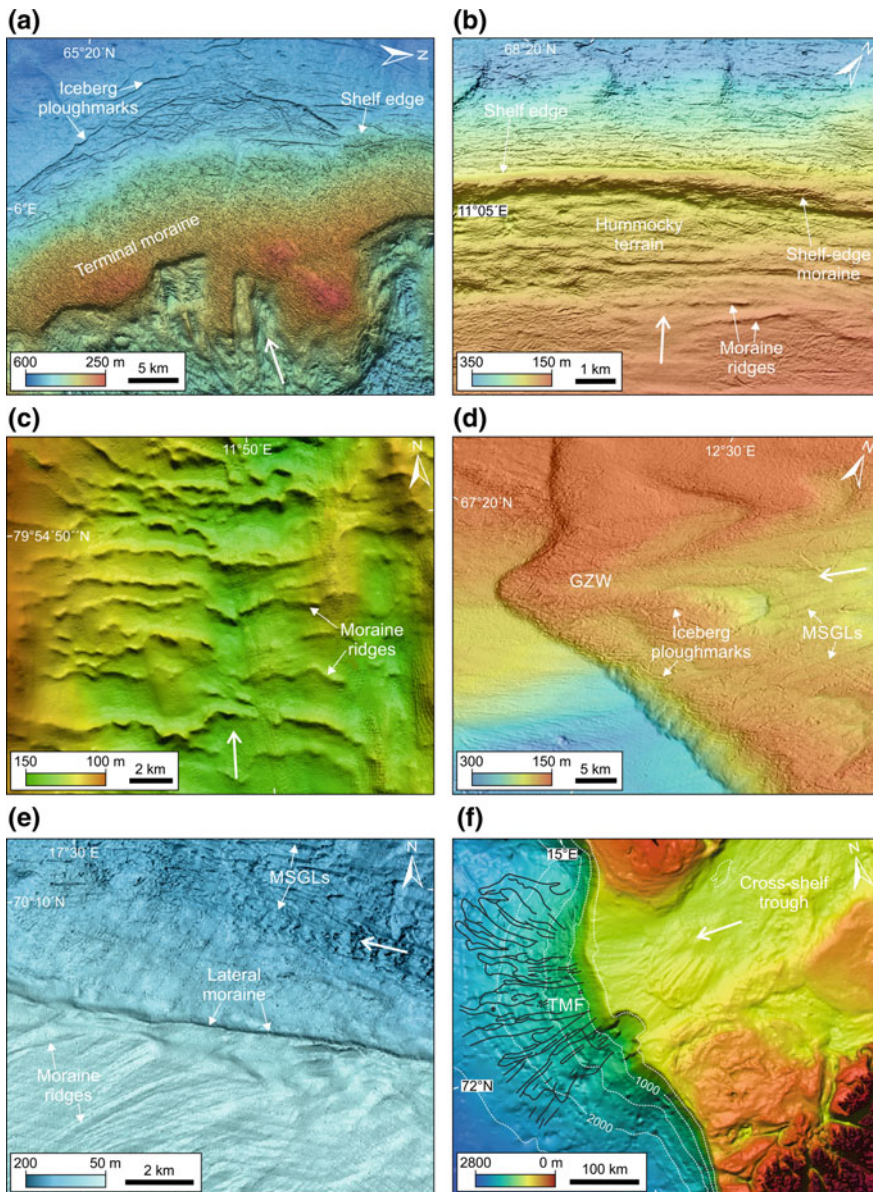


Fig. 3 Examples of submarine ice-marginal landforms. White arrows show former ice-flow directions. **a** The Skjoldryggen terminal moraine on the mid-Norwegian shelf. **b** A shelf-edge moraine and a belt of hummocky terrain close to the shelf edge of Røstbanken, west of the Lofoten Islands, Norway. **c** Series of small moraine ridges in Raudfjorden, northwest Spitsbergen. **d** Grounding-zone wedge (GZW) in Vestfjorden, south of the Lofoten Islands, Norway. **e** Lateral-moraine ridge at the southern lateral margin of Rebbenesdjupet, northern Norway. **f** Trough-mouth fan (TMF) at the mouth of Bear Island cross-shelf trough, Barents Sea. Black lines show seafloor glacigenic debris-flows (adapted from Taylor et al. 2002a)

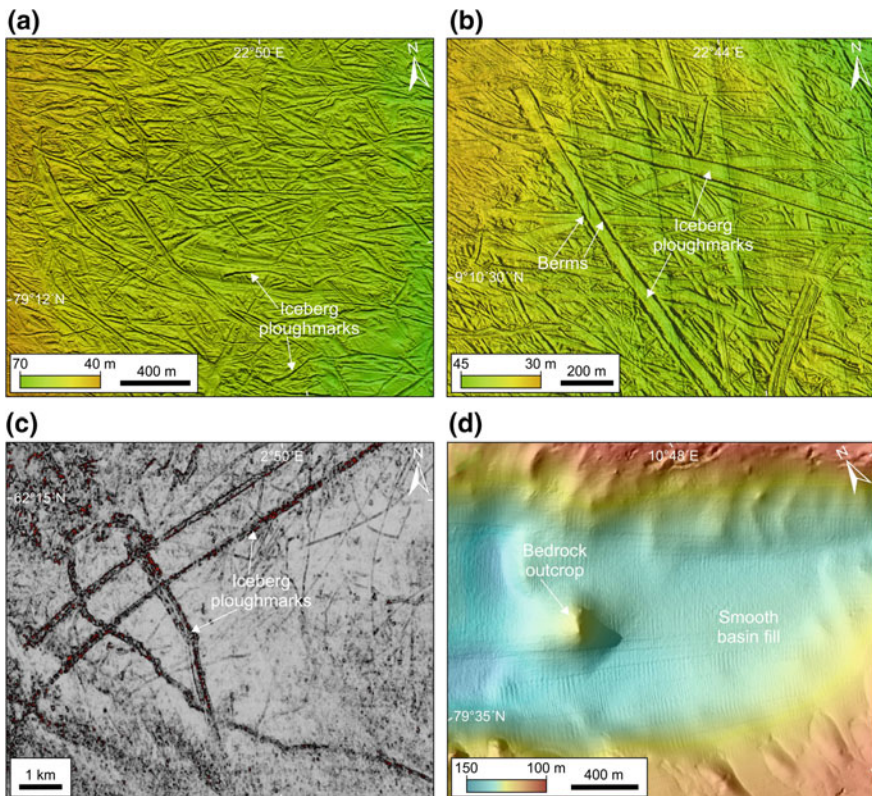


Fig. 4 Examples of glacimarine landforms. **a** Narrow linear to curvilinear iceberg ploughmarks on the seafloor outside Bråsvellbreen, eastern Svalbard. **b** Wide iceberg ploughmarks with raised berms on the seafloor of Bråsvellbreen, eastern Svalbard. **c** Iceberg ploughmarks on a buried surface around 100 m deep in the northern North Sea. **d** Bathymetric image of smooth basin-fill sediments in Magdalenefjorden, northwest Spitsbergen

sub-seafloor stratigraphy (e.g. Fig. 1b). The identification of MSGLs on palaeo-shelves provides direct evidence for the former presence of grounded, fast-flowing ice and can be used to infer palaeo-ice stream flow directions (e.g. Dowdeswell et al. 2006).

Whereas MSGLs represent the end-point of a spectrum of elongate subglacial landforms (Clark 1993), ice-flow parallel ridges with lower elongation ratios, such as flutes and drumlins, are also identified in association with relatively fast-flowing ice (e.g. Shipp et al. 1999; Wellner et al. 2001; Ó Cofaigh et al. 2002; Ottesen et al. 2005). Groups of parallel to subparallel flutes and drumlins have been identified on the seafloor of formerly glaciated fjords and continental shelves, where they are interpreted to indicate relatively fast ice flow within outlet glaciers or ice streams

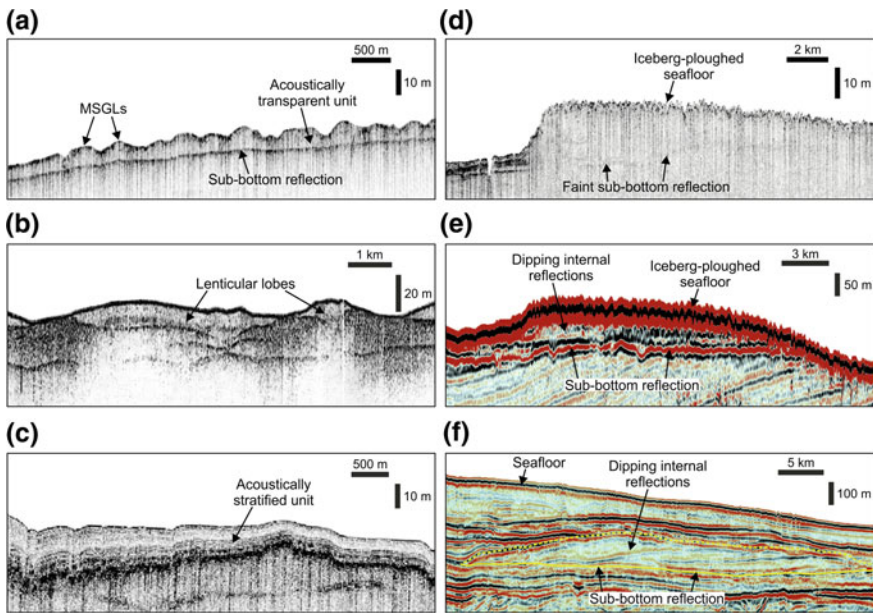


Fig. 5 Examples of the internal acoustic character of glacially-influenced landforms. **a–d** show TOPAS sub-bottom profiles (3.5 kHz), whereas **e–f** show seismic-reflection profiles. **a** Mega-scale glacial lineations (*MSGLs*) formed within acoustically transparent sediment in Marguerite Bay, Antarctic Peninsula (Reprinted from Ó Cofaigh et al. 2005, with permission from Elsevier)—past ice flow is towards the reader. **b** Cross-section through acoustically transparent glacigenic debris-flow lobes on the Bear Island trough-mouth fan, Barents Sea (Reprinted from Taylor et al. 2002b, with permission from Elsevier). **c** Acoustically stratified basin-fill sediment in the Uummannaq cross-shelf trough, West Greenland. **d** Long-profile of a grounding-zone wedge (*GZW*) in the Uummannaq cross-shelf trough, West Greenland. **c** and **d** are adapted from Dowdeswell et al. (2014). **e** Long-profile of a grounding-zone wedge (*GZW*) off West Greenland. **f** Long-profile of a grounding-zone wedge on a buried surface around 150 deep in Amundsen Gulf, Arctic Canada. **e** and **f** are adapted from Batchelor and Dowdeswell (2015)

(e.g. Solheim and Elverhøi 1997). Drumlins can be differentiated by their distinctive shape, with blunt up-glacier or stoss sides and tapered down-flow or lee sides, and have been interpreted to indicate former zones of ice acceleration (Shipp et al. 1999; Wellner et al. 2001).

Erosional subglacial landforms include streamlined crag-and-tails, which consist of an outcrop of bedrock with a tapering ridge of glacial sediment deposited on the lee side of the obstacle, and ice-moulded bedrock (Table 1 and Fig. 1c). These features are formed by the action of relatively fast-flowing ice and have been identified within fjords and on inner-continental shelves in areas where outcrops of bedrock are exposed on the seafloor (e.g. Fig. 1c) (Wellner et al. 2001; Dowdeswell et al. 2014).

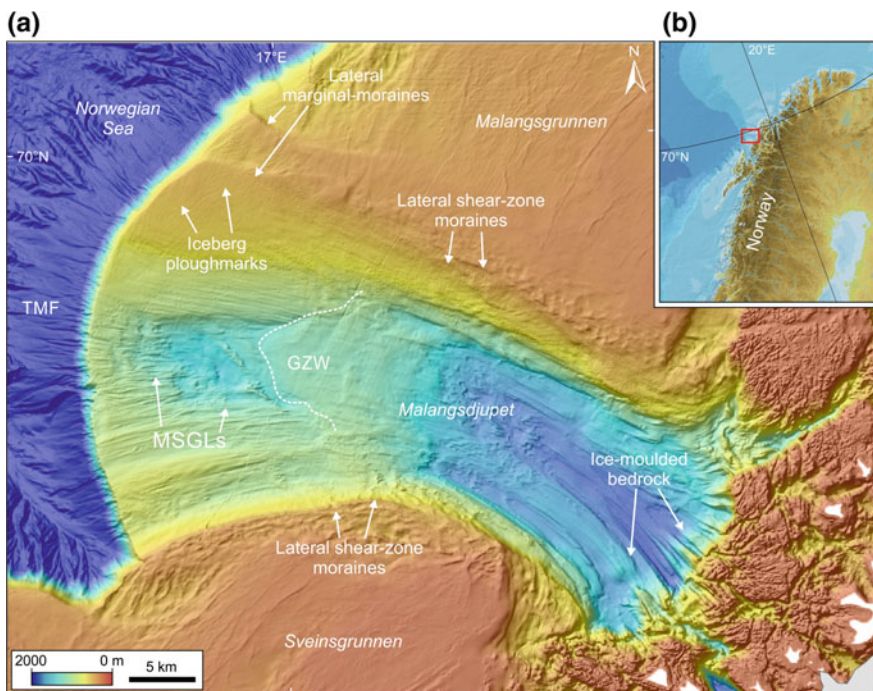


Fig. 6 **a** Bathymetric image of the seafloor of Malangsdjupet cross-shelf trough on the north Norwegian margin, illustrating the typical submarine architecture and landforms that are produced by a fast-flowing ice stream. The locations of ice-moulded bedrock, mega-scale glacial lineations (MSGLs), a grounding-zone wedge (GZW), ice-stream lateral shear-zone moraines, iceberg ploughmarks and a trough-mouth fan (TMF) are shown. The image is provided by the MAREANO project. **b** Location map (red box; map from IBCAO v. 3.0)

2.1.2 Hill-Hole Pairs

Hill-hole pairs are subglacially produced glacitectonic landforms that consist of a topographic depression or hole located up-glacier of a positive-relief arcuate hill of similar size (e.g. Fig. 2a). The former direction of ice flow is indicated by the orientation of the hill-hole axis. Individual hill-hole pairs have been identified on relatively shallow submarine banks off Norway and Svalbard (e.g. Sættem 1990; Ottesen et al. 2005; Dowdeswell et al. 2010), whilst an assemblage of several tens of pairs has been reported from the Arendal Terrace on the southern Norwegian margin (Ottesen et al. 2005; Rise et al. 2016). The formation of these landforms is suggested to involve the freezing-on of slabs of sediment at the ice-sheet base and the subsequent melting and release of this sediment in a downstream direction (Ottesen et al. 2005). Hill-hole pairs are therefore interpreted to be produced beneath relatively slow-flowing and probably thin ice, which facilitates the basal freeze-on of sediment.

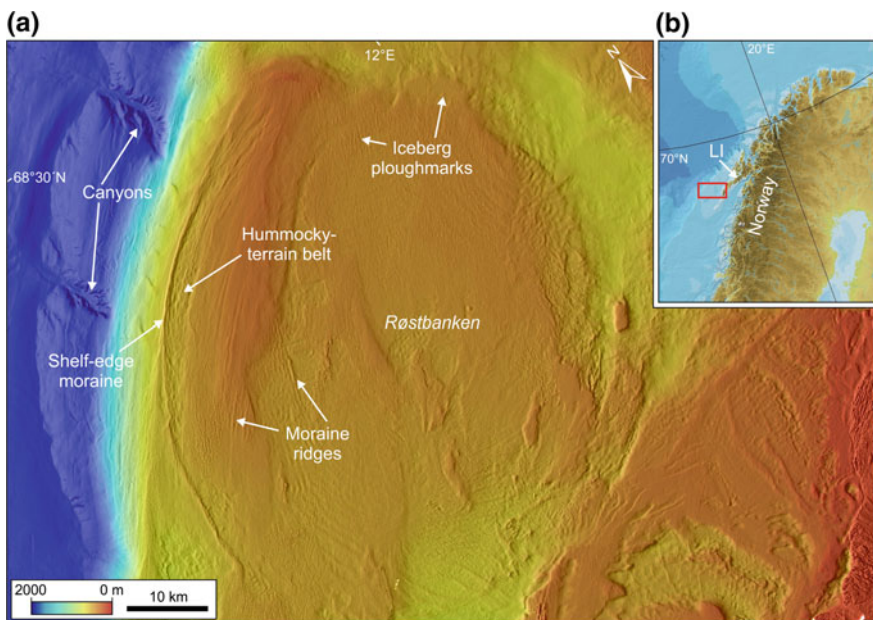


Fig. 7 **a** Bathymetric image of the seafloor of Røstbanken, west of the Lofoten Islands, Norway, illustrating the typical submarine architecture and submarine landforms that are produced by slow-flowing ice. The locations of a shelf-edge moraine, a hummocky-terrain belt, recessional moraine ridges, iceberg ploughmarks and submarine canyons are shown. The image is provided by the MAREANO project. **b** Location map (red box; map from IBCAO v. 3.0). LI is Lofoten Islands

2.1.3 Crevasse-Fill Ridges

Crevasse-fill ridges are non-orientated subglacial landforms that have a distinctive rhombohedral pattern consisting of a series of intersecting ridges a few metres high (Fig. 2b). They have been identified on the forefields of surging terrestrial glaciers (Sharp 1985; Evans and Rea 1999) and on the seafloor beyond the marine margins of several surge-type glaciers in Svalbard (Boulton et al. 1996; Ottesen et al. 2008). The ridges are interpreted to be produced during the post-surge ice stagnation phase by the squeezing of soft, deformable sediment into basal crevasses. These crevasses are formed at the glacier bed during the preceding active phase of the surge cycle.

2.1.4 Subglacial Glaci fluvial Landforms

Tunnel valleys and eskers are produced by the flow of subglacial meltwater (Table 1). They reveal the former pattern of meltwater drainage and are usually aligned parallel or sub-parallel to the direction of former ice flow.

Tunnel valleys are meltwater channels that have cut down beneath the ice into the underlying substrate (Boyd et al. 1988; Ó Cofaigh 1996). They can reach widths

of several kilometres and depths of up to around 400 m. Extensive networks of buried tunnel valleys have been identified on seismic-reflection profiles of the North Sea (e.g. Fig. 2c), where they record the pathways of subglacial meltwater beneath the former Eurasian Ice Sheet over a number of successive glaciations (e.g. Praeg 2003).

Conversely, eskers are sedimentary casts of supraglacial, englacial or subglacial meltwater channels (Warren and Ashley 1994). The majority of preserved eskers were formed subglacially by the sedimentary infilling of channels incised upwards into the base of the ice (known as 'R' channels; Röthlisberger 1972). Eskers are straight to sinuous in plan-form (Fig. 2d) and are composed of glaciifluvial sand and gravel. Eskers up to a few tens of metres high and 2 km wide have been identified on the seafloor of a number of Spitsbergen fjords, in the Baltic Sea, and in Hudson Bay, Canada (Ottesen et al. 2008; Dowdeswell and Ottesen 2016; Greenwood et al. 2016). The formation of eskers may reflect either the synchronous configuration of the hydrological system during high-magnitude drainage events, or the time-transgressive deposition of short esker segments beneath a retreating ice margin linked to normal intra-annual changes in meltwater discharge (Boulton and Hindmarsh 1987; Ó Cofaigh 1996).

2.2 *Ice-Marginal Landforms*

Ice-marginal landforms (Fig. 3) are produced during deglacial still-stands or re-advances of the ice margin. They can provide information about the former configuration of an ice mass and the style and relative speed of ice retreat (e.g. Dowdeswell et al. 2008).

2.2.1 Moraine Ridges

Moraine ridges (Fig. 3a–c) are formed transverse to ice-flow direction along a line source at the grounding zone, which is the point at which the ice-sheet base ceases to be in contact with the underlying substrate. Submarine moraines can be categorised into large terminal and recessional moraine ridges, hummocky-terrain belts and small retreat moraines (Fig. 3a–c).

Terminal and recessional moraines can reach several tens of metres thick and several kilometres wide in the former ice-flow direction (e.g. Sexton et al. 1992; Seramur et al. 1997; Ottesen and Dowdeswell 2009). They form through a combination of processes, including sediment lodgement and deformation, meltwater deposition, melt-out of basal and englacial debris, and squeezing and pushing of sediment from beneath the ice (Powell and Domack 1995; Powell and Alley 1997). Terminal and recessional moraines have been identified within high-latitude fjords in both hemispheres (e.g. Powell 1983; Dowdeswell and Vasquez 2013) and are

widespread on the continental shelves of Norway, Svalbard and Britain and Ireland (Elverhøi et al. 1983; Powell and Domack 2002; Vorren and Plassen 2002; Ottesen et al. 2005, 2007; Bradwell et al. 2008; Rydningen et al. 2013).

Submarine moraines are probably formed mainly at the margins of tidewater glaciers, which have unrestricted vertical accommodation space for the development of a high-amplitude ridge at the grounding zone (Powell and Alley 1997). They may be formed preferentially at the grounding zone of relatively slow-flowing regions of an ice sheet, as evidenced by their widespread occurrence on shallow, inter-trough areas of the continental shelf (Dowdeswell and Elverhøi 2002; Ottesen et al. 2005, 2007; Ottesen and Dowdeswell 2009). The Skjoldryggen moraine on the mid-Norwegian margin (Fig. 3a) provides an example of a large terminal-moraine ridge. Although this moraine is located in a region that has experienced high rates of sediment delivery during the last three glaciations (Rise et al. 2005), it is interpreted to have formed at times when fast ice flow and rapid sediment delivery to the shelf edge may have ceased (Ottesen et al. 2005).

Submarine hummocky-terrain belts have a distinctive morphology of irregular crests and depressions with amplitude of 5–20 m (Fig. 3b) (Ottesen and Dowdeswell 2009; Elvenes and Dowdeswell 2016). The crests are typically asymmetric with steeper ice-distal faces. Well-defined belts of hummocky terrain up to 6 km wide have been identified extending for tens of kilometres along the outermost continental shelf beyond inter-trough banks off north Norway and northwest Svalbard (Fig. 3b) (Ottesen and Dowdeswell 2009; Elvenes and Dowdeswell 2016). The formation of belts of hummocky-terrain, which have also been termed ‘lift-off moraine’, has been suggested to be linked to buoyancy-related tidal effects that cause small-scale variations in the position of the grounding zone (Elvenes and Dowdeswell 2016). This process has been observed beneath modern ice-shelf grounding zones (Bindschadler et al. 2003; Gudmundsson 2006).

Small retreat moraines, which are often referred to as De Geer moraines (Lindén and Möller 2005), are typically a few metres high and up to a few hundred metres wide (e.g. Fig. 3c). They are usually identified in assemblages of tens to hundreds of relatively evenly spaced sub-parallel ridges. Small transverse ridges, interpreted as retreat moraines, have been identified on the seafloor of shallow inter-trough regions of the shelf, as well as within cross-shelf troughs and high-latitude fjords (Boulton 1986; Ottesen et al. 2005; Mosola and Anderson 2006; Ottesen and Dowdeswell 2006, 2009; Todd et al. 2007; Ó Cofaigh et al. 2008). In contrast with larger terminal and recessional moraines (Fig. 3a), which probably build-up during grounding-zone still-stands of at least decades to centuries, small moraine ridges (Fig. 3c) are produced by the delivery and ice pushing of sediment during short-lived still-stands or re-advances of a grounded ice margin during overall retreat (Boulton et al. 1996; Ottesen and Dowdeswell 2009). They therefore indicate the relatively slow retreat of grounded ice (Dowdeswell et al. 2008). Although confirmation by dated sediment cores is relatively rare, small retreat moraines are often formed annually, with minor re-advances taking place as a result of the suppression of iceberg calving by sea-ice buttressing during winter months (Boulton 1986; Dowdeswell et al. 2008; Ó Cofaigh et al. 2008).

2.2.2 Grounding-Zone Wedges

Grounding-zone wedges (GZWs) are asymmetric sedimentary depocentres which form predominantly through the rapid accumulation of subglacial sediment at the grounding zone of marine-terminating ice sheets (Fig. 3d) (e.g. Powell and Alley 1997). GZWs are typically 15–100 m thick and less than 15 km long in the along-flow direction (Dowdeswell and Fugelli 2012; Batchelor and Dowdeswell 2015). They can be differentiated by their relatively subdued geometry compared with higher amplitude moraine ridges (Fig. 3a, d). Whereas submarine moraines probably develop preferentially at tidewater ice cliffs, GZWs have been suggested to form mainly where floating ice shelves constrain vertical accommodation space immediately beyond the grounding zone (Dowdeswell and Fugelli 2012; Batchelor and Dowdeswell 2015).

A large number of GZWs have been described from formerly-glaciated continental margins, where they are identified within major fjord systems and cross-shelf troughs (e.g. Anderson 1997; Powell and Alley 1997; Ó Cofaigh et al. 2005; Mosola and Anderson 2006; Ottesen et al. 2007; Larter et al. 2012). The association of GZWs with cross-shelf troughs and fjords suggests that high rates of sediment delivery to the grounding zone of a fast-flowing ice stream or outlet glacier is required for GZW formation. The presence of GZWs in the geological record indicates an episodic style of ice-stream retreat in which rapid retreat of the grounding zone is punctuated by still-stands of at least decades to centuries (Dowdeswell et al. 2008; Ó Cofaigh et al. 2008; Batchelor and Dowdeswell 2015). Many high-latitude GZWs occur at vertical or lateral pinning points in the shelf topography, which encourage grounding-zone stabilisation through increasing basal and lateral drag (Joughin et al. 2004; Ottesen et al. 2007).

Seismic-reflection profiles reveal that a number of GZWs contain seaward-dipping reflections, which indicate sediment progradation and wedge growth through the continued delivery of basal sediment (Fig. 5e and f) (Larter and Vanneste 1995). Although the majority of GZWs have been recognised on or close to the seafloor and were probably formed during the last deglaciation, a number of buried GZWs, interpreted to have been formed during earlier Quaternary glaciations, have been identified from seismic-reflection profiles of the Greenland and West Antarctic margins (Dowdeswell and Fugelli 2012; Gohl et al. 2013; Batchelor and Dowdeswell, 2015). Possible GZWs have also been identified in the Late Ordovician glacial sediments of North Africa (Decalf et al. 2016).

2.2.3 Ice-Proximal Fans

Ice-proximal fans are point-source depocentres that develop at the mouths of subglacial meltwater channels at the ice-sheet grounding zone (e.g. Powell 1990; Powell and Domack 1995). The formation of ice-proximal fans is therefore dependent on the availability of surface-derived meltwater and the existence of a channelised meltwater network beneath the ice sheet (Powell 1990; Siegert and Dowdeswell 2002).

Ice-proximal fans up to a few tens of metres thick have been identified on the seafloor of fjords in Alaska, Norway and Svalbard, where they mark the former locations of relatively stable grounding-zone positions (Powell 1990; Lønne 1995; Seramur et al. 1997; Dowdeswell et al. 2015). The absence of large ice-proximal fans on formerly glaciated continental shelves is probably a consequence of the highly-variable position of the ice-sheet grounding zone (Dowdeswell et al. 2015). Advancing ice sheets overrun and remove evidence of sediment delivered to the mouths of subglacial meltwater channels, whilst the majority of ice-margin still-stands during deglaciation are probably of insufficient duration to enable the development of large fans unless sediment delivery is very rapid.

2.2.4 Lateral Moraines

Submarine glacial landforms can also develop at the lateral margins of fast-flowing ice streams. Ice-stream lateral marginal-moraines build up at the lateral boundary between ice streams and terrain that is free of grounded ice, whilst ice-stream lateral shear-moraines form in the shear zone between ice streams and slower-flowing regions of the ice sheet (Stokes and Clark 2002; Batchelor and Dowdeswell 2016). Ice-stream lateral shear-moraines are orientated parallel to the former ice-flow direction (e.g. Fig. 3e) and their formation is probably linked to the high stress gradient in the shear zone at the boundary between fast- and slow-flowing ice (e.g. Bentley 1987). They are linear to curvilinear in plan-form and are typically a few tens of metres high and less than a few kilometres wide (Stokes and Clark 2002). Ice-stream lateral shear-moraines have been identified at one or both lateral margins of cross-shelf troughs off Norway and Svalbard, where they have been interpreted to define the lateral boundaries of former ice streams (Ottesen et al. 2005, 2008; Rydningen et al. 2013). Although ice-stream lateral shear-moraines are an important geomorphological indicator of past ice-stream activity, they are not always present in the geological record and may require relatively constrained conditions to form (Stokes and Clark 2002; Hindmarsh and Stokes 2008).

2.2.5 Trough-Mouth Fans

Trough-mouth fans (TMFs) are major glacial-sedimentary depocentres that build up on the continental slope beyond fast-flowing ice streams (Fig. 3f). TMFs are formed when large volumes of deformable sediment are delivered to the shelf edge by ice streams over successive full-glacial periods. This sediment is often remobilised on the upper continental slope to form glacigenic debris-flows (GDFs) (Alley et al. 1989; Laberg et al. 2000). TMFs have volumes of up to several hundred thousand cubic kilometres and are identified on bathymetric maps of the seafloor by a distinctive outward bulging of slope contours beyond the trough-mouth, indicating shelf progradation (Fig. 3f) (Dowdeswell et al. 1996, 1998; Ó Cofaigh et al. 2005). These sedimentary depocentres contain a record of

past glacial history and can provide information about long-term sediment delivery and ice-stream dynamics (Dowdeswell et al. 1996, 2006; Vorren and Laberg 1997; Dowdeswell and Siegert 1999; Ó Cofaigh et al. 2003).

TMFs composed predominantly of stacked acoustically-transparent lenses representing GDFs from episodes of cross-shelf glaciation (Figs. 3f and 5c) have been identified on the continental slope beyond many high-latitude cross-shelf troughs (Vorren et al. 1988; Laberg and Vorren 1995; Dowdeswell et al. 1996; King et al. 1996; Vorren and Laberg 1997; Ó Cofaigh et al. 2003; Batchelor and Dowdeswell 2014). However, the slope beyond former ice streams can also be characterised by channel and gully systems or mass transfer deposits resulting from slope failure (e.g. Dowdeswell et al. 1996, 2004b; Laberg and Vorren 2000; Ó Cofaigh et al. 2003; Piper et al. 2012). TMF development is encouraged by high debris flux, limited contour-current erosion of the slope and a relatively low (generally <4°) upper-slope gradient, which enables GDFs to accumulate on the upper-slope (Ó Cofaigh et al. 2003).

2.3 *Glacimarine Landforms*

Whereas terrestrial sections of an ice sheet lose mass through surface melting and run-off, and, rarely, sublimation, marine-terminating ice sheets additionally lose mass through iceberg calving and the melt-out of basal and englacial debris from icebergs, ice cliffs and floating ice shelves. The processes associated with mass loss by iceberg and meltwater production lead to the formation of distinctive glacimarine landforms and sediments.

2.3.1 *Iceberg Ploughmarks*

Iceberg ploughmarks (e.g. Fig. 4a–c) are linear to curvilinear depressions produced by the grounding of iceberg keels in seafloor sediments (Woodworth-Lynas et al. 1991; Dowdeswell et al. 1993). They have typical depths of a few metres to tens of metres and widths of up to several hundred metres, and many have distinctive raised berms a few metres high on either side of a central depression (Fig. 4b).

Linear to curvilinear depressions, interpreted as iceberg ploughmarks, are widespread on the seafloor of mid- and high-latitude continental margins in present-day water depths down to at least 500 m (e.g. Woodworth-Lynas et al. 1991; Dowdeswell et al. 1993; Metz et al. 2008). They are particularly common on relatively shallow inter-trough banks, where they are often responsible for the erosion and reworking of older subglacial and ice-marginal landforms and sediments. Some wide iceberg ploughmarks are probably formed by the grounding of tabular icebergs on the seafloor, whereas parallel to subparallel sets of ploughmarks may be produced by single large icebergs with multiple keels or by the keels of several icebergs that were trapped within multi-year sea ice, providing a uniform pattern of iceberg drift.

Whereas the majority of seafloor iceberg ploughmarks were probably formed during the last glacial-deglacial cycle, iceberg ploughmarks produced during earlier stages of the Quaternary can be identified from 3-D seismic-reflection data (e.g. Fig. 4c). Buried iceberg ploughmarks preserved on palaeo-shelf surfaces indicate the expansion of ice sheets beyond the coastline and provide information about palaeo-oceanographic conditions (e.g. Syvitski et al. 1996; Dowdeswell and Ottesen 2013).

2.3.2 Smooth Basin Fill from Meltwater Plumes

The discharge of sediment-laden meltwater from conduits at the grounding zone produces turbid jets of sediment-water mixtures, which typically transform into buoyant plumes in seawater (e.g. Powell 1990; Mugford and Dowdeswell 2011). The suspension settling of material derived from meltwater plumes provides a significant source of sediment in some glacimarine environments (e.g. Cowan and Powell 1990; Dowdeswell et al. 1998; Ó Cofaigh and Dowdeswell 2001). Sand and coarse silt are typically deposited within a few kilometres of the grounding zone, whereas finer-grained material is transported in plumes for greater distances. The rain-out of sediment through the water column results in the formation of a blanket of acoustically transparent to stratified basin-fill sediment on the seafloor (Cai et al. 1997), which has a smooth appearance on bathymetric images (Fig. 4d). These sediments often have a strong cyclical signature manifested as acoustic lamination as a result of variations in glacial meltwater discharge and the position of the ice margin (Fig. 5c).

Suspension settling occurs at present in high-latitude fjords and was a significant process in some shelf and slope settings during the Quaternary (e.g. Domack 1990; Dowdeswell et al. 1996, 2000). High rates of deglacial and post-glacial meltwater-derived sedimentation in temperate and subpolar glacimarine environments can lead to the burial of submarine glacial landforms (Elverhøi et al. 1983; Cowan and Powell 1990; Cai et al. 1997; Dowdeswell and Vasquez 2013). Suspension setting is less significant on polar continental margins, such as off Greenland and Antarctica, where there are lower rates of glacimarine sedimentation and ice mass is lost predominantly through iceberg calving rather than meltwater runoff (e.g. Dowdeswell et al. 1993, 1996).

2.4 Marine Landforms

Marine processes, including the action of waves and currents, and mass movement events such as submarine slides (Table 1) can result in the burial and reworking of submarine glacial landforms. Current and wave action can modify glacial landforms on relatively shallow areas of the seafloor (e.g. Howe and Pudsey 1999), whilst submarine slides with lengths of up to several kilometres take place as a result of

the failure of glacial sediments on steep fjord walls (e.g. Ottesen and Dowdeswell 2009; Forwick et al. 2010). Larger submarine slides with volumes of up to several tens of thousand cubic kilometres have been recognised on the continental slope beyond cross-shelf troughs and shallower banks in both hemispheres (e.g. Laberg and Vorren 1993, 2000; Hjelstuen et al. 2005; Piper et al. 2012). Slope failure on high-latitude continental margins can occur as a consequence of the build-up of excess pore pressure in fine-grained sediment as a result of rapid sedimentation during full-glacial periods, contour-current erosion of the lower slope under interglacial conditions, and tectonic activity and gas-hydrate disassociation (e.g. Mosher et al. 1994; Laberg and Vorren 2000; Mienert 2004).

3 Glacial Landforms on the Norwegian Margin: A Case Study

The typical distribution of glacial landforms on formerly-glaciated continental margins is illustrated using the case study of the Norwegian continental shelf and slope (Figs. 6 and 7).

3.1 *Landforms in Cross-Shelf Troughs*

The large-scale architecture and submarine glacial landforms that are typically produced by fast-flowing ice streams are shown by the Malangsdjupet cross-shelf trough on the north Norwegian margin (Fig. 6). Malangsdjupet has been interpreted to have been occupied by a marine-terminating ice stream during a number of Quaternary full-glacial periods, including during the Last Glacial Maximum (LGM) around 20 ka ago (Ottesen et al. 2005, 2008; Rydningen et al. 2013).

The trough is around 50 km long and has a maximum width and depth of 30 and 400 m, respectively (Fig. 6). Malangsdjupet has characteristic cross-shelf trough geometry, with over-deepened inner-shelf basins extending from fjords, well-defined lateral margins and an increasing width towards the shelf edge (Stokes and Clark 2001) (Fig. 6). It has a landward-dipping seafloor, which is probably a result of repeated erosion of the inner-shelf by ice over successive glaciations. Bathymetric data show a seaward change in the roughness of the seafloor, which corresponds with a transition from outcrops of crystalline bedrock on the inner-shelf to a sedimentary substrate on the mid- and outer-shelf (Fig. 6). The continental slope beyond the trough displays the progradational architecture and outward bulging upper-slope contours that are typical of glacial-sedimentary depocentres or TMFs (Dowdeswell et al. 1998; Ó Cofaigh et al. 2005). Malangsdjupet TMF has been interpreted to have been built up on the slope from around 1.5 million years

ago, when fast-flowing ice streams started delivering large quantities of deformable sediment to the Norwegian continental margin over successive full-glacial periods (Rise et al. 2005; Rydningen et al. 2016).

Several types of submarine glacial landform are preserved on the seafloor of Malangsdjupet; these include subglacially produced ice-moulded bedrock and MSGLs, ice-marginal GZWs and lateral moraines, and iceberg ploughmarks (Fig. 6) (Vorren and Plassen 2002; Ottesen et al. 2005, 2008; Rydningen et al. 2013). These landforms record the extent and dynamics of the ice stream in the trough during the last glacial-deglacial cycle.

Ice-moulded bedrock and MSGLs were produced subglacially during ice-stream advance and reveal former ice-flow directions. Ice-moulded bedrock on the inner-shelf shows that the ice emerged from the fjords and converged in the central trunk of the trough (Fig. 6). MSGLs with lengths of several kilometres are present on the mid- and outer-shelf, indicating that grounded, fast-flowing ice extended to the shelf edge during the LGM.

An ice-marginal GZW is present on the mid-shelf of Malangsdjupet (Fig. 6). This depocentre, which spans most of the trough width and is at least 20 km long in the ice-flow direction, was produced during a still-stand in the grounding-zone position of at least decades to centuries during ice-stream retreat. The presence of a mid-shelf GZW and preserved outer-shelf MSGLs suggest that the ice stream experienced an episodic style of retreat (Dowdeswell et al. 2008), with ice probably retreating relatively rapidly from the shelf edge to the GZW position on the mid-shelf.

Ice-stream lateral shear-zone moraines a few metres high are present along both lateral margins of Malangsdjupet (Fig. 6). These landforms delimit the former lateral boundaries between the ice stream in the trough and slower-flowing ice on the adjacent banks (Fig. 6). Ice-stream lateral marginal-moraines are also present at the northern outermost lateral margin of the trough, where they probably record the former boundary between the ice stream and terrain that was free of grounded ice during lateral-moraine formation (Rydningen et al. 2016; Batchelor and Dowdeswell 2016).

A number of linear to curvilinear iceberg ploughmarks are present at the northern margin of Malangsdjupet in water depths of between 100 and 200 m (Fig. 6). They record the drift tracks of deep-keeled icebergs that were produced during regional deglaciation. Iceberg ploughmarks are generally absent from the seafloor of the rest of the trough, which suggests that these regions were deeper than the maximum iceberg-keel depth. The relatively fresh appearance of glacial landforms on bathymetric images of the seafloor suggests that there is only a thin veneer of glacimarine sediments draping the shelf and slope off northern Norway. Accumulations of smooth basin-fill sediments derived from meltwater plumes are probably present in inner-shelf basins between bedrock outcrops and in the more ice-proximal fjords (e.g. Elverhøi et al. 1983).

3.2 Landforms on Inter-Trough Banks

The inter-trough bank of Røstbanken beyond Lofoten on the Norwegian margin illustrates the typical architecture and glacial landforms that are produced by relatively slow-flowing regions of an ice sheet (Fig. 7). Slow-moving ice is interpreted to have expanded to the shelf edge beyond Røstbanken during the LGM as well as probably also during a number of earlier Quaternary full-glacial periods (Ottesen et al. 2005).

Slow-moving ice is relatively passive; it does not typically cause considerable erosion of the continental shelf or deliver large volumes of deformable sediment to the shelf edge. Røstbanken therefore lacks the erosional cross-shelf trough and depositional TMF architecture that is characteristic of former ice-stream locations. Røstbanken has water depths of between 100 and 200 m and there is no evidence of a significant glacial-sedimentary depocentre on the upper continental slope (Fig. 7). The slope beyond the bank is instead characterised by small-scale mass-wasting features and submarine canyons.

Subglacially produced streamlined landforms that indicate the direction of former ice flow are largely absent from Røstbanken. By contrast, the bank is dominated by ice-marginal moraines that are orientated transverse to the former ice-flow direction (Fig. 7). A terminal-moraine ridge is present at the shelf edge, marking the maximum extent of grounded ice during the LGM (Ottesen et al. 2005). A several kilometre-wide belt of hummocky terrain, which was probably produced by tidally-related variations in the position of the grounding zone (Ottesen and Dowdeswell 2009), is also present on the outermost shelf (Fig. 7). The mid- and outer-shelf of Røstbanken is dominated by a number of recessional-moraine ridges that are a few tens of metres wide in the former ice-flow direction (Fig. 7). These ridges mark the former positions of still-stands or minor re-advances in the grounding zone and indicate the relatively slow retreat of grounded ice across the bank (Dowdeswell et al. 2008). Røstbanken is heavily scoured by linear to curvilinear depressions, which are interpreted to have been produced by the keels of icebergs ploughing into sediments on the relatively shallow seafloor (Fig. 7).

3.3 Landsystem Models for Fast- and Slow-Flowing Ice

The submarine glacier-influenced landforms described from Malangsdjupet and Røstbanken (Figs. 6 and 7) can be combined into schematic landsystem models for fast- and slow-flowing ice on formerly-glaciated continental margins (Fig. 8) (e.g. Ottesen et al. 2005, 2007; Ó Cofaigh et al. 2005; Ottesen and Dowdeswell 2009).

The locations of former ice streams can be identified by deep (typically >300 m) cross-shelf troughs that are formed by fast-flowing ice over successive full-glacial periods. In contrast, the former locations of slower-flowing, relatively passive ice are typically characterised by shallower banks (Fig. 8). Whereas large TMFs often

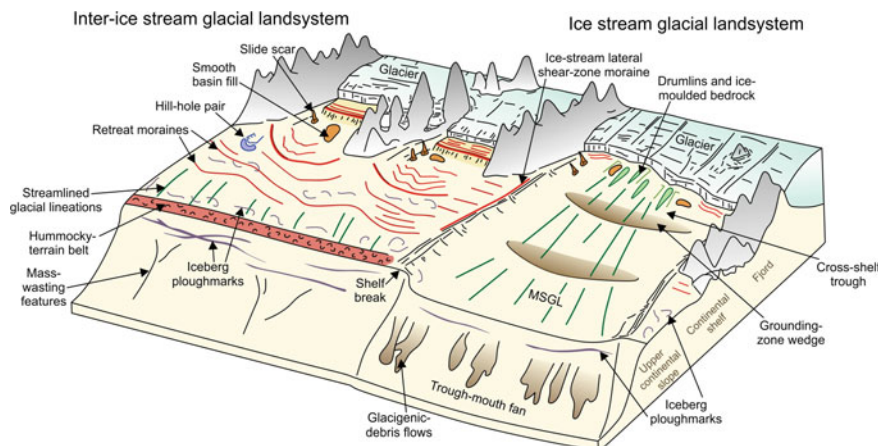


Fig. 8 Summary schematic landsystem models of the submarine landforms on the seafloor of inter-ice stream shallow banks and cross-shelf troughs formerly occupied by fast-flowing ice streams (adapted from Ottesen and Dowdeswell 2009)

develop beyond cross-shelf troughs, lower rates of sediment delivery to the shelf edge beyond inter-ice stream regions of the ice sheet preclude the development of major glacial-sedimentary depocentres in these locations.

A key feature of the ice-stream glacial landform-assemblage model is the presence of elongate streamlined landforms, such as MSGLs, that are orientated parallel to the former ice-flow direction (Fig. 8) (Stokes and Clark 2002; Ó Cofaigh et al. 2002). GZWs record the positions of still-stands in the grounding zone during deglaciation and indicate an episodic style of ice-stream retreat through the trough.

By contrast, the inter-ice stream glacial landform-assemblage model is dominated by ice-marginal landforms, such as moraine and hummocky-terrain belts, which are orientated transverse to the former ice-flow direction (Ottesen and Dowdeswell 2009). Groups of parallel to subparallel moraine-ridges provide evidence for the slow retreat of grounded ice across the bank (Dowdeswell et al. 2008). Some inter-ice stream locations contain glacitectonically formed hill-hole pairs that indicate the direction of past ice flow (Ottesen and Dowdeswell 2009). Ice-stream lateral shear-moraines are orientated parallel to the former ice-flow direction and delimit the lateral boundary between fast- and slow-flowing ice (Fig. 8) (Stokes and Clark 2002).

Iceberg ploughmarks have been identified on the seafloor of inter-trough banks, cross-shelf troughs and the upper continental slope (e.g. Woodworth-Lynas et al. 1991; Dowdeswell et al. 1993). They are most widespread on inter-trough banks that are the former locations of slow-flowing ice, as a result of the shallower seafloor in these locations (Fig. 8).

4 Future Research Objectives

Recent developments in geophysical imaging techniques have enabled the identification and interpretation of glacial landforms in a wide range of submarine environments. There are, however, three key areas in which future research may be directed.

First, there is a need for increased data coverage of formerly glaciated continental margins. Some offshore areas, such as the Norwegian margin and the western Barents Sea, have been the focus of extensive seafloor mapping programmes and subsurface investigations, facilitating detailed reconstructions of past ice-sheet configurations and dynamics (e.g. Ottesen et al. 2005, 2007; Andreassen et al. 2014). However, comparatively little is known about other formerly glaciated regions, such as the Kara Sea in the Russian Arctic and parts of the Queen Elizabeth Islands in the Canadian Arctic, where data collection has historically been hampered by sea ice.

Secondly, higher-resolution data of the seafloor and the subsurface are needed to capture complexity in ice-sheet behaviour, with a particular focus on dynamic behaviour of ice streams during the last deglaciation. Geophysical surveys have revealed that the geological record is more complex than previously envisaged, both in terms of the changing dynamics of individual sectors of former ice sheets, and the assemblages of submarine glacial landforms that are produced (e.g. Greenwood et al. 2012).

Finally, increased chronological control, derived from the dating of material within sediment cores, is needed to establish the timing of ice-sheet advances and retreats and to better constrain the rates of formation of submarine glacial landforms.

Acknowledgements We wish to thank the MAREANO project (www.mareano.no) for access to bathymetry data from the Norwegian margin.

References

- Alley AB, Blankenship DD, Rooney ST et al (1989) Sedimentation beneath ice shelves—the view from ice stream B. *Mar Geol* 85:101–120
- Anandakrishnan S, Alley RB (1997) Stagnation of ice stream C, West Antarctic by water piracy. *Geophys Res Lett* 24:265–268
- Anderson JB (1997) Grounding zone wedges on the Antarctic continental shelf, Weddell Sea. In: Davis TA, Bell T, Cooper AK, Josenhans H, Polyak L, Solheim A, Syoker MS, Stravers JA (eds) *Glaciated continental margins: an atlas of acoustic images*. Chapman & Hall, London, pp 968–970
- Andreassen K, Winsborrow MCM, Bjarnadóttir LR et al (2014) Ice stream retreat dynamics inferred from an assemblage of landforms in the northern Barents Sea. *Quat Sci Rev* 92:246–257

- Batchelor CL, Dowdeswell JA (2014) The physiography of high Arctic cross-shelf troughs. *Quat Sci Rev* 92:68–96
- Batchelor CL, Dowdeswell JA (2015) Ice-sheet grounding-zone wedges (GZWs) on high-latitude continental margins. *Mar Geol* 363:65–92
- Batchelor CL, Dowdeswell JA (2016) Lateral shear-moraines and lateral marginal-moraines at the margins of palaeo-ice streams. *Quat Sci Rev* 151:1–26
- Bentley CR (1987) Antarctic ice streams: a review. *J Geophys Res* 92:8843–8858
- Bindschadler RA, King MA, Alley RB et al (2003) Tidally controlled stick-slip discharge of a West Antarctica ice stream. *Science* 301:1087–1089
- Boulton GS (1986) Push-moraines and glacier-contact fans in marine and terrestrial environments. *Sedimentology* 33:677–698
- Boulton GS, Hindmarsh RCA (1987) Sediment deformation beneath glaciers: rheology and geological consequences. *J Geophys Res* 92:9059–9082
- Boulton GS, Van Der Meer JJM, Hart J et al (1996) Till and moraine emplacement in deforming bed surge—an example from a marine environment. *Quat Sci Rev* 15:961–987
- Boyd R, Scott DB, Douma M (1988) Glacial tunnel valleys and Quaternary history of the outer scotian shelf. *Nature* 333:61–64
- Bradwell T, Stoker MS, Golledge NR et al (2008) The northern sector of the last British ice sheet: maximum extent and demise. *Earth Sci Rev* 88:207–226
- Cai J, Powell RD, Cowan EA et al (1997) Lithofacies and seismic-reflection interpretation of temperate glacimarine sedimentation in Tarr Inlet, Glacier Bay, Alaska. *Mar Geol* 143:5–37
- Clark CD (1993) Mega-scale glacial lineations and cross-cutting ice-flow landforms. *Earth Surf Proc Land* 18:1–29
- Clark CD (1994) Large scale ice-moulded landforms and their glaciological significance. *Sed Geol* 91:253–268
- Clark CD, Tulaczyk SM, Stokes CR et al (2003) A groove-ploughing theory for the production of mega-scale glacial lineations, and implications for ice-stream mechanics. *J Glaciol* 49:240–256
- Cowan EA, Powell RD (1990) Suspended sediment transport and deposition of cyclically interlaminated sediment in a temperate glacial fjord, Alaska, U.S.A. In: Dowdeswell JA, Scourse JD (eds) *Glacimarine environments: processes and sediments*, Geological Society, London Special Publication 53, pp 75–90
- Damuth JE (1978) Echo character of the Norwegian-Greenland Sea: relationship to Quaternary sedimentation. *Mar Geol* 28:1–36
- Decalf C, Dowdeswell JA, Fugelli EMG (2016) Seismic character of possible buried grounding-zone wedges in the late Ordovician glacial rocks of Algeria. In: Dowdeswell JA, Canals M, Jakobsson M, Todd BJ, Dowdeswell EK, Hogan KA (eds) *Atlas of submarine glacial landforms: modern, Quaternary and ancient*. Geological Society, London, Memoirs 46, pp 245–246
- Domack EW (1990) Laminated terrigenous sediments from the Antarctic Peninsula: the role of subglacial and marine processes. In: Dowdeswell JA, Scourse JD (eds) *Glacimarine environments: processes and sediments*. Geological Society, London, Special Publication 53, pp 9–103
- Dowdeswell JA, Elverhøi A (2002) The timing of initiation of fast-flowing ice streams during a glacial cycle inferred from glacimarine sedimentation. *Mar Geol* 188:3–14
- Dowdeswell JA, Fugelli EMG (2012) The seismic architecture and geometry of grounding-zone wedges formed at the marine margins of past ice sheets. *Geol Soc Am Bull* 124:1750–1761
- Dowdeswell JA, Ottesen D (2013) Buried iceberg ploughmarks in the early Quaternary sediments of the central North Sea: a two-million year record of glacial influence from 3D seismic data. *Mar Geol* 344:1–9
- Dowdeswell JA, Ottesen D (2016) Eskers formed at the beds of modern surge-type tidewater glaciers in Spitsbergen. In: Dowdeswell JA, Canals M, Jakobsson M, Todd BJ, Dowdeswell EK, Hogan KA (eds) *Atlas of submarine glacial landforms: modern, Quaternary and ancient*. Geological Society, London, Memoirs 46, pp 83–84

- Dowdeswell JA, Siegert MJ (1999) Ice-sheet numerical modelling and marine geophysical measurements of glacier-derived sedimentation on the Eurasian Arctic continental margins. *Geol Soc Am Bull* 111:1080–1097
- Dowdeswell JA, Vásquez M (2013) Submarine landforms in the fjords of southern Chile: implications for glaciomarine processes and sedimentation in a mild glacier-influenced environment. *Quat Sci Rev* 64:1–19
- Dowdeswell JA, Villinger H, Whittington RJ et al (1993) Iceberg scouring in scoresby sund and on the East Greenland continental shelf. *Mar Geol* 111:37–53
- Dowdeswell JA, Kenyon N, Elverhøi A et al (1996) Large-scale sedimentation on the glacier influenced Polar North Atlantic margins: long-range side-scan sonar evidence. *Geophys Res Lett* 23:3535–3538
- Dowdeswell JA, Elverhøi A, Spielhagen R (1998) Glaciomarine sedimentary processes and facies on the Polar North Atlantic margins. *Quat Sci Rev* 17:243–272
- Dowdeswell JA, Whittington RJ, Jennings AE et al (2000) An origin for laminated glaciomarine sediments through sea-ice build-up and suppressed iceberg rafting. *Sedimentology* 47:557–576
- Dowdeswell JA, Ó Cofaigh C, Taylor J et al (2002) On the architecture of high-latitude continental margins: the influence of ice-sheet and sea-ice processes in the Polar North Atlantic. In: Dowdeswell JA, Ó Cofaigh C (eds) *Glacier-influenced sedimentation on high-latitude continental margins*, Geological Society, London, Special Publication 203, pp 33–54
- Dowdeswell JA, Ó Cofaigh C, Pudsey CJ (2004a) Thickness and extent of the subglacial till layer beneath an Antarctic paleo-ice stream. *Geology* 32:13–16
- Dowdeswell JA, Ó Cofaigh C, Pudsey CJ (2004b) Continental slope morphology and sedimentary processes at the mouth of an Antarctic palaeo-ice stream. *Mar Geol* 204:203–214
- Dowdeswell JA, Ottesen D, Rise L (2006) Flow-switching and large-scale deposition by ice streams draining former ice sheets. *Geology* 34:313–316
- Dowdeswell JA, Ottesen D, Evans J et al (2008) Submarine glacial landforms and rates of ice-stream collapse. *Geology* 36:819–822
- Dowdeswell JA, Evans J, Ó Cofaigh C (2010) Submarine landforms and shallow acoustic stratigraphy of a 400 km-long fjord-shelf-slope-transect, Kangerlussuaq margin, East Greenland. *Quat Sci Rev* 29:3359–3369
- Dowdeswell JA, Hogan KA, Ó Cofaigh C et al (2014) Late Quaternary ice flow in a West Greenland fjord and cross-shelf trough system: submarine landforms from Rink Isbrae to Uummannaq shelf and slope. *Quat Sci Rev* 92:292–309
- Dowdeswell JA, Hogan KA, Arnold NS et al (2015) Sediment-rich meltwater plumes and ice-proximal fans at the margins of modern and ancient tidewater glaciers: observations and modelling. *Sedimentology* 62:1665–1692
- Dowdeswell EK, Todd BJ, Dowdeswell JA (2016) Crag-and-tail features: convergent ice flow through Eclipse sound, Baffin Island, Arctic Canada. In: Dowdeswell JA, Canals M, Jakobsson M, Todd BJ, Dowdeswell EK, Hogan KA (eds) *Atlas of submarine glacial landforms: modern, Quaternary and ancient*. Geological Society, London, Memoirs 46, pp 55–56
- Dyke AS, Andrews JT, Clark PU et al (2002) The Laurentide and Innuitian ice sheets during the last glacial maximum. *Quat Sci Rev* 21:9–31
- Elvenes S, Dowdeswell JA (2016) Possible ‘lift-off moraines’ at grounded ice-sheet margins, North Norwegian shelf edge. In: Dowdeswell JA, Canals M, Jakobsson M, Todd BJ, Dowdeswell EK, Hogan KA (eds) *Atlas of submarine glacial landforms: modern, Quaternary and ancient*. Geological Society, London, Memoirs 46, pp 247–248
- Elverhøi A, Lønne O, Seland R (1983) Glaciomarine sedimentation in a modern fjord environment, Spitsbergen. *Polar Res* 1:127–149
- Elverhøi A, Andersen ES, Dokken T et al (1995) The growth and decay of the late Weichselian ice sheet in western Svalbard and adjacent areas based on provenance studies of marine sediments. *Quat Res* 44:303–316

- Elverhøi A, Hooke RLeB, Solheim A (1998) Late Cenozoic erosion and sediment yield from the Svalbard-Barents Sea region: implications for understanding erosion of glacierised basins. *Quat Sci Rev* 17:209–242
- Evans DJA, Rea BR (1999) Geomorphology and sedimentology of surging glaciers: a land-systems approach. *Ann Glaciol* 28:75–82
- Evans J, Pudsey CJ, Ó Cofaigh C et al (2005) Late Quaternary glacial history, flow dynamics and sedimentation along the eastern margin of the Antarctic Peninsula ice sheet. *Quat Sci Rev* 24:741–774
- Forwick M, Vorren TO, Hald M et al (2010) Spatial and temporal influence of glaciers and rivers on the sedimentary environment in Sassenfjorden and Tempelfjorden, Spitsbergen. In: Howe JA, Austin WEN, Forwick M, Paetzel M (eds) *Fjord systems and archives*, Geological Society, London, Special Publications 344, pp 163–193
- Fowler AC (2010) The instability theory of drumlin formation applied to Newtonian viscous ice of finite depth. *Proceedings of the Royal Society, London(A)* 466:2673–2694
- Garcia M, Dowdeswell JA, Ercilla G, Jakobsson M (2012) Recent glacially influenced sedimentary processes on the East Greenland continental slope and deep Greenland Basin. *Quaternary Sci Rev* 49:64–81
- Gohl K, Uenzelmann-Neben G, Larter RD et al (2013) Seismic stratigraphic record of the Amundsen Sea Embayment shelf from pre-glacial to recent times: evidence for a dynamic West Antarctic ice sheet. *Mar Geol* 344:115–131
- Greenwood SL, Gyllencreutz R, Jakobsson M et al (2012) Ice-flow switching and East/West Antarctic Ice Sheet roles in glaciation of the western Ross Sea. *Geol Soc Am Bull* 124: 1736–1749
- Greenwood SL, Jakobsson M, Hell B et al (2016) Esker systems in the Gulf of Bothnia. In: Dowdeswell JA, Canals M, Jakobsson M, Todd BJ, Dowdeswell EK, Hogan KA (eds) *Atlas of submarine glacial landforms: modern, Quaternary and ancient*. Geological Society, London, Memoirs 46, pp 209–210
- Gudmundsson GH (2006) Fortnightly variations in the flow velocity of Rutford ice stream, West Antarctica. *Nature* 444:1063–1064
- Hindmarsh RCA, Stokes CR (2008) Formation mechanisms for ice-stream lateral shear margin moraines. *Earth Surf Proc Land* 33:610–626
- Hjelstuen BO, Sejrup HP, Haflidason H et al (2005) Late Cenozoic glacial history and evolution of the Storegga Slide area and adjacent slide flank regions, Norwegian continental margin. *Mar Pet Geol* 22:57–69
- Howe JA, Pudsey CJ (1999) Antarctic circumpolar deep water: a Quaternary paleoflow record from the northern Scotia Sea, South Atlantic Ocean. *J Sediment Res* 69:847–861
- Joughin I, Rignot E, Rosanova E et al (2003) Timing of recent accelerations of Pine Island Glacier, Antarctica. *Geophys Res Lett* 30:1706
- Joughin I, Abdalati W, Fahnestock M (2004) Large fluctuations in speed on Greenland's Jakobshavn Isbrae glacier. *Nature* 432:608–610
- King EL, Sejrup HP, Haflidason H et al (1996) Quaternary seismic stratigraphy of the North Sea Fan: glacially fed gravity flow aprons, hemipelagic sediments, and large submarine slides. *Mar Geol* 130:293–315
- King EC, Hindmarsh RCA, Stokes CR (2009) Formation of mega-scale glacial lineations observed beneath a West Antarctic ice stream. *Nat Geosci* 2:585–588
- Laberg JS, Vorren TO (1993) A late Pleistocene submarine slide on the Bear island trough mouth fan. *Geo-Mar Lett* 13:227–234
- Laberg JS, Vorren TO (1995) Late Weichselian debris flow deposits on the Bear island trough mouth fan. *Mar Geol* 127:45–72
- Laberg JS, Vorren TO (2000) The Trænadjupet slide, offshore Norway—morphology, evacuation and triggering mechanisms. *Mar Geol* 171:95–114
- Laberg JS, Vorren TO, Dowdeswell JA et al (2000) The Andøya slide and the Andøya Canyon, north-eastern Norwegian-Greenland Sea. *Mar Geol* 162:259–275

- Larter RD, Vanneste LE (1995) Relict subglacial deltas on the Antarctic Peninsula outer shelf. *Geology* 23:33–36
- Larter RD, Graham ACG, Hillenbrand CD et al (2012) Late Quaternary grounded ice extent in the Filchner Trough, Weddell Sea, Antarctica: new marine geophysical evidence. *Quat Sci Rev* 53:111–122
- Lindén M, Möller P (2005) Marginal formation of De Geer moraines and their implications to the dynamics of grounding-line recession. *J Quat Sci* 20:113–133
- Lønne I (1995) Sedimentary facies and depositional architecture of ice-contact glaciomarine systems. *Sed Geol* 98:13–43
- MacAyeal DR (1993) Binge/purge oscillations of the Laurentide ice sheet as a cause of the North Atlantic's Heinrich events. *Paleoceanography* 8:775–784
- Metz JM, Dowdeswell JA, Woodworth-Lynas CMT (2008) Sea-floor scour at the mouth of Hudson Strait by deep-keeled icebergs from the Laurentide ice sheet. *Mar Geol* 253:149–159
- Mienert J (2004) COSTA—continental slope stability. *Mar Geol* 213:1–504
- Mosher DC, Moran K, Hiscock RN (1994) Late Quaternary sediment, sediment mass flow processes and slope stability on the Scotian Slope, Canada. *Sedimentology* 41:1039–1061
- Mosola AB, Anderson JB (2006) Expansion and rapid retreat of the west Antarctic ice sheet in eastern Ross Sea: possible consequence of over-extended ice streams? *Quat Sci Rev* 25: 2177–2196
- Mugford RI, Dowdeswell JA (2011) Modelling glacial meltwater plume dynamics and sedimentation in high-latitude fjords. *J Geophys Res* 116:F01023
- Ó Cofaigh C (1996) Tunnel valley genesis. *Prog Phys Geogr* 20:1–19
- Ó Cofaigh C, Dowdeswell JA (2001) Laminated sediments in glaciomarine environments: diagnostic criteria for their interpretation. *Quat Sci Rev* 20:1411–1436
- Ó Cofaigh C, Pudsey CJ, Dowdeswell JA et al (2002) Evolution of subglacial bedforms along a paleo-ice stream, Antarctic Peninsula continental shelf. *Geophys Res Lett* 29:1199
- Ó Cofaigh C, Taylor J, Dowdeswell JA et al (2003) Palaeo-ice streams, trough mouth fans and high-latitude continental slope sedimentation. *Boreas* 32:37–55
- Ó Cofaigh C, Dowdeswell JA, Allen CS et al (2005) Flow dynamics and till genesis associated with a marine-based Antarctic palaeo-ice stream. *Quat Sci Rev* 24:709–740
- Ó Cofaigh C, Dowdeswell JA, Evans J et al (2008) Geological constraints on Antarctic palaeo-ice-stream retreat. *Earth Surf Process Land* 33:513–525
- Ó Cofaigh C, Andrews JT, Jennings AE, Dowdeswell JA, Hogan KA, Kilfeather AA, Sheldon C (2013) Glaciomarine lithofacies, provenance and depositional processes on a West Greenland trough-mouth fan. *J Quaternary Sci* 28:13–26
- Ottesen D, Dowdeswell JA (2006) Assemblages of submarine landforms produced by tidewater glaciers in Svalbard. *J Geophys Res* 111:F01016
- Ottesen D, Dowdeswell JA (2009) An inter-ice stream glaciated margin: submarine landforms and a geomorphic model based on marine-geophysical data from Svalbard. *Geol Soc Am Bull* 121:1647–1665
- Ottesen D, Dowdeswell JA, Rise L (2005) Submarine landforms and the reconstruction of fast-flowing ice streams within a large Quaternary ice sheet: the 2500-km-long Norwegian-Svalbard margin (57°–80°N). *Geol Soc Am Bull* 117:1033–1050
- Ottesen D, Dowdeswell JA, Lanvik JY et al (2007) Dynamics of the late Weichselian ice sheet on Svalbard inferred from high-resolution sea-floor morphology. *Boreas* 36:286–306
- Ottesen D, Stokes CR, Rise L et al (2008) Ice-sheet dynamics and ice streaming along the coastal parts of northern Norway. *Quat Sci Rev* 27:922–940
- Piper DJW, Deptuck ME, Mosher DC et al (2012) Erosional and depositional features of glacial meltwater discharges on the eastern Canadian continental margin. In: Application of the principles of seismic geomorphology to continental-slope and base-of-slope systems: case studies from seafloor and near-seafloor analogues. SEPM Special Publication 99
- Powell RD (1983) Glacial-marine sedimentation processes and lithofacies of temperate tidewater glaciers, Glacier Bay, Alaska. In: Molnia BF (ed) *Glacial-marine sedimentation*. Plenum Press, New York, pp 185–232

- Powell RD (1990) Processes at glacial grounding-line fans and their growth to ice-contact deltas. In: Dowdeswell JA, Scourse JD (eds) *Glacimarine environments: processes and sediments*. Geological Society, London, Special Publication 53, pp 53–73
- Powell RD, Alley RB (1997) Grounding-line systems: processes, glaciological inferences and the stratigraphic record. In: Barker PF, Cooper AC (eds) *Geology and seismic stratigraphy of the Antarctic margin II*. Antarctic Research Series, American Geophysical Union, Washington, DC, 71, pp 169–187
- Powell RD, Domack EW (1995) Modern glaciomarine environments. In: Menzies J (ed) *Glacial Environments*, vol 1. *Modern glacial environments: processes. Dynamics and Sediments*. Butterworth-Heinemann, Oxford, pp 445–486
- Powell R, Domack E (2002) Modern glaciomarine environments. In: Menzies J (ed) *Modern and past glacial environments*. Butterworth-Heinemann, Boston, pp 361–389
- Praeg D (2003) Seismic imaging of mid-Pleistocene tunnel-valleys in the North Sea Basin—high resolution from low frequencies. *J Appl Geophys* 53:273–298
- Rise L, Ottesen D, Berg K et al (2005) Large-scale development of the mid-Norwegian margin during the last 3 million years. *Mar Pet Geol* 22:33–44
- Rise L, Bellec V, Ottesen D et al (2016) Hill-hole pairs on the Norwegian continental shelf. In: Dowdeswell JA, Canals M, Jakobsson M, Todd BJ, Dowdeswell EK, Hogan KA (eds) *Atlas of submarine glacial landforms: modern, Quaternary and ancient*. Geological Society, London, Memoirs 46, pp 203–204
- Röthlisberger H (1972) Water pressure in intra- and subglacial channels. *J Glaciol* 11:177–203
- Rydningen TA, Vorren TO, Laberg JS et al (2013) The marine-based NW Fennoscandian ice sheet: glacial and deglacial dynamics as reconstructed from submarine landforms. *Quat Sci Rev* 68:126–141
- Rydningen TA, Laberg JS, Kolstad V (2016) Seabed morphology and sedimentary processes on high-gradient trough mouth fans offshore Troms, northern Norway. *Geomorphology* 246:205–219
- Sættem J (1990) Glaciotectonic forms and structures on the Norwegian continental shelf: observations, processes and implications. *Norske Geologisk Tidsskrift* 70:81–94
- Seramur KC, Powell RD, Carlson PR (1997) Evaluation of conditions along the grounding line of temperate marine glaciers: an example from Muir Inlet, Glacier Bay, Alaska. *Mar Geol* 140:307–327
- Sexton DJ, Dowdeswell JA, Solheim A et al (1992) Seismic architecture and sedimentation in north-west Spitsbergen fjords. *Mar Geol* 103:53–68
- Sharp M (1985) ‘Crevasse-fill’ ridges—a landform type characteristic of surging glacier? *Geogr Ann* 67A:213–220
- Shipp SS, Anderson JB, Domack EW (1999) Late Pleistocene-Holocene retreat of the West Antarctic ice-sheet system in the Ross Sea: part 1—geophysical results. *Geol Soc Am Bull* 111:1486–1516
- Shipp SS, Wellner JA, Anderson JB (2002) Retreat signature of a polar ice stream: subglacial geomorphic features and sediments from the Ross Sea, Antarctica. In: Dowdeswell JA, Ó Cofaigh CS (eds) *Glacier-influenced sedimentation on high latitude continental margins*. Geological Society of London, London, UK, pp 277–304
- Siegert MJ, Dowdeswell JA (2002) Late Weichselian iceberg, meltwater and sediment production from the Eurasian ice sheet: results from numerical ice-sheet modelling. *Mar Geol* 188: 109–127
- Solheim A (1991) The depositional environment of surging sub-polar tidewater glaciers: a case study of the morphology, sedimentation and sediment properties in a surge-affected marine basin outside Nordaustlandet, northern Barents Sea. *Norsk Polarinstitutt Skrifter*, p 194
- Solheim A, Elverhøi A (1997) Submarine glacial flutes and De Geer moraines. In: Davies TA, Bell T, Cooper AK, Josenhans H, Polyak L, Solheim A, Stoker MS, Stravers JA (eds) *Glaciated continental margins: an atlas of acoustic images*. Chapman & Hall, London, pp 56–57

- Solheim A, Russwurm L, Elverhøi A et al (1990) Glacial geomorphic features in the northern Barents Sea: direction evidence for grounded ice and implications for the pattern of deglaciation and late glacial sedimentation. In: Dowdeswell JA, Scourse JD (eds) *Glacimarine environments processes and sediments*. Geological Society, London, Special Publication 53, pp 253–268
- Spagnolo M, Clark CD, Ely JC et al (2014) Size, shape and spatial arrangement of mega-scale glacial lineations from a large and diverse dataset. *Earth Surf Proc Land* 39:1432–1448
- Stokes CR, Clark CD (1999) Geomorphological criteria for identifying Pleistocene ice streams. *Ann Glaciol* 28:67–75
- Stokes CR, Clark CD (2001) Palaeo-ice streams. *Quat Sci Rev* 20:1437–1457
- Stokes CR, Clark CD (2002) Ice stream shear margin moraines. *Earth Surf Proc Land* 27:547–558
- Stokes CR, Margold M, Clark CD et al (2016) Ice stream activity scaled to ice sheet volume during Laurentide ice sheet deglaciation. *Nature* 530:322–326
- Svendsen JI, Astakhov VI, Bolshiyann D Yu et al (1999) Maximum extent of the Eurasian ice sheet in the Barents and Kara Sea region during the Weichselian. *Boreas* 28:234–242
- Syvitski JPM, Lewis CFM, Piper DJW (1996) Palaeoceanographic information derived from acoustic surveys of glaciated continental margins: examples from eastern Canada. In: Andrews JT, Austin WEN, Bergsten H, Jennings AE (eds) *Late Quaternary palaeoceanography of the North Atlantic margins*. Geological Society Special Publication 111, pp 51–76
- Taylor J, Dowdeswell JA, Siegert MJ (2002a) Late Weichselian depositional processes, fluxes, and sediment volumes on the margins of the Norwegian Sea (62–75°N). *Mar Geol* 188:61–77
- Taylor J, Dowdeswell JA, Kenyon NH et al (2002b) Late Quaternary architecture of trough-mouth fans: debris flows and suspended sediments on the Norwegian margin. In: Dowdeswell JA, O’Cofaigh C (eds) *Glacier-influenced sedimentation on high-latitude continental margins*. Geological Society, London, Special Publications 203, pp 55–71
- Todd BJ, Valentine PC, Longva O et al (2007) Glacial landforms on German Bank, scotian shelf: evidence for late Wisconsinan ice-sheet dynamics and implications for the formation of De Geer moraines. *Boreas* 36:148–169
- Vanneste M, Mienert J, Bünz S (2006) The Hinlopen slide: a giant, submarine slope failure on the northern Svalbard Margin, Arctic Ocean. *Earth Planet Sci Lett* 245:373–388
- Vorren TO, Laberg JS (1997) Trough mouth fans—palaeoclimate and ice-sheet monitors. *Quat Sci Rev* 16:865–881
- Vorren TO, Plassen L (2002) Deglaciation and palaeoclimate of the Andfjord-Vågsfjord area, North Norway. *Boreas* 31:97–125
- Vorren TO, Hald M, Lebesbye E (1988) Late Cenozoic environments in the Barents Sea. *Paleoceanography* 3:601–612
- Warren WP, Ashley GM (1994) Origins of the ice-contact stratified ridges (eskers) of Ireland. *J Sediment Res (A)* 64:433–449
- Wellner JS, Lowe AL, Shipp SS et al (2001) Distribution of glacial geomorphic features on the Antarctic continental shelf and correlation with substrate: implications for ice behavior. *J Glaciol* 47:397–411
- Whillans IM, Bentley CR, van der Veen CJ (2001) Ice streams B and C. In: Alley RB, Bindschadler RA (eds) *The west Antarctic ice sheet: behavior and environment*, Am Geophys Union Antarct Res Ser 77:257–281
- Woodworth-Lynas CMT, Josenhans HW, Barrie JV et al (1991) The physical processes of seabed disturbance during iceberg grounding and scouring. *Cont Shelf Res* 11:939–951

Submarine Landslides

Joshu Mountjoy and Aaron Micallef

Abstract Robust interpretation of geomorphology is a primary method of understanding failure modes, emplacement mechanisms and post-failure modification of submarine landslides. Since high-resolution hull-mounted multibeam systems became widely available in the last 20 years, our understanding of submarine landslides has improved dramatically. Techniques such as 3D seismic and cm-resolution seafloor mapping has revealed both surface and sub-surface geomorphology in unprecedented detail, and we are making rapid advancements towards refining our understanding of the processes that lead to specific geomorphological signatures associated with slope failure. One of the greatest challenges in the geomorphological analysis of submarine landslides is in accounting for post-failure modification processes. As erosional processes, such as gullying, erode the easily recognisable landslide geomorphology, or sediment drape smothers landslide features, it becomes increasingly more challenging to identify where landslides have occurred. In some depositional environments (e.g. a slope basin) the landslide debris may be preserved in the stratigraphy and analysed using 3D data. However, in erosional environments, such as submarine canyons, there is often little or no remaining deposit and interpretation of landslide processes must be based solely on the landslide scar, which is often heavily modified due to the dynamic nature of the canyon environment. Accurate interpretation and quantification of landslide parameters becomes important for determining magnitude frequency for landslide populations, which is a key piece of information for hazard studies.

J. Mountjoy (✉)

National Institute of Water and Atmospheric Research,
301 Evans Bay Parade, Greta Point, Wellington, New Zealand
e-mail: Joshu.mountjoy@niwa.co.nz

A. Micallef

Department of Geosciences, Marine Geology and Seafloor Surveying,
University of Malta, Msida MSD 2080, Malta

1 Introduction

Submarine landslides are among the largest natural events on Earth, occurring along all continental margins and at all water depths (Masson et al. 2006; Urlaub et al. 2013; Moscardelli and Wood 2015). They can occur at low slope gradients (<2°) and over large distances (>1000 km) (Huhnerbach and Masson 2004). In terms of volume, submarine landslides can be three orders of magnitude larger than their terrestrial counterparts, which makes them one of the most important agents transferring sediments across the planet (Hampton et al. 1996; Korup 2012). They can generate or enhance damaging tsunamis, posing a significant risk to coastal communities (Bondevik et al. 2005; Tappin et al. 2014). Submarine landslides can also damage seafloor infrastructure, such as that used to recover oil and gas, or seafloor telecommunication cables, which carry more than 95% of global internet traffic (Carter et al. 2012; Talling et al. 2014). Submarine landslides have been shown to play a role defining hydrocarbon reservoir location and geometry, facies distributions, and development of stratigraphic traps and of seal intervals (Lamarche et al. 2015).

Submarine landslides have been reported on active and passive continental margins (McAdoo et al. 2000; Weaver et al. 2000; Urgeles and Camerlenghi 2013), within submarine canyons (Micallef et al. 2012), fjords (Lastras et al. 2013) and submarine deltas and fans of large rivers (Prior et al. 1982b), as well as oceanic islands (Watt et al. 2014). The Agulhas Slide is by far the largest submarine landslide reported in the literature (Dingle 1977; Dingle and Robson 1985). Its estimated volume is 20,000 km³, which is one order of magnitude larger than the Nuuanu debris avalanche, a volcanic flank collapse offshore Oahu (Hawaii) (Moore et al. 1989), or the Storegga Slide, which failed on the glaciated margin offshore Norway (Bryn et al. 2005). The workshop on marine slides and other mass movements organised by NATO in 1980 was the first attempt to bring submarine slope instability in the international spotlight. Since then, numerous initiatives (e.g. ADFEX (Arctic Delta Failure Experiment, 1989–1992), GLORIA (1984–1991), STEAM (Sediment Transport on European Atlantic Margins, 1993–1996), ENAM II (1996–1999), STRATAFORM (1995–2001), COSTA (Continental slope Stability, 2000–2002) have addressed issues related to submarine landslides. The latest of these initiatives is S4SLIDE (2015–2020), funded by UNESCO IGCP-640.

As on terrestrial hillslopes, the term landslide refers to the displacement of a mass of soil or rock when the downslope driving forces acting on the material are greater than the forces acting to resist major deformations. There are a number of distinctions within the definition for submarine landslides, which relate to factors such as velocity, coherency and the ratio of sediment/rock to fluid. Masson et al. (2006) distinguish between slides, debris flows, debris avalanches and turbidity currents according to the following definitions:

- Slide: The movement of a coherent mass of sediment bounded by distinct failure planes (can be translational or rotational);
- Debris flow: The laminar, cohesive flow of clasts in a fine-grained matrix;

- Debris avalanche: The rapid flow of cohesionless rock fragments, blocks and clasts with energy dissipation by grain contact;
- Turbidity current: A gravity flow in which sediment grains are maintained in suspension by fluid turbulence.

Others (Mulder and Cochonat 1996; Locat and Lee 2002) have also included spreads, creep and falls in their classification schemes and many landslides are a complex combination of different failure styles.

A wide variety of factors have been proposed to explain how submarine slope failure is preconditioned or triggered (Locat and Lee 2002); (Canals et al. 2004; Masson et al. 2006). These include the geological characteristics of the landslide material (e.g. presence of a weak layer (Bryn et al. 2005; Locat et al. 2014), rapid sediment accumulation, overpressure development (Dugan and Flemings 2000) and transient external factors (e.g. oversteepening (Assier-Rzadkiewicz et al. 2000), seismic loading (Piper et al. 1999), gas hydrate dissociation (Kennett et al. 2003; Maslin et al. 2004), gas charging (Field 1990), storm-wave and tidal loading (Bea et al. 1983), glacial loading (Mulder and Moran 1995), seepage (Orange and Breen 1992), volcanic island processes (Masson 1996), tectonic movements, diapirism and human activities (Dan et al. 2007).

2 Geomorphic Expression of Submarine Landslides

All landslide processes may have some distinctive geomorphic expression related to the presence of blocks or the flow-type deformation of soft sediment. However, all landslides share a large number of common geomorphic features that can be used to describe them. At the first order, the features of terrestrial and submarine landslides are the same and subsequently much of the submarine literature has initially drawn on key terrestrial publications (e.g. Varnes 1978). The primary geomorphic features of submarine landslides are illustrated in Fig. 1. The characteristic behaviour of a submarine (and terrestrial) landslide is extensional deformation or stretching through the upper part of the slide as material moves out of the source zone, transitioning to compressional deformation in the distal deposition zone as material velocity decreases from the leading edge and debris accumulates against itself, intact stratigraphy, or other obstructions such as previous landslide deposits. In some cases, however, this idealised behaviour will not apply and a range of compressional and extensional features are observed throughout the landslide (Mountjoy et al. 2014).

The cutaway schematic diagram in Fig. 1 illustrates some of the process observations that can be made from surface geomorphic features alone. Features of the source zone, such as the head and lateral scarp (which can be >100 m high), define the contact between intact slope sediment/rock and displaced material. Near the headscarp, displaced blocks remaining in the source zone are normal faulted and back rotated, which is reflected at the surface by concave downslope steps, fractures

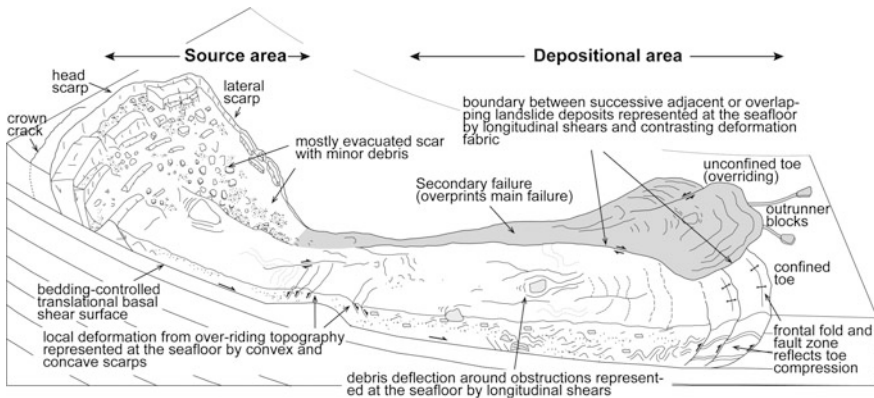


Fig. 1 Cutaway perspective line drawing of the geomorphic anatomy of a submarine landslide modified, adapted from (Prior et al. 1984; Bull et al. 2009)

or scarps. If material has been evacuated from the landslide scar, a smooth seafloor occurs. In the distal region of the landslide, where debris has impacted into intact stratigraphy, raised ridges aligned perpendicular to the direction of movement reflect structural-type faulting at depth and define a frontal compressional fold and fault zone. On the surface, the diagnostic geomorphic feature of this process will be convex downslope ridges. Individual blocks, up to several kilometres in width, may travel beyond the edge of the distal region.

3 Investigating Submarine Landslides

The earliest complete imaging of submarine landslides used side scan sonar surveying in shallow water to image near-coastal landslides (e.g. Prior et al. 1982a). Deeper water landslides were subsequently mapped with larger side scan sonar systems and 12 kHz multibeam (e.g. GLORIA, Seamarc, MR1, EM12). These deeper water studies achieved horizontal resolutions of 50–100 m over large areas, which enabled mapping of the extent and first order features of very large landslides at scales up to thousands of square kilometres (Lipman et al. 1988; McAdoo et al. 2000; Collot et al. 2001). In addition, high resolution 2D seismic reflection (e.g. Chirp, 3.5 kHz, boomer, sparker) surveys were used to reveal the internal architecture of submarine landslides in reasonable detail and estimate their thickness, although with limited lateral context (Bugge et al. 1987; Locat and Lee 2002).

The advent of shipboard 30 kHz multibeam echosounders from the mid to late 1990s resulted in a dramatic increase in the complete imaging of the geomorphology of submarine landslides. This has led to significant advances in seafloor analysis at resolutions similar to that available for terrestrial landslides, and it is now routine to map landslides in their entirety at 10–25 m horizontal resolution.

In addition, whole margins are now being mapped at this resolution and the identification of submarine landslides from their geomorphic fingerprint has also significantly improved.

Geomorphological analysis of submarine landslides covers a wide range of approaches. The majority of submarine landslide studies use surface and subsurface analysis and detailed surveying to describe first order features of a landslide, or multiple landslides, and make inferences about the processes, controls and triggers associated with them. The geomorphological analysis of submarine landslides can involve the following key approaches:

3.1 Geomorphometric Analyses

There is significant value in user-driven (informed-subjective) interpretation, which requires training and experience, and the effective application of it is non-trivial. By forcing the user to put lines on the map that represent the geomorphic expression of sub-surface processes, there is a requirement to develop a 3-dimensional understanding of the geomorphic system.

In contrast to “informed-subjective interpretation”, quantitative geomorphic analysis or morphometric techniques are used to objectively identify and quantify geomorphic features. Micallef et al. (2007) list a number of benefits that the morphometric approach offers, including (1) a greater spatial detail of analysis, (2) production of topographic information in quantitative format, (3) the generation of consistent and rapid results based on an established set of rules for landform delineation.

Figure 2 shows an example of objective morphometric analysis of the Storegga Slide offshore Norway. Micallef et al. (2007) mapped ridge crests within the Storegga Slide to define the key features of the landslide debris, namely spreading ridges. They were then able to analyse parameters such as ridge spacing, orientation and length to distinguish domains within the landslide. The result of this analysis is

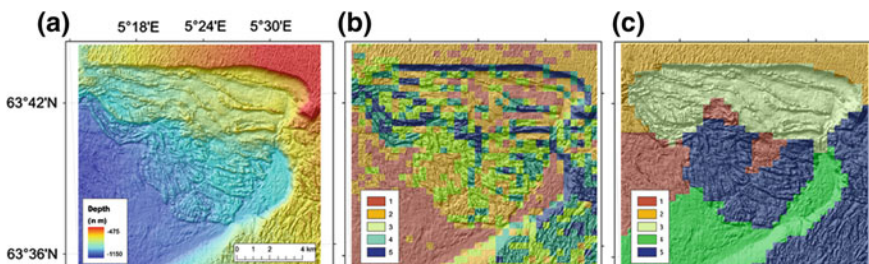


Fig. 2 Morphometric analysis of the Storegga Slide. (Reprinted from Micallef et al. (2007), with permission from John Wiley and Sons, Inc.) **a** Bathymetric map. **b** ISODATA analysis from slope gradient, profile, and plan curvature as input layers. **c** ISODATA analysis from ridge characteristics and slope gradient standard deviation as the input layers

shown in Fig. 2c, where the geomorphic domains of the landslide are clearly distinguished. In contrast, analysis of basic surface derivatives of slope and curvature does not usefully separate distinct domains (Fig. 2b).

It is important to be aware that all objective mapping techniques require experienced user interpretation and often intervention or guidance to be of any relevance. Most often, a combination of both objective and subjective approaches will result in the most efficient, robust and insightful results.

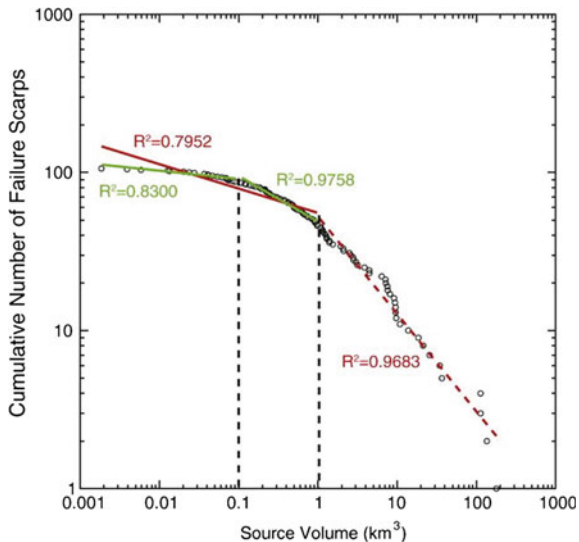
3.2 *Landslide Population Statistics*

Mapping the distribution and metrics of regional submarine landslide populations is a critical requirement to assess the impact of submarine landslides on the seafloor, whether for hazard assessment, understanding their role in landscape evolution, or determining the environmental controls on landslide occurrence. While surface geomorphological mapping is a relatively straight forward exercise where landslide geomorphology is well preserved, landslide mapping can be a challenge when the information is incomplete. A certain level of interpretation is required to define, for example, the extent of the deposit on the seafloor, the edge of the landslide scar and, critically, composite events that make up one landslide scar or deposit. As larger areas of continental margins are getting complete coverage with high resolution (10–20 m) multibeam bathymetric data, the opportunity to map complete regional landslide populations is increasing.

Major efforts have been undertaken to map landslide populations across continental margins and use these datasets to determine controls on landslide occurrence, controlling factors, and as a basis for hazard assessment (Owen et al. 2007; Lee 2009; Ten Brink et al. 2009; Twichell et al. 2009; Urgeles and Camerlenghi 2013; Moscardelli and Wood 2015). These studies have been able to define the magnitude distribution of submarine landslides (Fig. 3), making a significant step towards understanding the true magnitude frequency of submarine landslides. Landslide population analysis has revealed some key insights into landside occurrence, including a peak of landslide headscars in 1000–1300 m water depth and the limited influence of slope gradient on landslide distribution (Huhnerbach and Masson 2004). Studies have identified the presence of many small failures on active margins in contrast to fewer large landslides on passive margins (Urgeles and Camerlenghi 2013). It is worth noting that the uncertainties in comparing landslide populations, distribution and relationships to other parameters should include the level of confidence at which all landslides have been identified and properly characterised in their respective areas.

A common comment in studies of mapped populations of landslides across large continental areas is that the databases are incomplete due to data quality and/or

Fig. 3 Landslide size distributions based on databases derived from geomorphic mapping of landslides. (Reprinted from Chaytor et al. (2009), with permission from Elsevier.)



coverage. It is also true that the mapped landslides only represent a portion of the total population due to variable rates of post landslide modification. It is common that only parts of submarine landslides are preserved in seafloor geomorphology, and in fact it is rare that the entire source area to depositional zone is preserved for individual failures. Landslide debris can be removed by other processes (e.g. submarine canyon flushing), parts of the landslide may be buried by sediment (e.g. Mosher and Campbell 2010) or local erosional processes may modify the landslide geomorphology so that the features are no longer immediately recognisable (Mosher and Piper 2007).

Away from open continental slopes, landslide geomorphology can be modified rapidly through the interaction with submarine canyons, tectonics and other sediment failures. Figure 4 shows three adjacent landslide scars that have very similar scar width, head scarp height and scar gradient, and all having a lower slope boundary defined by the Kaikoura Canyon, known to be active during the Holocene (Lewis and Barnes 1999). What varies markedly, however, is the preservation of landslide geomorphology. The surface preservation of landslide features such as debris and planar basal surfaces (Fig. 4a), drainage network bifurcation (a qualitative proxy for maturity), and the diffusion of sharp slope breaks (Fig. 4b) leads to the qualitative conclusion that there is a progressive down canyon younging of these failures (i.e. T1 is the most recently active failure). In the absence of difficult to acquire and expensive data for landslide failure age, inferences about relative landslide scar maturity can be useful to understand landscape evolution in similar environments. Any assumptions of relative age must be made with the caveat that surface processes may modify geomorphology at different rates and quantitative information from processes such as scarp diffusion is challenging (Mitchell 1996).

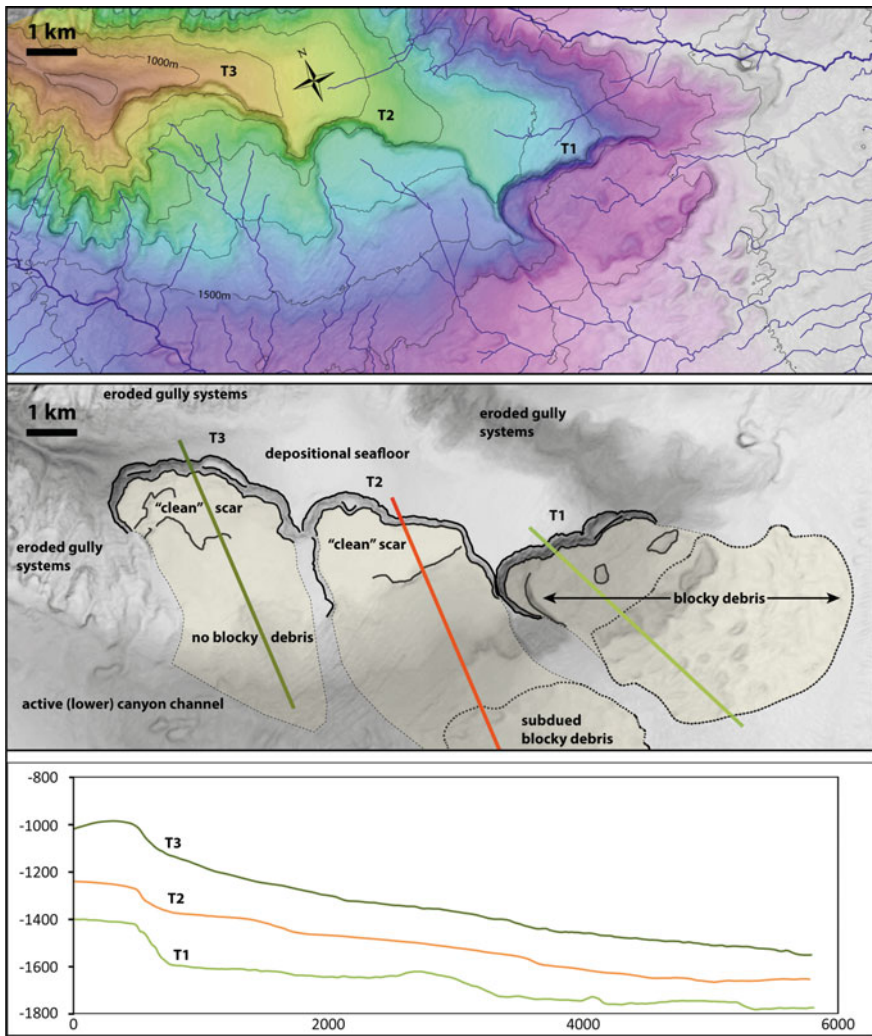


Fig. 4 Kaikoura canyon sequential landslides. *Top panel* multibeam bathymetric map showing the three landslide scars T1–T3 with automated drainage network (blue lines). *Middle panel* slope gradient map with annotated geomorphic interpretation. *Bottom panel* Longitudinal profiles across the landslide scars T1–T3, locations indicated in *middle panel*. Axes are in metres

3.3 Very High Resolution Imaging and Repeat Surveying

Ultra-high resolution acoustic imaging (typically from instruments mounted on Autonomous Underwater Vehicles or AUVs), and recording of visual imagery (typically mounted on Remote Operated Vehicles or ROVs), offer the opportunity to understand the fine scale details of submarine landslide geomorphology. AUVs

are deployed where the geomorphology is already well known and a specific area needs to be mapped in detail. To gain insight into mass failure processes in 1000–2000 m water depths offshore California, an AUV was used to map landslide scars at 1 m resolution (Gwiazda et al. 2016; Paull et al. 2016). The fine scale geomorphology of the landslide scars reveals extensive post failure modification of the slide scars. The Tubeworm Slump in Monterey Canyon has a ~6 km headscarp length composed of approximately 20 smaller scarps, indicating multiphase failure to create the initial scar or, alternatively, extensive small scale failure following the initial event. The Eel Slump has extensive post failure erosional modification of the head scarp, with linear erosional gullies at a spacing of 150 m as well as a smoothed drape of sediment over the main slide scar. In these two cases, the detail of geomorphology from AUV data reveals key information about the scale of processes operating to shape landslide scars that is not available from other techniques.

In a new and novel application, Huvenne et al. (2016) used a ROV with a forward looking 400 kHz multibeam system to map a landslide scarp in >1000 m water depth in the Rockall Trough at up to 10 cm resolution. Huvenne et al. (2016) are able to distinguish the geomorphology of the vertical to overhanging headscarp and resolve individual blocks and lithological features such as bedding. With further development and application this approach has the potential to make major advances in understanding submarine landslides due to the very high (cm) resolution and ability to image vertical and overhanging seafloor. ROVs also offer the opportunity to analyse cm scale geomorphology using optical imagery, which can reveal individual block angularity and surficial sediment shedding processes (Watt et al. 2015; Chaytor et al. 2016).

Repeat bathymetric surveys have the potential to capture the extent and geomorphological signature of individual failure events, as well as the post failure evolution of landslide scars. Numerous repeat surveys have been conducted to study landslide processes in a range of environments including canyons, open slopes, volcanic flanks and river deltas (e.g. Wright et al. 2008; Hughes-Clarke et al. 2012). An example of the evolution of a landslide on a near-shore slope offshore Gabon is shown in Fig. 5 (Biscara et al. 2012). Results show a small channel migrating upslope to near the shoreline followed by $2.4 \times 10^6 \text{ m}^3$ slope failure with the channel defining the lateral margin of the landslide. Within a short period of time significant modification of the slide scar occurs via small scale submarine landslides and channel development in the slide scar. Infill of the slide scar starts to occur and, assuming continued sedimentation, the scar would be completely filled within 20 years.

To see rapidly changing geomorphological processes in action, it is typically necessary to use dynamic shallow water environments as analogous natural laboratories for deeper ocean processes. A campaign of very high temporal frequency monitoring of the dynamic evolution of the Squamish Delta in Canada using repeat multibeam surveys over a 1 year time period reveal large scale ($>20,000 \text{ m}^3$) failures occurring at the delta lip (Clare et al. 2016). These landslides set in motion

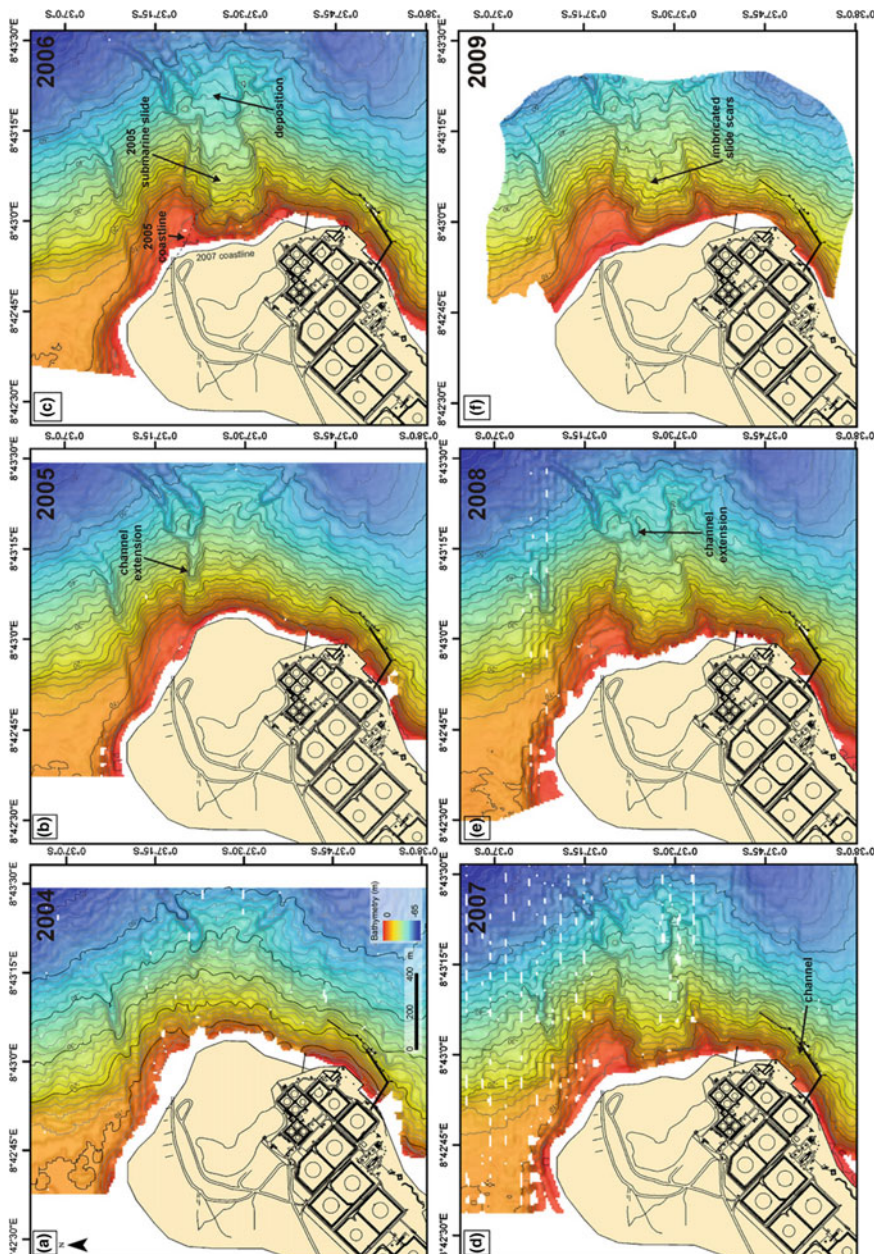


Fig. 5 Repeat bathymetric survey showing the development of submarine landslide scar geomorphology over a 5 year period. (Reprinted from Biscara et al. (2012), with permission from Elsevier.) Annual bathymetric grids are compiled from densely-spaced single beam echosounder surveys

trains of successive deposition and erosion associated with ephemeral bedforms in the channel floor. Monitoring by repeat surveying demonstrates the interaction between erosion and deposition that is accelerated in this high-sedimentation-rate environment. Gullies are created and removed in a short period of time and failures occur at ridges in the slope typically thought to be areas of stability. Monitoring processes on seafloor slopes in the deep ocean is more challenging as high resolution imaging is more difficult and process rates are likely to be slower. Repeat surveys have shown that active arc volcanoes experience small and frequent mass-wasting events and associated cone regrowth that are an important geomorphological process that can occur over short time periods (Wright et al. 2008).

Observations from repeat surveys show a range of dynamic processes operating over just 1–5 years. To capture active slope failure processes with repeat surveying requires a dynamic environment with a high temporal occurrence of events. Rapid geomorphic evolution is not common in the deep ocean but highly dynamic shallow water environments provide excellent analogies to unravel the geomorphic expression of processes in deeper water environments.

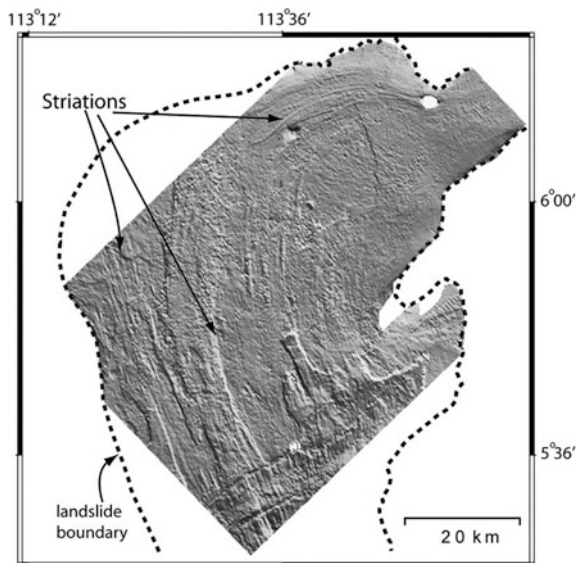
3.4 3D Seismic Geomorphology of Submarine Landslides

A major advancement in submarine landslide geomorphology was the application of analysis techniques to petroleum industry 3D seismic reflection datasets (Frey-Martínez et al. 2006; Gee et al. 2007). Smaller scale 3D seismic systems, such as the P-Cable, are optimally suited for analysis of landslides preserved at or near the seafloor, are cost effective for research voyages, and have very high resolution (5–10 m) within the upper 500 m of the sedimentary sequence (Berndt et al. 2012). The major advantage of 3D data is the ability to derive surfaces at depth by interpreting landslide features and analyse the seismic attributes associated with such surfaces (e.g. Dalla Valle et al. 2013). Seismic attributes derived from 3D data are optimal for analysing fluid flow features, fracture networks and the relationship of these to landslide deformation (Bünz et al. 2005). 3D seismic geomorphology of the erosional basal surface of submarine landslides can reveal striations that define the direction of movement during landslide emplacement, and can be used to distinguish single from multiple event failures (Fig. 6). The ability to use 3D seismic data to reveal the geomorphology of old, buried landslide features as if they were still on the seafloor has opened up a new area of research that continues to dramatically increase our understanding of landslide processes.

4 Major Challenges and Future Directions

We still lack a deep understanding of many crucial aspects associated with the pre-conditioning, triggering and dynamic behaviour of submarine landslides that can in part be addressed using geomorphic analysis. Among the major gaps in our knowledge are:

Fig. 6 Seafloor-like DEM created from a subsurface horizon in 3D seismic data reveals the erosional character of the basal surface of a landslide. (Reprinted from Gee et al. (2007), with permission from Elsevier.)



- How do submarine landslides evolve after initiation and how do their dynamics affect their impact on coastal areas, including the generation of tsunamis?
- What are the indicators of incipient submarine slope instability in different geological-tectonic settings?
- What are the time recurrence periods for submarine landslides? Do they cluster in space and time?
- What is the impact of climatic variations on the occurrence of submarine landslides?
- Can changes in the methane hydrate stability zone on continental margins trigger submarine landslides?

The strategy that we and the S4SLIDE community propose to address the above research questions entails:

- Continue to invest in sub-seafloor characterisation and sampling to reduce data uncertainty in the third dimension.
- Generate statistically significant submarine landslide data sets to allow robust probabilistic stability and hazard assessment.
- Repeat multibeam surveys to address dynamic slope behaviour during failure and transient phenomena in slope failure preconditioning and triggering.
- Advance monitoring of the geomorphic evolution of submarine landslides in deeper water environments as well as highly dynamic shallow water environments, also via scientific drilling (Flemings et al. 2008).

- Advance the capability to model submarine landslide triggered tsunamis, particularly by better constraining the disintegration of material during failure.
- Promote multi-scale quantitative geomorphological investigations by integrating field measurements, remote sensing, and numerical models.

5 Conclusions

Landslides are defined by their geomorphology. Headscarp morphometry can be used to define landslide volume, failure mode (block slide vs. rotational disintegrative failure), the number of failures that have occurred and subsequent erosional processes. Landslide deposit morphology can define transitional modes of emplacement and interaction with extant topography. While we can often use seismic reflection data to image subsurface processes that influence seafloor morphology, these data are not always available, or located in ideal locations, and it is valuable to be able to derive subsurface process information from surface morphology.

Developing techniques such as high resolution (sub-metre) imaging, 3D seismic reflection and seafloor monitoring are providing major advancements in the field. The ability to reveal fine scale geomorphology allows insight into geomorphic processes at the scale of terrestrial LiDAR data. By using 3D seismic data, it is now possible to analyse the geomorphology of paleo-seafloor horizons and erosional surfaces in the same way we analyse the modern seafloor.

One of the major challenges in the field is the identification of the full population of landslides. Landslide monitoring shows that the geomorphic evidence for landslide occurrence can be created and destroyed within a very short period of time, from days to years depending on the environment. We rely on identification of landslide sources for hazard assessments for tsunami studies and so the accurate identification of landslide populations, and increased understanding of landslide processes, has significant implications for society.

References

- Assier-Rzadkiewicz S, Heinrich P, Sabatier PC et al (2000) Numerical modelling of a landslide-generated tsunami: the 1979 Nice event. *Pure Appl Geophys* 157:1717–1727
Bea RG, Wright SG, Sircar P et al (1983) Wave-induced slides in south pass block 70, Mississippi Delta. *J Geotech Eng* 109:619–644
Berndt C, Costa S, Canals M et al (2012) Repeated slope failure linked to fluid migration: the ANA submarine landslide complex, Eivissa channel, Western Mediterranean Sea. *Earth Planet Sci Lett* 319–320:65–74

- Biscara L, Hanquiez V, Leynaud D et al (2012) Submarine slide initiation and evolution offshore pointe odden, Gabon—analysis from annual bathymetric data (2004–2009). *Mar Geol* 299: 43–50
- Bondevik S, Løvholt F, Harbitz C et al (2005) The Storegga Slide tsunami—comparing field observations with numerical simulations. *Mar Pet Geol* 22:195–208
- Bryn P, Berg K, Forberg CF et al (2005) Explaining the Storegga Slide. *Mar Pet Geol* 22(1–2): 11–19
- Bugge T, Befring S, Belderson RH et al (1987) A giant three-stage submarine slide off Norway. *Geo-Mar Lett* 7:191–198
- Bull S, Cartwright J, Huuse M (2009) A review of kinematic indicators from mass-transport complexes using 3D seismic data. *Mar Pet Geol* 26(7):1132–1151
- Bünz S, Mienert J, Bryn P et al (2005) Fluid flow impact on slope failure from 3D seismic data: a case study in the Storegga Slide. *Basin Res* 17(1):109–122
- Canals M, Lastras G, Urgeles R et al (2004) Slope failure dynamics and impacts from seafloor and shallow sub-seafloor geophysical data: case studies from the COSTA project. *Mar Geol* 213(1–4):9–72
- Carter L, Milliman J, Talling PJ et al (2012) Near-synchronous and delayed initiation of long run-out submarine sediment flows from a record-breaking river flood, offshore Taiwan. *Geophys Res Lett* 39:L12603
- Chaytor JD, Ten Brink U, Solow AR et al (2009) Size distribution of submarine landslides along the US atlantic margin. *Mar Geol* 264(1):16–27
- Chaytor JD, Demopoulos AW, Uri S et al (2016) Assessment of canyon wall failure process from multibeam bathymetry and remotely operated vehicle (ROV) observations, US atlantic continental margin, submarine mass movements and their consequences. Springer, pp 103–113
- Clare M, Clarke JH, Talling P et al (2016) Preconditioning and triggering of offshore slope failures and turbidity currents revealed by most detailed monitoring yet at a fjord-head delta. *Earth Planet Sci Lett* 450:208–220
- Collot J-Y, Lewis KB, Lamarche G et al (2001) The giant Ruatoria debris avalanche on the northern Hikurangi margin, New Zealand: result of oblique seamount subduction. *J Geophys Res* 106(B9):19271–219297
- Dalla Valle G, Gamberi F, Rocchini P et al (2013) 3D seismic geomorphology of mass transport complexes in a foredeep basin: examples from the Pleistocene of the central adriatic basin (Mediterranean Sea). *Sed Geol* 294:127–141
- Dan G, Sultan N, Savoye B (2007) The 1979 Nice harbour catastrophe revisited: trigger mechanism inferred from geotechnical measurements and numerical modelling. *Mar Geol* 245:40–64
- Dingle RV (1977) The anatomy of a large submarine slump on a sheared continental margin (SE Africa). *J Geol Soc Lond* 134:293–310
- Dingle RV, Robson S (1985) Slumps, canyons and related features on the continental margin off East London, SE Africa (SW Indian Ocean). *Mar Geol* 67(1–2):37–54
- Dugan B, Flemings P (2000) Overpressure and fluid flow in the New Jersey continental slope: implications for slope failure and cold seeps. *Science* 289(5477):288–291
- Field ME (1990) Submarine landslides associated with shallow seafloor gas and gas hydrates off Northern California. In: AAPG (ed) Fifth circum-pacific energy and mineral resources conference, Honolulu, Hawaii
- Flemings PB, Long H, Dugan B et al (2008) Pore pressure penetrometers document high overpressure near the seafloor where multiple submarine landslides have occurred on the continental slope, offshore Louisiana, Gulf of Mexico. *Earth Planet Sci Lett* 269:309–325
- Frey-Martínez J, Cartwright J, James D (2006) Frontally confined versus frontally emergent submarine landslides: a 3D seismic characterisation. *Mar Pet Geol* 23(5):585–604
- Gee M, Uy H, Warren J et al (2007) The Brunei slide: a giant submarine landslide on the North West borneo margin revealed by 3D seismic data. *Mar Geol* 246(1):9–23
- Gwiazda R, Paull CK, Caress DW et al (2016) Eel Canyon slump scar and associated fluid venting, Submarine Mass movements and their consequences. Springer, pp 411–418

- Hampton MA, Lee HJ, Locat J (1996) Submarine landslides. *Rev Geophys* 34(1):33–59
- Hughes-Clarke J, Brucker S, Muggah J et al (2012) The Squamish prodelta: monitoring active landslides and turbidity currents. In: Proceedings of the Canadian hydrographic conference 2012, p 15
- Huhnerbach V, Masson DG (2004) Landslides in the North Atlantic and its adjacent seas: an analysis of their morphology, setting and behaviour. *Mar Geol* 213(1–4):343–362
- Huvenne VA, Georgiopoulou A, Chaumillon L et al (2016) Novel method to map the morphology of submarine landslide headwall scarps using remotely operated vehicles, submarine mass movements and their consequences. Springer, pp 135–144
- Kennett JP, Cannariato KG, Hendy IL et al (2003) Methane hydrates in quaternary climate change: the Clathrate Gun Hypothesis. *Am Geophys Union Spec Publ* 54:216
- Korup O (2012) Earth's portfolio of extreme sediment transport events. *Earth Sci Rev* 112: 115–125
- Lamarche G, Mountjoy J, Bull S et al (2015) Submarine mass movements and their consequences: progress and challenges. In: Lamarche G, Mountjoy J, Bull S, Hubble T, Krastel S, Lane E, Micallef A, Moscardelli L, Mueller C, Pecher I, Woelz S (eds) *Submarine mass movements and their consequences*. Springer International Publishing, Heidelberg, pp 1–12
- Lastras G, Amblas D, Calafat AM et al (2013) Landslides cause tsunami waves: insights from Aysén fjord, Chile. *EOS Trans Am Geophys Union* 94(34):297–298
- Lee HJ (2009) Timing of occurrence of large submarine landslides on the Atlantic Ocean margin. *Mar Geol* 264(1–2):53–64
- Lewis KB, Barnes PM (1999) Kaikoura Canyon, New Zealand: active conduit from near-shore sediment zones to trench-axis channel. *Mar Geol* 162(1):39–69
- Lipman PW, Normark WR, Moore JG et al (1988) The giant submarine Alika debris slide, Mauna Loa. *Hawaii J Geophys Res* 93(B5):4279–4299
- Locat J, Lee HJ (2002) Submarine landslides: advances and challenges. *Can Geotech J* 39: 191–212
- Locat J, Leroueil S, Locat A et al (2014) Weak layers: their definition and classification from a geotechnical perspective. In: Krastel S, Berhmann JH, Volker D, Stipp M, Berndt C, Urgeles R, Chaytor JD, Huhn K, Strasser M, Harbitz CB (eds) *Submarine mass movements and their consequences*. Springer International Publishing, Switzerland, pp 3–12
- Maslin M, Owen M, Day S et al (2004) Linking continental slope failures and climate change: testing the clathrate gun hypothesis. *Geology* 32:53–56
- Masson DG (1996) Catastrophic collapse of the volcanic island of Hierro 15 ka ago and the history of landslides in the Canary Islands. *Geology* 24(3):231–234
- Masson DG, Harbitz CB, Wynn RB et al (2006) Submarine landslides: processes, triggers and hazard prediction. *Philos Trans R Soc* 364(1845):2009–2039
- McAdoo BG, Pratson LF, Orange DL (2000) Submarine landslide geomorphology, US continental slope. *Mar Geol* 169:103–136
- Micallef A, Berndt C, Masson DG et al (2007) A technique for the morphological characterization of submarine landscapes as exemplified by debris flows of the Storegga Slide. *J Geophys Res F Earth Surf* 112(2):F02001
- Micallef A, Mountjoy JJ, Canals M et al (2012) Deep-seated bedrock landslides and submarine canyon evolution in an active tectonic margin: Cook Strait, New Zealand. In: Yamada Y, Kawamura K, Ikebara K, Ogawa Y, Urgeles R, Mosher D, Chaytor JD, Strasser MC (eds) *Submarine mass movements and their consequences*. Springer, London, pp 201–212
- Mitchell NC (1996) Creep in pelagic sediments and potential for morphologic dating of marine fault scarps. *Geophys Res Lett* 23(5):483–486
- Moore JG, Clague DA, Holcomb RT et al (1989) Prodigious submarine landslides on the Hawaiian Ridge. *J Geophys Res* 94:17465–17484
- Moscardelli L, Wood L (2015) Morphometry of mass-transport deposits as a predictive tool. *Geol Soc Am Bull* B31221-1

- Mosher DC and Campbell DC (2010) The Barrington submarine landslide, western Scotian Slope. In: Shipp C, Weimer P and Posamentier H (eds) The importance of mass-transport deposits in deepwater settings. SEPM Spec Pub 91
- Mosher DC, Piper DJ (2007) Analysis of multibeam seafloor imagery of the Laurentian Fan and the 1929 Grand Banks landslide area, submarine mass movements and their consequences. Springer, pp 77–88
- Mountjoy JJ, Pecher I, Henrys S et al (2014) Shallow methane hydrate system controls ongoing, downslope sediment transport in a low-velocity active submarine landslide complex. Hikurangi Margin, New Zealand. *Geochem Geophys Geosyst* 15
- Mulder R, Cochonat P (1996) Classification of offshore mass movements. *J Sediment Res* 66(1):43–57
- Mulder T, Moran K (1995) Relationship among submarine instabilities, sea-level variations and the presence of an ice shelf on the continental shelf: an example from the Verrill Canyon area, Scotian Shelf. *Palaeogeography* 10:137–154
- Orange DL, Breen NA (1992) The effects of fluid escape on accretionary wedges 2. Seepage force, slope failure, headless submarine canyons and vents. *J Geophys Res* 97(B6):9277–9295
- Owen M, Day S, Maslin M (2007) Late Pleistocene submarine mass movements: occurrence and causes. *Quatern Sci Rev* 26(7–8):958–978
- Paull CK, Anderson K, Caress DW et al (2016) Fine-scale morphology of tubeworm slump, Monterey Canyon, submarine mass movements and their consequences. Springer, Berlin, pp 155–162
- Piper DJW, Cochonat P, Morrison ML (1999) The sequence of events around the epicentre of the 1929 Grand Banks earthquake: initiation of debris flows and turbidity currents inferred from sidescan sonar. *Sedimentology* 46:79–97
- Prior DB, Bornhold BD, Coleman JM et al (1982a) Morphology of a submarine slide, Kitimat Arm. *Brit Columbia Geol* 10(11):588–592
- Prior DB, Coleman JM, Bornhold BD (1982b) Results of a known seafloor instability event. *Geo Mar Lett* 2:117–122
- Prior DB, Bornhold BD, Johns MW (1984) Depositional characteristics of submarine debris flow. *J Geol* 92:707–727
- Talling PJ, Clare M, Urlaub M et al (2014) Large submarine landslides on continental slopes: geohazards, methane release, and climate change. *Oceanography* 27(2):32–45
- Tappin DR, Grilli ST, Harris JC et al (2014) Did a submarine landslide contribute to the 2011 Tohoku tsunami? *Mar Geol* 357:344–361
- Ten Brink US, Barkan R, Andrews BD et al (2009) Size distribution and failure initiation of submarine and subaerial landslides. *Earth Planet Sci Lett* 287:31–42
- Twichell DC, Chaytor JD, ten Brink US et al (2009) Morphology of late quaternary submarine landslides along the U.S. Atlantic continental margin. *Mar Geol* 264(1):4–15
- Urgeles R, Camerlenghi A (2013) Submarine landslides of the Mediterranean Sea: trigger mechanisms, dynamics, and frequency-magnitude distribution. *J Geophys Res Earth Surf* 118(4):2600–2618
- Urlaub M, Talling PJ, Masson DG (2013) Timing and frequency of large submarine landslides: implications for understanding triggers and future geohazard. *Quatern Sci Rev* 72:63–82
- Varnes DJ (1978) Landslide types and processes. In: Schuster RL, Krizek RJ (eds) Special report 176: landslides: analysis and control. Transportation Research Board, Washington, DC, pp 11–33
- Watt S, Jutzeler M, Talling P et al (2015) New insights into landslide processes around volcanic islands from remotely operated vehicle (ROV) observations offshore Montserrat. *Geochem Geophys Geosyst* 16(7):2240–2261
- Watt SFL, Talling PJ, Hunt JE (2014) New insights into the emplacement dynamics of volcanic island landslides. *Oceanography* 27(2):46–57
- Weaver PPE, Wynn RB, Kenyon NH et al (2000) Continental margin sedimentation, with special reference to the north-east Atlantic margin. *Sedimentology* 47(1):239–256
- Wright IC, Chadwick WW, de Ronde CE et al (2008) Collapse and reconstruction of Monowai submarine volcano, Kermadec arc, 1998–2004. *J Geophys Res Solid Earth* 113(B8)

Submarine Canyons and Gullies

**David Amblas, Silvia Ceramicola, Thomas P. Gerber, Miquel Canals,
Francesco L. Chiocci, Julian A. Dowdeswell, Peter T. Harris,
Veerle A.I. Huvenne, Steven Y.J. Lai, Galderic Lastras,
Claudio Lo Iacono, Aaron Micallef, Joshu J. Mountjoy,
Charles K. Paull, Pere Puig and Anna Sanchez-Vidal**

Abstract Submarine canyons are deep incisions observed along most of the world's continental margins. Their topographic relief is as dramatic as that of any canyon or river valley on land but is hidden beneath the surface of the ocean. Our knowledge of canyons has therefore come primarily from remote sensing and sampling, and has involved contributions from various oceanographic disciplines. Canyons are a critical link between coastal and shelf waters and abyssal depths; water masses, sediment, nutrients, and even litter and pollutants are carried through them. Advances in technology continue to provide new insights into canyon environments by pushing the frontier of deep marine observations and measurements. In this chapter we describe the main geomorphic features of submarine

D. Amblas (✉) · J.A. Dowdeswell
Scott Polar Research Institute, University of Cambridge, Cambridge, UK
e-mail: da435@cam.ac.uk

S. Ceramicola
Istituto Nazionale di Oceanografia e di Geofisica Sperimentale, Trieste, Italy

T.P. Gerber
Statoil Research and Technology, Austin, TX, USA

M. Canals · G. Lastras · A. Sanchez-Vidal
GRC Geociències Marines, University of Barcelona, Barcelona, Spain

F.L. Chiocci
Dipartimento di Scienze della Terra, University of La Sapienza, Rome, Italy

P.T. Harris
GRID-Arendal, Arendal, Norway

V.A.I. Huvenne · C.L. Iacono
Marine Geoscience, National Oceanography Centre, University of Southampton,
Waterfront Campus, Southampton, UK

S.Y.J. Lai
Department of Hydraulic and Ocean Engineering, National Cheng Kung University,
Tainan, Taiwan

A. Micallef
Department of Geosciences, Marine Geology and Seafloor Surveying,
University of Malta, Msida, Malta

canyons and what is known about their formation and the processes that shape them. We also consider submarine gullies, which are small valleys commonly found within or alongside submarine canyons on the continental slope and may represent an incipient stage of canyon development.

1 Introduction

1.1 Definitions and Nomenclature

In general terms submarine canyons are defined as steep-sided, V-shaped valleys with heads at or near the continental shelf edge. They extend across the continental slope and are commonly linked to numerous tributaries, similar to unglaciated river-cut canyons on land (Neuendorf et al. 2005). The basis for this commonly accepted definition was established in 1963 by Francis P. Shepard, among the first geologists to devote his life's work to marine geology. Although the term "submarine canyon" is occasionally used for all seafloor valleys, in this chapter we focus mainly on canyons that fit this description. We therefore exclude other seafloor valley types, which were also distinguished by Shepard in 1963, such as delta-front troughs, fan valleys, fault valleys, shelf valleys and glacial troughs. The submarine channels observed in the continental rise and abyssal plains are also not considered in this chapter, although they frequently represent the final morphological expression of submarine canyons in the deep sea (see Chapter "[Submarine Fans and their Channels, Levees, and Lobes](#)").

The striking geomorphic resemblance between submarine canyons and river valleys (Fig. 1; see Sect. 2.2) has led, unsurprisingly, to a shared terminology for their description. We define, for instance, the sinuous course of submarine canyons as meanders, the line connecting the deepest points along the canyon as the thalweg, the smaller canyons that join into larger ones as tributaries, and the different reaches of a submarine canyon as the upper, middle and lower courses (see Sect. 2.1). Beyond nomenclature, the concepts and methodologies used to study the formative processes in submarine and subaerial canyons are also comparable in many ways (see Sect. 2.2).

On submarine canyon walls and steeper sections of the open continental slope it is very common to observe gullies (Figs. 1 and 2). Again the concept of "submarine

J.J. Mountjoy

National Institute of Water and Atmospheric Research, Wellington, New Zealand

C.K. Paull

Monterey Bay Aquarium Research Institute, Moss Landing, USA

P. Puig

Institut de Ciències del Mar—CSIC, Barcelona, Spain

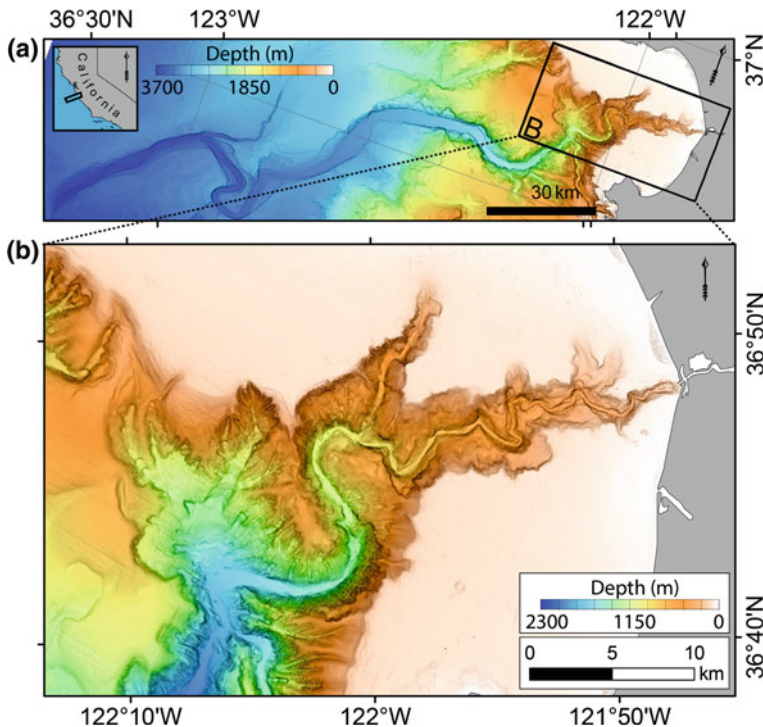


Fig. 1 Shaded relief images of Monterey Canyon, California, based on multibeam echosounder data collected by Monterey Bay Aquarium Research Institute (Greene et al. 2002). **a** 180 km long segment of the canyon extending from the shoreline to water depths of 3800 m. **b** Detail of the upper canyon revealing numerous meanders and gullied canyon walls

“gully” is taken from its subaerial counterpart, which refers to “a very small valley, such as a small ravine in a cliff face, or a long, narrow hollow or channel worn in earth or unconsolidated material (as on a hillside) by running water and through which water runs only after a rain or the melting of ice or snow” (Neuendorf et al. 2005). Here we define a submarine gully in similar terms: small-scale (<10 km), first-order and confined channels, generally on the order of tens of meters deep and often linear in planform.

1.2 *The Origin of Submarine Canyons*

The occurrence of submarine canyons was first noted in the late 19th century and followed up with several pioneering observations in the early 20th century (Dana 1863; Spencer 1903; Shepard 1932; Daly 1936; Bucher 1940a, b). One of the first hydrographic charts showing well-defined canyons was prepared by Veatch and

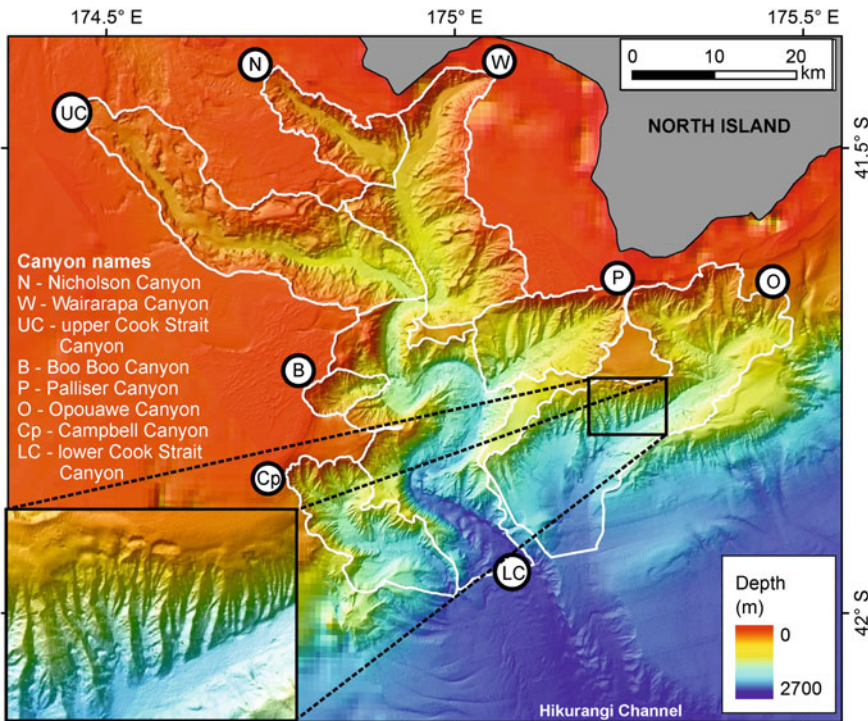


Fig. 2 **a** Shaded relief image of the Cook Strait Canyon, New Zealand. **b** Detail of the submarine gullies dissecting the walls of the canyon. Adapted from Micallef et al. (2014b)

Smith (1939) for the east coast of the United States. Their maps show straight or sinuous valleys running from the continental shelf down to the continental slope.

Early researchers were puzzled by what might cause such large-scale features on the seafloor. More detailed observations followed from the evolution of sonar mapping techniques, which prompted even more discussion about the origin of submarine canyons. During the early days of canyon research, the prevailing view was that marine processes, as they were known at that time, could not account for such large-scale landforms. Hence, canyon formation must have required either extreme changes in sea level that exposed continental margins to the eroding action of rivers (Veatch and Smith 1939), or catastrophic submarine events like erosion by tsunami waves (Bucher 1940b). But whereas there is evidence for exposure of some canyon heads during Pleistocene low stands of sea level, the question of which processes are active in the middle and lower courses of canyons—that have never been exposed above sea level—remained. In 1936, Reginald A. Daly addressed this question by hypothesising that sediment-laden gravity flows, or turbidity currents, might be responsible for canyon erosion (see Sect. 2.4). This idea was later

supported by Kuenen (1937) and is now, after nearly a century of work on deep marine stratigraphy, sedimentology and geomorphology, the prevailing model for canyon formation.

What is less certain is the sequence of canyon development from incipient to mature stages of evolution. Observational evidence suggests that canyons can propagate both upslope and downslope. The downslope model of development follows from the ideas of Daly (1936), who proposed that canyons were probably formed during periods of low sea level when turbidity currents generated near the shelf edge spilled down the slope, eroding channels that were enlarged and lengthened by subsequent flows. The upslope model came from observations like those of Twichell and Roberts (1982), who described canyons and gullies on the Atlantic seaboard of North America that showed no connection to the continental shelf (so-called blind canyons) and were interpreted to represent different stages of evolution. Orange and Breen (1992) attributed the origins of some blind canyons to slope failure induced by fluid seepage. Such blind canyons are evidently not related to river systems or to the supply of sediment to the shelf edge. Based on similar observations, Farre et al. (1983) proposed a model of canyon formation in which mass failures on the slope occur retrogressively, with the head of the canyon migrating upslope towards the shelf where it is more likely to capture turbidity currents that further erode its course. Pratson et al. (1994) and Pratson and Coakley (1996) combined and broadened these ideas by showing that (1) some apparently slope-confined canyons actually have buried upslope reaches that connect to the shelf, and (2) downslope turbidity current erosion and retrogressive slope failure can occur in tandem, resulting in a canyon formation sequence that progresses from small slope-confined gullies to large, headward-eroding canyons that breach the shelf break. A thorough review of the processes involved in the formation of canyons can be found in Pratson et al. (2007).

2 Submarine Canyon Morphology and Evolution

2.1 *The Physiography of Submarine Canyons*

Shelf-incising submarine canyons are characterised by several common features (Fig. 3): (1) a canyon head, often showing a distinct rim with a pointed to amphitheater-like shape that cuts the upper continental slope and the shelf edge; (2) an upper course, deeply incised into the slope with steep-sided walls covered by gullies and mass movement scars, and a meandering V-profile valley resembling a river-cut canyon; (3) a middle course, where the relief is smoother, the sinuous valley wider and the cross-sectional profile more U-shaped; and (4) a lower course with low-relief side walls and a U-shaped profile that is commonly transitional to a channel confined by depositional levées. This mostly depositional lower course is often considered a channel rather than a canyon, together forming a canyon-channel system, as described by Covault (2011). Submarine canyons commonly have

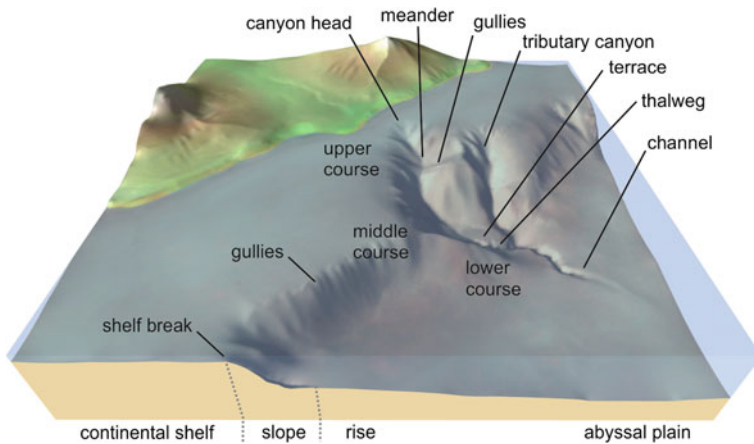


Fig. 3 Sketch showing the main physiographic elements of a shelf-incising submarine canyon

tributaries feeding their upper and middle courses. At the bottom of many canyons it is also common to observe a well-defined thalweg bounded by one or more terraces.

The above description is necessarily general and, as such, cannot capture the full spectrum of canyon morphologies. It is mainly based on large canyons that are eroded into bedrock in their upper courses, are floored with relatively coarse-grained sediments, and have a direct or indirect connection to rivers or longshore drift cells (e.g. Paull et al. 2005; Covault et al. 2007; Mountjoy et al. 2009; Lombo Tombo et al. 2015). As noted in Sect. 1.2, there are numerous submarine canyons that do not incise the continental shelf but instead begin somewhere down the slope, known as blind, headless or slope-confined canyons (Fig. 4; Harris and Whiteway 2011; Lastras et al. 2011a; Brothers et al. 2013; Huang et al. 2014; Lo Iacono et al. 2014). Some canyons are evidently aggradational and progradational instead of erosional (Wonham et al. 2000; Bertoni and Cartwright 2005; Straub and Mohrig 2009; Amblas et al. 2012), others show smooth walls lacking terraces or mass movement scars (Blum and Okamura 1992; Straub and Mohrig 2009; Jobe et al. 2011), and not all connect to leveed channels or deep sea fans (Lastras et al. 2011b).

2.2 A Brief Comparison with Fluvial Systems

The intriguing similarity between submarine canyons and river valleys was first recognised in early bathymetric measurements along continental margins (Daly 1936). The apparent geomorphic similarities between fluvial and deep-water systems—similarities that are now well documented in swath sonar maps of the

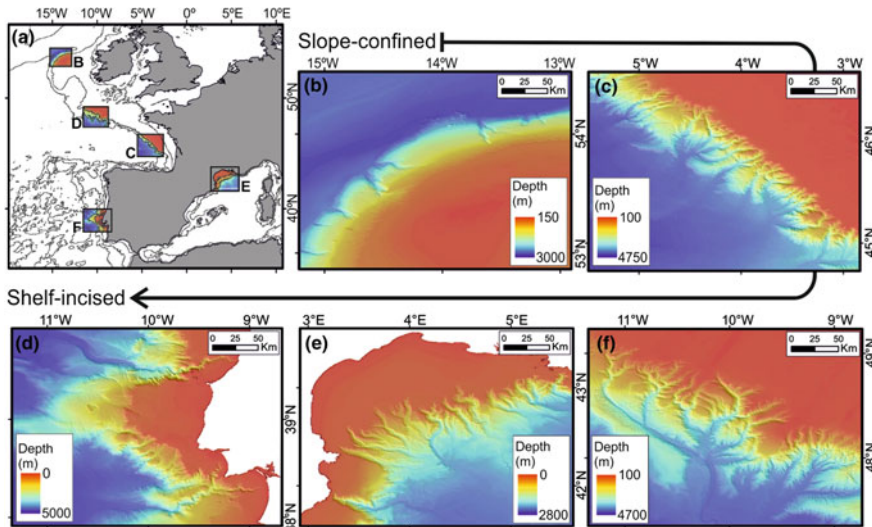


Fig. 4 Different types of submarine canyons, from slope-confined to shelf-incised. **a** Location map. **b** Irish margin (Porcupine Bank). **c** South-Armoricaine margin (Bay of Biscay). **d** Celtic margin (Whittard Canyon). **e** Gulf of Lion and North-Catalan margin. **f** Portuguese margin (Nazaré, Cascais and Setúbal/Lisbon canyons). Bathymetric data source: EMODnet Bathymetry

seafloor (Fig. 5)—have motivated numerous comparative studies (Shepard 1981; McGregor et al. 1982; Pratson and Ryan 1996; Mitchell 2005, 2006; Straub et al. 2007; Amblas et al. 2011, 2015). Central to these studies is the question of why such similar landforms should exist in subaerial and submarine environments when (1) few continental slopes have ever been exposed to subaerial processes and (2) the surface processes that shape landscapes and seascapes differ in some important ways. Clearly these differences are in many cases less important than the similarities in the formative processes.

On land, drainage patterns are associated with the action of rivers and mass flows. Similarly, it is generally assumed that submarine turbidity currents and mass flows generate the corresponding patterns on the seafloor (Shepard 1981; Parker 1982; Pratson and Coakley 1996; Imran et al. 1998). So it is unsurprising that process analogies have been drawn to explain geomorphic features on the seafloor. Many studies have explored this question and some brief examples are given in Sect. 2.4.2.

2.3 Global Distribution of Submarine Canyons

Global assessments of submarine canyons have been published by Harris and Whiteway (2011) and by Harris et al. (2014). Harris and Whiteway (2011) mapped 5849 large canyon thalwegs based on an analysis of the ETOPO-1 (1 nautical

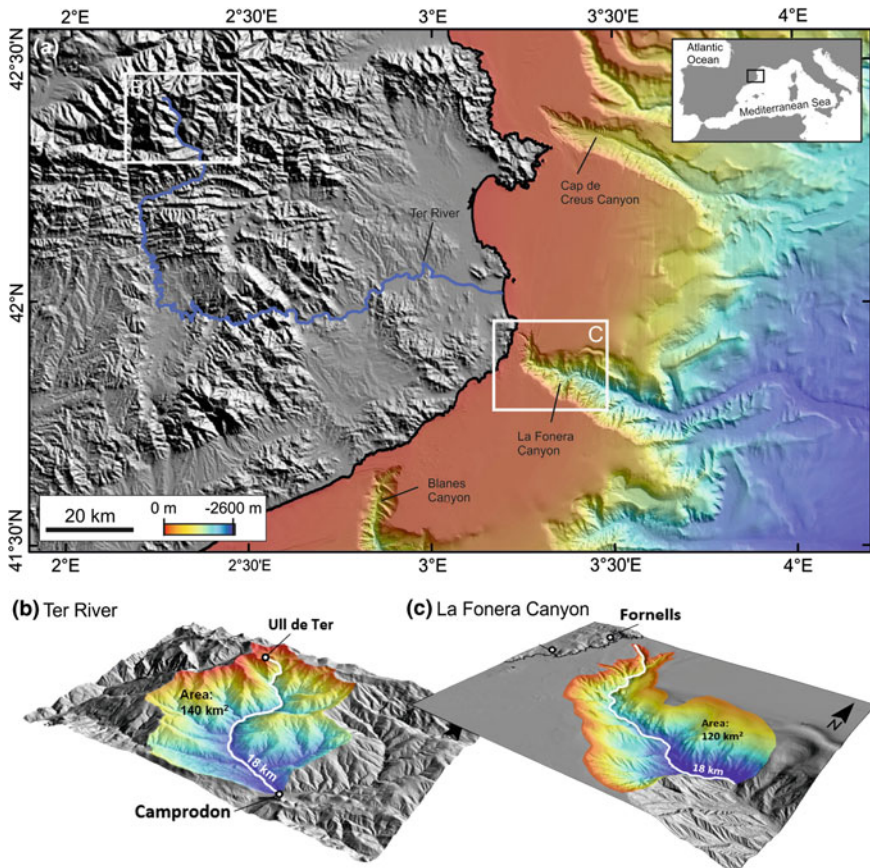


Fig. 5 a. Shaded relief image of the NW Mediterranean margin. The elevation data combine different multibeam bathymetry data sets from the University of Barcelona, the Spanish Institute of Oceanography, IFREMER, and global digital databases. Morphological comparison between the upper courses of b a river (Ter River, in the Pyrenees Mountain Range) and c a submarine canyon (La Fonera Canyon). The resolution of the DTMs is the same in both cases (15 m). Both drainage systems share similar morphologies that include a main sinuous valley surrounded by tributaries with steep flanks cut by well-developed gullies. Note that at 18 km downstream in both the subaerial and submarine valleys we observe the same height difference (1300 m) and comparable contributing drainage areas (140 km² in the river and 120 km² in the canyon)

mile = 1.852 km) bathymetric grid, in which “large” is defined as those canyons that extend over a depth range of at least 1000 m and are incised at least 100 m into the slope at some point along their thalweg. Harris et al. (2014) mapped 9477 “large” canyon polygons based on the interpretation of the Shuttle Radar Topography Mapping (SRTM30_PLUS) 30-arc second (~1 km) database (Becker et al. 2009). Both assessments compared and contrasted canyon geomorphic properties along active versus passive continental margins as well as between 8

major ocean regions (Fig. 6; Table 1), with the more recent (Harris et al. 2014) map providing estimations of canyon area and other related dimensional data.

Active continental margins contain over 50% more canyons than passive margins and the canyons are steeper, shorter, more dendritic, and are more closely spaced on active than on passive continental margins (Harris and Whiteway 2011). River-associated, shelf-incising canyons are more numerous on active continental margins ($n = 119$) than on passive margins ($n = 34$). They are most common on the western margins of South and North America, where they comprise 11.7% and 8.6% of canyons respectively, but are absent from the margins of Australia and Antarctica.

On average, shelf incising canyons are over twice the mean size of blind canyons (780 km^2 and 380 km^2 , respectively). They are also greater in mean length (54.8 and 37.3 km, respectively) and less incised (1395 and 2963 m, respective mean depths). Canyons comprise an average of 11.2% of the continental slope area, attaining maxima of 16.1% of the continental slope of the Arctic Ocean and 14.1% of the Southern Ocean (Antarctic) continental slope. In contrast, the slope of the South Atlantic Ocean has only 8.9% of its area incised by canyons (Harris et al. 2014).

Canyons in the Mediterranean and Black Seas have the shortest mean length, smallest depth of incision and smallest average area of the ocean regions, for both shelf incising and blind canyons. In contrast, shelf incising canyons in the Arctic Ocean have the greatest mean length, greatest depth of incision and greatest average area. For blind canyons, it is the Southern Ocean that has the greatest mean length, greatest depth of incision and greatest average area (Table 1). In general, polar

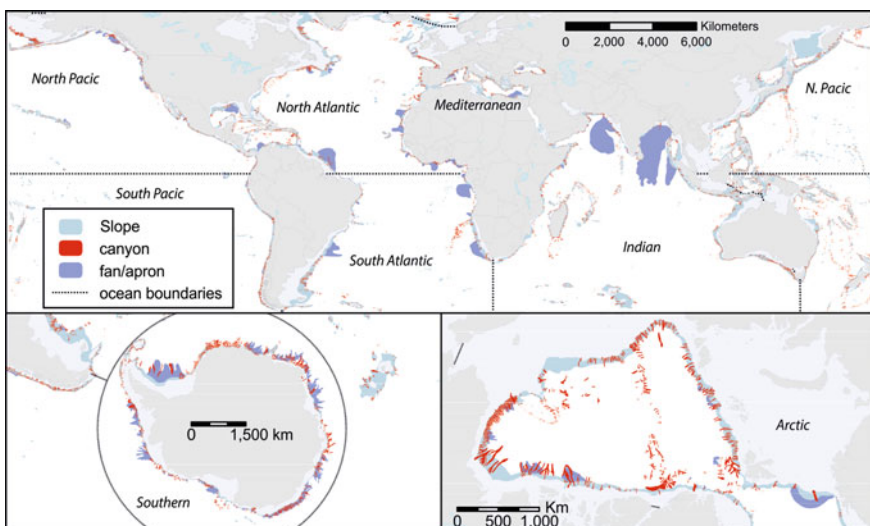


Fig. 6 Maps showing the location of large submarine canyons based on the analysis of the modified SRTM30_PLUS 30-arc second (~1 km) database as interpreted by Harris et al. (2014)

Table 1 Geomorphic statistics for “all canyons (AC)”, “shelf-incising canyons (SHI)” and “blind canyons (BC)”

Ocean	AC area (km ²)	AC no.	AC mean area (km ²)	AC mean length (km)	AC mean incision depth (m)	AC mean spacing (km)	SHI area (km ²)	
Arctic Ocean	359,650	404	890	58.9	2132	13.5	162,020	
Indian Ocean	760,420	1590	480	44.4	2399	11.9	222,690	
Mediterranean Black Sea	163,040	817	200	26.6	1601	6.2	94,430	
North Atlantic	738,430	1548	480	42.0	2433	10.0	292,330	
North Pacific	816,580	2085	390	38.8	2360	10.2	367,710	
South Atlantic	291,290	453	640	49.2	2441	14.6	65,320	
South Pacific	694,790	2009	350	35.7	2378	14.3	214,960	
Southern Ocean	569,440	571	1000	59.4	2300	8.2	194,410	
All Oceans	4,393,650	9477	460	41.1	2308	11.2	1,613,860	
Ocean	SHI No.	SHI average size (km ²)	SHI mean length (km)	SHI incision depth (m)	BC No.	BC average size (km ²)	BC mean length (km)	BC incision depth (m)
Arctic Ocean	75	2160	99.6	1619	329	600	49.7	2249
Indian Ocean	295	754	56.0	1401	1295	415	41.7	2627
Mediterranean Black Sea	307	307	33.1	1093	510	134	22.7	1907
North Atlantic	293	997	63.8	1565	1255	355	36.8	2636
North Pacific	489	751	56.9	1424	1596	281	33.2	2647
South Atlantic	73	894	66.0	1349	380	594	46.0	2650
South Pacific	368	584	46.6	1346	1641	292	33.2	2609
Southern Ocean	176	1104	63.7	1575	395	949	57.5	2623
All Oceans	2076	777	54.8	1395	7401	375	37.3	2563

Extreme values are in bold. (Source Harris et al. 2014)

submarine canyons are twice the size of those in non-polar regions. Canyons in the Arctic have an average size of 890 km² and in the Southern Ocean the average canyon size is 997 km², compared to the overall (global) average size of 463 km² (Table 1). The largest submarine canyon on Earth is the Bering-Bristol-Pribylov Canyon complex in Alaska (Normark and Carlson 2003), which covers an area of 33,340 km². Earth’s largest four canyons are all located on polar slopes that have been influenced by Quaternary glaciation.

2.4 Geomorphic Processes in Submarine Canyons

2.4.1 Sea Level and Regional Tectonic Forcing

Regional tectonics and global sea level fluctuations are the dominant alloogenetic controls on continental margin evolution. The stair-step shape of continental margins is primarily a result of the transition from continental to oceanic crust, with secondary effects produced by the loading of sediments along the margin. The relief and gradient of continental slopes depends largely on the accommodation space available for sediments to accumulate. On passive margins this is determined by the thermal subsidence that follows rifting and formation of an ocean basin, whereas on active margins it is determined by deformation associated with subduction (Hays and Pitman 1973; Pitman 1978). This difference translates into some notable contrasts in the distribution and morphology of canyons between passive and active margins (Pratson et al. 2007; Harris et al. 2014). Beyond that, the underlying geology and the presence of faults or other structures act as key controlling factors of canyon development (e.g. Laursen and Normark 2002; Chiang and Yu 2006; Noda et al. 2008; Micallef et al. 2014b).

Sea level changes also play an important role in submarine canyon evolution, as they modify the accommodation space along a margin, move the supply of terrigenous sediments towards or away from the shelf break, and force a back and forth translation of marine surface processes (Pratson et al. 2007). As recently as 20,000 years ago (the “Last Glacial Maximum”, or LGM), vast ice sheets covered much of North America and northern Eurasia, causing a ~120 m lowering of global sea level due to the reduction of water volume in the ocean basins (Imbrie and Imbrie 1979). As a result, shorelines migrated seaward, leaving much of the continental shelf exposed as a coastal plain and shortening the distance between the head of slope canyons and river mouths. This increased slope erosion rates and the delivery of terrigenous sediment to the deep ocean, most of which was funnelled through submarine canyons with a direct river connection (Forde 1981; Farre et al. 1983; Posamentier et al. 1991; Haq 1991; Lombo Tombo et al. 2015). In some cases, LGM ice-sheets crossed continental shelves to the shelf edge and actually encroached into parts of some shelf-incising canyons, partly infilling them with glacial debris that was eroded during subsequent ice retreat (Cameron et al. 2016).

The well-studied natural experiment from the recent past provided by ice-sheet driven global sea level change offers clues as to how sea level fluctuations of varying magnitude may have affected canyon growth and evolution in the more distant past. A special mention should be made here of the Mediterranean and Black seas, where a km-scale lowering of sea level (the ‘Messinian salinity crisis’) ca. 5.5 Ma ago exposed not only shelves but also much of the slope (Ryan et al. 1973), exposing some modern Mediterranean submarine canyons to subaerial erosion at that time (Ceramicola et al. 2015).

So, does the compelling evidence for increased canyon activity during periods of low sea level mean that canyons are relict features that are inactive when sea level is

high, as it is today? This was the general belief during most of the 20th century, but there is now strong evidence that many submarine canyons are still active today, as indicated by measurements of flows capable of transporting sediment and thus modifying canyon thalwegs (Canals et al. 2006; Chiang and Yu 2006; Ogston et al. 2008; Paull et al. 2010; Sanchez-Vidal et al. 2012; Puig et al. 2014; Amaro et al. 2016).

2.4.2 Sedimentary and Hydrodynamic Processes

As mentioned above, erosion by turbidity currents is thought to be the dominant canyon sculpting process (Sects. 1.2 and 2.2). Turbidity currents are mixtures of sediment and water that, because of their suspended sediment content, are denser than the surrounding water (Parsons et al. 2007). This excess density causes them to flow downslope as an undercurrent, where they can exchange sediment with the bed. Hence, if they move swiftly enough (favoured on steeper slopes and in laterally confined conduits) they can entrain more sediment than they deposit and cause net erosion of the seafloor (Pratsos et al. 2000; Piper and Normark 2009; Mohrig and Marr 2003). As they descend to lower slopes and/or lose their confinement, they tend to become depositional and eventually die out as the sediment driving their movement settles out.

There are several ways in which a turbidity current can form (Piper and Normark 2009), although the relative importance of each in any given setting can be difficult to recognise. Mass failures—either on the open slope, within a canyon or tributary, or along the front of a river delta in shallow water—can generate debris flows (which can also erode the seafloor) that may evolve via water entrainment and dilution into turbidity currents (Piper and Normark 2009). River discharge or subglacial meltwater with high concentrations of suspended sediment can flow hyperpycnally to the sea bed, generating turbidity currents directly at river mouths or marine-terminating glacier fronts (Mulder and Syvitski 1995). Storm waves can suspend sediments in bottom boundary layers that then flow downslope, gaining enough speed to keep sediment in suspension and thus transforming into turbidity currents (Friedrichs and Wright 2004; Puig et al. 2003).

Dense waters generated in shallow marine environments by changes in temperature and salinity may also evolve into gravity flows and drain through submarine canyons. Like turbidity currents, such dense water flows can transport sediment and mobilize and erode the seabed along submarine canyon axes (Canals et al. 2006; Lastras et al. 2007; Puig et al. 2008). Similarly, thermohaline ocean currents (or ‘contour’ currents) that flow in geostrophic balance parallel to isobaths at shelf to upper slope depths may be steered downslope through canyons and can also affect canyon evolution in some regions (Wåhlin 2002, 2004).

Numerical and experimental studies

Mathematical modelling has been used to address questions about the geomorphology of submarine canyons. Most models developed to study the flow of

turbidity currents and their interaction with the seabed are based on the same formalism used in models of open-channel river flow (Parsons et al. 2007). Of particular relevance to submarine canyons is the phenomenon of turbidity current initiation. Because turbidity currents are driven by the sediment suspended in the flow, if they begin to erode the seabed their density will increase, setting up a positive feedback by which a current of modest size can evolve into a powerful canyon-cutting flow (Bagnold 1962; Pantin 1979; Parker 1982; Fukushima et al. 1985). Also noteworthy are analyses aimed at understanding the spontaneous formation of submarine gullies and small channels beneath laterally extensive, unconfined flows. In particular, these studies have identified the scale of lateral spacing (a few hundred meters to a few km) at which gullying is expected (Izumi 2004). Assuming that many submarine canyons evolve from gullies (e.g., Farre et al. 1983; Pratson and Coakley 1996; Micallef et al. 2014a), this spacing will in turn control the eventual location of large canyon systems. Some researchers have adopted the approach of landscape evolution modellers in seeking simple ‘geomorphic transport laws’ applicable to slopes and canyons (Pratson and Coakley 1996; Mitchell 2006; Gerber et al. 2009). These relate surface sediment transport directly to surface morphology, allowing for a tractable representation of submarine landscape (or ‘seascape’) evolution on timescales of interest to submarine geomorphologists.

Researchers have also turned to reduced-scale physical experiments to better understand the formation of submarine canyons. Despite scaling limitations, reduced-scale experimental landscapes subjected to relative uplift and distributed fluid flow readily develop erosional topography with realistic drainage networks and channel patterns (see Paola et al. 2009 and references therein). Although different in some important respects, the resemblance of submarine canyons and their tributaries to upland drainage networks has motivated work on reduced-scale formation of submarine canyons. Lai et al. (2016) show that by isolating two key processes—the progressive growth of slope relief and a constant source of unconfined gravity flows—they are able to produce a canyon growth sequence and morphologies that appear similar to what is observed at field scale (Fig. 7). While their setup may be simple and resulting slopes purely erosional, their experiments have evidently captured some of the main formative processes driving canyon growth.

2.4.3 The Human Imprint

Their location within continental margins and their physiography make many submarine canyons prone to human direct impacts of different types, which include marine litter accumulation, transfer and deposition of chemical pollutants, and seafloor modification at large scale by bottom trawling. Canyons with their heads at a short distance from the shoreline are particularly sensitive to marine coastal processes, ultimately becoming efficient pathways for the transfer of the human signal to the deep (Canals et al. 2013). Amongst the main physiographic features of

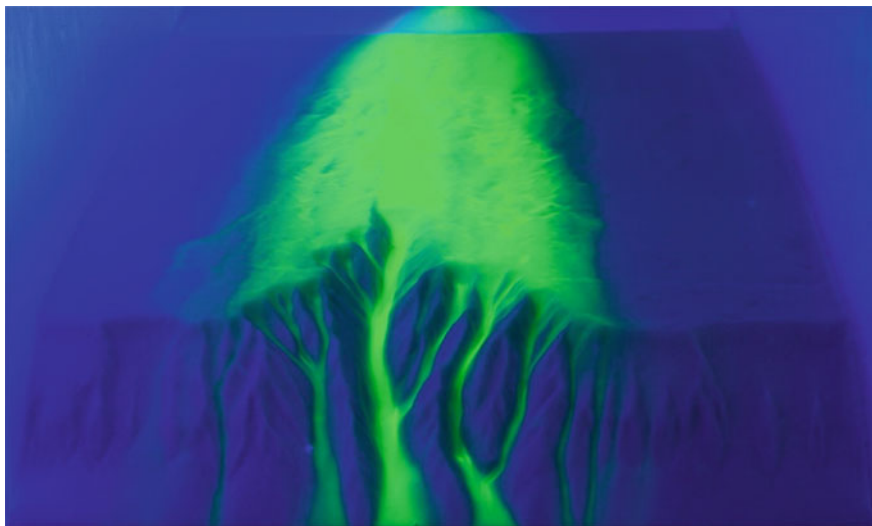


Fig. 7 Perspective view of submerged sandbox during the experiment summarised in Lai et al. (2016). The saline underflow (highlighted with *green* fluorescent dye) spreads as it flows down the featureless, sloping shelf. The flow is then funnelled through the evolving network of canyons on the steeper slope that was excavated by previous flows

the deep-sea floor, submarine canyons exhibit the highest litter density (densities in excess of 10,000 items km⁻²), well ahead of seamounts, banks and mounds, continental slopes, and ocean ridges (Pham et al. 2014; Tubau et al. 2015). Very high concentrations of small-sized plastics and settling fluxes of persistent organic pollutants (POPs) have also been found in deep submarine canyons (Salvadó et al. 2012; Woodall et al. 2014). This transfer role may be enhanced by the ability of canyons to trap off-shelf fluxes and channel them downslope.

The massive modification of the seascape by deep-water bottom trawling has a global dimension, with a strong incidence within submarine canyons. Persistent bottom trawling is able to sculpt and terrace canyon flanks otherwise dominated by contour-normal, branching gully systems. This has been documented by combining high-resolution multibeam data with a Vessel Monitoring System data over most practiced fishing grounds in submarine canyons of the northwestern Mediterranean Sea (Puig et al. 2012). The destruction of the canyon floor integrity comes with the generation of trawling-induced resuspension plumes and enhanced down-slope sediment transport (Martín et al. 2014a), causing severe erosion and impacts on the ecosystems of trawled canyon flanks (Martín et al. 2014b; Pusceddu et al. 2014). However, such a disturbed environment may benefit commercial species commonly occurring in submarine canyons, such as some deep-sea shrimps, thus leading to the contradictory situation of a sustainable productive fishery whereas the original habitat has been fully destroyed.

2.4.4 Marine Geohazards

Hazards related to submarine canyons are most often of concern on active margins where the shelf is narrow and the slope is steep. The Mediterranean provides several examples (e.g. Calabrian Ligurian, Sicilian and Algerian margins). As mentioned above, canyons usually develop retrogressively with the head migrating upslope via mass wasting. On some narrow shelves, canyon heads lie as close as a kilometre or less from the coastline. Recent studies on the Calabria Ionian margin of Italy show retrogressive canyon headwalls that are a few kilometres wide and as close as a few hundred meters from the coastline (Casalbore et al. 2012; Ceramicola et al. 2014).

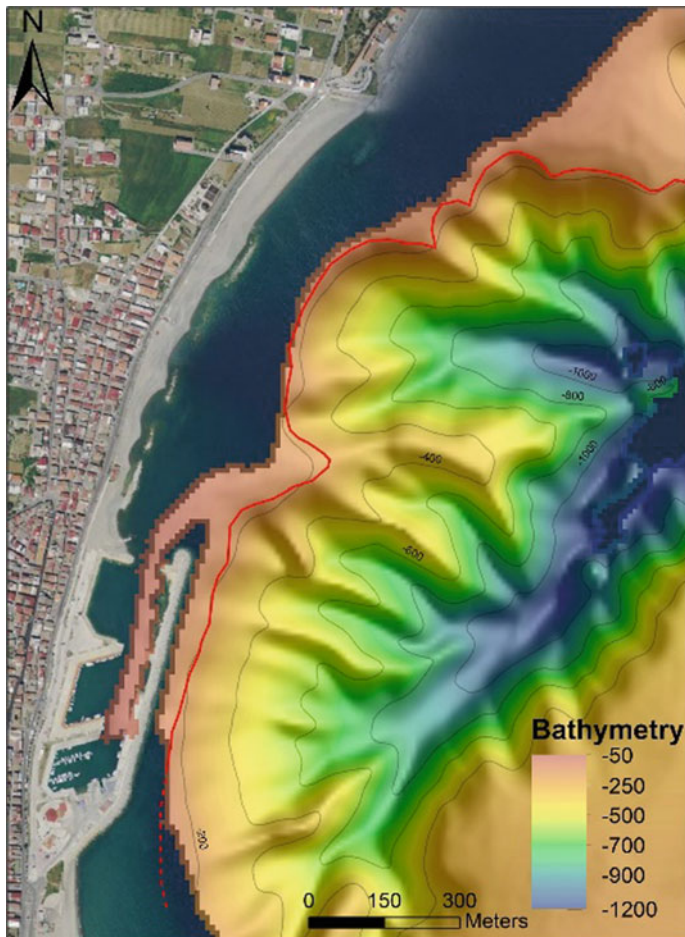


Fig. 8 Image of the Cirò marina harbour and offshore (Calabria, Italy) where Cirò submarine canyon head is present. The canyon headwall escarpment is located only a few tens of meters from the harbour pier

Their headward extension therefore represents a significant hazard for coastal areas and infrastructure (e.g. settlements, harbours, highways and railways). A well-known case is that of the Calabria harbour of Cirò Marina where the harbour pier was built on the headwalls of the upward retrogressive Cirò canyon (Fig. 8) and has consequently undergone episodic damage at its foundations (Ceramicola et al. 2014). In areas like these, regular monitoring of the position of canyon headwalls and the occurrence of major erosional events should be a priority.

Mass wasting at canyon heads and on submarine canyon walls has the potential to generate tsunamis. This is demonstrated by the events that occurred in Gioia Tauro harbour in 1977 (Zaniboni et al. 2010; Casalbore et al. 2014; Casas et al. 2016) and Nice airport in 1979 (Ioualalen et al. 2010; Migeon et al. 2011). Large scale mass wasting can also reach the deepest parts of canyons, sometimes at very high velocities (Piper et al. 1999), thus representing a potential hazard for pipelines and other offshore infrastructure (Carter et al. 2012). Moreover, canyon location has strong effects on tsunami wave build-up and run-up at the coastline (Iglesias et al. 2014).

3 Towards an Integrated Approach to Submarine Canyon Research

The extent of research activity focused on submarine canyons demonstrates their importance to our understanding of continental margins and deep-sea ecosystems across a range of temporal and spatial scales. Submarine canyons can be considered as main conduits for source-to-sink sedimentary processes, posing geohazard threats, forcing and focusing meso-scale oceanographic patterns, enhancing localised primary productivity and in many cases creating peculiar habitats for species of environmental and economic importance (Fernandez-Arcaya et al. 2016). For this reason the marine scientific community, supported by several governmental organisations and conservation agencies, has increasingly worked towards a more coordinated and integrated approach to canyon research (Huvenne and Davies 2014).

In addition to the wide range of individual canyon studies currently being undertaken, there is a strong need for comparative observations from different canyon systems, which will help to understand canyon functioning, mitigate potential geohazard threats and also to define environmental baselines for submarine canyons (which are actually missing), providing scientific support to the management of natural resources. However, information and data from submarine canyons are generally still scarce, and are widely spread across different geographical areas. A few noteworthy case studies have taken an integrated approach to the study of a single canyon system (Whittard Canyon, Amaro et al. 2016; Nazaré Canyon, Tyler et al. 2009) and should serve as examples for future work.

An integrated, holistic approach to the study of canyon systems will also require repeated observations of the seafloor topography and habitats, coupled with the contemporary acquisition of biological, chemical and physical oceanographic data. In line with this point, recent advances in marine technology are increasingly enabling the cost- and time-effective collection of integrated ‘4D’ data, including in complex terrains that were previously out of reach for conventional survey and sampling methodologies (along steep walls, under overhangs etc., Huvenne et al. 2011, 2016). AUV and ROV systems are increasingly available and are able to collect high resolution data from the seafloor (see Chapter “[ROVs and AUVs](#)”). Similarly, glider systems can now provide information on water column properties at temporal and spatial scales that are closer to the natural processes driving canyon dynamics than has ever been possible. By deploying these tools in repeated and coordinated surveys we can dramatically increase the observational basis that will drive the next generation of canyon research.

Acknowledgments This work was supported by the European Union’s Horizon 2020 research and innovation programme under the Marie Skłodowska-Curie grant agreement No 658358 (D. Amblas).

References

- Amaro T, Huvenne VAI, Allcock AL et al (2016) The Whittard Canyon—a case study of submarine canyon processes. *Prog Oceanogr* 146:38–57
- Amblas D, Gerber TP, Canals M et al (2011) Transient erosion in the Valencia Trough turbidite systems, NW Mediterranean Basin. *Geomorphology* 130:173–184
- Amblas D, Gerber TP, De Mol B et al (2012) Survival of a submarine canyon during long-term outbuilding of a continental margin. *Geology* 40(6):543–546
- Amblas D, Canals M, Gerber TP (2015) The long-term evolution of submarine canyons: insights from the NW Mediterranean. *CIESM Monogr* 47:171–181
- Bagnold RA (1962) Autosuspension of transported sediment: turbidity currents. *Proc R Soc Lond Ser A* 265:315–319
- Becker JJ, Sandwell DT, Smith WHF et al (2009) Global bathymetry and elevation data at 30 arc seconds resolution: SRTM30_PLUS. *Mar Geodesy* 32:355–371
- Bertoni C, Cartwright J (2005) 3D seismic analysis of slope-confined canyons from the Plio-Pleistocene of the ebro continental margin (Western Mediterranean). *Basin Res* 17:43–62
- Blum P, Okamura Y (1992) Pre-holocene sediment dispersal systems and effects of structural controls and holocene sea-level rise from acoustic facies analysis: SW Japan forearc. *Mar Geol* 108(3):295–322
- Brothers DS, ten Brink US, Andrews BD et al (2013) Geomorphic process fingerprints in submarine canyons. *Mar Geol* 337:53–66
- Bucher WH (1940a) Origin of the submarine valleys on the continental slopes of the North Atlantic. *Nature* 146(3699):407–408
- Bucher WH (1940b) Submarine valleys and the related geologic problems of the North Atlantic. *Geol Soc Am Bull* 51:489–512
- Cameron GDM, King EL, Todd BJ (2016) A large, glacially modified shelf-edge canyon, scotian shelf, Atlantic Canada. In: Dowdeswell JA, Canals M, Jakobsson M, Todd BJ, Dowdeswell EK, Hogan KA (eds) *Atlas of submarine glacial landforms: modern, quaternary and ancient*, vol 46. Geological Society, London, pp 403–404

- Canals M, Puig P, Heussner S et al (2006) Flushing submarine canyons. *Nature* 444:354–357
- Canals M, Company JB, Martin D et al (2013) Integrated study of Mediterranean deep canyons: novel results and future challenges. *Prog Oceanogr* 118:1–27
- Carter L, Milliman JD, Talling PJ et al (2012) Near-synchronous and delayed initiation of long run-out submarine sediment flows from a record-breaking river flood, offshore Taiwan. *Geophys Res Lett* 39:L12603
- Casalbore D, Bosman A, Chiocci FL (2012) Study of recent small-scale landslides in geologically active marine areas through repeated multibeam surveys: examples from the southern Italy. In: Yamada Y et al (eds) *Submarine mass movements and their consequences*, vol 31. Advances in natural and technological hazards research. Springer, Dordrecht, pp 573–582
- Casalbore D, Bosman A, Ridente D et al (2014) Coastal and submarine landslides in the tectonically-active Tyrrhenian Calabrian margin (Southern Italy): examples and geohazard implications. In: Krastel S et al (eds) *Submarine mass movements and their consequences*, vol 37. Advances in natural and technological hazards research. Springer, Heidelberg, pp 261–269
- Casas D, Chiocci F, Casalbore D, et al (2016) Magnitude-frequency distribution of submarine landslides in the Gioia Basin (southern Tyrrhenian Sea). *Geo-Marine Letters*, in press
- Ceramicola S, Praeg D, Coste M et al (2014) Submarine mass-movements in the Ionian Calabrian margin and their consequences for marine geohazards. In: Krastel S et al (eds) *Submarine mass movements and their consequences*, vol 37. Advances in natural and technological hazards research. Springer, Heidelberg, pp 295–306
- Ceramicola S, Amaro T, Amblas D et al (2015) Submarine canyon dynamics in the Mediterranean and Black seas, an integrated geological, oceanographic and ecosystems perspective. Briand F, Castaldi A (eds) CIESM workshop monograph, vol 47. Sorrento, pp 7–20
- Chiang CS, Yu H-S (2006) Morphotectonics and incision of the Kaoping submarine canyon, SW Taiwan orogenic wedge. *Geomorphology* 80:199–213
- Covault JA (2011) Submarine fans and canyon-channel systems: a review of processes, products, and models. *Nat Educ Knowl* 3(10):4
- Covault JA, Normark WR, Romans BW, Graham SA (2007) Highstand fans in the California borderland: the overlooked deep-water depositional system. *Geology* 35:783–786
- Daly RA (1936) Origin of submarine “canyons”. *Am J Sci* 31:401–420
- Dana JD (1863) Manual of geology, treating of the principles of the science with special reference to American geological history. Philadelphia, 798 pp
- Farre JA, McGregor BA, Ryan WBF et al (1983) Breaching the shelfbreak: passage from youthful to mature phase in submarine canyon evolution. *SEPM Spec Publ* 33:25–39
- Fernandez-Arcaya U, Ramirez-Llodra E, Aguzzi J et al (2016) Ecological role of submarine canyons and need for canyon conservation: a review. *Front Mar Sci* 4:5. doi: [10.3389/fmars.2017.00005](https://doi.org/10.3389/fmars.2017.00005)
- Forde EB (1981) Evolution of Veatch, Washington, and Norfolk submarine canyons— inferences from strata and morphology. *Mar Geol* 39:197–214
- Friedrichs CT, Wright LD (2004) Gravity-driven sediment transport on the continental shelf: implications for equilibrium profiles near river mouths. *Coast Eng* 51:795–811
- Fukushima Y, Parker G, Pantin HM (1985) Prediction of ignitive turbidity currents in Scripps submarine canyon. *Mar Geol* 67:55–81
- Gerber TP, Amblas D, Wolinsky MA et al (2009) A model for the long-profile shape of submarine canyons. *J Geophys Res Earth Surf* 114:f03002
- Greene HG, Maher N, Paull CK (2002) Physiography of the monterey bay national marine sanctuary and implications about continental margin development. *Mar Geol* 181:55–62
- Haq BU (1991) Sequence stratigraphy, sea-level change, and significance for the deep sea. *Spec Publ Int Assoc Sedimentol* 12:3–39
- Harris PT, Whiteway T (2011) Global distribution of large submarine canyons: geomorphic differences between active and passive continental margins. *Mar Geol* 285:69–86
- Harris PT, MacMillan-Lawler M, Rupp J et al (2014) Geomorphology of the oceans. *Mar Geol* 352:4–24
- Hays JD, Pitman WC III (1973) Lithospheric plate motion, sea level changes and climatic and ecological consequences. *Nature* 246:18–22

- Huang Z, Nichol SL, Harris PT et al (2014) Classification of submarine canyons of the Australian continental margin. *Mar Geol* 357:362–383
- Huvenne VAI, Davies JS (2014) Towards a new and integrated approach to sub-marine canyon research. *Deep-Sea Res II* 104:1–5
- Huvenne VAI, Tyler PA, Masson DG et al (2011) A picture on the wall: innovative mapping reveals cold-water coral refuge in submarine canyon. *PLoS ONE* 6:e28755
- Huvenne VAI, Georgioupolou A, Chaumillon L et al (2016) Novel method to map the morphology of submarine landslide headwall scarps using remotely operated vehicles. Springer International Publishing Switzerland 2016. In: Lamarche G et al (eds) Submarine mass movements and their consequences, vol 41. Advances in natural and technological hazards research. Springer, Heidelberg, pp 135–144
- Iglesias O, Lastras G, Souto C et al (2014) Effects of coastal submarine canyons on tsunami propagation and impact. *Mar Geol* 350:39–51
- Imbrie J, Imbrie KP (1979) Ice ages: solving the mystery. MacMillan, New York 224 pp
- Imran J, Parker G, Katapodes N (1998) A numerical model of channel inception on submarine fans. *J Geophys Res* 103:1219–1238
- Ioualalen M, Migeon S, Sardoux O (2010) Landslide tsunami vulnerability in the Ligurian Sea: case study of the 1979 October 16 Nice international airport submarine landslide and of identified geological mass failures. *Geophys J Int* 181:724–740
- Izumi N (2004) The formation of submarine gullies by turbidity currents. *J Geophys Res* 109: C03050
- Jobe ZR, Lowe DR, Uchytil S (2011) Two fundamentally different types of submarine canyons along the continental margin of Equatorial Guinea. *Mar Pet Geol* 28:843–860
- Kuenen PhH (1937) Experiments in connection with Daly's hypothesis on the formation of submarine canyons. *Leidse Geol Mededel* 8:327–335
- Lai SYJ, Gerber TP, Amblas D (2016) An experimental approach to submarine canyon evolution. *Geophys Res Lett* 43:1–7
- Lastras G, Canals M, Urgeles R et al (2007) A walk down the Cap de Creus canyon, NW Mediterranean Sea: recent processes inferred from morphology and sediment bedforms. *Mar Geol* 246:176–192
- Lastras G, Acosta J, Muñoz A et al (2011a) Submarine canyon formation and evolution in the Argentine Continental Margin between 44°30'S and 48°S. *Geomorphology* 128(3–4):116–136
- Lastras G, Canals M, Amblas D et al (2011b) Understanding sediment dynamics of two large submarine valleys from seafloor data: Blanes and La Fonera canyons, northwestern Mediterranean Sea. *Mar Geol* 280(1–4):20–39
- Laursen J, Normark WR (2002) Late quaternary evolution of the San Antonio submarine canyon in the central Chile forearc ($\sim 33^{\circ}$ S). *Mar Geol* 188(3–4):365–390
- Lo Iacono C, Sulli A, Agate M (2014) Submarine canyons of north-western Sicily (Southern Tyrrhenian Sea): variability in morphology, sedimentary processes and evolution on a tectonically active margin. *Deep-Sea Res II* 104:93–105
- Lombo Tombo S, Dennielou B, Berné S et al (2015) Sea-level control on turbidite activity in the Rhone canyon and the upper fan during the last glacial maximum and early deglacial. *Sed Geol* 323:148–166
- Martín J, Puig P, Palanques A, Ribó M (2014a) Trawling-induced daily sediment resuspension in the flank of a Mediterranean submarine canyon. *Deep Sea Research II* 104:174–183
- Martin J, Puig P, Masqué P et al (2014b) Impact of bottom trawling on deep-sea sediment properties along the flanks of a submarine canyon. *PLoS ONE* 9(8):e104536
- McGregor B, Stubblefield WL, Ryan WBF et al (1982) Wilmington submarine canyon: a marine fluvial-like system. *Geology* 10(1):27–30
- Micallef A, Ribó M, Canals M et al (2014a) Space-for-time substitution and the evolution of a submarine canyon-channel system in a passive progradational margin. *Geomorphology* 221:34–50
- Micallef A, Mountjoy J, Barnes PM et al (2014b) Geomorphic response of submarine canyons to tectonic activity: Insights from the Cook Strait canyon system. *N Z Geosphere* 10(5):905–929

- Migeon S, Cattaneo A, Hassoun V et al (2011) Morphology, distribution and origin of recent submarine landslides of the Ligurian margin (North-western Mediterranean): some insights into geohazard assessment. *Mar Geophys Res* 32:225–243
- Mitchell NC (2005) Interpreting long-profiles of canyons in the USA Atlantic continental slope. *Mar Geol* 214:75–99
- Mitchell NC (2006) Morphologies of knickpoints in submarine canyons. *GSA Bull* 118:589–605
- Mohrig D, Marr JG (2003) Constraining the efficiency of turbidity current generation from submarine debris flows and slides using laboratory experiments. *Mar Pet Geol* 20:883–899
- Mountjoy JJ, Barnes PM, Pettinga JR (2009) Morphostructure and evolution of submarine canyons across an active margin: Cook Strait sector of the Hikurangi margin. *N Z Mar Geol* 260(1–4):45–68
- Mulder T, Syvitski JPM (1995) Turbidity currents generated at river mouths during exceptional discharges to the world oceans. *J Geol* 103:285–299
- Neuendorf KKE, Mehl JP Jr, Jackson JA (2005) Glossary of geology. American Geological Institute, Alexandria, p 382
- Noda A, Tuzino T, Furukawa R et al (2008) Physiographical and sedimentological characteristics of submarine canyons developed upon an active forearc slope: the Kushiro submarine canyon, northern Japan. *Geol Soc Am Bull* 120(5/3):750–767
- Normark WR, Carlson PR (2003) Giant submarine canyons: is size any clue to their importance in the rock record? *Geol Soc Am Spec Pap* 370:175–190
- Ogston AS, Drexler TM, Puig P (2008) Sediment delivery, resuspension, and transport in two contrasting canyon environments in the southwest Gulf of Lions. *Cont Shelf Res* 28(15): 2000–2016
- Orange DL, Breen NA (1992) The effects of fluid escape on accretionary wedges 2. Seepage force, slope failure, headless submarine canyons, and vents. *J Geophys Res* 97:9277–9295
- Pantin HM (1979) Interaction between velocity and effective density in turbidity flow: phase-plane analysis, with criteria for auto-suspension. *Mar Geol* 31:59–99
- Paola C, Straub K, Mohrig D et al (2009) The “unreasonable effectiveness” of stratigraphic and geomorphic experiments. *Earth Sci Rev* 97(1–4):1–43
- Parker G (1982) Conditions for the ignition of catastrophically erosive turbidity currents. *Mar Geol* 46:307–327
- Parsons JD, Friedrichs CT, Traykovski PA et al (2007) The mechanics of marine sediment gravity flows. In: Nittrouer CA et al (eds) Continental margin sedimentation: from sediment transport to sequence stratigraphy. International Association of Sedimentologists Special Publication 37, Blackwell Publishing, Oxford, UK, pp 275–336
- Paull CK, Mitts P, Ussler W III et al (2005) Trail of sand in upper Monterey canyon: offshore California. *Bull Geol Soc Am* 117(9–10):1134–1145
- Paull CK, Ussler W III, Caress D et al (2010) Origins of large crescent-shaped bedforms within the axial channel of Monterey canyon. *Geosphere* 6:755–774
- Pham CK, Ramirez-Llodra E, Alt CHS et al (2014) Marine litter distribution and density in European Seas, from the shelves to deep basins. *PLoS ONE* 9(4):e95839
- Piper DJW, Normark WR (2009) Processes that initiate turbidity currents and their influence on turbidites: a marine geology perspective. *J Sediment Res* 79:347–362
- Piper DJW, Cochonat P, Morrison ML (1999) The sequence of events around the epicentre of the 1929 Grand Banks earthquake: initiation of debris flows and turbidity current inferred from sidescan sonar. *Sedimentology* 46:79–97
- Pitman WC III (1978) Relationship between eustacy and stratigraphic sequences of passive margins. *Geol Soc Am Bull* 89:389–1403
- Posamentier HW, Erskine RD, Mitchum RM (1991) Models for submarine fan deposition within a sequence stratigraphic frameworks. In: Weimer P, Link M (eds) *Seismic facies and sedimentary processes of submarine fans and turbidite systems*. Springer, pp 197–222
- Pratson LF, Coakley BJ (1996) A model for the headward erosion of submarine canyons induced by downslope-eroding sediment flows. *Geol Soc Am Bull* 108(2):225–234

- Pratson LF, Ryan WBF (1996) Automated drainage extraction for mapping the Monterey submarine drainage system, California margin. *Mar Geophys Res* 18:757–777
- Pratson LF, Ryan WBF, Mountain GS et al (1994) Submarine canyon initiation by downslope-eroding sediment flows; evidence in late cenozoic strata on the New Jersey continental slope. *Geol Soc Am Bull* 106(3):395–412
- Pratson LF, Imran J, Parker G et al (2000) Debris flows vs. turbidity currents: a modeling comparison of their dynamics and deposits. In: Bouma AH, Stone CG (eds) *Fine-grained Turbidite Systems*. American Association of Petroleum Geologists Memoir 72, vol 68. SEPM Spec Publ, pp 57–72
- Pratson LF, Nittrouer CA, Wiberg PL et al (2007) Seascape evolution on clastic continental shelves and slopes. In: C.A. Nittrouer JA et al (eds) *Continental margin sedimentation: from sediment transport to sequence stratigraphy*. International Association of Sedimentologists Special Publication 37. Blackwell Publishing, Oxford, UK, pp 339–380
- Puig P, Ogston AS, Mullenbach BL et al (2003) Shelf-to canyon sediment-transport processes on the Eel continental margin (northern California). *Mar Geol* 193(1–2):129–149
- Puig P, Palanques A, Orange DL et al (2008) Dense shelf water cascades and sedimentary furrow formation in the Cap de Creus Canyon, northwestern Mediterranean Sea. *Cont Shelf Res* 28:2017–2030
- Puig P, Canals M, Company JB et al (2012) Ploughing the deep sea floor. *Nature* 489:286–290
- Puig P, Palanques A, Martín J (2014) Contemporary sediment-transport processes in submarine canyons. *Annu Rev Mar Sci* 6:53–77
- Pusceddu A, Bianchelli S, Martín J et al (2014) Chronic and intensive bottom trawling impairs deep-sea biodiversity and ecosystem functioning. *Proc Natl Acad Sci* 111(24):8861–8866
- Ryan WBF, Hsue KJ, Cita MB et al (1973) Initial reports of the Deep Sea drilling project, covering Leg 13 of the cruises of the drilling vessel Glomar Challenger Lisbon, Portugal to Lisbon, Portugal, Aug–Oct 1970. Texas A & M University, Ocean Drilling Program, College Station, TX
- Salvadó JA, Grimalt JO, López JF et al (2012) Role of dense shelf water cascading in the transfer of organochlorine compounds to open marine waters. *Environ Sci Technol* 46:2624–2632
- Sanchez-Vidal A, Canals M, Calafat AM et al (2012) Impacts on the deep-sea ecosystem by a severe coastal storm. *PLoS ONE* 7(1):e30395
- Shepard FP (1932) Landslide modifications in submarine valleys. *EOS Trans Am Geophys Union* 13(1):226–230
- Shepard FP (1963) *Submarine Geology*. Harper & Row, New York 557 p
- Shepard FP (1981) Submarine canyons; multiple causes and long-time persistence. *Am Assoc Petrol Geol Bull* 65:1062–1077
- Spencer JW (1903) Submarine valleys off the American coasts and in the North Atlantic. *Geol Soc Am Bull* 14:207–226
- Straub KM, Mohrig D (2009) Constructional canyons built by sheet-like turbidity currents: observations from offshore Brunei Darussalem. *J Sediment Res* 79:24–39
- Straub KM, Jerolmack DJ, Mohrig D, Rothman DH (2007) Channel network scaling laws in submarine basins. *Geophys Res Lett* 34:L12613
- Tubau X, Canals M, Lastras G et al (2015) Marine litter on the floor of deep submarine canyons of the Northwestern Mediterranean Sea: the role of hydrodynamic processes. *Prog Oceanogr* 134:379–403
- Twichell DC, Roberts DG (1982) Morphology, distribution, and development of submarine canyons on the United States Atlantic continental slope between Hudson and Baltimore Canyons. *Geology* 10(8):408–412
- Tyler P, Amaro T, Arzola R et al (2009) Europe's Grand canyon: Nazare submarine canyon. *Oceanography* 22:48–57
- Veatch AC, Smith PA (1939) Atlantic submarine valleys of the United States and the Congo submarine valley. Geological Society of America special papers, vol 7. New York, 106 pp
- Wählin AK (2002) Topographic steering of dense currents with application to submarine canyons. *Deep Sea Res Part I* 49:305–320

- Wählin AK (2004) Downward channeling of dense water in topographic corrugations. Deep Sea Res Part I 51:577–590
- Wonham JP, Jayr S, Mougamba R et al (2000) 3D sedimentary evolution of a canyon fill (Lower Miocene-age) from the mandrove Formation, offshore Gabon. Mar Pet Geol 17:175–197
- Woodall LC, Sanchez-Vidal A, Canals M et al (2014) The deep sea is a major sink for microplastic debris. R Soc Open Sci 1:140317
- Zaniboni F, Armigliato A, Pagnoni G et al (2010) Continental margins as a source of tsunami hazard: The 1977 Gioia Tauro (Italy) landslide–tsunami investigated through numerical modeling. Mar Geol 357:210–217

Submarine Fans and Their Channels, Levees, and Lobes

Mark E. Deptuck and Zoltán Sylvester

Abstract Submarine fans are complex morphological features that develop on the continental slope, rise and abyssal plain, normally at the mouths of submarine canyons. They are constructed principally from the deposits of sediment gravity flows (mainly turbidity currents and debris flows) as terrigenous and shallow marine sediment is redistributed into deeper water. In this chapter we focus on the most important building blocks of submarine fans: leveed submarine channels and the submarine lobes they feed. Mass transport deposits are also important components of many submarine fans; they are described in the Chapter on “[Submarine Canyons and Gullies](#)”. Submarine channels are the most noticeable geomorphic features on submarine fans, linking net erosional elements like canyons and gullies to net depositional elements like submarine lobes. They develop through both erosional and depositional processes, and have straight to highly sinuous planform geometries. Where they are flanked by aggradational levees or are entrenched into the seabed, they provide stable pathways through which sediment is transported and partitioned into different fan settings. Coarse-grained sediment commonly accumulates on the floors or at the mouths of submarine channels; finer-grained sediment preferentially accumulates on channel banks and on adjacent aggradational levees. In this chapter we describe the wide range of morphological features recognised on the surfaces of submarine fans, and the physical processes that shape the seabed in areas where submarine channels, levees, and lobes develop.

M.E. Deptuck (✉)

Canada-Nova Scotia Offshore Petroleum Board, Halifax, Nova Scotia, Canada
e-mail: mdeptuck@cnsopb.ns.ca

Z. Sylvester

Chevron Energy Technology Company, Houston, TX, USA
e-mail: zoltan.sylvester@gmail.com

1 Introduction

Submarine fans form the largest sediment accumulations on Earth: they can be hundreds of kilometres long and several kilometres thick, especially where an ample supply of terrigenous material is available. Although the surface of these submarine fans may appear relatively smooth and featureless when compared to erosional landscapes, higher-resolution bathymetry and three-dimensional reflection seismic datasets increasingly reveal a complex array of erosional and depositional features, the most notable of which are submarine channels that have variably sinuous planform geometries and commonly resemble rivers on land (e.g. Damuth et al. 1983; Kenyon et al. 1995) (Fig. 1).

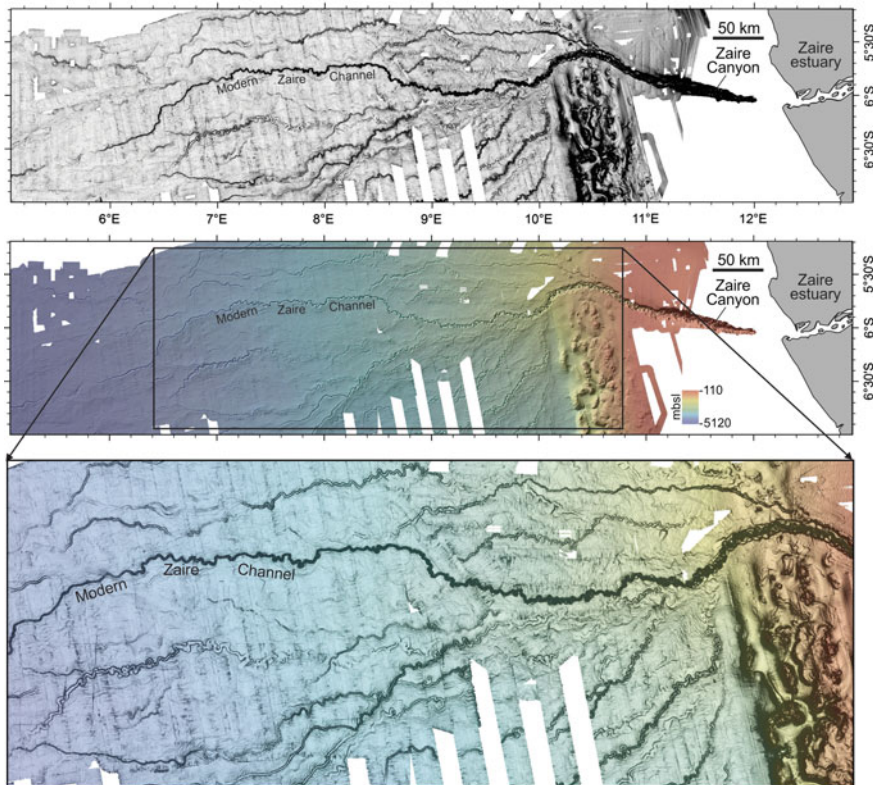


Fig. 1 Dip map (*top*), shaded relief bathymetry (*middle*) and close-up of dip map draped by bathymetry (*lower*) from multibeam echo sounder surveys seaward of the Zaire River, showing the complex pattern of sinuous submarine channels that bifurcate from the Zaire Canyon and ancestral Zaire Channel (images provided by Marie Picot and Nathalie Babonneau). For more details on the evolution of channel-levee systems and lobes in this well-studied system see Picot et al. (2016) and references therein

Although the best known and largest submarine fans like Amazon, Indus, Bengal, Mississippi, and Zaire develop seaward of Earth's largest rivers or their deltas (Wetzel 1993), submarine channels and fans also develop seaward of much smaller deltas supplied both by high-gradient bed-load dominated rivers that cross narrow continental shelves (like the Golo fans off eastern Corsica; Gervais et al. 2006; and the Hueneme Fan off southern California; Piper et al. 1999), and low-gradient suspension-load dominated rivers that cross wide continental shelves (like the Fuji-Einstein system offshore Alabama, eastern Gulf of Mexico; Sylvester et al. 2012; Fig. 2). Submarine fans may also develop in areas remote from direct fluvial-deltaic input, for example at the mouths of shelf-indenting canyons that intercept littoral drift cells (e.g. Covault et al. 2007; Boyd et al. 2008) or along glaciated margins where the advance and retreat of shelf-crossing glaciers, and associated meltwater events, transport large quantities of poorly sorted and unstable glacial material onto the outer continental shelf and slope (Piper et al. 1985, 2012; Klaucke et al. 1998). Submarine fans form on both active and passive margins, in relatively shallow (<500 m) to very deep water (>4000 m), at both high and low latitudes, in oceans and in lakes.

The diverse range of submarine fan settings is matched by their architectural variability and wide range of dimensions. For example, the Crati Fan in the tectonically active Ionian Sea is a small system supplied by a coarse-grained, high gradient river with a small catchment area. It is less than 20 km long and covers just $7.0 \times 10^1 \text{ km}^2$ (Ricci Lucchi 1985). At the other end of the spectrum, the Bengal

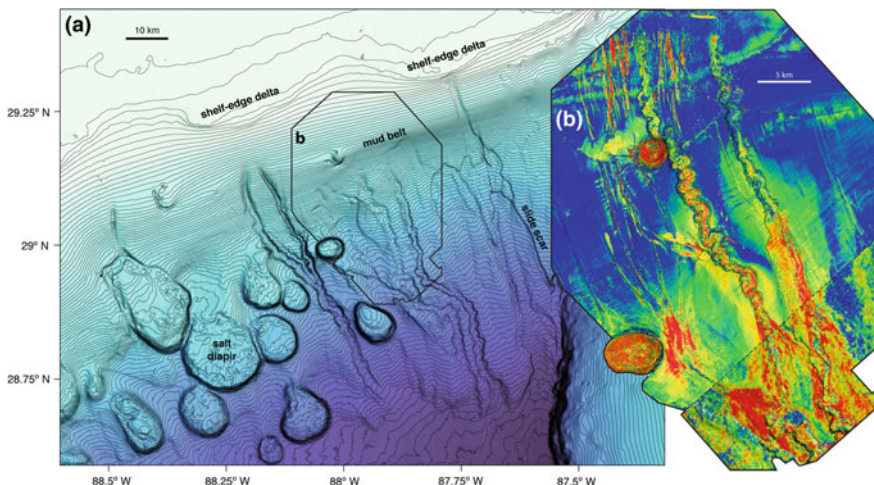


Fig. 2 Seafloor bathymetry in the eastern Gulf of Mexico, showing salt diapirs and largely inactive submarine channels affected by slide scars (contour interval is 20 m; bathymetry data from NOAA). Inset on the right shows the basal seismic surface of the Fuji-Einstein system, coloured by seismic amplitude (blue low amplitude, red high amplitude; modified from Sylvester et al. 2012). The two main channels start at the shelf edge and are directly linked to two delta lobes. Changes in slope gradient, salt diapirs, and faults affect these channels

Fan is a giant, long-lived system supplied by the Ganges-Brahmaputra rivers whose catchment areas encompass the southern Himalayas. It is more than 2900 km long and covers an astounding $2.8 \times 10^6 \text{ km}^2$ (Emmel and Curray 1985). Fan lengths in these end-member examples vary across three orders of magnitude; the area they cover varies across five orders of magnitude.

Despite the diversity of submarine fan settings and overall size, studies of individual turbidite systems show that most submarine fans are made up of a combination of submarine channels that progressively build up levees, and submarine lobe-like deposits that accumulate where sediment-gravity flows lose channel confinement. Submarine fans may contain one main channel-levee system (CLS) or a series of CLSs that develop in succession through avulsions. The main channel may be relatively straight and wide, flanked by highly asymmetric levees—as is the case for the Laurentian, Var, and Kramis fans along relatively steep margins (e.g., Piper et al. 1985; Savoye et al. 1993; Babonneau et al. 2012)—or it may be highly sinuous and narrow, flanked by relatively symmetric levees—as is the case for the Mississippi, Amazon, and Zaire fans (e.g., Damuth et al. 1983; Bouma et al. 1985a; Picot et al. 2016). These basic building blocks of submarine fans are commonly interlayered with deposits from large submarine landslides (slumps, slides, and debris flows—collectively referred to as mass transport deposits) and pelagic or hemipelagic drape, all of which can be variously modified by other marine processes like ocean currents.

While the overall size and bulk composition of submarine fans reflects the volume and composition of terrestrial material delivered to the canyon over longer time frames (Wetzel 1993; Reading and Richards 1994) and overall margin physiography (e.g. slope length and gradient; Sømme et al. 2009), submarine fan architecture and geomorphology also reflect the frequency and nature of triggering mechanisms for sediment gravity flows (Piper and Normark 2001), and processes active on the fan itself or within the substrate above which the fan sits. Seabed deformation associated with basement or thin-skinned tectonics (e.g. the development of normal faults and salt diapirs in Fig. 2), may produce a wide variety of structures that impact fan or channel development (see Steffens et al. 2003; Covault and Romans 2009; Clark and Cartwright 2009; Mayall et al. 2010). Indeed, the dynamically evolving surfaces of submarine fans produce some of the most fascinating and beautiful submarine landscapes on Earth.

2 Five Decades of Submarine Fan Research—Challenges and Progress

Over the past five decades, the most profound challenge faced by those who study submarine fans is the dearth of direct observations and measurements from sediment gravity flows in nature and hence limited direct constraints on the physical processes that shape (via erosion and deposition) the surfaces of submarine fans

(Talling et al. 2015). With rare exceptions—e.g. the timing of submarine cable breaks (Heezen and Ewing 1952), instrumentation placed in the path of sediment gravity flows (e.g. Normark and Dickson 1976), or sonar images of a turbidity current as it passes through a channel (Hay 1987)—early fan depositional models were largely based on the seafloor morphology of a limited number of fans (mostly off California), coupled with sparse shallow coring (e.g. Normark 1970, 1978) and early observations from outcrops (e.g. Mutti and Ricci Lucchi 1972; Walker 1978). Generic representative fan models produced in the 1970s distinguished three reaches: an *upper fan* consisting of a leveed ‘fan-valley’ that passes into a channelled convex-upward bulge located on the *middle fan*, where turbidity currents dissipated after leaving fan-valley confinement, and terminating in a *lower fan* consisting of flat-lying, unchannellised, unconfined sediment that grade into basin plain deposits (e.g. Normark 1978). The coarsest material in these models was linked to the floors of submarine channels and near their mouths, and finer-grained material was mainly found on levees adjacent to upper fan channels (interpreted as deposits from overbanked turbidity currents) and in distal lower fan settings.

Recognising that a single general fan model could not capture the increasingly wide array of observations from ancient and modern fans, a number of fan classification schemes emerged in the 20 years that followed, using criteria like the efficiency of sand transport to distal fan reaches (Mutti 1985), tectonic setting (Shanmugam and Moiola 1988), sea level position (Posamentier et al. 1991), or sediment calibre coupled with the number of feeder canyons (Reading and Richards 1994). Concerted efforts were also made to compile results from numerous modern and ancient fan systems through the 1980s (COMFAN I and COMFAN II meetings), resulting in the publication of two seminal volumes (Bouma et al. 1985b; Weimer and Link 1991) that summarised the state-of-the-art and highlighted the wide variability in turbidite systems that exist in nature. These compilations provided a clearer picture of the basic building blocks of submarine fans, with Mutti and Normark (1991) describing a common suite of architectural elements in both modern and ancient turbidite systems that are still used today. Key elements included channel and closely associated overbank deposits (levees), a number of smaller scale features like scours and bedforms near the mouths of submarine channels (referred to as the channel-lobe transition), lobes, and mass transport deposits.

Coring in the 1980s and 1990s, in particular long cores collected during DSDP Leg 96 and ODP Leg 155, provided hundreds of meters of direct calibration through different parts of the Mississippi and Amazon fans, respectively. These cores confirmed the finer-grained composition and sedimentology of thick levees (e.g. Hiscott et al. 1997; Piper and Deptuck 1997), the coarser-grained composition (up to gravel size) of submarine channel deposits (Bouma et al. 1985a; Manley et al. 1997) and high amplitude reflection packages or ‘HARPs’ found at the base of many CLSs (interpreted to form in response to levee avulsions and the temporary loss of flow confinement; e.g., Pirmez et al. 1997; Piper and Normark 2001), as well as the generally muddy composition of large mass transport deposits (Piper et al. 1997).

The proliferation and improved imaging of 3D seismic data, particularly since the early 2000s, heralded a new era in submarine fan research. The concept of *seismic geomorphology* evolved from such data-sets (e.g., Cartwright and Huuse 2005; Davies et al. 2007; Prather et al. 2012). Not only did 3D seismic data provide stunning images of the modern seabed, but it also enabled interpreters to map buried surfaces, providing insight into how the geomorphology of submarine fans or their components evolved through time. Large 3D seismic volumes have also been used to demonstrate the importance of the shape and evolution of the receiving basin (e.g. Prather et al. 1998; Pirmez et al. 2000; Steffens et al. 2003; Adeoba et al. 2005; Ferry et al. 2005; Gee and Gawthorpe 2006), demonstrating that local variations in gradient trigger changes in the erosional or depositional behaviour of sediment-gravity flows (e.g. Mulder and Alexander 2001), and hence geomorphology.

In parallel with the widespread acquisition of 3D seismic data-sets, improvements in modern deep-towed sidescan sonar (e.g., Babonneau et al. 2002), multi-beam data from autonomous underwater vehicles (AUVs) (e.g., Normark et al. 2009; Maier et al. 2013), and ultra-high resolution sub-bottom imaging tools capable of resolving m-scale beds (e.g. Piper et al. 1999; Deptuck et al. 2008; Maier et al. 2013), have provided some of the clearest images to date of modern fan systems (e.g., Figs. 1 and 3). These data-sets have enabled a new generation of targeted coring programs (e.g., Babonneau et al. 2004; Gervais et al. 2006; Pirmez et al. 2012; Jobe et al. 2015, 2016) and together should continue to narrow the resolution gap between modern turbidite systems and a new generation of detailed outcrop studies (e.g., Nilsen et al. 2007; Schwarz and Arnott 2007; Prelat et al. 2009; Hubbard et al. 2008) and flume tank experiments (e.g., Straub et al. 2008; Parsons et al. 2010; Fernandez et al. 2014).

3 Processes

Sediment that is ultimately delivered to a submarine fan via sediment-gravity flows may be stored temporarily near the shelf edge or along canyon margins, awaiting an array of potential triggering mechanisms. The triggering mechanism is important because it influences the volume, composition, and duration of individual flows, and may be modulated by sea level variations (Piper and Normark 2001). Once initiated, flow behaviour ultimately controls how coarse- and fine-grained material is partitioned into different fan settings, and is strongly influenced by the overall gradient (Normark and Piper 1991) and seabed morphology (Mulder and Alexander 2001), including the degree of channel-confinement. Sediment-gravity flows may be triggered by earthquakes, large storms or rip currents, or simply by sedimentation once a threshold in slope stability is exceeded (Normark and Piper 1991). Alternatively, rivers in flood may deliver sediment directly into canyon heads via hyperpycnal flows (Mulder and Syvitski 1995), a mechanism that may be most important during periods of low sea level or in systems with canyons that extend

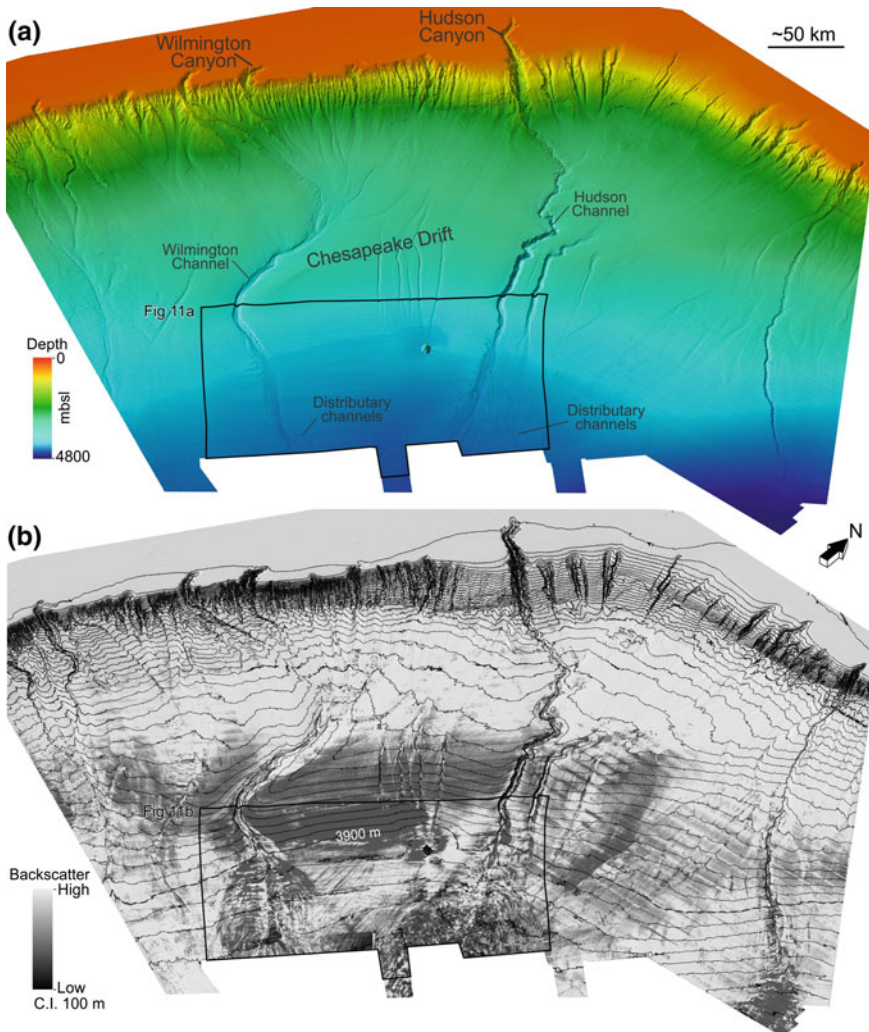


Fig. 3 Perspective view from the southeast showing **a** shaded-relief bathymetry and **b** backscatter (draped above bathymetry) from the continental shelf, slope, and rise off the northeastern United States (offshore Delaware, New Jersey, and New York). Heavily canyoned slope passes seaward into the Wilmington and Hudson submarine fans. Variations in the continental rise morphology, associated with a contourite drift, produced variations in the degree of channel entrenchment or diversion. An abrupt loss of channel-confinement near the 3900 m isobath coincides with a 0.5° decrease in gradient and a change to low-relief ephemeral submarine channels and scoured lobe deposits. Multibeam bathymetry data extracted from the National Geophysical Data Center (www.ngdc.noaa.gov/mgg/bathymetry). Data from the continental rise also available from the University of New Hampshire, Joint Hydrographic Center—Center for Coastal and Ocean Mapping (Gardner 2004). Data gridded at 100 m and illuminated from the southwest. See also Sweeney et al. (2012) and Brothers et al. (2013)

across the shelf, providing a longer-term connection between the canyon head and river mouth. However, the large fluvial suspended sediment concentrations necessary for hyperpycnal flows to exceed the density of the saline seawater may make these events uncommon in larger low-gradient rivers (Mulder and Syvitski 1995).

The idea that sand-size or coarser sediment can be transported in the deep sea over long distances by turbidity currents is only a few decades old (Kuenen and Migliorini 1950), but it is widely accepted today that submarine channels are carved, built, and maintained by these underwater density flows. The driving force that keeps turbidity currents in motion over large distances is the density difference between the sediment-water mixture and the surrounding seawater. Sediment in the current is kept in suspension mostly through turbulence, although it is likely that other processes play a role as well in their lowermost, high-concentration layer (e.g., Talling et al. 2015). Turbidity currents are highly stratified, with sediment concentration rapidly decreasing from a maximum value close to the bottom; the grain size of suspended sediment also decreases upward, so that sand or coarser sediment is commonly restricted to the lowermost part of the submarine channel. This produces predominantly fine-grained (mud- and silt-rich) levee deposits with coarser sediment restricted to the lower few tens of metres of the channel (Hiscott et al. 1997).

Another characteristic feature of turbidity currents is their velocity profile. In contrast with rivers, where the velocity maximum is very close to the water surface, the largest velocity in turbidity currents is somewhere between the upper and lower boundaries of the flow, often closer to the bottom (e.g., Peakall and Sumner 2015). The nature of the velocity profile has implications for the structure of secondary flow and resulting development of sinuosity in submarine channels. Some experimental and modelling work suggests that the direction of secondary flow is river-like (e.g., Imran et al. 2007; Abad et al. 2011). However, other experiments and field data indicate that the flow pattern in the lower part of the flow is reversed relative to that in rivers (e.g., Corney et al. 2008; Parsons et al. 2010). Regardless of the exact nature of the secondary flow and the role it plays in sediment distribution within channels, both geomorphologic and seismic stratigraphic observations suggest that the majority of submarine channels develop higher sinuosities through preferential preservation of deposits on the inner bank and long-term erosion on the outer bank (e.g., Deptuck et al. 2003; Sylvester et al. 2011; Maier et al. 2012; Kolla et al. 2012), much like in rivers.

In addition to turbidity currents, sediment gravity flows with higher sediment concentrations, such as slides, slumps, and debris flows, also play a role in the evolution of submarine channels. Large-scale sliding and slumping can cover or remobilise significant portions of a submarine fan (Piper et al. 1997). Smaller-scale slides are often present along channel margins and likely contribute to meander-bend erosion. In addition, larger-scale and more mobile debris flows can travel tens of kilometres downslope along the channel axis and can partially or entirely fill the channel with mass wasted material, in some cases with large blocks that were eroded upstream.

4 Morphology of Submarine Channels and Their Levees

Submarine channels may be stable and long-lived where they are entrenched into the seabed or flanked by aggradational wedge-shaped levees, or ephemeral where both levee heights and entrenchment depths are low. Their dimensions and architecture vary widely; in general, small fans are composed of smaller CLSs than larger fans (see also Skene 1998; Deptuck et al. 2003). The dimensions of CLSs probably scale with some combination of its lifespan and the volume, composition, and recurrence intervals of sediment gravity flows. In general, levees decrease in size and relief further away from their source as does the amount of erosion, if any, along its base (e.g., Fig. 4). However, enhanced erosion or sedimentation (particularly at the base of CLSs) may take place locally anywhere along the path of a CLS in response to changes in seabed morphology produced by underlying tectonic structures or pre-existing sedimentary bodies like levees, lobes, or contourite drifts.

Most large, long-lived river-fed submarine fans (e.g., Amazon, Indus, Bengal, Zaire, and Mississippi) develop down-slope from a well-established canyon and are composed of a number of stacked submarine channels flanked by wedge-shape levees (Fig. 4). Successive CLSs originate through large-scale avulsions, as illustrated in Fig. 5. The location and frequency of avulsions varies within and between different fan systems (Kolla 2007); the surface expression of the Zaire Fan in Fig. 1 records fifty-two channel-levee-lobe systems, each developing in response to an avulsion that took place anywhere between the canyon mouth and the distal reaches of the fan (Picot et al. 2016). On the Indus Fan, some of the largest CLSs on Earth experience major avulsions near the canyon mouth, with successive CLSs heavily cannibalising previous ones near the avulsion node. Preservation increases down system where individual CLSs are offset from each other by their thick wedge-shaped levees (Fig. 5). A closer view of the morphology of an upper fan avulsion on Amazon Fan is shown in Fig. 6a. The abandoned segments of CLSs down-slope from avulsion nodes remain largely inactive as sediment delivery is re-routed to other parts of the fan. As such, proximal avulsions have a greater impact on overall sediment routing than distal ones. Abandoned CLSs, however, may be resuscitated if they are intercepted and re-occupied by younger submarine channels, complicating fan geomorphology (e.g. Jégou et al. 2008; Jobe et al. 2015).

One of the most striking characteristics of many submarine channels is their pronounced sinuosity (Wynn et al. 2007). Braiding in submarine channels in contrast appears to be rare (Foreman et al. 2015). The discovery of highly sinuous channels on the surface of the Amazon Fan (Damuth et al. 1983) was a surprise and an important moment in the history of submarine geomorphology. Later bathymetric surveys and more recent three-dimensional seismic datasets across many submarine fans have shown that sinuous submarine channels are the norm, not the exception. While the sinuous planform patterns are quite similar to fluvial systems, aggradation rates in submarine CLSs can be more than an order of magnitude larger than those observed in rivers (Peakall et al. 2000; Jobe et al. 2016).

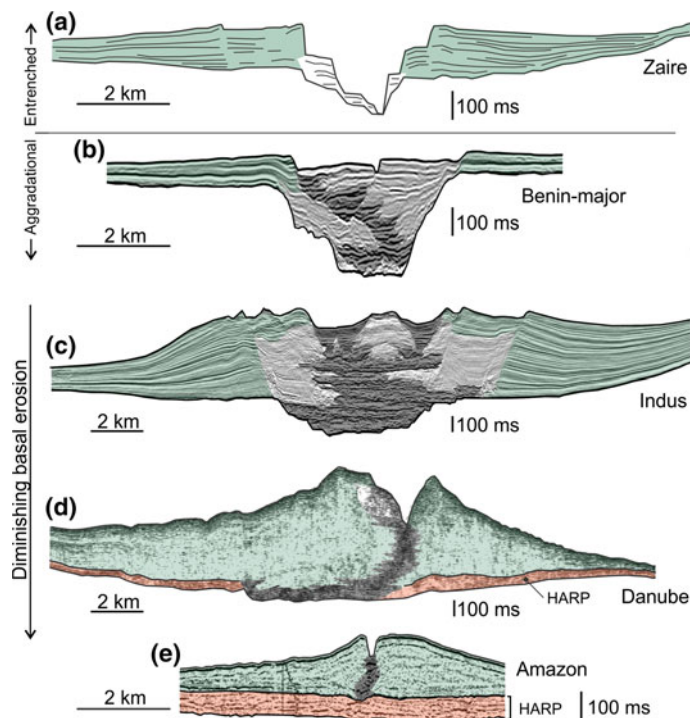


Fig. 4 Architectural variations in long-lived channel-levee systems (CLS). **a** Zaire Channel (redrawn from Babonneau et al. 2002); **b** Benin-major CLS, western Niger Delta slope (see Deptuck et al. 2012); **c** Indus Fan CLS C (modified from Deptuck 2003); **d** Danube CLS, Black Sea (Reprinted from Marine Geology, 179, Popescu et al., Late Quaternary channel avulsions on the Danube deep-sea fan, Black Sea, 2001, with permission from Elsevier); **e** Amazon Channel (Amazon Fan; Reprinted from Pirmez et al. 2000, with permission from GCSSEPM Foundation). In **a** and **b** inner levees (light grey) are well-developed and are at least in part contemporaneous with outer levee deposits (green). Channel deposits shown in dark grey, and avulsion-related lobe deposits (HARPs—‘high amplitude reflection packages’) are shown in orange. Diminished erosion near the base of the highly aggradational CLSs in **b** to **e** strongly influence their overall architecture

Individual submarine channels may be perched above the surrounding seafloor, flanked directly by the crests of relatively simple wedge-shaped levees (e.g. Figs. 4d, e and 6) or they may be flanked by much more complex deposits that form multi-tiered bench-like terraces adjacent to the active channel floor (e.g. Figs. 4a–c and 7). Measuring the width and depth of submarine channels is not as straightforward as in rivers, especially if multiple terraces are present. In general, however, submarine channels are wider, deeper, and steeper than their subaerial counterparts—their widths range from ~100 m to more than 10 km, their depths from a few meters to ~200 m, and their slopes cover the range from 0.0001 to 0.01 (Konsoer et al. 2013). Gradients along submarine channels can be up to two orders of

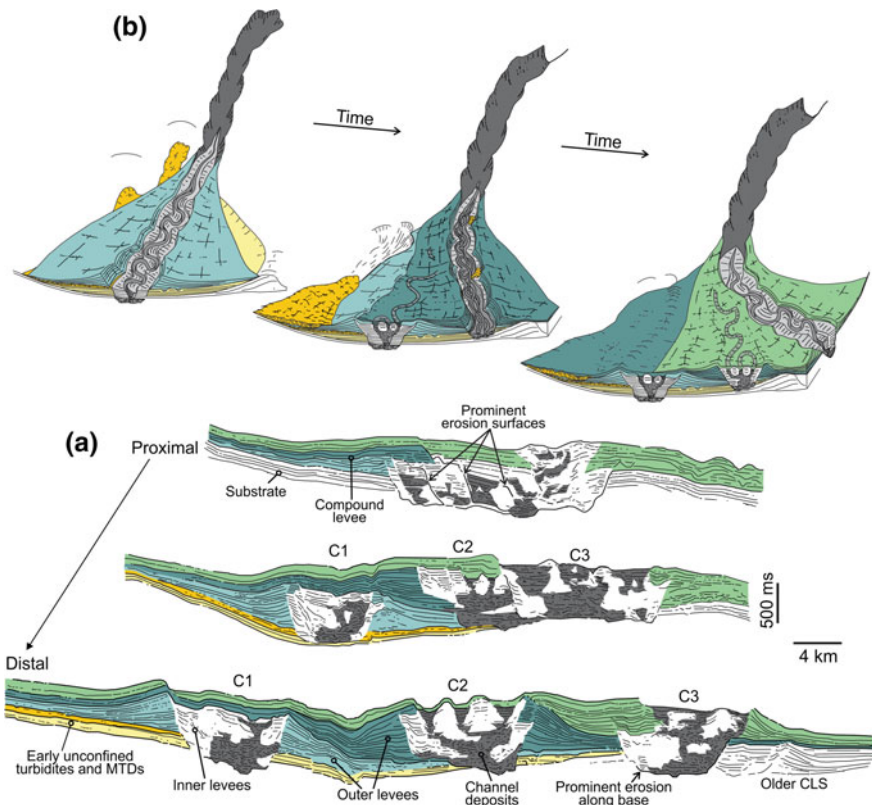


Fig. 5 **a** Three transects across part of the Indus fan—one of the largest submarine fans in the world—showing changes in fan architecture with increasing distance from the canyon-mouth. Highly self-cannibalized channel-levee systems (CLSs) with prominent erosive surfaces near the canyon-mouth pass down-system into well-preserved compensatorially stacked CLSs, each bordered by prominent wedge-shaped outer levees with erosion limited to the base of each system. **b** Schematic illustrations showing a succession of upper fan avulsions on the Indus fan and resulting fan architecture. From Deptuck (2003)

magnitude steeper than rivers of similar size. The size of the channel bends scales with the overall channel size, according to a scaling relationship that is close to the one observed in the case of rivers (Clark et al. 1992). However, for the same meander wavelength, submarine channels seem to be wider than rivers (Pirmez and Imran 2003).

These differences in size and slope are due to the fact that the driving force per unit volume is smaller in the case of turbidity currents than in rivers, a consequence of the much smaller density difference between the low-concentration sediment suspension and ambient seawater. In addition, the majority of submarine channels, certainly the ones on large submarine fans, are fundamentally different from rivers in two aspects: (1) they commonly do not have tributaries and instead originate

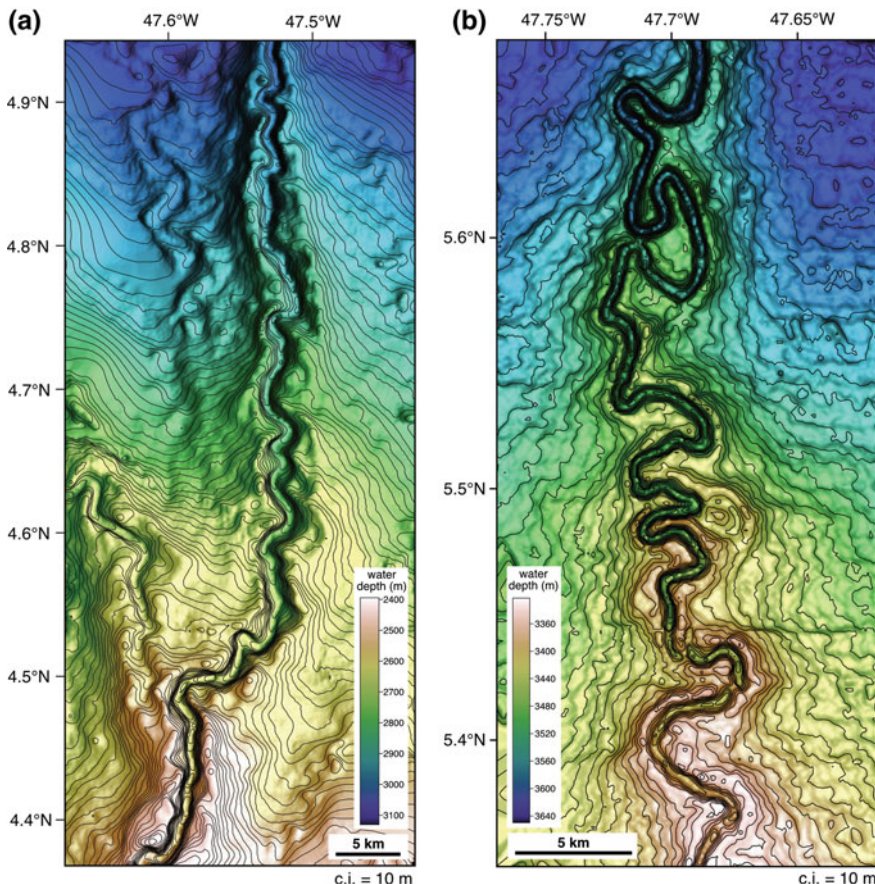


Fig. 6 Sinuous submarine channels on the Amazon Fan. **a** Avulsion on the upper fan, **b** Higher sinuosity and recent and incipient cutoffs on the middle fan. Bathymetry data from NOAA

from a single source, usually a canyon; and (2) their size systematically decreases downstream. There are notable exceptions—some of the largest submarine channels, like the North Atlantic Mid-Ocean Channel (NAMOC; Klaucke et al. 1998), are fed by a number of tributaries, and some canyons (or channels extending from them) may intersect and re-occupy pre-existing channels, producing tributary-like channel patterns (e.g. landward parts of the Wilmington fan in Fig. 3a).

The decrease in width, depth, and channel cross-sectional area is the result of decreasing discharge towards the distal parts of fan systems as some of the sediment in the flow is deposited on the channel floor and levees (Pirmez and Imran 2003; Spinewine et al. 2011). The width and height of levees also decline in a downdip direction (Skene et al. 2002), allowing increasingly deeper parts of the turbidity current to spill and deposit sediment over the levees. This produces generally coarser-grained levees in the distal parts of CLSs (Hiscott et al. 1997).

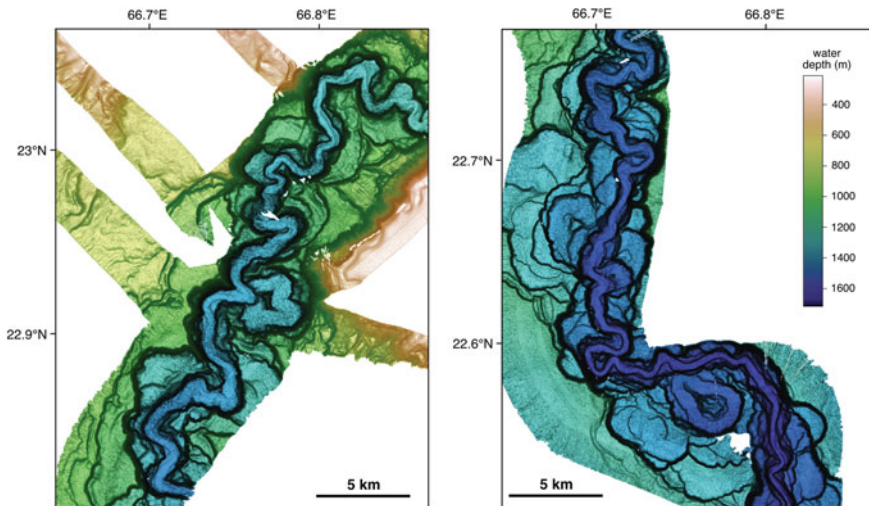


Fig. 7 Morphology of large channel-levee systems: the canyon-channel transition zone on the upper part of the Indus Fan, with terraces and cutoffs. Data from Clift and Henstock (2015)

Finer-Scale Geomorphic Features In addition to avulsions and their common sinuous planform geometries, the improved quality of seabed and shallow sub-surface imaging tools reveals a number of other geomorphic features in leveed submarine channels like sediment waves (e.g. Normark et al. 2002), thalweg deposits like plugs (Deptuck et al. 2007), bars (Nakajima et al. 2009), and coarse-grained bedforms (Wynn et al. 2002b), and erosional features like scours, knickpoints and erosional terraces (Clark and Pickering 1996; Heiniö and Davies 2007; Micallef et al. 2014; Sylvester and Covault 2016), as well as a range of near-channel or channel-margin features including lateral accretion packages and inner levees (e.g., Abreu et al. 2003; Deptuck et al. 2003; Babonneau et al. 2004). These features provide clues about the finer-scale controls on channel-levee geomorphology.

Although the aggradation rates in CLSs are generally higher than in rivers, in some cases aggradation is preceded by a period of vertical incision that exerts a long-lasting influence on younger aggrading channels (e.g. Figs. 4b, c, 7, 8). Overbank deposits adjacent to these early aggradational channels are commonly confined within the initial incision and have been referred to as ‘inner levees’, to distinguish them from ‘outer levees’ that form outside of the erosional surface (Deptuck et al. 2003). Long-lived sinuous channel systems that aggrade within the initial incision commonly have complex morphologies and stratigraphic architectures, characterised by scalloped valley margins, draped terraces, and a complicated network of time-transgressive erosional surfaces (Sylvester et al. 2011). Fine-grained overbank deposits are commonly unable to erase earlier erosional products like cut-off loops, scalloped canyon margins, or different generations of inner levees, and as a result some aspects of the seabed geomorphology in channel

systems reflect the draped expression of older submarine landforms that are no longer active (e.g. Figs. 7 and 8). As such, it is important to consider *geomorphic inheritance* when deducing modern processes from seabed images.

Similar to many meandering rivers, the banks immediately adjacent to submarine channels are commonly asymmetric (e.g. Babonneau et al. 2002; Reimchen et al. 2016), with the steepest and highest bank coinciding with the cut-bank where erosion is focused (see Fig. 8c). The asymmetry in levee height also reflects increased overspill due to the inertia of flows as they adjust to sharp changes in channel orientation (Piper and Normark 1983). Asymmetry in some large CLSs has also been linked to the Coriolis effect where thick muddy flows are diverted to the

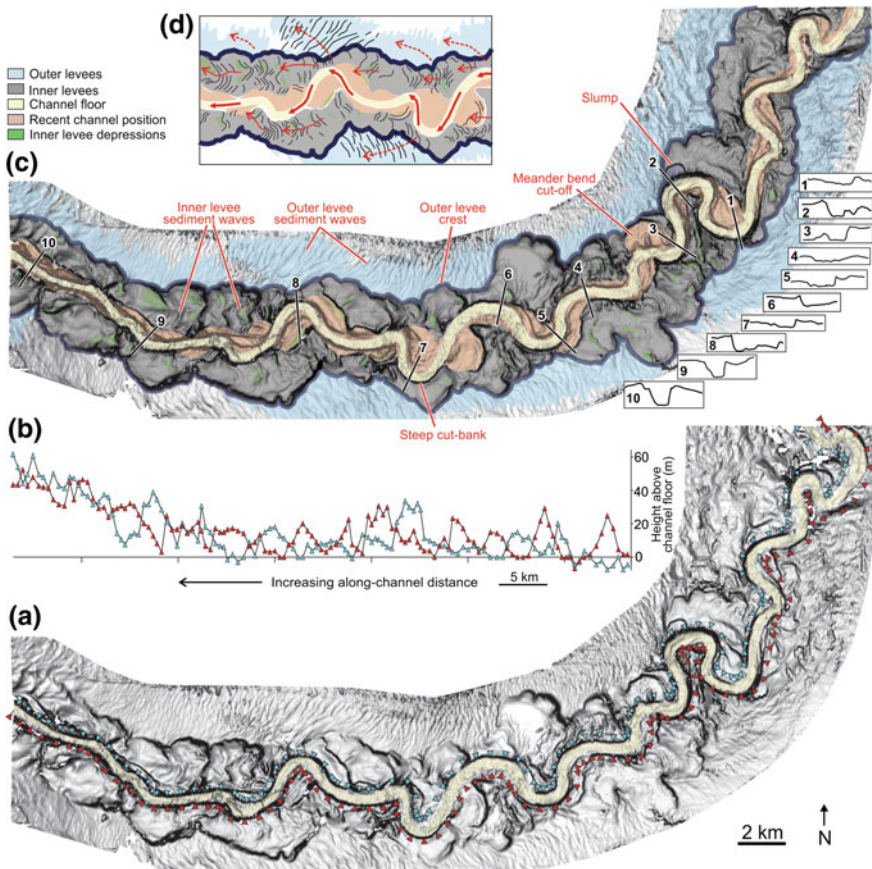


Fig. 8 **a** Dip map of the Benin Channel, western Niger Delta slope. Flow direction is to the *left*. **b** the left- and right-hand channel banks are highly asymmetric, showing the greatest elevation adjacent to cut-banks (see also Deptuck et al. 2007). **c** Dip map colour coded according to different submarine channel-levee settings, with representative channel cross sections. **d** Flow vectors inferred from the thalweg and the crests of both inner and outer levee sediment waves

right (facing down the channel) in the northern hemisphere (Klaucke et al. 1998; Popescu et al. 2001). Overbank deposits in some systems form distinct up-flow migrating sediment waves (Normark et al. 2002). These are most commonly reported in outer levee settings, particularly outboard sharp meander bends, but have also been recognized in inner levee settings (e.g. Deptuck et al. 2012). In some cases, rather than forming net depositional features, flows that overspill levee crests at sharp meander bends can be erosive, producing regularly spaced scours called cyclic steps that may be precursors to new submarine channels (Fildani et al. 2006).

The crests of sediment waves in Fig. 8 provide insight into variations in flow trajectory at different elevations above the channel thalweg (Fig. 8d) (see also Kane and Hodgson 2011). The deepest and coarsest material follows the most sinuous path along the channel floor. Finer-grained material carried higher up in the flow has contributed to inner levee sediment waves with crests generally normal to the overall channel-belt trend, but only loosely tied to the more sinuous channel thalweg. The more elevated parts of flows were guided by the confining crests of outer levees, but the relatively uniform, normal to oblique orientation of sediment wave crests on outer levees suggests that sediment carried at the highest elevation above the channel floor escaped confinement and travel obliquely away from the overall trend of the CLS.

Channel Initiation, Migration and Planform Adjustments In existing submarine channels, stratified sediment-gravity flows will contribute finer-grained material to the levees if the through-put flow is thicker than the channel banks, sustaining or increasing flow confinement unless the channel floor aggrades correspondingly. But how are submarine channels initiated in the first place? A number of studies have documented trains of up-stream migrating scours or bedforms, referred to as cyclic steps, which appear to be pre-cursors to at least some submarine channels (Fildani et al. 2006, 2013; Heiniö and Davies 2009; Kostic 2011). Cyclic steps range from net-erosional to net-depositional features and also appear to be common on floors of established canyons and channels, particularly those with steep gradients (Covault et al. 2014; Hughes-Clarke 2016). Turbidity currents that shape these bedforms are relatively shallow and supercritical over the steep sides of the cyclic steps and undergo a hydraulic jump at the upslope end of lower-gradient sections (Kostic 2011; Hughes-Clarke 2016). Fildani et al. (2013) interpreted early linear channels to evolve through erosion and linkage of net-erosional cyclic steps (trains of scours).

The Lucia Chica channels in Fig. 9 provide several clues about the inception and subsequent development of submarine channels. The system consists of a single deeper, longer-lived and more sinuous feeder channel (inset B) that is replaced downslope by at least four separate lower-relief, ephemeral and less sinuous channels (near a subtle reduction in slope angle) that, in turn, rejoin a single deep channel 12 km further down the slope (inset A—where the gradient abruptly increases and a number of prominent knickpoints are evident; Maier et al. 2013). In settings where channels are preserved in early stages of their evolution, as in Fig. 9, there are indications that sinuosity develops gradually from straight channels or gullies (Gee and Gawthorpe 2007; Sylvester et al. 2012; Maier et al. 2013).

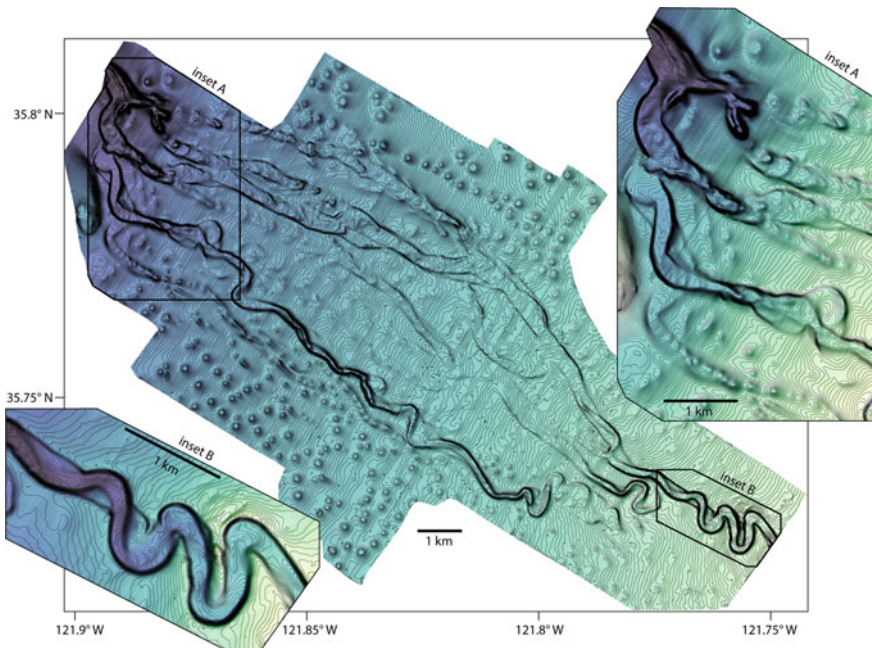


Fig. 9 Lucia Chica channel system, located off the central California coast, showing the diversity of low relief channel systems that developed above a lower-gradient step of the slope. There are multiple channel avulsions and channels with diverse morphologies that reflect, at least in part, the maturity of the channel. Flow from *lower right to upper left*. For more details see Maier et al. (2013)

The sharp contrasts in the geomorphology of immediately adjacent submarine channels in Fig. 9—ranging from narrow and sinuous to wide and straight—probably reflect variations in channel maturity, with avulsions terminating the development of some channels before they could evolve more sinuous planform geometries (Maier et al. 2013). As such, the Lucia Chica system illustrates the connection between geomorphology and time; all else being equal, it takes more time (and more flows) for sinuous channels to develop than straight channels, and differences in channel lifespan (as measured by the number of transited flows prior to an avulsion) allows channels with very different morphologies to sit adjacent to each other on seemingly similar slope segments, or upslope and downslope from avulsion nodes.

A spectrum of depositional and erosional processes may explain how submarine channels migrate, ranging from the development of barforms on inner channel bends to alternating periods of cut-and-fill. In the latter, a period of vertical fill (e.g. emplacement of a debrite plug along a long channel reach) onlaps channel walls and raises the elevation of the channel floor without a corresponding change in the elevation of the channel banks or levee crests. Such events widen the channel floor

and may prompt a stepwise change in channel migration and planform geometry during the passage of subsequent flows, and can lead to the development of chute-like cut-offs (Deptuck et al. 2007; Maier et al. 2012). In extreme cases, thick channel-plugging deposits may block the passage of subsequent turbidity currents (Bouma et al. 1985a), increasing the potential for major avulsions. In a number of fans, systematic patterns of channel migration, with signs of relatively gradual inner bend growth and lateral accretion, are increasingly evident on seismic profiles (e.g., Abreu et al. 2003; Sylvester et al. 2011; Kolla et al. 2012). Well-imaged examples are still rare, but it appears that both types of channel migration can be present at the same time; the longer-term result is deposition on the inner bend and erosion on the outer bend (Conway et al. 2012; Biscara et al. 2013). While meander cutoffs seem to be less common in submarine channels than in rivers (Peakall et al. 2000), their importance in long-lived, high-sinuosity systems is increasingly clear (Babonneau et al. 2004; Sylvester et al. 2011; Kolla et al. 2012; Jobe et al. 2015; Sylvester and Covault 2016; Hansen et al. 2017).

Although there is a natural tendency for many submarine channels to develop and maintain high sinuosity, their planform geometry and cross-sectional shape can be strongly influenced by local tectonic deformation (Clark and Cartwright 2009; Mayall et al. 2010). For example, the relatively straight channel segment on the left side of Fig. 8 developed in response to amplification of an underlying fold, prompting both vertical incision and a decrease in sinuosity (Deptuck et al. 2007). This was accomplished through knickpoint migration (e.g., Pirmez et al. 2000; Heiniö and Davies 2007) as the channel adjusted to a new gradient profile.

5 Morphology of Submarine Lobes

Submarine lobes are deposited where turbidity currents exit channel confinement and lose competence or capacity to carry some or all of their load. This mostly happens at the channel-mouth where levee relief is low, but may also form in response to a local ‘en-route’ reduction in gradient (e.g. ‘transient fans’ described by Adeogba et al. 2005), or as an initial response to a channel-levee avulsion where the confining levee is eroded (e.g. ‘avulsion lobes’ or ‘HARPs’ described by Pirmez et al. 1997). Lobes are elongate low-relief features with gradients that usually do not exceed 1°. The distribution of lobe deposits at the seaward ends of submarine channels is closely linked to the channel-levee avulsion history in both large (e.g., Jégou et al. 2008; Picot et al. 2016) and small (e.g., Piper and Normark 2001; Deptuck et al. 2008) fan systems. The largest known submarine lobes are on the Amazon and Zaire fans and can reach several tens of kilometres in length (Jégou et al. 2008; Picot et al. 2016), but represent relatively small features compared to the length-scale of the channels that feed them. Submarine lobes in smaller fans are volumetrically more important compared to the overall fan size (e.g. complex stacked lobes at the mouths of the South Golo channel in Fig. 10a).

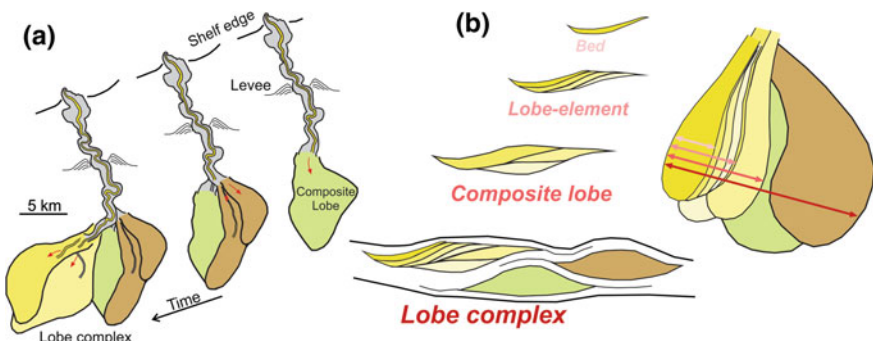


Fig. 10 **a** Development of the lobe complex seaward of the South Golo channel-levee system, offshore eastern Corsica, composed of three main composite lobes, each in turn composed of a number of higher-order lobe elements. **b** Schematic diagram showing the general hierarchy of compensation stacking in submarine lobes (terminology from Deptuck et al. 2008)

Within the same system, planview lobe dimensions correlate well with thickness (Deptuck et al. 2008), but the correlation does not hold well across a variety of systems, potentially due to a difference between entirely unconfined lobes and ones that are affected by the underlying basin topography (Prelat et al. 2010). Still, relatively little is known about the fine-scale internal structure and depositional history of large lobes like those of the Amazon and Zaire Fan. Lobe architecture is ultimately controlled by smaller-scale avulsions near the channel mouth that, to varying degrees, redirect sediment to different lobe settings. A number of hierarchies in lobe compensation stacking are evident (Fig. 10b). Individual beds or bed-sets stack to form lobe-elements; lobe-elements stack to form composite lobes; and composite lobes stack to form lobe complexes (Deptuck et al. 2008). The dimensions, shape, and architecture of lobe deposits reflect a number of interrelated factors including: flow properties (volume, duration, composition); the number of flows and their degree of variation through time; sea floor morphology at the mouth of the leveed channel; and lobe lifespan prior to avulsion or abandonment (Deptuck et al. 2008). As in submarine channels, lobe lifespan is important because even very large fan systems supplied by large-volume turbidity currents like Amazon may not produce correspondingly large lobes if frequent avulsions prematurely terminate sediment delivery to the lobe (Prelat et al. 2010). In general, longer-lived lobes contain a larger volume of sediment, cover larger areas, are longer and have the potential to be architecturally more complex.

Finer-Scale Geomorphic Features Although submarine lobes are net depositional features, their finer-scale morphology is shaped both by erosion and sedimentation. Seafloor images (Decker et al. 2004) and extractions from 3D seismic data (e.g., Prelat et al. 2010; Oluboyo et al. 2014) reveal some of the finer-scale geomorphic characteristics of lobes, and suggest that many consist of an intricate network of bifurcating channels of decreasing dimensions. The depth of these ephemeral channels is commonly not more than a few metres and often less than 1 m (Decker et al. 2004). In Fig. 11, the change from confined to relatively

unconfined flows takes place where the gradient abruptly drops by 0.5° . A number of relict and more recently active channels are recognized near the channel-mouth, as are large-scale bedforms (Fig. 12). A number of spoon- to chevron-shaped scours are also present that locally amalgamate into broad erosive surfaces (Fig. 12d). Scours, in some cases exceeding 20 m depth and 2 km width, are recognised near the channel-lobe transition zone in a number of submarine fans, and reflect the erosive behaviour of flows that undergo hydraulic jumps upon exiting channel-confinement (e.g., Piper and Normark 1983; Mutti and Normark 1991; Wynn et al. 2002a). In some instances, an abnormally large flow may erode and rework older lobe deposits as it continues towards more basinal settings, as may have been the case in Fig. 11 where a number of wider, low-relief channels eroded even the distal parts of lobes (Fig. 12b).

6 Key Research Questions and Future Directions

Significant progress has been made over the past five decades in unravelling the geomorphology of submarine fans, particularly following the initial discovery of sinuous submarine channels on the Amazon Fan. However, only a small fraction of present-day submarine fans is covered with high-resolution bathymetric data, and our knowledge is even more limited when it comes to processes that govern the formation of these systems. Measurements of velocities and concentrations of large turbidity currents are difficult to obtain and are exceedingly sparse compared to what is available in the case of rivers (Talling et al. 2015). Recent direct observations of turbidity currents are very promising (Cooper et al. 2013; Hughes-Clarke 2016). The increasing utilisation of autonomous underwater vehicles (AUVs) in the collection of multibeam bathymetry data, with repeat surveys, will certainly contribute to a larger and more diverse dataset of morphologies and to a better understanding of the associated processes (e.g., Covault et al. 2014). 3D seismic surveys have been and will be among the most important sources of information, as they also provide insight into how geomorphology translates into stratigraphy; and their resolution and quality will continue to improve, further reducing the scale gap between conventional surveys and fine-scale observations.

Some of the subjects that are still relatively poorly understood and form active areas of research include: (1) the concentration and degree of turbulence in the lowermost parts of turbidity currents; (2) the role of subcritical versus supercritical flow and the types of bedforms linked to each; (3) relative importance of punctuated versus gradual meander bend growth and mechanisms responsible for the development of cutoffs in submarine environments; (4) mechanisms for sinuosity development and the nature of secondary circulation in submarine channels; (5) controls on the timing and location of channel-levee avulsions; (6) investigations of the full range of submarine channel geometries, including whether braided or multi-thread channels are present in nature; and (7) latitudinal controls and the influence of the Coriolis force on channel-levee morphology.

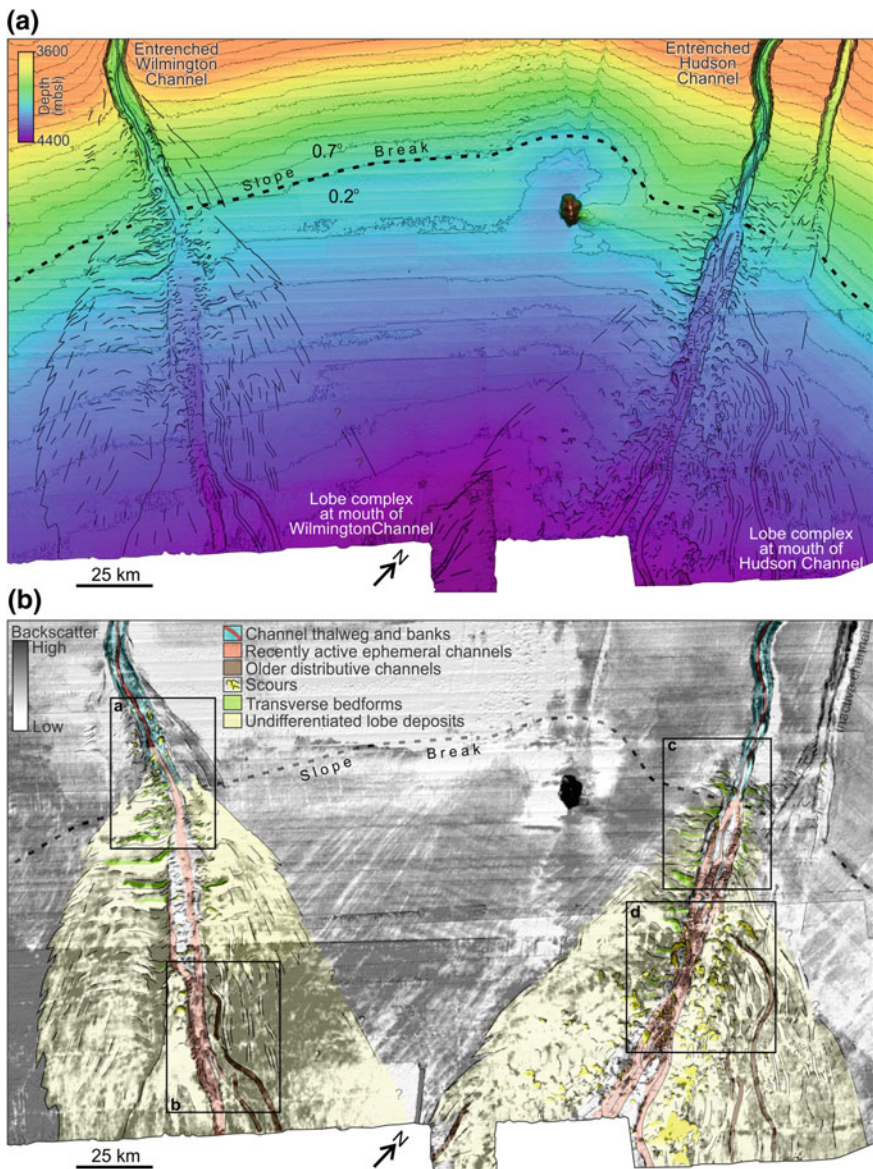


Fig. 11 Interpretation of geomorphic features near the channel-lobe transition seaward of Wilmington and Hudson channels. **a** Bathymetry; **b** Backscatter. See Fig. 3 for location. Data collected by the University of New Hampshire Joint Hydrographic Center (Center for Coastal and Ocean Mapping) (see Gardner 2004)

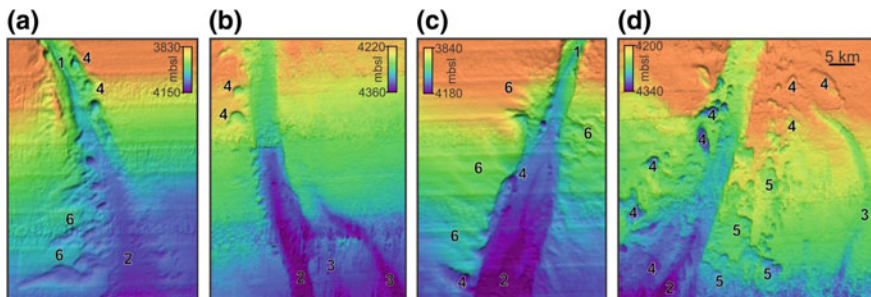


Fig. 12 Close-up multibeam bathymetric images near the channel-lobe transition of the Wilmington (**a**, **b**) and Hudson (**c**, **d**) fans. 1 Channel thalweg; 2 Recent lower-relief erosive channel; 3 Relict distributary channel; 4 Chevron to spoon-shaped scours; 5 Amalgamated scours; 6 Orthogonal bedforms (sediment waves). Location shown in Fig. 11b

As these research topics advance, variations in submarine fan geomorphology—both between different modern systems and temporal changes within individual systems—will increasingly be used to constrain the flow processes responsible for building submarine fans (Peakall and Sumner 2015). Improved understanding of the links between process and geomorphology will likely lead to increased usage of geomorphology—and temporal changes in geomorphology—as kinematic indicators for reconstructing the deformation history of passive and active margin slopes. Finally, recent studies examining first-order scaling relationships between different segments of the sediment delivery and repository system (i.e. source-to-sink studies; Sømme et al. 2009) may provide the best approach for classifying the broad-scale morphology of submarine fans.

Acknowledgements Our sincere appreciation goes to Marie Picot and Nathalie Babonneau for providing the seafloor images from Zaire Fan and to Peter Clift for permission to use the Indus fan data. We thank Andrea Fildani for helpful comments.

References

- Abad JD, Sequeiros OE, Spinewine B et al (2011) Secondary current of saline underflow in a highly meandering channel: experiments and theory. *J Sediment Res* 81:787–813
- Abreu V, Sullivan M, Mohrig D et al (2003) Lateral accretion packages (LAPs): an important reservoir element in deep water sinuous channels. *Mar Pet Geol* 20:631–648
- Adeogba AA, McHargue TR, Graham SA (2005) Transient fan architecture and depositional controls from near-surface 3-D seismic data, Niger Delta continental slope. *AAPG Bull* 89:627–643
- Babonneau N, Savoye B, Cremer M et al (2002) Morphology and architecture of the present canyon and channel system of the Zaire deep-sea fan. *Mar Pet Geol* 19:445–467
- Babonneau N, Savoye B, Cremer M et al (2004) Multiple terraces within the deep incised Zaire Valley (ZaiAngo Project): are they confined levees? *Geological Society London Special Publications*, vol 222, pp 91–114

- Babonneau N, Cattaneo A, Savoye B et al (2012) The Kramis deep-sea fan off western Algeria: role of sediment waves in turbiditic levee growth. In: Prather B, Deptuck M, Mohrig B et al (eds) Application of the principles of seismic geomorphology to continental slope and base-of-slope systems: case studies from seafloor and near-seafloor analogues. SEPM Special Publication, vol 99, pp 293–308
- Biscara L, Mulder T, Hanquez V et al (2013) Morphological evolution of Cap Lopez Canyon (Gabon): illustration of lateral migration processes of a submarine canyon. *Mar Geol* 340:49–56
- Bouma AH, Coleman JM, DSDP Leg 96 Shipboard Scientists (1985a) Mississippi fan: Leg 96 program and principal results. In: Bouma AH, Normark WR, Barnes NE (eds) Submarine fans and related turbidite systems. Springer, New York, pp 247–252
- Bouma AH, Barnes NE, Normark WR (eds) (1985b) Submarine fans and related turbidite sequences. Springer, New York
- Boyd R, Ruming K, Goodwin I et al (2008) Highstand transport of coastal sand to the deep ocean: a case study from Fraser Island, southeast Australia. *Geology* 36:15–18
- Brothers DS, ter Brink US, Andrews BD et al (2013) Geomorphic characterization of the U.S. Atlantic continental margin. *Mar Geol* 338:46–63
- Cartwright JA, Huuse M (2005) 3D seismic technology: the geological “Hubble”. *Basin Res* 17:1–20
- Clark JD, Pickering KT (1996) Architectural elements and growth patterns of submarine channels: application to hydrocarbon exploration. *AAPG Bull* 80:194–221
- Clark IR, Cartwright JA (2009) Interactions between submarine channel systems and deformation in deepwater fold belts: examples from the Levant Basin, Eastern Mediterranean sea. *Mar Pet Geol* 26:1465–1482
- Clark JD, Kenyon NH, Pickering K (1992) Quantitative analysis of the geometry of submarine channels: implications for the classification of submarine fans. *Geology* 20:633–636
- Clift P, Henstock T (2015) Kongsberg EM302 processed bathymetry data, Indus Canyon and shelf, Pelagia cruise PE300 (year 2008–2009, investigators Peter Clift and Tim Henstock). Integrated Earth Data Applications (IEDA)
- Conway KW, Barrie JV, Picard K et al (2012) Submarine channel evolution: active channels in fjords, British Columbia, Canada. *Geo-Mar Lett* 32(4):301–312
- Cooper C, Wood J, Andrieux O (2013) Turbidity current measurements in the Congo canyon. In: Offshore technology conference, OTC 23992
- Corney R, Peakall J, Parsons DR et al (2008) The orientation of helical flow in curved channels. *Sedimentology* 53:249–257
- Covault JA, Romans BW (2009) Growth patterns of deep-sea fans revisited: Turbidite-system morphology in confined basins, examples from the California Borderland. *Mar Geol* 265:51–66
- Covault JA, Normark WR, Romans BW et al (2007) Highstand fans in the California Borderland: the overlooked deep-water depositional systems. *Geology* 35:783–786
- Covault JA, Paull CK, Kostic S et al (2014) Submarine channel initiation, filling and maintenance from sea-floor geomorphology and morphodynamic modelling of cyclic steps. *Sedimentology* 61:1031–1054
- Damuth JE, Kowsmann RO, Flood RD et al (1983) Age relationships of distributary channels on Amazon deep-sea fan: implications for fan growth pattern. *Geology* 11:470–473
- Davies RJ, Posamentier HW, Wood LJ et al (2007) Seismic geomorphology: applications to hydrocarbon exploration and production. Geological Society of London Special Publication, vol 277, 274 p
- Decker J, Teas PA, Schneider RD et al (2004) Modern deep sea sedimentation in the Makassar Strait: insights from high-resolution multibeam bathymetry and backscatter, sub-bottom profiles, and USBL-navigated cores. In: IPA-AAPG deepwater and frontier symposium, pp 377–387
- Deptuck ME (2003) Post-rift geology of the Jeanne d'Arc Basin, with a focus on early Paleogene submarine fans and insights from modern deep-water systems. Dissertation, Dalhousie University, Canada

- Deptuck ME, Steffens GS, Barton M et al (2003) Architecture and evolution of upper fan channel-belts on the Niger Delta slope and in the Arabian Sea. *Mar Pet Geol* 20:649–676
- Deptuck ME, Sylvester Z, Pirmez C et al (2007) Migration-aggradational history and 3D seismic geomorphology of submarine channels in the Pleistocene Benin-major Canyon, western Niger Delta slope. *Mar Pet Geol* 24:406–433
- Deptuck ME, Piper DJW, Savoye B et al (2008) Dimensions and architecture of late Pleistocene submarine fan lobes off the northern margin of east Corsica. *Sedimentology* 55:869–898
- Deptuck ME, Sylvester Z, O'Byrne C (2012) Pleistocene seascape evolution above a ‘simple’ stepped slope, western Niger Delta. In: Prather B, Deptuck M, Mohrig B et al (eds) Application of the principles of seismic geomorphology to continental slope and base-of-slope systems: case studies from seafloor and near-seafloor analogues. SEPM Special Publication, vol 99, pp 199–222
- Emmel FJ, Curran JR (1985) Bengal Fan, Indian Ocean. In: Bouma AH, Barnes NE, Normark WR (eds) Submarine fans and related turbidite sequences. Springer, New York, pp 107–112
- Fernandez RL, Cantelli A, Pirmez C et al (2014) Growth patterns of subaqueous depositional channel lobe systems developed over a basement with a downdip break in slope: laboratory experiments. *J Sediment Res* 84:168–182
- Ferry JN, Mulder T, Parize O et al (2005) Concept of equilibrium profile in deep-water turbidite systems: effects of local physiographic changes on the nature of sedimentary processes and the geometry of deposits. In: Hodgson DM, Flint SS (eds) Submarine slope systems: processes and product. Geological Society London Special Publication, vol 244, pp 181–193
- Fildani A, Normark WR, Kostic S et al (2006) Channel formation by flow stripping: large-scale scour features along the Monterey East channel and their relation to sediment waves. *Sedimentology* 53(6):1265–1287
- Fildani A, Hubbard SM, Covault JA et al (2013) Erosion at inception of deep-sea channels. *Mar Pet Geol* 41:48–61
- Foreman BZ, Lai SYJ, Komatsu Y et al (2015) Braiding of submarine channels controlled by aspect ratio similar to rivers. *Nat Geosci* 8:700–704
- Gardner JV (2004) Cruise Report USNS Henson (T-AGS-63) U.S. Law of the Sea cruise to map the foot of the slope and 2500-m isobaths of the Northeast US Atlantic continental margin. <http://ccom.unh.edu/theme/law-sea/reports>. Accessed 20 Feb 2017
- Gee M, Gawthorpe R (2006) Submarine channel controlled by salt tectonics: examples from 3D seismic data offshore Angola. *Mar Pet Geol* 23:443–458
- Gee M, Gawthorpe R (2007) Early evolution of submarine channels offshore Angola revealed by three-dimensional seismic data. Geological Society London Special Publications, vol 277, pp 223–235
- Gervais A, Mulder T, Savoye B et al (2006) Sediment distribution and evolution of sedimentary processes in a small sandy turbidite system (Golo system, Mediterranean Sea): implications for various geometries based on core framework. *Geo-Mar Lett* 26:373–395
- Hansen L, Janocko M, Kane I et al (2017) Submarine channel evolution, terrace development, and preservation of intra-channel thin-bedded turbidites: Mahin and Avon channels, offshore Nigeria. *Mar Geol* 383:146–167
- Hay AE (1987) Turbidity currents and submarine channel formation in Rupert Inlet, British Columbia 2. The roles of continuous and surge-type flow. *J Geophys Res* 92:2882–2900
- Heezen BC, Ewing M (1952) Turbidity currents and submarine slumps, and the 1929 Grand Banks earthquake. *Am J Sci* 250:849–873
- Heiniö P, Davies RJ (2007) Knickpoint migration in submarine channels in response to fold growth, western Niger Delta. *Mar Pet Geol* 24:434–449
- Heiniö P, Davies RJ (2009) Trails of depression and sediment waves along submarine channel on the continental margin of Espírito Santo Basin, Brazil. *GSA Bull* 121:698–711
- Hiscott RN, Hall RR, Pirmez C (1997) Turbidity-current overspill from the Amazon Channel: texture of the silt/sand load, paleoflow from anisotropy of magnetic susceptibility, and implications for flow processes. In: Flood RD, Piper DJW, Klaus A et al (eds) Proceedings of the ocean drilling program, Scientific Results Leg 155, pp 53–78

- Hubbard SM, Romans BW, Graham SA (2008) Deep-water foreland basin deposits of the Cerro Toro formation, Magallanes basin, Chile: architectural elements of a sinuous basin axial channel belt. *Sedimentology* 55:1333–1359
- Hughes-Clarke JE (2016) First wide-angle view of channelized turbidity currents links migrating cyclic steps to flow characteristics. *Nat Commun* 7:11896
- Imran J, Islam M, Huang H et al (2007) Helical flow couplets in submarine gravity underflows. *Geology* 35:659–662
- Jégou I, Savoye B, Pirmez C et al (2008) Channel-mouth lobe complex of the recent Amazon Fan: the missing piece. *Mar Geol* 252:62–77
- Jobe ZR, Sylvester Z, Parker AO et al (2015) Rapid adjustment of submarine channel architecture to changes in sediment supply. *J Sediment Res* 85:1–25
- Jobe ZR, Howes NC, Auchter NC (2016) Comparing submarine and fluvial channel kinematics: implications for stratigraphic architecture. *Geology* 44:931–934
- Kane EA, Hodgson DM (2011) Sedimentological criteria to differentiate submarine channel levee subenvironments: exhumed examples from the Rosario Fm. (Upper Cretaceous) of Baja California, Mexico, and the Fort Brown FM. (Permian), Karoo Basin, S. Africa. *Mar Petrol Geol* 28:807–823
- Kenyon NH, Amir A, Cramp A (1995) Geometry of the younger sediment bodies of the Indus Fan. In: Pickering KT, Hiscott RN, Kenyon NH, et al (eds) *Atlas of deep-water environments: architectural styles in turbidite systems*, Chapman & Hall, London, pp 89–93
- Klaucke I, Hesse R, Ryan W (1998) Seismic stratigraphy of the Northwest Atlantic Mid-Ocean channel: growth pattern of a mid-ocean channel-levee complex. *Mar Pet Geol* 15:575–585
- Kolla V (2007) A review of sinuous channel avulsion patterns in some major deep-sea fans and factors controlling them. *Mar Pet Geol* 24:450–469
- Kolla V, Bandyopadhyay A, Gupta P et al (2012) Morphology and internal structure of a recent upper Bengal Fan-valley complex. In: Prather B, Deptuck M, Mohrig B et al (eds) *Application of the principles of seismic geomorphology to continental slope and base-of-slope systems: case studies from seafloor and near-seafloor analogues*. SEPM Special Publication, vol 99, pp 347–369
- Konsoer K, Zinger J, Parker G (2013) Bankfull hydraulic geometry of submarine channels created by turbidity currents: Relations between bankfull channel characteristics and formative flow discharge. *J Geophys Res Earth Surf* 118:216–228
- Kostic S (2011) Modeling of submarine cyclic steps: controls on their formation, migration, and architecture. *Geosphere* 7:294–304
- Kuenen PhH, Migliorini CI (1950) Turbidity currents as a cause of graded bedding. *J Geol* 58:91–127
- Maier KL, Fildani A, McHargue TR et al (2012) Punctuated deep-water channel migration: high-resolution subsurface data from the Lucia Chica channel system, offshore California, U.S. A. *J Sediment Res* 82:1–8
- Maier KL, Fildani A, Paull CK et al (2013) Deep-sea channel evolution and stratigraphic architecture from inception to abandonment from high-resolution autonomous underwater vehicle surveys offshore central California. *Sedimentology* 60:935–960
- Manley PL, Pirmez C, Busch W et al (1997) Gran-size characterization of Amazon Fan deposits and comparison to seismic facies units. In: Flood RD, Piper DJW, Klaus A et al (eds) *Proceedings of the ocean drilling program, Scientific Results Leg 155*, pp 35–52
- Mayall M, Lonergan L, Bowman A (2010) The response of turbidite slope channels to growth-induced seabed topography. *AAPG Bull* 94:1011–1030
- Micallef A, Mountjoy JJ, Barnes PM et al (2014) Geomorphic response of submarine canyons to tectonic activity: insights from the cook strait canyon system, New Zealand. *Geosphere* 10:905–929
- Mulder T, Syvitski JPM (1995) Turbidity currents generated at mouths of rivers during exceptional discharges to the world oceans. *J Geol* 103:285–299
- Mulder T, Alexander J (2001) Abrupt change in slope causes variation in the deposit thickness of concentrated particle-driven density currents. *Mar Geol* 175:221–235

- Mutti E (1985) Turbidite systems and their relations to depositional sequences. In: Zuffa GG (ed) *Provenance of arenites*, Reidel Publishing Company, pp 65–93
- Mutti E, Ricci Lucchi F (1972) Le turbiditi dell'Appennino Settentrionale: introduzione all'analisi di facies. *Memorie della Società Geologica Italiana* 11:161–199
- Mutti E, Normark WR (1991) An integrated approach to the study of turbidite systems. In: Weimer W, Link MH (eds) *Seismic facies and sedimentary processes of modern and ancient submarine fans*. Springer, New York, pp 75–106
- Nakajima T, Peakall J, McCaffrey WD et al (2009) Outer-bank bars: a new intra-channel architectural element within sinuous submarine slope channels. *J Sediment Res* 79:872–886
- Nilsen TH, Shew RD, Steffens GS et al (eds) (2007) AAPG studies in geology 56—*atlas of deep-water outcrops*. Tulsa, Oklahoma, 504 p
- Normark WR (1970) Growth patterns of deep sea fans. *AAPG Bull* 54:2170–2195
- Normark WR (1978) Fan valleys, channels, and depositional lobes on modern submarine fans; characters for recognition of sandy turbidite environments. *AAPG Bull* 62:912–931
- Normark WR, Dickson FH (1976) Sublacustrine fan morphology in Lake Superior. *AAPG Bull* 60:1021–1036
- Normark WR, Piper DJW (1991) Depositional consequences of turbidity currents reflecting initiation processes and flow evolution. *SEPM Special Publication*, vol 46, pp 207–230
- Normark WR, Piper DJW, Posamentier H et al (2002) Variability in form and growth of sediment waves on turbidite channel levees. *Mar Geol* 192:23–58
- Normark WR, Paull CK, Caress DW et al (2009) Fine-scale relief related to Late Holocene channel shifting within the floor of the Upper Redondo Fan, offshore Southern California. *Sedimentology* 56:1690–1704
- Oluboyo AP, Gawthorpe RL, Bakke K et al (2014) Salt tectonic controls on deep-water turbidite depositional systems: Miocene, southwestern Lower Congo Basin, offshore Angola. *Basin Res* 26:597–620
- Parsons DR, Peakall J, Aksu A et al (2010) Gravity-driven flow in a submarine channel bend: direct field evidence of helical flow reversal. *Geology* 38:1063–1066
- Peakall J, Sumner EJ (2015) Submarine channel flow processes and deposits: a process-product perspective. *Geomorphology* 244:95–120
- Peakall J, McCaffrey B, Kneller B (2000) A process model for the evolution, morphology, and architecture of sinuous submarine channels. *J Sediment Res* 70:434–448
- Picot M, Droz L, Marsset T et al (2016) Controls on turbidite sedimentation: insights from a quantitative approach of submarine channel and lobe architecture (Late Quaternary Congo Fan). *Mar Pet Geol* 72:423–446
- Piper DJW, Normark WR (1983) Turbidite depositional patterns and flow characteristics, Navy Submarine fan, California Continental Borderlands. *Sedimentology* 30:681–694
- Piper DJW, Deptuck ME (1997) Fine-grained turbidites of the Amazon Fan: facies characterization and interpretation. In: Flood RD, Piper DJW, Klaus A et al (eds) *Proceedings of the ocean drilling program, Scientific Results Leg 155*, pp 79–108
- Piper DJW, Normark WR (2001) Sandy fans—from Amazon to Hueneme. *AAPG Bull* 85:1407–1438
- Piper DJW, Stow DAV, Normark WR (1985) Laurentian fan, Atlantic Ocean. In: Bouma AH, Barnes NE, Normark WR (eds) *Submarine fans and related turbidite sequences*. Springer, New York, pp 137–142
- Piper DJW, Pirmez C, Manley PL et al (1997) Mass-transport deposits of the Amazon Fan. In: Flood RD, Piper DJW, Klaus A et al (eds) *Proceedings of the ocean drilling program, Scientific Results Leg 155*, pp 109–146
- Piper DJW, Hiscott RN, Normark WR (1999) Outcrop-scale acoustic facies analysis and latest quaternary development of Hueneme and Dume submarine fans, offshore California. *Sedimentology* 46:47–78
- Piper DJW, Deptuck ME, Mosher DC et al (2012) Erosional and depositional features of glacial meltwater discharges on the eastern Canadian continental margin. In: Prather B, Deptuck M, Mohrig B et al (eds), *Application of the principles of seismic geomorphology to continental slope and base-of-slope systems: case studies from seafloor and near-seafloor analogues*. SEPM Special Publication, vol 99, pp 61–80

- Pirmez C, Imran J (2003) Reconstruction of turbidity currents in Amazon Channel. *Mar Pet Geol* 20:823–849
- Pirmez C, Hiscott R, Kronen J (1997) Sandy turbidite successions at the base of channel-levee systems of the Amazon Fan revealed by FMS logs and cores: unraveling the facies architecture of large submarine fans. In: Flood RD, Piper DJW, Klaus A et al (eds) *Proceedings of the ocean drilling program, Scientific Results Leg 155*, pp 7–33
- Pirmez C, Beaubouef RT, Friedmann SJ et al (2000) Equilibrium profile and baselevel in submarine channels: examples from Late Pleistocene systems and implications for the architecture of deepwater reservoirs. In: GCSSEPM foundation 20th annual research conference, vol 20, pp 782–805
- Pirmez C, Prather BE, Mallarino G et al (2012) Chronostratigraphy of the Brazos-Trinity depositional system, western Gulf of Mexico: implications for deepwater depositional models. In: Prather B, Deptuck M, Mohrig B et al (eds) *Application of the principles of seismic geomorphology to continental slope and base-of-slope systems: case studies from seafloor and near-seafloor analogues*. SEPM Special Publication, vol 99, pp 107–139
- Popescu I, Lericolais G, Panin N et al (2001) Late Quaternary channel avulsions on the Danube deep-sea fan, Black Sea. *Mar Geol* 179:25–37
- Posamentier HW, Erskine RD, Mitchum RM (1991) Chapter 6—models for submarine-fan deposition within a sequence-stratigraphic framework. In: Weimer P, Link MH (eds) *Seismic facies and sedimentary processes of modern and ancient submarine fans*. Springer, New York, pp 127–136
- Prather BE, Booth JR, Steffens GS et al (1998) Classification, lithologic calibration and stratigraphic succession of seismic facies from intraslope basins, deep water Gulf of Mexico, U.S.A. *AAPG Bull* 82:701–728
- Prather BE, Deptuck ME, Mohrig D et al (eds) (2012) *Application of the principles of seismic geomorphology to continental slope and base-of-slope systems: case studies from seafloor and near-seafloor analogues*. SEPM Special Publication, vol 99. Tulsa, Oklahoma
- Prelat A, Hodgson DM, Flint S (2009) Evolution, architecture and hierarchy of distributary deep-water deposits: a high-resolution outcrop investigation from the Permian Karoo Basin, South Africa. *Sedimentology* 56:2132–2154
- Prelat A, Covault JA, Hodgson DM et al (2010) Intrinsic controls on the range of volumes, morphologies, and dimensions of submarine lobes. *Sed Geol* 232:66–76
- Reading HG, Richards M (1994) Turbidite systems in deep-water basin margins classified by grain size and feeder system. *AAPG Bull* 78:792–822
- Reimchen AP, Hubbard SM, Straight L et al (2016) Using sea-floor morphometrics to constrain stratigraphic models of sinuous submarine channel systems. *Mar Pet Geol* 77:92–115
- Ricci Lucchi F (1985) Chapter 9: Crati fan. In: Bouma AH, Barnes NE, Normark WR (eds) *Submarine fans and related turbidite sequences*. Springer, New York, pp 59–64
- Savoye B, Piper DJW, Droz L (1993) Plio-Pleistocene evolution of the Var deep-sea fan off the French Riviera. *Mar Pet Geol* 10:550–571
- Schwarz E, Arnott RWC (2007) Anatomy and evolution of a slope channel-complex set (Neoproterozoic Isaac Formation, Windermere Supergroup, southern Canadian Cordillera): implication for reservoir characterization. *J Sediment Res* 77:89–109
- Shanmugam G, Moiola RJ (1988) Submarine fans: characteristics, models, classification and reservoir potential. *Earth Sci Rev* 24:383–428
- Skene KI (1998) Architecture of submarine channel levees. Dissertation, Dalhousie University, Canada
- Skene KI, Piper DJW, Hill PS (2002) Quantitative analysis of variations in depositional sequence thickness from submarine channel levees. *Sedimentology* 49:1411–1430
- Sømme TO, Helland-Hansen W, Martinsen OJ et al (2009) Relationships between morphological and sedimentological parameters in source-to-sink systems: a basis for predicting semi-quantitative characteristics in subsurface systems. *Basin Res* 21:361–387
- Spinewine B, Sun T, Babonneau N et al (2011) Self-similar long profiles of aggrading submarine leveed channels: analytical solution and its application to the Amazon channel. *J Geophys Res AGU* 116:F03004

- Steffens GS, Biegert EK, Sumner S et al (2003) Quantitative bathymetric analyses of selected deepwater siliciclastic margins: receiving basin configurations for deepwater fan systems. *Mar Pet Geol* 20:547–561
- Straub KM, Mohrig D, McElroy B et al (2008) Interactions between turbidity currents and topography in aggrading sinuous submarine channels: a laboratory study. *Geol Soc Am Bull* 120:368–385
- Sweeney EM, Gardner JV, Johnson JE et al (2012) Geological interpretation of a low-backscatter anomaly found on the New Jersey continental margin. *Mar Geol* 326–328:46–54
- Sylvester Z, Pirmez C, Cantelli A (2011) A model of submarine channel-levee evolution based on channel trajectories: implications for stratigraphic architecture. *Mar Pet Geol* 28:716–727
- Sylvester Z, Deptuck ME, Prather B et al (2012) Seismic stratigraphy of a shelf-edge delta and linked submarine channels in the NE Gulf of Mexico. In: Prather B, Deptuck M, Mohrig B et al (eds) Application of the principles of seismic geomorphology to continental slope and base-of-slope systems: case studies from seafloor and near-seafloor analogues. SEPM Special Publication, vol 99, pp 31–59
- Sylvester Z, Covault JA (2016) Development of cutoff-related knickpoints during early evolution of submarine channels. *Geology* 44:835–838
- Talling PJ, Allin J, Armitage DA et al (2015) Key future directions for research on turbidity currents and their deposits. *J Sediment Res* 85:153–169
- Walker RG (1978) Deep-water sandstone facies and ancient submarine fans: models for exploration for stratigraphic traps. *AAPG Bull* 62:932–966
- Weimer P, Link MH (eds) (1991) Seismic facies and sedimentary processes of modern and ancient submarine fans. Springer, New York
- Wetzel A (1993) The transfer of river load to deep-sea fans: a quantitative approach. *AAPG Bull* 77:1679–1692
- Wynn RB, Kenyon NH, Masson DG (2002a) Characterization and recognition of deep-water channel-lobe transition zones. *AAPG Bull* 8:1441–1462
- Wynn RB, Piper DJW, Gee MJR (2002b) Generation and migration of coarse-grained sediment waves in turbidity current channels and channel-lobe transition zones. *Mar Geol* 192:59–78
- Wynn RB, Cronin BR, Peakall J (2007) Sinuous deep-water channels: genesis, geometry and architecture. *Mar Pet Geol* 24:341–387

Contourite Drifts and Associated Bedforms

Ibimina Esentia, Dorrik Stow and Zeinab Smillie

Abstract Contourites, also known as alongslope deposits, are sediments that have been deposited or significantly affected by the persistent action of contour (bottom) currents. Contourite drifts are the large-scale morphological expression of contourite deposition, up to 10^6 km^2 in area and $>1 \text{ km}$ in thickness. They are a common feature in some parts of the ocean basins and are found covering large areas of the present-day seafloor beneath modern bottom current systems. They typically co-occur with erosional features caused by bottom currents in very large-scale contourite depositional systems. Contourite drifts are classified into four principal types—sheeted drifts, mounded-elongate drifts, patch drifts, and channel-related drifts—and four specific types linked to their mode or location of formation, including confined drifts, infill drifts, fault-controlled drifts, and mixed-drift systems. The principal erosional elements include: depositional hiatuses; regional erosive surfaces—erosional terraces, abrasive surfaces, channel scour and sub-circular scour; and linear erosion—contourite channels, moats, marginal valleys and isolated furrows. Seismic criteria for the identification of drifts and erosional elements must be applied carefully at three scales of observation—whole drift, seismic element and seismic facies. Bottom-current bedforms are common over drifts and erosive features and provide important insights into the flow characteristics and depositional mechanisms. The wide range of longitudinal and transverse bedforms can be linked to flow velocity and sediment grain-size in a bedform-velocity matrix. The principal controls on contourite systems are: the nature and style of bottom current flow; the slope gradient and other topographic features; and the sediment supply.

I. Esentia · D. Stow (✉) · Z. Smillie
Heriot-Watt University, Edinburgh, Scotland, UK
e-mail: dorrik.stow@pet.hw.ac.uk

1 Introduction

1.1 Scope and Terminology

Contourites are sediments that have been deposited, or significantly affected, by the persistent action of contour (bottom) currents (Stow et al. 2002, 2008; Rebisco 2005; Rebisco et al. 2008, 2014; Stow and Faugères 2008). They are a group of closely related deepwater facies, deposited under the influence of semi-permanent current action, and are commonly referred to as alongslope deposits resulting from semi-continuous depositional processes. This distinguishes them from other deep-water facies that have been deposited either by episodic downslope processes or events (turbidites, debrites, hybrid deposits, slides and hyperpycnites), or from continuous vertical settling—the so-called background processes (pelagites and hemipelagites).

Several different bottom current processes can be recognised as operating in deep water settings (Shanmugam 2003, 2006; Rebisco et al. 2014) (a) thermohaline bottom currents, (b) wind-driven bottom currents, (c) deepwater tidal bottom currents, and (d) internal waves and tides (baroclinic currents). Types (a) and (b) are both *contour currents* capable of depositing contourites and contourite drifts. Types (c) and (d) can both influence contour currents, and so contribute to contourite deposition, and can also act independently, both on the open slope and where focussed in deep-water channels and passageways. Bottom current velocity is also affected by intermittent processes, such as giant eddies, benthic storms and tsunamis.

Contourite drifts are the large-scale morphological expression of contourite deposition (Faugères and Stow 2008). They are a very common feature in some parts of the ocean basins and are found covering large areas of the present-day seafloor beneath modern bottom current systems. In some regions they are expressed as the build-up of large contourite mounds or drifts through semi-continuous deposition over a period of millions of years (Rebisco and Stow 2001; Faugères and Stow 2008). They also occur as less morphologically distinct sheet-like deposits, which may be closely interbedded with the other deepwater facies.

Contourite erosional elements are the non-depositional zones and erosional features on the seafloor often closely associated with and adjacent to contourite drift deposition. They occur where the bottom current velocity is sufficiently strong to prevent deposition or cause substrate erosion (Hernández-Molina et al. 2008; Rebisco and Camerlenghi 2008; Garcia et al. 2009).

Contourite bedforms are the small-scale seafloor sedimentary features (waves, dunes, ripples, scours, etc.) that result from the depositional and erosional processes that form contourites (Wynn and Masson 2008; Stow et al. 2009; Casas et al. 2015). They are visible on the present-day seafloor under the influence of contour currents. Their external form and internal structures may then be preserved in the sediment record.

Contourite facies range from very fine-grained (mud and silt) to relatively coarse-grained (sand and gravel) contourite deposits, and include siliciclastic, bioclastic, volcaniclastic and chemogenic compositional varieties, so that contourite drifts and contourite bedforms are equally varied in composition and grain size (Stow et al. 2002; Stow and Faugères 2008).

Based on the large amount of information gleaned from modern contourite systems, it is possible to construct a fairly accurate picture of just how, where and when contourite deposition occurs and contourite drifts are formed. An associated picture emerges of when and where deposition gives way to non-deposition and erosion by bottom currents, and how long-term accumulation of contourites can result from the alternation of deposition and erosion in time and space. Following a brief history of past research on the topic, this chapter aims to provide a state-of-the-art review of contourite drifts, contourite erosional elements and contourite bedforms. In each case, we will address: (a) the types, examples and occurrence, (b) the processes/mode of formation, and (c) their recognition and implications. We then briefly highlight key research questions for the future.

1.2 Brief History of Study

Early work by the German physical oceanographer Georg Wüst (1933) initially proposed that bottom currents driven by thermohaline circulation might be sufficiently strong to influence sediment flux in the deep ocean basins. But his work was largely ignored until the early 1960s when Bruce Heezen of Woods Hole Oceanographic Institute took up the challenge from a marine geological perspective. In their now seminal paper of 1966, Heezen et al. (1966) demonstrated the very significant effects of contour following bottom currents or contour currents in shaping sedimentation on the deep continental rise off eastern North America. The deposits of these semi-permanent alongslope currents soon became known as contourites, clearly distinguishing them from the deposits of downslope event processes known as turbidites. The ensuing decade saw a profusion of research on contourites and bottom currents in and beneath the present-day oceans, and the demarcation of slope-parallel, elongate, mounded sediment bodies made up largely of contourites that became known as contourite drifts (Hollister and Heezen 1972; McCave and Tucholke 1986). Their initial identification in ancient rocks exposed on land, however, proved mostly inaccurate. Subsequent work has greatly improved on these earlier interpretations (Stow and Lovell 1979; Stow et al. 1998; Hueneke and Stow 2008) although controversy still exists (Shanmugam 2000, 2012).

Standard sedimentary facies models for contourites were developed from detailed observations on modern systems (Stow 1979, 1982; Stow and Piper 1984; Faugères et al. 1984; Gonthier et al. 1984). The direct link between bottom current strength and nature of the contourite facies, especially grain size, was demonstrated (Stow et al. 1986). This has been taken forward through the work by Nick McCave and associates (Robinson and McCave 1994; McCave et al. 1995) in decoding the

often very subtle signatures captured in contourites in terms of variation in deep-sea paleocirculation. Discrimination was made between contourites and other deep-sea facies, such as turbidites deposited by catastrophic downslope flows and hemipelagites that result from continuous vertical settling in the open ocean (Stow and Lovell 1979; Stow and Tabrez 1998). Much progress has been made on the types and distribution of sediment drifts (McCave et al. 1980; Faugères and Stow 1993, 2008; Howe et al. 1994; Stoker et al. 1998), as well as on their seismic characteristics (Faugères et al. 1999; Nielsen et al. 2008).

For the most part, physical oceanographers have worked independently of geologists on the nature and variability of bottom currents, so that much integration is still required between these disciplines. Important contributions that to some extent bridge this divide have come from the HEBBLE project on the Nova Scotian Rise (Hollister and McCave 1984; Nowell and Hollister 1985; McCave et al. 1988), work along the Brazilian continental margin (Viana et al. 1998a, b), and an extensive programme of research in the Gulf of Cadiz (Maldonado and Nelson 1999), culminating in IODP Expedition 339 (Stow et al. 2013a; Hernández-Molina et al. 2014a, b). Prior to this latest mission, the international deep-sea drilling programme in its various guises (DSDP, IPOD, ODP, IODP) has contributed enormously to contourite research—the paleoceanographic context and study of oceanic gateways remain primary targets at present (Knutz 2008). Several edited volumes of papers dealing in part or wholly with contourite systems serve to synthesise much of the knowledge up to the end of the last century. These include: Nowell and Hollister (1985), McCave et al. (1988), Stow and Faugères (1993, 1998), Gao et al. (1998), Stoker et al. (1998), Mienert (1998), Stow and Mayall (1999), Wynn and Stow (2002), Rebescos and Stow (2001), and Stow et al. (2002).

Both the recent IODP expedition (Stow et al. 2002; Hernández-Molina et al. 2014a, b) and the recognition of the economic potential of contourites by the oil industry has seen a renewed explosion of research (Viana and Rebescos 2007; Rebescos and Camerlenghi 2008). Key synthesis papers and edited volumes on contourites and related research that have appeared in the past few years include those by Rebescos et al. (2014), Pickering and Hiscock (2016), Acosta et al. (2015) and Hernández-Molina et al. (2014a, b, 2016a, b). The following synthesis draws together findings from all of this prior research.

2 Contourite Drifts

At the large scale, contourite deposition is focused in contourite drifts, which range in scale from around 0.5×10^2 to $>10^6 \text{ km}^2$, and in larger *contourite depositional systems* that comprise several related drifts and associated erosional elements (Faugères et al. 1993; Stow et al. 2002; Hernández-Molina et al. 2008; Rebescos 2005). Contourite depositional systems develop along continental margins that have been under the influence of bottom currents for relatively long periods of time ($>2\text{--}3 \text{ My}$). They show the development of mounded, elongate, sheeted and patch

drifts, as well as contourite moats and channels. The long-term action of bottom currents generally occurs in association with other deepwater processes, including both downslope and pelagic processes. The larger drifts clearly demonstrate long-term continuity of deposition over several millions of years that allows the accumulation of several hundreds of metres of contourite sediment.

The four principal types of contourite drift that have been identified include (Fig. 1): sheeted drifts, mounded-elongate drifts, patch drifts, and channel-related drifts. Several other drift types have been recognised, which are all variations of the principal types, but determined in relation to their specific topographic or sediment supply controls. These include (Fig. 1): confined drifts, infill drifts, fault-controlled drifts, and mixed drift systems (McCave and Tucholke 1986; Faugères et al. 1993; Rebesco and Stow 2001; Rebesco 2005; Faugères and Stow 2008; Rebesco et al. 2014). These different types of contourite system are controlled largely by a combination of factors: the nature and style of bottom current flow (e.g. tabular vs. multicore flow of Hernández-Molina et al. 2008); the slope gradient and other topographic features; and the sediment supply. There is also a distinct overlap between the drift types identified, such that they form a continuous spectrum of deposits.

Selected examples of these drifts, together with typical range of sizes and key reference, are provided in Table 1.

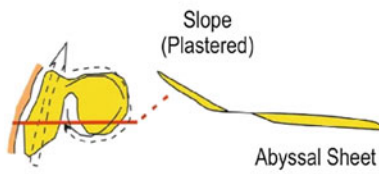
2.1 Sheeted Drifts

Sheeted drifts (Fig. 1; Table 1) typically represent relatively slow rates of deposition of fine-grained contourites over a large area of seafloor (slope plastered drifts and abyssal sheet drifts). They can be very extensive in area from 10^3 to $>10^6 \text{ km}^2$. The flow is mostly simple and tabular, broad and regionally stable, although it may also include strands of more intense flow and giant eddy circulation. For *mud-rich sheeted drifts*, contourite deposition appears to take place directly from suspension more or less evenly across the whole flow width, with a mean accumulation rate of $<20 \text{ cm/ky}$. *Sand-rich sheeted drifts*, however, are a depositional-erosional body linked with more localised zones of higher energy flow, as found in erosive terraces and abrasive surfaces below very active bottom currents. Erosion, winnowing and deposition as bedload alternate continuously such that localised higher rates of accumulation ($>60 \text{ cm/ky}$) may give way to longer periods of non-deposition or erosion.

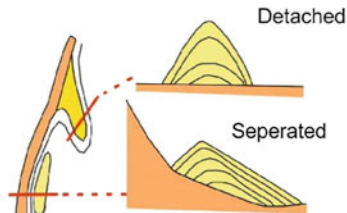
Sheeted drifts can also be distinguished on the basis of their occurrence, yielding: *abyssal sheeted drifts*, *slope sheeted drifts* and *channel sheeted drifts*. Slope sheeted drifts are also referred to as *plastered drifts*. Many examples are known, especially from the Atlantic Ocean, as summarised in Faugères et al. (1999), Stow et al. (2002), Rebesco and Camerlenghi (2008) and Rebesco et al. (2014).

Principal Drift Types

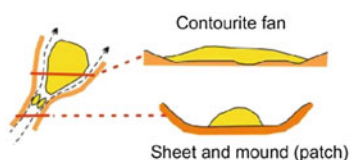
Sheeted Drifts



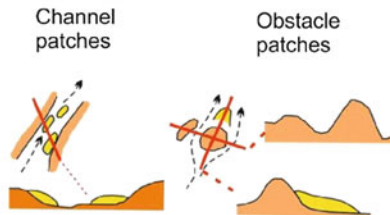
Mounded Elongate Drifts



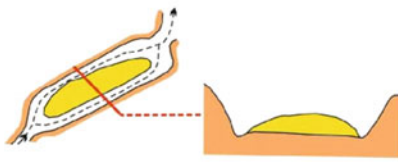
Channel-Related Drifts



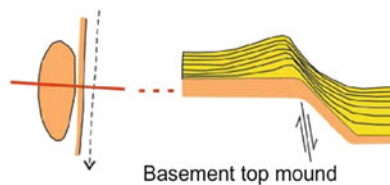
Patch Drifts



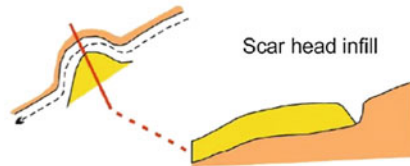
Confined Drifts



Fault-Controlled Drifts



Infill Drifts



Downwelling Drifts

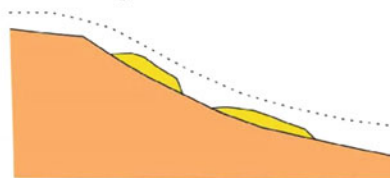


Fig. 1 Summary of principal contourite drift types showing sketches of both plan view and cross-section. Examples are provided for each type in the text and in Table 1. Modified from Rebesco and Stow (2001), Stow et al. (2002), Faugères and Stow (2008) and Rebesco et al. (2014)

There is probably a complete gradation in depositional style between sheeted drifts (with very low mounded geometry), and mixed drifts in which thinner sheets (or beds) of contourites closely interbedded with other deepwater facies (hemipelagites, turbidites, etc.).

Table 1 Principal morpho-genetic types of contourite systems—depositional drifts and erosional elements

	Subdivisions	Size (km ²)	Examples
<i>Depositional drifts</i>			
Contourite sheet drift	(a) Abyssal sheet	$10^5\text{--}10^6$	(a) Ewing drift; Gloria drift, Rockall basin
	(b) Slope (plastered) sheet	$10^3\text{--}10^4$	(b) Gulf of Cadiz CDS; Campos margin; Chatham drift; Gardar drift
	(c) Channel (patch) sheet	< 10^3	(c) Within Vema channel; Cadiz channel
Mounded-elongate drift	(a) Detached drift	$10^3\text{--}10^5$	(a) Eirik drift; Blake drift (many other examples of mounded drifts worldwide)
	(b) Separated drift	$10^3\text{--}10^4$	(b) Feni drift; Faro drift; Flemish drift; Agulhas drift
Channel-related drift	(a) Sheeted patch-drift	$10\text{--}10^3$	(a) NE Rockall trough; Vema channel; Cadiz channel
	(b) Mounded patch-drift	$10\text{--}10^3$	(b) Alavarez-Cabral moat; Vema channel
	(c) Contourite-fan	$10^3\text{--}10^5$	(c) Vema channel exit
Patch drift	(a) Channel patch-drifts	$10\text{--}10^3$	Many different examples worldwide, but most are not specifically named
	(b) Slope patch-drifts	$10\text{--}10^3$	
	(c) Downwelling patch-drifts	$10\text{--}10^3$	
Confined drift		$10^3\text{--}10^5$	Sumba drift; Davies drift; Sicilian channel drift; Louisville drift; Lake Baikal drifts
Infill drift	(a) Slide scar infill	$10^3\text{--}10^4$	Many small examples exist; some larger drifts (e.g. Feni, Lofoten) are generally known as plastered drifts that have evolved from infill drifts
	(b) Irregular relief infill	$10^2\text{--}10^3$	
	(c) Channel infill	$10^2\text{--}10^3$	
Fault-controlled drift		$10\text{--}10^3$	Examples known from Gulf of Cadiz and Antarctic margin

(continued)

Table 1 (continued)

	Subdivisions	Size (km ²)	Examples
Mixed drifts turbidite-contourite systems	(a) Extended turbidite bodies	$10^3\text{--}10^4$	(a) Columbia levee, S Brazil basin; Hikurangi fan drift, New Zealand margin
	(b) Sculptured turbidite bodies	$10^3\text{--}10^4$	(b) Antarctic margins; SE Weddell sea
	(c) Intercalated turbidites-contourites-hemipelagites	Can be very extensive	(c) Hatteras rise; East North American margins; Hebridean margin
<i>Erosional elements</i>			
Depositional hiatuses		$10^3\text{--}10^6$	Standard features of very many CDS systems; see especially Gulf of Cadiz CDS
Regional erosional surfaces	(a) Contourite terraces	$10^3\text{--}10^5$	Argentine margin; Uruguayan margin; Iberian margin
	(b) Abraded surfaces	$10^3\text{--}10^4$	Argentine margin; Uruguayan margin; Iberian margin
	(c) Subcircular scour	$10^2\text{--}10^3$	Iberian margin; Antarctic margin
Linear erosional features	(a) Contourite channels	$10^2\text{--}10^3$	Linear erosional features are well studied from the Gulf of Cadiz, but also occur in many other areas of contourite deposition and erosion
	(b) Contourite moats	$10^2\text{--}10^3$	
	(c) Contourite marginal valleys	$10\text{--}10^2$	
	(d) Large isolated contourite furrows	$10\text{--}10^2$	

The table shows approximate size ranges for each type and selected examples only. Further examples and bibliographic references are given in the text and in previous synthesis publications by Faugères et al. (1999), Rebesco and Stow (2001), Stow et al. (2002), Faugères and Stow (2008), and Rebesco et al. (2014).

2.2 Mounded-Elongate Drifts

Mounded-elongate drifts (Fig. 1; Table 1) represent relatively enhanced rates of deposition (typically 20–60 cm/ky) of fine-to-medium-grained contourites, commonly focused into slope-parallel, elongate sediment bodies over moderate to large areas of seafloor ($10^3\text{--}10^6$ km²). The flow may be either simple (as above) or part of multiple current pathways (multicore flow), and tends to be markedly intensified at

drift margins, in some cases causing narrow erosional zones—contourite channels, moats and marginal valleys. Slower flow and large eddies dominate over the drift itself and lead to enhanced deposition and hence to gradual build-up of the drift mound. It remains somewhat unclear on which side of the current core drift build-up is most likely to occur, and whether or not this is primarily a result of Coriolis deflection. There are a number of apparently contrasting examples in the literature (e.g. Faro-Albufeira drift, Stow et al. 2002; Eirik drift, Hunter et al. 2007), so that we consider it more likely that drift deposition is focused in-between different strands of a multicore flow pattern, whereas erosion, non-deposition and coarse-grained contourite facies occur directly beneath the high velocity cores. Over time, and in response to sea-level, climate or other forcing factors, the flow pattern varies both spatially and in intensity, so that individual drifts build up by differential aggradation, progradation, and erosion (Hernández-Molina et al. 2007; Llave et al. 2001, 2006, 2007).

Mounded drifts can be subdivided according to their morphological relationship with the slope on which they occur, yielding *detached drifts* and *separated drifts*. The former are those drifts that extend outwards from the continental margin, whereas the latter are completely separated from the margin by a distinct contourite moat. More examples are provided in compilations by Faugères et al. (1999), Stow et al. (2002), Rebesco and Camerlenghi (2008) and Rebesco et al. (2014).

2.3 Channel-Related Drifts

Channel-related drifts (Fig. 1; Table 1) are those associated with deepwater channels, passageways or gateways through which bottom circulation is constrained, therefore leading to an increase in flow intensity and velocity. Such features range from those that are relatively shallower sills between basins, such as the Gibraltar Gateway (>300 m), to those at oceanic depths, such as the Vema Channel (>4000 m). Where channels are broad, they are typified by multicore flow pathways that may result from topographic interaction and channel margin effects. Smaller channels, by contrast, may show simple flow, although flow meandering and edge effects are also common. The channel region is characterised by erosion, non-deposition and coarse-grained *sheeted contourites*, together with deposition of finer-grained contourites in localised *patch drifts* (either mounded or sheet-form). The channel exit region experiences flow broadening and deceleration, together with re-combination of distinct current strands. Deposition occurs as a sheet-like *contourite-fan*, typically with down-flow decrease in contourite grain size (Faugères et al. 1998, 2002; Masse et al. 1998).

There is not sufficient data on channel-related drifts to provide an average accumulation rate. It is also likely that deposition and erosion will both be evident and show temporal and lateral variation across the channel system. Typical sizes range from 10 to 10^3 km^2 for channel patch drifts to $10^3\text{--}10^6 \text{ km}^2$ for contourite fans.

2.4 Patch Drifts

Patch drifts (Fig. 1; Table 1) include a wide range of smaller-scale contourite depositional bodies that may be mounded or sheet-like in geometry and with either an elongate or more irregular shape. They occur in different settings including: (a) within channels or gateways (as in 2.3 above); (b) slope systems associated with the generation and downwelling of bottom water masses; and (c) anywhere that contourite drifts occur, where they represent the earlier (younger) precursor of a larger-scale mounded-elongate, sheeted or other drift type.

The size ($10\text{--}10^3 \text{ km}^2$), rates of accumulation and occurrence are very variable.

2.5 Confined Drifts

Confined drifts (Fig. 1; Table 1) are lesser known systems which, to some extent, appear similar to the broad channel systems (above). They are probably affected by multicore flow pathways and typified by zones of both erosion and deposition. A clear example has been described from the Sumba Gateway in the Indonesian archipelago (Reed et al. 1987). Data from the Sicilian gateway in the central Mediterranean have suggested an interesting aspect of flow behaviour and contourite deposition (Reeder et al. 2002). There are a number of confined basins through which the Levantine Sea bottom water flows and in one of these the nature of sediments and high rate of sedimentation suggest that a process of bottom current flow lofting has occurred. The result is one of a mixed contourite-hemipelagite sheet-like deposit.

2.6 Infill Drifts

Infill drifts (Fig. 1; Table 1) occur directly in response to the excavation of topographic lows or scours, which can be the result of downslope mass transport processes, such as slides and slumps. Along such slump-scarred continental margins that are swept by bottom currents, the portion of slope that has been excavated may become progressively back-filled by contourite drift deposits. These are referred to as infill drifts and their size relates to the size of the scour feature being filled and the length of time over which deposition has occurred.

Downslope turbidity current channels crossing bottom-current pathways may also receive infill drift deposition, although such contourite material will be subject to erosion by the normal downslope processes. Complete drift infill of a channel of unknown origin is observed within the Faro-Albufeira drift in the Gulf of Cadiz (Stow et al. 2002).

2.7 Fault-Controlled Drifts

Fault-controlled drifts (Fig. 1; Table 1) are characterised by the direct influence of faulting on their location and nature of growth. The fault activity creates a change in seafloor relief, either instantaneously or as a result of continuing fault movement, and this then causes a perturbation in the bottom-current flow pathway. Drift development may occur either at the base or top of the fault-controlled relief.

2.8 Mixed Drift Systems

The interaction of deepwater depositional processes (downslope, alongslope and pelagic) is the norm along many continental margins, leading to a range of modified or mixed drifts systems (Fig. 1; Table 1). The interaction of pelagic/hemipelagic processes with bottom currents does not result in any morphological effect on the drift morphology, so that the term *mixed drift* generally refers to the interaction of downslope and alongslope flow processes. This may be of several types and different terms have been introduced to describe them. Examples from four different margins are described below:

- (a) Eastern North American Margin: Process interaction is evident from the regular interbedding of thin muddy contourite sheets deposited during interglacial periods and fine-grained turbidites dominant during glacials; and from the marked asymmetry of channel levees on the Laurentian Fan, with the larger levees and extended tail in the direction of the dominant bottom current flow. Along the Cape Hatteras Margin, the complex imbrication of downslope and alongslope deposits on the lower continental rise has been referred to as a *companion drift-fan*.
- (b) The New Zealand Margin: Along the Chatham-Kermadec margin offshore New Zealand, the deep western boundary current scours and erodes the Bounty Fan south of the Chatham Rise and directly incorporates fine-grained material from turbidity currents that have travelled down the Hikurangi Channel. This material, together with hemipelagic sediment, is swept north from the downstream end of the turbidity current channel to form a *fan-drift* deposit. Other mixed drift systems from the region are outlined by Carter and McCave (1994, 2002).
- (c) Antarctic Margins: Eight large sediment mounds off the West Antarctic Peninsula Margin (Rebesco et al. 2002; Camerlenghi et al. 1997) are elongated perpendicular to the margin and separated by turbidity current channels, with an asymmetry that indicates construction by entrainment of the suspended load of down-channel turbidity currents within the ambient southwesterly directed bottom currents and their deposition downcurrent. A complex mix of turbidite and bottom-current controlled sedimentation is evident on the Wilkes Land slope (Escutia et al. 2002).

- (d) Hebridean Margin: This shows a complex pattern of intercalation of downslope (slides, debrites and turbidites), alongslope contourites and glaciomarine hemipelagites in both time and space; the alongslope distribution of these mixed facies types by the northward-directed slope current has led to the term *composite slope-front fan* for the Barra Fan (Knutz et al. 2002).

3 Contourite Erosional Elements

The semi-continuous action of bottom current processes over an extended period of time (e.g. thousands to millions of years) does not only lead to the formation of depositional features (i.e. contourite drifts) but also to the development of non-depositional zones and erosional features on the sea floor. The principal erosional elements identified (Hernández-Molina et al. 2008; Rebesco and Camerlenghi 2008; García et al. 2009; Rebesco et al. 2014) include (Fig. 2; Table 1): (a) depositional hiatuses; (b) regional erosion: erosional terraces, abrasive surfaces, channel scour and sub-circular scour; and (c) linear erosion: contourite channels, contourite moats, marginal valleys and furrows. In general, these areas display erosive winnowing of the seafloor leading to depositional hiatuses and to the accumulation of coarser-grained (sand and gravel) contourites. These features have been relatively less studied than the associated drifts, but we do now have a clear understanding of the importance of erosional elements alongside their depositional counterparts.

3.1 Depositional Hiatuses

A characteristic feature of the seafloor beneath active bottom current systems is that large areas are subject to prolonged periods of non-deposition and/or erosion. Such hiatuses (Fig. 2; Table 1) may extend along a linear channel or moat, across a broad depositional drift or even an entire contourite depositional system. The seafloor beneath the hiatus may be characterised by a hardened substrate (e.g. over-consolidated mud), a coarse-grained lag deposit (e.g. sand or gravel), or a rocky substrate. The overall morphology is either smooth or with an irregular pitted/erosive aspect.

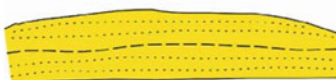
Examples of depositional hiatuses are common to most contourite drifts (Faugères et al. 1999), and have been well described from the Vema Contourite fan in the South Atlantic (Mezerais et al. 1993) and from the Cadiz CDS (Stow et al. 2013a, b; Hernández-Molina et al. 2014a, b). In the case of the Cadiz CDS, IODP drilling results revealed the widespread nature of such hiatuses (10^4 – 10^5 km 2) and their variable duration from <10 ky to >1 my.

3.2 Regional Erosive Surface

Relatively large areas of the seafloor (10^2 – 10^4 km 2) under the influence of bottom currents may undergo substantial erosion. This results in *regional erosive surfaces*, which are also known as *areal erosional features* (Rebesco et al. 2014). Three types have been identified as follows (Fig. 2; Table 1).

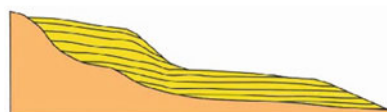
Contourite Erosional Elements

Depositional Hiatus

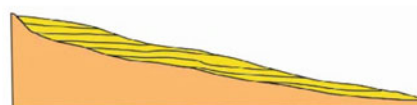


Planar Erosional Surfaces

Contourite Terrace

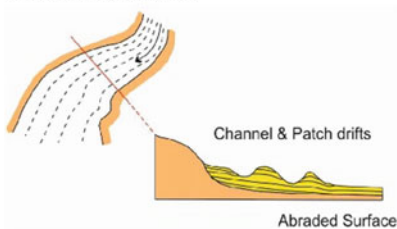


Abraded Surface

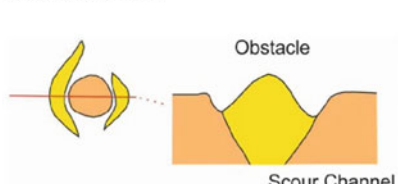


Linear Erosional Features

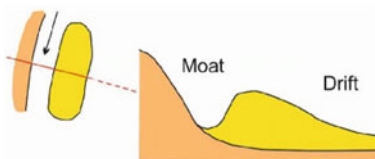
Contourite Channels



Crescentic Scour



Contourite Moat



Marginal Valley



Fig. 2 Summary of the principal contourite erosional elements showing sketches of each type. Examples are provided for each type in the text and in Table 1. Modified from Hernández-Molina et al. (2008), García et al. (2009) and Rebesco et al. (2014)

Contourite terraces have been recognised on several continental slopes. These are extensive scoured surfaces that are cut into the slope topography forming a horizontal to gently seaward-sloping terrace, or series of terraces that are elongated parallel to the margin. They have been described from the Gulf of Cadiz contourite depositional system and from the Argentine margin (Hernández-Molina et al. 2009, 2014a, b). The former is covered with a mixture of coarse-grained lag contourites, intervening mounded contourites (more mud-rich), and a variety of bedforms and larger erosional elements, such as channels. The Argentine terraces are relatively finer-grained in sediment cover and smoother in morphology. Both types represent prolonged erosion and non-deposition associated with bottom currents that impinge on the slope seafloor. They are believed to occur in particular at the interface between different water masses.

Abraded surfaces are very similar to the terraces (above) in terms of morphology and sediment cover, except that they do not form as a slope terrace. They may occur anywhere on the seafloor, and have been documented extensively from the Gulf of Cadiz region (Ercilla et al. 2015). Those that occur within larger-scale channels or oceanic gateways are known as *channel scour surfaces*.

Large-scale *subcircular scour* features have been found in an upper or middle-slope position where strong, dynamic, stratified water masses appear to have formed powerful eddies in the water column that create localised erosion at the seafloor (Hernández-Molina et al. 2008; Rebesco et al. 2014). Little more is known about the nature and genesis of these features.

3.3 Linear Erosional Features

Large-scale linear erosional features (Fig. 2; Table 1) are well known from beneath existing and strong bottom current systems. They typically occur in association with seafloor topographic highs, including mounded drifts, ridges, banks, seamount chains, diapirs, mud volcanoes and plateaus (Maldonado et al. 2005; Hernández-Molina et al. 2008; García et al. 2009; Rebesco et al. 2014). According to these authors, they include a variety of types: channels, moats, marginal valleys, and large isolated furrows. However, the distinction between these types is rather subtle in some cases and overlapping in others. The features range in size from 100 m wide and 1–10 km long (large isolated furrows) to 3–10 km wide and >100 km long (channels and moats).

Contourite Channels are elongate erosional depressions that are generated by the erosive action of bottom currents. They can be sinuous, slightly sinuous or straight depending on their position on the slope, the surrounding morphology, type of seafloor obstacle encountered, and the strength of the current acting during their formation or evolution. They are typically orientated alongslope, oblique to slope or around a topographic obstacle, and generally follow the direction of the dominant bottom current flow pathway. The Cadiz Contourite Channel in the middle slope of the Gulf of Cadiz is an example of a well-studied contourite channel that originates

from the distal end of the Cadiz Terrace and is then deflected when it encounters a diapiric ridge as an obstacle to flow. Several other channels in the Gulf of Cadiz are detailed by García et al. (2009).

A *Contourite Marginal Valley* is a particular type of channel that is formed by the interaction of a bottom current with existing seafloor relief such as a seamount, diapiric ridge, diapiric dome, or mud volcano. Erosion occurs around the flank of the structure as the bottom current is accelerated by being constrained by the relief.

A *Contourite Moat* is an erosional channel that occurs specifically along the flank of a mounded-elongate drift, usually taken as the moat that separates a mounded elongate separated drift from the adjacent slope, as a result of non-deposition or localised erosion below the bottom current core.

A *Large Isolated Contourite Furrow* is a relatively small contourite channel, which may be caused by the erosive action of a small flow that has separated from the main bottom current, probably as a result of some topographic feature obstructing and splitting the flow. It could also represent the incipient formation of a larger channel. Since they are commonly small, narrow and with a relatively smaller incision than contourite channels, Rebesco et al. (2014) prefer to classify them as a large bedform.

4 Seismic Characteristics

In many cases, the first means of identification of contourite drifts will be on seismic profiles. However, with growing recognition of the widespread occurrence of drifts in the deep sea, their variety of types, scales and depositional settings, as

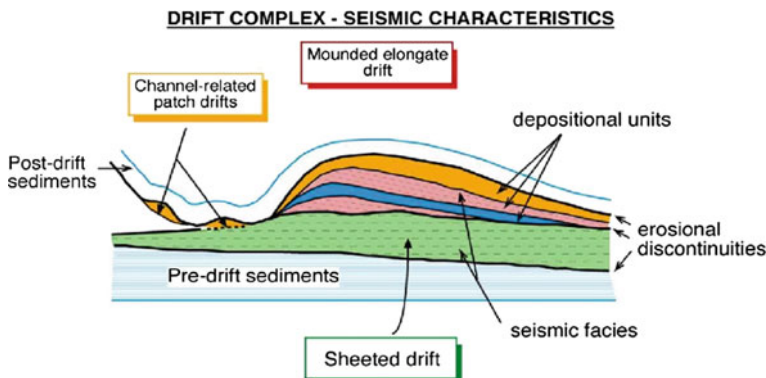


Fig. 3 Conceptual model of the seismic characteristics of contourite drift and adjacent erosional elements. Modified from Stow et al. (2002) and Nielsen et al. (2008). For seismic recognition of contourite systems a threefold approach is required: **a** identify drift type, geometry, elongation and discontinuity surfaces; **b** identify depositional seismic units with a down-current to oblique progradation; and **c** identify typical seismic facies and cyclicity

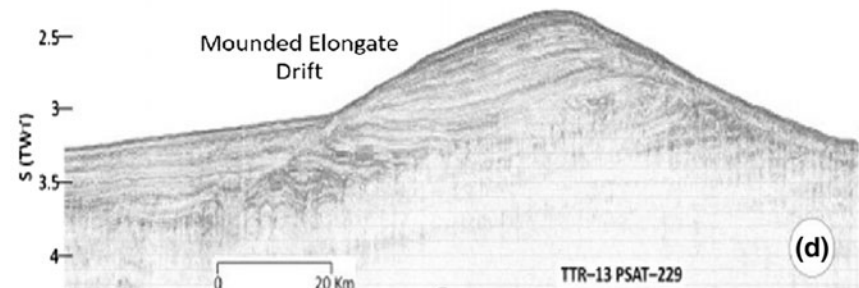
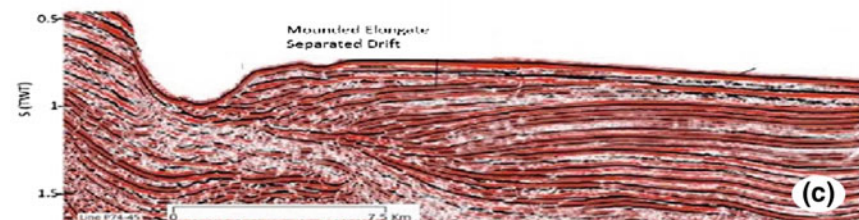
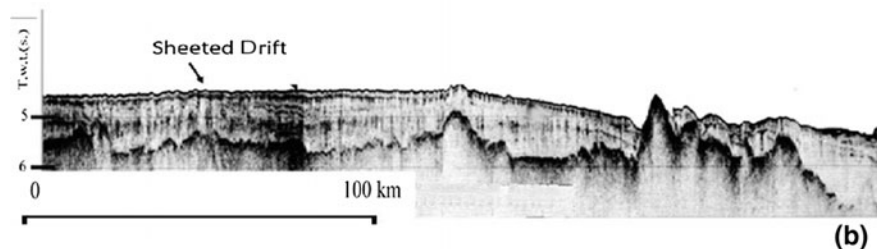
Fig. 4 Examples of seismic profiles across contourite drift depositional systems. **a** Sheeted drift: ► Isfjorden plastered (slope) drift from West Spitzbergen margin (Reprinted from Deep Sea Research Part I, 79, Rebesco et al., Quaternary contourite drifts of the Western Spitsbergen margin, 2013, with permission from Elsevier). **b** Sheeted drift: Gloria (abyssal) drift from the NW Atlantic Ocean (after Egloff and Johnson 1975). **c** Mounded elongate drift: Faro-Albufeira (separated) drift, Northern Gulf of Cadiz (Reprinted from Marine Geology, 352, Rebesco et al., Contourites and associated sediments controlled by deep-water circulation processes: State-of-the-art and future considerations, 2014, with permission from Elsevier). **d** Mounded elongate drift: Eirik (detached) drift, southern Greenland margin (from Hunter et al. 2007). **e** Confined drift: Louisville (confined) drift, eastern New Zealand margin (after Carter and McCave 1994). **f** Channel-related drift: Vema contourite fan, South Brazilian basin, South Atlantic Ocean (after Faugères et al. 1998). **g** Drift complex: Sheeted drift within NE Rockall Trough passes laterally into a mounded-elongate drift, and patch drifts within the adjacent moat (after Faugères et al. 1999). **h** Infill drift: Faeroe plastered infill (slope) drift, southern margin Norwegian Sea.

well as their similarity to features typical of other deep-sea facies (such as turbidite lobes, levees and fans), it has become necessary to erect a set of seismic criteria that will help distinguish drifts from other similar bodies. This becomes much more difficult, of course, where close interbedding of different facies has occurred as in the mixed drift systems noted above. The current set of seismic criteria for enabling positive identification has been modified from the three-scale approach presented by Faugères et al. (1999), and further developed by Rebesco and Stow (2001), Stow et al. (2002) and Nielsen et al. (2008). The key attributes are shown schematically in Fig. 3 and a range of examples of different drift types in Fig. 4.

4.1 First-Order Seismic Element (i.e. Drift Scale)

This involves identification of the large-scale elements of the drift such as the overall architecture, the external geometry, the internal reflector character, and the upper and lower bounding surfaces. This first order seismic element of drifts reflects long-lasting (temporally) stable conditions in the bottom-current regime and/or oceanographic setting. The bounding surfaces represent a record of major changes in the depositional environment. The large-scale features observed include:

- (a) *Drift geometry.* The variety of drift geometries now known to exist have been described in the previous section. Those with a more distinctly mounded rather than low-relief sheet-like geometry are most easily identified. This is especially true where the sediment body occurs beneath an existing bottom current system and is clearly isolated from other possible sediment sources (such as downslope supply routes).
- (b) *Drift elongation.* An overall down-current elongation is typical of most drifts. The elongation direction is therefore wholly alongslope or at some small angle of deviation (generally <30°) from the slope contours. In order to observe the planform geometry of drifts, it is necessary to obtain either a closely-spaced 2D seismic survey or 3D seismic survey.



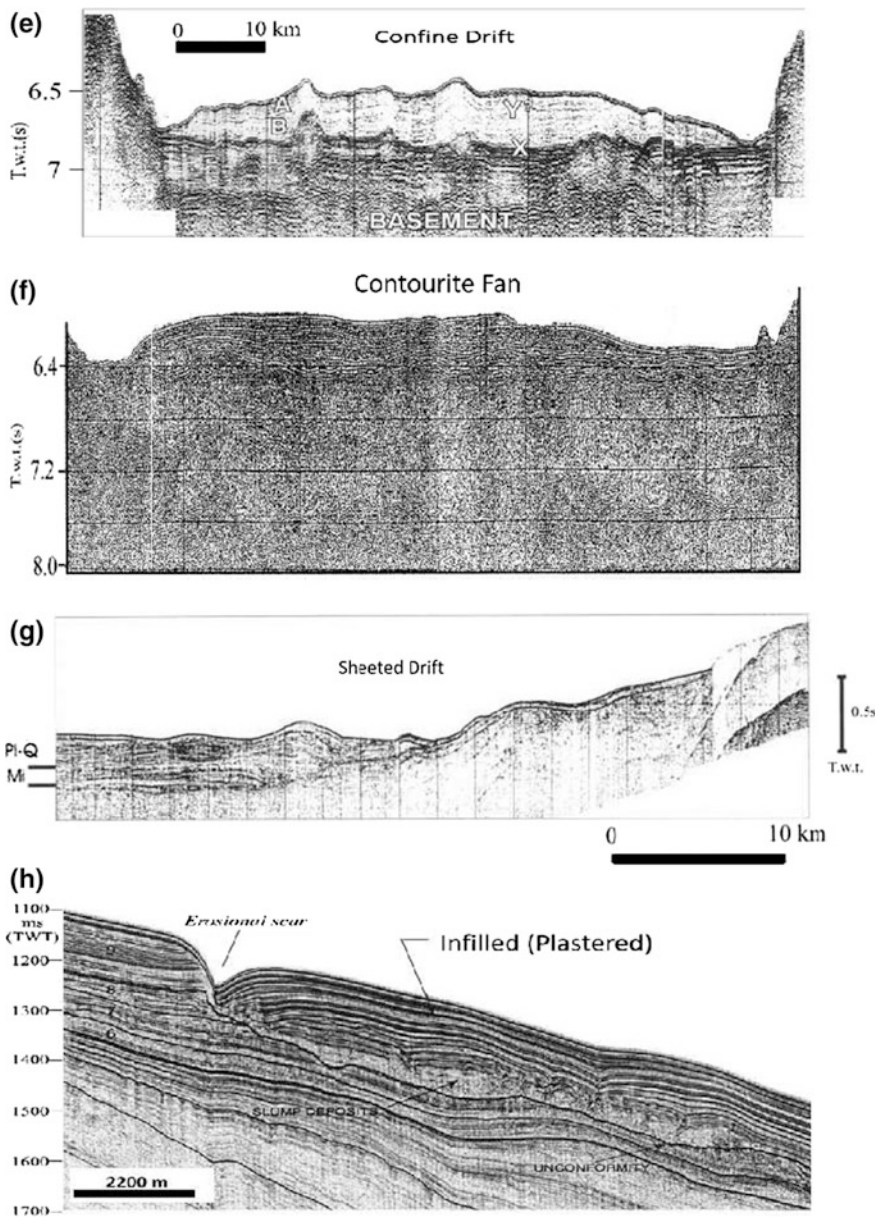


Fig. 4 (continued)

- (c) *Erosional discontinuities.* These are typically widespread discontinuities both at the base and within the drift, extending across the accumulation as a whole. These are commonly marked by continuous high-amplitude reflectors, which may also underline a change in seismic facies. Some of these unconformities will be on a sub-regional scale, beyond the confines of the drift, while others (such as the basal horizon) may even link into ocean-wide discontinuities. These reflect periodic changes in bottom-current conditions.
- (d) *Uniform reflector pattern.* Drifts are commonly represented by extensive, sub-parallel, moderate to low-amplitude reflectors, with mainly gradational changes typical between seismic facies, in addition to the erosional discontinuities noted above. These reflect the long-lasting stable conditions, both laterally and temporally, that are the norm for drift accumulation.

4.2 Second-Order Seismic Element (i.e. Depositional Seismic Units)

This involves the analysis of the internal architecture of the first-order drift and identification of medium-scale seismic units, their shape and stacking pattern, and reflector terminations. Internal architecture within a drift is generally complex, as a result of local variation in processes and accumulation rates linked to changes in current activity. In many cases, the history of drift construction is marked by an alternation of periods of sedimentation and periods of erosion or non-deposition. Medium and small-scale features reflect these changes.

- (a) *Seismic units.* Most of the larger drifts will comprise a series of broadly lenticular, upwardly-convex, seismic units.
- (b) *Stacking pattern.* Progradational, aggradational and uniform stacking patterns occur in different drift systems. These may change through the history of drift development.
- (c) *Migration direction.* The individual seismic units may show migration in down-current to oblique direction, coincident with the elongation direction of the drift as a whole. Any lateral migration direction is likely to be influenced by the Coriolis Force (to the right in the Northern Hemisphere, and to the left in the Southern Hemisphere), providing the right morphological context, current direction and latitude.
- (d) *Reflector terminations.* Down-lapping and sigmoid progradational reflector patterns are typical, whereas a top-lapping pattern is less common.

4.3 Third-Order Seismic Element (i.e. Seismic Facies)

At the fine-scale of seismic resolution, the nature of individual seismic facies reflects changes in both depositional processes and in sediment types. They are not unique to contourite drifts and also depend very closely on the methods employed for seismic acquisition and processing. However, once a drift origin has been established, using a combination of seismic and other characteristics, much interesting detail can be gleaned from this small-scale approach.

- (a) *Seismic facies*. A wide variety of seismic facies are typical of contourites, most of which are equally present in turbidite and/or hemipelagic systems. These include: (i) semi-transparent, reflector-free intervals, (ii) continuous, sub-parallel, moderate to low-amplitude reflectors, (iii) regular, migrating-wave, moderate to low-amplitude reflectors, (iv) irregular, wavy to discontinuous, moderate-amplitude reflectors, and (v) an irregular, continuous, single high-amplitude reflector. Stow et al. (2002) suggest that this order of seismic facies (i–v) reflects increasing strength in the bottom-current regime. Particular seismic facies associations may be more diagnostic of contourite systems, although this area also needs more work.
- (b) *Seismic facies cyclicity*. There is now much evidence of a cyclic pattern in some drifts between a more transparent facies (T) and a moderate-amplitude continuous reflector seismic facies (R) (Fig. 5). Preliminary interpretation suggests seismic facies R reflects a greater proportion of silt/sand content contourites, more hiatuses and condensed sedimentation sections, due to increased bottom current intensity. Seismic facies T, by contrast, is due to low silt/sand content within a more continuous and homogeneous muddy contourite section, reflecting decreased bottom current intensity. The driver for this cyclic model is most likely bottom-current variation linked to climate change.

5 Bottom Current Bedforms

At a small scale, the seafloor is smoothed and/or sculpted into a wide variety of bedforms at dimensions that range over several orders of magnitude (Heezen and Hollister 1971; Kenyon and Belderson 1973; Wynn and Masson 2008; Masson et al. 2004; Stow et al. 2009, 2013a, b). These provide important insights into both flow characteristics and depositional-erosional mechanisms of bottom currents. Surface lineation and ripples are ubiquitous at the centimetre scale, sand waves and dunes are common metric scale features, mud furrows and sand ribbons occur with a spacing of tens of metres and length up to several kilometres.

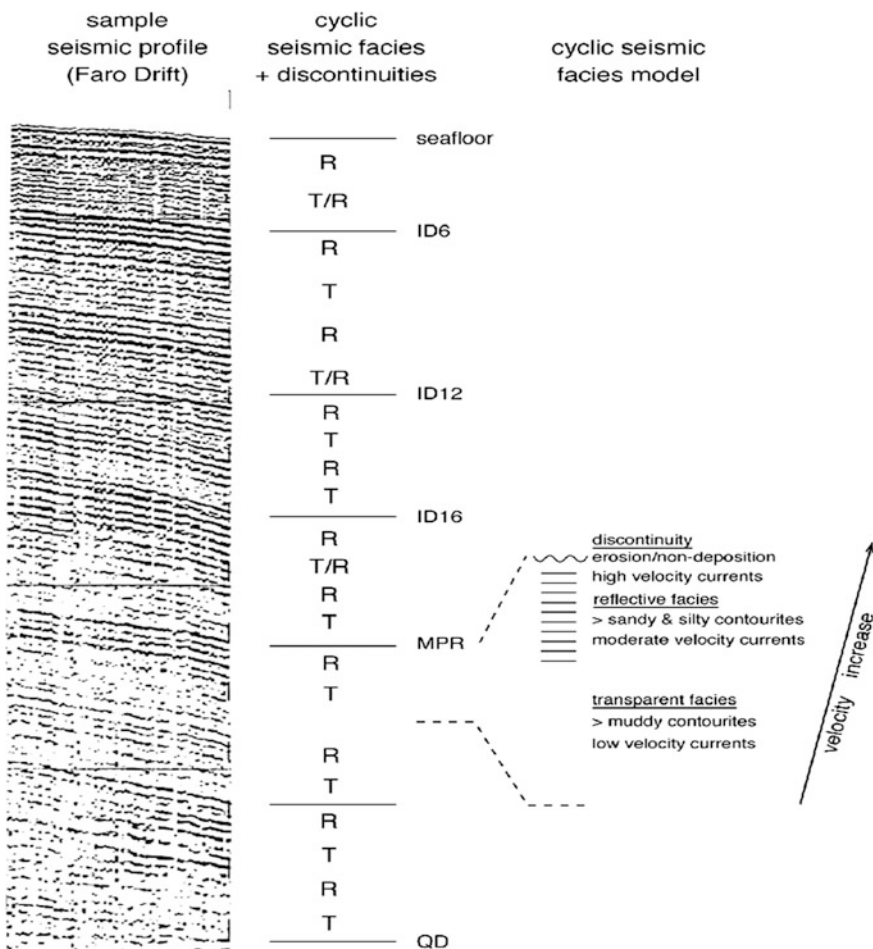


Fig. 5 Seismic facies typical of contourite drifts, Faro Drift, Gulf of Cadiz (from Stow et al. 2002). Note seismic cyclicity of transparent and reflective packages separated by discontinuity surfaces. Interpreted in terms of long-term variation in bottom current strength

Bedforms can be divided into two main groups: longitudinal and transverse bedforms (Fig. 6). We briefly outline below the main bedforms within these two groups. It should be noted that none of these bedforms is exclusive to formation under bottom currents, nor do they occur solely in deepwater settings.

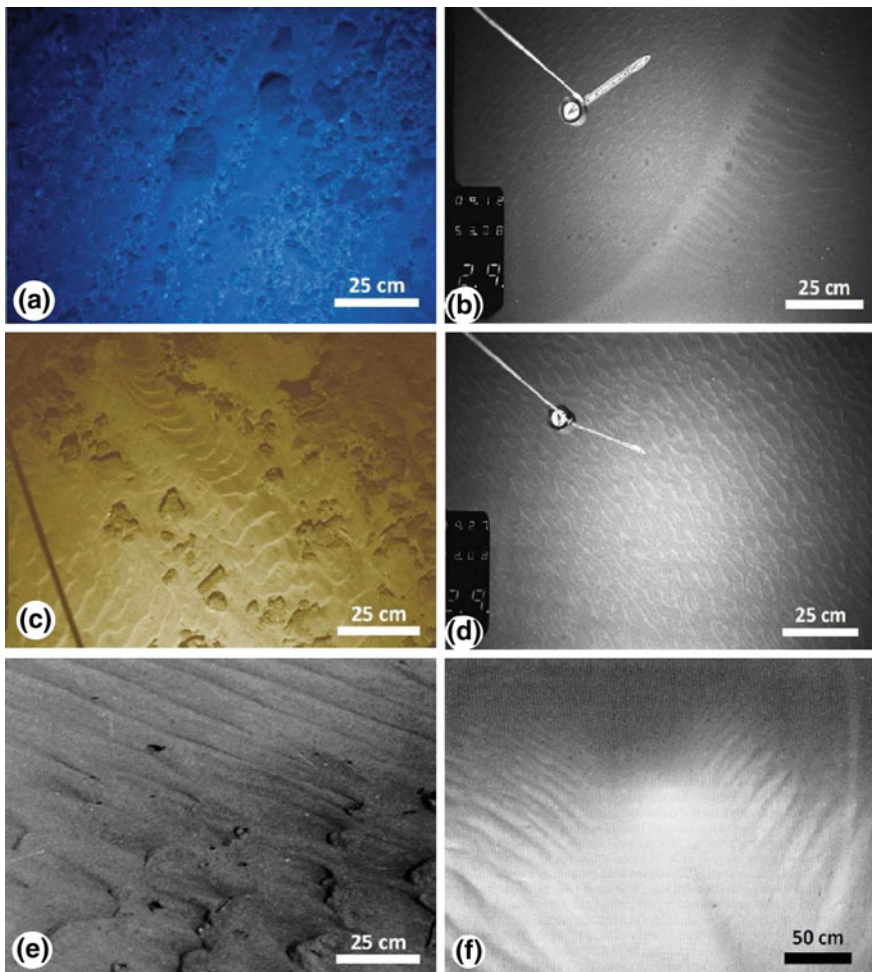


Fig. 6 Examples of bottom photographs showing selected bedforms on the present-day seafloor. **a–f** From Gulf of Cadiz. **a** Lineation in coarse-grained sand-gravel sediment. **b** Sand wave or dune covered in smaller-scale ripples, with curved crest and avalanche stringers down the lee face. **c** Transverse sand ripples between gravel patches and stringers. **d** Small sand ripples, most transverse to flow but with some interference. **e** Lineation in sands (longitudinal ripples), with more linguoid ripples in foreground. **f** Part of longitudinal furrow, deeply erosive into muddy seafloor

5.1 Longitudinal Bedforms

This is a range of bedforms that are all generally elongated parallel to flow direction and that can be developed on mud, sand and gravel substrates. They include four main types:

- Surface lineations of very low relief (mm) and spacing (mm to cm) occur on muddy and silty substrates at low flow speed (<0.15 m/s). They also occur at slightly greater relief (cm) and spacing on sand and gravel substrates at correspondingly higher flow speeds (0.1–0.5 m/s).
- Ribbon marks are large mounded and elongate sand ridges up to metres in height that can run for several kilometres over a sand sheet, in some cases with a more or less anastomosing pattern. Gravel ribbons or stringers are similar features formed on a sand-gravel substrate. Both features require high flow speeds (0.5–1.5 m/s).
- Crag and tail features refer to the elongate depositional mound that forms behind a seafloor obstacle. Comet scours are crescentic to elongate erosional scours that form around the margins of and extend downstream from an obstacle. Both structures occur at all different scales, from centimetres to hundreds of metres, and at flow speeds of 0.1–0.5 m/s.
- Furrows are commonly occurring, regularly-spaced, elongate, sub-parallel and mainly erosive bedforms that occur at a wide range of scales in different substrate types. Those that have been excavated under powerful bottom currents over muddy substrates can reach several metres in depth, tens of metres in width and extend for many kilometres down-current. Equivalent furrows are known from sandy and gravel substrates. All three types probably have an element of deposition on the ridge segments between furrows, and form at flow speeds from 0.5 m/s (mud furrows) to 2 m/s (gravel furrows).

5.2 *Transverse Bedforms*

These bedforms are oriented transverse to the flow direction and form on substrates of fine sand/coarse silt up to gravel-size. They include three main types:

- Ripples are the smallest of the transverse bedforms (wavelength decimetres, height centimetres), and occur in straight, sinuous, and linguoid planform. Flow speed ranges from 0.15 (small straight-crested) to 0.5 m/s (linguoid).
- Dunes and sand waves show similar variations to ripples but with longer wavelengths and heights and are formed under correspondingly higher flow speeds—up to 1.0 m/s for the larger barchan dunes. Gravel waves are relatively less common but do occur under still higher flow speeds up to around 1.3–1.4 m/s.
- Giant mud waves occur in very fine-grained sediments at low flow speeds (0.1–0.2 m/s), with wavelengths of 1–3 km and wave heights up to around 50 m. Whereas the other transverse bedforms are formed under tractional grain movement and show down-flow migration, the giant mud waves mostly show up-stream migration and accumulate from the settling of suspension loads.

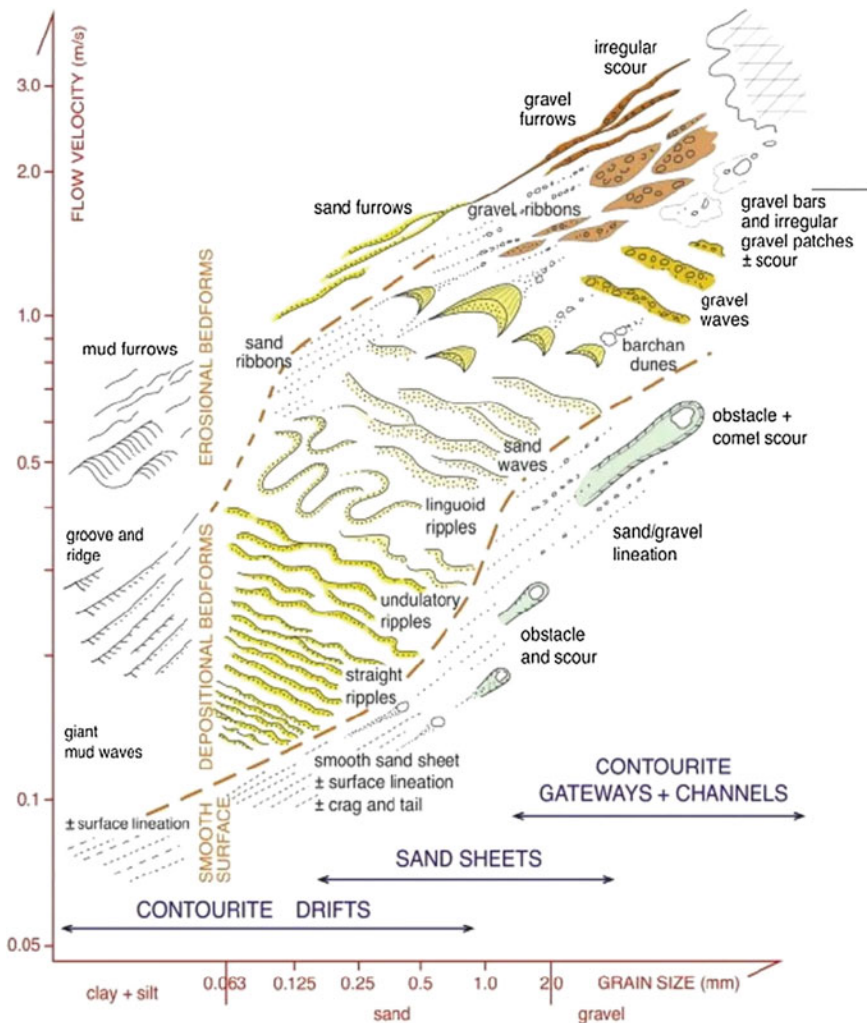


Fig. 7 Bedform-velocity matrix. Modified from Stow et al. (2009) and Rebescu et al. (2014). The plot shows the range of depositional and erosive bedforms commonly associated with bottom currents in deepwater, with an indication of where different bedforms occur (drifts, sand sheets, gateways and channels). The bedforms are controlled in part by flow velocity (y-axis) and in part by grain size of the sediment (x-axis). Both axes are plotted as log scales

Stow et al. (2009) have synthesised a large amount of this data into a bedform-velocity matrix (Fig. 7), from which we can derive information on flow direction, velocity, variability and continuity. The nature and distribution of bedforms also allows comment on various aspects of contourite deposition.

- (1) The widespread fine-grained contourites of many drifts, with smoothed sediment surfaces and/or surface lineation, represent deposition of silt and clay directly from suspension through a laminar boundary layer, which in places is subject to well-ordered small-scale helical flow vortices creating the linear sediment fabric.
- (2) The common presence of ripple bedforms at all scales on silt-sand substrates indicates that tractional movement of bedload at the base of flow is the normal mode of transport and deposition of fine-to-medium grained granular material in bottom currents.
- (3) In zones subjected to higher velocity currents, tractional movement of coarser materials is evidenced by sand waves, barchan dunes and, more rarely, gravel waves and bars. That these bedforms are often covered by smaller-scale ripples is evidence of bottom current variability, probably over timescales of hours (tidal influence) to weeks (benthic storm effects). Periods of intense bedload transport therefore alternate with periods of lesser transport and deposition.
- (4) Some linear bedforms, known as furrows, are formed at relatively higher flow velocities in both mud and sand-gravel substrates. These represent mainly erosive conditions at the base of flow leading to sediment entrainment and transport. Groove and ridge structures (also known as longitudinal triangular ripples) appear to be a smaller scale equivalent of mud furrows, formed at moderate flow velocities over fine substrates and involving both deposition and erosion.
- (5) The lateral juxtaposition of bedform types occurs over a horizontal scale of metres, indicating the variability in velocity of strands of flow (or regions of flow) at this order of magnitude. There is also the larger-scale of variation over hundreds of metres from more dominantly erosive to mainly depositional. This can occur in an across-flow sense, from erosive marginal moat to central depositional drift, and in a down-flow sense, away from a gateway or channel exit.
- (6) The development of large-area fields of giant sediment waves and their persistence in time through the sedimentary record (thousands to a few million years), reflects the broad tabular flow and long-term stability of low-velocity bottom currents in their region of formation. Deposition of the fine clays and silts that make up these bedforms is almost certainly directly from suspension, under the influence of internal lee waves in a weakly stratified bottom current (Flood 1988).

6 Future Research

Amongst many important research topics that remain outstanding with respect to contourite studies, we suggest the following as the most significant:

- (a) *Processes.* (i) Understanding the processes of bottom current flow, how these vary laterally and longitudinally within the current system, and what controls the variability of the flow in both time and space. (ii) Recognition of boundaries between water masses flowing at different velocities and of the effects of these boundaries on sedimentation, seafloor morphology and geotechnical properties of contourites. (iii) Understanding the influence and impact of different processes (e.g. turbidity currents, internal tides and waves) on bottom currents and contourites. (iv) Improvement in knowledge of the link between physical oceanography and contourite deposition/erosion.
- (b) *Deposition and budget.* (i) Understanding the exact mechanisms of how the carrying capacity and deposition is distributed across a current system. (ii) Analysing the sediment budget for different drift systems—how much and what types of sediment are derived from different sources. (iii) Careful consideration of the control of coarser layers on contourites from turbidity current input, increased bottom current velocity and increased primary productivity.
- (c) *Climate change.* (i) Decoding the links between bottom current flow variation, contourite deposits and climate change. Consideration of how different bottom water masses and hence different bottom current systems are affected by climate.
- (d) *Fossil contourites.* (i) Clear characterisation of the criteria for recognition of contourites in the ancient record (subsurface and on land) and their distinction from related deposits in deep water—e.g. turbidites, hemipelagites and the deposits from other bottom current systems. (ii) Establishment of good type examples in the field and in subsurface cores for the different facies types. (iii) Recognition of hybrid facies that have been influenced by one or several processes during sedimentation.
- (e) *Economic significance.* (i) Recognition of the role of contourites as a deepwater play for hydrocarbon reservoirs in deepwater, and the discovery and characterisation of oil/gas in contourite reservoirs. (ii) Documenting and understanding the variation of organic carbon content of contourites. (iii) Recognising the role and impact of both bottom currents and contourite sediments in the field of ocean geohazards. (iv) Detailed study of the role of bottom currents in the development of ferro-manganese nodules.
- (f) *Biological significance.* (i) Detailed study of the ichnofacies characterisation of contourites in terms of the nature, diversity and distribution of trace fossils, and the specific controls of water mass, organic matter supply, and rates of sedimentation. (ii) Clear understanding of the role of bottom currents in deepwater benthic ecosystems, including those of black smoker vents and cold-water corals.

The multidisciplinary research discussed by Howe (2008) and amplified by Rebesco et al. (2014) points towards the most appropriate methodologies that should be employed to address the above questions.

References

- Acosta J, Berné S, Chiocci F, Palanques A, Guillen J (eds) (2015) *Atlas of bedforms in the Western Mediterranean*. Elsevier, Netherlands
- Camerlenghi A, Rebesco M, Pudsey CJ (1997) High resolution terrigenous sedimentary record of a sediment drift on the continental rise of the Antarctic Peninsula Pacific margin. In: Ricci CA (ed) *The Antarctic Region: Geological Evolution and Processes*. Terra Antarctica Publication, pp 705–710
- Carter L, McCave IN (1994) Development of sediment drifts approaching an active plate margin under the S.W. Pacific deep western boundary current. *Paleoceanography* 9:1061–1085
- Carter L, McCave IN (2002) Eastern New Zealand Drifts, Miocene-Recent. In: Stow D, Pudsey C, Howe J, Faugères J, Viana A (eds) *Deep-Water contourite systems: modern drifts and ancient series, seismic and sedimentary characteristics*. Geological Society, London, Memoirs, vol 22, pp 385–407
- Casas D, Ercilla G, Hernández-Molina FJ, MOWER Cruise Team (2015) Bottom current-generated bedforms: the action of the MOW (Mediterranean outflow). In: Abstracts of the 31st IAS meeting of sedimentology, Krakow, Poland, 22–25 June 2015
- Egloff J, Johnson GL (1975) Morphology and structure of the southern Labrador Sea. *Can J Earth Sci* 12:2111–2134
- Ercilla G, Casas D, Hernández-Molina FJ et al (2015) Bottom current-generated bedforms: the action of the MOW (Mediterranean outflow) at the exit of the Strait of Gibraltar. In: Acosta J, Berné S, Chiocci F, Palanques A, Guillen J (eds) *Atlas of bedforms in the Western Mediterranean*. Elsevier, Netherlands
- Escutia C, Nelson CH, Acton GD, Ettreim SL, Cooper AK, Warnk, DA, Jaramillo JM (2002) Current controlled deposition on the Wilkes Land continental rise, Antarctica. In: Stow D, Pudsey C, Howe J, Faugères J, Viana A (eds) *Deep-Water contourite systems: modern drifts and ancient series, seismic and sedimentary characteristics*. Geological Society, London, Memoirs, vol 22, pp 373–384
- Faugères JC, Stow DAV (1993) Bottom-current-controlled sedimentation: a synthesis of the contourite problem. *Sedimentary Geology* 82:287–297
- Faugères JC, Stow DAV (2008) Contourite drifts: nature, evolution and controls. In: Rebesco M, Camerlenghi A (eds) *Contourites. Developments in sedimentology*, vol 60, pp 259–288
- Faugères JC, Stow DAV, Gonthier E (1984) Contouritic drift moulded by deep Mediterranean outflow. *Geology* 12:296–300
- Faugères JC, Mezerais ML, Stow DAV (1993) Contourite drift types and their distribution in the North and South Atlantic Ocean basins. *Sed Geol* 82(1–4):189–203
- Faugères JC, Imbert P, Mezerais ML et al (1998) Seismic patterns of a muddy contourite fan Vema Channel, South Brazilian Basin and a sandy deepsea fan Cap Ferret system Bay of Biscay: a comparison. *Sed Geol* 115(1–4):81–110
- Faugères JC, Stow DAV, Imbert P et al (1999) Seismic features diagnostic of contourite drifts. *Mar Geol* 162(1):1–38
- Faugères J, Lima A, Masse L et al (2002) The Columbia channel-levee system: a fan drift in the southern Brazil Basin. In: Stow D, Pudsey C, Howe J, Faugères J, Viana A (eds) *Deep-Water contourite systems: modern drifts and ancient series, seismic and sedimentary characteristics*. Geological Society London Special Publication, vol 22, pp 223–238
- Flood RD (1988) A lee wave model for deep sea mud-wave activity. *Deep Sea Res* 35:973–983
- Gao ZZ, Eriksson KA, He YB et al (1998) Deep-water traction current deposits. Science Press, Beijing, New York
- García M, Hernández-Molina FJ, Llave E et al (2009) Contourite erosive features caused by the Mediterranean outflow water in the Gulf of Cadiz: quaternary tectonic and oceanographic implications. *Mar Geol* 257:24–40

- Gonthier EG, Faugères JC, Stow DAV (1984) Contourite facies of the Faro Drift, Gulf of Cadiz. In: Stow DAV, Piper DJW (eds) *Fine-grained Sediments: deep water processes and facies*. Geological Society London, Special Publications, vol 22, pp 775–797
- Heezen BC, Hollister CD (1971) *The face of the deep*. Oxford University Press, New York
- Heezen BC, Hollister CD, Ruddiman WF (1966) Shaping of the continental rise by deep geostrophic contour currents. *Science* 152:502–508
- Hernández-Molina FJ, Llave E, Stow DAV et al (2006) The contourite depositional system of the Gulf of Cadiz: a sedimentary model related to the bottom current activity of the Mediterranean outflow water and its interaction with the continental margin. *Deep-Sea Res Part II Topical Stud Oceanogr* 53(11–13):1420–1463
- Hernández-Molina FJ, Llave E, Stow DAV et al (2007) The contourite depositional system of the Gulf of Cadiz: a sedimentary model related to the bottom current activity of the Mediterranean outflow water and the continental margin characteristics. *Deep-Sea Res II* 53(11–13):1420–1463
- Hernández-Molina FJ, Llave E, Stow DAV (2008) Continental slope contourites. In: Rebesco M, Camerlenghi A (eds) *Contourites. Developments in sedimentology*, vol 60, pp 379–408
- Hernández-Molina FJ, Paterlini M, Violante R et al (2009) Contourite depositional system on the argentine slope: an exceptional record of the influence of Antarctic water masses. *Geology* 37:507–510
- Hernández-Molina FJ, Serra N, Stow DAV (2011) Along-slope oceanographic processes and sedimentary products around the Iberian margin. *Geo-Mar Lett* 31:315–341
- Hernández-Molina FJ, Llave E, Preu B et al (2014a) Contourite processes associated with the Mediterranean outflow water after its exit from the gibraltar strait: global and conceptual implications. *Geology* 42:231–234
- Hernández-Molina FJ, Stow DAV, Alvarez-Zarikian CA et al (2014b) Onset of Mediterranean outflow into the North Atlantic. *Science* 344(6189):1244–1250
- Hernández-Molina FJ, Llave E, Sierro FJ et al (2016a) Evolution of the Gulf of Cadiz Margin and west Portugal contourite depositional system: tectonic, sedimentary and paleoceanographic implications from IODP expedition 339. *Mar Geol* 377:7–39
- Hernández-Molina FJ, Wåhlin A, Bruno M et al (2016b) Oceanographic processes and products around the Iberian margin: a new multidisciplinary approach. *Mar Geol* 378:127–156
- Hernández-Molina FJ, Ercilla G, Casas D et al (2016c) Larger morphological sea-floor features and bedforms associated to the Mediterranean outflow water in the Gulf of Cadiz. Marine and river dune dynamics—MARID V, 4–5 April 2016, North Wales, UK. Abstract volume: 1–4
- Hollister CD, Heezen BC (1972) Geological effects of ocean bottom currents: Western North Atlantic. In: Gordon AL (ed) *Studies in physical oceanography* 2. Gordon & Breach, New York, pp 37–66
- Hollister CD, McCave IN (1984) Sedimentation under deep-sea storms. *Nature* 309:220–225
- Howe J (2008) Methods for contourite research. In: Rebesco M, Camerlenghi A (eds) *Contourites. Developments in Sedimentology*, vol 60, pp 19–34
- Howe JA, Stoker MS, Stow DAV (1994) Late Cenozoic sediment drift complex, NE Rockall Trough, North Atlantic. *Paleoceanography* 9:989–999
- Hueneke H, Stow DAV (2008) Progress and problems in the identification of fossil contourites. In: Rebesco M, Camerlenghi A (eds) *Contourites. Developments in sedimentology*, vol 60, pp 323–344
- Hunter S, Wilkinson D, Stanford J, Stow DAV, Bacon S, Akhmetzhanov A, Kenyon N (2007) The Eirik Drift: a long-term barometer of North Atlantic deepwater flux south of Cape Farewell, Greenland. In: Viana AR, Rebesco M (eds) *Economic and Palaeoceanographic Significance of Contourite Deposits*, Geological Society London Special Publications vol 276, pp 245–263
- Kenyon NH, Belderson RH (1973) Bed forms of the Mediterranean undercurrent observed with side-scan sonar. *Sed Geol* 9:77–100
- Knutz PC (2008) Palaeoceanographic significance of contourite drifts. *Dev Sedimentol* 60: 511–535

- Knutz PC, Jones EJW, Howe JA, Van Weering TJC, Stow DAV (2002) Wave-form sheeted contourite drift on the Barra Fan, NWUK continental margin. In: Stow D, Pudsey C, Howe J, Faugères J, Viana A (eds) Deep-Water contourite systems: modern drifts and ancient series, seismic and sedimentary characteristics. Geological Society, London, Memoirs, vol 22, pp 85–98
- Llave E, Hernández-Molina FJ, Somoza L et al (2001) Seismic stacking pattern of the Faro-Albufeira contourite system (Gulf of Cadiz): a quaternary record of paleoceanographic and tectonic influences. *Mar Geophys Res* 22(5–6):487–508
- Llave E, Schönfeld J, Hernández-Molina FJ, Mulder T, Somoza L, Díaz del Río V, Sánchez-Almazo I (2006) High-resolution stratigraphy of the Mediterranean outflow contourite system in the Gulf of Cadiz during the late Pleistocene: the impact of Heinrich events. *Mar Geol* 227:241–262
- Llave E, Hernández-Molina FJ, Stow DAV et al (2007) Reconstructions of the Mediterranean outflow water during the quaternary based on the study of changes in buried mounded drift stacking pattern in the Gulf of Cadiz. *Mar Geophys Res* 28:379–394
- Maldonado A, Nelson CH (eds) (1999) Marine geology of the Gulf of Cadiz. *Marine Geology Special Issue* 155
- Maldonado A, Barnolas A, Bohoyo F et al (2005) Miocene to Recent contourite drifts development in the northern Weddell Sea (Antarctica). *Global and Planetary Change* 45: 99–129
- Masse L, Faugères JC, Hrovatin D (1998) The interplay between turbidity and contour current processes on the Columbia Channel fan drift, Southern Brazilian Basin. *Sed Geol* 115:111–132
- Masson DG, Wynn RB, Bett BJ (2004) Sedimentary environment of the Faeroe Shetland Channel and Faeroe Bank channels, NE Atlantic, and the use of bedforms as indicators of bottom current velocity in the deep ocean. *Sedimentology* 51:1–35
- McCave IN, Lonsdale PF, Hollister CD, Gardner WD (1980) Sediment transport over the Hatton and Gardar contourite drifts. *J. sed. Petrol.*, 50:1049–62
- McCave IN, Tucholke BE (1986) Deep current-controlled sedimentation of the western North Atlantic. In: Tucholke BE, Vogt PE (eds) *Western North Atlantic Region, The Geology of North America*, vol M. Geological Society of America, pp 451–468
- McCave IN, Hollister CD, Nowell ARM (eds) (1988) Deep ocean sediment transport: HEBBLE collected reprints 1980–1987. Woods Hole Oceanographic Institute, Woods Hole
- McCave IN, Manighetti B, Robinson SG (1995) Sortable silt and fine sediment size/composition slicing: parameters for paleocurrent speed and paleoceanography. *Paleoceanography* 10:593–610
- Mezerais ML, Faugères JC, Figueiredo AG, Masse L (1993) Contour current accumulation off Vema Channel mouth, southern Brazil Basin: pattern of a “contourite fan”. *Sediment Geol* 82:173–188
- Mienert J (ed) (1998) European North Atlantic Margin (ENAM): sediment pathways, processes and flux. *Marine Geology Special Issue* 152
- Nielsen T, Knutz P, Kuijpers A (2008) Seismic expression of contourite depositional systems. In: Rebesci M, Camerlenghi A (eds) *Contourites. Developments in sedimentology*, vol 60, pp 301–321
- Nowell ARM, Hollister CD (eds) (1985) Deep ocean sediment transport—preliminary results of the high energy benthic boundary layer experiment. *Mar Geol* 66
- Pickering KT, Hiscott RN (2016) Deep marine systems: processes, deposits, environments, tectonics and sedimentation. American Geophysical Union and Wiley
- Preu B, Hernández-Molina FJ, Violante R (2013) Morphosedimentary and hydrographic features of the northern Argentine margin: the interplay between erosive, depositional and gravitational processes and its conceptual implications. *Deep-Sea Res Part I Oceanogr Res Pap* 75:157–174
- Rebesci M (2005) Contourites. In: Richard C, Selley RC, Cocks LRM, Plimer IR (eds) *Encyclopedia of geology*. Elsevier, Oxford, vol 4, pp 513–527
- Rebesci M, Stow DAV (eds) (2001) Seismic expression of contourites and related deposits. *Marine Geophysical Researches Special Issue* 22 (5–6)

- Rebesco M, Camerlenghi A (eds), 2008. Contourites. Developments in sedimentology, vol 60. Elsevier, Amsterdam
- Rebesco M, Camerlenghi A, Van Loon AJ (2008) Contourite research: a field in full development. In: Rebesco M, Camerlenghi A (eds) Contourites, Developments in Sedimentology, vol 60, pp 3–10
- Rebesco M, Pudsey CJ, Canals M et al (2002) Sediment drifts and deep-sea channel systems, Antarctic Peninsula Pacific margin. In: Stow DAV, Pudsey CJ, Howe JA, Faugères J-C, Viana AR (eds) Deep-water contourite systems: modern drifts and ancient series, seismic and sedimentary characteristics. Geological Society London Memoirs 22, pp 353–372
- Rebesco M, Wåhlin A, Laberg JS, Schauer A, Brezcynska-Möller A, Lucchi RG, Noormets R, Accettella D, Zarayskaya Y, Diviacco P (2013) Quaternary contourite drifts of the Western Spitsbergen margin. Deep-Sea Res Part I Oceanogr Res Pap 79:156–168
- Rebesco M, Hernández-Molina FJ, Van Rooij D et al (2014) Contourites and associated sediments controlled by deep-water circulation processes: state of the art and future considerations. Mar Geol 352:111–154
- Reed DL, Meyer AW, Silver EA, Prasetyo H (1987) Contourite sedimentation in an intra-oceanic forearc system: eastern Sunda Arc, Indonesia. Marine Geology, 76:223–242
- Reeder MS, Rothwell G, Stow DAV (2002) The sicilian gateway: anatomy of the deep-water connection between East and West Mediterranean basins. In: Stow DAV, Pudsey CJ, Howe JA, Faugères J-C, Viana AR (eds) Deep-water contourite systems: modern drifts and ancient series, seismic and sedimentary characteristics. Geological Society London Memoirs 22, pp 171–190
- Robinson SG, McCave IN (1994) Orbital forcing of bottom currents enhanced sedimentation on Feni drift, NE Atlantic, during the Mid-Pleistocene. Paleoceanography 9(6):943–972
- Shanmugam G (2000) 50 years of the turbidite paradigm (1950s to 1990s): deep-water processes and facies models—a critical perspective. Mar Pet Geol 17:285–342
- Shanmugam G (2003) Deep-marine tidal bottom currents and their reworked sands in modern and ancient submarine canyons. Mar Pet Geol 20(5):471–491
- Shanmugam G (2006) Deep-water bottom currents. Handb Petrol Explor Prod 5:85–139
- Shanmugam G (2012) New perspectives on deep-water sandstones: origin recognition, initiation, and reservoir quality. Elsevier, Oxford
- Shanmugam G, Spalding TD, Rosheart DH (1993) Process, sedimentology and reservoir quality of deep-marine bottom current reworked sands sandy contourites: an example from the Gulf of Mexico. AAPG Bull 77(7):1241–1259
- Stoker MS (1998) Sediment drift development on the Rockall continental margin, off NW Britain. In: Stoker MS, Evans D, Cramp A (eds) Geological processes on continental margins: sedimentation, mass wasting and stability. Geological Society London 129, pp 229–254
- Stoker MS, Akhurst C, Howe JA et al (1998) Sediment drifts and contourites on the continental margin, off Northwest Britain. Sed Geol 115(1–4):33–52
- Stow DAV (1979) Distinguishing between fine-grained turbidites and contourites on the Nova Scotian deep water margin. Sedimentology 26:371–387
- Stow DAV (1982) Bottom currents and contourites in the North Atlantic. Bulletin de l'Institut de Géologie du Bassin d'Aquitaine 31:151–166
- Stow DAV, Lovell JPB (1979) Contourites: their recognition in modern and ancient sediments. Earth-Sci Rev 14:251–291
- Stow DAV, Piper DJW (1984) Deep-water fine grained sediments: facies models. In: Stow DAV, Piper DJW (eds) Fine-grained sediments: deep-water processes and facies. Geological Society London Special Publication, vol 15, pp 611–646
- Stow DAV, Faugères JC (eds) (1993) Contourites and bottom currents. Sediments Geology (Special Issue) 82
- Stow DAV, Tabrez A (1998) Hemipelagites: facies, processes and models. Geological Society London Special Publication 129, pp 317–338
- Stow DAV, Mayall M (eds) (1999) Deep-water sedimentary systems: new models for the 21st century. Marine and Petroleum Geology Special Issue 17

- Stow DAV, Faugères JC (2008) Contourite facies and faces model. In: Rebesco M, Camerlenghi, A (eds) *Contourites. Developments in sedimentology*, vol 60, pp 223–250
- Stow DAV, Faugères JC, Gonthier E (1986) Facies distribution and textural variation in Faro drift contourites: velocity fluctuation and drift growth. *Mar Geol* 72:71–100
- Stow DAV, Faugères J, Viana A et al (1998) Fossil contourites: a critical review. *Sed Geol* 115(1–4):3–31
- Stow DAV, Faugères JC, Howe J et al (2002) Bottom currents, contourites and deep-sea sediment drifts: current state-of-the-art. In Stow DAV, Pudsey C, Howe J, Faugères JC, Viana A (eds) *Deep-water contourite systems: modern drifts and ancient series, seismic and sedimentary characteristics*. Geological Society London Memoirs 22, pp 7–20
- Stow DAV, Hunter S, Wilkinson D, Hernandez-Molina J (2008) The nature of contourite deposition. In: Rebesco M, Camerlenghi A (eds) *Contourites. Developments in Sedimentology*, vol 60, pp 143–156
- Stow DAV, Hernández-Molina FJ, Llave E et al (2009) Bedform-velocity matrix: the estimation of bottom current velocity from bedform observations. *Geology* 37:327–330
- Stow DAV, Hernández-Molina FJ, Alvarez Zarikian C et al (2013a) Mediterranean outflow: environmental significance of the Mediterranean outflow water. Integrated Ocean Drilling Program Management International Inc, Tokyo
- Stow DAV, Hernández-Molina FJ, Llave E et al (2013b) The Cadiz Contourite Channel: Sandy contourites, bedforms and dynamic current interaction. *Mar Geol* 343:99–114
- Viana A, Rebesco M (eds) (2007) Economic and paleoceanographic significance of contourite deposits. Geological Society London Special Publications 276
- Viana A, Faugeres JC, Stow DAV et al (1998a) Bottom-current controlled sand deposits: a review from modern shallow to deep water environments. *Sed Geol* 115:53–80
- Viana A, Faugeres JC, Kowsmann RO et al (1998b) Hydrology, morphology and sedimentology of the Campos continental margin, offshore Brazil. *Sed Geol* 115:133–158
- Wüst G (1933) Bodenwasser und Bodenkonfiguration der atlantischen Tiefsee. In: *Zeitschrift der Gesellschaft für Erdkunde*, pp 1–18
- Wynn RB, Stow DAV (eds) (2002) Recognition and interpretation of deep-water sediment waves. *Marine Geology Special Issue* 192 (1–3)
- Wynn RB, Masson DG (2008) Sediment waves and bedforms. In: Rebesco M, Camerlenghi A (eds) *Contourites. Developments in sedimentology*, vol 60, pp 289–300

Volcanic Islands and Seamounts

Daniele Casalbore

Abstract Recent advances in seafloor imagery systems have enabled the extensive mapping of submarine volcanic areas, depicting with unprecedented detail a large spectrum of landforms. They can be grouped in two main types: volcanic and erosive-depositional landforms, reflecting the interplay between constructive and destructive forces that control the growth and morphological evolution of volcanic edifices. Volcanic landforms mainly include primary volcanic constructs (cones, lava flows and delta, undifferentiated bedrock outcrops), but also volcano-tectonic features, such as caldera collapses. Erosive-depositional landforms typically cover most part of the volcanic flanks and include features related to wave erosion and sea-level fluctuations (insular shelves and guyots), gravity-driven instability processes (landslide scars), and density gravity flows (gullies, canyons, fan-shaped features, sediment waves). However, despite the large number of marine studies realized until now, we are still far from having a complete mapping of these areas as well as reliable models for the correct interpretation of several landforms, mainly because of the paucity of direct observations. A systematic monitoring of active processes is essential to understand the genesis and evolution of such phenomena; repeated multibeam surveys are playing a key role in this regard. Also the comparison and parameterization of these landforms in different settings can provide insights on the main factors controlling their genesis. But it is necessary to set shared and standardized protocols for the interpretation and analysis of morpho-bathymetric data, also in consideration of the exponential increase in data availability from these areas, whose study is becoming crucial for several disciplines.

D. Casalbore (✉)

Università Sapienza di Roma, Piazzale Aldo Moro 5, Rome, Italy
e-mail: daniele.casalbore@uniroma1.it

1 Introduction

Few geological processes capture the popular imagination and boost scientist's question for knowledge about our planet more than active volcanism. Volcanoes have played a major role in the evolution of our planet, but also represent one of the main geohazards for human communities, being able to alter social evolution, as demonstrated by the Minoan eruption of Santorini that buried flourishing Bronze Age settlements (Friedrich 2000). It has been estimated that volcanic hazard caused more than 270,000 casualties in the last five centuries (Auker et al. 2013), most of them being the direct or indirect (tsunamis) result of sector collapses affecting the flanks of insular volcanoes. Although decades of subaerial geological mapping have contributed to the understanding of how volcanic islands evolve, they often represent only the tip of large edifices rising for thousands of meters above the seafloor, as observed at Stromboli, where the 98% of the edifice lies underwater (Fig. 1). This implies that we are not able to reconstruct the thorough morpho-structural evolution of volcanic edifice without marine studies. These latter are essential for the study of seamounts, i.e. isolated underwater volcanic edifices that reach at least 1000 m in height (Menard 1964). Actually, modern studies identify seamounts as small as 50–100 m in height using high-resolution bathymetry (Smith and Cann 1990). Based on global satellite altimetry, Kim and Wessel (2011) recently identified ca. 25,000 potential seamounts with height >100 m (yellow points in Fig. 1).

However, we are still far from having real number of seamounts distribution, mainly due to lack of a full coverage of oceans by using swath bathymetry. Seafloor

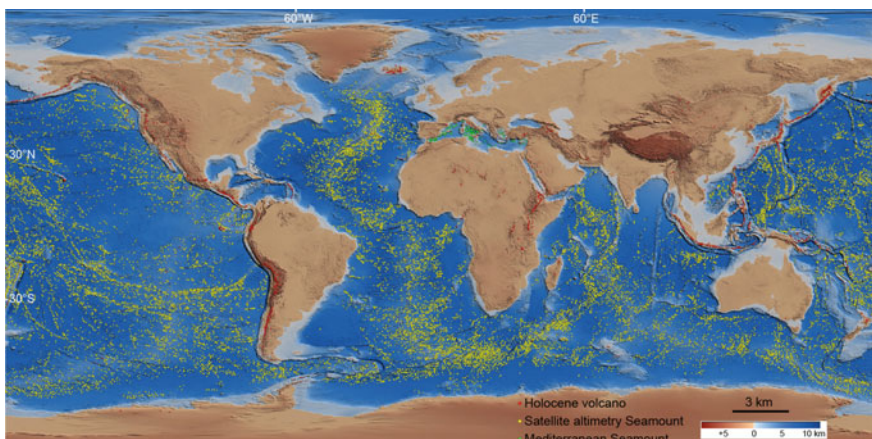


Fig. 1 Shaded relief map of the world (data from Ryan et al. 2009), with the distribution of Holocene volcanoes (data from the website volcano.si.edu/ge/GVPWorldVolcanoes.kml), seamounts derived from global satellite altimetry (Kim and Wessel 2011) and from the Atlas of the Mediterranean seamounts (Wurthz and Rovere 2015)

imagery systems are, in fact, playing a key role in the exploration of the oceans, changing our vision on the extent, distribution and variability of landforms. Moreover, the growing availability of detailed Digital Elevation Models is leading to the systematic parametrization of the volcanic edifices and associated landforms, providing insights on the complex interplay between volcanic, tectonic, erosive-depositional and eustatic processes controlling their genesis (e.g., Mitchell 2001; Ramalho et al. 2013; Grosse et al. 2014). In this regard, the present chapter would represent an outgrowth of the expanding interest in the geomorphology of submarine flanks of volcanic islands and seamounts. The study of these areas is becoming crucial for several disciplines, because of (a) the strong interaction between seamounts and geostrophic currents, (b) their role as hotspots of biodiversity, (c) the future harvesting of mineral resources, and (d) the geohazard related to volcanic activity and slope failures affecting volcanic edifices.

2 Submarine Geomorphology of Volcanic Islands and Seamounts

Morpho-bathymetric data collected in submarine volcanic areas has revealed a large suite of geomorphic features referable to two main types: volcanic and erosive-depositional landforms (Sect. 3). The growth and morphological evolution of volcanoes are, in fact, the result of interaction between constructive and destructive forces. The constructional processes prevail during the relatively short periods of eruptive activity, whereas destructive forces become dominant during the longer inter-eruption periods or when volcanic activity has ended. In order to evidence differences between “constructional” and “failed” flanks (i.e., dominated by mass-wasting processes), bathymetric cross-sections and graphs of cumulative surface gradients can be useful (Fig. 2, Mitchell et al. 2002). In the case of Stromboli edifice, characterized by a quasi-bilateral symmetry of the flanks with respect to its SW-NE rift axis (Romagnoli et al. 2009a), the NE and SW flanks show a large variability of slope gradients, reflecting the uneven morphology of constructional slopes. In contrast, the failed SE and NW flanks show a narrower distribution of slope values that linearly decrease with depth (Fig. 2).

3 Volcanic and Erosive-Depositional Landforms

Volcanic landforms include primary constructional and volcano-tectonic features, often representing the end-members of a continuum process. The most common volcanic landforms are cones (Sect. 3.1), lava flows and delta (Sect. 3.2), caldera collapses (Sect. 3.3) and undifferentiated bedrock outcrops. These latter are coherent and linear ridges, often oriented in a radial direction from the island.

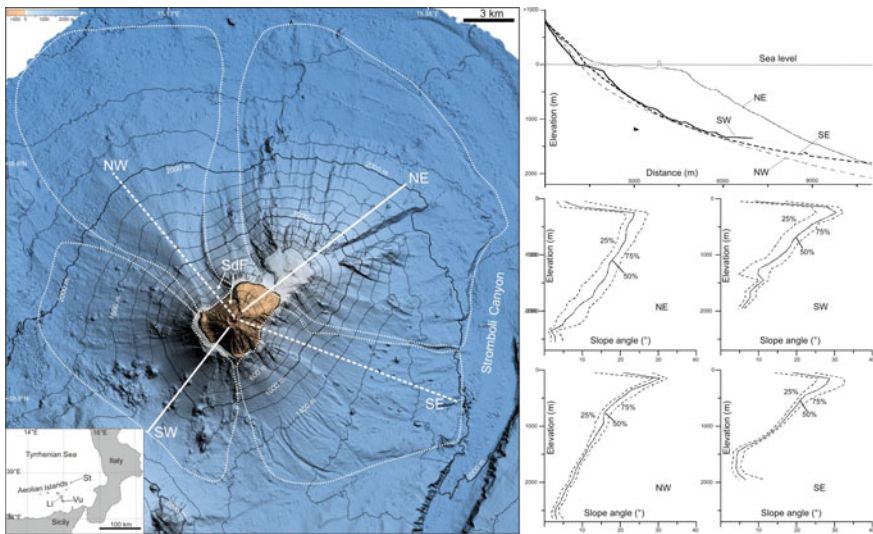


Fig. 2 On the *left*, shaded relief map of Stromboli edifice, with the location of the bathymetric cross-sections (white lines) shown in the *upper right*; *Sdf* Sciara del Fuoco. Dotted white lines delimit the areas where slope graphs, shown in the *lower right*, were computed (modified from Casalbore et al. 2010). Slope graphs were realized by sorting slope gradients within each flank for prefixed depth intervals, and a slope cumulative distribution is computed for each depth interval. Location of Aeolian Islands is shown in the *inset*; *St* Stromboli Island; *Li* Lipari Island, *Vu* Vulcano Island

Because of their degraded morphology, they are commonly interpreted as old remnants of bedrock outcrops carved by marine erosive activity.

Erosive-depositional landforms may cover instead most part of the submarine extent of a volcanic edifice, leading to its progressive enlargement and formation of a large volcanoclastic apron (Carey 2000). These landforms show a large variability in size and morphology, being the result of a large spectrum of sedimentary processes acting at different magnitudes and time scales. Based on the dominant processes involved in their formation, we can distinguish landforms associated to (a) wave erosion and sea-level fluctuations (Sect. 3.4), (b) gravity-driven instability processes (Sect. 3.5), (c) confined and unconfined gravity flows (Sect. 3.6).

3.1 Volcanic Cones

Volcanic cones may have conical or sub-conical shapes, be elongated along preferential directions or show a more complex shape. Moreover, they can be isolated, aligned along the main regional tectonic trend, or occur in clusters. The different distribution and shape of the cones provide insights into the interaction between magmatism and tectonics. Volcanic features radially oriented to the flank of the

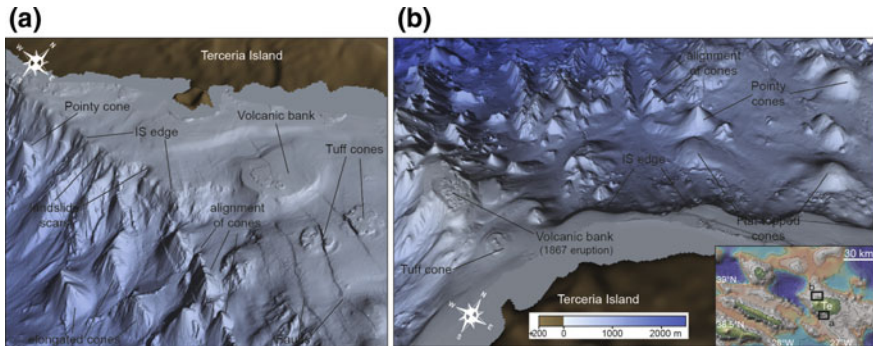


Fig. 3 3-D view (vertical exaggeration $\times 2.5$) of the SE (a) and NW (b) offshore of Terceira Island; see Sect. 3.1 for details

volcanic edifices, suggest that they are mainly the result of local magmatic stress (e.g., Tibaldi and Lagmay 2006). In contrast, elongated or aligned features indicate a main role played by regional tectonic lineaments. These latter are typically observed in tectonically-controlled setting, where they formed through systems of volcanic and tectonic fissures, which provide a preferential pathway for the ascent of magmas through the crust (e.g., Gudmundsson 1986; Searle et al. 2010). An example of these features is reported from Terceira offshore in the Azores (Fig. 3, Casalbo et al. 2015).

Based on their morphology, volcanic cones can be further divided into two main sub-types: pointy and flat-topped.

Pointy cones are found in all water depths and geodynamic settings, so that their shape is not indicative of specific environmental conditions and/or eruptive mechanisms. However, since high hydrostatic pressure reduces gas exsolution from magma and favors effusive eruptions, the deeper pointy cones should be presumably dominated by effusive activity with respect to shallow-waters cones, where the pyroclastic component increase. This latter becomes dominant in the case of tuff cones formed during surtseyan eruptions, i.e., phreatomagmatic eruptions characterized by violent explosions caused by rising magma coming into contact with sea-water. Tuff cones are commonly found in shallow-water sectors and are characterized by a flat summit, sub-concentric furrows and ridges, and other small circular features, that likely arose from episodic eruptions into shallow-water and subsequent wave erosion (Fig. 3). Wave erosion is a very efficient process in destroying volcanic cones made of poorly consolidated materials, as reported at Surtla and surrounding satellite vents during the 1963–1966 eruption (Romagnoli and Jakobsson 2015). More in general, submarine flat-topped cones are found at depths <-200 m as a consequence of wave reworking during sea-level fluctuations (Sect. 3.4). When the flat summit is much larger than their height, flat-topped cones are also named volcanic banks (Fig. 3).

Differently, flat-topped cones with larger basal diameters (1–5 km) and height of few hundreds of meters, were reported at depths >700 m along the submarine flanks

of Hawaiian Islands and Puna Ridge (Clague et al. 2000). These features appear to be monogenetic and they are probably formed during prolonged low to moderate effusion of magma, with low viscosities and volatile content on gentle slopes.

From a morphometric point of view, one of the main parameters used for the characterization of volcanic cones is the ratio between cone height and average basal diameter, providing insights both on the degree of erosion of the cones and on the geodynamic setting where they form (Fornaciai et al. 2012). It is noteworthy the most significant advances in our understanding of the formation and morphological evolution of volcanic cones come from repeated bathymetric surveys, as reported from the Monowai Seamount (Watts et al. 2012) or offshore El Hierro Island (Rivera et al. 2013).

3.2 *Lava Flows and Lava-Fed Deltas*

Submarine lava flows are generally characterized by distinctive lobate outlines, high acoustic reflectivity, low relief, and a rugged surface texture. In some cases, submarine effusive activity can form complex lava fields, where it is difficult to recognize the single lava flows.

Because of the paucity of direct observations of active submarine eruptions, lava flow morphology can provide insights on eruptive processes. Most of the studies on submarine lava flows were realized along the Mid-Oceanic Ridges, where ship-based bathymetry allowed to depict only the gross morphology of lava flows, so their emplacement mechanisms were mainly reconstructed through visual inspections. Only a few, recent studies are trying to merge visual observations with ultra-high resolution multibeam bathymetry collected using AUV to map the variability of morpho-facies and structures of the submarine lava flows at metric or sub-metric scale (Caress et al. 2012; McClinton and White 2015).

It is even more surprisingly that very few studies were realized on submarine lava flows in shallow-water setting and more in general on the behavior of subaerial lava flows penetrating into the water. In general, this behavior seems to be mostly controlled by the lava flow type: pāhoehoe and ‘a’ā. The latter flows show a more coherent behavior under water with respect to pāhoehoe flows, which are often completely disintegrated to form breccias. This is likely due to the lower thickness and greater vesicularity, permeability, and joint density characterizing pāhoehoe lava flows with respect to the ‘a’ā type (Stevenson et al. 2012 and reference therein). Moreover, it is noteworthy that ‘a’ā and more generally silica-rich flows are able to form a thick carapace that would favor the thermal insulation of lava flows from the sea water, and thus their movement on the seafloor in a caterpillar-like fashion. An impressive example of submarine extent of silica-rich flows is recognizable in the NE part of Lipari, where they move down ~900 m for a length of ca. 3 km (Fig. 4a, Casalbore et al. 2016).

Prolonged lava flows penetrating into the sea are also able to form lava-fed delta along the coastline. Also in this case, the emergent part of these landforms has been

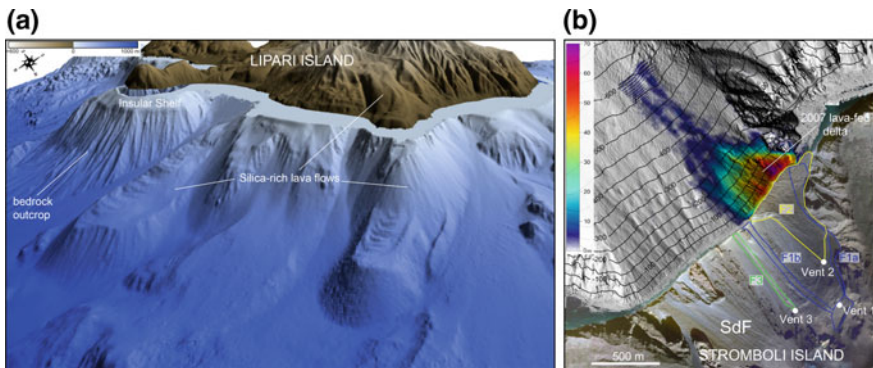


Fig. 4 3-D view of the NE flank of Lipari, where two lava flows are recognizable, representing the offshore extent of subaerial silica-rich coulee. On the right, aerial photo of Sciara del Fuoco (*SdF* location in Fig. 2) and bathymetric residual map between the pre- and post-2007 eruption surveys draped over post-2007 eruption bathymetry (modified from Bosman et al. 2014). The values in the *scale bar* indicate the thickness in meters of seafloor accretion due to the emplacement of the delta fed by subaerial lava flows emitted during the 2007 eruption, whose limits are indicated by the *green, blue and yellow lines*

studied and monitored in detail, whereas little is known about their subaqueous counterpart (Mitchell et al. 2008). The only example of bathymetric monitoring of an active lava-fed deltas was realized during the 2007 eruption at Stromboli Volcano (Fig. 4b, Bosman et al. 2014), allowing to constrain the main processes responsible for its emplacement and growth. In detail, this study have shown that (a) the position and rate of delta accretion are strongly dependent on feeding points and effusion rates; (b) the slope gradients and morphology of the basal surface control the overall delta architecture and the amount of volcaniclastic debris, (c) sudden collapse of portions of the submarine delta may occur simultaneously with volcanic accretion, with implication on the correct estimation of the emplaced volume and effusion rates.

3.3 Caldera Collapses

Calderas are circular depressions observed on many volcanoes, with diameters ranging from few up to tens of kms. They occur in all geodynamic setting and their formation has been commonly related to vertical collapse of the roof of a magma chamber during large eruptions. Because of their hazard potential, but also their link to ore deposits and geothermal energy resources, a worldwide database of calderas has been recently realized (Geyer and Marty 2008). In submarine setting, most studies on submarine calderas focused on basaltic volcanoes associated with mid-ocean ridges or intraplate hotspot volcanism. In these cases, caldera formation is thought to represent the result of syn- or post-eruption collapse following magma

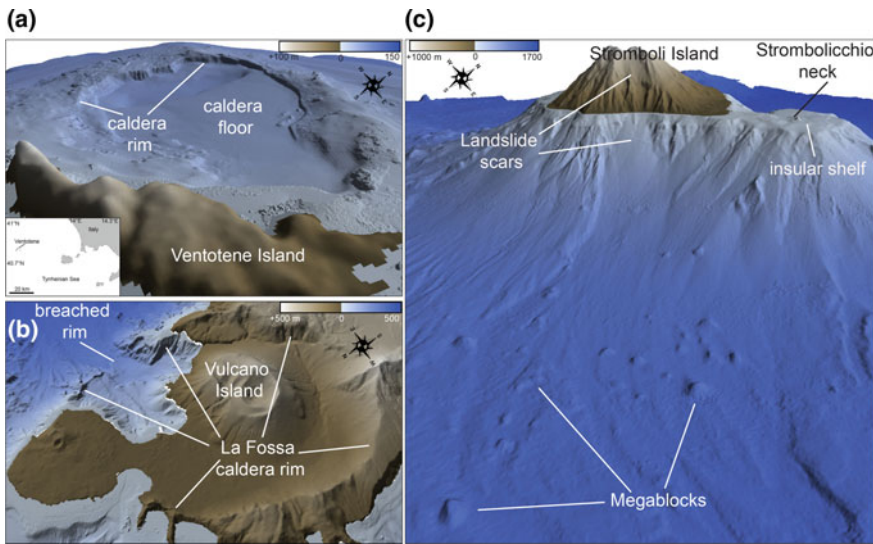


Fig. 5 On the left, 3-D view (vertical exaggeration $\times 2$) of the caldera depressions recognized off Ventotene (**a** location in the inset) and Vulcano (**b** location in the inset of Fig. 2) Islands; see Sect. 3.3 for further details. On the right, 3-D view of the eastern, failed (Sect. 3.5) flank of Stromboli island; note also the presence of a wide insular shelf around Strombolicchio neck (Sect. 3.4)

withdrawal, from a central magmatic conduit to supply flank eruptions (e.g., Fornari et al. 1984). Calderas are also frequently observed at submarine arc volcanoes, where they have been associated to large explosive eruptions (e.g., Wright and Gamble 1999).

A caldera collapse typically displays a flat floor bounded by high and steep scarp forming the caldera rim, as shown in Fig. 5a off Ventotene Island (Casalbore et al. 2014a). This caldera is 4×2.5 km in size and its formation has been related to a large explosive eruption occurred at between 0.15–0.3 Ma. In other cases, caldera depressions can be the result of multiple coalescing collapses, as for instance observed at La Fossa Caldera (Vulcano Island, Fig. 5b; Romagnoli et al. 2012 and reference therein). The NE part of the caldera lies under water and its rim was partially breached by marine retrogressive erosion, leading to the successive dismantling of the submarine caldera infilling.

3.4 Landforms Associated to Wave Erosion and Sea-Level Fluctuations

These landforms typically display a planar summit surface and are found at depths <200 m, exception made for areas affected by long-term subsidence. In the Sect. 3.1,

we have already seen as shallow-water flat-topped cones can be interpreted as the result of wave erosion cutting the summit of pointy cones. Wave erosion is, in fact, responsible for the development around volcanic islands of shore platforms that initiate as soon as volcanism wanes during stable relative sea levels (Trenhaile 2000). These features progressively evolve into reefless insular shelves as surf migrates landward and seaward with changing sea levels (Quartau et al. 2010). At Stromboli, for instance, a wide shelf formed around the Strombolicchio neck (Fig. 5c), representing the remnant of an older eroded volcano dated at ca. 200 ka (Gillot and Keller 1993) whose conical summit has been completely dismantled by erosion. The shelf edge is located at ca. -130 m, just corresponding to the lowest level reached by the sea during the Last Glacial Maximum about 20 ka ago.

Once these shelves are formed, their size and morphology is mainly controlled by the competition between wave erosion that enlarges them and volcanic progradation that reduces their size. Shelf width generally tends to increase with exposure to wave action through time and a direct relationship between shelf age and shelf width is often observed (Quartau et al. 2014 and reference therein).

Another typical landform associated to wave erosion is guyot, i.e. seamount having a smooth and flat top. Its formation is similarly related to wave cut of a volcanic island, but it also undergo coral reef or atoll formation and lagoonal infilling, and then subside through the bank stage (at depths <200 m) to become a guyot.

3.5 Landforms Related to Gravity-Driven Instability Processes

Because of their rapid growth, volcanoes may become unstable and experience failure at any spatial from minor rock falls up to catastrophic collapses involving volumes up to thousands of cubic kilometers. The predisposing factors for volcano instability are manifold, encompassing internal and external causes (McGuire 2006). The triggering of the collapse is typically associated to a short-live dynamic event, such as an earthquake or dyke intrusion.

A collapsed flank is morphologically characterized by horseshoe-shaped scars in source area, and by fan-shaped features with hummocky terrains and megablocks (i.e. debris avalanche deposits) in depositional area, as observed along the E flank of Stromboli (Fig. 5c). Multiple collapses are observed in many volcanoes, such as in the NW Stromboli affected by 4 coaxial collapses in the last 13 ka (Tibaldi 2001), forming a large fan-shaped bulge at the base of the Sciara del Fuoco (SdF in Fig. 2; Romagnoli et al. 2009b). This is likely due to the fact that a failed flank becomes a weakness zone within the edifice and can lead to a depressurization of the underlying magma chamber, focusing subsequent volcanic activity within and along the collapsed area (Tibaldi et al. 2009 and reference therein). Likewise, the occurrence of large-scale collapses perpendicular to the main axial rift zone (Fig. 2)

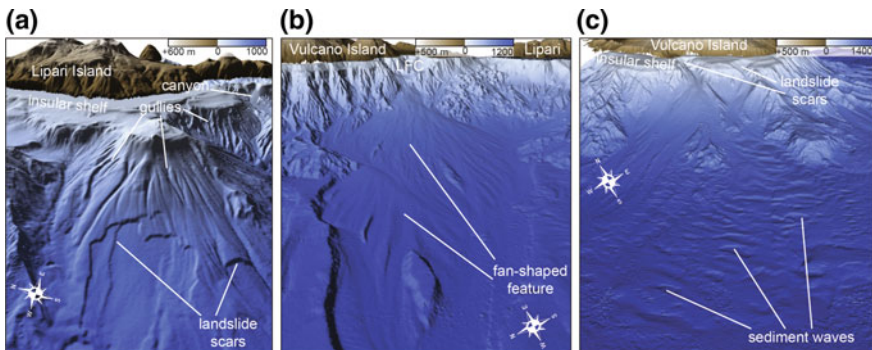


Fig. 6 3-D view (vertical exaggeration $\times 2$) of the W flank of Lipari Island (a), NE (b) and SW (c) flanks of Vulcano Island, where several erosive-depositional landforms were identified (see Sects. 3.4, 3.5 and 3.6 for further details). Location of the islands is shown in the inset of Fig. 2

is a common feature observed for volcanic edifices lying in extensional regimes. It can be explained by the outward flank displacement due to the dykes intrusion along the rift zone (Voight and Elsworth 1997).

Smaller landslides are also widespread along the flanks of volcanic edifices, commonly occurring at higher frequency with respect to the large events. In the active NW flank of Stromboli, a tsunamigenic submarine landslide occurred on the 30th December 2002, with a maximum observed run-up of 10 m. The extent and geometry of the failure were reconstructed through the comparison of pre- and post-slide bathymetries, allowing to compute a mobilized volume of ca. $10 \times 10^6 \text{ m}^3$ (Chiocci et al. 2008). The same authors interpreted the high gradients and the presence of volcaniclastic layers within the slope as the main predisposing factors for the slope failure. Volcaniclastic layers, in fact, may act as weakness levels due to their particular shear behavior (low grain resistance) if sudden strain/stress increments occur.

Slide scars at hundred-meters scale are often recognized at the edge of the insular shelf or along the older volcanic flanks draped by a relevant sedimentary cover (Fig. 6a). Deposits related to these scars are often not recognizable on the bathymetry, likely due to the fact that landslide mass either lost cohesion during failure or failed as a cohesive mass and disintegrated downslope.

3.6 Landforms Related to Confined/Unconfined Density Gravity Flows

Landforms typically related to confined density gravity flows are mainly gullies and canyons. Gullies are narrow channelized features at hundred-meter length, commonly having a V-shape section. They are mostly located in the upper part of the

submarine slope, mainly carving the volcanic bedrock. However, gullies can also radially affect the sedimentary blanket covering the flanks of old volcanic cones (Fig. 6a).

Canyons are larger and longer channelized features, often draining the entire submarine flanks. The most active canyons strongly indent the insular shelf, arriving up to few hundreds of meters far from the coast (Fig. 6a). Small and crescent-shaped seafloor waveforms within their thalweg are considered as a proxy of active sedimentary dynamics (e.g., Babonneau et al. 2013).

The most common landforms associated to unconfined gravity flows are fan-shaped deposits, often found at the base of the channelized features, where a marked decrease of slope gradients occur. These landforms can range in width from some hundreds of meters up to thousands of kms (Cilaos fan off La Reunion Island, Sisavath et al. 2011). Their size mainly depends on the availability of sediments from the source area (the drainage basin of a river, climate conditions, abundance of loose volcaniclastic material) as well as by the morphological link between sub-aerial and submarine slope. An example of large fan-shaped feature is shown at the base of La Fossa Caldera (Fig. 6b), covering an area of 20 km² between –350 and –1150 m. This feature is characterized both by a swale and ridge morphology and the lacking of hummocky terrains, indicating that its formation is likely the result of the gradual stacking of gravity flows, fed by the dismantling of the La Fossa caldera infill (Sect. 3.3).

Large sediment waves, with wavelength of several hundreds of meters and wave height up to tens of meters are another common landform associated to unconfined gravity flows along the flank of volcanic islands (Fig. 6c; Wynn et al. 2000; Leat et al. 2010; Sisavath et al. 2011; Casalbore et al. 2014b).

4 Gaps in Present-Day Knowledge and Perspectives for the Future

The previous sections have shown how the submarine flanks of volcanic islands and seamounts are characterized by several volcanic and erosive-depositional landforms. Of course, the presented landforms do not exhaust the list of the landforms recognisable in these areas, but they are likely the most common features. For the sake of clarity, only landforms whose formation can be attributed to well-defined processes have been presented, but the interpretation of submarine volcanic landforms is often more problematic. This is intrinsically due to the fact that a landform can be the result of different processes or a complex interplay of multiple processes operating at different temporal scale. In addition, reliable models for the genesis of several landforms in the submarine environment are often lacking, mainly in relation to the paucity of direct observations. Their interpretation is often based on the results of laboratory studies and/or the comparison with similar phenomena observed onland, where their formation can be more easily monitored. However,

some landforms and associated processes are exclusive of the marine environment and their study requires *in situ* monitoring. In this regard, repeated bathymetric surveys are a fundamental tool for monitoring the evolution of a landform and link it with own genetic process, especially if integrated by direct observations.

The comparison and systematic parameterisation of submarine volcanic landforms in different settings can represent a further and low-cost step to better constraints the factors controlling their formation and development. In contrast to terrestrial applications, the use of such techniques in the marine environment is still in its infancy (Lecours et al. 2016). In order to exploit the full potential of such analysis, methods and interpretations need to be standardized, particularly in view of issues specific to the marine environment. This means that a great effort has to be realized by geoscientist working in submarine and subaerial volcanic areas to set shared protocols for the interpretation and analysis of submarine volcanic landforms, taking into account the lessons learned from terrestrial volcanic geomorphology (Thouret 1999). In the next years, it is predictable an exponential increase in data availability from submarine volcanic areas, considering (a) the recent advances in quality and cost-effectiveness of available technologies, (b) the growing interest for the functioning of deep-sea systems and (c) the large areas that have not been surveyed, yet.

As volcanic island is concerned, another main gap remains the link between their subaerial and submarine morphology. Indeed, although the evolution of volcanic islands is continuous above and below sea level, scientists are not always able to reconcile the onshore and offshore data in a consistent way (Quartau et al. 2014). This is due to the fact that bathymetric surveys in shallow-water are very time-consuming, but also to the paucity of multidisciplinary studies involving field volcanologists and marine geologists. However, it is fundamental to improve our ability to integrate these data, because submarine information provides complementary evidence not visible above sea level and vice versa, mainly in consideration that coastal volcanic processes can directly impact the life of local communities.

Acknowledgements This chapter is the result of several fruitful discussions with many colleagues in the last 15 years. Particular thanks are due to Francesco Latino Chiocci, Claudio Romagnoli, Alessandro Bosman and Eleonora Martorelli that introduced me in the marine study of insular volcanoes. Similarly, the data presented in this work are the results of several projects and cruises realized in the last 20 years by IGAG-CNR, University Sapienza of Rome and Bologna. Specifically, data around Italian insular volcanoes were collected aboard R/V *Urania* and *Thetis* (CNR) and *Universitatis* (CoNISMA), mainly in the framework of DPC-GNV projects and the MaGIC Project. Data around Terceira Island were collected aboard the launch *Haliotis* and the R/V *L'Atalante* within the framework of the EUROFLEET project “Features of Azores and Italian Volcanic Islands”, <http://dx.doi.org/10.17600/11120030>. I would also acknowledge Alessandro Tibaldi for his suggestions that improved the quality of the paper.

References

- Auker MR, Sparks RSJ, Siebert L, Crosweller HS, Ewert J (2013) A statistical analysis of the global historical volcanic fatalities record. *J Appl Volcanol* 2(1):1–24
- Babonneau N, Delacourt C, Cancouët R, Sisavath E, Bachélery P, Mazuel A, Jorry SJ, Deschamps A, Ammann J, Villeneuve N (2013) Direct sediment transfer from land to deep-sea: insights into shallow multibeam bathymetry at La Réunion Island. *Mar Geol* 346:47–57
- Bosman A, Casalbore D, Romagnoli C, Chiocci FL (2014) Formation of an ‘āā lava delta: insights from time-lapse multibeam bathymetry and direct observations during the Stromboli 2007 eruption. *Bull Volcanol* 76(7):1–12
- Caress DW, Clague DA, Paduan JB, Martin J, Dreyer B, Chadwick WW Jr, Denny A, Kelley DS (2012) Repeat bathymetric surveys at 1-metre resolution of lava flows erupted at Axial Seamount in April 2011. *Nat Geosci* 5:483–488
- Carey S (2000) Volcaniclastic sedimentation around island arcs. In: Sigurdsson H (ed) *Encyclopedia of volcanoes*. Academic Press, San Diego, pp 627–642
- Casalbore D, Romagnoli C, Chiocci FL, Frezza V (2010) Morphosedimentary characteristics of the volcaniclastic apron around Stromboli volcano (Italy). *Mar Geol* 269:132–148
- Casalbore D, Bosman A, Martorelli E, Sposato A, Chiocci FL (2014a) Mass wasting features on the submarine flanks of Ventotene volcanic edifice (Tyrrhenian Sea, Italy). In: Krastel et al. (eds) *Submarine mass movements and their consequences advances in natural and technological hazards research*. vol 37, Springer, Heidelberg, pp 285–293
- Casalbore D, Bosman A, Romagnoli C, Chiocci FL (2014b) Large-scale seafloor waveforms on the flanks of insular volcanoes (Aeolian Archipelago, Italy), with inferences about their origin. *Mar Geol* 355:318–329
- Casalbore D, Romagnoli C, Pimentel A, Quartau R, Casas D, Ercilla G, Hipolito A, Sposato A, Chiocci FL (2015) Volcanic, tectonic and mass-wasting processes offshore Terceira Island (Azores) revealed by high-resolution seafloor mapping. *Bull Volcanol* 77:1–19
- Casalbore D, Bosman A, Romagnoli C, Di Filippo M, Chiocci FL (2016) Morphology of Lipari offshore (Southern Tyrrhenian Sea). *J Maps* 12(1):77–86
- Chiocci FL, Romagnoli C, Tommasi P, Bosman A (2008) Stromboli 2002 tsunamigenic submarine slide: characteristics and possible failure mechanisms. *J Geophys Res* 113:B10102
- Clague DA, Moore JG, Reynolds JR (2000) Formation of submarine flat-topped volcanic cones in Hawai‘i. *Bull Volcanol* 62(3):214–233
- Formaciai A, Behncke B, Favalli M, Neri M, Tarquini S, Boschi E (2012) Morphometry of scoria cones, and their relation to geodynamic setting: a DEM-based analysis. *J Volcanol Geotherm Res* 217–218:56–71
- Fornari DJ, Ryan WBF, Fox PJ (1984) The evolution of craters and calderas on young seamounts: insights from sea MARC 1 and SEABEAM sonar surveys of a small seamount group near the axis of the East Pacific Rise at 108° N. *J Geophys Res* 89:11069–11083
- Friedrich W (2000) *Fire in the sea, the Santorini Volcano: natural history and the legend of Atlantis*. Cambridge University Press, Cambridge
- Geyer A, Martí J (2008) The new worldwide Collapse Caldera Database (CCDB): a tool for studying and understanding caldera processes. *J Volcanol Geotherm Res* 175:334–354
- Gillot PY, Keller J (1993) Radiochronological dating of Stromboli. *Acta Vulcanol* 3:69–77
- Grosse P, van Wyk de Vries B, Euillardes PA, Euillardes LD (2014) A global database of composite volcano morphometry. *Bull Volcanol* 76:784
- Gudmundsson A (1986) Mechanical aspects of postglacial volcanism and tectonics of the Reykjanes Peninsula, southwest Iceland. *J Geophys Res* 91(B12):12711–12721
- Kim SS, Wessel P (2011) New global seamount census from altimetry-derived gravity data. *Geophys J Int* 186(2):615–631

- Leat P, Tate AJ, Tappin DR, Day SJ, Owen MJ (2010) Growth and mass wasting of volcanic centers in the northern south sandwich arc, South Atlantic, revealed by new multibeam mapping. *Mar Geol* 275:110–126
- Lecours V, Dolan MF, Micallef A, Lucieer VL (2016) Characterising the ocean frontier: a review of marine geomorphometry. *Hydrol Earth Syst Sci Discuss.* doi:[10.5194/hess-2016-73](https://doi.org/10.5194/hess-2016-73)
- McClinton JT, White SM (2015) Emplacement of submarine lava flow fields: a geomorphological model from the Niños eruption at the Galapagos Spreading Center. *Geochem Geophys Geosyst* 16:899–911
- McGuire W (2006) Lateral collapse and tsunamigenic potential of marine volcanoes. In: Troise C, De Natale G, Kilburn CRJ (eds) Mechanisms of activity and unrest at large calderas. *Geol Soc, London, Spec Publ* 269:121–140
- Menard HW (1964) Marine geology of the Pacific. McGraw-Hill, New York
- Mitchell NC (2001) Transition from circular to stellate forms of submarine volcanoes. *J Geophys Res* 106:1987–2003
- Mitchell NC, Masson DG, Watts AB, Gee MJR, Urgeles R (2002) The morphology of the submarine flanks of volcanic ocean islands. A comparative study of the Canary and Hawaiian hotspot islands. *J Volcanol Geoth Res* 115:83–107
- Mitchell NC, Beir C, Rosin PL, Quartau R (2008) Tempera F (2008) Lava penetrating water: submarine lava flows around the coasts of Pico Island Azores. *Geochem Geophys Geosyst* 9: Q03024. doi:[10.1029/2007GC001725](https://doi.org/10.1029/2007GC001725)
- Quartau R, Trenhaile AS, Mitchell NC, Tempera F (2010) Development of volcanic insular shelves: insights from observations and modelling of Faial Island in the Azores Archipelago. *Mar Geol* 275:66–83
- Quartau R, Hipólito A, Romagnoli C, Casalbore D, Madeira J, Tempera F, Roque C, Chiocci FL (2014) The morphology of insular shelves as a key for understanding the geological evolution of volcanic islands: insights from Terceira Island (Azores). *Geochem Geophys Geosyst* 15:1801–1826
- Ramalho RS, Quartau R, Trenhaile AS, Mitchell NC, Woodroffe CD, Avila SP (2013) Coastal evolution on volcanic oceanic islands: a complex interplay between volcanism, erosion, sedimentation, sea-level change and biogenic production. *Earth Sci Rev* 127:140–170
- Rivera J, Lastras G, Canals M, Acosta J, Arrese B, Hermida N, Micallef A, Tello O, Amblas D (2013) Construction of an oceanic island: insights from the El Hierro (Canary islands) 2011–2012 submarine volcanic eruption. *Geology* 41:355–358
- Romagnoli C, Jakobsson SP (2015) Post-eruptive morphological evolution of island volcanoes: Surtsey as a modern case study. *Geomorphology* 250:384–396
- Romagnoli C, Casalbore D, Chiocci FL, Bosman A (2009a) Offshore evidence of large-scale lateral collapses on the eastern flank of Stromboli, Italy, due to structurally controlled, bilateral flank instability. *Mar Geol* 262:1–13
- Romagnoli C, Kokelaar P, Casalbore D, Chiocci FL (2009b) Lateral collapses and active sedimentary processes on the northwestern flank of Stromboli volcano, Italy. *Mar Geol* 265:101–119
- Romagnoli C, Casalbore D, Chiocci FL (2012) La Fossa caldera breaching and submarine erosion (Vulcano island, Italy). *Mar Geol* 303–306:87–98
- Ryan WBF, Carbotte SM, Coplan JO et al (2009) Global multi-resolution topography synthesis. *Geochem Geophys Geosyst* 10:Q03014
- Searle RC, Murton BJ, Achenbach K et al (2010) Structure and development of an axial volcanic ridge: Mid-Atlantic Ridge, 45° N. *Earth Planet Sci Lett* 299(1):228–241
- Sisavath E, Babonneau N, Saint-ange F, Bachélery P, Jorry SJ, Deplus C, De Voogd B, Savoye B (2011) Morphology and sedimentary architecture of a modern volcaniclastic turbidite system: the Cilaos fan, offshore La Réunion Island. *Mar Geol* 288:1–17
- Smith DK, Cann JR (1990) Hundreds of small volcanoes on the median valley floor of the Mid-Atlantic Ridge at 24–30° N. *Nature* 348:152–155

- Stevenson JA, Mitchell NC, Mochrie F, Cassidy M, Pinkerton H (2012) Lava penetrating water: the different behaviours of pahoehoe and ‘a‘a at the Nesjahraun, Pingvellir, Iceland. *Bull Volcanol* 74:33–46
- Thouret JC (1999) Volcanic geomorphology—an overview. *Earth Sci Rev* 47(1):95–131
- Tibaldi A (2001) Multiple sector collapses at Stromboli volcano, Italy: how they work. *Bull Volcanol* 63:112–125
- Tibaldi A, Lagmay AMF (2006) Interaction between volcanoes and their basement. *J Volcanol Geotherm Res* 158(1):1–5
- Tibaldi A, Corazzato C, Marani MP, Gamberi F (2009) Subaerial–submarine evidence of structures feeding magma to Stromboli Volcano, Italy, and relations with edifice flank failure and creep. *Tectonophysics* 469:112–136
- Trenhaile AS (2000) Modeling the development of wave-cut platforms. *Mar Geol* 166:163–178
- Voight B, Elsworth D (1997) Failure of volcano slopes. *Geotechnique* 47:1–31
- Watts AB, Peirce C, Grevemeyer I, Paulatto M, Stratford W, Bassett D, Hunter JA, Kalnins LM, de Ronde CEJ (2012) Rapid rates of growth and collapse of Monowai submarine volcano in the Kermadec Arc. *Nat Geosci* 5:510–515
- Wright IC, Gamble JA (1999) Southern Kermadec submarine caldera arc volcanoes (SW Pacific): caldera formation by effusive and pyroclastic eruption. *Mar Geol* 161:207–227
- Wurthz M, Rovere M (2015) Atlas of the Mediterranean seamounts and seamount-like structures. IUCN, Malaga
- Wynn RB, Masson DG, Stow DAV, Weaver PPE (2000) Turbidity current sediment waves on the submarine slopes of the western Canary Islands. *Mar Geol* 163:185–198

Mid-ocean Ridges

Neil C. Mitchell

Abstract Mid-ocean ridges illustrate well how volcanic, tectonic, hydrothermal and sedimentary processes sculpt geomorphology in the deep ocean. Because of their poor accessibility (lying 2700 m below sea level on average) and remote locations, the development and deployment of new technology has been important for the discovery and investigation of new features. In contrast with continental environments, erosion has only modestly affected these areas, so features can be well preserved, in particular, volcanic landforms. The eruption of lavas creates volcanic cones, ridges of hummocky flows, widespread low-relief flows and drain-back features in lava lakes. Plate-tectonic extension creates faults, many with moderate dips, as inferred from the earthquakes they produce. However, other faults with presently shallower dips are suggested by corrugated slip surfaces exposed at the seabed on slow-spreading ridges. Steep scarps, comprising fractured rock and in places weak lithologies such as serpentinite, are easily destabilized, producing landslides, talus cones and talus ramps. Seawaters penetrating the crust and heated by it produce hydrothermal springs, such as spectacular “black smokers”. Precipitation of sulphides from those exhaling fluids and their deposition produces smooth mats of sediment and chimneys that can collapse to contribute to the sedimentary deposits as talus. This combination of processes makes mid-ocean ridges fascinating environments to work on, representing how >60% of Earth’s solid (oceanic) crust has been created. Despite poor accessibility of such areas, researchers will likely continue to deploy new instruments as they are developed to reveal more details of mid-ocean ridge geomorphology and understanding of how it develops.

N.C. Mitchell (✉)

School of Earth and Environmental Sciences, University of Manchester,
Williamson Bldg, Oxford Road, Manchester M139PL, UK
e-mail: Neil.mitchell@manchester.ac.uk

1 Introduction

Mid-ocean ridges occur where Earth's oceanic tectonic plates are separating and the gap between them is being filled by hotter upwelling mantle rocks (Fig. 1a). Those hotter rocks have lower density than mantle rocks beneath older oceanic crust, hence their relative buoyancy has created ridges on Earth's solid surface. In practice, these are only visible as ridges in topographic cross-sections of large vertical exaggeration. At the ridge crest itself (the "axis"), the lithosphere is rifting. This process has produced many normal faults, which form linear escarpments on the seabed. Where the plates are separating slowly, the uppermost mantle has become colder and more rigid than where plates are separating rapidly. In slow-spreading ridges, where the lithosphere is thick, we commonly find a rift valley, a feature that has been ascribed to a steady-state necking of the lithosphere (Tapponier and Francheteau 1978) or to viscous head loss in the asthenospheric mantle rising between the plates (Ribe 1988). At fast spreading ridges, in contrast, the lithosphere is hotter and thinner, so the axial valley is commonly very narrow and shallow or non-existent, commonly replaced with a narrow ridge. Also a result of the plate separation, pressure in the upwelling mantle progressively decreases, causing partial melting. Those 'melts' percolate up towards the surface, where they intrude the crust (which hence is largely formed of gabbroic intrusions). Injections of melt into the brittle crust create the dyke complex and occasional eruptions at the solid surface produce a variety of volcanic landforms (lava flows, ridges, cones and seamounts).

The spreading described above is organized into segments of the ridge, which can be viewed roughly as composite rifting volcanoes. Between those "spreading segments", the movement can be accommodated by strike-slip faults, which commonly lie within deep "transform valleys" oriented perpendicular to the

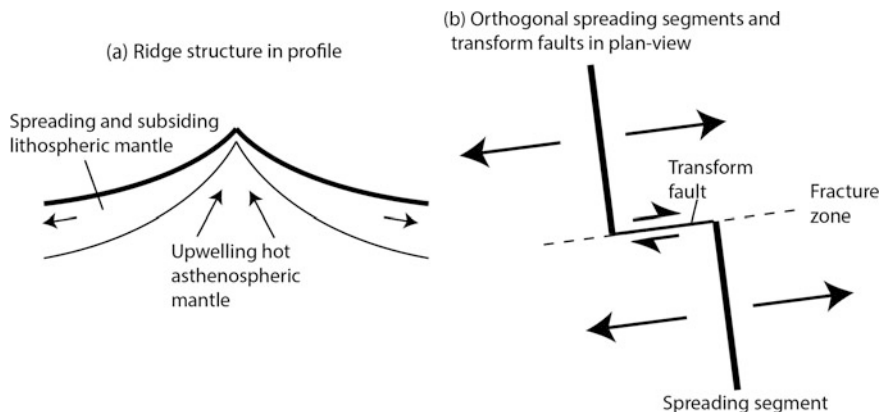


Fig. 1 **a** Regional profile of a mid-ocean ridge illustrating seafloor spreading. **b** Plan-view pattern of orthogonal spreading segments and transform faults

spreading segments (Figs. 1b and 2a). In contrast, in places where the distances between segments are small, the strike-slip movement instead can be accommodated without a through-going fault, in a more complicated way involving both

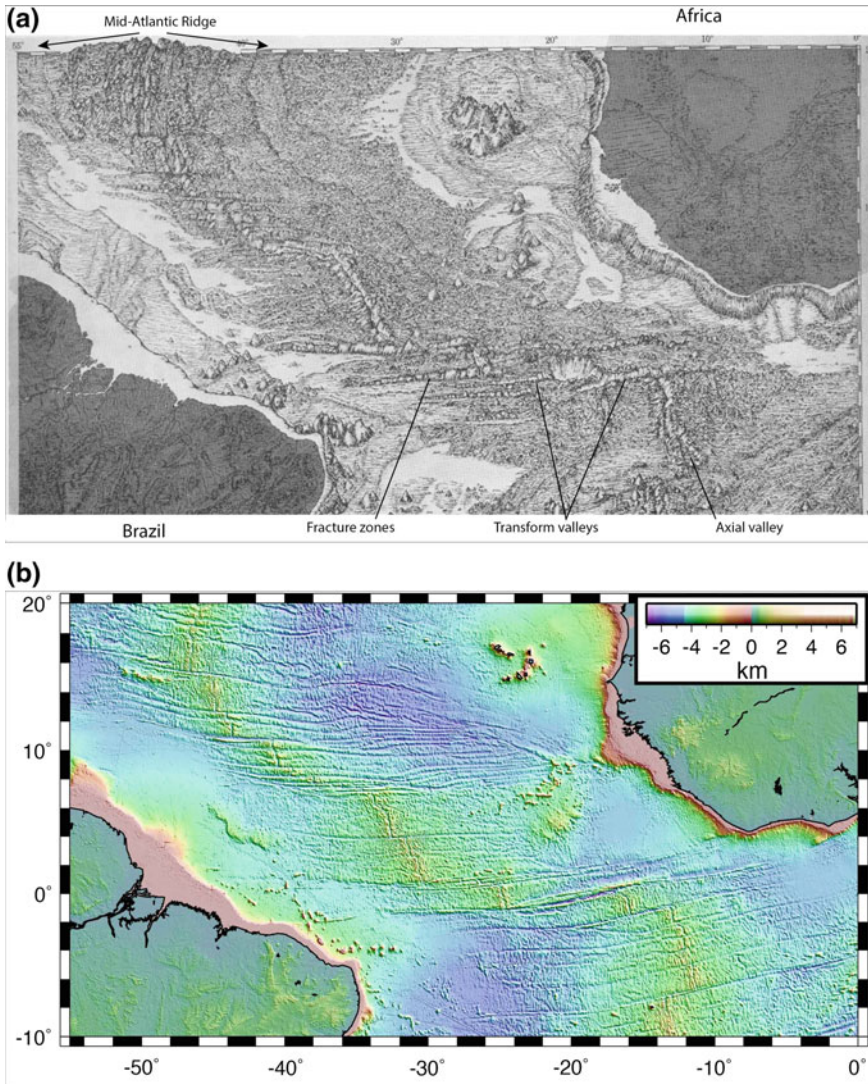


Fig. 2 Bathymetry maps of the central-north Atlantic illustrating our improved view of regional geomorphology that has accompanied technological improvements. **a** Physiography based on sparse echo-soundings of research vessels (Heezen and Tharp 1961). **b** Bathymetry obtained by interpolating between echo-soundings with the gravity field derived from sea-surface shape from satellite altimeters (Becker et al. 2009; Smith and Sandwell 1997). (Reprinted from Mitchell 2015, with permission from Elsevier.)

extension and strike-slip movement (by “transtensional” fault movements and/or by oblique volcanic intrusions). These features are called “non-transform discontinuities”.

Mid-ocean ridges lie above sea level in only a few isolated places (such as on Iceland and in the Afar region of Africa). Elsewhere, their crests lie at an average water depth of 2700 m. Because of their poor accessibility, the development and deployment of new technology has been important in the history of how the mid-ocean ridges have been explored, starting with the early lead-line soundings for telephone cable routes in the 19th Century, which first outlined the regional shapes of the ridges, to modern research using high-resolution multibeam sonars deployed near the bed. Whereas in subaerial geomorphology, hypothesis and enquiry have been prompted by structures that have always been visible, in submarine geomorphology, advances of understanding have typically occurred when new features have been discovered or imaged with instruments at higher resolution. Also because of the limited accessibility, our knowledge of the marine geological processes creating these morphological features has relied mostly on a forensic type of analysis (reconstructing events based on analyses of samples or other geophysical data) rather than by monitoring of processes more directly, although monitoring has been possible in some instances, some of which are outlined below.

Although not untouched by erosion, mid-ocean ridges have been modified much less than continental landscapes sculpted by rivers, glaciers and coastal erosion. They therefore provide excellent examples of how the shape of the seabed provides clues to the processes that formed it. Many of the original maps of ocean bathymetry drafted by Bruce Heezen and Marie Tharp (e.g., Fig. 2a) contributed information on mid-ocean ridge features that needed to be explained ultimately by the seafloor spreading theory. Those maps were created by interpolating between widely spaced lines of echo-soundings from research ship traverses. If a more continental style of erosion of such landscapes had occurred, it is doubtful that the orthogonal pattern of straight axial valleys and transform valleys would have been revealed so easily.

The following Sects. 2–7 review the different components of ridge geomorphology, while providing some history of that development. A personal view of likely developments follows in Sect. 8. For more detailed reading on mid-ocean ridge geomorphology, Searle (2013) is recommended.

2 Regional Geomorphology

Features broader than 10 km are now well revealed by the free air gravity field derived from satellite altimetry measurements (Sandwell et al. 2014). Figure 2b shows the regional bathymetry derived partly using the altimetry measurements where echo-soundings are sparse [exploiting the effect of the seabed density contrast on free air gravity anomalies to derive bathymetry variation (Smith and Sandwell 1997)]. As shown in that figure, the pattern of fracture zones (valleys)

crossing the Atlantic is revealed more clearly than in the earlier map (Fig. 2a), as well as features with trends intermediate between the fracture zones and spreading segments, which are produced by migrating spreading segments (Briais and Rabinowicz 2002).

Early in the development of the seafloor spreading hypothesis and as different parts of the oceanic basement were dated using seafloor spreading magnetic anomalies and Deep Sea Drilling Project samples, it was found that the seafloor subsides in proportion to the square root of crustal age (Parsons and Sclater 1977). Where a ridge overlies hotter mantle (near hotspots or mantle plumes), temperature gradients through the lithosphere might be expected to be steeper, so the lithosphere should cool more rapidly. The oceanic crust has indeed been found to subside more rapidly near hotspots than elsewhere, with subsidence rates correlating strongly with the ridge axis depth—Crosby and McKenzie (2009) found >10% greater initial subsidence rate for ridges 2400 m deep compared with those 2800 m deep.

“Morphometric” studies involve characterizing the shapes of structures and determining how the derived shape characteristics vary with parameters representing potential influences on the morphology. The method has been used to investigate the transition from an axial rift valley at slow-spreading ridges to a ridge at fast-spreading ridges, which occurs over intermediate spreading rates of 40–60 mm year⁻¹, though also varies with absolute depth of the ridge axis, as ridges near mantle hotspots (where ridges are elevated) can have axial highs like fast-spreading ridges (Malinverno 1993; Small 1994).

Regional bathymetry maps such as Fig. 2b are now capable of resolving some of the topographic fabric of abyssal hills (small ridges oriented parallel to the main spreading ridge, north-south in Fig. 2b). As described in Sect. 3, these hills were created mainly by the faults at the spreading ridges. Malinverno (1991) showed that the transition from a rift valley to an axial high is accompanied by a change in the relief of the abyssal hills, such that their root-mean-square relief varies inversely with the square root of spreading rate.

The lithosphere at ridges is thinner and therefore weaker than that beneath the older parts of the oceanic plates. Where weights act on the young lithosphere, it is deflected over shorter distances. The weight of Ascension Island, for example, has depressed the young lithosphere around it to ~40 km from the island (Minshull and Brozena 1997) compared with >200 km deflection by the Hawaii islands on Cretaceous oceanic lithosphere. Other deflections can occur because of rifting, where fault movements remove weight of hanging wall rocks from lithospheric footwalls.

3 Faults

First motions of teleseismic recordings of earthquakes generated at mid-ocean ridges have suggested that normal fault movements occur with moderately dipping fault planes, of ~45° dip (Huang and Solomon 1988). This observation has

supported a view up until the late 1990s that such moderately dipping normal faults have generated much of the seabed relief observed at ridges, such as illustrated from the interpretation of Deep-Tow bathymetry profiles in Fig. 3a. With continued seafloor spreading, such relief is inherited by the abyssal hills that form the rugosity of basement underlying the majority of the ocean basins.

Faults on land have been studied with traditional surveying and space-based techniques (InSAR and GPS) to record how the deformation that occurs during individual earthquakes contributes to the development of rift topography. Unfortunately, for most mid-ocean ridges, inaccessibility and attenuation of radar waves in seawater has prevented a similar approach, but there have been successful efforts to record deformation in the Afar and Iceland. For example, Stein et al. (1991) recorded the elevation changes associated with a volcanic rifting event, in which movements of normal faults accompanied intrusion of a dyke. Those displacements partly mimicked the shape of the inner rift, suggesting how individual events contribute to the geomorphology. Mechanical modelling suggested that activated faults had steep dips of 60° – 80° , supporting the view of steep faulting at ridges mentioned earlier. Significant work has been carried out in the Afar and on Iceland to characterize such events. However, as Afar and Iceland both overlie mantle hotspots where the crust is unusually thick, the rifting process may not be exactly analogous to the deeper mid-ocean ridges.

Contradicting the above view of steep faults, a closer examination of data from hull-mounted multibeam sonars by Cann et al. (1997) uncovered shallow-dipping corrugated surfaces at the seabed. The example in Fig. 3b was identified by them and shows a rounded surface with corrugations aligned with the seafloor spreading direction, as though a fault footwall has slipped at low angle or moderately steeply in the crust and rotated towards a horizontal inclination at the seabed. Paleomagnetic measurements on samples recovered by scientific drilling (at the open star symbol in Fig. 3b) indeed showed evidence for $\sim 46^\circ$ rotation (Morris et al. 2009). Although such faults were previously suspected to be associated with weak serpentinite rocks, the drilling recovered mainly gabbros in the footwall. Escartín et al. (2008) estimated that around half of the northern Mid-Atlantic Ridge is spreading by such ‘detachment’ faults, the remainder spreading by intrusion of dykes and high angle fault movements.

The evidence of strike-slip earthquakes in transform valleys, inferred from fault plane solutions (Sykes 1967), was important support for the seafloor-spreading hypothesis (Fig. 1b). Although seismic moment release rates of transform valleys are 1–2 orders of magnitude greater than those of spreading segments, seismic coupling is nevertheless $\sim <10\%$ (Rundquist and Sobolev 2002), so most fault movements do not generate detectable earthquakes. Furthermore, the large and varied vertical relief of these valleys implies that there must be some dip-slip fault movements in transform valleys. Indeed, escarpments produced by such movements have been sites of submersible traverses investigating the structure of the crust (Karson 1998; Mitchell et al. 2000).

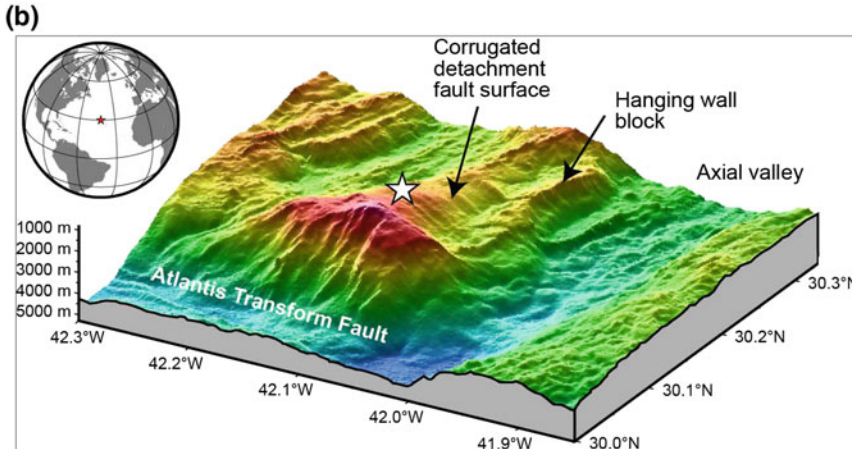
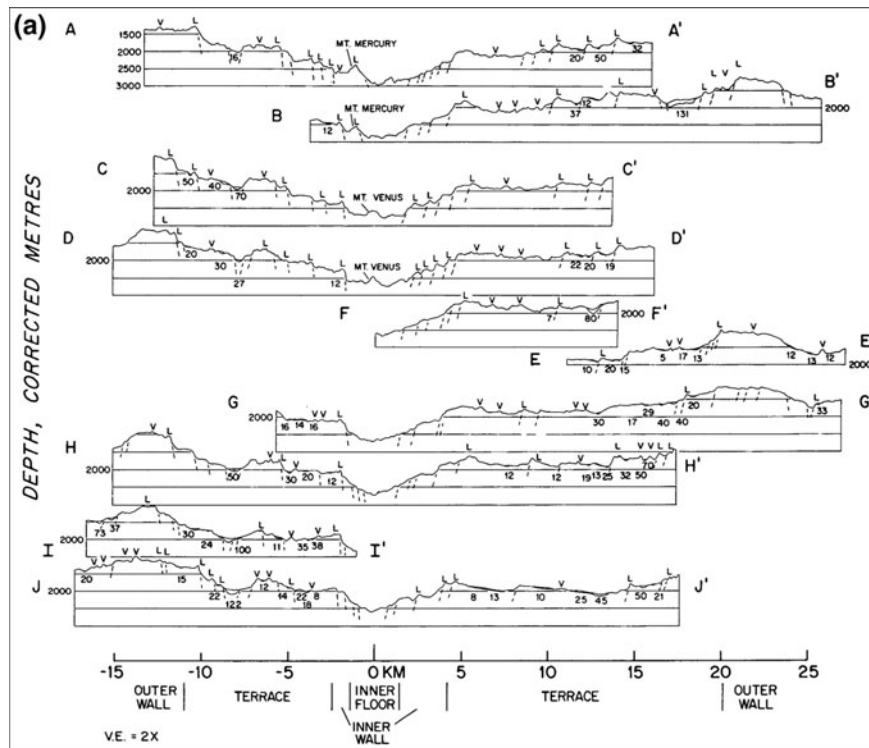


Fig. 3 Figures illustrating evolving ideas on how tectonic extension occurs at mid-ocean ridges. **a** Profiles of the Mid-Atlantic Ridge interpreted in terms of steeply dipping normal faults creating most seabed relief. (Reprinted from Macdonald and Luyendyk 1977, with permission from Geological Society of America.) **b** Perspective view of bathymetry from a shipboard multibeam sonar showing a corrugated surface interpreted as the exposed fault plane of a normal fault (Reprinted from Morris et al. 2009, with permission from Elsevier.)

4 Landslides

Bathymetry data collected with multibeam sonars installed in the hulls of research vessels have poor resolution and can reveal only the largest landslides at ridges (Tucholke 1992). However, higher resolution seabed images from sidescan sonars towed closer to the ocean floor have revealed talus ramps and cones formed from the degradation of fault scarps (Kong et al. 1988; Searle et al. 1998). Such features develop within only a few millions of years of the crust forming, possibly from rock slopes destabilized by frequent earthquakes. Following this initial stage, scarps apparently continue degrading over 10s of millions of years, forming trellis channel networks (Tucholke et al. 1997).

Scientific drilling on the flanks of the Mid-Atlantic Ridge has recovered inter-layered serpentinite rock breccias and lavas. Lithological sequences of rocks observed in submersible dives and in rock dredges also do not obviously follow the simple “classical” oceanic crustal structure of lavas successively overlying diabase (dykes), gabbro and mantle rocks (Mitchell 2001). Landslides may explain some heterogeneity, by mixing up the lithologies locally; high-resolution maps of serpentinite-rich basement (Cannat et al. 2013) have revealed landslides in serpentinite, such as those shown in Fig. 4. The breccias created by landsliding can then be over-erupted by lavas, leading to the lithological sequences found in the drill cores.

5 Volcanic Geomorphologic Features

Early detailed investigation of volcanic landforms was carried out with shipboard multibeam sonars and manned submersibles during a joint French-American study on the slow-spreading Mid-Atlantic Ridge (Ballard and Van Andel 1977), and during a similar study on the medium-spreading Galapagos Spreading Centre (Ballard et al. 1979). Since then, there have been many volcanic investigations involving submersibles, ROVs, AUVs and deeply towed devices, centred mainly on the Mid-Atlantic Ridge and fast-spreading East Pacific Rise.

On fast-spreading ridges, erupted lavas tend to have low viscosities and therefore spread out easily, leaving flat-lying (“sheet” and “lobate”) flows, as well as steeper slopes (Soule et al. 2007). Lava lakes containing pillars where the lava became chilled by trapped water venting through them are common, with pillar “bathtub rings” caused by subsequent lava drain back. The more recent high-resolution bathymetry from AUVs has revealed channels, pathways travelled by the distributing lava (Soule et al. 2005).

In contrast, eruptions on slow-spreading ridges produce a more rugged geomorphology. The terrain is commonly described as ‘hummocky’ and in photographs typically contains stacks of pillow lavas, although flat-lying lava flows also occur (Perfit and Chadwick 1998). Hummocky flows can be arranged in ridges

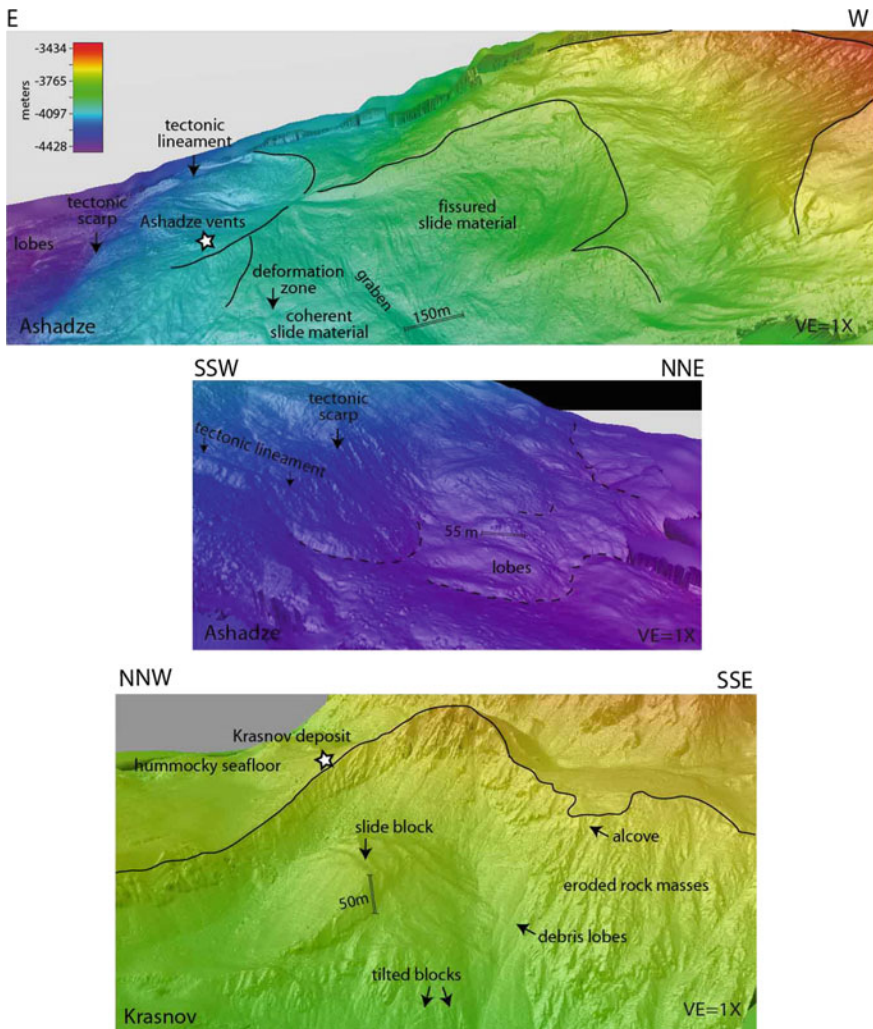


Fig. 4 Perspective views of bathymetry collected with a high-resolution multibeam sonar installed on an ROV revealing slumps and other landslide features (Cannat et al. 2013) (Reprinted from Cannat et al. 2013, with permission from Wiley.)

and tumuli (Bryan et al. 1994), likely originally erupted over dykes or dyke swarms. Some superimposed cones may represent late-stage focused effusion from the dykes, as occurs in subaerial eruptions (Head et al. 1996). Some cones may be rootless (Bryan et al. 1994) and fed by lava tubes (Smith and Cann 1999). Photographs of both fast and slow ridges typically show abundant fissures from the on-going extension.

Illustrating how the new high-resolution topography available from AUVs and ROVs is helping to study volcanic landforms, Fig. 5 shows data collected from the East Pacific Rise (Deschamps et al. 2014). Despite faster cooling and high ambient pressure, many features such as those shown are comparable with those found in lava flow fields on land and can be interpreted in terms of lava flowage, inflation, cooling and drainback.

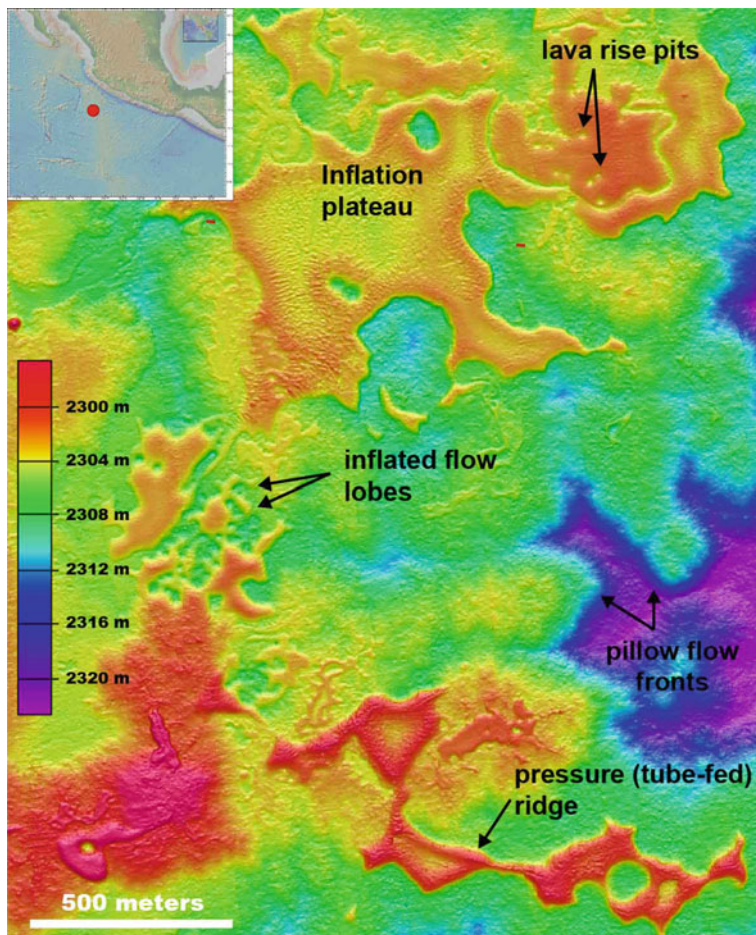


Fig. 5 Detail of volcanic lava flow structures in high-resolution bathymetry from the northern East Pacific Rise (Deschamps et al. 2014). (Reprinted from Deschamps et al. 2014, with permission from Wiley.)

6 Hydrothermal Springs

Emissions of hydrothermal fluids can produce hot ‘black smokers’ (jets of fluids containing precipitating sulphide particles) or clearer diffuse venting. The particles in black smokers can settle to form smooth mounds of hydrothermal sediment. Precipitating silicate and sulphide minerals from the fluids can also produce chimneys many metres to >10 m tall, such as illustrated in Fig. 6. Chimneys are unstable and can topple during earthquakes or otherwise fracture to contribute talus to the sedimentary mounds the chimney fields stand on. Petrological and geochemical analyses of samples obtained from these chimneys have revealed that they were formed of layers of different minerals, suggesting cycles in the hydrothermal fluid composition and temperature, as well as mineral reactions during seawater ingress. While many hydrothermal springs are associated with fluid circulation above the hot magma, some are associated with circulation through ultramafic rocks brought towards the seabed by detachment faults.

7 Sediment Transport and Deposition

Where ridges lie far from the continents, only pelagic particles accumulate on them, generally at slower rates than other forms of sediment near continents, so that hints of the oceanic basement relief commonly remain visible in seabed morphology even on crust of many millions of years in age. Those pelagic sediments can accumulate like snow with little redistribution so that they drape the underlying basement topography. Commonly, though, some lateral (usually downslope) movement occurs to leave concave up-wards deposits (Mitchell 1995) or flat lying turbidite ‘ponds’ (van Andel and Komar 1969). Where ridges lie near to continental sources of sediment, more frequent turbidity currents can flood the axial valley with sediment, such as the northern Juan de Fuca Ridge (Davis and Lister 1977). Even more exotically, the invading sediments can include flows of evaporites, such as in the Red Sea (Augustin et al. 2014).

8 Remaining Issues and Developments

Our understanding of mid-ocean ridge geomorphology should continue to improve as new technology is developed and deployed. Modern multibeam sonars are capable of imaging acoustic backscattering from the water column as well as the seabed and could be used to record emissions and biota over vent sites along with more optimized acoustic imaging of them (Bemis et al. 2015). Synthetic aperture sonar (adapted from synthetic aperture radar) may further improve seabed imaging. Acoustic backscattering strength in sidescan sonar images depends on seabed

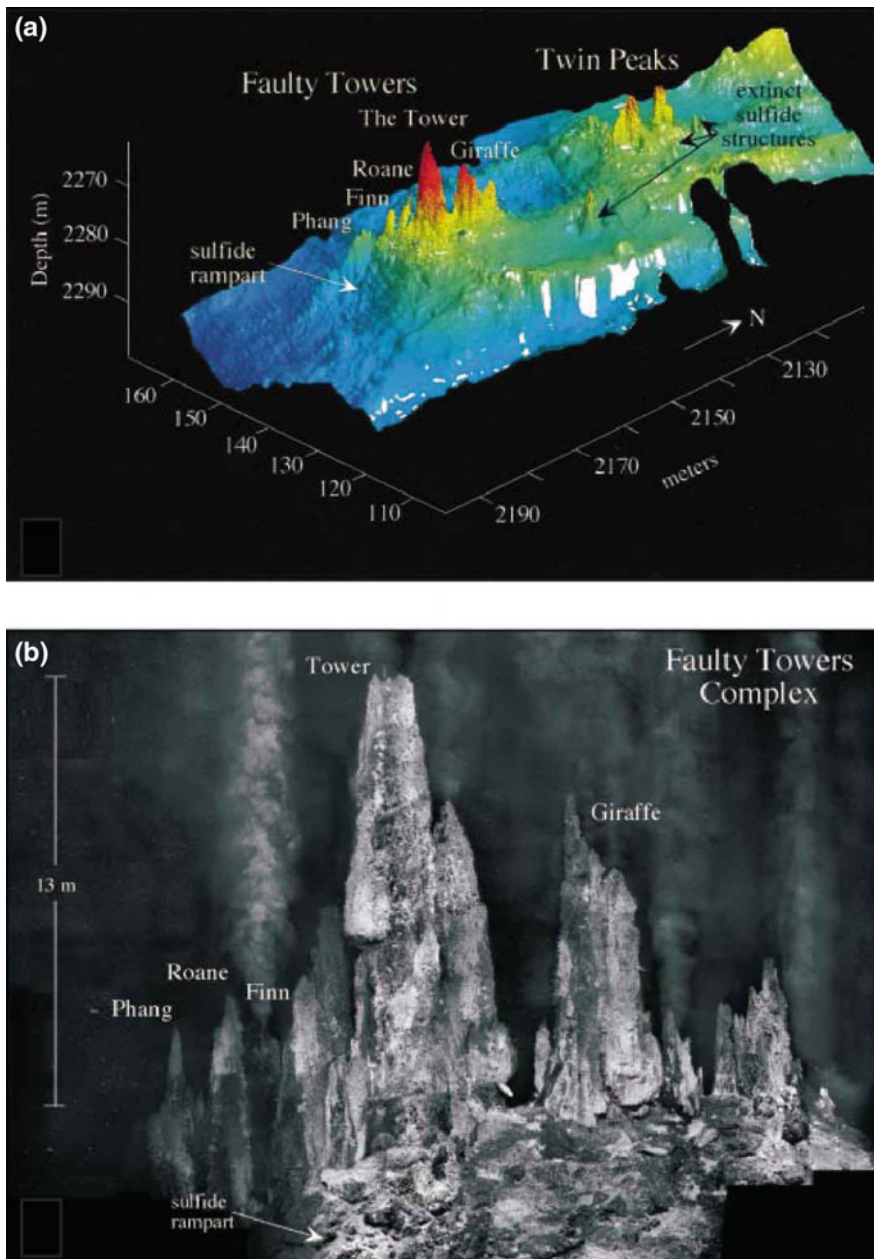


Fig. 6 Pinnacles in a hydrothermal vent field on the Juan de Fuca Ridge (Kelley et al. 2001) (Reprinted from Kelley et al. 2001, with permission from Geological Society of America.). **a** Perspective view derived from elevation data collected with a 675 kHz scanning sonar mounted on an ROV. **b** Mosaic of 73 still images

micro-roughness at the scale of the sonar acoustic frequency, any sediment cover and incidence angle of the signal with the bed (which varies with bed topography). For example, the low backscattering of smooth sheet flows (Soule et al. 2005) illustrates the effect of roughness. As attenuation in any sediment cover also varies with acoustic frequency (Mitchell 1993), we might expect data collected with multi-frequency sonars to reveal useful information. More generally, increasing use of deeply towed systems, ROVs and AUVs with seabed imaging systems (cameras, sonars and LiDAR) should progressively enlarge the database of observations we have of high-resolution geomorphology.

Knowledge of the subsurface lithologic structure would be helpful, as on land, for working out how the geomorphology develops, in particular, for volcanic landforms. However, structure is difficult to image with geophysical methods and sampling by scientific drilling has been limited because of cost and technical issues (holes in friable volcanic rock are unstable). Illustrating the problem with geophysical datasets, seismic refraction methods can reveal boundaries in the upper crust that are not lithological boundaries exactly, because seismic velocities vary with the porosity of the rock, affecting its bulk rigidity (Carlson 2010), and porosity may vary within units. Alteration also varies velocities, illustrated by reflections in seismic data collected over the detachment fault in Fig. 3b (Collins et al. 2009). Similar issues apply to electro-magnetic measurements, where electrical resistivity varies with connected porosity and pore fluid resistivity (sensitive to conducting brines and magmatic fluids). Nevertheless, further progress will be made by carefully designed experiments combining geophysical experiments with information from scientific drilling and observing rock sequences exposed at fault escarpments (Karson 1998).

Much of the effort on ridges has involved ‘forensic science’, i.e., we have imaged seabed features and attempted to reconstruct the processes that formed them, aided by analyses of samples and geophysical data. There has been less progress in observing geological events or processes as they occur. Although seismicity can forewarn a volcanic eruption in some instances, the times of occurrence of volcanic eruptions, fault movements and landslides are largely unpredictable, making planning of any in situ observation problematic.

This is important for physical volcanology. On land, infrared measurements are routinely made on erupting lavas to monitor temperature; lava viscosity is strongly non-linear with temperature, so the final geometries of flows strongly depend on lava temperature and eruption rate. Temperature measurements in submarine mid-ocean ridges have not been possible. Individual lava flows are the basic units of the uppermost crust and thus important for determining how the crust develops, but mapping their geometries at the seabed is difficult because lava types can vary with effusion rate and gradient so their surface morphology is insufficiently characteristic for distinguishing them (on land a single lava flow can change between a'a' and pahoehoe types during the same eruption). To overcome this, boundaries to some historical lava flows have been mapped out based on the extent of un-sedimented lava (e.g., Soule et al. 2007). Caress et al. (2012) characterized the shapes and thickness distributions of ~10 m thick lava flows erupted in 2011 on the Juan de

Fuca Ridge using repeated high-resolution bathymetry from an AUV. As these studies illustrate, information should accumulate over time with further surveying, encompassing lavas newly erupted since previous surveys were carried out.

Further information on eruptions and crustal deformations will arise from bottom observatories (cabled or autonomous packages of instruments). For example, Chadwick et al. (2012) documented inflation-deflation cycles from pressure sensors on the Juan de Fuca Ridge, including a sudden uplift immediately prior to the 2011 eruption associated with intrusion of a dyke. The same event was recorded with ocean bottom seismometers, which revealed changes in seismicity leading up to the eruption and constrained the eruption duration (Dziak et al. 2012). Cabled observatories off western North America will likely yield more information on eruptions over time.

More generally recording how the seabed changes its topography during earthquakes (Stein et al. 1991), will be challenging as associated depth changes of ~1 m are typically smaller than the depth precision of hull-mounted multibeam sonars. Nevertheless, recordings of earthquake T-waves using hydrophones moored in the oceans can be used to detect and locate small magnitude earthquakes, allowing volcano-tectonic earthquakes to be studied (Smith et al. 2003). Such information provided in real-time may allow opportunistic inspection of earthquake ruptures and deformation in the future. Observatory pressure sensors and acoustic ranging to bottom-moored transponders may also ultimately reveal tectonic movements.

As the above notes illustrate, we have made enormous progress in understanding mid-ocean ridge geomorphology, despite their deep and commonly remote locations, and we can expect further exciting developments to emerge over the decades to come.

References

- Augustin N, Devey CW, van der Zwan FM, Feldens P, Tominaga M, Bantan R, Kwasnitschka T (2014) The transition from rifting to spreading in the Red Sea. *Earth Planet Sci Lett* 395: 217–230
- Ballard RD, van Andel TH (1977) Morphology and tectonics of the inner rift valley at lat 36°50'N on the Mid-Atlantic Ridge. *Geol Soc Am Bull* 88:507–530
- Ballard RD, Holcomb RT, van Andel TH (1979) The Galapagos Rift at 86°W: 3. Sheet flows, collapse pits, and lava lakes of the Rift valley. *J Geophys Res* 84:5407–5422
- Becker JJ, Sandwell DT, Smith WHF, Braud J, Binder B, Depner J, Fabre D, Factor J, Ingalls S, Kim S-H, Ladner R, Marks K, Nelson S, Pharaoh A, Trimmer R, Von Rosenberg J, Wallace G, Weatherall P (2009) Global bathymetry and elevation data at 30 arc seconds resolution: SRTM30_PLUS. *Mar Geodesy* 32:355–371
- Bemis KG, Silver D, Xu G, Light R, Jackson D, Jones C, Ozer S, Liu L (2015) The path to COVIS: a review of acoustic imaging of hydrothermal flow regimes. *Deep Sea Res II* 121: 159–176

- Briaïs A, Rabinowicz M (2002) Temporal variations in the segmentation of slow to intermediate spreading mid-ocean ridges 1. Synoptic observations based on satellite altimetry data. *J Geophys Res* 107:Paper 2098. doi:10.1029/2001JB000533
- Bryan WB, Humphris SE, Thompson G, Casey JF (1994) Comparative volcanology of small axial eruptive centers in the MARK area. *J Geophys Res* 99:2973–2984
- Cann JR, Blachman DK, Smith DK, McAllister E, Janssen B, Mello S, Avgerinos E, Pascoe AR, Escartín J (1997) Corrugated slip surfaces formed at ridge-transform intersections on the Mid-Atlantic Ridge. *Nature* 385:329–332
- Cannat M, Mangeney A, Ondréas H, Fouquet Y, Normand A (2013) High-resolution bathymetry reveals contrasting landslide activity shaping the walls of the Mid-Atlantic Ridge axial valley. *Geochem Geophys Geosyst* 14. doi:[10.1002/ggge.20056](https://doi.org/10.1002/ggge.20056)
- Caress DW, Clague DA, Paduan JB, Martin JF, Dreyer BM, Chadwick WW, Denny A, Kelley DS (2012) Repeat 1 m resolution bathymetric surveys reveal April 2011 lava flows at axial seamount. *Nature Geosc* 5:483–488
- Carlson RL (2010) How crack porosity and shape control seismic velocities in the upper oceanic crust: Modeling downhole logs from Holes 504B and 1256D. *Geochem Geophys Geosyst* 11: Paper Q04007. doi:04010.01029/02009GC002955
- Chadwick WW, Nooner SL, Butterfield DA, Lilley MD (2012) Seafloor deformation and forecasts of the April 2011 eruption at axial seamount. *Nature Geosci* 5:474–477
- Collins JA, Blackman DK, Harris A, Carlson RL (2009) Seismic and drilling constraints on velocity structure and reflectivity near IODP Hole U1309D on the central dome of Atlantis Massif, Mid-Atlantic Ridge 30°N. *Geochem Geophys Geosyst* vol 10, article Q01010. doi:[10.1029/2008GC002121](https://doi.org/10.1029/2008GC002121)
- Crosby AG, McKenzie D (2009) An analysis of young ocean depth, gravity and global residual topography. *Geophys J Int* 178:1198–1219
- Davis EE, Lister CRB (1977) Tectonic structures on the Juan de Fuca Ridge. *Geol Soc Am Bull* 88:346–363
- Deschamps A, Grigné C, Saout ML, Soule SA, Allemand P, Lanoe BVV, Floc'h F (2014) Morphology and dynamics of inflated subaqueous basaltic lava flows. *Geochem Geophys Geosyst* 15. doi:[10.1002/2014GC005274](https://doi.org/10.1002/2014GC005274)
- Dziak RP, Haxel JH, Bohnenstiehl DR, Chadwick WW, Nooner SL, Fowler MJ, Matsumoto H, Butterfield DA (2012) Seismic precursors and magma ascent before the April 2011 eruption at axial seamount. *Nature Geosci* 5:478–482
- Escarthán J, Smith DK, Cann J, Schouten H, Langmuir CH, Escrig S (2008) Central role of detachment faults in accretion of slow-spreading oceanic lithosphere. *Nature* 455:790–794
- Head JW, Wilson L, Smith DK (1996) Mid-ocean ridge eruptive vent morphology and substructure: Evidence for dike widths, eruption rates, and axial volcanic ridges. *J Geophys Res* 101:28265–28280
- Heezen BC, Tharp M (1961) Physiographic diagram of the South Atlantic, the Caribbean, the Scotia Sea, and the eastern margin of the South Pacific Ocean. *Geol Soc Am*
- Huang PY, Solomon SC (1988) Centroid depths of mid-ocean ridge earthquakes: dependence on spreading rate. *J Geophys Res* 93:13445–13477
- Karson JA (1998) Internal structure of oceanic lithosphere: a perspective from tectonic windows. In: Buck WR, Delaney PT, Karson JA, Lababrielle Y (eds) *Faulting and magmatism at mid-ocean ridges*. American Geophysical Union, Washington, D.C., pp 177–218
- Kelley DS, Delaney JR, Yoerger DR (2001) Geology and venting characteristics of the Mothra hydrothermal field, Endeavour segment, Juan de Fuca Ridge. *Geology* 29:959–962
- Kong LSL, Detrick RS, Fox PJ, Mayer LA, Ryan WBF (1988) The morphology and tectonics of the MARK area from Sea Beam and SeaMARC I observations (Mid-Atlantic Ridge 23°N). *Mar Geophys Res* 10:59–90
- Macdonald KC, Luyendyk BP (1977) Deep-tow studies of the structure of the Mid-Atlantic Ridge crest near latitude 37°N. *Geol Soc Am Bull* 88:621–636
- Malinverno A (1991) Inverse square-root dependence of mid-ocean-ridge flank roughness on spreading rate. *Nature* 352:58–60

- Malinverno A (1993) Transition between a valley and a high at the axis of mid-ocean ridges. *Geology* 21:639–642
- Minshull TA, Brozena JM (1997) Gravity anomalies and flexure of the lithosphere at Ascension Island. *Geophys J Int* 131:347–360
- Mitchell NC (1993) A model for attenuation of backscatter due to sediment accumulations and its application to determine sediment thickness with GLORIA sidescan sonar. *J Geophys Res* 98:22477–22493
- Mitchell NC (1995) Diffusion transport model for pelagic sediments on the Mid-Atlantic Ridge. *J Geophys Res* 100(B10):19991–920009
- Mitchell NC (2001) Random sequences of lithologies exposed on the Mid-Atlantic Ridge. *J Geophys Res* 106:26365–326378
- Mitchell NC (2015) Submarine geomorphology. In: Sinclair H (ed) Reference module in earth systems and environmental sciences. Elsevier, Amsterdam
- Mitchell NC, Tivey MA, Gente P (2000) Slopes of mid-ocean ridge fault scarps from submersible observations. *Earth Planet Sci Lett* 183:543–555
- Morris A, Gee JS, Pressling N, John BE, MacLeod CJ, Grimes CB, Searle RC (2009) Footwall rotation in an oceanic core complex quantified using reoriented Integrated Ocean Drilling Program core samples. *Earth Planet Sci Lett* 287:217–228
- Parsons B, Sclater JG (1977) An analysis of the variation of ocean floor bathymetry and heat flow with age. *J Geophys Res* 82:803–827
- Perfit MR, Chadwick JW (1998) Magmatism at mid-ocean ridges: constraints from volcanological and geochemical investigations. In: Buck WR, Delaney PT, Karson JA, Lagabrielle Y (eds) Faulting and magmatism at mid-ocean ridges. American Geophysical Union, pp 59–115
- Ribe NM (1988) On the dynamics of mid-ocean ridges. *J Geophys Res* 93:429–436
- Rundquist DV, Sobolev PO (2002) Seismicity of mid-oceanic ridges and its geodynamic implications: a review. *Earth Sci Rev* 58:143–161
- Sandwell D, Müller RD, Smith WHF, Garcia E, Francis R (2014) New global marine gravity model from CryoSat-2 and Jason-1 reveals buried tectonic structure. *Science* 346:65–67
- Searle RC (2013) Mid-ocean ridges. Cambridge University Press, New York, p 318
- Searle RC, Cowie PA, Mitchell NC, Allerton S, MacLeod CJ, Escartin J, Russell SM, Slootweg PA, Tanaka T (1998) Fault structure and detailed evolution of a slow spreading ridge segment: the Mid-Atlantic Ridge at 29°N. *Earth Planet Sci Lett* 154:167–183
- Small C (1994) A global analysis of mid-ocean ridge axial topography. *Geophys J Int* 116:64–84
- Smith DK, Cann JR (1999) Constructing the upper crust of the Mid-Atlantic Ridge: a reinterpretation based on the Puna Ridge, Kilauea Volcano. *J Geophys Res* 104:25379–25399
- Smith WHF, Sandwell DT (1997) Global sea floor topography from satellite altimetry and ship soundings. *Science* 277:1956–1962
- Smith DK, Escartin J, Cannat M, Tolstoy M, Fox CG, Bohnenstiel DR, Bazin S (2003) Spatial and temporal distribution of seismicity along the northern Mid-Atlantic Ridge (15–35°N). *J Geophys Res* 108:2167. doi:[10.1029/2002JB001964](https://doi.org/10.1029/2002JB001964)
- Soule SA, Fornari DJ, Perfit MR, Rubin KH (2007) New insights into mid-ocean ridge volcanic processes from the 2005–2006 eruption of the East Pacific Rise, 9°46'N–9°56'N. *Geology* 35:1079–1082
- Soule SA, Fornari DJ, Perfit MR, Tivey MA, Ridley WI, Schouten H (2005) Channelized lava flows at the East Pacific Rise crest 9°–10°N: the importance of off-axis lava transport in developing the architecture of young oceanic crust. *Geochem Geophys Geosyst* 6:Q08005. doi:[10.1029/2005GC000912](https://doi.org/10.1029/2005GC000912)
- Stein RS, Briole P, Ruegg J-C, Tapponnier P, Gasse F (1991) Contemporary, Holocene and Quaternary deformation of the Asal Rift, Djibouti: implications for the mechanics of slow spreading ridges. *J Geophys Res* 96:21789–21806
- Sykes LR (1967) Mechanism of earthquakes and nature of faulting on mid-ocean ridges. *J Geophys Res* 72:2131–2153

- Tapponier P, Francheteau J (1978) Necking of the lithosphere and the mechanics of slowly accreting plate boundaries. *J Geophys Res* 83:3955–3970
- Tucholke BE (1992) Massive submarine rockslide in the rift-valley wall of the Mid-Atlantic Ridge. *Geology* 20:129–132
- Tucholke BE, Stewart WK, Kleinrock MC (1997) Long-term denudation of ocean crust in the central North Atlantic Ocean. *Geology* 25:171–174
- Van Andel TH, Komar PD (1969) Ponded sediments of the Mid-Atlantic Ridge between 22° and 23° North latitude. *Geol Soc Am Bull* 80:1163–1190

Cold Seep Systems

Silvia Ceramicola, Stéphanie Dupré, Luis Somoza and John Woodside

Abstract ‘Cold’ seeps (or cold vents) are seafloor manifestations of fluid migration through sediments from the subsurface to the seabed and into the water column, and may reach the atmosphere. They are an important but not fully understood process in our oceans that has important repercussions on human society and on the climate. Modern sonar systems can obtain seafloor images of cold seep features from tens to thousands of meters wide with metric resolution, providing key information on the formation and evolution of the various seabed expressions of cold seeps. In this chapter we attempt to address cold seep systems with an emphasis on their origin, evolution, form, and occurrence, approaching them primarily from their morphologies and the acoustic character of the seafloor and near bottom erupted sediments. We address morphological characteristics of mud volcanoes, pockmarks, carbonate-related structures including MDAC, AOM and giant carbonate mounds and ridges, offering various examples mainly from recent discoveries in Mediterranean region which are among the most spectacular and most frequently cited examples. Detailed focus on topics such as acoustic backscatter, brine pools, etc. have been described in separate gray boxes of text with the aim to highlight their particular significance. Finally, gaps in knowledge and key research questions on cold seep studies have been outlined with the aim of orienting young researchers

S. Ceramicola (✉)

Istituto Nazionale di Oceanografia e di Geofisica Sperimentale—OGS,
Borgo Grotta Gigante 42/c, 34010 Sgonico, Trieste, Italy
e-mail: sceramicola@inogs.it

S. Dupré

IFREMER Laboratoire Aléas géologiques et Dynamique Sédimentaire
Centre Bretagne, ZI de la Pointe du Diable—CS, 10070-29280 Plouzané, France

L. Somoza

Marine Geology Dv, Geological Survey of Spain—IGME,
Ríos Rosas 23, 28003 Madrid, Spain

J. Woodside

Lyngby Marine Geophysical Research, Mgr. Nolenslaan 5,
1181 VL Amstelveen, The Netherlands

and students towards those topics that deserve the highest attention as they are still unresolved.

Box 1: Acoustic Backscatter Data

Backscatter signal differs from acoustic reflection as it includes acoustic energy returned (in many different directions) from reflectors within the sediments to a depth dictated by the frequency and energy of the acoustic source. It therefore can provide information about the upper sediments on the seafloor. Backscatter data is used to detect active seepage at the seafloor because of the carbonate crusts and rough surface around seeps and the volume scatterers (rock fragments in mud breccia, gas, broken carbonate crust, etc.) in the upper seep sediments. The strong acoustic impedance contrast (reflectivity) between the sediments and both gas and crusts causes a stronger backscatter signal from these spots than from the normal seafloor sediments (e.g. Volgin and Woodside 1996; Zitter et al. 2005). On the other hand, brine pools appear as areas of practically no backscatter because most of the sonar energy is dispersed away from the sensors by specular reflection at the density interface between brine and normal sea water (e.g. Woodside and Volgin 1996), except for vertical incidence sonar signals. Both multi-beam echosounders and side scan sonars (hull mounted or deep towed) can be used to collect acoustic backscatter data.

Box 2: Anaerobic Oxidation of Methane (AOM)

Methane is a powerful greenhouse gas with a greater influence than CO₂. If all the methane coming from deep submarine reservoirs emitted into the water column, through cold seeps systems, were to reach the atmosphere, it would have a significant impact on the climate change of the Earth. Therefore, anaerobic oxidation of methane (AOM) is considered an important filter and sink for methane, preventing its expulsion into the water column and ultimately into the atmosphere. AOM is mainly mediated by a consortium of anaerobic methanotrophic (ANME) archaea and sulfate reducing bacteria (SRB) (e.g. Boetius et al. 2000). The sulfate is made available from seawater infiltrating the upper seafloor sediments. Bicarbonate is a by-product of the reactions involved and can result in the deposition of authigenic carbonates (see Box 3).

Box 3: Methane-Derived Authigenic Carbonates

Methane-derived authigenic carbonates (MDACs) are formed as a by-product of the AOM described in the previous grey box. As results of the symbiosis between ANME and SRB, high amounts of Fe-enriched carbonates may form

around cold seeps. The depth and the type of carbonates of MDACs depends basically on the rate of flux of the methane in the seeps (e.g. Magalhaes et al. 2012). Therefore, in seeps with high flux rates of methane, MDACs can be generated at the sediment-seawater interface forming pavements or crusts composed mainly of aragonite. In contrast, in seeps with low flux rates of methane, MDACs are formed below seafloor by cementation along the fluid conduits or pre-existing channels within the sedimentary column, forming chimney-like pipe structures mainly composed of dolomites. Extensive fields of these carbonates forming chimneys, crusts, pavements or slabs are found offshore in areas like the Gulf of Cádiz, South China Sea, New Zealand and Costa Rica, and other areas with extensive cold seep emissions (e.g. Díaz del Río et al. 2003). In anoxic bottom waters, such as the Black Sea, microbial consortia fuelled by methane seeps generate MDACs chimneys that form in the subsoil and rise several meters in height in the water column.

Box 4: Hydrothermal Vents

Cold seeps differ from hydrothermal vents occurring at mid oceanic ridges as the temperatures of vents are lower than 100 °C in contrast to ‘hot’ hydrothermal fluids that may reach temperatures of 200–400 °C. Generally, temperatures of cold seeps are warmer than the surrounding seawater reflecting the geothermal gradient of the seeping material, whether it comes from deep or shallow sediments.

Box 5: Brine Pools

In the Mediterranean region a thick layer up to 3 or 4 km of evaporitic deposits resulted from a late Miocene (~5 Ma, Messinian stage) desiccation of the sea (Hsu et al. 1973). Salt underlies a large part of the Messinian Mediterranean Basin. Water released from sediments below the salt creates a salty brine during its ascent through the salt to the seafloor. The brines are denser than the sea water and form pools in depressions on the seafloor. Often these depressions are pockmarks created by the fluid seeps, but they can also be formed by sedimentary deformation (e.g. along the Mediterranean Ridge, sediments folded during compression between the European and African plates south of Greece). The pools appear bizarrely as seafloor lakes.

1 Introduction

'Cold' seeps (or cold venting) are seafloor manifestations of fluid migration through sediments from the subsurface to the seabed and into the water column until they may reach the atmosphere. They may be generated by the activity of microbes in shallow sediments or by processes occurring deeper in the sediments (thermogenic). They are widespread natural processes found mostly (and in their most active state) on portions of land and seabed that are (or have been) characterised by the expulsion of free or hydrated gas (methane and higher hydrocarbons), oil (asphalt), water (salt brines, fresh or mixed waters) and sediments (mud breccia) in different proportions according to the processes that are responsible for their formation and the depth at which they have been generated. On land seepage has been known since ancient times by our ancestors (e.g. Romans, Native Americans, Azeris) who used the extruded material for curative purposes or for their everyday life. Some of these sites gained religious or cultural significance (e.g. Azerbaijan 'eternal flames').

Discoveries of submarine seeps occurred in the sixties when deep sea exploration achieved the first great discoveries. After that they have been recognised on the seafloors of all oceans (Fig. 1) including inland seas such as the Mediterranean and Black Seas (Judd and Hovland 2007), where some of the most diverse and

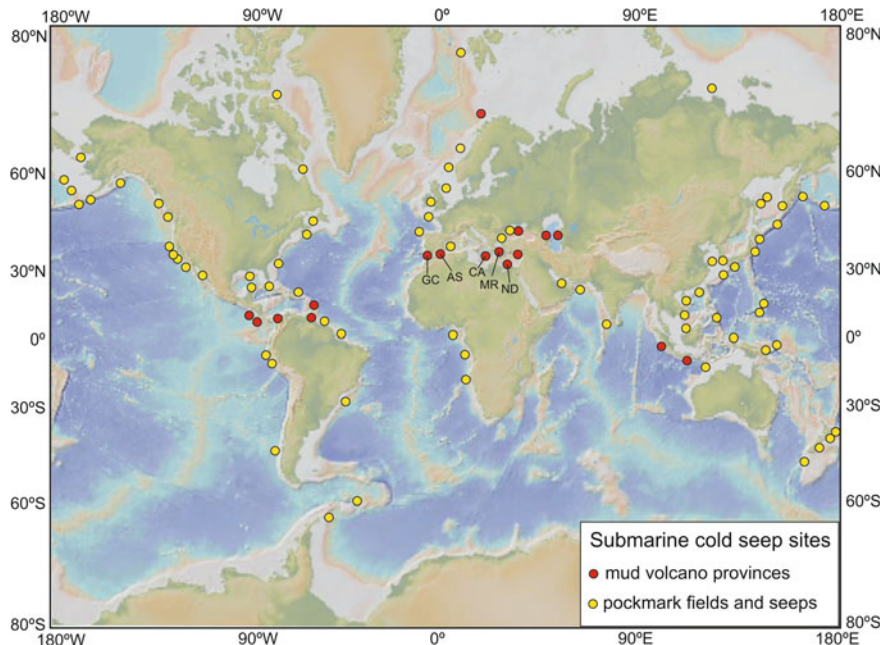


Fig. 1 Map showing distribution of cold seeps in the world (Modified from Milkov 2000; Kopf 2002). GC Gulf of Cádiz; AS Alboran Sea; CA Calabrian Arc; MR Mediterranean Ridge; ND Nile Delta Deep Sea Fan

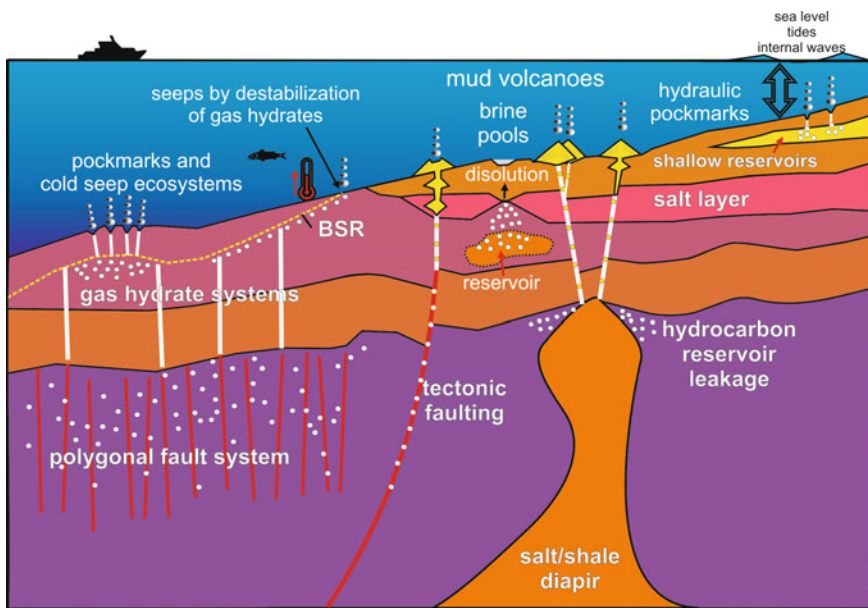


Fig. 2 Sketch of a portion of a continental margin affected by circulation of fluids (Modified from Berndt 2005)

spectacular examples have been discovered during the last 20 years (Ceramicola et al. 2014; Dupré et al. 2007, 2008, 2010, 2014; Huguen et al. 2005; Mascle et al. 2014; Woodside et al. 1996; Somoza et al. 2002, 2003; Zitter et al. 2005).

Seabed fluid flows have been identified on both active and passive continental margins in areas affected by compressional tectonics (e.g. subduction zones), or in deltaic environments characterised by rapid sediment deposition associated with high subsidence (e.g. Nile delta); however, they may occur as well in areas where the geothermal gradient is high or when thermogenic hydrocarbon reservoirs reach their final stages of natural gas generation (Fig. 2).

The great advances in underwater technology developed to explore the seafloor (ROVs, AUVs) since the end of the last century have greatly improved the capabilities of observing cold seep morphologies from a close distance, revealing their near bottom characteristics at metric resolution. This knowledge was key in unraveling important aspects of cold seep activity, resulting in better models of their formation and explanations of their spatio-temporal evolution.

Cold seeps are associated with a number of different seafloor structures such as mud volcanoes (including gryphons), pockmarks, diaps, carbonate-related constructions (mounds, chimneys, crusts, plates), brine pools, oil and gas vents. In the present chapter the diverse seafloor geomorphologies of cold seeps, and how these are indicative of their formation, functioning, and evolution in time, will be touched upon and their most typical characteristics illustrated.

Cold venting can host important ecosystems (e.g. Sibuet and Olu 1998; Olu et al. 2004) and act as hotspots for geo-biosphere interactions. It is also important to be aware of their occurrence on the seafloor of continental margins as they may represent hazards for marine infrastructures (communication cables, oil drilling platforms, pipelines). Fluid and gas circulation in sediments is able to modify sediment pore pressure and thus favour the inception of failures and/or other types of slope erosion (i.e. gullies, canyons). Cold seeps expel methane and other greenhouse gases, so being able to quantify the global occurrence of submarine methane emissions in the global carbon budget and their impact on climate is of great relevance.

2 Methods to Detect Cold Seeps Systems

Long-range side scan sonars were used in the 1980s to obtain the first large scale bathymetric/morphological maps of the ocean floor. The GLORIA (Geological LOng Range Inclined Asdic) side scan sonar was one of the first sonars operated by UK and US to detect and investigate the continental margins worldwide. Sound source and receivers were built into a “fish” that was towed about 200 m behind a ship.

Knowledge of cold seeps greatly advanced thanks to the widespread use of modern echo-sounders capable of recording both bathymetry (depth) and reflectivity (backscatter) of the seafloor, as well as acoustic anomalies in the water column. Integrating these three types of acoustic information is key in characterising cold seep morphologies and activity at the seafloor. Seafloor bathymetry acquired using low frequency sounders (resolutions tens of meters), is particularly important as it allows large scale mapping and thus identification of the occurrence of large (kilometer scale) seafloor morphologies (i.e. multiple cones, large calderas, domes, pries, etc.). High frequency sounders allow higher-resolution (meter scale) bathymetry. These seabed maps are used to reveal details of cold seep morphologies such as striations along the lobes of mud flows, circular rims around the calderas, fractures in the carbonatic pavement, providing evidence to reconstruct their activity through time. High-resolution bathymetry maps can be used to differentiate ‘fresher’ morphologies of younger mud flows from older ones buried under marine sediments. This information combined with the locations of high reflectivity patches of the seafloor is used to guide the sampling of mud flow sediment. This is particularly important in determining the timing of the different flows and thus the different seep events.

150 circular to subcircular high-backscatter patches were recognised on the shallow inner part of the Mediterranean Ridge and Calabrian accretionary complexes, during extensive surveying by the GLORIA system in the Eastern and Central Mediterranean (Fusi and Kenyon 1996). Some of these patches were interpreted as evidence of mud volcanoes and mud ridges already identified by Cita

et al. (1981), and provided some of the first geophysical evidences of cold seeps in the Mediterranean sea (Limonov et al. 1996).

Bathymetric maps acquired from Autonomous Underwater Vehicles (AUV) and Remotely Operated Vehicles (ROV), which are able to fly closer to the seafloor, show details as small as one meter across. These are among the most detailed maps ever made of the deep seafloor (Dupré et al. 2008; Sen et al. 2016).

Because bathymetry alone cannot be used to infer activity at the seafloor, backscatter (see Box 1) is used to reveal active or recently active cold seep structures (depending on the penetration of the sounding device used to investigate the seafloor sediments). Multibeam sonars are also able nowadays to record the anomalies in the water column due to gas bubbles (hydroacoustic flares), another indication of activity at a cold seep which is the source of the bubbles.

When surveying a new portion of the seafloor in search of cold seeps, the integrated use of the above described acoustic methods, including subbottom profiler data (Ceramicola et al. 2014), can be very effective (Fig. 3). However ground truthing information with near-bottom visual surveys, together with core sampling (gravity, piston, mini cores) remain the only methods able to prove mud

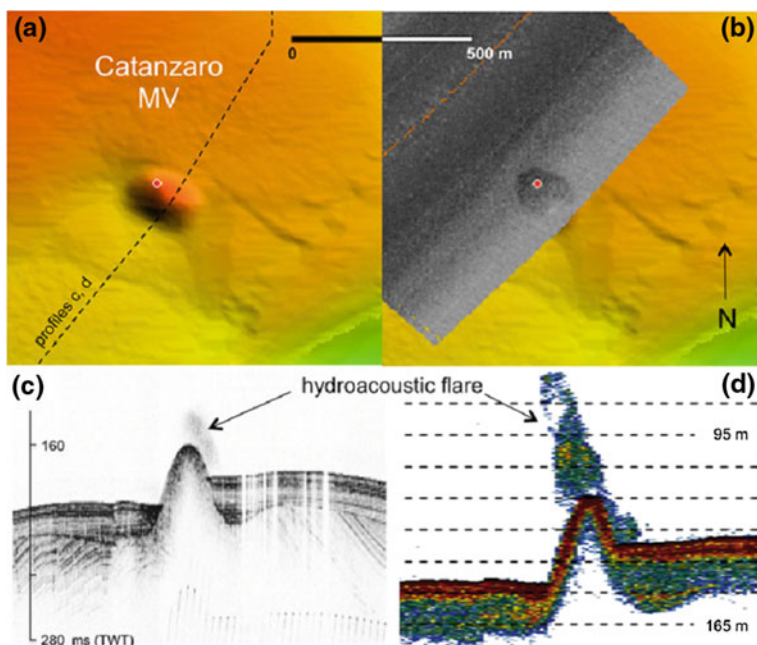


Fig. 3 Integrated acoustic methods to detect active seepage at the Catanzaro mud volcano (Ionian margin). **a** Multibeam bathymetry; **b** backscatter mosaic superimposed on bathymetry data; **c** subbottom data showing an acoustic flare in the water column; **d** echo sounder single beam data showing the flare in the water column above the mud volcano. The Catanzaro mud volcano has not been proven by coring or visual imaging yet. However, the combination of four different geophysical characteristics strongly suggests that this is a mud volcano (Ceramicola et al. 2014)

extrusion (e.g. mud breccia) on the seafloor. Core sediments are used to define the age of the different mud flows and when possible, to determine how long the cold seep structure has been active. Submersibles and ROVs equipped with cameras are commonly used to observe whether life is present at active or recently active cold seeps, to collect samples, to make measurements (e.g. temperature), and sometimes to further insonify the seafloor with acoustic signals.

3 Geomorphological Indicators of Cold Seeps

Fluid seepage through seafloor sediments is ubiquitous. For example, the rolling topography of sediment drape over a rough seafloor basement is related to loss of water due to compaction and differential subsidence, often along fine fractures in the sediment. In this chapter we restrict ourselves to more obvious structures on the seafloor that form in response to localised and concentrated fluid fluxes. These structures comprise mud volcanoes and mud flows, pockmarks (depressions) and brine pools, methane-derived carbonate structures (mounds, chimneys, sheets, etc.), and methane hydrates with their related structures (Fig. 2). On the scale of oceans, these structures are small but they can form large local landforms and fields of them.

3.1 Mud Volcanoes

Mud volcanoes are in no way ‘volcanic’ in the strict sense but derive their name from their similar shape and manner of formation by extrusion or eruption of material from below onto the surface above. They differ from mud diapirs in that the material forming them has actually breached the seafloor, which is not the case for mud or shale diapirs.

Mud volcanoes are generally the largest of these seafloor landforms: often sub-circular in plan view, with diameters of up to a few kilometers and typical heights of up to about 200 m. They are formed by eruption onto the seafloor of sediments from over-pressured formations on the order of kilometers deep (Fig. 4). There is thus a central feeder channel (sometimes with several branches) through which major eruptions occur and fluids (often rich in methane) seep continuously, or intermittently with lower intensity during the dormant phase. The driving pressure can be the result of compressional tectonics (e.g. at subduction zones or thrusts) or sedimentary pressure (e.g. on the Nile deep sea fan). Often, the sediments forming the surface of a mud volcano support a variety of clasts from indurated sediment below; thus, combined with methane-derived carbonate structures, they may form a rough surface and contain rocks and sediment very much older than the normal seafloor sediments. These deposits forming the mud volcano are known as mud breccia (Cita et al. 1981) and are responsible for the volume

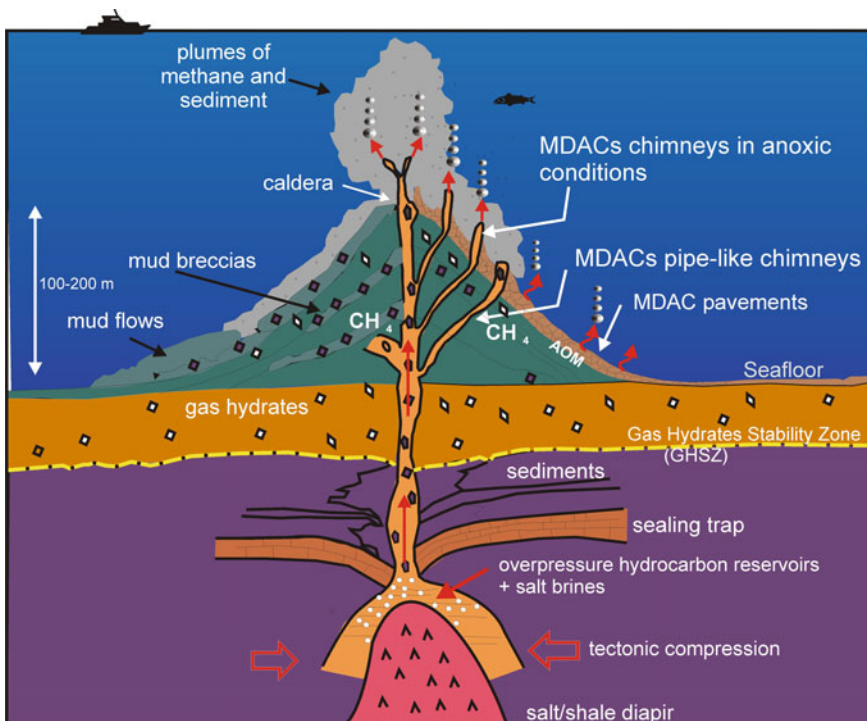


Fig. 4 Scheme showing the general functioning of mud volcanoes (Not all these features may be present)

backscattering of acoustic energy that makes them visible to sidescan sonar and multibeam mapping systems.

A more detailed discussion of the driving mechanism of mud volcanoes can be found in Chapter “[Drivers of Seafloor Geomorphic Change](#)” of this book.

Mud volcanoes have different morphologies that reflect their origins and structure (Fig. 5). These forms vary from broad flat mud pies such as those on the Nile Deep Sea Fan, to conical forms resembling volcanoes (such as Ginsburg Mud Volcano in the Gulf of Cadiz), but they are found mostly in the shape of an inverted bowl (such as the Mercator and Napoli mud volcanoes; e.g. [Masclle et al. 2014](#)). Sometimes they are composed of multiple conical shaped edifices, such as the twin cones of the Madonna dello Ionio or the Venere MV in the fore-arc basin of the Calabrian arc, one adjacent to the other sharing similar shapes and morphologies ([Praeg et al. 2009](#)), or the double cone at Chephren Mud Volcano on the Nile Deep sea Fan ([Dupre et al. 2014](#); [Masclle et al. 2014](#)). The flat mud pies on the Nile Fan are located above broad ‘gas chimneys’. They are kilometre scale wide but not high (typically about 50 m), and have distinctive concentric ridges and valleys of a few metres relief across the relatively flat summit (Fig. 5a).

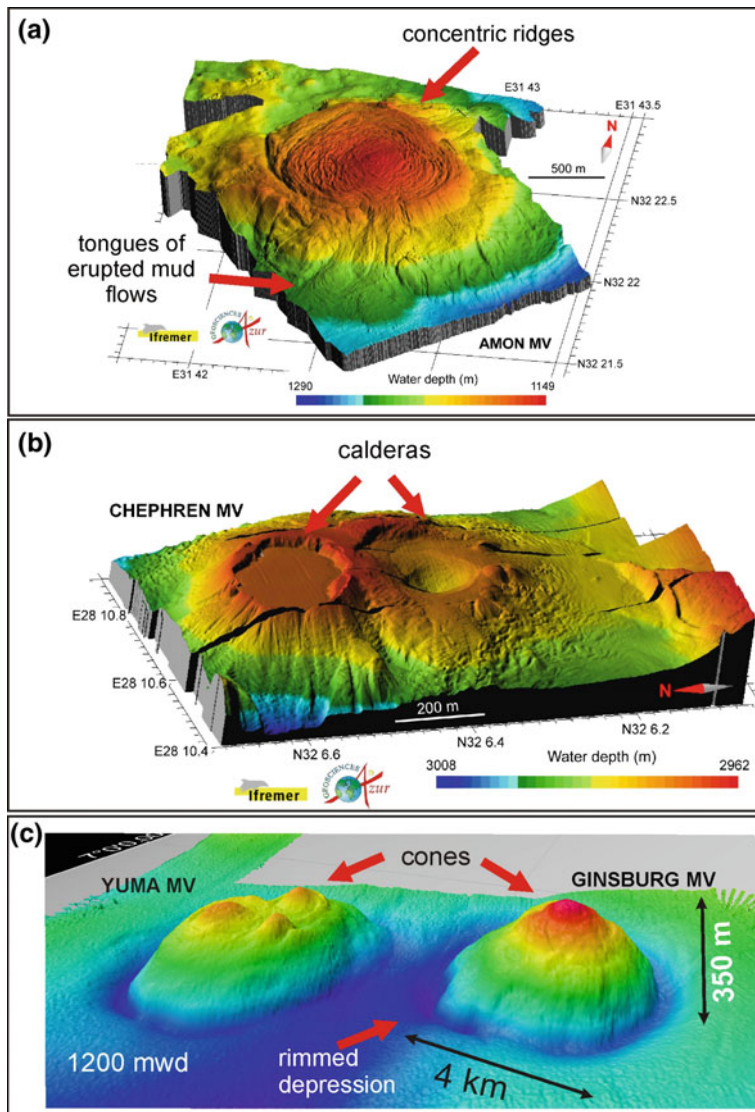


Fig. 5 Examples of mud volcanoes with different morphologies: Mud volcanoes with a central caldera such as **a** Amón and **b** Chephren MVs from Nile Deep Sea Fan (Dupré et al. 2008); and **c** mud volcanoes formed by an accumulation of cones and surrounded by a depression, like the Yuma and Ginsburg MVs from the Gulf of Cádiz (Modified from Toyos et al. 2016)

The ridges may show striations indicative of mud flow extrusion from the centre (Dupré et al. 2007) (see Fig. 5a). Activity occurs commonly near the centre of the volcano, however it may take place also locally closer to the rim. The physical

consistency of erupted material is responsible for the shape of the edifice and the steepness of its slope (Fig. 5b).

When collapse affects only the summit of the mud volcano, probably as a result of a fresh eruption of low consistency mud, a sag depression is formed resembling a volcanic caldera (e.g. Amsterdam, Madonna dello Ionio, Mercator, and Napoli MVs). Often the different tongues of erupted mud flows are visible down the flanks of the mud volcano and in some cases out onto the surrounding sea floor (e.g. Amsterdam, Sartori MVs). Depending on the consistency of the mud breccia, these mud flows and lobes can in some cases be as thick as 300 m, as at Amsterdam (Woodside et al. 1998) or Mercator MV (Somoza et al. 2003; Toyos et al. 2016). The Amsterdam mud volcano also shows a well developed caldera where the south rim has been breached resulting in massive flows. The flows themselves can bury some seafloor topography such as the anticlines and synclines formed by folding of the compressional accretionary prism at subduction zones, thus modifying the geomorphology.

In contrast, eruptions of higher consistency flows tend to build up circular to elongated cone-like mud volcanoes like Ginsburg MV (Fig. 5c) in the Gulf of Cádiz (e.g. Toyos et al. 2016). Sometimes, the upper cones of the mud volcanoes are formed by two or three cones as occurs at Yuma MV (Fig. 5c). At their base, most of these mud volcanoes show rimmed depression as the Hespérides or Anastasya MVs (Somoza et al. 2003), and scarps interpreted as flank failures developed by collapse, faulting and compaction processes.

Gryphons and salsas, common on land mud volcanoes, as in Azerbaijan (e.g. Mazzini et al. 2009) or the LUSI mud volcano in Indonesia (Mazzini et al. 2007), are also found associated with underwater mud volcanoes. The salsas can form pools on the summit of mud volcanoes (e.g. Napoli and Cheops mud volcanoes; e.g. Mascle et al. 2014) if the fluid is denser than the surrounding sea water, like salt rich brines (see below). Gryphons, steep-sided cones generally shorter than 3 m extrude fluid mud in active sub-centres of the mud volcano (features described onshore but identified also offshore). One gryphon on the west side of Amsterdam Mud Volcano rises to about 90 m (Zitter et al. 2005) and is therefore more of a parasitic cone than a gryphon.

Caldera morphologies are related to more fluid-rich seeps mainly associated with passive margins, whereas cones are more typical of mud volcanoes in compressional tectonic environments where eruptions result from buildup and release of pressure below; however both types may be present in either environment.

The age and duration of mud volcanic activity probably has a lot to do with the geological setting. In the Anaximander Mountains, examination of mud flows on Kula mud volcano suggest the occurrence of eruptions at a 5–10 kyr interval (Lykousis et al. 2009), although this need not be standard for all mud volcanoes. To the west, on the Mediterranean Ridge and the Calabrian accretionary prism, sediment cores and 12 kHz backscatter signatures from hundreds of mud volcanoes indicate the occurrence of mud breccias within a few metres of seabed, implying at least one eruption over the last 60 ka, i.e. the last glacial-interglacial cycle (Rabaute

and Chamot-Rooke 2007; Ceramicola et al. 2014). However, many mud volcanoes may have been active over much longer timescales. Scientific drilling of Napoli and Milano mud volcanoes on the Mediterranean Ridge show them to have been in operation for more than 1 million years (Robertson and Kopf 1998). On the Calabrian prism, seismic reflection investigations of the Madonna dello Ionio and Pythagoras MVs suggest they have operated over the last 3 Ma (Praeg et al. 2009). In the Alborán Sea, complex mud volcanoes formed with multiple cones are the longest living mud volcanoes, constructed by at least six extrusion episodes since the mid-Pliocene 3.3 million years ago. In the Gulf of Cádiz, the largest mud volcanoes, Ginsburg and Yuma MVs (Fig. 5e), initiated in the Messinian (5.3 million years ago) after the tectonic emplacement of the Betic-Rifean Arc onto the Atlantic margin (Toyos et al. 2016).

3.2 Pockmarks

Pockmarks are depressions on the seafloor resulting from collapse of the sediments upon upward migration of overpressured fluids (Judd and Hovland 2007; King and MacLean 1970). Pockmarks form where seeps occur without eruption of deep sediments, although they can occur on mud volcanoes (Dimitrov and Woodside 2003). The fluids involved in the formation of pockmarks are mostly gases, more specifically methane, of microbial or thermogenic in origin. However, submarine water seeps may occur e.g. groundwater releases (Whiticar 2002) and dewatering of sediments (Harrington 1985; Loncke et al. 2015). Where the fluids have passed through salt formations, as in many parts of the Mediterranean Sea, dense brines (water saltier than the surrounding seawater) may fill the pockmarks, forming seafloor brine pools (Huguen et al. 2005) or lakes (Dupré et al. 2014) (see brine lake gray box).

Pockmarks are widespread in the marine environment from shallow water areas like estuaries (Garcia-Gil 2003), continental shelves (King and MacLean 1970; Ingrassia et al. 2015) and slopes (Bøe et al. 1998; Pilcher and Argent 2007), to deep water basins (Bayon et al. 2009; Gay et al. 2006; Marcon et al. 2014).

Driving mechanisms for pockmark formation and/or reactivation especially in the shallower examples are seismic activity, tidally driven hydraulic pumping (over the short-term time scale) and variation in hydrostatic pressure driven by sea level changes (over large-time scale) (Fig. 2). More information can be found in Chapter “Drivers of Seafloor Geomorphic Change” of this book.

The morphology of the pockmarks can be easily inferred from bathymetry if the resolution of the sonar is higher than the size of the pockmark. Combined with multi-frequency seafloor backscatter, the bathymetry may provide key information with regard to the detection and characterization of the pockmarks. A high amplitude of the backscatter signal may indicate the presence of methane-derived authigenic carbonates (MDACs), debris or coarse sediments within the pockmark.

The morphology and the spatial distribution of pockmarks are important guides in marine exploration with regard to their detection but also to the processes involved. They may provide information on the nature of the fluids involved (gas, hydrates, water, brines), the conditions of pockmark formation and evolution (the relative age, fluxes) and indications of the occurrence of post-formation processes (hydrodynamism, sedimentation rates).

Pockmarks and seafloor pools are commonly circular to oval (Fig. 6a, b, d) and can be 1–10s of meters across, and they may merge to form even larger structures up to several hundreds of m across (Ingrassia et al. 2015; Somoza et al. 2012). Their depths are usually up to about 10 m but may be greater than 200 m. Giant pockmarks may reach diameters >500 m and up to 1–1.5 km across (León et al. 2014; Pilcher and Argent 2007; Sultan et al. 2010; Somoza et al. 2003).

Pockmarks may be isolated, arranged in clusters or coalescent. They may form strings or chains in relation to fault traces (Soter 1999) or buried paleochannels (Gay et al. 2003). Widespread pockmarks may reach densities of over a few thousands per km² (Judd and Hovland 2007; Baltzer et al. 2014), and occupy wide surface areas, e.g. 30% of the seabed in the North Sea is scattered with pockmarks (Judd and Hovland 2007).

The pockmark shape can be asymmetric, e.g. due to slumping, or elongate, e.g. in relation to erosive features and the removal of sediments by bottom currents (Boe

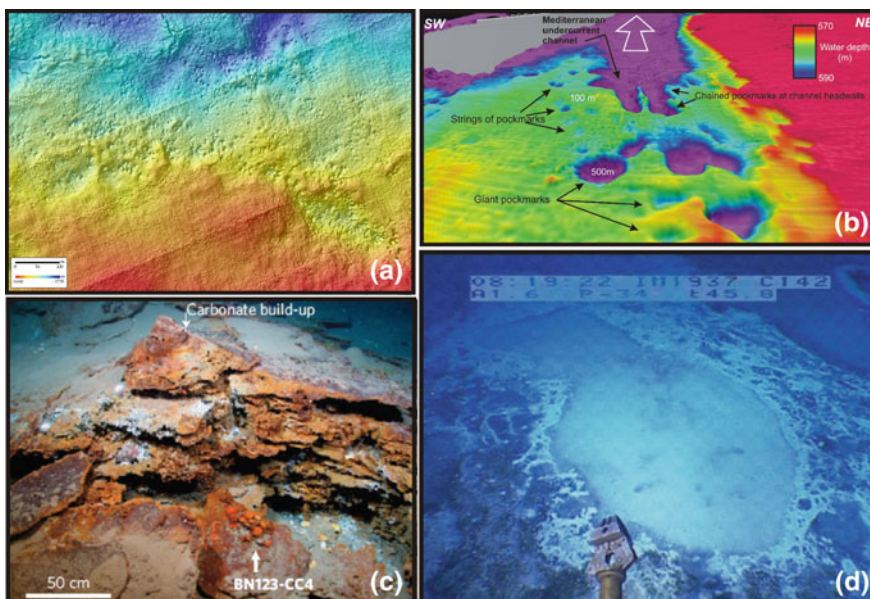


Fig. 6 Multibeam bathymetry and submarine images of pockmarks. **a** Field of pockmarks in the Nile Deep Sea Fan. **b** Chains of pockmarks in the Gulf of Cádiz. **c** Submarine image of methane-derived authigenic carbonates forming in a pockmark. **d** Submarine image of a pockmark filled with brine

et al. 1998; Josenhans et al. 1978). Pockmarks may be filled and associated with MDAC structures (Bayon et al. 2009) and fauna (Baltzer et al. 2014; Sen et al. 2016) or sediments deposited post-formation. Hydrate-bearing pockmarks are much more irregular depressions as a result of the formation and decomposition of gas hydrates in underlying sediments (Riboulot et al. 2016; Sultan et al. 2010).

The size of the pockmarks may be controlled by the fluid fluxes (Roberts 2001), by the underlying lithology (King and MacLean 1970) and by the thickness and architecture of near bottom sediments (Baltzer et al. 2014).

3.3 *Carbonate-Related Structures*

Most methane and other hydrocarbons associated with cold seeps are transformed into Methane-Derived Authigenic Carbonates (MDACs) due to the symbiotic activity of microbial-mediated consortia of archaea and bacteria (see grey boxes). The transformation of cold seep fluids to carbonates tends to strengthen structures such as mud volcanoes or pockmarks by providing both a hard framework and protective patches resistant to erosion (Fig. 6c).

3.3.1 Methane-Derived Authigenic Carbonates (MDACs)

The MDACs may form tubular chimneys (when oxidation of methane took place within the subsurface plumbing system) or build-ups of pavements or slabs when they occur near the surface of cold seeps (Fig. 6c). MDAC chimneys are typically cylindrical pipes with a central orifice up to 10 cm across and straight, tortuous, ramified or helical tubes showing a wide range of sizes (5–30 cm in diameter and 0.15–1.5 m in length). The central orifice acts as the seep conduit for methane and is thus the location of the AOM process (see gray box) which progressively cements the walls of the tubes with MDACs. The rate of cementation within the methane conduits is unknown. Some carbonate MDACs are associated with gas hydrate destabilization within mud volcanoes or seeps (Aloisi et al. 2000; Roberts 2001) (Fig. 4).

3.3.2 “Forest” of Carbonate Chimneys

Some of the most intriguing features we can observe rising from the seafloor of our continental margins, or lying on their side if collapsed, are seep-associated carbonate chimneys. Vast “forests” of these carbonate chimneys related to hydrocarbon-enriched fluid seepage have been reported in modern oceans as in the Kattegat (Jørgensen 1992), in the Gulf of Cádiz (Díaz-del-Río et al. 2003), in the

Adriatic Sea (Angeletti et al. 2015), in the Monterey Bay in California (Stakes et al. 1999), in the Campos basin off Brazil (Wirsig et al. 2012), in the Congo deep sea fan (Haas et al. 2010), in the Black Sea (Peckmann et al. 2001), in the Gulf of Mexico (Roberts 2001), off the Otago Peninsula in New Zealand (Orpin 1997), in the Dongsha area in the South China Sea (Han et al. 2013), and in the Cascadia subduction zone, offshore Oregon (Bohrmann et al. 1998). Some spectacular examples of forests of carbonate chimneys are observed in the Gulf of Cádiz. Here, carbonate mounds appear as irregular shaped clusters with a diameter of up to 6 km or clusters forming ridges up to 20 km long as in the Diasom chimney field (Somoza et al. 2003). The Diasom field is a prominent structural high with steep slopes between 25° and 35° and irregular crests formed by cone-shaped mounds rising 250 m above the seabed, such as the Cornide or Coruña Mounds. Observations from underwater camera revealed that these mounds are composed of large numbers of cylindrical pipe-like carbonate chimneys, pavements and crusts. Isotopic values from the chimneys show moderate to low depletion of $\delta^{13}\text{C}$ values (−20 to −40‰), reflecting that they were formed by AOM from a mixed source of biogenic and thermogenic gases (Díaz-del-Río et al. 2003).

The ramified pattern of the chimneys as observed in underwater photos indicates that they were formed by AOM (see Box 3) around the conduits that fed submarine cold seeps, and are now exposed probably as a result of winnowing by the strong Mediterranean outflow undercurrent (Díaz del Río et al. 2003). At the same time large vertical carbonate walls up to 50 m high, resulting from fissure-like seeps, may also have been exposed. In this way, giant carbonate mounds may form hard-rock morphological barriers that are able to channel strong deep water currents like the Mediterranean Outflow Water into the Atlantic Ocean.

The formation of vast expanses of MDACs around cold seeps also provides a hard substratum for growing seabed benthic organisms. Especially important are those forming reefs from what are known as cold-water corals (CWC), most of them belonging to the Scleractinia family as *Lophelia Pertusa* or *Madrepora Oculata*. These corals are able to live at water depths between 800 and 1200 m without the occurrence of light for photosynthesis. The deep water corals may grow around and above dormant cold seeps, being able to build up mounds (up to 50 m high) and/or linear ridges (up to 5 km long). The term CWC “reefs” is only used when the mounds or ridges are formed by living corals. The largest CWC reefs have been reported from the Porcupine, Rockall Trough (van Weering et al. 2003). There is strong scientific debate however as to whether the corals are fuelled by cold seeps or simply grow on cold seeps where a hard substrate is available and where there is upwelling food for them possibly related also to turbulence created by the formation of AOM carbonates. Further information may be found in Chapter “[Cold-Water Carbonate Bioconstructions](#)” in this book.

4 Geohazards and Ecosystem Habitats

Fluids at continental margins are major players in numerous geological, bio-chemical and oceanographic processes that may be associated with marine geohazards and can substantially alter the seafloor geomorphology. Some of the most dramatic hazards in which fluids may be involved are (i) sedimentary slope instabilities, (ii) association with earthquakes, and (iii) sudden methane release into the ocean. Fluids may thus be the predisposing or triggering factor, the geohazard itself, or a consequence of the geohazards. Developing large scale seafloor mapping programmes to acquire a good knowledge of the occurrence and distribution of active cold seep systems along continental margins, as well as understanding the processes that regulate venting and their implications regarding geohazards, are key to the security of the submarine nearshore, offshore, and coastal infrastructures. Hazards related to cold seeps may be natural or triggered by human activity (e.g. hydrocarbon spill, shallow gas blow-out). Monitoring the ocean floors at sites of venting using seabed observatory (EMSO, FluSO etc....) represents an important scientific challenge. Detailed discussion of some of these topics can be found in Chapters “[Submarine Canyons and Gullies](#)”, “[Submarine landslides](#)” and “[Applied Geomorphology and Geohazard Assessment for Deepwater Development](#)” in this book.

On the other hand, cold seeps provide benefits to the marine environment by favouring life in deep water and hosting important ecosystems. Cold seeps areas hosting such vulnerable ecosystems should receive the attention of European and international regulations aimed at protecting and preserving these singular deep sea habitats for chemosynthetic organisms.

5 Gaps in Knowledge and Key Research Questions

The purpose of this subchapter is to highlight gaps in knowledge and key research questions on cold seep studies as a guide for young researchers and students to those topics that deserve the highest attention for future investigations.

Despite the growing interest in cold seep research and the many recent discoveries, the study of cold seep systems remains a relatively recent research topic. For this reason, processes and mechanisms regulating extrusion at seabed and their evolution in space and time are still largely unknown. Thus, the identification and analysis of the key questions represent an important scientific challenge.

Seabed morphology is an important tool that is able to reveal key information regarding the regulation of cold seep activity and the driving mechanisms. Microbathymetry maps, repeated multibeam acquisition of the same features in time, equalised backscatter analyses to reconstruct activity through time and the search for hydroacoustic anomalies in the water column are some of the modern tools that should be used to fill this gap in knowledge.

Some of the key research questions that deserve attention and specific investigation are:

1. How does the morphological variability of seeps relate to their specific driving processes? Different cold seep morphologies (e.g. mud pie, conic edifices, gryphons) are often observed adjacent to each other, occurring in a similar lithological and geological setting, and it is not clear on what this variability is dependant.
2. What is the timing of dormant versus active phases, the episodicity, and recurrence times?
3. How much gas is emitted into the water column, and what consequently is the impact of the gas released into the atmosphere on the global carbon cycle?
4. What is the impact of fluid release along faults during earthquakes, and what is their influence on geohazards?

Acknowledgements Because this chapter is based on the research of so many colleagues and projects, it is difficult to single out individual scientists and funding agencies for acknowledgment. This in no way diminishes the debt of thanks we have for their ground-breaking work. The names of a few of the many are to be found in the list of references. Reviewer G.G. Akhmanov is thanked for his positive and supporting comments on the chapter.

References

- Aloisi G, Pierre C, Rouchy JM, Foucher JP, Woodside J (2000) Methane-related authigenic carbonates of eastern Mediterranean Sea mud volcanoes and their possible relation to gas hydrate destabilisation. *Earth Planet Sc Lett* 184:321–338
- Angeletti L, Canese S, Franchi F, Montagna P, Reitner J, Walliser EO, Taviani M (2015) The “chimney forest” of the deep Montenegrin margin, south-eastern Adriatic Sea. *Mar Petrol Geol*. doi:[10.1016/j.marpetgeo.2015.04.001](https://doi.org/10.1016/j.marpetgeo.2015.04.001)
- Baltzer A, Ehrhold A, Rigolet C, Souron A, Cordier C, Clouet H, Dubois S (2014) Geophysical exploration of an active pockmark field in the Bay of Concarneau, southern Brittany, and implications for resident suspension feeders. *Geo-Mar Lett* 34(2–3):215–230
- Bayon G, Loncke L, Dupré S, Caprais JC, Ducassou E, Duperron S, Etoubleau J, Foucher JP, Fouquet Y, Gonharet S, Henderson GM, Huguen C, Klaucke I, Mascle J, Migeon S, Olu-Le Roy K, Ondréas H, Pierre C, Sibuet M, Stadnitskaia A, Woodside J (2009) Multi-disciplinary investigation of fluid seepage on an unstable margin: the case of the Central Nile deep sea fan. *Mar Geol* 261(1–4):92–104
- Berndt C (2005) Focused fluid flow in passive continental margins. *Philos T R Soc A* 363 (1837):2855–2871
- Bøe R, Rise L, Ottesen D (1998) Elongate depressions on the southern slope of the Norwegian Trench (Skagerrak): morphology and evolution. *Mar Geol* 146(1–4):191–203
- Boetius A, Ravenschlag K, Schubert CJ, Rickert D, Widdel F, Gieseke A, Amann R, Jørgensen BB, Witte U, Pfannkuche O (2000) A marine microbial consortium apparently mediating anaerobic oxidation of methane. *Nature* 407:623–626
- Bohrmann G, Greinert J, Suess E, Torres M (1998) Authigenic carbonates from the Cascadia subduction zone and their relation to gas hydrate stability. *Geology* 26(7):647–650

- Ceramicola S, Praeg A, Cova D, Accettella M, Zecchin M (2014) Seafloor distribution and last glacial to postglacial activity of mud volcanoes on the Calabrian accretionary prism, Ionian Sea. *Geo-Mar Lett* 34:11–129
- Cita MB, Ryan WFB, Paggi I (1981) Prometheus mud breccia: an example of shale diapirism in the western Mediterranean ridge. *Annales Géologiques des Pays Helléniques* 3:543–570
- Díaz-del-Río V, Somoza L, Martínez-Frías J, Mata MP, Delgado A, Hernández-Molina FJ, Lunar R, Martín-Rubí JA, Maestro A, Fernández-Puga MC, León R, Llave E, Medialdea T, Vázquez JT (2003) Vast fields of hydrocarbon-derived carbonate chimneys related to the accretionary wedge/olistostrome of the Gulf of Cadiz. *Mar Geol* 195(1–4):177–200
- Dimitrov L, Woodside J (2003) Deep sea pockmark environments in the eastern Mediterranean. *Mar Geol* 195:263–276
- Dupré S, Woodside J, Foucher J-P, De Lange G, Mascle J, Boetius A, Mastalerz V, Stadnitskaia A, Ondréas H, Huguen C, Harmegnies F, Gontharet S, Loncke L, Deville E, Niemann H, Omoregie E, Olu-Le Roy K, Fiala-Medioni A, Dählmann A, Caprais J-C, Prinzhofer A, Sibuet M, Pierre C, Sinnonghe Damsté J, NAUTINIL Scientific Party (2007) Seafloor geological studies above active gas chimneys off Egypt (Central Nile Deep Sea Fan). *Deep Sea Res P I* 54(7):1146–1172
- Dupré S, Buffet G, Mascle J, Foucher J-P, Gauger S, Boetius A, Marfia C, the AsterX AUV Team, The Quest ROV Team, the BIONIL Scientific Party (2008) High-resolution mapping of large gas emitting mud volcanoes on the Egyptian continental margin (Nile Deep Sea Fan) by AUV surveys. *Mar Geophys Res* 29(4):275–290. doi:[10.1007/s11001-009-9063-3](https://doi.org/10.1007/s11001-009-9063-3)
- Dupré S, Woodside J, Klaucke I, Mascle J, Foucher J-P (2010) Widespread active seepage activity on the Nile Deep Sea Fan (offshore Egypt) revealed by high-definition geophysical imagery. *Mar Geol* 275(1–4):1–19. doi:[10.1016/j.margeo.2010.04.003](https://doi.org/10.1016/j.margeo.2010.04.003)
- Dupré S, Mascle J, Foucher J-P, Harmegnies F, Woodside J, Pierre C (2014) Warm brine lakes in craters of active mud volcanoes, Menes caldera off NW Egypt: evidence for deep-rooted thermogenic processes. *Geo-Mar Lett* 34(2–3):153–168. doi:[10.1007/s00367-014-0367-1](https://doi.org/10.1007/s00367-014-0367-1)
- Fusi N, Kenyon NH (1996) Distribution of mud diapirism and other geological structures from long-range sidescan sonar (GLORIA) data, in the Eastern Mediterranean Sea. *Mar Geol* 132:21–38
- Garcia-Gil S (2003) A natural laboratory for shallow gas: the Rías Baixas (NW Spain). *Geo-Mar Lett* 23(3):215–229
- Gay A, Lopez M, Cochonat P, Sultan N, Cauquil E, Brigaud F (2003) Sinuous pockmark belt as indicator of a shallow buried turbiditic channel on the lower slope of the Congo Basin, West African margin. *Geol Soc Spec Publ Subsurf Sediment Mobil* 216:173–189
- Gay A, Lopez M, Ondreas H, Charlou JL, Sermondadaz G, Cochonat P (2006) Seafloor facies related to upward methane flux within a Giant Pockmark of the Lower Congo Basin. *Mar Geol* 226(1–2):81–95
- Haas A, Peckmann J, Elvert M, Sahling H, Bohrmann G (2010) Patterns of carbonate authigenesis at the Kouilou pockmarks on the Congo deep-sea fan. *Mar Geol* 268:129–136
- Han XQ, Yang KH, Huang YY (2013) Origin and nature of cold seep in north-eastern Dongsha area, South China Sea: evidence from chimney-like seep carbonates. *Chin Sci Bul.* 30:3689–3697
- Harrington PK (1985) Formation of pockmarks by pore-water escape. *Geo-Mar Lett* 5(3):193–197. doi:[10.1007/bf02281638](https://doi.org/10.1007/bf02281638)
- Hsü KJ, Ryan WBF, Cita MB (1973) Late Miocene desiccation of the Mediterranean. *Nature* 242:240–244
- Huguen C, Mascle J, Woodside J, Zitter T, Foucher JP (2005) Mud volcanoes and mud domes of the Central Mediterranean Ridge: Near-bottom and in situ observations. *Deep-Sea Res P I* 52 (10):1911–1931
- Ingrassia M, Martorelli E, Bosman A, Macelloni L, Sposato A, Chiocci FL (2015) The Zannone Giant Pockmark: first evidence of a giant complex seeping structure in shallow-water, central Mediterranean Sea, Italy. *Mar Geol* 363:38–51

- Jørgensen NO (1992) Methane-derived carbonate cementation of marine sediments from Kattegat, Denmark: geochemical and geological evidence. *Mar Geol* 103:1–13
- Josenhans HW, King LH, Fader GB (1978) A side-scan sonar mosaic of pockmarks on the Scotian Shelf. *Can J Earth Sci* 15:831–840
- Judd A, Hovland M (2007) Seabed fluid flow: the impact on geology, biology and the marine environment. Cambridge University Press, Cambridge
- Kopf AJ (2002) Significance of mud volcanism. *Rev Geophys* 40(2-1-2-52):1005
- King LH, MacLean B (1970) Pockmarks on the Scotian Shelf. *Geol Soc Am Bull* 81:3142–3148
- León R, Somoza L, Medialdea T, González FJ, Giménez-Moreno CJ, Pérez-López R (2014) Pockmarks on either side of the Strait of Gibraltar: formation from overpressured shallow contourite gas reservoirs and internal wave action during the last glacial sea-level lowstand? *Geo-Mar Lett* 34(2–3):131–151
- Limonov AF, Woodside JM, Cita MB, Ivanov MK (1996) The Mediterranean Ridge and related mud diapirism: a background. *Mar Geol* 132:7–19
- Loncke L, Maillard A, Basile C, Roest WR, Bayon G, Gaullier V, Pattier F, Mercier de Lépinay M, Grall C, Droz L, Marsset T, Giresse P, Caprais JC, Cathalot C, Graindorge D, Heuret A, Lebrun JF, Bermell S, Marcaillou B, Sotin C, Hebert B, Patriat M, Bassetti MA, Tallobre C, Buscail R, Durrieu de Madron X, Bourrin F (2015) Structure of the Demerara passive-transform margin and associated sedimentary processes. Initial results from the IGUANES cruise. Geological Society, London, Special Publications 431. doi:[10.1144/sp431.7](https://doi.org/10.1144/sp431.7)
- Lykousis V, Alexandri S, Woodside J, de Lange G, Daehlmann A, Perissoratis C, Heesch K, Chr Ioakim, Sakellariou D, Nomikou P, Rousakis G, Casas D, Ballas D, Ercilla G (2009) Mud volcanoes and gas hydrates in the Anaximander mountains (Eastern Mediterranean Sea). *Mar Petrol Geol* 26:854–872
- Magalhães VH, Pinheiro LM, Ivanov MK, Kozlova E, Blinova V, Kolganova J, Vasconcelos C, McKenzie J, Bernasconi SM, Kopf AJ, Díaz-del-Río V, González FJ, Somoza L (2012) Formation processes of methane-derived authigenic carbonates from the Gulf of Cadiz. *Sediment Geol* 243–244(1):155–168
- Marcon Y, Ondreas H, Sahling H, Bohrmann G, Olu K (2014) Fluid flow regimes and growth of a giant pockmark. *Geology* 42(1):63–66. doi:[10.1130/g34801.1](https://doi.org/10.1130/g34801.1)
- Mascle J, Mary F, Praeg D, Brosolo L, Camera L, Ceramicola S, Dupré S (2014) Distribution and geological control of mud volcanoes and other fluid/free gas seepage features in the Mediterranean Sea and nearby Gulf of Cadiz. *Geo-Mar Lett* 34:89–110
- Mazzini A, Svensen H, Planke S, Guliyev I, Akhmanov GG, Fallik T, Banks D (2009) When mud volcanoes sleep: insight from seep geochemistry at the Dashgil mud volcano, Azerbaijan. *Mar Petrol Geol* 26(9):1704–1715
- Mazzini A, Svensen H, Akhmanov GG, Aloisi G, Planke S, Malthe-Sorensen A, Istadi B (2007) Triggering and dynamic evolution of the LUSI mud volcano, Indonesia. *Earth Planet Sc Lett* 261(3–4):375–388
- Milkov AV (2000) Worldwide distribution of submarine mud volcanoes and associated gas hydrates. *Mar Geol* 167(1):29–42
- Olu-Le Roy K, Sibuet M, Fiala-Medioni A, Gofas S, Salas C, Mariotti A, Fouche JP, Woodside J (2004) Cold seep communities in the deep eastern Mediterranean Sea: composition, symbioses and spatial distribution on mud volcanoes. *Deep-Sea Res PT I* 51(12):1915–1936
- Orpin AR (1997) Dolomite chimneys as possible evidence of coastal fluid expulsion, uppermost Otago continental slope, southern New Zealand. *Mar Geol* 138:51–67
- Peckmann J, Reimer A, Lüth U, Lüth C, Hansen BT, Heinicke C, Hoefs J, Reitner J (2001) Methane-derived carbonates and authigenic pyrite from the northwestern Black Sea. *Mar Geol* 177(1–2):129–150
- Pilcher R, Argent J (2007) Mega-pockmarks and linear pockmark trains on the West African continental margin. *Mar Geol* 244(1–4):15–32
- Praeg D, Ceramicola S, Barbieri R, Unnithan V, Wardell N (2009) Tectonically-driven mud volcanism since the late Pliocene on the Calabrian accretionary prism, central Mediterranean Sea. *Mar Petrol Geol* 26:1849–1865

- Rabaute A, Chamot-Rooke N (2007) Quantitative mapping of active mud volcanism at the western Mediterranean Ridge-backstop contact. *Mar Geophys Res* 28:271–293
- Riboulot V, Sultan N, Imbert P, Ker S (2016) Initiation of gas-hydrate pockmark in deep-water Nigeria: geo-mechanical analysis and modelling. *Earth Planet Sci Lett* 434:252–263. doi:[10.1016/j.epsl.2015.11.047](https://doi.org/10.1016/j.epsl.2015.11.047)
- Roberts HH (2001) Fluid and gas expulsion on the northern Gulf of Mexico continental slope: Mud-prone to mineral-prone responses. In: Natural gas hydrates: occurrence, distribution, and detection, vol 124. Geophysical monograph series. AGU, Washington, DC, pp 145–161. doi:[10.1029/GM124p0145](https://doi.org/10.1029/GM124p0145)
- Robertson AHF, Kopf A (1998) Origin of clasts and matrix within the Milano and Napoli mud volcano, Mediterranean Ridge accretionary prism. In: Robertson AHF, Emeis KC, Richter C, Camerlenghi A (eds), Proceedings of the ODP, scientific reports, vol 160. College Station, TX (Ocean Drilling Program), pp 575–596
- Sen A, Ondréas H, Gaillot A, Marcon Y, Augustin JM, Olu K (2016) The use of multibeam backscatter and bathymetry as a means of identifying faunal assemblages in a deep-sea cold seep. *Deep Sea Res Pt I* 110:33–49. doi:[10.1016/j.dsr.2016.01.005](https://doi.org/10.1016/j.dsr.2016.01.005)
- Sibuet M, Olu K (1998) Biogeographic biodiversity and fluid dependence of deep-sea cold-seep communities at active and passive margins. *Deep-Sea Res Pt II* 45(1–3):517–567
- Somoza L, Gardner JM, Díaz-del-Río V, Vázquez T, Pinheiro L, Hernández-Molina FJ, TASYO/ANASTASYA Shipboard Scientific Parties (2002) Numerous methane gas related seafloor structures identified in the Gulf of Cádiz. *Eos Transactions of the American Geophys Union* 47:541–547
- Somoza L, Diaz-del-Rio V, Leon R, Ivanov M, Fernández-Puga MC, Gardner JM, Hernández-Molina FJ, Pinheiro LM, Rodero J, Lobato A, Maestro A, Vázquez JT, Medialdea T, Fernández-Salas LM (2003) Seabed morphology and hydrocarbon seepage in the Gulf of Cadiz mud volcano area: acoustic imagery, multibeam and ultra-high resolution seismic data. *Mar Geol* 195(1–4):153–176
- Somoza L, Medialdea T, León R, Ercilla G, Vázquez JT, Farran M, Hernández-Molina FJ, González FJ, Juan C, Fernández-Puga MC (2012) Structure of mud volcano systems and pockmarks in the region of the Ceuta Contourite Depositional System (Western Alborán Sea). *Mar Geol* 332–334:4–26
- Soter S (1999) Macroscopic seismic anomalies and submarine pockmarks in the Corinth-Patras rift, Greece. *Tectonophysics* 308(1–2):275–290. doi:[10.1016/S0040-1951\(99\)00090-6](https://doi.org/10.1016/S0040-1951(99)00090-6)
- Stakes DS, Orange D, Paduan JB, Salamy KA, Maher N (1999) Cold-seeps and authigenic carbonate formation in Monterey Bay, California. *Mar Geol* 159(1–4):93–109
- Sultan N, Marsset B, Ker S, Marsset T, Voisset M, Vernant AM, Bayon G, Cauquil E, Adamy J, Colliat JL, Drapeau D (2010) Hydrate dissolution as a potential mechanism for pockmark formation in the Niger delta. *J Geophys Res-Sol Ea* 115 (B8):n/a–n/a. doi:[10.1029/2010jb007453](https://doi.org/10.1029/2010jb007453)
- Toyos MH, Medialdea T, León R, Somoza L, Gonzalez FJ, Meléndez N (2016) Evidence of episodic long-lived eruptions in the Yuma, Ginsburg, Jesús Baraza and Tasyo mud volcanoes, Gulf of Cádiz. *Geo-Mar Lett.* doi:[10.1007/s00367-016-0440-z](https://doi.org/10.1007/s00367-016-0440-z)
- Van Weering TJ, de Haas H, Akhmetzamov AM, Kenyon NH (2003) Giant carbonate mounds along the Porcupine and SW Rockall Trough margins. In: Mienert J, Weaver P (eds) European margin sediment dynamics, side-scan sonar and seismic images. Springer, Berlin, pp 211–216
- Volgin AV, Woodside JM (1996) Sidescan sonar images of mud volcanoes from the Mediterranean Ridge: causes of variation in backscatter intensity. *Mar Geol* 132(1–4):39–53
- Whiticar MJ (2002) Diagenetic relationships of methanogenesis, nutrients, acoustic turbidity, pockmarks and freshwater seepages in Eckernförde Bay. *Mar Geol* 182(1–2):29–53. doi:[10.1016/s0025-3227\(01\)00227-4](https://doi.org/10.1016/s0025-3227(01)00227-4)
- Wirsig C, Kowsmann RO, Miller DJ, de Oliveira Godoy JM, Mangini A (2012) U/ Th-dating and post-depositional alteration of a cold seep carbonate chimney from the Campos Basin offshore Brazil. *Mar Geol* 329–331:24–33

- Woodside JM, Ivanov MK, Limonov AF, Shipboard Scientists of the Anaxiprobe Expeditions (1998) Shallow gas and gas hydrates in the Anaximander Mountains regions, eastern Mediterranean Sea. In: Henriet JP, Mienert J (eds) Gas hydrates: relevance to world margin stability and climate change, vol 137. Geological Society, London, Special Publications, pp 177–193
- Woodside JM, Volgin AV (1996) Brine pools associated with Mediterranean Ridge mud diapirs: an interpretation of echo-free patches in deep two sidescan sonar data. *Mar Geol* 132(1–4):55–61
- Zitter TAC, Huguen C, Woodside JM (2005) Geology of mud volcanoes in the Eastern Mediterranean from combined sidescan and submersible surveys. *Deep-Sea Res Pt I* 52 (3):457–475

Abyssal Hills and Abyssal Plains

Marie-Helene Cormier and Heather Sloan

Abstract Abyssal hills and abyssal plains makeup the majority of the seafloor, and thus cover vast amount of the Earth's surface. Abyssal hills form in the young oceanic lithosphere near mid-ocean ridges. These elongate, ridge-parallel hills and intervening valleys provide the characteristic fabric of the recently accreted and sparsely sedimented seafloor. Near-bottom investigations document that abyssal hills owe most of their morphology to extensional faulting. Their tectonically-driven growth continues as far as ~ 35 km from the spreading axis, thus defining a broader plate boundary zone within which the parting plates acquire their steady-state motion. Abyssal hill morphology is sensitive to key aspects of seafloor accretion, and thus preserves accurate records of changing spreading rate, lithospheric thermal structure, and plate boundary geometry. In general, the slower the spreading rate, the larger their dimensions are. This relationship is modulated by regional variations in the thermal structure of the lithosphere, such as may be produced by proximity to hot spots, cold spots, or transform faults and non-transform ridge offsets. As divergent plate motion rafts the aging, subsiding oceanic lithosphere away from the mid-ocean ridge, abyssal hills are generally slowly buried beneath layers of sediments. However, extreme variability in sedimentation rates means that the burial of abyssal hills by sediments is not predictably related to the age of the lithosphere. In fact, the rugged fabric of the abyssal hills is transformed into the remarkably flat surface of the abyssal plains only where oceanic basins are within reach of the fast-moving turbidity currents that originate along the continental margins.

M.-H. Cormier (✉)

Graduate School of Oceanography, University of Rhode Island, Narragansett,
RI 02882, USA

e-mail: mhgormier@uri.edu

H. Sloan

Lehman College, City University of New York,
250 Bedford Park Blvd West, Bronx, NY 10468, USA
e-mail: heather.sloan@lehman.cuny.edu

1 Abyssal Hills

Aligned sub-parallel to spreading centers, the repetitive pattern of elongate abyssal hills and intervening valleys creates the distinctive fabric of the young seafloor (Figs. 1 and 2). They were first detected in the mid-twentieth century thanks to the advent of sonar technology (Heezen et al. 1959). As more of the seafloor was ensonified, it became apparent that abyssal hills were a product of seafloor spreading and a ubiquitous feature of the younger oceanic crust. Abyssal hills are often introduced as the most common morphological feature on Earth's surface (Menard 1964; Macdonald et al. 1996; Goff et al. 2004; Buck et al. 2005).

Early near-bottom sonar instruments and direct observations from submersible documented the interplay of normal faulting and volcanism that results in abyssal hill relief (Luyendyk 1970; Rea 1975; Lonsdale 1977; Macdonald and Luyendyk 1985). Later, emerging swath (multibeam) sonar systems produced the first detailed bathymetric maps with a resolution similar to that of land-based topographic maps, revealing the full three-dimensionality of these features (Goff 1992). As data coverage of the ridge flanks continues to expand, so does our understanding of abyssal hill morphology. Many questions about the formation and evolution of abyssal hills remain unsolved or debatable.

This chapter summarizes decades of investigations on abyssal hills and presents a consensus understanding of how spreading rates, lithosphere thermal structure, and changing plate boundary geometry combine to define the varying characteristics of abyssal hills.

1.1 Abyssal Hills Are Shaped by Extensional Tectonics

Direct visual observations, side-scan sonar imagery, and swath bathymetry have established that abyssal hill relief results primarily from slip on normal (extensional) faults (Macdonald 1982; Searle et al. 1984; Macdonald et al. 1996; Goff 2015; Olive et al. 2015). Normal faults initiate about 2–3 km from the axis of accretion, regardless of spreading rates (Macdonald et al. 1982; Searle 1984). Fault length and fault throw (vertical component of slip) continue to increase with distance from the ridge axis for at least 35 km (Alexander and Macdonald 1996; Sloan and Patriat 2004a). This distance is consistent with the broad region of seismicity that surrounds the mid-ocean ridge (Smith et al. 2003). Abyssal hills are therefore produced by a system of interconnected steeply- to moderately-dipping normal faults that continue to accumulate slip up to tens of kilometers away from the ridge axis. Their ultimate morphology thus represents an integrated response to processes that occurred within the broad (at least 70 km-wide) plate boundary zone.

Several tectonic models (Fig. 3) account for the variable morphology of abyssal hills, each one applicable to a particular region (see Goff 1991 and Macdonald et al. 1996 for reviews, and Sauter et al. 2013 for the definition of a new class of abyssal

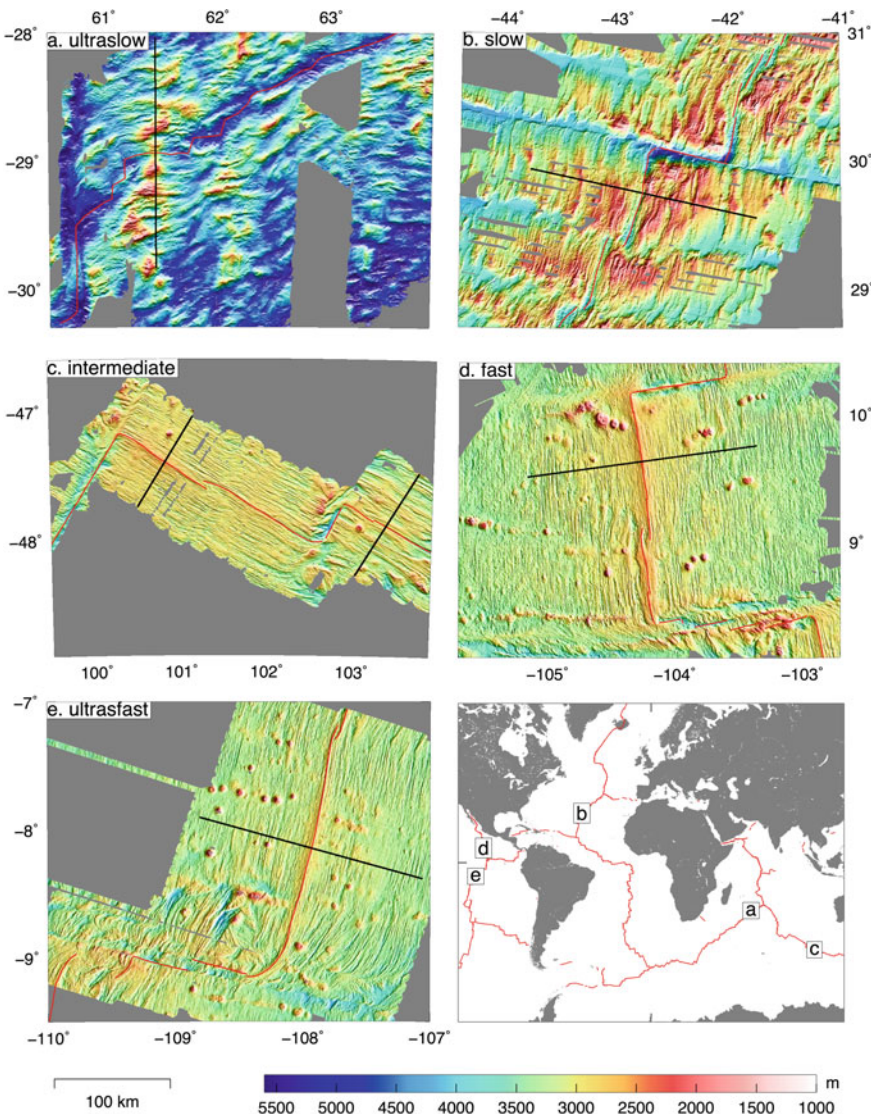


Fig. 1 Five bathymetric maps displaying representative examples of abyssal hill morphology formed at a range of spreading rates, from **a** ultraslow to **e** ultrafast. Thin red lines mark the spreading axes and transform faults. Black lines locate the bathymetric profiles displayed in Fig. 2. Index map at bottom right shows the locations of these five examples

hills). Most models distinguish between “inward-dipping” normal faults, those producing scarps that face toward the spreading center, versus “outward-dipping” faults (those producing scarps that face away from the spreading centers). In the most classic model abyssal hills are the results of “horst and graben” tectonics

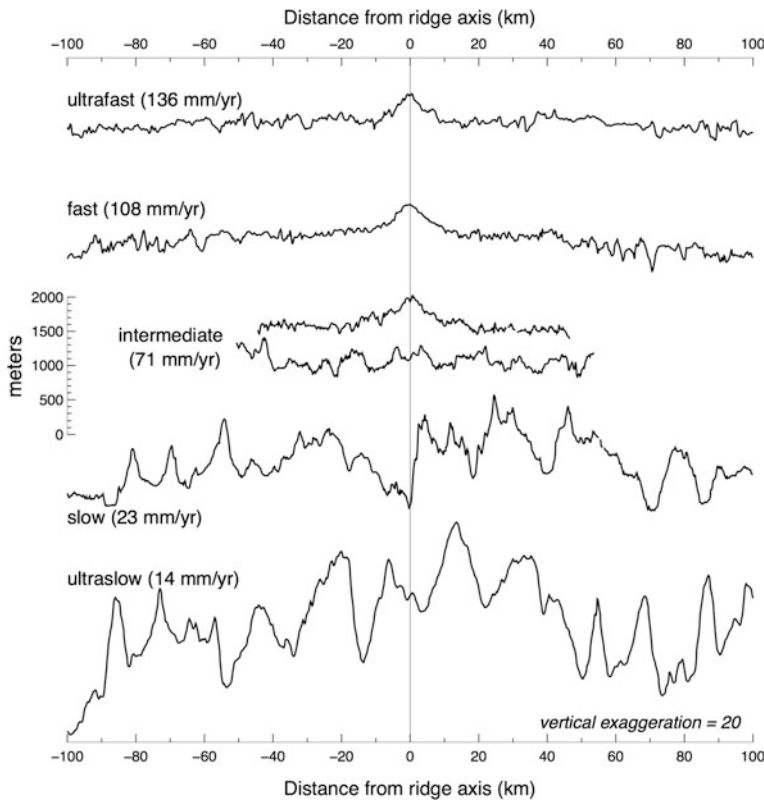


Fig. 2 Bathymetric profiles across the long axis of abyssal hills for a representative range of spreading rates, from ultrafast (*top*) to ultraslow (*bottom*). Profiles are located with black lines in Fig. 1. All profiles are displayed at the same scale with a vertical exaggeration of 20:1. Note the similarity of the top three profiles, all of which correspond to spreading centers marked by an axial high, from intermediate to ultrafast spreading rates. This is in contrast to the variability of the bottom three profiles, which correspond to spreading centers marked by a rifted axis, from ultra-slow to intermediate spreading rates

(Fig. 3a), with each individual hill bounded by an inward-dipping fault and an outward-dipping fault. For fast and intermediate spreading ridges where the spreading axis corresponds to a 15–20 km-wide axial high (see Chapter “[Mid-Ocean Ridges](#)”; Figs. 1 and 2), lavas erupting from the summit area may flow outward for long distances and repeatedly drape over nascent outward-dipping fault scarps; where lavas reach the base of the axial high, their flow is dammed by inward-dipping scarps bounding the youngest abyssal hills, thus reducing vertical relief (Fig. 3b). In this case, outward-dipping faults are known as “volcanic growth faults” (Macdonald et al. 1996) and might account for the somewhat gentler slope on the outward-facing side of abyssal hills compared to the inward-facing side

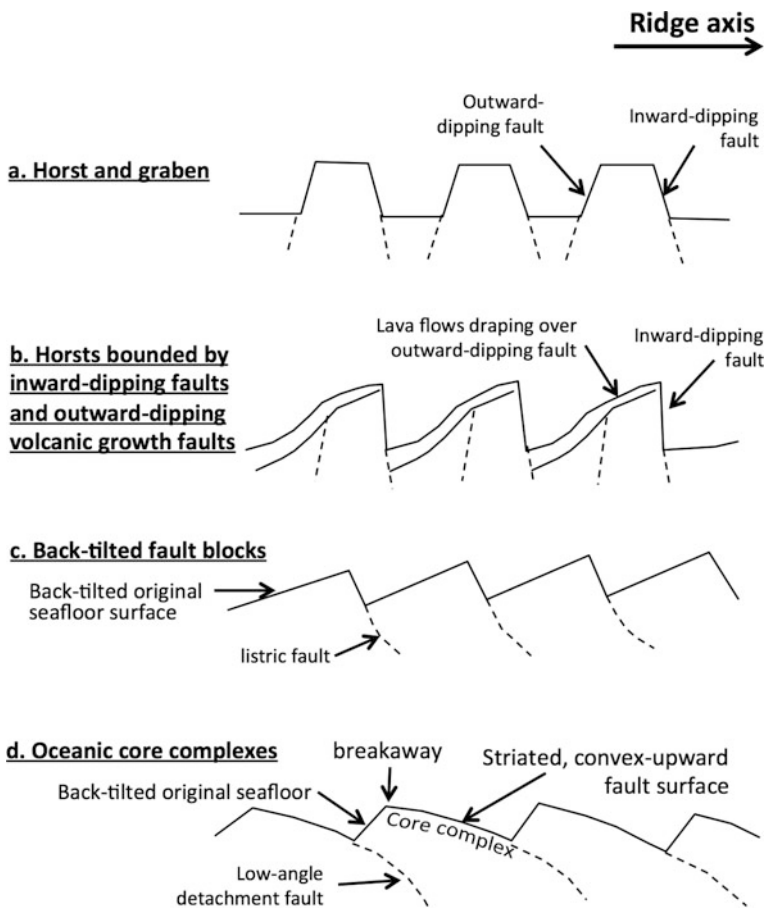


Fig. 3 Four models for the development of abyssal hills. All four models imply the existence of extensional faults that dip toward the ridge axis (inward-dipping) and/or away from the ridge axis (outward-dipping). **a** Horst and graben terrain resulting from inward- and outward-dipping normal faults forming episodically off-axis; **b** Horsts bounded by inward-dipping normal faults and by outward-dipping normal faults that are partly draped by lava flows issued from the ridge axis (volcanic growth faults); **c** Back-tilted fault blocks forming by horizontal axis rotation on inward-dipping normal faults; **d** Oceanic core complex forming through inward-dipping low-angle detachment faults. Detachment fault displays a convex-upward profile, suggesting that rotation of the slip plane occurs as isostatic uplift takes place as a result of prolonged extension on that detachment fault. Modified from Macdonald et al. (1996) and Cann et al. (1997)

(Fig. 4c). Other models may explain marked asymmetries between the inward-facing and outward-facing flanks of abyssal hills. Inward-dipping faults may be listric faults, meaning that the fault surface flattens with depth. Listric faulting results in the outward rotation, or back-tilting, of the intervening fault blocks. In such cases, the back-tilted seafloor constitutes the outward flanks of

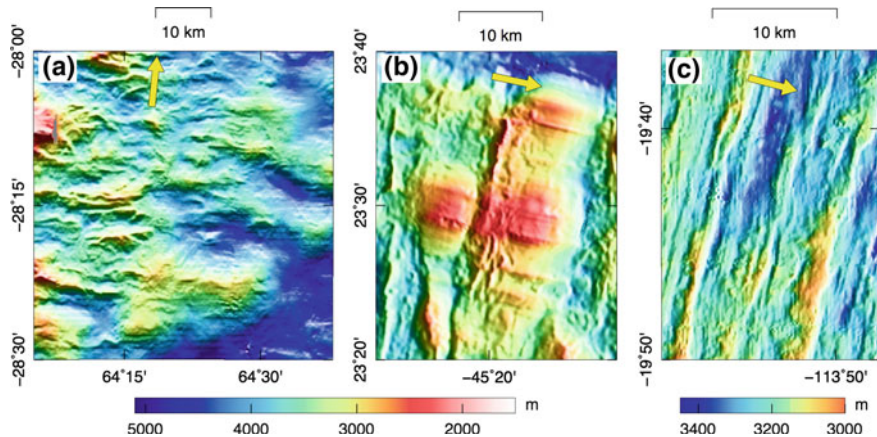


Fig. 4 Shaded-relief bathymetric maps illustrating three styles of abyssal hills. Yellow arrows point in the direction of the spreading centers. Different scales and different color scales apply to each map. **a** Abyssal hills formed at the ultraslow-spreading Southwest Indian Ridge. Abyssal hills on the west side are bounded by both inward- and outward-dipping linear fault scarps, and hummocky volcanic features such as cones are recognizable in places. In contrast, abyssal hills on the east side display a smooth relief consisting of broader ridges with rounded profiles (“smooth seafloor”). These hills lack any volcanic texture and, accordingly, almost exclusively mantle-derived rocks have been sampled from their surfaces. **b** Oceanic core complexes formed at the slow-spreading Mid-Atlantic Ridge. Subtle spreading-parallel striations mark the domed surface of the exhumed detachment fault. **c** Abyssal hills formed at the fast-spreading East Pacific Rise. Inward-dipping and outward-dipping linear fault scarps bound individual abyssal hills, with the outward-facing scarps being overprinted in places by lava lobes (“volcanic growth faults”)

abyssal hills (Fig. 3c). Occasionally, the inward-facing side and the top surface of an abyssal hill is produced by a large detachment fault (Fig. 3d), known as an oceanic core complex (Cann et al. 1997). In this case, the shallow-dipping fault plane is exhumed over up to tens of kilometers and is marked in plan-view by subtle ridge-perpendicular striations produced by asperities on the fault interface (Fig. 4b). In profile-view, these exhumed fault surfaces are convex-upward and can produce kilometer-scale vertical relief. The steeper outward-facing sides of oceanic core complexes correspond to the original seafloor surface that has been back-tilted by as much as 30° – 40° (MacLeod et al. 2009).

While abyssal hills are a product of extensional tectonics within the broader plate boundary zone, their detailed characteristics are modulated by variations in the thermal structure of the lithosphere, spreading rates, and ridge segmentation.

1.2 Influence of the Thermal Structure of the Lithosphere

Although no more than approximately 10% of the oceans has been mapped with high-resolution multibeam bathymetric sonar, existing data are sufficient to outline

some marked regional variations in the morphological characteristics of abyssal hills. The heights of abyssal hill vary by an order of magnitude, from ~ 50 to >1000 m, and their widths range from ~ 2 to >10 km (Macdonald and Luyendyk 1985; Goff 1991; Goff et al. 1995, 1997; Cochran et al. 1997; Sauter et al. 2011; Sloan et al. 2012).

This morphological variability primarily reflects regional variations in thermal structure of the lithosphere. When cooler conditions prevail near the axial region, the lithosphere is thicker and stronger (McNutt 1984; Phipps Morgan and Chen 1993). Conversely, warmer thermal structures produce thinner and weaker lithosphere. Numerical models predict that lithospheric strength and thickness are the main factors that control spacing and throw of normal faults in response to tensional stress (Shaw and Lin 1993; Buck et al. 2005; Behn and Ito 2008). This in turn, will determine abyssal hill dimensions (Escartin et al. 1999; Sauter et al. 2011; Sloan et al. 2012). Cooler, and therefore thicker and stronger lithosphere, is capable of sustaining faults that are spaced further apart and accommodate larger amount of slip, resulting in the formation of broader and taller abyssal hills.

1.3 *Influence of Spreading Rate*

Spreading rate, which varies from 10 to 150 mm/year, has a dominant influence on abyssal hill morphology (Figs. 1, 2, and 5): Namely, the slower the spreading rate, the taller and wider the abyssal hills become (Malinverno 1991; Goff et al. 1997; Kriner et al. 2006; Goff 2015). This correlation primarily reflects the fact that the slower the spreading rate, the thicker and stronger the lithosphere is within the axial region (see Chapter “[Mid-Ocean Ridges](#)”). This thicker and stronger lithosphere is expected to sustain longer-lived faults that will develop larger throw to produce larger abyssal hills. In detail, the relationship between abyssal hill dimensions and spreading rates differs depending on the morphology of the ridge axis (Goff 2015). The correlation is strong for abyssal hills that formed near spreading centers characterized by an axial valley (<70 mm/year), with ultraslow spreading ridges producing the most rugged, highest amplitude abyssal hill relief. But all abyssal hills that formed at spreading centers characterized by an axial high (>70 mm/year) have similar smaller dimensions (Figs. 1, 2, and 5). Abyssal hills formed at intermediate spreading rates (50–90 mm/year), a rate at which the axial morphology transitions between axial valley and axial high, illustrate this dichotomy: At equal spreading rates, smaller abyssal hills are produced where an axial high is present rather than an axial valley (Figs. 1c and 2).

Overall, normal faults account for a small portion of the full spreading rate, with the remainder being accommodated by magmatic accretion of new seafloor within the ~ 5 km-wide neovolcanic zone. However, as spreading rate decreases, the percentage of extension accommodated by normal faults increases from an estimated $\sim 5\%$ at the fast-spreading East Pacific Rise (Macdonald and Luyendyk 1977; Cowie et al. 1993; Alexander and Macdonald 1996) to about 10% at the

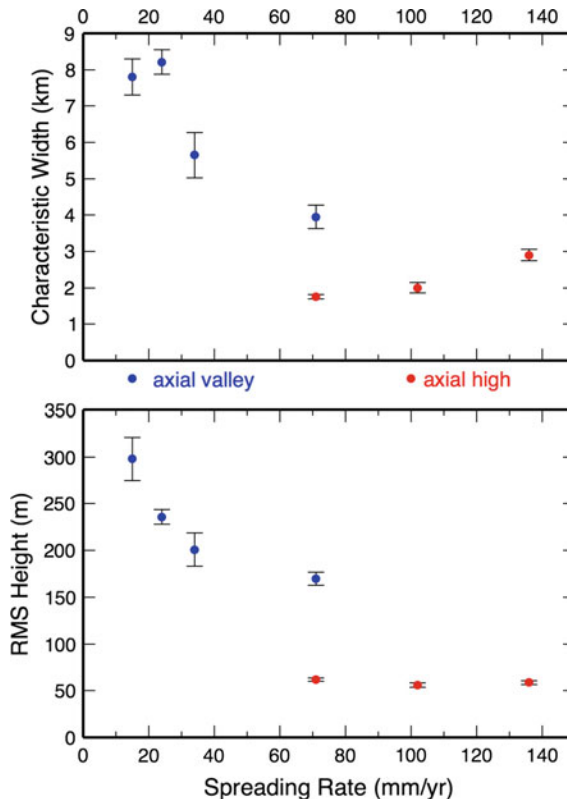


Fig. 5 Relationship between spreading rates and the heights or widths of abyssal hills. Here, the RMS height approximates the average deviation of bathymetry from the mean local depth, and thus corresponds to less than half the average height of the abyssal hills; nonetheless, this parameter objectively evaluates seafloor roughness and applies to all abyssal hills similarly and proportionally. *Blue dots* correspond to spreading centers with a rifted axis, and *red dots* correspond to spreading centers with an axial high. *Error bars* indicate 1 standard deviation. The dimensions of abyssal hills generally decrease with increasing spreading rates. However, abyssal hills formed at spreading centers defined by an axial high display smaller dimensions that remain similar across a broad range of spreading rates (70–140 mm/year). After Goff et al. (1997) and Sloan et al. (2012) (color figure online)

slow-spreading Mid-Atlantic Ridge (Searle et al. 1998a; Escartin et al. 1999). At slow spreading rates, prolonged slip on inward-dipping detachment faults (Figs. 3d and 4b) may occasionally account for most or all of the spreading rate (Cann et al. 1997; Smith et al. 2008; Cannat et al. 2006; Cann et al. 2015). Magma supply at ultraslow spreading rates (<15 mm/year) may become so restricted that lithosphere with little or no extrusive crust is produced for extended periods (>1 Myr), directly exposing mantle on the slip surface of low-angle detachment faults (Cannat et al. 2006;

Sauter et al. 2013). This exposed upper mantle produces an unusually smooth seafloor and, likewise, produces abyssal hills that are strikingly smooth compared to adjacent abyssal hills that expose volcanic rocks (Fig. 4a). In marked contrast, long-lived detachments faults and core complexes have never been reported at fast and ultrafast spreading rates (>90 mm/year). Instead, fast-spreading abyssal hills (Figs. 3a, 3b and 4c) are mostly the product of horst-and-graben tectonics, although volcanic growth faults may mask their true nature in places (Macdonald et al. 1996).

1.4 *Influence of Mantle Hot Spots and Cold Spots*

Although spreading rate is a general predictor of abyssal hill characteristics, regional thermal anomalies can have an overriding effect. The presence of a hot spot at or near a spreading center creates a warmer thermal structure capable of producing smaller, less rugged abyssal hills than expected. The northern Mid-Atlantic Ridge near the robust Iceland hot spot is a well-known example: Abyssal hills produced along the Reykjanes Ridge south of Iceland display unexpectedly small dimensions that are more akin to those produced at fast spreading centers (Searle et al. 1998b). The opposite effect occurs in areas with anomalously low mantle temperatures (cold spots), such as along the intermediate-spreading Southeast Indian Ridge near the Australian-Antarctic Discordance: There, the ridge axis and the adjacent abyssal hills display all the characteristics of a slow-spreading ridge (Sempéré et al. 1991). The effect of cooler mantle temperatures has also been shown to be the dominant factor controlling the increasingly rougher fabric of abyssal hills along the Southwest Indian Ridge as it approaches the Rodriguez triple junction (Sauter et al. 2011; Sloan et al. 2012). Thus, abyssal hill morphology across the world's ocean records the impact of anomalous mantle temperatures, an impact that may locally dominate that of spreading rates.

1.5 *Influence of Ridge Segmentation*

The mid-ocean ridge is segmented and offset at intervals by transform faults and by smaller (<30 km) non-transform discontinuities. The off-axis traces of these offsets are pervasive morphologic features on the ridge flanks that interrupt the regular pattern of ridge-parallel abyssal hills, and strongly affect the morphology of abyssal hills terminations.

Transform faults remain stable over long periods of time and create linear fracture zones on the flanks that parallel the spreading direction. Non-transform offsets, on the other hand, tend to migrate along the ridge axis. As a result, their off-axis traces, called discordant zones, often strike obliquely to the ridge. Discordant zones occur symmetrically on both flanks of a ridge axis, producing

V-patterns that point in the direction the discontinuity has been migrating over time (Figs. 6c, d, and 7). The evolving geometry of the spreading axis is thus conveniently recorded in the patterns of fracture zones and discordant zones that are preserved on the ridge flanks (Sloan and Patriat 1992; Cormier et al. 1996).

Spreading rate has a strong influence on the style of non-transform discontinuities, and therefore on the morphology of the discordant zones they create. At slow-spreading rates, non-transform discontinuities offset the axial valley with little or no overlap between ridge segments. The off-axis discordant zones they produce are broad, deep corridors usually containing a series of closed-contour basins (Figs. 1b and 6c). At fast spreading rates, the two offset ridge segments curve toward each other and overlap, enclosing a deep nodal basin between them (Chapter “Mid-Ocean Ridges”; Fig. 6d). This type of non-transform offset is called an overlapping spreading centers, or OSC (Macdonald and Fox 1983). OSCs migrate along the axis, the retreating segment episodically cutting inside of itself and transferring onto one side of the ridge axis the abandoned curved ridge tip and adjacent nodal basin (Fig. 6d). As a result, where OSCs are steadily migrating in one direction, the V-shaped discordant zone consists of a broad zone of curved abandoned ridge tips and intervening nodal basins on one side of the ridge axis,

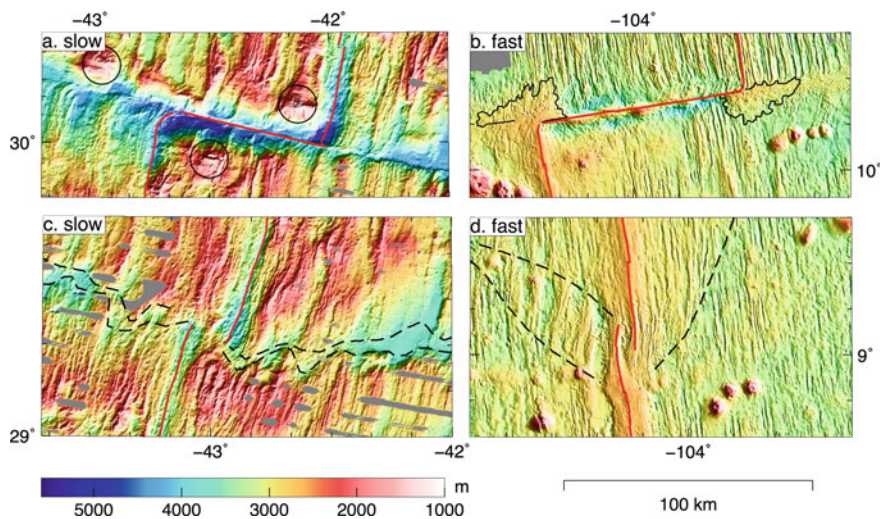


Fig. 6 Varying abyssal hill morphologies in proximity to ridge offsets. *Red lines* mark the plate boundary. **a** Atlantis Transform Fault at the slow-spreading Mid-Atlantic Ridge. *Black circles* outline oceanic core complexes that formed at the inside corner of the ridge-transform intersections; **b** Clipperton transform fault at the fast-spreading East Pacific Rise. *Black lines* highlight the “rooster’s combs” that form at some ridge-transform intersections, when magma is injected beyond the segment end and erupts onto the adjacent older plate; **c** non-transform offset at the slow-spreading Mid-Atlantic Ridge. *Dashed lines* outline the off-axis discordant zone and highlight the changing position of this offset through time; **d** OSC at the fast-spreading East Pacific Rise. This non-transform offset has migrated southward, forming a V-shaped discordant zone (*dashed lines*) that points in the direction of migration

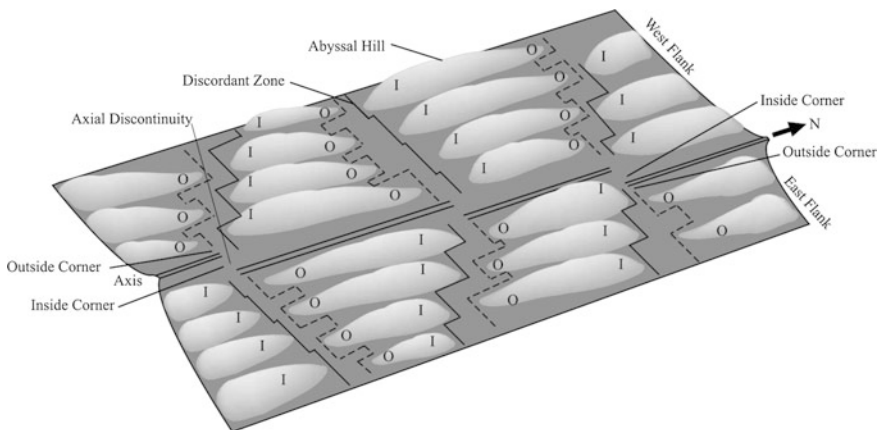


Fig. 7 Schematic of inside corners (*I*) and outside corners (*O*) bathymetry at slow-spreading ridges (Sloan and Patriat, 2004b) (Reprinted from Geochemistry Geophysics Geosystem, 5, Sloan and Patriat, Reconstruction of the flanks of the Mid-Atlantic Ridge, 28° to 29°N: implications for evolution of young oceanic lithosphere at slow-spreading centers, 3, 2004, with permission from John Wiley and Sons). A series of axial segments (*double lines*) generate swaths of abyssal hills separated by discordant zones. Higher abyssal hills form at the inside corners of axial offsets and smaller abyssal hills form near outside corners. This inside corner/outside corner asymmetry is preserved on the ridge flanks, resulting in an asymmetric pattern of abyssal hills terminations: The older seafloor across a discordant zone or a fracture zone is counter-intuitively shallower than the younger side (see also Fig. 6a, c)

while on the other side it consists of a more subtle but well defined lineament separating curved abyssal hills from linear abyssal hills (Wilson 1990).

Ridge offsets also have a marked influence on the morphology of abyssal hill terminations. At slow spreading rates, abyssal hills formed at “inside corners” of a ridge-transform intersection, the corner formed by the ridge axis and the active transform fault, have greater heights and widths than abyssal hills formed at “outside corners”, the corner formed by the ridge axis and the inactive fracture zone (Collette 1986; Severinghaus and Macdonald 1988; Sloan and Patriat 2004a) (Fig. 6). This inside-outside corner depth asymmetry is particularly pronounced where high-relief oceanic core complexes have formed at inside corners; core complexes have never been observed to form at outside corners. Such asymmetry is generally ascribed to a contrast in lithospheric coupling across a ridge-transform intersection, whereby newly created seafloor at the inside corner can adjust vertically where it abuts the active plate boundary, but becomes welded to the older, deeper lithosphere across the inactive fracture zone at the outside corner (Severinghaus and Macdonald 1988).

No such consistent depth asymmetry is observed at offsets of the fast spreading ridges. There, magma is sometime injected beyond the end of the ridge segment, through the ridge-transform intersection, and onto the older adjacent lithosphere, the associated volcanism creating a volcanic carapace with lobate edges that

overprints the older abyssal hills (Barth et al. 1994). These features produce subdued ridge-transform intersection highs, which, in map view, have outlines reminiscent of a rooster's comb. The formation of these ridge-transform intersection highs obliterates the trough that developed along the active transform fault and as a result, fracture zones that formed at fast spreading ridges may have a subtle bathymetric expression (Fig. 5a, b).

As the ridge axis approaches a transform fault, it tends to curve toward the segment on the other side of the offset in response to local rotation of the stress field, in the transition from tension to shear (Fox and Gallo 1984; Phipps Morgan and Parmentier 1984; Grindlay and Fox 1993; Croon et al. 2010). Accordingly, at all spreading rates, abyssal hills that form near the outside corners of a ridge-transform intersection echo the shape of the ridge axis and curve towards the offset (Fig. 6a, b). On the other hand, those abyssal hills that formed near the inside corners may display curvature in either direction or no curvature at all. There, strong coupling across the active transform domain may be partially accommodated by distributed strike-slip deformation and result in a curvature in the direction opposite to that of the ridge axis (Sonder and Pockalny 1999; Croon et al. 2010).

2 The Abyssal Plains

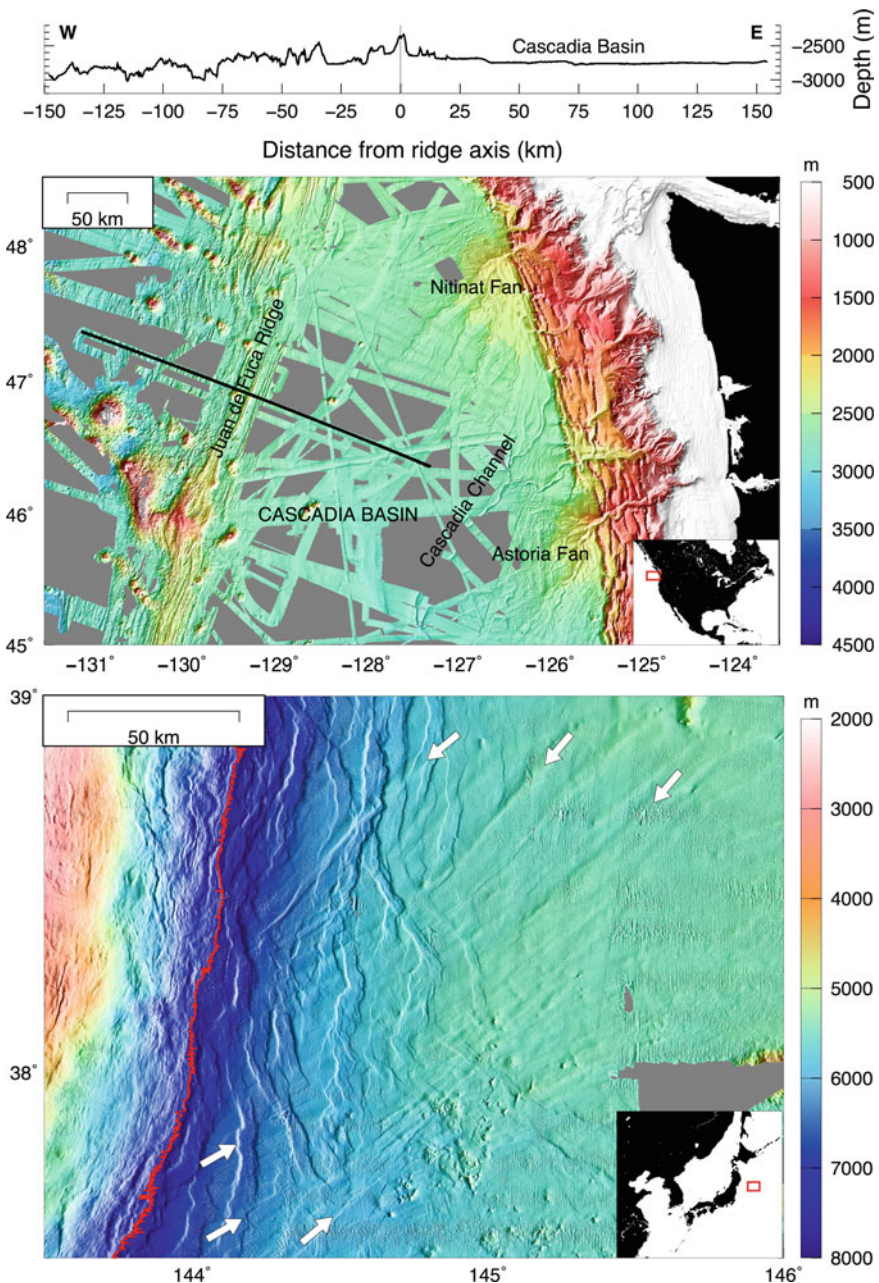
As young oceanic lithosphere is rafted away from the mid-ocean ridges, sediments slowly accumulate over the aging and subsiding seafloor and gradually smother the rugged relief of the abyssal hills. The aging lithosphere becomes part of an oceanic basin, these deeper areas delimited by mid-ocean ridges, continental margins, and/or oceanic plateaus (see Chapter “[Origin and Geomorphic Characteristics of Ocean Basins](#)”). Deep oceanic basins have water depths ranging between ~ 3 and ~ 6 km and constitute $\sim 40\%$ of the World’s oceans. Some are thickly sedimented and present a remarkably flat (slope $< 0.05^\circ$) seafloor known as an abyssal plain. Because abyssal plains are commonly thought of as vast, monotonous submarine deserts, they remain largely under-investigated. Perhaps unexpected features await discovery in these vast, little-explored regions of seafloor.

Two main sedimentary processes deliver sediments to deep oceanic basins: Clastic sedimentation, the delivery of terrigenous material via episodic, fast-moving turbidity currents through the canyons and deep-sea channels that punctuate the continental slopes, and pelagic sedimentation, the slow, steady raining of particulates through the water column (see Chapter “[Submarine Canyons and Gullies](#)”). Only one of these two processes, turbidity currents, can generate the flat, sub-horizontal seafloor of the abyssal plains. A turbidity current consists of a slurry of seawater and sediments that is set in motion by earthquakes, tsunamis, or storms. Turbidity currents originate on continental margins and flow far, even on very gentle slopes. The sedimentary deposits they produce, known as turbidites, produce flat, regular sediment layers that may extend far from the continental margins. Where oceanic basins are bounded by passive margins on their landward side,

such as in the Atlantic Ocean or the Antarctic Ocean, turbidity currents can flow unabated by any obstacle and produce smooth abyssal plains over time. However, where oceanic basins are bounded on their landward side by deep subduction trenches, such as around most of the Pacific Ocean, terrigenous sediments carried by turbidity currents become trapped within these trenches and do not reach the adjacent oceanic basins. There, the abyssal hill fabric typically remains visible through the thin drape (<0.5 km) of slowly-accumulating pelagic sediments.

The extreme variability of sediment accumulation in the oceanic basins is well illustrated by the contrasting seafloor fabrics of the Juan de Fuca Plate and that of the Pacific Plate at its western border (Fig. 8). The Juan de Fuca Plate, which is everywhere younger than 10 Ma, is blanketed by up to 2 km of sediments as a result of the exceptionally high rate of terrigenous sediments supplied from North America during the Pleistocene glacial periods (Normark and Reid 2003). In fact, the trench associated with the Cascadia subduction zone is entirely filled with turbidites, with deep sea fans and deep-sea channels extending seaward of the subduction zone, delivering sediments directly to the Cascadia Basin and producing a young, smooth abyssal plain. In stark contrast, the Pacific plate where it approaches the Japan Trench is an order of magnitude older (130–140 Myr), and yet the seafloor still faintly displays its inherited abyssal hill fabric. The comparatively thin (~500 m) sediment cover for this old seafloor is primarily explained by two factors: this area of the Pacific plate has never drifted through regions with high pelagic sedimentation rates, and only scant terrigenous sediments is supplied from central Japan. In fact, some oceanic basins have never accumulated any significant sediment cover, such as the Southwest Pacific Basin. There, a vast area of seafloor 34–85 Myr-old remains essentially bare of sediments (Rea et al. 2006).

Whether lying beneath the sediments of an abyssal plain or mostly bare of sediments, ancient abyssal hills are reactivated on the outer rise of subduction zones, the area where the subducting plate bends slightly upward and then steeply downward as it approaches the trench (see Chapter “[Oceanic Trenches](#)”). Where the abyssal hill fabric is aligned sub-parallel to the subduction zone, the normal faults that define the flanks of abyssal hills are reactivated to accommodate the bending of the plate. Where abyssal hill fabric strikes obliquely to the subduction zone, the plate brakes along a new set of normal faults that strike sub-parallel to the subduction zone (Fig. 8). These new faults appear to be affected by the pre-existing abyssal hill fabric, terminating or stepping-over where they intersect abyssal hills; this geometry suggests that even obliquely striking abyssal hill faults are to some extent reactivated at subduction zones. Thus, at the end of their life cycle, abyssal hills may provide a convenient pathway for seawater to penetrate through the oceanic crust and the lithospheric mantle, possibly leading to the lubrication of the interface between subducting plate and overriding plate. Their reactivation may thus facilitate the input of water in the mantle wedge above the subducting plate, enhancing arc volcanism and possibly leading to serpentinization in the upper mantle.



◀Fig. 8 Abyssal hills and abyssal plains near the end of their life cycle at two contrasting subduction zones; insets locate the displayed areas. *Top map* Bathymetry of the Juan de Fuca Ridge and Juan de Fuca Plate off the west coast of North America. An exceptionally high sedimentation rate completely obscures subduction trench and abyssal hills. The *black line* locates the bathymetric profile shown above to illustrate the flat bathymetry of the Cascadia Basin. *Bottom map* Bathymetry of the Pacific plate off the Japan Trench (Fujiwara et al. 2011). Some of the world's oldest seafloor (~ 140 Myr) is subducting beneath Japan and yet, the abyssal hill fabric (*white arrows*) remains visible through the relatively thin sediment cover. A new set of normal faults oriented sub-parallel to the trench axis (*red*) cross-cuts the pre-existing fabric of the abyssal hills to accommodate the bending of the subducting plate

3 Some Outstanding Questions

Developments in deep-submergence and marine geophysical technology over the past few decades have lead to a much improved characterization of abyssal hills. Yet, many questions regarding their formation and evolution remain either unanswered or debatable. Some are listed below.

3.1 What Is the Width of the Plate Boundary Zone at Mid-Ocean Ridges?

The distance over which abyssal hills continue to grow, and thus the distance over which lithospheric deformation accumulates, is a direct measurement of the width of plate boundary zone. The documented growth of abyssal hills out to at least 35 km from the ridge axis (see Sect. 1.1) indicates that the plate boundary zone is at minimum 70 km wide. However, data are lacking that could test some follow-up questions, such as: What is the maximum extent of the plate boundary zone? How does the width of the plate boundary zone depend (or not) on spreading rates, patterns of axial segmentation, or regional variations in the thermal structure of the lithosphere?

At two slowly-diverging plate boundaries on land, in Iceland and along the Afar Rift in Ethiopia, geodetic investigations indicate deformation zones as wide as 100–150 km (Wright et al. 2012). However, underwater geodesy is still an emerging technology and the true extent of the deformation zone at submerged mid-ocean ridges remains to be quantified. Alternative and/or complementary methods that could contribute useful evidence include: (1) the acquisition of high-resolution bathymetric data that extend as far as 100–150 km to either side of various mid-ocean ridges, presumably encompassing the entire plate boundary zone; (2) the acquisition of high-resolution seismic reflection profiles where sediments accumulate sufficiently fast to record the full history of tectonic deformation in their stratigraphy; (3) the long-term deployment of arrays of ocean bottom seismometers across the plate boundary zone in order to determine the width of the zone of background seismicity.

3.2 Do Abyssal Hills Offer Long-Lived Pathways for Fluids Through the Oceanic Crust?

Various observations, including fossil hydrothermal sites and enhanced heat flow measurements, suggest that the faults bounding the abyssal hills may favor hydrothermal circulation off-axis (Abbott et al. 1992; Haymon et al. 2005). If fluid circulation continued to focus along the flanks of abyssal hills long after they become buried under a thick sediment cover, this process may be expressed in the sedimented seafloor as clusters of dissolution structures or pockmarks that align with the trend of the buried abyssal hills. More extensive investigation of the vast abyssal plains using high-resolution multibeam bathymetric and sidescan sonars should record the subtle expression of such features, if present.

3.3 How Does Mass Wasting Affect Abyssal Hill Morphology?

Talus is commonly observed at the base of young abyssal hills and landslide scars have been mapped along the walls of rift valleys and transform faults (Mitchell et al. 2000; Cannat et al. 2013). However, it remains unclear whether fresh talus or landslides only occur where faults are recently active, or whether they can also be indicative of slope instability and the progressive erosion of abyssal hill flanks. Detailed geophysical and near-bottom investigations that extend beyond the broader plate boundary zone may provide an answer.

3.4 Are the Abyssal Plains as Featureless as We Think?

The abyssal plains remain largely unexplored: Do subtle features occur across their vast expanses that have escaped detection? For example, does low-level fluid circulation lead to the formation of pockmarks or dissolution structures across the abyssal plain? Recent investigations suggest that turbidity currents may evolve into erosional debris flows capable of crossing the flat abyssal plain (Talling et al. 2007): Do such events leave characteristic signatures on the seafloor? Are rare, large magnitude intraplate earthquakes producing liquefaction features equivalent to the clusters of sand blows observed on land, or some subtle fault scarps and fissures? The morphological signature of volcanism related to hotspots is obvious, but how common are the “petit-spot” volcanoes that erupt on subducting plates seaward of trenches in response to plate flexure, as characterized by Hirano et al. (2006)?

Acknowledgements We are grateful for the public availability of multibeam bathymetric data through the National Geophysical Data Center (<https://www.ngdc.noaa.gov/mgg/bathymetry/multibeam.html>) and GeoMapapp (<http://www.geomapapp.org>). These bathymetric data have been processed with MB-System and all figures have been generated with GMT, both freely available software (Caress et al. 2015; Wessel et al. 2013). We thank D. Sauter for the gridded bathymetric data of the Southwest Indian Ridge, T. Fujiwara for the gridded bathymetric data of the Japan Trench, a dataset compiled by the Japan Oceanographic Data Center and JAMSTEC, and D.K. Blackman for review.

References

- Abbott DH, Stein CA, Diachuk O (1992) Topographic relief and sediment thickness: their effects on the thermal evolution of the oceanic crust. *Geophys Res Lett* 19:1975–1978
- Alexander RT, Macdonald KC (1996) Sea Beam, SeaMARC II, and Alvin-based studies of faulting on the East Pacific Rise 9°20'–9°50'N. *Mar Geophys Res* 18:557–587
- Barth GA, Kastens KA, Klein E (1994) The origin of bathymetric highs at ridge-transform intersections: a multi-disciplinary case study at the Clipperton Fracture Zone. *Mar Geophys Res* 16:1–50
- Behn MD, Ito G (2008) Magmatic and tectonic extension at mid-ocean ridges: 1. Controls on fault characteristics. *Geochem Geophys Geosyst*. doi:[10.1029/2008GC001965](https://doi.org/10.1029/2008GC001965)
- Buck WR, Lavier LL, Poliakov ANB (2005) Modes of faulting at mid-ocean ridges. *Nature* 434:719–723
- Cann JR, Blackman DK, Smith DK, McAllister E, Janssen B, Mello SLM, Avgerinos A, Pascoe AR, Escartin J (1997) Corrugated slip surfaces formed at ridge-transform intersections on the Mid-Atlantic Ridge. *Nature* 385:329–332
- Cann JR, Smith DK, Escartin J, Schouten H (2015) Tectonic evolution of 200 km of Mid-Atlantic Ridge over 10 million years—interplay of volcanism and faulting. *Geochem Geophys Geosyst*. doi:[10.1002/2015GC005797](https://doi.org/10.1002/2015GC005797)
- Cannat M, Sauter D, Mendel V, Ruellan E, Okino K, Escartin J, Combier V, Baala M (2006) Modes of seafloor generation at a melt-poor ultraslow-spreading ridge. *Geology* 34:605–608
- Cannat M, Mangeney A, Ondréas H, Fouquet Y, Normand A (2013) High resolution bathymetry reveals contrasting landslide activity shaping the walls of the Mid-Atlantic Ridge axial valley. *Geochem Geophys Geosyst* 14:996–1011
- Cochran JR, Sempéré J-C, The SEIR Scientific Team (1997) The Southeast Indian Ridge between 88°E and 120°E: Gravity anomalies and crustal accretion at intermediate spreading rates. *J Geophys Res* 102(B7):15463–15487. doi:[10.1029/97JB00511](https://doi.org/10.1029/97JB00511)
- Collette BJ (1986) Fracture zones in the North Atlantic: morphology and a model. *J Geol Soc* 143:763–774
- Cormier MH, Scheirer DS, Macdonald KC (1996) Evolution of the East Pacific Rise at 16°–19°S since 5 Ma: bisection of overlapping spreading centers by new, rapidly migrating propagating ridge segments. *Mar Geophys Res* 18:53–84
- Cowie PA, Scholtz CH, Edwards MH, Malinverno A (1993) Fault strain and seismic coupling on mid-ocean ridges. *J Geophys Res* 98:17911–17920
- Croon MB, Cande SC, Stock JM (2010) Abyssal hill deflections at Pacific-Antarctic ridge-transform intersections. *Geochem Geophys Geosyst*. doi:[10.1029/2010GC003236](https://doi.org/10.1029/2010GC003236)
- Caress DW, Chayes DN, dos Santos Ferreira, C (2015) MB-system seafloor mapping software—processing and display of swath sonar data. <http://www.mbari.org/data/mbsystem>
- Escartín J, Cowie PA, Searle RC, Allerton S, Mitchell NC, MacLeod CJ, Slootweg AP (1999) Quantifying tectonic strain and magmatic accretion at a slow spreading ridge segment, Mid-Atlantic Ridge, 29°N. *J Geophys Res* 104(B5):10421–10437

- Fox PJ, Gallo DG (1984) A tectonic model for ridge-transform-ridge plate boundaries: implications for the structure of oceanic lithosphere. *Tectonophysics* 104:205–242
- Fujiwara T, Kodaira S, No T, Kaiho Y, Takahashi N, Kaneda Y (2011) The 2011 Tohoku-Oki earthquake: displacement reaching the trench axis. *Science* 334:1240
- Goff JA (1991) A global and regional stochastic analysis of near-ridge abyssal hill morphology. *J Geophys Res* 96:21, 713–21,737. doi:[10.1029/91JB02275](https://doi.org/10.1029/91JB02275)
- Goff JA (1992) Quantitative characterization of the abyssal hill morphology along flow lines in the Atlantic Ocean. *J Geophys Res* 97:9183–9202
- Goff JA (2015) Comments on “Glacial cycles drive variations in the production of oceanic crust”. *Science* 349:1065a
- Goff JA, Tucholke BE, Lin J, Jaroslow GE, Kleinrock MC (1995) Quantitative analysis of abyssal hills in the Atlantic Ocean: a correlation between axis crustal thickness and extensional faulting. *J Geophys Res* 100:22509–22522. doi:[10.1029/95JB02510](https://doi.org/10.1029/95JB02510)
- Goff JA, Ma Y, Shah AK, Cochran JR, Sempéré J-C (1997) Stochastic analysis of seafloor morphology on the flank of the Southeast Indian Ridge: the influence of ridge morphology on the formation of abyssal hills. *J Geophys Res* 102:15521–15534
- Goff JA, Smith WHF, Marks KM (2004) The contributions of abyssal hills morphology and noise to altimetric gravity fabric. *Oceanography* 17:24–37
- Grindlay NR, Fox PJ (1993) Lithospheric stresses associated with nontransform offsets of the Mid-Atlantic Ridge: implications from a finite element analysis. *Tectonics* 12:982–1003
- Haymon RM, Macdonald KC, Benjamin SB, Ehrhardt CJ (2005) Manifestations of hydrothermal discharge from young abyssal hills on the fast-spreading East Pacific Rise flank. *Geology* 33:153–156
- Heezen BC, Tharp M, Ewing M (1959) The floors of the oceans: I. The North Atlantic. Geological Society of America, Special Paper vol 65, p 126
- Hirano N, Takahashi E, Yamamoto J, Abe N, Ingle SP, Kaneoka I, Hirata T, Kimura JI, Ishii T, Ogawa Y, Machida S, Suyehiro K (2006) Volcanism in response to plate flexure. *Science* 313:1426–1428
- Kriner K, Pockalny RA, Larson RL (2006) Bathymetric gradients of lineated abyssal hills: inferring seafloor spreading vectors and a new model for hills formed at ultra-fast rates. *Earth Planet Sci Lett* 242:98–110
- Lonsdale P (1977) Structural geomorphology of a fast-spreading rise crest: the East Pacific Rise near 3°25'S. *Mar Geophys Res* 3:251–293
- Luyendyk B (1970) Origin and history of abyssal hills in the northeast Pacific. *Geol Soc Am Bull* 81:2237–2260
- Macdonald KC (1982) Mid-ocean ridges: fine scale tectonic, volcanic and hydrothermal processes within the plate boundary zone. *Annu Rev Earth Planet Sci* 10:155–190
- Macdonald KC, Fox PJ (1983) Overlapping spreading centers: new accretion geometry on the East Pacific Rise. *Nature* 302:55–58
- Macdonald KC, Luyendyk BP (1977) Deep-Tow studies of the structure of the Mid-Atlantic Ridge crest near lat 37°N. *Geol Soc Am Bull* 88:621–636
- Macdonald KC, Luyendyk BP (1985) Investigation of faulting and abyssal hill formation on the flanks of the East Pacific Rise (21°N) using ALVIN. *Mar Geophys Res* 7:515–535
- Macdonald KC, Fox PJ, Alexander RT, Pockalny R, Gente P (1996) Volcanic growth faults and the origin of Pacific abyssal hills. *Nature* 380:125–129
- MacLeod CJ, Searle RC, Murton BJ, Casey JF, Mallows C, Unsworth SC, Achenbach KL, Harris M (2009) Life cycle of oceanic core complexes. *Earth Planet Sci Lett* 287:333–344
- Malinverno A (1991) Inverse square-root dependence of mid-ocean ridge flank roughness on spreading rate. *Nature* 352:58–60
- McNutt M (1984) Lithospheric flexure and thermal anomalies. *J Geophys Res* 89:11180–11194
- Menard HW (1964) Marine geology of the Pacific. McGraw Hill, New York
- Mitchell NC, Tivey MA, Gente P (2000) Seafloor slopes at mid-ocean ridges from submersible observations and implications for interpreting geology from seafloor topography. *Earth Planet Sci Lett* 183:543–555

- Normark WR, Reid JA (2003) Extensive deposits on the Pacific plate from late Pleistocene North American glacial lake outbursts. *J. Geology* 111:617–637
- Olive JA, Behn MD, Ito GT, Buck WR, Escartín J, Howell S (2015) Sensitivity of seafloor bathymetry to climate-driven fluctuations in mid-ocean ridge magma supply. *Science* 350:310–313
- Phipps Morgan J, Chen YJ (1993) Dependence of ridge-axis morphology on magma supply and spreading rate. *Nature* 364:706–708
- Phipps Morgan J, Parmentier EM (1984) Lithospheric stress near a ridge-transform inter-section. *Geophys Res Lett* 11:113–116
- Rea DK (1975) Model for the formation of topographic features of the East Pacific Rise crest. *Geology* 3:77–80
- Rea DK, Lyle MW, Liberty LM, Hovan SA, Bolyn MP, Gleason JD, Hendy IL, Latimer JC, Murphy BM, Paul CF, Rea THC, Stancin AM, Thomas DJ (2006) Broad region of no sediment in the southwest Pacific Basin. *Geology* 34:873–876
- Sauter D, Sloan H, Cannat M, Goff J, Patriat P, Schaming M, Roest WR (2011) From slow to ultra-slow: how does spreading rate affect seafloor roughness and crustal thickness? *Geology* 39:911–914. doi:[10.1130/G32028](https://doi.org/10.1130/G32028)
- Sauter D, Cannat M, Rouméjón S, Andreani M, Birot D, Bronner A, Brunelli D, Carlut J, Delacour A, Guyader V, MacLeod CJ, Manatschal G, Mendel V, Ménez B, Pasini V, Ruellan E, Searle R (2013) Continuous exhumation of mantle-derived rocks at the Southwest Indian Ridge for 11 million years. *Nat Geosci* 6:314–320
- Searle RC (1984) GLORIA survey of the East Pacific Rise near 3.5°S: tectonic and volcanic characteristics of a fast spreading mid-ocean rise. *Tectonophysics* 101:319–344
- Searle RC, Cowie PA, Mitchell NC, Allerton S, MacLeod CJ, Escartin J, Russell SM, Slootweg PA, Tanaka T (1998a) Fault structure and detailed evolution of a slow spreading ridge segment: the Mid-Atlantic Ridge at 29°N. *Earth Planet Sci Lett* 154:167–183
- Searle RC, Keeton JA, Owens RB, White RS, Mecklenburgh R, Parsons B, Lee S-M (1998b) The Reykjanes Ridge: structure and tectonics of a hot-spot influences, slow-spreading ridge, from multibeam bathymetry, gravity and magnetic investigations. *Earth Planet Sci Lett* 160:463–478
- Sempére J-C, Palmer J, Christie DM, Phipps Morgan J, Shor AN (1991) The Australian-Antarctic discordance. *Geology* 19:429–432
- Severinghaus JP, Macdonald KC (1988) High inside corners at ridge-transform intersections. *Mar Geophys Res* 9:353–367
- Shaw PR, Lin J (1993) Causes and consequences of variations in faulting style at the Mid-Atlantic Ridge. *J Geophys Res* 98:21839–21851
- Sloan H, Patriat P (1992) Kinematics of the North American-African plate boundary between 28° and 29°N during the last 10 Ma: evolution of the axial geometry and spreading rate and direction. *Earth Planet Sci Lett* 113:323–341
- Sloan H, Patriat P (2004a) Generation of morphotectonic fabric on the Mid-Atlantic Ridge flanks, 28° to 29°N: Implications for the limits of tectonic deformation and abyssal hill formation. *Geochem Geophys Geosyst* 5. doi:[10.1029/2004GC000584](https://doi.org/10.1029/2004GC000584)
- Sloan H, Patriat P (2004b) Reconstruction of the flanks of the Mid-Atlantic Ridge, 28° to 29°N: Implications for evolution of young oceanic lithosphere at slow-spreading centers. *Geochem Geophys Geosyst* 5. doi:[10.1029/2004GC000727](https://doi.org/10.1029/2004GC000727)
- Sloan H, Sauter D, Goff JA, Cannat M (2012) Abyssal hill characterization at the ultraslow spreading Southwest Indian Ridge. *Geochem Geophys Geosyst* 13. doi:[10.1029/2011GC003850](https://doi.org/10.1029/2011GC003850)
- Smith DK, Escartín J, Cannat M, Tolstoy M, Fox CG, Bohnenstiehl DR, Bazin S (2003) Spatial and temporal distribution of seismicity along the northern Mid-Atlantic Ridge (15°–35°N). *J Geophys Res* 108 doi:[10.1029/2002JB001964](https://doi.org/10.1029/2002JB001964)
- Smith DK, Escartín J, Schouten H, Johnson JR (2008) Fault rotation and core complex formation: Significant processes in seafloor formation at slow-spreading mid-ocean ridges (Mid-Atlantic Ridge, 13°–15°N). *Geochem Geophys Geosyst* 9. doi:[10.1029/2007GC001699](https://doi.org/10.1029/2007GC001699)

- Sonder LJ, Pockalny RA (1999) Anomalously rotated abyssal hills along active transforms: distributed deformation of oceanic lithosphere. *Geology* 27:1003–1006
- Talling PJ, Wynn RB, Masson DG, Frenz M, Cronin BT, Schiebel R, Akhmetzhanov AM, Dallmeier-Tiessen S, Benetti S, Weaver PPE, Georgioupolou A, Zühlstorff C, Amy LA (2007) Onset of submarine debris flow deposition far from original giant landslide. *Nature* 450:541–544
- Wessel P, Smith WHF, Scharroo R, Luis JF, Wobbe F (2013) Generic mapping tools: improved version released. *EOS Trans AGU* 94(45):409–410. doi:[10.1002/2013EO450001](https://doi.org/10.1002/2013EO450001)
- Wilson DS (1990) Kinematics of overlapping rift propagation with cyclic rift failure. *Earth Planet Sci Lett* 96:384–392
- Wright TJ, Sigmundsson F, Pagli C, Belachew M, Hamling II, Brandsdottir B, Keir D, Pedersen R, Ayele A, Ebinger CJ, Einarsson P, Lewi E, Calais E (2012) Geophysical constraints on the dynamics of spreading centers from rifting episodes on land. *Nat Geosci* 5:242–250

Oceanic Trenches

Jacob Geersen, David Voelker and Jan H. Behrmann

Abstract Although only recognized in the middle of the last century, oceanic trenches are among the most spectacular structural and morphological features in the deep oceans. Caused by the collision and subduction of tectonic plates and shaped by the interplay of tectonic and sedimentary processes, the morphology of oceanic trenches can be manifold. In this chapter we discriminate between sediment starved trenches, partly sediment filled trenches, and sediment flooded trenches. In sediments starved trenches the tectonic signature is usually well preserved everywhere in the trench, including at the outer slope, the depression, and the inner slope. In contrast, in sediment flooded trenches the outer slope and the trench depression usually correspond to a flat seafloor that results from the deposition of thick sedimentary sequences that overprint all fault scarps. Here, a tectonic signature is only found at the trench inner slope where accretion of trench sediments results in thrust faulting. The remarkable differences in trench morphologies underline that for a comprehensive understanding of the structural evolution of a convergent margin, detailed knowledge on the sedimentary and tectonic history of the adjacent oceanic trench is necessary.

The original version of this chapter was revised: For detailed information please see Erratum.
The erratum to this chapter is available at https://doi.org/10.1007/978-3-319-57852-1_28

J. Geersen (✉) · J.H. Behrmann
GEOMAR Helmholtz Centre for Ocean Research Kiel,
Wischhofstrasse 1–3, 24148 Kiel, Germany
e-mail: jgeersen@geomar.de

J.H. Behrmann
e-mail: jbehrmann@geomar.de

D. Voelker
MARUM—Center for Marine Environmental Science,
Leobener Strasse, 28359 Bremen, Germany
e-mail: dvoelker@marum.de

1 Introduction

1.1 Discovery of Oceanic Trenches

Oceanic trenches are long, narrow depressions of the deep seabed (Fig. 1). Water depths are often more than one or two kilometers greater than in the adjacent deep ocean basin. In the modern plate tectonic context oceanic trenches are genetically connected to convergent plate boundaries, defining the zones where a lower, mostly oceanic plate is subducted beneath an overriding plate, which can be made up of oceanic or continental crust and lithosphere (compare Fig. 2 for global distribution of oceanic trenches). They were essentially discovered by the gravity measurements at sea of Vening Meinesz (1929, 1932) in the twenties and thirties of the past century. As a result of an increase in bathymetric measurements during the Second World War, mainly in the western Pacific Ocean, the linear nature of deep sea trenches became obvious. The picture became more complete by the widespread use of echosounders in the fifties and sixties of the past century, and on 23 January 1960 the manned bathyscaphe “Trieste” reached a water depth of 10,911 m below sea floor at the Challenger Deep in the Mariana Trench.

The bathymetric profiles across oceanic trenches are fundamentally asymmetric, a fact that was recognized early. Topography of the oceanward side of the trench is dictated by the elastic downbending of the lower plate in response to loading of the overriding plate. The bending radius is mainly dependent on the elastic thickness of the lithosphere and, in turn, on the age of the subducting plate (e.g. Bodine and Watts 1979). The slope angle of the other side of the trench is principally controlled by the angle of repose of the rocks making up the leading edge of the upper plate, and the relative strengths of these rocks and the basal plate boundary shear zone

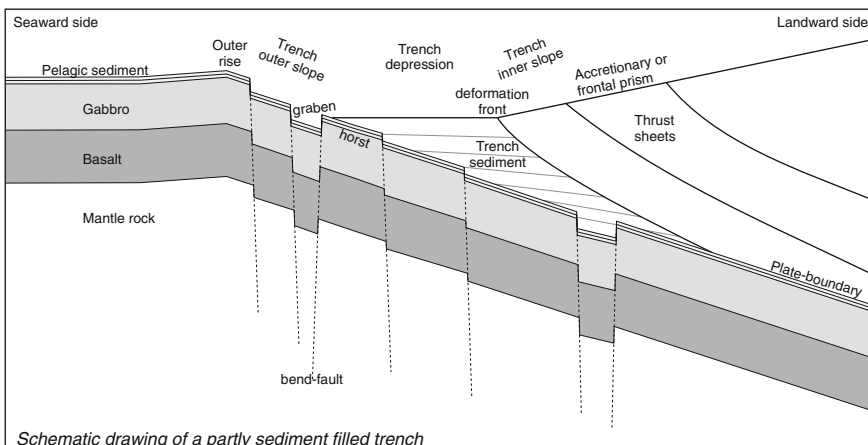


Fig. 1 Schematic drawing of a partly sediment filled trench highlighting most of the structural elements that we discuss in the context of this chapter

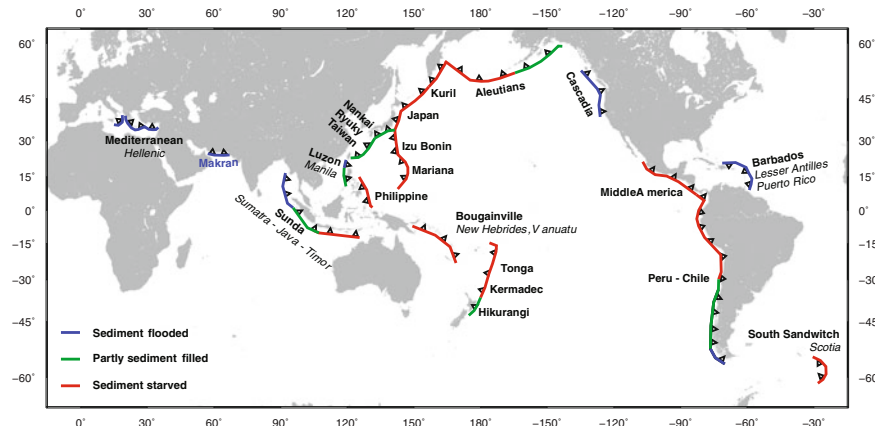


Fig. 2 Global map of oceanic trenches including the most common names used for the respective trenches. Colors are used to distinguish between sediment starved (red), partly sediment filled (green), and sediment flooded (blue) trenches. However, we note that the nature of a trench can change over short (kilometer-scale) distances, e.g. if morphologic features such as seamount are located in the trench axis. The classification therefore only provides an overview not accounting for small scale variations (Color figure online)

(e.g. Davis et al. 1983). As very different parameters define the two angles of slope, these are bound to be different. Below we discuss the main processes that generate and shape the morphology of oceanic trenches. We first discuss processes that impact on the trench outer slope before concentrating on the trench depression and the trench inner slope (Fig. 1).

1.2 Outer Rise and Trench Outer Slope

As stated above, the most important, among the many geologic processes that generate and shape the morphology of an oceanic trench is bending of the oceanic lithosphere prior to subduction (e.g. Bodine and Watts 1979). Caused by the negative buoyancy of the under-thrusted slab, and promoted by the elastic behavior of the lithosphere, plate-bending usually starts some tens of kilometers seaward of the trench-axis (in the context of this chapter, the term seaward refers to the side of the trench where the oceanic plate is located whereas the term landward is used to refer to the side of the subduction-zone—compare Fig. 1). The onset of bending is marked by the outer rise, a topographic high on the seaward side of the trench (Fig. 1). Because the outer-rise elevates from the surrounding oceanic plate only by some tens of meters, and due to the often complex morphology of the oceanic plate (see paragraph below), it is difficult to recognize the outer-rise as a spatially continuous morphologic expression in map-view. When bending stresses exceed the tensile strength of the plate, brittle failure occurs resulting in the development of

normal-faults (bend-faults) that can offset the seafloor up to some hundreds of meters. Bend-faulting often induces a prominent horst-and-graben topography parallel to the trench axis that is characteristic for the trench outer slope (Figs. 3, 4 and 5). A second group of morphological features that (in the case of thin sediment cover) often dominates trench outer slopes is the seafloor spreading fabric aligned parallel to the spreading center (Figs. 3, 4 and 5). Spreading fabric and bend faults often strike at different angles making it easy to distinguish them in map-view (Figs. 3 and 4). Masson (1991) and Ranero et al. (2005) showed that pre-existing spreading fabric oriented $<30^\circ$ oblique to the axis of bending can get reactivated during plate-bending thereby suppressing the development of new bend-faults. Examples for this setting are found offshore Northern Chile and Southern Peru where the South American coastline and the trench axis swing to the west (Geersen et al. 2015) or off the Pacific shore of Nicaragua (Ranero et al. 2005). Both, bend-faults and spreading fabric, are sometimes overprinted by crustal edifices on the oceanic plate such as seamounts, basement ridges or oceanic fracture zones (e.g. Figs. 3 and 4). The impact of elevated basement topography on the shape of a trench outer slope can be manifold. While basement ridges or large seamounts often suppress the development of bend faults or alter their strike direction, smaller seamounts are often cut and intersected by bend faults (Fig. 3).

1.3 Trench Depression

The absolute depth of a trench is controlled by the degree (wavelength) of bending and the depth of the oceanic plate before it starts to bend (in isostatic equilibrium). Both parameters primarily depend on the age of the oceanic plate. Lithospheric age at oceanic trenches ranges between ~ 170 Ma (east of the Mariana trench) to 0 Ma (where active spreading ridges subducted—e.g. Chile Ridge off Southern Chile) (Müller et al. 2008). The age of the oceanic lithosphere further controls the amount of pelagic sediment that accumulates on the oceanic basement. The longer the timespan and the higher the biogenic productivity in the respective areas the thicker the pelagic sediment section on the basement.

A second parameter that controls the absolute depth of a trench is the influx of sediment from land and the continental slope. Sediment supply is mainly controlled by the climate of the hinterland and related weathering processes, combined with the existence of drainage and transport systems to the sea and across the shelf and slope. In dry areas, where denudation rates of the hinterland are low, usually very little sediment reaches the trench. Here, absolute trench sediment thickness is often only a couple of tens or hundreds of meters. In such sediment starved trenches, the tectonic morphology of the trench is usually well preserved (e.g. Northern Chile—Fig. 3). In areas of moderate sediment supply, the trench depression is only partly filled with sediments that onlap on the pelagic sediment or the oceanic basement. In these settings, the trench depression appears as a first order morphologic features in bathymetric data (e.g. Central Chile—Fig. 4). If sediment supply from land is high,

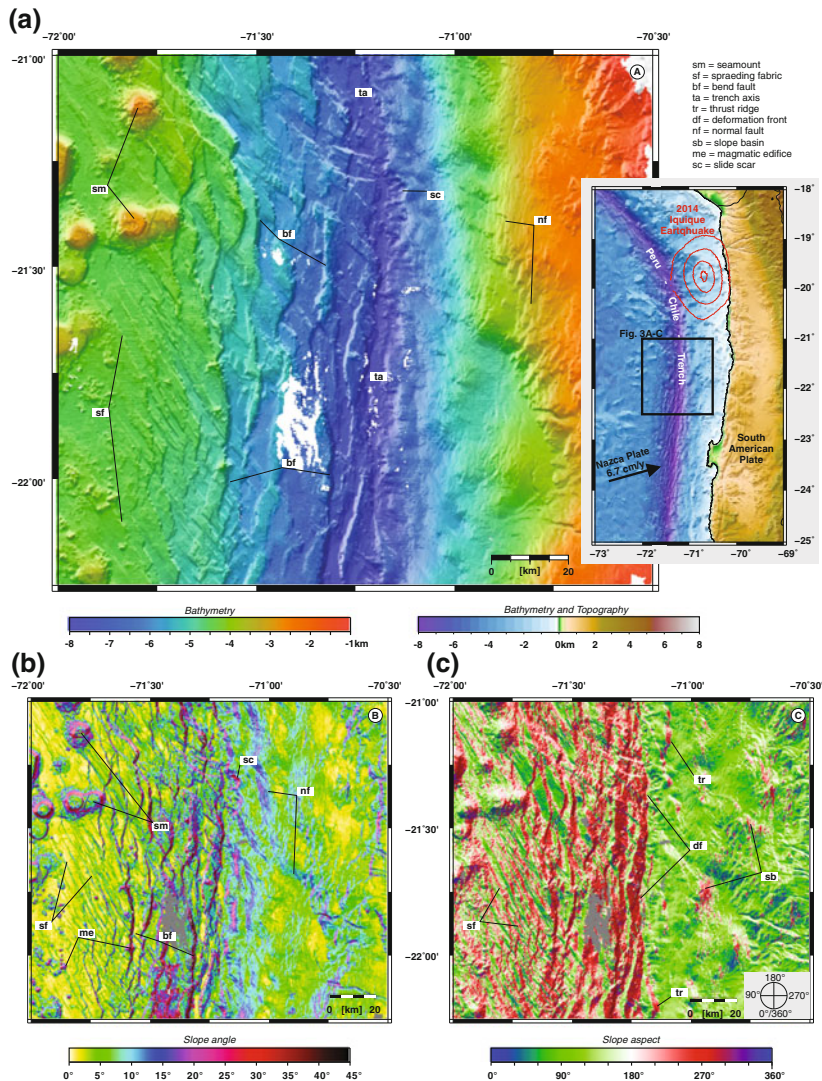


Fig. 3 The sediment starved trench of Northern Chile. **a** Seafloor bathymetry, **b** slope angle, and **c** slope aspect

e.g. because of the presence of large river systems or the proximity of glaciers to the coast, the trench sediment fill can be many kilometers thick. In such sediment flooded trenches, the trench depression and the outer rise are often not recognizable as bathymetrical features (e.g. Cascadia—Fig. 5). Prominent examples for

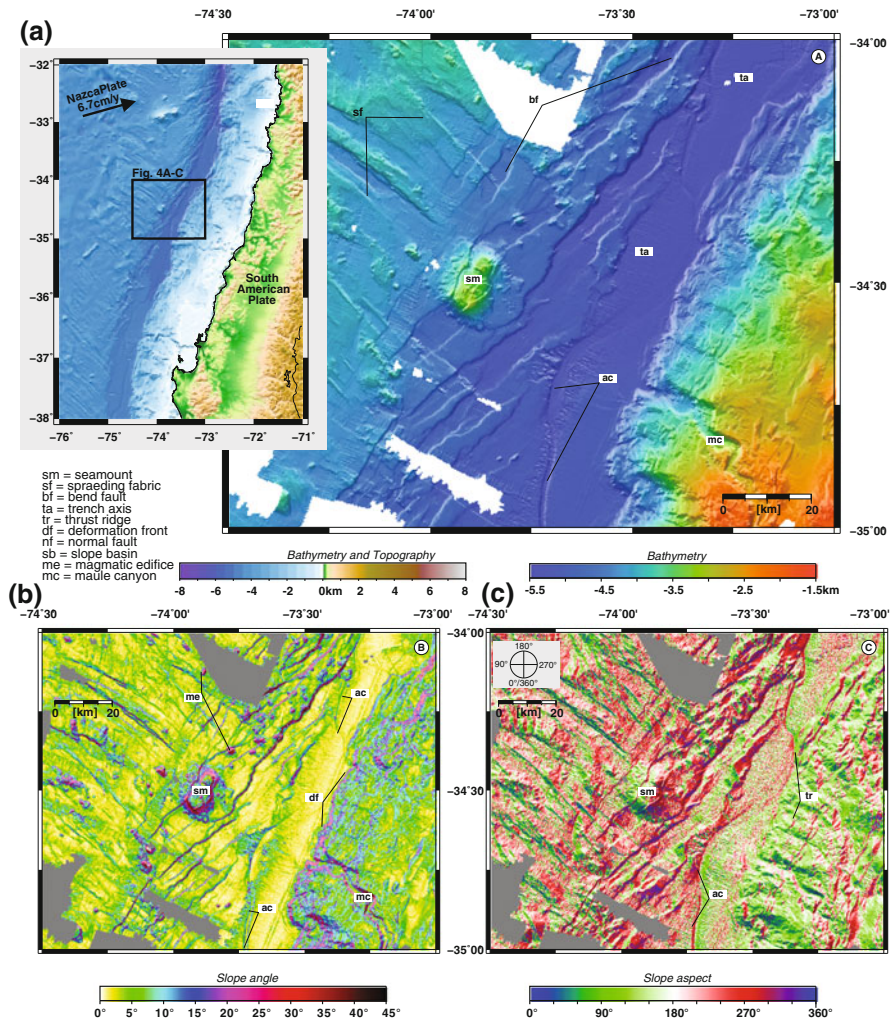


Fig. 4 The partly sediment filled trench of Central Chile. **a** Seafloor bathymetry, **b** slope angle, and **c** slope aspect

sediment-flooded trenches are the Makran trench with a sediment thickness of up to 7.5 km (Smith et al. 2012), the Cascadia trench with a sediment thickness of 3–4 km (Flueh et al. 1998), or the trench off Northernmost Sumatra that has sediment thicknesses of up to 6 km (Geersen et al. 2013). Bend-faulting can continue under the trench sediments but will only result in a morphological seafloor expression if its rate exceeds the sedimentation rate in the trench.

In general, sedimentation in the trench tends to level out all topography, thus creating a plain seafloor. However, in addition to bend-faulting that may outpace

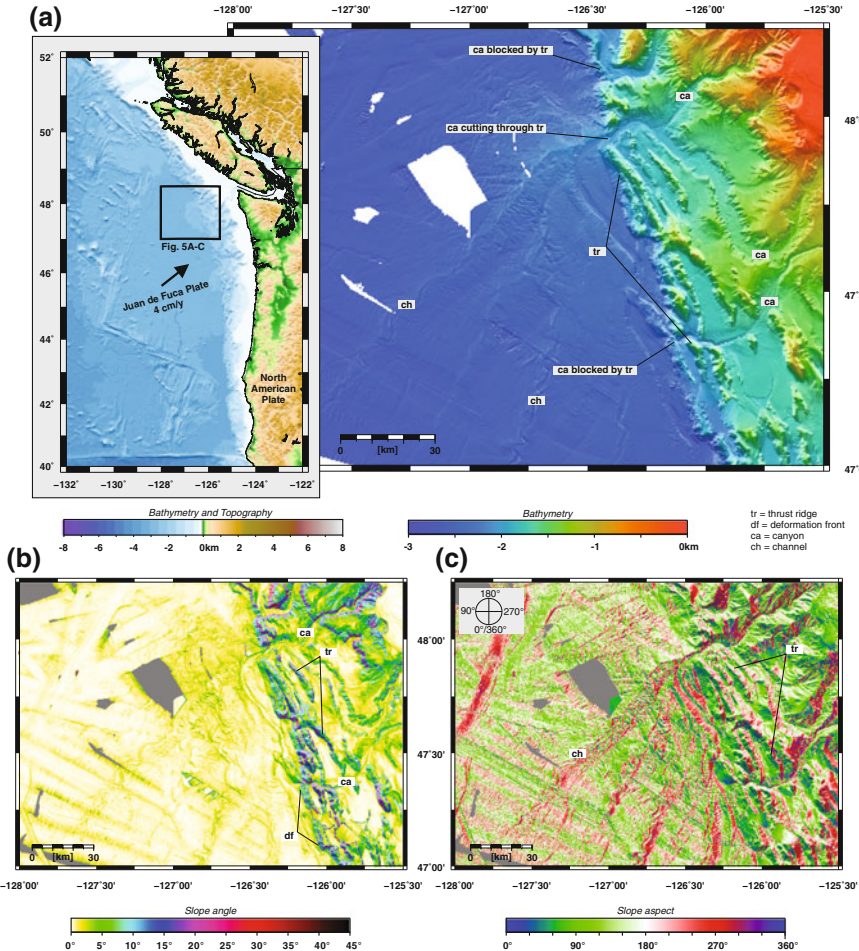


Fig. 5 The sediment flooded trench of Cascadia. **a** Seafloor bathymetry, **b** slope angle, and **c** slope aspect

the trench sedimentation rate, a number of sedimentary processes potentially shape the seafloor in the trench depression. Where large canyon systems are present, the channeling of sediment through the canyon axis leads to local ponding of sediment in front of the canyon exits and the formation of sediment fans. In this case, gravitational driven trench parallel sediment transport directed away from the canyon exit helps to evenly distribute the sediment in the trench depression. Trench parallel sediment transport is often manifested by the existence of channel systems that meander along the trench axis (e.g. axial channel off Central Chile, Fig. 4) (Voelker et al. 2013). A second driver for trench parallel sediment transport is a progression in the age and thus absolute depth of the oceanic basement along the subduction-zone. Another type of sediment transport that may shape the seafloor

morphology in the trench depression is gravitationally driven failure of the continental slope. Tectonic steepening of the continental slope in combination with seismic shaking resulting from frequent strong earthquakes, potentially triggers submarine landslides, the deposits of which are often found on the seafloor in the trench depression. The Reloca Slide for example that removed a part of the accretionary prism of Central Chile deposited multiple kilometer-scale blocks on the trench floor (Voelker et al. 2009).

1.4 Trench Inner Slope

In contrast to the trench outer slope that is shaped by bend-faulting and sediment influx, the trench inner slope on the landward side of the trench is primarily shaped by processes related to plate-collision and subduction. Here, a fundamental difference exists between (a) erosive margins that develop in areas where the trench is sediment starved and (b) accretionary margins that develop in the case of sediment flooded or partly sediment filled trenches.

In sediment starved trenches, where the morphology of the oceanic plate is not leveled-out by sediment, the roughness of the seafloor can cause tectonic abrasion and erosion of material from the toe and/or the base of the upper plate. Subduction of the eroded material leads to a decrease in the volume of the upper-plate. In erosive margins, the removal of material from the upper-plate often causes subsidence and steepening of the continental slope and widespread normal faulting. The latter often results in trench-parallel escarpments that offset the seafloor over some tens of kilometers. Individual thrust ridges that dominate the trench inner slope at accretionary margins (see paragraph below) are usually not found in erosive margins or they are limited to the very distal part of the continental slope (Fig. 3).

In the case of sediment flooded and partly sediment filled trenches, a portion of the sediment gets accreted to the upper-plate leading to the formation of an accretionary prism (Figs. 1, 4 and 5). This results in a net growth of the upper plate. At accretionary margins the inner trench slope has a moderate slope that develops on top of imbricate thrust sheets of former trench sediments. Ongoing accretion, thrust faulting and related gravitational instability of (over)steepened slopes often induces a rough seafloor morphology that is characteristic for many trench inner slopes (e.g. Geersen et al. 2011). Sedimentary basins that potentially level out the rough seafloor morphology develop in some places but the spatial extend of such basins is usually restricted to a few kilometers along and across the continental slope.

As already mentioned above, tectonic activity combined with strong earthquakes may lead to gravitational failure of the continental slope at the trench inner slope. The scarp of a submarine landslide often shows a semi-circular shape that opens towards the trench (Voelker et al. 2012). Slope gradients across the headwall and the sidewalls are often high (above 20°) but decrease with time due to erosion of the exposed cliffs.

2 Results

We now discuss three examples for different trench morphologies. In addition to the bathymetric data we show slope gradient and slope aspect maps, both of which are derived from the bathymetric data. Figure 3 shows the sediment starved trench offshore Northern Chile where terrigenous sediment influx is limited due to the location within the subtropical belt of deserts with little to no precipitation in the hinterland of the Atacama Desert. Subsequently we discuss the Central Chilean trench which is partly filled with sediment (Fig. 4). All data from offshore Chile were collected over the last two decades during multiple seagoing campaigns of German (RV Sonne, RV Meteor) and British (R.R.S. James Cook) research vessels. Finally we examine the Cascadia trench off Washington and Vancouver Island that is not recognizable as bathymetric expression due to the thick sediment blanket of the Astoria and Nitinat fans (Fig. 5). Bathymetric data from the Cascadia margin was extracted from the Global Multi-Resolution Topography (GMRT) synthesis (Ryan et al. 2009). Insets in Figs. 3, 4 and 5, showing a combination of bathymetric and topographic data, are based on GEBCO_08 Grid, version 20091120 [www.gebco.net/data_and_products/gridded_bathymetry_data].

2.1 *Sediment Starved Trench Off Northern Chile*

The tectonic framework of the North Chilean continental margin is controlled by the subduction of the Eocene oceanic Nazca Plate underneath the South American Plate (inset Fig. 3). The Nazca Plate subducts obliquely at an angle of 80.1° and a rate of about 6.7 cm/y (Angermann et al. 1999). Bending of the Nazca Plate starts about 50 km seaward of the deformation front. Whereas it is difficult to recognize the outer-rise in the seafloor data, a number of morphological features dominate the oceanic plate seaward of the trench and along the trench outer slope. These features include (a) seamounts that relate to the Iquique Ridge, (b) NW-SE striking seafloor spreading fabric, and (c) N-S trending bend faults (Fig. 3). The seamounts rise up to 1500 m above the surrounding seafloor that has an average depth of about 4300 m before it descends into the trench. Most of the conical seamounts host a rather flat top with slope gradients below 5° and steep flanks with slope gradients up to 45° (Fig. 3b). Their diameters range from 5 to 10 km. In addition to the seamounts many small edifices that also formed due to magmatic activity are imaged around the seamounts. All of the magmatic features overprint the seafloor spreading fabric which is found pervasively across the oceanic plate. The seafloor spreading fabric can be easily recognized as NW-SE striking lineation in the slope aspect map (Fig. 3c). Vertical seafloor offsets across the individual fault blocks are often only 50–100 m. The small offsets are the main reason that most of the spreading lineation disappears towards the trench axis where it is buried under a thin sediment

section. The bulk of the thin sediment fill that accumulates in the trench likely represents slope debris resulting from gravitational failure of the steep continental slope (von Huene and Ranero 2003).

In contrast to the spreading fabric, the N-S striking bend faults offset the seamounts, thus indicating that they formed after the seamount formation. Vertical offsets of the seafloor across the bend faults increase landwards from a couple of hundred meters at the seaward side of the trench to ~ 800 m close to the trench axis. In the deepest part of the trench depression the offsets across the bend-faults decrease in height, which is again caused by the accumulation of some trench sediment together with erosion of the exposed horst structures. Slope gradients across the bend faults are generally high (above 20°) with maximum values up to 45° . The landward most part of the trench depression coincides with the deformation front which marks the change from a predominantly eastward (landward) dipping seafloor on the trench outer slope and in the trench depression to an almost uniformly westward (seaward) dipping seafloor on the trench inner slope and the continental slope (Fig. 3c). The almost complete lack of landward facing scarps on the trench inner slope (Fig. 3c) is a characteristic feature of erosive margins where thrust ridges are not or only marginally developed due to the lack of sufficient volumes of trench sediment which would be available for frontal accretion.

Slope gradients on the trench inner slope range between $\sim 3\text{--}8^\circ$ and increase locally to values above 10° across some of the widespread seaward facings scarps that dominate the lower continental slope (Fig. 3b). These scarps represent the surface outcrops of normal faults that develop due to tectonic erosion at the toe and the base of the upper plate and resulting subsidence of the continental slope. Some of the hanging walls of the normal faults show an almost flat seafloor (whitish to yellowish patches in Fig. 3b) that slopes (if it slopes at all) in different directions (Fig. 3c). These areas represent small sedimentary slope basins (half-grabens) that develop due to activity of the underlying normal fault (compare Fig. 3 in Geersen et al. 2011). A few semi-circular features are present that may describe scars of submarine landslides (Fig. 3a, b). However, gravitational driven sediment transport seems to occur in form of small events that do not leave characteristic traces in the swath bathymetric data.

2.2 Partly Sediment Filled Trench Off Central Chile

Around $\sim 32^\circ\text{S}$ the Peru-Chile trench changes from a sediment starved trench in the north to a partly sediment filled trench in the south (e.g. Voelker et al. 2013). The increase in trench sediment thickness and the resulting change in the tectonic mode, from erosion in the north to accretion in the south, are mainly controlled by a change in the climate of the hinterland. In contrast to the North Chilean trench, which is located offshore the Atacama Desert, the Central and South Chilean trench is located in an area where Westerlies bring abundant moisture that precipitates at the western slopes of the Andes. The resulting increase in the mean annual

precipitation rate from ~ 0.5 m/a at around 30° S to $2\text{--}3$ m/a south of 38° S (Hoffmann 1975) together with the glaciation of the Patagonian Andes in the south results in a high terrigenous sediment input to the trench.

Off Central Chile, oceanic lithosphere of the Nazca Plate that was formed in the Oligocene (Müller et al. 2008) subducts beneath the South American Plate at a rate of ~ 6.7 cm/y (Angermann et al. 1999) (inset Fig. 4). Bending of the oceanic plate starts about 60 km seaward of the deformation front, which is about the same distance as off Northern Chile. This similarity in elastic behavior, in spite of the contrasting age of the subducting plate, demonstrates that in addition to absolute plate age, parameters such as in-plane force and plate rheology further impact on the elastic behavior of oceanic lithosphere (e.g. Craig and Copley 2014).

Similar to Northern Chile, the seafloor morphology on the trench outer slope and on the oceanic plate is dominated by seamounts, smaller magmatic edifices, seafloor spreading fabric (NW-SE striking), and bend faults (NE-SW trending). Where not overprinted by these large-scale morphological structures, the trench outer slope exhibits slope angles $<5^{\circ}$. The bathymetric difference between the oceanic plate that has an average depth of around 4100 m and the trench axis at about 5200 m is mainly produced by the NE-SW striking bend-faults that offset the seafloor some hundreds of meters. The bend-faults also offset the NW-SE striking seafloor spreading fabric and the seamount at 34.5° S, indicating that they represent the youngest morphological feature group. All the morphological features disappear 10–20 km seaward of the deformation front in favor of an almost flat seafloor (slope gradient $<2^{\circ}$). The flat seafloor corresponds to the top of the sedimentary trench fill that has a thickness of about 2400 m in the area (Voelker et al. 2013) and that levels out all oceanic plate topography. The only morphological feature in the area of the trench depression is a 3–5 km wide and up to 150 m deep channel that meanders along the trench axis (Voelker et al. 2013). The trench axial channel, which stretches over more than 1000 km from the Chacao Canyon at 41° S to north of the Juan Fernandez Ridge (32° S), witnesses the presence and importance of trench parallel sediment transport off Central Chile.

Landward of the trench axis both seaward dipping (W to NW) and landward dipping (E to SE) scarps are visible at the trench inner slope (Fig. 4c). The scarps that host slope gradients between $5\text{--}20^{\circ}$ correspond to thrust ridges that formed by the accretion of trench sediment packages. Off Central Chile, frontal accretion and the buildup of the modern accretionary prism at the trench inner slope started about 6 Ma ago after the onset of glaciation in the Patagonian Andes and resulting increased sediment flux to the trench (e.g. Bangs and Cande 1997; Melnick and Echtler 2006). Where not intersected by thrust ridges, the trench inner slope dips at an angle of $5\text{--}10^{\circ}$. Between $34.5^{\circ}\text{--}35^{\circ}$ S the Maule Canyon cuts about 600 m into the seafloor of the trench inner slope.

2.3 *Sediment Flooded Trench off Cascadia*

Figure 5 shows the seafloor morphology of the Cascadia trench offshore Washington and Vancouver Island. Here, the actual trench depression cannot be recognized in the shape of the seafloor, indicating that the trench is completely filled (flooded) with sediment. However, even though the bathymetric expression is missing, the name trench is also applied in the case of sediment flooded trenches, owing to the structural importance of the feature.

Off Cascadia, the Miocene Juan de Fuca Plate subducts under the North American Plate at a rate of about 4 cm/y (Riddihough 1984). Sediment input is dominated by fluvially and glacially-derived sediments that are delivered to the shelf edge during sea level low stands and transported to the trench and oceanic plate by a network of submarine canyons. As a result, the Quaternary submarine Astoria and Nitinat Fans did not only fill the trench depression completely but also levelled out all topography on the oceanic plate. Instead of seamounts, bend-faults and seafloor spreading fabric, the only morphological feature on the oceanic plate is a series of channels that connect to the exit of the Nitinat canyon. The channels are best recognized in the slope aspect map due to their oppositely dipping sidewalls (Fig. 5c).

The lack of topography on the oceanic plate stands in contrast to a high structural and morphological complexity on the trench inner slope. Here, multiple steep thrust ridges (up to 25°) (Fig. 5b) that dip to the northeast and southwest (Fig. 5c) dominate the lower continental slope. Similar to Central Chile, the thrust ridges develop due to continuous frontal accretion of trench sediment. Multiple canyons that incise the trench inner slope indicate active sediment transport from the continental slope and shelf to the oceanic plate. In this setting, thrust ridge growth continuously competes with canyon erosion. At their exits, the canyons are either blocked by thrust ridges (if thrust ridge growth outpaces canyon erosion) or they cut through the ridges (if canyon erosion outpaces thrust ridge growth) (Fig. 5a).

3 Discussion

Below we illustrate research topics related to oceanic trenches. Although the topics are not solely related to trench morphologies, they underline how knowledge on the structure and morphology of the oceanic plate in the trench region can help to understand geologic processes such as sediment transport or seismicity.

3.1 Impact of Lower Plate Morphology on Earthquake Rupture

The subduction process not only creates oceanic trenches as large scale structural features on the seafloor, but also causes the largest and most destructive earthquakes on the planet Earth. The magnitude and spatial extend of such earthquakes depends on the physical state of the interface between the upper overriding and lower subducting plate (e.g. Kelleher and Cann 1976). An important factor that influences the physical state of the plate-interface is the structure of the subducting oceanic plate. For instance, topographic anomalies such as seamounts, fracture zones and basement ridges have been suspected to impact on earthquake rupture (e.g. Bilek et al. 2003). The southern boundary of the 2014 Mw 8.1 Iquique earthquake (North Chile) coincides with multiple subducting seamounts (Fig. 3, also compare Geersen et al. 2015). The subducted seamounts are interpreted to cause pervasive fracturing around the initial plate boundary, therewith creating favorable conditions for aseismic creep and small earthquakes that rupture individual fractures and unfavorable conditions for large earthquake rupture to propagate across that area (Wang and Bilek 2011; Geersen et al. 2015). Another parameter that impacts on earthquake rupture is the amount, structure and composition of trench sediment. The deeper sections of these sediments are often subducted along with the down-going plate and thus alter the physical state of the plate-interface. Contrasting sediment properties that result in different rupture behaviors have been inferred on either side of the segment boundary between the 2004 (Mw 9.2) and 2005 (Mw 8.7) Sumatran earthquakes (Dean et al. 2010). Furthermore, the amount of subducted sediment can impact on plate coupling through smoothing of the subduction interface; i.e. where a thick sedimentary sequence is subducted, a homogeneous coupled plate boundary is expected that allows rupture propagation over long distances (e.g. Scholl et al. 2015).

3.2 Transport and Redistribution of Sediment in Oceanic Trenches

As long as they are not completely filled, oceanic trenches act as traps for gravity-driven sediment flows. They thus provide very effective barriers for the transport of material from the continent onto the oceanic plates. The effectiveness in trapping sediment flows such as turbiditic currents is due to the high slope gradient of the trench outer slope and the total height difference between the trench axis and the outer rise. The fact that trenches are narrow, but linear and continuous features along convergent margins, adds to the effectiveness in shielding the oceanic plate from continent-derived sediment. As soon as the trench gets subdued or erased as bathymetrical feature by continuous sediment infill, turbidity currents from the continent can freely extend far onto the oceanic plate (Fig. 5).

Sediment input to trenches at ocean-continent boundaries is mainly gravitationally transported from the continental slope, while sedimentation by particle rain from the open water column is normally lower. Submarine canyons that connect to river systems are one way of funneling sediment to the trench thus bypassing the shelf, but sediment is also derived from the open continental slope, mainly in the form of turbidity currents. In the trench, these sediments intercalate with the steady hemipelagic background sedimentation.

If the trench axis is non-horizontal, one reason of which is along-axis variations in oceanic plate age, then turbidity currents that are “caught” in the trench will follow the slope gradient and inner-trench sediment transport features will develop. Prominent expressions of such transport are “trench-axial channels” such as in the Central Chile Trench (Voelker et al. 2013) and in the Nankai Trench. In these cases, outlets of submarine canyons to the trench connect to a single central channel that runs in the deepest part of the trench over distances of some hundreds of kilometers and that shares many attributes with feeder channels at low-gradient submarine fan systems such as meanders, banks, subdued levees, and internal meanders.

3.3 Outer Rise Seismicity

Subduction-zone earthquakes are generated at the seismogenic part of the plate-boundary underneath the forearc. This is the area which releases about 90% of seismic energy on a global scale (Pacheco and Sykes 1992), partly in earthquakes with magnitudes exceeding Mw 8. However, there is a second region of seismicity related to trenches, located at the outer rise and trench outer slope.

Outer-rise earthquakes seldom exceed magnitudes of Mw 6. They can be separated into two basic categories based on the mechanical nature of the earthquake nucleation (focal mechanism), namely compressional and tensional events that reflect either compressional or tensional outer-rise stress regimes. Changes in the stress regime in the outer rise region are a direct consequence of the degree of plate-coupling and the occurrence of large subduction earthquakes under the marine forearc. Thus, the temporal and spatial occurrence of outer-rise earthquakes is directly related to the seismic cycle of the subduction zone.

Compressional outer-rise events tend to occur off subduction zones where intraplate-coupling is high and where no large subduction earthquake has occurred for a long time. A simple model to explain this observation is that the ongoing convergence of both plates is mainly converted into elastic deformation of the forearc as long as the coupling zone remains locked, creating a compressional stress regime. This compression acts on the outer rise region. If the frictional strength of inherited or newly formed faults is overcome, occasional slip along faults expresses as (compressional) outer rise seismicity.

Tensional earthquakes in the outer rise region on the other hand tend to occur after large subduction events. The idea behind this observation is that tensional

stress from the sinking slab (slab pull) is temporarily transmitted to the outer-rise in the moment of a large subduction zone earthquake. The sudden failure and large displacement along the coupling zone act back onto the oceanic plate that is “pulled” landwards. As the oceanic crust of the outer rise region is mechanically weakened by bend faulting, normal failure along faults, expressing as tensional seismic events is most likely to occur here.

4 Conclusion

Oceanic trenches that stretch over thousands of kilometers along convergent plate boundaries are a first order structural feature in the deep oceans. Depending on the dominance of sedimentary or tectonic processes they can develop very different shapes. Profound knowledge on the structure, morphology and geologic history of oceanic trenches, including the amount and composition of the sedimentary trench-fill, can help to understand the structural evolution of the adjacent active margin.

References

- Angermann D, Klotz J, Reigber C (1999) Space-geodetic estimation of the Nazca-South America Euler vector. *Earth Planet Sci Lett* 171:329–334 doi:[10.1016/S0012-821X\(99\)00173-9](https://doi.org/10.1016/S0012-821X(99)00173-9)
- Bangs NL, Cande SC (1997) Episodic development of a convergent margin inferred from structures and processes along the southern Chilean margin. *Tectonics* 16:489–503
- Bilek SL, Schwartz SY, DeShon HR (2003) Control of seafloor roughness on earthquake rupture behaviour. *Geology* 31:455–458
- Bodine JH, Watts AB (1979) On lithospheric flexure seaward of the Bonin and Mariana trenches. *Earth Planet Sci Lett* 43:132–148 doi:[10.1016/0012-821X\(79\)90162-6](https://doi.org/10.1016/0012-821X(79)90162-6)
- Craig TJ, Copley A (2014) An explanation for the age independence of oceanic elastic thickness estimates from flexural profiles at subduction zones, and implications for continental rheology. *Earth Planet Sci Lett* 392:207–216 doi:[10.1016/j.epsl.2014.02.027](https://doi.org/10.1016/j.epsl.2014.02.027)
- Davis D, Suppe J, Dahlen FA (1983) Mechanics of fold-and-thrust belts and accretionary wedges. *J Geophys Res* 88:1153–1172 doi:[10.1029/JB088iB02p01153](https://doi.org/10.1029/JB088iB02p01153)
- Dean SM, McNeill LC, Henstock TJ et al (2010) Contrasting décollement and prism properties over the Sumatra 2004–2005 earthquake rupture boundary. *Science* 329(5988):207–210 doi:[10.1126/science.1189373](https://doi.org/10.1126/science.1189373)
- Flueh ER, Fisher MA, Bialas J et al (1998) New seismic images of the Cascadia subduction zone from cruise SO108—ORWELL. *Tectonophysics* 293:69–84
- Geersen J, Behrmann JH, Völker D et al (2011) Active tectonics of the South Chilean marine fore arc (35°S–40°S). *Tectonics* 30:TC3006 doi:[10.1029/2010TC002777](https://doi.org/10.1029/2010TC002777)
- Geersen J, McNeill L, Henstock TJ et al (2013) The 2004 Aceh-Andaman earthquake: early clay dehydration controls shallow seismic rupture. *Geochem Geophys Geosyst* 14(9):3315–3323 doi:[10.1002/ggge.20193](https://doi.org/10.1002/ggge.20193)
- Geersen J, Ranero CR, Barckhausen U et al (2015) Subducting seamounts control interplate coupling and seismic rupture in the 2014 Iquique earthquake area. *Nat Commun* 6:8267 doi:[10.1038/ncomms9267](https://doi.org/10.1038/ncomms9267)

- Hoffmann JA (1975) Atlas climatico de America del Sur. World Meteorol Organ
- Kelleher J, McCann W (1976) Buoyant zones, great earthquakes, and unstable boundaries of subduction. *J Geophys Res* 81:4885–4896
- Masson DG (1991) Fault patterns at outer trench walls. *Mar Geophys Res* 13:209–225 doi:[10.1007/bf00369150](https://doi.org/10.1007/bf00369150)
- Melnick D, Echtler HP (2006) Inversion of forearc basins in south-central Chile caused by rapid glacial age trench fill. *Geology* 34:709–712 doi:[10.1130/G22440.1](https://doi.org/10.1130/G22440.1)
- Müller RD, Sdrolias M, Gaina C et al (2008) Age, spreading rates and spreading symmetry of the world's ocean crust. *Geochem Geophys Geosyst* 9:Q04006 doi:[10.1029/2007GC001743](https://doi.org/10.1029/2007GC001743)
- Pacheco JF, Sykes LR (1992) Seismic moment catalog for large shallow earthquakes from 1900 to 1989. *Bull Seismol Soc* 82:1306–1349
- Ranero CR, Villaseñor A, Phipps Morgan J et al (2005) Relationship between bend-faulting at trenches and intermediate-depth seismicity. *Geochem Geophys Geosyst* 6:Q12002 doi:[10.1029/2005GC000997](https://doi.org/10.1029/2005GC000997)
- Riddihough R (1984) Recent movements of the Juan de Fuca plate system. *J Geophys Res Solid Earth* 89:6980–6994 doi:[10.1029/JB089iB08p06980](https://doi.org/10.1029/JB089iB08p06980)
- Ryan WBF, Carbotte SM, Coplan JO et al. (2009) Global multi-resolution topography synthesis. *Geochem Geophys Geosyst* 10:Q03014 doi:[10.1029/2008gc002332](https://doi.org/10.1029/2008gc002332)
- Scholl DW, Kirby SH, von Huene R et al (2015) Great (\geq Mw 8.0) megathrust earthquakes and the subduction of excess sediment and bathymetrically smooth seafloor. *Geosphere* 11:236–265 doi:[10.1130/GES01079.1](https://doi.org/10.1130/GES01079.1)
- Smith G, McNeill L, Henstock TJ et al (2012) The structure and fault activity of the Makran accretionary prism. *J Geophys Res Solid Earth* 117:B07407 doi:[10.1029/2012jb009312](https://doi.org/10.1029/2012jb009312)
- Vening Meinesz F (1929) Theory and practice of pendulum observations at sea. Nederlandse Commissie voor Geodesie, J. Waltman Jr., Delft, 95 pp
- Vening Meinesz FAV (1932) Gravity expeditions at sea 1923–1930. Vol. 1. The expeditions, the computations and the results. Nederlandse Commissie voor Geodesie, J. Waltman Jr., Delft, 109 pp
- Voelker D, Weinrebe W, Behrmann JH et al (2009) Mass wasting at the base of the south central Chilean continental margin: the Reloca Slide. *Adv Geosci* 22:155–167 doi:[10.5194/adgeo-22-155-2009](https://doi.org/10.5194/adgeo-22-155-2009)
- Voelker D, Geersen J, Contreras-Reyes E et al (2012) Morphology and geology of the continental shelf and upper slope of southern Central Chile (33°S–43°S). *International J of Earth Sci* 1–23 doi:[10.1007/s00531-012-0795-y](https://doi.org/10.1007/s00531-012-0795-y)
- Voelker D, Geersen J, Contreras-Reyes E et al (2013) Sedimentary fill of the Chile Trench (32°S–46°S): volumetric distribution and causal factors. *J Geol Soc* 2012–119 doi:[10.1144/jgs2012-119](https://doi.org/10.1144/jgs2012-119)
- von Huene R, Ranero CR (2003) Subduction erosion and basal friction along the sediment-starved convergent margin off Antofagasta, Chile. *J Geophys Res Solid Earth* 108,2079 doi:[10.1029/2001JB001569](https://doi.org/10.1029/2001JB001569)
- Wang K, Bilek SL (2011) Do subducting seamounts generate or stop large earthquakes? *Geology* 39:819–822 doi:[10.1130/G31856.1](https://doi.org/10.1130/G31856.1)

Cold-Water Carbonate Bioconstructions

Claudio Lo Iacono, Alessandra Savini and Daniela Basso

Abstract Cold-water carbonate bioconstructions are the product of complex interactions between calcifying organisms and the surrounding environment, and deeply contribute in affecting the evolution of the submarine landscape in space and time. Important variables contributing to their development, growth and/or demise include sedimentary dynamics, food supply, physical and chemical characteristics of water masses and local hydrodynamic regimes. Geomorphological studies of bioconstructions are therefore critical in deciphering the physical and biological processes contributing to their development. The aim of this chapter is to summarise the state of the art of geomorphic studies on temperate coralligenous bioconstructions and cold-water coral reefs/mound systems, both representing the two most important and largest carbonate bioconstructions in temperate and deep-sea waters. The importance of these biogenic constructions covers several aspects. They can represent important carbonate factories of the deep sea, archives of past climate and oceanographic conditions and they support increased species diversity and complex biotic interactions with respect to the surrounding seafloor. Because of their remote location (from hundreds to thousands of meters below sea level), only since the last tens of years, technological advances are allowing fine-scale physical and ecological investigations of these bioconstructions, containing ecosystem engineers able to strongly modify the landscape heterogeneity. An increased

The original version of this chapter was revised: For detailed information please see Erratum.
The erratum to this chapter is available at https://doi.org/10.1007/978-3-319-57852-1_28

C. Lo Iacono (✉)

National Oceanography Centre, University of Southampton
Waterfront Campus, European Way, Southampton SO14 3ZH, UK
e-mail: cllo@noc.ac.uk

A. Savini · D. Basso

Department of Earth and Environmental Sciences,
University of Milano-Bicocca, Piazza della Scienza 4, 20126 Milan, Italy
e-mail: alessandra.savini@unimib.it

D. Basso

e-mail: daniela.basso@unimib.it

awareness of their potential extension and significance as natural resource, is now steering scientific efforts towards the need to overcome the gaps in knowledge and contribute to prevent their vulnerability to an increasing human pressure.

1 Introduction

Many marine organisms can contribute to the creation, development and maintenance of complex biogenic three dimensional structures, commonly named bioconstructions, which develop through the accretion or accumulation of organogenic deposits, and are able to affect the evolution of the submarine seascape in space and time. From a semantic point of view, “bioconstruction” is a term having a landform connotation as well as a process meaning. Bioconstruction, bioerosion and bio-protection represent biologically mediated components of earth surface processes and constitute the main subjects of bio-geomorphological studies (Naylor 2005). Within the marine realm, bioconstructions are produced all over the submerged environment, from coastal areas to the deep-sea, by different organisms belonging to extremely diverse taxa (bacteria, algae, numerous species of metazoans). Bioconstructions can form through biologically-induced or biologically-controlled calcification, or may result from material bind from other sources (e.g. using organic cement or sediment baffling) or develop from a combination of the two processes (Lowenstam 1981; Riding 2002; Naylor 2005). Plants and animals generally having a calcareous composition create a new hard substrate by skeletal deposition followed by superposition and overgrowing, or adhere to pre-existent hard substrates, and persist as solid elements after their death. Within time, the accumulation of these limy remains may lead to the development of solid and complex constructions which may give rise to relevant landforms, with living communities generating new frameworks over a build-up of cemented skeletal remains of dead organisms (Wood 1999; Riding 2002). The growing dynamics and ecological functioning of building organisms clearly affect the morphological variability of bioconstructions. Sedimentary dynamics, physical and chemical characteristics of water masses and local hydrodynamic regimes (waves and currents) are in most cases critical variables exerting a major control on growth and demise of bioconstructions in space and time. The study of the origin, configuration and evolution of landforms created by bioconstructors requires therefore a strongly multidisciplinary approach to comprehensively understand the links between biotic and physical processes involved in their formation. Furthermore, geomorphological studies are revealing to be critical in deciphering the physical and biological processes that contributed to the development and distribution of bioconstructions. A rich and diverse terminology has been adopted to describe the calcareous biogenic landforms created by sessile organisms. Some of the most adopted terminology does not specifically refer to the natural processes involved in their formation, neither to their composition or structure. This is the case of the terms “concretion” or “build-up” (see Riding 2002 for a deeper analysis and a comprehensive list of references). Others debated definitions are aimed to address the sedimentological, geomorphological and ecological characteristics contributing to

the formation of bioconstructions. This is the case of the term reef. Riding (2002) presented a comprehensive review of the composition and structure of biogenic reefs, occurring at a large variety of scales and depths, drawing the attention to the high diversity and variable sedimentary composition of the reef-forming deposits. Despite classical common definitions of reefs generally being based on the dominant constituent organisms (e.g.: microbial, algal, archaeocyath, stromatoporoid, coral, rudist, etc.—see Table 1 in Cocito 2004), these generally lack a focus on their geomorphic aspect. The term reef refers here to a persistent bioconstructed morphologic framework (generally formed by several interacting organisms) with a clear three dimensional expression, which influences the local sedimentary dynamics and oceanography and supports living benthic communities. Other terms which refer to biogenic-mediated geomorphic features with a distinct shape are banks, originally indicating biogenetic accumulations resulting from baffling and binding processes of benthic organisms (Lowenstam 1950; Klement 1967; Riding 2002), but now largely adopted to generically indicate sub-horizontal biogenic frameworks surrounded by marked breaks of slope, and mounds (Toomey and Finks 1969; Wilson 1975; James and Bourque 1992; Bosence and Bridges 1995; Riding 2002; Roberts et al. 2006; Fouberet and Henriet 2009; Rodríguez-Martínez 2011), indicating positive reliefs, from few to hundreds of meters tall, and generally displaying rounded, semicircular, ellipsoid or elongated shapes. Mounds can be composed of a variety of dominant organisms capable of trapping or baffling fine sediments (e.g. cold water corals, bryozoans, polychaetes) and therefore occurring in a variably-composed sedimentary matrix. Mound structures have been recognized in several geological records (Hebbeln and Samankassou 2015), with the oldest features being of early Palaeozoic age (Monty 1995). A rigorous nomenclature explaining the different origin, composition and structure of banks and mounds is in any case still missing, as confirmed by the rich sequence of adopted adjectives (mud-mounds, detritial mounds, carbonate mounds, carbonate mud mound, lime mud mound, microbial mounds, mud-banks, reef mounds, stromatactis mounds, etc.) (see Table 4.2 in Roberts et al. 2009).

Bioconstructions of coastal and shelf seas have been the subject of comprehensive studies since more than a century. Tropical coral reefs, for example, are the most studied bioconstructions on a global scale, mainly owing to the ecological relevance of these large ecosystems, considered among the most important hotspots of marine biodiversity. Tropical corals are able to create entire bio-constructed coastal landforms, several hundreds of kilometres long and hundreds of meters across, whose extension is easily visible in satellite images. These reefs are widely addressed in all basic texts on marine biology, coastal geomorphology and stratigraphy (Wood 1999; Montaggioni and Braithwaite 2009; Woodroffe and Webster 2015). Other widely studied coastal and shallow water bioconstructions are found in temperate seas (James and Clarke 1997; Pedley and Carannante 2006). These concretions create complex structures in moderate to strong hydrodynamic regimes, from the coastal intertidal environment to the infralittoral setting, whose deepest limit is marked by a strong decrease of light, insufficient to support the photosynthetic rate of photophilous plants. The dominant coastal temperate bioconstructors are coralline algae such as *Lithophyllum byssoides* (Lamarck) Foslie, vermetid gastropods, other species of coralline algae and several bryozoans,

polychaetes and oysters, able to develop solid and few meters thick calcareous rims, sub-horizontal benches and sporadic reefs along the coastline (Laborel 1987; Relini 2009; Kružić 2013).

The extension and the geomorphological characteristics of important submerged bioconstructions, able to form large reefs and mound structures in partially unexplored deeper environments, have been revealed only over the last 30 years thanks to the availability of seafloor acoustic mapping techniques and the development of scientific Remotely Operated Vehicles (ROV). This is the case for the coralligenous formations and cold-water coral reefs and mounds, the latter developing in a wide depth range, from tens up to a few thousands of meters. The importance of these biogenic constructions covers several aspects. They can represent important carbonate factories of the deep sea (Titschack et al. 2008), and archives of past climate and oceanographic conditions (Frantz et al. 2005; Montagna et al. 2006; Ries 2006; Kamenos et al. 2012; Thierens et al. 2013). They support increased species diversity and complex biotic interactions with respect to the surrounding seafloor.

The aim of this chapter is to summarise the state of the art on geomorphology, distribution and main composition of the temperate coralligenous bioconstructions and cold-water coral reefs/mound systems, representing the two most important and largest carbonate bioconstructions in the deep ocean.

2 Coralligenous Bioconstructions

Coralligenous (C) bioconstructions represent calcareous build-ups of biogenic origin (i.e.: organic frame-reefs; Riding 2002), formed since the Holocene transgression in the Mediterranean, through the multi-stratified accretion in dim light condition of encrusting coralline algae and invertebrate associations (Sartoretti et al. 1996; Ballesteros 2006). They are generally distributed from a few meters (Sarà 1971) down to about 120–150 m water depth, the deepest C occurrence corresponding to the oligotrophic, transparent waters of the Eastern Mediterranean basin (Laubier 1966; Hong 1982; Ballesteros 2006). C produces distinct biogenic reef-like frameworks from few to tens of meters large and up to 4–6 m thick on sub-horizontal seafloors across different depths, or covering hard and complex surfaces along the lower limit of submerged rocky-coast and circalittoral slopes, displaying variable lateral continuity and thickness. C thrives with low to moderate level of nutrient inputs, temperatures from 10 to 23 °C and low to moderate hydrodynamics (Relini 2009), promoting the development of the biogenic framework and limiting the deposition of terrigenous sediments (Morganti et al. 2001; Balata et al. 2006). Low light conditions represent the key parameter that controls the growth of coralline algae in C (Relini 2009). The depth-range of C is therefore variable through the photic zone, since a number of environmental parameters and physical settings determine the total illumination reaching the seafloor. Submarine topography for instance has a significant effect on modulating the seafloor

illumination, since seafloor irregularities (escarpments, overhanging walls, caves, etc.) can create a number of favourable low-light conditions even at shallow depths.

The term Coralligenous (or Coralligène, the original French name) refers to a complex of biocoenoses (C complex) and to the habitat it represents (Laborel 1961). The main dominating communities correspond to calcareous algae (shallower sectors of the bioconstruction), suspension feeders (deeper sectors, cavities and overhangs), borers (inner sectors) and even soft-bottom fauna (within sediments deposited in cavities, depressions and holes) (Fig. 1). The volumetrically most important framework builders in C are calcareous red algae Corallinophycidae (CCA), bryozoans, polychaetes and cnidarians (Laubier 1966; Di Geronimo et al. 2002; Novosel et al. 2004; Cocito 2004; Basso et al. 2007; Ballesteros 2006; Giaccone et al. 2009; Rosso and Sanfilippo 2009). The interplay of biotic and abiotic factors (mainly: light penetration, availability of trophic resources, substrate exposition, sedimentation rate, freshwater influence, biotic interactions) produces several C facies, unevenly distributed along geographical and depth gradients (Pérès 1982; Bellan-Santini et al. 1994; Sartoretto 1994; Canals and Ballesteros 1997; Casellato and Stefanon 2008; Bonacorsi et al. 2012). Ballesteros (2006) provided a first quantification of the number of species (about 1670) forming the coralligenous communities and identified an algal-dominated assemblage in the relatively shallow C, contrasting with an animal-dominated C in the deep. An overview of the environmental factors influencing their development and distribution, illustrating most of the complex biotic relationships and ecological processes that create and destroy the calcareous frameworks was also provided (Ballesteros 2006).

Significant literature has been also produced on the physical/geological characterization of the reef-like structures formed by the coralligenous biocoenoses, including their fossil counterparts (Bosence and Pedley 1982; Carannante and Simone 1996; Rasser 2000; Nelson et al. 2001; Rasser and Piller 2004; Nalin et al. 2006; Bracchi et al. 2016).

First pioneer studies carried out by Johannes Walther (1860–1937, see Ginsburg et al. 1994) and Abel (1961) interestingly outlined a number of similarities between Mediterranean C and Red Sea coral reefs, in terms of structural complexity. As for coral-reefs (and most of bioconstructions), C are indeed complex features in terms of their physical structure, associated biota and the ecological processes they generate (Laubier 1966). Their morphology can reach a high degree of complexity, with rugged surfaces and many cavities and overhangs due to irregular growth of the benthic calcifiers, erosional processes, boring organisms, or a combination of these factors. In these dark crevices and under overhangs the shade-loving assemblages develop, including sponges and, in some cases, the precious red coral *Corallium rubrum*, whose occurrence suggested the name Coralligène (= generating the coral, Marion 1883; Basso et al. 2007; Virgilio et al. 2006; Relini 2009). Space competition among encrusting calcifiers, differential growth rates, cementation, episodes of sedimentation and partial erosion generates through time a significant

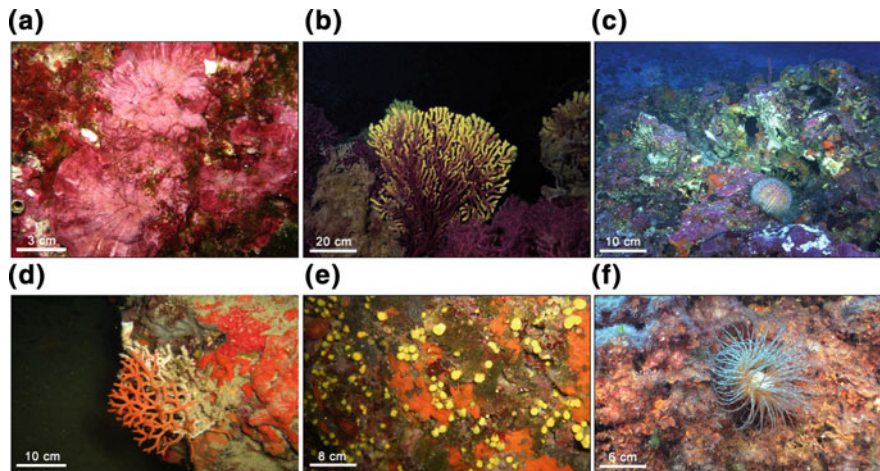


Fig. 1 Characteristic organisms of coralligenous formations. **a** Pink layered/foliose encrusting calcareous red algae growing at the surface of a biogenic substrate (coralligenous). Serpulid tubes also occur; **b** Fan-shaped red to yellow branching colonies of Octocorallia (*Paramuricea clavata*) growing at the top of a coralligenous build-up. The colonies are typically oriented on a plane that is normal to the direction of the main current; **c** Sub-horizontal coralligenous substrate encrusted by various species of purple coralline algae and orange sponges. Note the small branching colonies of the Octocorallia *Eunicella* sp. and the large sea urchin *Echinus melo* feeding on algae; **d** Branching colony of the bryozoan *Pentapora fascialis* growing on the flank of a coralligenous build-up, where several species of encrusting sponges also occur. One *Halocynthia papillosa* ascidian (sea-squirt) is attached below the *Pentapora* colony and tiny tube-dwelling serpulids grow at its base; **e** *Cerianthus membranaceus* (Anthozoa) on coralligenous substrate covered by coralline red algae and *Peyssonnelia* spp.; **f** Overhanging surface of coralligenous substrate bordering a submarine cave, encrusted by numerous solitary corals (the yellow Scleractinia *Leptopsammia pruvoti*), the ascidians *H. papillosa*, sponges and algae. Photos courtesy of F. Mastrotoraro

structural complexity and environmental heterogeneity (Jones et al. 1994), which in turn controls the distribution and abundance of coexisting species, and increasing the C habitat biodiversity.

2.1 Geomorphology of Coralligenous Bioconstructions

The extent to which the C biota can modify the submarine environment, affecting the evolution of submerged landforms is extremely variable. C can cover and drape quite homogeneously the pre-existing hard substrate enhancing its topographic complexity, or produce new distinct geomorphic features on the seafloor, of variable shapes and dimensions, that characterize the seascape in wide areas of the continental shelf. A precise description of their 3D morphological development and extension is however often overlooked. In literature C formations are generally indicated as reefs, concretions, frameworks, build-ups, pillars, outcrops, but they

still lack a detailed systematic classification of morphotypes and associated processes, since the drivers that control their differentiation have been poorly investigated (Bracchi et al. 2015, 2016; Doxa et al. 2016).

A first attempt of showing the relevance of C in marine geomorphological research has been provided by Laborel (1961), with the description of five coral-ligenous types: cave and overhang concretions, wall concretions, concretions at the base of submarine walls, concretions over flat rocky surfaces and platform coral-ligenous assemblages. These types were distinguished according to their position and exposure to light penetration along an almost steep coastal belt and submerged shelf and the type of substrate on which they grow. Pérès and Picard (1951, 1964) introduced the term “coralligène de plateau” to describe C settled on a coarse bioclastic sub-horizontal bottom and originated from the coalescence of algal concretions (rhodoliths; Bosellini and Ginsburg 1971; Nalin et al. 2006), distinguishing this type of C from the one growing on sloping and complex rocky surfaces. Following Pérès and Picard (1964), most authors indicate C as *banks* when they develop on flat bottoms (e.g.: coralligène de plateau), whereas the term *rim* is used to refer to those lips and rims growing on sub-vertical substrates (e.g.: cliffs or slopes in the circalittoral), and also occurring at the opening of submarine caves (Laborel 1987; Ballesteros 2006). These authors thus introduced a first “geomorphological” classification, trying to merge two different criteria to distinguish C: the “morphology” and the “genesis”, this latter related to the type of substrate on which C develops. However, in several cases the genesis of banks is not related to the coralligène de plateau, and on the other hand, a vertical C structure could develop with no need of an underlying cliff (Basso et al. 2007; Bracchi et al. 2015).

Both coralligenous rims and coralligenous banks vary considerably in their 3D morphological development, showing a wide range of morphotypes (Fig. 2). Rims may be poorly developed or grow to extreme sizes reaching widths of more than 3 m (Laborel 1987; Ballesteros 2006). They can be single or multiple features and may set up at regular or irregular intervals. Rocky vertical or sub-vertical walls, which can be found along the open shelf or in submerged caves, represent the typical settings for the development of coralligenous rims (Laborel 1987).

When forming banks, C generally occurs in groups rather than as isolated structures. A rich descriptive terminology (e.g.: heads, blocks, vertical pillars, columns, ridges etc.) has been used to refer to the variety of morphotypes they can develop and since the availability of advanced hydro-acoustic mapping systems (such as MB swath bathymetry) calibrated by visual systems such as ROV and drop cameras, research on the geomorphology of submerged bioconstructions has advanced (Figs. 1 and 2). Bracchi et al. (2015) described the morphological diversity across and between individual C structures, mainly featured in columns and ridges and covering more than 436 km² of the whole Apulian continental shelf, in the southern-central Mediterranean (Campiani et al. 2014). The proposed classification can be considered descriptive, since it is based on the C morphological aspects, whereas the interpretation of genetic relationships and processes between C and substrata are on purpose not explored. According to Bracchi et al. (2015) ridges

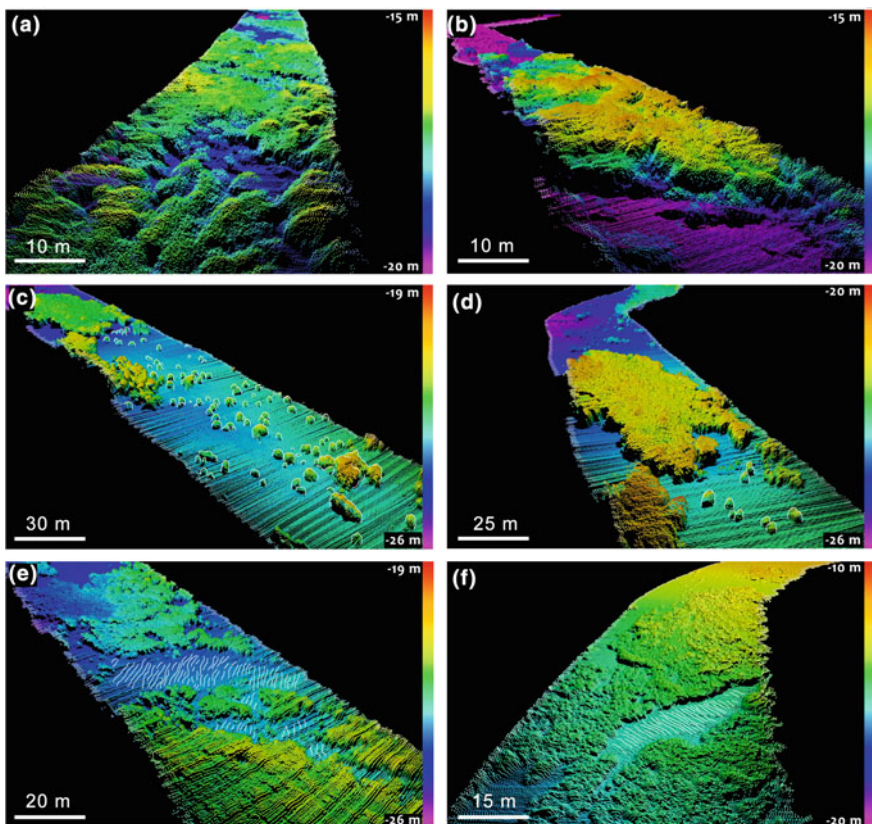


Fig. 2 Multibeam point data acquired along different continental shelf regions of the Mediterranean. **a** Large continuous coralligenous bioconstructions showing an almost flat top with a typical bumpy aspect; **b** Edge of a large coralligenous bioconstruction, rising almost 5 m from a flat seafloor, with a rugged and pitted surface and vertical to stepped, irregular boundaries; **c** Single isolated coralligenous bioconstructions (smaller are roughly 1 m large and no more than 1 m high), distributed along a flat seafloor. Larger coralligenous bioconstructions with distinct boundaries are visible at the end of the multibeam line; **d** Large (ca. 40 m wide) coralligenous bioconstructions rising from 1 to 2 m from the seafloor, with a flat surface and distinct vertical boundaries. Minor isolated coralligenous bioconstructions (ca. 1 m large and no more than 1 m height) are also visible on the *right*; **e** Large coralligenous bioconstructions (more than 40 m wide and from 1 to 2 m high) with indistinct boundaries and separated by a channel. Note the subaqueous dunes documenting the action of unidirectional bottom currents; **f** Coralligenous bioconstructions with internal sediment patches where subaqueous dunes are visible

can reach lateral extensions of tens of meters with heights ranging between 2 and 5 m. Columns represent more distinct features on the seafloor, which may occur in clusters or be isolated, often in association with *Posidonia oceanica* meadows, or with coarse detritic sediments. In most cases, the action of bottom currents and low sedimentation rates seem to represent favourable conditions, which promote

coralligenous development instead of the deposition of terrigenous sediments. Bedforms documenting the action of unidirectional bottom currents are often mapped along the edges of bioconstructions and between them, where sediments and detritic sediment accumulate within the more depressed areas (Fig. 2). Coralligenous atolls, with a radius ranging from 20 to 30 m, have been recently mapped offshore northern Cap Corse (Bonacorsi et al. 2012), northern Mediterranean, between 106 and 112 m water depth. These features form a circular crown structure (made up of coralligenous bioconstructions combined with praline rhodoliths and many invertebrates) with a central core formed by a rounded C formation up to 3 m wide and 0.5 m high (Bonacorsi et al. 2012) surrounded by soft sediments. Similar morphologies have never been observed in other locations, likely owing to the lack of extensive high-resolution acoustic mapping of the (Mediterranean) seafloor, specifically below 50 m of water depth. The shape of these unique and peculiar features has been related to external inherited processes responsible for the initial creation of hard substrates (i.e. gas venting associated to pockmark formation—see Chapter “[Cold Seep Systems](#)”).

Despite the lack of a comprehensive investigation on the role of Quaternary geomorphic processes on the C distribution and growing processes, the inherited geomorphic landscape of the seafloor likely plays a fundamental role affecting the morphological diversity of C. A quite good documentation exists on the relevance of some major environmental parameters such as slope, current exposure, water transparency, temperature and sedimentation in controlling the differentiation in coralligenous biocoenoses. Nevertheless, most research lacks the investigation of the relationships between the variability of the framework morphologies and changes in the associated biological community and parameters. Some authors documented how the observed differentiation in shape and dimension of C is often inherited from the morphology of the hard substrates that allowed the settlement and growth of coralline algae. Most of them are represented by continental shelf rocky outcrops (Bracchi et al. 2015, 2016) and/or modified relic morphologies originated during previous low-stand or transgressive stages of the sea level (e.g. beach-rocks, sediment bars, etc. Navone et al. 1992) and located in areas subject to low sedimentation rate. After the initial settlement of coralline algae and during the time of coralligenous development, rising in sea-level caused changes in hydrodynamic regime, sediment input and light penetration. The interplay of these ecological controls influenced different growth rates of benthic calcifiers and the development dynamics of C, in turn affecting its 3D morphology (Pérès and Picard 1951, 1964; Sartoretto et al. 1996; Di Geronimo et al. 2005; Nalin et al. 2006; Bracchi et al. 2016).

C formations were thus affected by Mediterranean sea-level oscillations during the Quaternary. Since the present-day C depth distribution coarsely corresponds to that portion of seafloor that was emerged during the last glacial maximum, the build-up of C must have occurred during the last transgression. Investigations in the north-western Mediterranean provided evidence that circalittoral C formed mostly in the early Holocene (from about 8.5 kyr BP) at a paleodepth not greater than 10–15 m and with a maximum accumulation rate (about 0.83 mm y^{-1}) between 5 and 8

kyrs BP (Sartoretto et al. 1996). After that period a decrease in accumulation rate (about 0.006 mm y⁻¹ or nil) has been documented for C deeper than 50 m of water depth, suggesting that significant accumulation rates presently occur only at shallow water depth (Sartoretto 1994; Sartoretto et al. 1996; Ballesteros 2006).

2.2 *Coralligenous Distribution*

C is common in the whole Mediterranean Sea, although the bioconstructions seem to be more abundant in the Adriatic, Aegean and Tyrrhenian Seas and in the Algero-Provençal Basin. A much lower number of occurrences have been reported for the Levantine Sea and Tunisian Plateau/Gulf of Sidra (Martin et al. 2014), although lack of reports of C at any particular site does not necessarily imply their absence, especially for the deep circalittoral, which has not been fully investigated by acoustic mapping and ground truthing (i.e.: video inspections). For the same reason, most of the C occurrences reported in literature are located between 10 and 50 water depth, while less information exists for the deeper sites (50–150 m). Several efforts have been promoted in order to fill these gaps (Campiani et al. 2014), although insufficient data are still available on the regional distribution of C across the whole Mediterranean Sea. The only available quantitative information on C extension actually corresponds to the Apulian continental shelf, where a total surface of 436 km² of seafloor is covered by coralligenous habitats (Campiani et al. 2014).

A tentative large-scale assessment of the predicted distribution of C on a basin scale has been modelled on the basis of existing records of a total 2763.4 km² of Mediterranean C (Martin et al. 2014). Bathymetry, slope of the seafloor and nutrient input were the three main contributors to the model (combined contribution of 84.1%), whilst the remaining three predictors (euphotic depth, phosphate concentration and geostrophic velocity of sea surface current) had a minor contribution. Unfortunately, the resulting model has a weak support by direct observations and published data. Considering the available polygon data and their associated surface areas, it is estimated that as much as 95% of coralligenous habitat may still need to be mapped across the Mediterranean basin, especially in deeper areas (Martin et al. 2014).

3 Cold-Water Coral Reefs and Carbonate Mounds

3.1 *Cold Water Corals and Physical Habitats*

Corals are marine animals belonging to the phylum Cnidaria, a large and complex taxonomic group. According to Cairns (2007) the generic term “coral” includes all cnidarians belonging to the classes Anthozoa and Hydrozoa that produce calcium

carbonate secretions. This definition encompasses over 5000 colonial and solitary species, ranging from stony corals (or true corals), provided with continuous carbonate exo- or endoskeletons (e.g. Scleractinia, Styelidae, Coralliidae), to soft corals (most Alcyonacea) formed by organic tissues and secondarily by microscopic biomineralised sclerites. Among the stony corals, able to build a hard carbonatic skeleton, there are some species known as “framework building” corals, owing to their ability to form complex three-dimensional carbonate structures, providing shelter and resources for a wide range of organisms. Most framework-building corals belong to the order Scleractinia and produce aragonite skeletons. Over 95% of them (around 765 species) consists of zooxanthellate species (Roberts et al. 2009) that live in warm, shallow and oligotrophic waters and contribute to the formation of colourful and diverse tropical reefs through photosynthetic processes of symbiotic algae. Very few species of framework building corals are azooxanthellate (18), i.e. they lack symbiotic dinoflagellates, 17 of them thriving in cold and generally deep waters. The latter are generally defined as stony “cold-water corals” (CWC) and, unlike tropical corals, they do not require the occurrence of light neither of warm and shallow waters. They cover a wide range of depths (39–3000 m) and latitudes (70°N–60°S) and feed on organic particles and organisms advected by water masses. CWC bioconstructions therefore develop where oceanography plays an important role in food transport processes (Mienis et al. 2014). Recent studies suggest a coupling between the CWC reef fauna and the surface productivity in relation to the local hydrography and sedimentary dynamics (Mienis et al. 2014; Mohn et al. 2014; Moreno Navas et al. 2014).

The most common framework building cold water corals are *Lophelia pertusa* and *Madrepora oculata*, observed worldwide, with larger occurrence in the North Atlantic and Mediterranean waters (Roberts et al. 2009). *L. pertusa* and *M. oculata* are most commonly observed in waters between 7 and 10 °C although they are able to tolerate a wider temperature range, between 4 and 15 °C (Brooke et al. 2013; Naumann et al. 2014) (Fig. 3). These species have been found on a depth range from tens of meters up to 1500/2000 m (Zibrowius 1980), and along different physiographic and geomorphologic settings. Other CWC species able to create bioconstructions are *Solenosmilia variabilis*, *Enallopsammia profunda*, *Oculina varicosa* and *Goniocorella dumosa* (Roberts et al. 2006; Hebbeln et al. 2016).

The occurrence of hard substrates on which coral colonies can start to settle is probably the most relevant pre-requisite for CWC bioconstructions to grow. However, oceanographic forcing and food input also represent key environmental variables for their survival (Duineveld et al. 2004, 2007; Van Oevelen et al. 2009). Suitable environments for cold-water coral settlement are regions where the interaction between large scale seafloor morphology and water mass dynamics (bottom currents, internal waves controlled by tides or density interfaces) create moderate to strong hydrodynamics and turbulent mixing, coupled with reduced terrigenous input and a constant delivery of organic matter. These settings generally coincide with outer shelf/upper slope regions (Thiem et al. 2006; Dullo et al. 2008), fjords (Freiwald et al. 2004; Försterra et al. 2005), seamounts (De Vogelaere et al., 2005; Tracey et al., 2011), landslides (De Mol et al. 2009; Lo Iacono et al. 2014a;

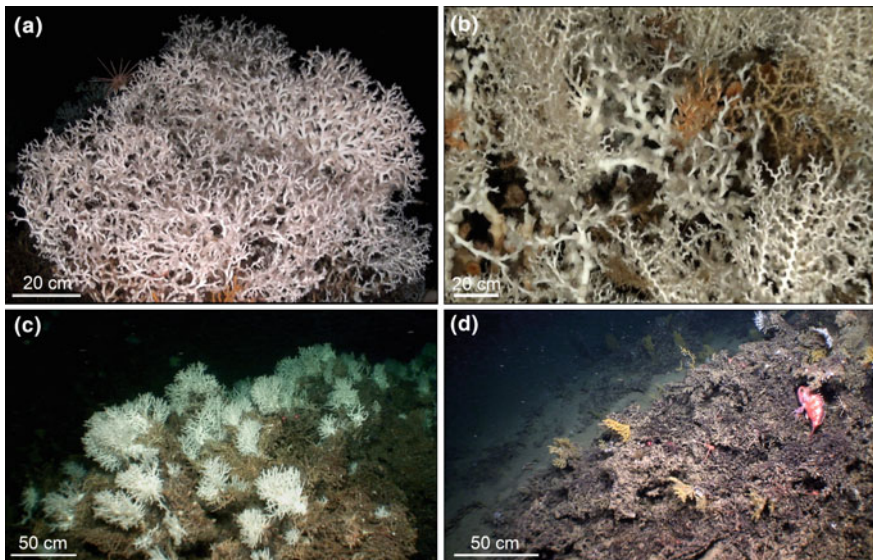


Fig. 3 Dominant species of a CWC reef. **a** A colony of *Lophelia pertusa*; **b** *L. pertusa*, white and pink *M. oculata*; **c** CWC reef with living colonies of *Madrepora oculata*; **d** CWC reef with dead frameworks of *L. pertusa* and living colonies of the gorgonian *Acanthogorgia hirsuta*. Photos in (a) and (b): © Oceana

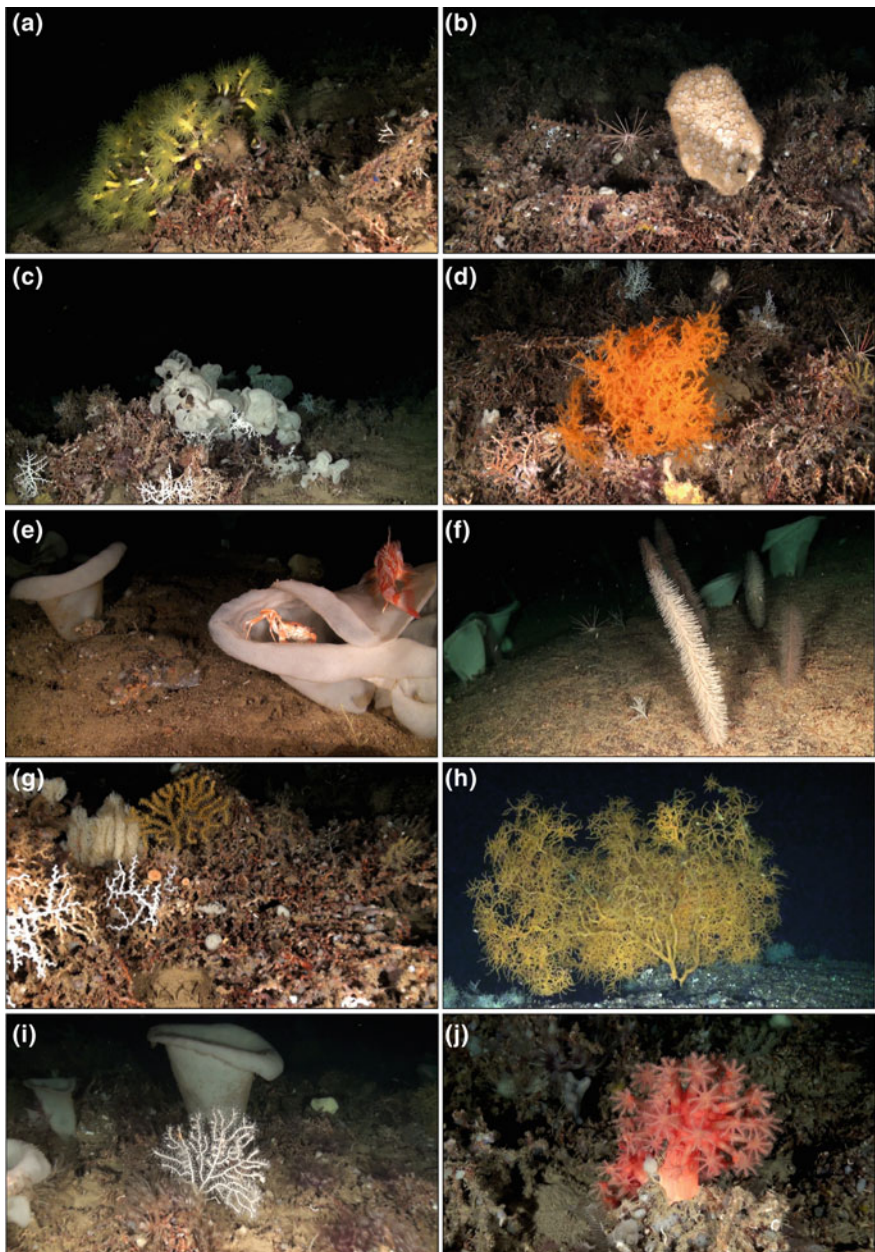
Savini et al. 2016), canyons (Orejas et al. 2009; Huvenne et al. 2011; Gori et al. 2013) and ocean gateways (Lo Iacono et al. 2014b; Lo Iacono et al. 2016). CWC are often observed along outer shelves and fjords of sub-polar and high latitude regions, settling on iceberg plough-marks and other erosive features produced during the last glacial cycle (Freiwald et al. 1999, 2002; Lindberg et al. 2007). Along the open slope, substrates providing suitable habitats for CWC settlement generally coincide with abrupt geomorphologies inherited from previous geologic events, such as landslides or fault scarps (Fosså et al. 2002; Colman et al. 2005; De Mol et al. 2009; Lo Iacono et al. 2014a; Savini et al. 2016). Following a feedback mechanism, the complex terrain of these settings enhances moderate to strong hydrodynamics, in turn maintaining exposed morphologies and low sedimentation rates along the CWC reefs. Steep or vertical walls of submarine canyons flushing organic-rich sediments to the deep-sea are also suitable habitats for CWC. The abrupt morphology and complex terrains of canyons naturally protect benthic ecosystems from the impact of destructive trawl fishing, taking a strategic role in designing new strategies for the conservation of natural resources (Orejas et al. 2009; Huvenne et al. 2011). Finally, seamounts and volcanic banks are prominent topographic highs, able to increase the upwelling of nutrient-rich waters resulting in a remarkable diversity and richness of fish and benthic fauna, including CWC (Genin et al. 1986; Duineveld et al. 2004; Rogers et al. 2007).

3.2 Cold Water Coral Reefs

If suitable environmental conditions (temperature, salinity, dissolved oxygen and pH values, turbulent current regimes and food availability) persist in time, framework building CWC are able to form extensive and complex carbonate reefs. CWC reefs develop in a delicate interplay between coral growth and bioerosion processes, giving rise to a complex ecosystem consisting of live coral colonies trapping and baffling suspended fine sediments, interspersed with dead reef framework, coral rubble and bioturbated sandy muds (Freiwald et al. 2004; Roberts et al. 2009), where other organisms (gorgonians, anthipatarians, sponges, polychaetes, molluscs, crustaceans, bryozoans, echinoderms, cirripeds and brachiopods) also contribute to the carbonate build-up (Fig. 4).

When unidirectional bottom currents prevail, the most pronounced geomorphic features along reefs generally correspond to ridge-like elongated reliefs, or “cigar shaped” reefs, few to hundreds of meters long, whose orientation is generally controlled by the main current patterns and where different sectors generally correspond to distinct habitats (Freiwald et al. 2002; Buhl-Mortensen and Lepland 2007; Buhl-Mortensen et al. 2016a). The specific dominance of living coral communities decreases from the head to the tail of the reef along the current direction, in parallel with an increase of dead framework and coral rubble supporting higher biodiversity (Fig. 6 in Buhl-Mortensen and Lepland 2007 and Fig. 8 in Freiwald et al. 2004). The generally asymmetric geomorphology of the reef and the orientation of the living colonies facing the bottom currents along its front may indicate a migration of the reef against the direction of local currents, which generally range between 5 and 20 cm s⁻¹ (Buhl-Mortensen et al. 2016a), suggesting these features as dynamic geomorphic elements developing under an interacting mechanism between coral growth rates and hydrodynamic regimes.

The most thriving reefs mapped until the present are located along the western Norwegian (Sula and Røst reefs) and Scottish margins (Mingulay reef) within a depth range of 30–450 m, and are mainly dominated by *Lophelia pertusa* communities (Freiwald et al. 2002; Roberts et al. 2005, 2009). More than 370 species associated to CWC bioconstructions are reported from the Mingulay reef and more than 1100 from the Norwegian reefs (Freiwald et al. 2002). The Norwegian Røst Reef, the world’s largest known cold-water coral reef, has a length of about 35 km, a width of up to 2.8 km and is around 35 m thick (Fosså et al. 2005), probably developed through merging processes of several single reefs. Uranium/Thorium dating indicates that many of the Norwegian reefs started to develop around 9 kyr BP, during the sea level rise of the last glacioeustatic cycle (Rokoengen and Østmo 1985; Buhl-Mortensen 2000). Morphometric analyses suggest a linear relationship between reef height and width, with their width being two to five times larger than their height (Buhl-Mortensen et al. 2001). Despite possible hiatuses and demise stages, vertical reef accretion rates for the Norwegian margin are estimated to be around 1.2 mm y⁻¹ (Buhl-Mortensen 2000).



◀Fig. 4 Examples of accompanying species in habitat forming CWC reefs. **a** Dendrophyllia cornigera. **b** Sea urchin *Cidaris cidras* and an unidentified sponge, **c** Sponge *Pachastrella molinifera* and living colonies of *M. oculata*. **d** The black coral *Leiopathes glaberrima* and the gorgonian *Acanthogorgia hirsuta* (along the right side). **e** The sponge *Asconema setubalense*, the fish *Helicolenus dactylopterus*, the crab *Bathynectes* sp. **f** The black coral *Parantipathes larix* and the sponges *Asconema setubalense*. **g** The gorgonian *Acanthogorgia hirsuta*, an unidentified sponge and living colonies of *Madrepora oculata*. **h** The back coral *Leiopathes glaberrima*. **i** The gorgonian *Villogorgia bebrycoides* and the sponge *Asconema setubalense*. **j** The cnidarian *Anthomastus grandiflorus*. Photos © Oceana

3.3 Development of Cold Water Coral Reefs and Mounds

A key characteristic for reef development both in space and time is the cyclic alternation between reef growth, bioerosion and sediment accumulation. Corals can gradually form coalescing thickets (Squires 1964) starting from small isolated colonies, owing to their *capability to form* extensive skeletal carbonate structures. Subsequently, passing through the stage of coral coppice (Squires 1964), they may give rise to CWC reefs, displaying a complex 3D structure and reaching dimension of up to hundreds of meters. Wilson (1979) presented a pioneering work on the spatial development of a reef. According to this model, different stages of coral growth give rise to a progressive outwards expansion of the bioconstruction, where colonies are spatially organized in concentric rings, named “Wilson rings” (Fig. 3 in Wilson 1979). This process of reef generation starts when small and adjacent coral patches nucleate around an initial coral colony (“ticket stage” of the reef development). During the following coral coppice stage, an increased production of coral rubble through bioerosion processes provides new available substrate for the growth of young colonies along the external border and within the innermost regions of the bioconstruction, which gradually become a complex 3D reef structure, where the amount of dead corals and coral debris by far exceeds the number of living colonies (Wilson 1979; Roberts et al. 2009). Actual models consider the cyclic alternation of distinct environmental stages as the most important factor for reef development in time. Changing environmental conditions induce crucial shifts in the dominating processes along the reef including oceanographic and sedimentary regimes, physical/chemical processes, biodiversity and species composition (Roberts et al. 2009; Douarin et al. 2009). After an initial settlement of colonies on hard substrates, a following expansion of coral frameworks coincides with suitable environmental conditions persisting in time, during which sediments trapped and baffled by thriving corals constitute an important structural component of the reef (Dorschel et al. 2007; Frank et al. 2009; Douarin et al. 2009). A general demise stage of living reefs occurs during the transition towards less suitable environmental conditions (e.g.: changing temperature, decreased food supply and productivity), bringing the start of coral collapse and increased production of coral debris and associated fauna. A consequent decrease of the reef seafloor complexity reduces the hydrodynamic regimes at the bottom and may increase the hemipelagic sediment accumulation (Douarin et al. 2009).

Within tens to hundreds of thousands of years, the alternation of suitable and unsuitable environmental conditions along reefs generally corresponds to cyclic interchanges between dominance of coral growth (thriving stages of the reefs) and fine sediment accumulation (demise stages). These long scale variations, generally related to the Quaternary glacioeustatic oscillations and associated changes in oceanographic conditions (Dorschel et al. 2005; Roberts et al. 2006, 2009), can give origin to pronounced morphologies defined as Cold-Water Coral mounds, forming through several cycles of reef development and representing sensitive carbonatic archives of past climatic and oceanographic changes (Kano et al. 2007; Raddatz et al. 2011; Fink et al. 2013; Thierens et al. 2013). CWC mounds correspond to positive reliefs generally occurring in clusters or as isolated features, distributed across a depth range of 70–1200 m and whose geomorphology corresponds to semi-circular, conical, tear-drop or linear ridge-like shapes (Kenyon et al. 2003; Masson et al. 2003; Van Rooij et al. 2003; van Weering et al. 2003; Huvenne et al. 2009; Lo Iacono et al. 2014a, b) (Fig. 5).

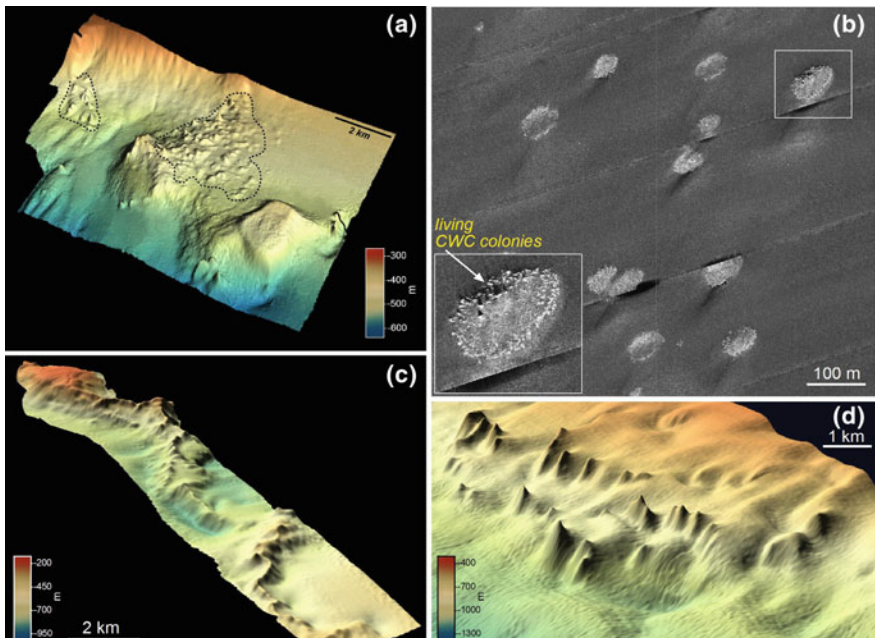
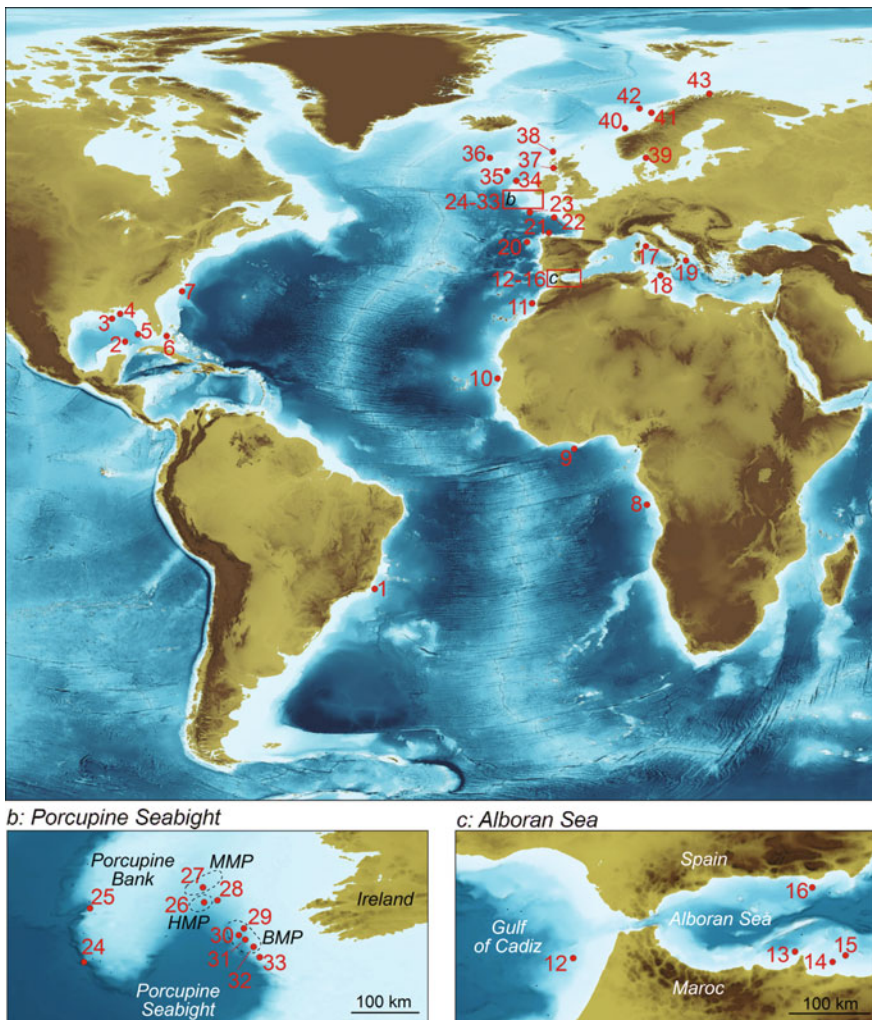


Fig. 5 **a** MB 3D model showing the two clusters of the West Melilla CWC mounds (max 45 m tall), Alboran Sea, Western Mediterranean. The larger cluster developed on a buried submarine landslide, as suggested by its lobular shape (see Lo Iacono et al. 2014a); **b** side-scan sonar mosaic showing the elliptic Darwin CWC mounds (Eastern Atlantic). The inset highlights the sharp and contrasting acoustic facies associated to living CWC colonies (see Huvenne et al. 2009; Victorero-Gonzalez et al. 2016); **c** MB 3D model showing the linear CWC Cabliers mound system, Alboran Sea, Western Mediterranean, developed on a volcanic substrate. Note the deep incised erosive moat along the base of the mound (see also Lo Iacono et al. 2014b); **d** MB 3D model showing the circular Magellan mounds, eastern Atlantic (data from GSI—INFOMAR Project)

The height of cold-water coral mounds can vary from a few meters to up to hundreds of meters whereas the width of their base can reach hundreds of meters for sub-circular shapes to up to few tens of kilometres for linear features. Geo-acoustic mapping of such important geomorphic features has unveiled hundreds of CWC mound fields, mainly spread along the NE and NW Atlantic margins and the central-western Mediterranean (Fig. 6), where they deeply affect the present-day seascapes configuration. The largest mounds, observed along the North East region of the Atlantic Sea (Irish Margin, Porcupine Seabight and Rockall Trough) are also defined as Giant Mounds. These features can reach dimensions of up to 350 m high and few kilometres wide (Kenyon et al. 2003; Mienis et al. 2007) and correspond to carbonate factories reaching back to Pliocene times (2.6 Ma; Kano et al. 2007). However, recent studies revealing the existence of new large mound fields along the western African margin reinforce the need for further mapping expeditions along less known areas. Interestingly, the large-scale distribution patterns of mounds coincide in most cases with the boundaries between prominent water masses in the Atlantic and developed close to prominent density interfaces, once more suggesting the primary role of the oceanography in the development and maintenance processes of CWC ecosystems.

Living reefs and coral assemblages are generally observed along and around the top of the mounds, coinciding with increased rugosity values of the seafloor (Guinan et al. 2009). The flanks of the mounds, that can reach steep slope gradients, are smoother and commonly characterized by dead coral framework, coral rubble and fine sediments, sometimes transported to deeper depths through the action of gravitational processes, reflected in small down flank organogenic sedimentary trails and lobes (Roberts et al. 2005). The elevated morphology of mounds, protruding into the water column, creates topographic obstacles, which steer the intensity and direction of bottom currents, in turn contributing in maintaining and enhancing their shapes. Fine grained deposits can be observed along the lee sides of mounds, sheltered from dominant bottom currents and extending from few to hundreds of meters, whereas large sediment wave fields composed of coarse coral debris can be found along the inter-mound areas, more exposed to the action of vigorous hydrodynamics (Kenyon et al. 2003; Huvenne et al. 2009). However, these processes are still poorly understood at small spatial scales (meters to tens of meters), mainly owing to the paucity of high resolution morpho-sedimentary models and oceanographic records, allowing to observe these interactions at the spatial scales they occur.

Elongated mounds extending for up to tens of kilometres have often been observed above tectonic trusts or linear volcanic ridges (Lo Iacono et al. 2014b) and related to the action of unidirectional bottom currents (Messing et al. 1990; Correa et al. 2012; Hebbeln et al. 2014). Unidirectional currents flowing along linear geomorphic features (tectonic ridges, shelf margins) probably contribute in merging adjacent sub-circular isolated mounds in longer linear coalescent systems (Eisele et al. 2014; Buhl-Mortensen et al. 2016b). Supporting this observation, a global pyramidal distribution of mound dimensions shows several small mounds compared to few larger features (Huvenne et al. 2003; Roberts et al. 2009).



The erosive action of strong bottom currents, enhanced by the morphology of the mound itself, can generate tens of meters deep and hundreds of meters wide linear scoured depressions along the bases of mounds, defined as “moats” Esentia et al. (2018). These erosive features are generally associated with “contourite drifts”, corresponding to elongated sedimentary deposits with variable size and thickness developing under moderate to strong persistent current regimes (Van Rooij et al. 2003; Hebbeln et al. 2016; Esentia et al. 2018). The side by side development of contouritic systems and CWC mounds suggests a complex interaction between transport of organic and clastic sediments under moderate to strong hydrodynamic regimes and the development of these prominent bioconstructions. As for the CWC

◀Fig. 6 Distribution map of the largest CWC mounds and living reefs along the Atlantic margins and the Mediterranean Sea. 1 Campos Basin Mounds—Lopes and Hajdu (2014), 2 Campeche Mounds—Hebbeln et al. (2014), 3 Gulf of Mexico Mounds—Georgian et al. (2016), 4 Visca Knoll Mounds—Brooke and Schroeder (2007), 5 West Florida Mounds—Neumann et al. (1977), 6 Florida Mounds—Grasmueck et al. (2006), 7 Cape Lookout Mounds—Mienis et al. (2014), 8 Angola Mini Mounds—Le Guillox et al. (2009), 9 Ghana Mounds—Buhl-Mortensen et al. (2016b), 10 Banda Mounds—Eisele et al. (2014), 11 Eugen Seibold Mounds—Glogowski et al. (2015), 12 Pen Duick Mounds—Van Roij et al. (2011), 13 West Melilla Mounds—Lo Iacono et al. (2014a), 14 East Melilla Mounds—Fink et al. (2013), 15 Cabliers Mound—Lo Iacono et al. (2014b), 16 Chella Mound—Lo Iacono et al. (2018), 17 Tuscan Archipelago Mounds—Remia and Taviani (2005), 18 Pantelleria Mounds—Martorelli et al. (2011), 19 Santa Maria di Leuca Mounds—Savini et al. (2014), 20 Breoghan Mounds—Somoza et al. (2014), 21 Ferrol and Coruña Canyon mini Mounds—unpublished, 22 Penmarc'h and Guivinec mini Mounds—De Mol et al. (2011), 23 Explorer and Dangeard mini Mounds—Stewart et al. (2014), 24 Arc Mounds—Mohn et al. (2014), 25 Porcupine Bank Canyon Mounds—Mazzini et al. (2012), 26 Hovland Mounds—Hovland et al. (1994), 27 Magellan Mounds—Hovland et al. (1994), 28 Viking Mounds—Foubert et al. (2011), 29 Galway Mounds—Dorschel et al. (2007), 30 Therese Mounds—De Mol et al. (2007), 31 Challenger Mound—Kano et al. (2007), 32 Macnas Mounds—Wilson et al. (2007), 33 Enya Mounds—Van Rooij et al. (2009), 34 Pelagia Mounds—Kenyon et al. (2003), 35 Logachev Mounds—Kenyon et al. (2003), 36 Francken Mounds—Wienberg et al. (2008), 37 Mingulay Mounds—Roberts et al. (2005), 38 Darwin Mounds—Masson et al. (2003), 39 Tisler Reef—Wild et al. (2009), 40 Sula Reef—Freiwald et al. (2002), 41 Traena Reef/Mounds—Lindberg (2004), 42 Røst Reef—Freiwald et al. (2004), 43 Stjernsund Reef/Mounds—Freiwald et al. (1997). MMP Magellan Mound Province (Hovland et al. 1994); HMP Hovland Mound Province (Hovland et al. 1994); BMP Belgica Mound Province (Henriet et al. 1998)

mounds, the sedimentary records of contouritic drifts are controlled by regional changes of sedimentary regimes controlled by past glacioeustatic changes (Hernández-Molina et al. 2014).

4 Biodiversity of Deep-Sea Bioconstructions: Environmental Issues, Management Strategies and Future Perspectives

CWC reefs and mounds and coralligenous bioconstructions are considered hotspots of biodiversity in the deep marine realm, contributing to regulate the dynamics of natural resources in the ocean, including fish stocks of economic importance (Guidetti et al. 2002, Salomidi et al. 2012, Paoli et al. 2016, Tribot et al. 2016 Roberts et al. 2009 and references therein). They have been declared as sensitive and vulnerable marine ecosystems by national and international legislations and are actually included in the list of endangered habitats by governmental organizations and conservation agencies (OSPAR 2008) (red list habitats).

CWC reefs for instance, serve as important spawning, nursery, feeding and refuge areas for a multitude of fishes and invertebrates (Fosså et al. 2002; Husebø et al. 2002; Colman et al. 2005; Stone 2006; Ross and Quattrini 2007; Baillon et al. 2012; Henry et al. 2013). Diversity within these reefs has been found to be orders of

magnitude higher than the surrounding seafloor, in some case rivalling shallow-water reefs (Rogers 1999; Henry and Roberts 2007). Their rough morphology, made up of crevices cavities and small build-ups, provides habitats for several other species. Norwegian authorities and EU have introduced regulations to ban destructive bottom trawling activities along such vulnerable ecosystems (Fosså and Skjoldal 2010), assigning to Norway the largest European deep-sea area protected from the threat of industrial activities.

Despite their relevant role in marine ecosystems and ocean biodiversity, the existence and conservation of these benthic communities is being seriously compromised by human-related activities. The physico-chemical perturbations caused by the increasing emissions of CO₂, such as the increasing temperature and the decreasing pH (i.e. ocean acidification), have a negative impact on the calcification of the skeleton of calcareous algae and invertebrates (Rodolfo-Metalpa et al. 2010; Basso 2012). It is expected that ocean acidification will enhance both bioerosion and chemical dissolution of carbonates in the future, with undersaturation expected to affect especially the deep, cold-water carbonates (Guinotte et al. 2006; Tribollet et al. 2009; Lunden et al. 2013; Murray et al. 2016; Wissak et al. 2014). The presence of commercial fisheries in these habitats induced destructive bottom trawling which strongly threatened the habitat complexity and biodiversity of deep-sea bioconstructions. Trawling over deep coral areas can be compared to land deforestation for the relevant loss of biodiversity that both processes involve (Watling and Norse 1997). Conservation groups are making scientific and political communities aware of the vulnerability of deep coral habitats to such massive exploitation in several Exclusive Economic Zones around the world. In an effort to protect these unique resources, researchers are refining acoustic mapping techniques and statistical models that are able to perform solid prediction of their distribution (Tittensor et al. 2009; Ross and Howell 2012; Robert et al. 2015, 2016). The Barcelona Convention's Action plan adopted in 2008 for the conservation of coralligenous outcrops and other calcareous bio-concretions declared the need of legal measures for their protection. Deep-sea bioconstructions are also considered with particular attention in the EU's Habitats Directive (under 1170 "Reefs"), and in the Bern Convention. More recently, the Marine Strategy Framework Directive (MSFD; European Parliament and Council of the European Union 2008; European Commission 2010), aimed at achieving the "Good Environmental Status" (GES) of all marine waters by 2020, required each Member State to develop a strategy of knowledge-based sustainable management for its marine waters. On the basis of the Barcelona Convention and other international initiatives for the environmental protection of deep-sea ecosystems (UNEP-MAPRAC/SPA 2008, 2010; UNEP-MAP 2011), a group of habitat types, among which C ad CWC, has been identified as of special scientific or biodiversity interest (MSFD, Annex III, Table 1). The implementation of appropriate monitoring measures is indeed instrumental to guarantee a sustainable management of C and CWC.. Although an extensive array of increasing high quality data on CWCs exists for the northeast Atlantic margin, there are still several gaps in understanding the functioning and evolution of these complex habitats, even regarding any potential relationship

between their ecological dynamics and the resulting geomorphic expression. Furthermore, the lack of full coverage high-resolution seafloor maps in the deep-sea may introduce a bias in the recorded extension of these relevant geomorphic features. For instance, recent oceanographic expedition along the western African and South American margins are revealing the existence of new CWC mound fields, where living reefs are supporting a high biodiversity (Le Guillox et al. 2009; Eisele et al. 2014; Lopes and Hajdu 2014; Glogowski et al., 2015; Buhl-Mortensen et al. 2016b).

New data on less explored areas may be of great significance, both regionally and globally, for:

- (1) refining the assessment of biodiversity at a global scale
- (2) better define the resilience of deep-sea habitats to human induced climatic forcing
- (3) better estimating the contribution to the ocean carbon budget of cool-water carbonatic systems
- (4) better constraining on a basin scale the main paleoceanographic events in recent time, including high-resolution focus on late Pleistocene and Holocene rapid climate events.

References

- Abel EF (1961) Über die Beziehung mariner Fische zu Hartbodenstrukturen. Sper Osterr Akad Wiss (Math Nat Kl Abt A) 170:223–263
- Baillon S, Hamel JF, Wareham VE, Mercier A (2012) Deep cold-water corals as nurseries for fish larvae. *Front Ecol Environ* 10(7):351–356
- Balata D, Acunto S, Cinelli F (2006) Spatio-temporal variability and vertical distribution of a low rocky subtidal assemblage in the north-west Mediterranean. *Estuar Coast Shelf Sci* 67:553–561. doi:[10.1016/j.ecss.2005.12.009](https://doi.org/10.1016/j.ecss.2005.12.009)
- Ballesteros E (2006) Mediterranean coralligenous assemblages: a synthesis of present knowledge. *Oceanogr Mar Biol Annu Rev* 44:23–195
- Basso D (2012) Carbonate production by calcareous red algae and global change. In: Basso D, Granier B (eds) *Calcareous algae and global change: from identification to quantification*. Geodiversitas 34:13–33
- Basso D, Nalin R, Massari F (2007) Genesis and composition of the Pleistocene Coralligène de plateau of the Cutro Terrace (Calabria, Southern Italy). *N Jb Geol Paläont* 244(2):73–182
- Bellan-Santini D, Lacaze JC, Poizat C (1994) Les biocénoses marines et littorales de Méditerranée, synthèse, menaces et perspectives. Collection Patrimoines Naturels. Secrétariat de la Faune et de la Flore/M.N.H.N. 19:1–246
- Ben Haj S, Boero F, Cebrian D, De Juan S, Limam A, Leonart J, Torchia G, Rais C (eds), RAC/SPA, Tunis, pp 100
- Bonacorsi M, Pergent-Martini C, Clabaut P, Pergent G (2012) Coralligenous “atolls”: discovery of a new morphotype in the Western Mediterranean Sea. *C R Biol* 335:668–672
- Bosellini A, Ginsburg NR (1971) Form and internal structure of recent algal nodules (Rhodolites) from Bermuda. *J Geol* 79:669–682

- Bosence DWJ, Pedley HM (1982) Sedimentology and palaeoecology of a Miocene coralline algal biostrome from the Maltese Islands. *Palaeogeogr Palaeoclimatol Palaeoecol* 38:9–43. [10.1016/0031-0182\(82\)90062-1](https://doi.org/10.1016/0031-0182(82)90062-1)
- Bosence DWJ, Bridges PH (1995) A review of the origin and evolution of carbonate mud-mounds. In: Monty CLV, Bosence DWJ, Bridges PH, Pratt BR (eds) Carbonate mud-mounds, their origin and evolution. Special Publications International Association Sedimentologists, vol 23. Blackwell, Oxford, pp 3–9
- Bracchi VA, Savini A, Marchese F, Palamara S, Basso D, Corselli C (2015) Coralligenous habitat in the Mediterranean Sea: a geomorphological description from remote data. *Ital J Geosci* 134(1):32–40. doi:[10.3301/IJG.2014.16](https://doi.org/10.3301/IJG.2014.16)
- Bracchi VA, Nalin R, Basso D (2016) Morpho-structural heterogeneity of shallow-water coralligenous in a Pleistocene marine terrace (Le Castella, Italy). *Pal Pal Pal* 454:101–112
- Brooke S, Schroeder WW (2007) State of deep coral ecosystems in the Gulf of Mexico Region: Texas to the Florida straits. In: Lumsden SE, Hourigan TF, Bruckner AW, Dorr G (eds) The state of deep coral ecosystems of the United States. NOAA Technical Memorandum CRCP-3, Silver Spring, MD, pp 271–306
- Brooke S, Ross SW, Bane JM, Seim HE, Young CM (2013) Temperature tolerance of the deep-sea coral *Lophelia pertusa* from the southeastern United States. *Deep-Sea Res II* 92:240–248
- Buhl-Mortensen PB (2000) *Lophelia pertusa* (Scleractinia) in Norwegian waters. Distribution, growth, and associated fauna. Dr. Scient thesis, Department of Fisheries and Marine Biology, University of Bergen, Norway
- Buhl-Mortensen PB, Lepland A (2007) Ecological consequences of exploration drilling on coral reefs. *Fiskennog Høvet* 7:123
- Buhl-Mortensen PB, Hovland MT, Fosså JH, Furevik DM (2001) Distribution, abundance and size of *Lophelia pertusa* coral reefs in mid-Norway in relation to seabed characteristics. *J Mar Biol Assoc UK* 81:581–597
- Buhl-Mortensen P, Buhl-Mortensen L, Purser A (2016a) Trophic ecology and habitat provision in cold-water coral ecosystems. In: Rossi S, Bramanti L, Gori A, Orejas Sacco del Valle C (eds) *Marine animal forests, the ecology of benthic biodiversity hotspots*, Springer International Publishing, Switzerland, pp 2–23
- Buhl-Mortensen L, Serigstad B, Buhl-Mortensen P, Olsen MN, Ostrowski M, Błażewicz-Paszkowycz M, Appoh E (2016b) First observations of the structure and megafaunal community of a large *Lophelia* reef on the Ivorian-Ghanaian margin (the Gulf of Guinea). *Deep-Sea Res Part II*. [10.1016/j.dsr2.2016.06.007](https://doi.org/10.1016/j.dsr2.2016.06.007)
- Cairns S (2007) Deep-water corals: an overview with special reference to diversity and distribution of deep-water scleractinian corals. *Bull Mar Sci* 81(3):311–322
- Campiani E, Foglini F, Fraschetti S, Savini A, Angeletti L (2014) Conservation and management of coralligenous habitat: experience from the BIOMAP project. GEOHAB meeting 2014, Lorne, Australia, 6–9 May, Abstract Volume
- Canals M, Ballesteros E (1997) Production of carbonate particles by phytobenthic communities on the Mallorca-Menorca shelf, Northwestern Mediterranean Sea. *Deep-Sea Res II Top Stud Oceanogr* 44:611–629. doi:[10.1016/S0967-0645\(96\)00095-1](https://doi.org/10.1016/S0967-0645(96)00095-1)
- Carannante G, Simone L (1996) Rhodolith facies in the central-southern Appenines Mountains, Italy. In: Franseen EK, Esteban M, Ward WC, Rouchy JM (eds) Models for carbonate stratigraphy from miocene reef complexes of Mediterranean regions. SEPM concepts in sedimentology and palaeontology, vol 5, pp 261–275
- Casellato S, Stefanon A (2008) Coralligenous habitat in the northern Adriatic Sea: an overview. *Mar Ecol* 29:321–341
- Cocito S (2004) Bioconstruction and biodiversity: their mutual influence. *Sci Mar* 68(1):137–144
- Colman JG, Gordon DM, Lane AP, Forde MJ, Fitz PJ (2005) Carbonate mounds off Mauritania, Northwest Africa: status of deep-water corals and implications for management of fishing and oil exploration activities. In: Freiwald A, Roberts JM (eds) *Cold-water corals and ecosystems*. Springer, Berlin, pp 417–441

- Correa TBS, Eberli GP, Grasmueck M, Reed JK, Correa AMS (2012) Genesis and morphology of cold-water coral ridges in a unidirectional current regime. *Mar Geol* 326–328:14–27
- De Mol B, Kozachenko M, Wheeler A, Alvares H, Henriet JP, Le Roy O (2007) Thérèse Mound: a case study of coral bank development in the Belgica Mound Province, Porcupine Seabight. *Int J Earth Sci* 96:103–120
- De Mol B, Huvenne VAI, Canals M (2009) Cold-water coral banks and submarine landslides: a review. *Int J Earth Sci* 98(4):885–899
- De Mol L, Van Rooij D, Pirlet H, Greinert J, Frank N, Quemmerais F, Henriet JP (2011) Cold-water coral habitats in the Penmarc'h and Guilvinec Canyons (Bay of Biscay): Deep-water versus shallow-water settings. *Mar Geol* 282:40–52
- De Vogelaere A, Burton EJ, Trejo T, King CE, Clague DA, Tamburri MN, Cailliet GM, Kochevar RE, Douros WJ (2005) Deep-sea corals and resource protection at the Davidson Seamount, California, U.S.A. In: Freiwald A, Roberts JM (eds) *Cold-water corals and ecosystems*. Springer, Berlin, pp 1189–1198
- Di Geronimo I, Di Geronimo R, Rosso A, Sanfilippo R (2002) Structural and taphonomic analysis of a columnar coralline algal build-up from SE Sicily. *Géobios* 24:86–95
- Di Geronimo I, Messina C, Rosso A, Sanfilippo R, Sciuto F, Vertino A (2005) Enhanced biodiversity in the deep: early pleistocene coral communities from southern Italy. In: Freiwald A, Roberts JM (eds) *Cold-water corals and ecosystems*. Springer, Berlin, pp 61–86
- Dorschel B, Hebbeln D, Foubert A, White M, Wheeler AJ (2007) Hydrodynamics and cold-water coral facies distribution related to recent sedimentary processes at Galway Mound west of Ireland. *Mar Geol* 244:184–195
- Dorschel B, Hebbeln D, Ruggeberg A, Dullo W, Freiwald A (2005) Growth and erosion of a cold-water coral covered carbonate mound in the Northeast Atlantic during the Late Pleistocene and Holocene. *Earth Planet Sc Lett* 233(1–2):33–44
- Douarin M, Sinclair DJ, Elliot M, Henry LA, Long D, Mitchison F, Roberts JM (2009) Changes in fossil assemblage in sediment cores from Mingulay Reef Complex (NE Atlantic): implications for coral reef build-up. *Deep Sea Res Part II* 99:286–296
- Doxa A, Holon F, Deter J, Villeger S, Boissery P, Mouquet (2016) Mapping biodiversity in three-dimensions challenges marine conservation strategies: the example of coralligenous assemblages in North-Western Mediterranean Sea. *Ecol Ind* 61:1042–1054
- Duineveld GCA, Lavaleye MSS, Berghuis EM (2004) Particle flux and food supply to a seamount cold-water coral community Galicia Bank, NW Spain. *Mar Ecol Prog Ser* 277:13–23
- Duineveld GCA, Lavaleye MSS, Bergman MJN, De Stigter H, Mienis F (2007) Trophic structure of a cold-water coral mound community (Rockall Bank, NE Atlantic) in relation to the near-bottom particle supply and current regime. *Bull Mar Sci* 81(3):449–467
- Dullo WC, Flögel S, Rüggeberg A (2008) Cold-water coral growth in relation to the hydrography of the Celtic and Nordic European continental margin. *Mar Ecol Prog Ser* 371:165–176
- Eisele M, Frank N, Wienberg C, Titschack J, Mienis F, Beuck L, Tisnerat-Laborde N, Hebbeln D (2014) Sedimentation patterns on a cold-water coral mound off Mauritania. *Deep-Sea Res II* 99:307–315
- Esentia I, Stow D, Smillie Z (2018) Contourite drifts and associated bedforms. In: Micallef A, Krastel S, Savini A (eds) *Submarine Geomorphology*. Springer
- European Commission (2010) Commission decision of 1 September 2010 on criteria and methodological standards on good environmental status of marine waters. *Off J Eur Union* L232/14
- European Parliament, Council of the European Union (2008) Directive 2008/56/EC of the European Parliament and of the Council of 17 June 2008 establishing a framework for community action in the field of marine environmental policy (Marine Strategy Framework Directive). *Off J Eur Union* L164/19
- Fink HG, Wienberg C, Hebbeln D, McGregor HV, Schmiedl G, Taviani M, Freiwald A (2013) Oxygen control on Holocene cold-water coral development in the eastern Mediterranean Sea. *Deep-Sea Res-I* 62:89–96

- Försterra G, Beuck L, Häussermann V, Freiwald A (2005) Shallow-water *Desmophyllum dianthus* (Scleractinia) from Chile: characteristics of the biocoenoses, the bioeroding community, heterotrophic interactions and (paleo)-bathymetric implications. In: Freiwald A, Roberts JM (eds) Cold-water corals and ecosystems. Springer, Berlin, pp 937–977
- Fosså JH, Skjoldal HR, (2010) Conservation of cold water coral reefs in Norway. In Grafton RQ Hilborn R, Squires D, Tait M, Williams M (eds) Handbook of marine fisheries conservation and management. Oxford University Press, New York, pp 215–230
- Fosså JH, Mortensen PB, Furevik DM (2002) The deep-water coral *Lophelia pertusa* in Norwegian waters: distribution and fishery impacts. *Hydrobiologia* 471:1–12
- Fosså JH, Lindberg B, Christensen O, Lundälv T, Svellingen I et al (2005) Mapping of *Lophelia* reefs in Norway: experiences and survey methods. In: Freiwald A, Roberts JM (eds) Cold-water corals and ecosystems. Springer, Berlin, pp 359–391
- Foubert A, Henriet JP (2009) Nature and significance of the recent carbonate mound record: the mound challenger code. Lecture notes in earth sciences, vol 126. Springer, 298 pp. ISBN: 978-3-642-00289-2
- Foubert A, Huvenne VAI, Wheeler A, Kozachenko M, Opderbecke J, Henriet JP (2011) The Moira Mounds, small cold-water coral mounds in the Porcupine Seabight, NE Atlantic: Part B —Evaluating the impact of sediment dynamics through high-resolution ROV-borne bathymetric mapping. *Mar Geol* 282:65–78
- Frank N, Ricard E, Lutringer-Paquet A, Van Der Land C, Colin C, Blamart D, Foubert A, Van Rooij D, Henriet J-P, De Haas H, Van Weering T (2009) The Holocene occurrence of cold water corals in the NE Atlantic: implications for coral carbonate mound evolution. *Mar Geol* 266:129–142
- Frantz BR, Foster MS, Riosmena-Rodriguez R (2005) *Clathromorphum nereostratum* (Coralinales, Rhodophyta): the oldest alga? *J Phycol* 41:770–773
- Freiwald A, Henrich R, Pätzold J (1997) Anatomy of a deep-water coral reef mound from Stjernsund, West-Finnmark, northern Norway. Cool-water carbonates. In: James NP (ed) SEPM Special Publication, 56, pp 141–161
- Freiwald A, Wilson JB, Henrich R (1999) Grounding pliocene icebergs shape recent deep-water coral reefs. *Sed Geol* 125:1–8
- Freiwald A, Huhnerbach V, Lindberg B, Wilson JB, Campbell J (2002) The Sula Reef complex, Norwegian Shelf. *Facies* 47:179–200
- Freiwald A, Fosså JH, Grehan A, Koslow T, Roberts JM (2004) Cold-water coral reefs. UNEP-WCMC, Cambridge, UK
- Genin A, Dayton PK, Lonsdale PF, Spiess FN (1986) Corals on seamount peaks provide evidence of current acceleration over deep-sea topography. *Nature* 322:59–61
- Georgian SE, DeLeo D, Durkin A, Gomez CE, Kurman M, Lunden JJ, Cordes EE (2016) Oceanographic patterns and carbonate chemistry in the vicinity of cold-water coral reefs in the Gulf of Mexico: implications for resilience in a changing ocean. *Limnol Oceanogr* 61:648–665
- Giaccone G, Giaccone T, Catra M (2009) Association with *Laminaria rodriguezii* on a detritic bottom and on rocks: *cystoseiretum zosteroidis* Giaccone 1973 subass. *Laminarietosum rodriguezii* Giaccone 1973. In: Priority habitats according to the SPA/BIO protocol (Barcelona Convention) present in Italy. Identification sheets 16:204–208
- Ginsburg RN, Gischler E, Schlager W (1994) Johannes Walther on reefs. Geological milestones, vol II. Comparative Sedimentology Laboratory, Rosenthal School of Marine and Atmospheric Science, University of Miami, 141 pp
- Głogowski S, Dullo WC, Feldens P, Liebetrau V, Von Reumont J, Hühnerbach V, Krastel S, Wynn RB, Flögel S (2015) The Eugen Seibold coral mounds offshore western Morocco: oceanographic and bathymetric boundary conditions of a newly discovered cold-water coral province. *Geo-Mar Lett* 35:257–269
- Gori A, Orejas C, Madurell T, Bramanti L, Martin M, Quintanilla E, Martí-Puig P, Lo Iacono C, Puig P, Requena S, Greeacre M, Gili JM (2013) Bathymetrical distribution and size structure of coldwater coral populations in the Cap de Creus and Lacaze-Duthiers canyons (northwestern Mediterranean). *Biogeosciences* 10:2049–2060

- Grasmueck M, Eberli GP, Viggiano DA, Correa T, Rathwell G, Luo J (2006) Autonomous underwater vehicle (AUV) mapping reveals coral mound distribution, morphology, and oceanography in deep water of the Straits of Florida. *Geophys Res Lett* 33:L23616. doi:[10.1029/2006GL027734](https://doi.org/10.1029/2006GL027734)
- Guidetti P, Terlizzi A, Fraschetti S, Boero F (2002) Spatio-temporal variability in fish assemblages associated with coralligenous formations in south eastern Apulia (SE Italy). *Ital J Zool* 69: 325–331
- Guinan J, Grehan AJ, Dolan MFJ, Brown C (2009) Quantifying relationships between video observations of cold-water coral cover and seafloor features in Rockall Trough, west of Ireland. *MEPS* 375:125–138
- Guinotte JM, Orr J, Cairns S, Freiwald A, Morgan L, George R (2006) Will human-induced changes in seawater chemistry alter the distribution of deep-sea scleractinian corals? *Front Ecol Environ* 4:141–146
- Hebbeln D, Samankassou E (2015) Where did ancient carbonate mounds grow—in bathyal depths or in shallow shelf waters? *Earth Sci Rev* 145:56–65
- Hebbeln D, Wienberg C, Wintersteller P, Freiwald A, Becker M, Beuck L, Dullo C, Eberli GP, Glogowski S, Matos L, Forster N, Reyes-Bonilla H, Taviani M, The MSM 20-4 Shipboard Scientific Party (2014) Environmental forcing of the Campeche cold-water coral province, southern Gulf of Mexico. *Biogeosciences* 11:1799–1815
- Hebbeln D, Van Rooij D, Wienberg C (2016) Good neighbours shaped by vigorous currents: cold-water coral mounds and contourites in the North Atlantic. *Mar Geol* 378:171–185
- Henriet J-P, De Mol B, Pillen S, Vanneste M, Van Rooij D, Versteeg W, Croker PF, Shannon PM, Unnithan V, Bouriaak S, Chachkine P, Porcupine-Belgica 97 Shipboard Party (1998) Gas hydrate crystals may help build reefs. *Nature* 391:648–649
- Henry LA, Roberts JM (2007) Biodiversity and ecological composition of macrobenthos on cold-water coral mounds and adjacent off-mound habitat in the bathyal Porcupine Seabight, NE Atlantic. *Deep Sea Res Part I Oceanogr Res* 54(4):654–672
- Henry LA, Navas JM, Roberts JM (2013) Multi-scale interactions between local hydrography, seabed topography, and community assembly on cold-water coral reefs. *Biogeosciences* 10(4): 2737–2746
- Hernández-Molina FJ, Llave E, Preu B, Ercilla G, Fontan A, Bruno M, Serra N, Gomiz JJ, Brackenridge RE, Sierra FJ, Stow DAV, García M, Juan C, Sandoval N, Arnaiz A (2014) Contourite processes associated with the Mediterranean outflow water after its exit from the Strait of Gibraltar: global and conceptual implications. *Geology* 42:227–230
- Hong JS (1982) Contribution à l'étude des peuplements d'un fond coralligène dans la région marseillaise en Méditerranée Nord-Occidentale. *Bull KORDI* 4:27–51
- Hovland M, Croker PF, Martin M (1994) Fault-associated seabed mounds (carbonate knolls?) off western Ireland and northwest Australia. *Mar Pet Geol* 11:232–246
- Husebø Å, Nøtttestad L, Fosså JH, Furevik DM, Jørgensen SB (2002) Distribution and abundance of fish in deep-sea coral habitats. *Hydrobiologia* 471:91–99
- Huvenne VAI, De Mol B, Henriet JP (2003) A 3D seismic study of the morphology and spatial distribution of buried coral banks in the Porcupine Basin, SW of Ireland. *Mar Geol* 198:5–25
- Huvenne VAI, Masson DG, Wheeler AJ (2009) Sediment dynamics of a sandy contourite: the sedimentary context of the Darwin cold-water coral mounds, Northern Rockall Trough. *Int J Earth Sci (Geol Rundsch)* 98:865–884
- Huvenne VAI, Tyler PA, Masson DG, Fisher EH, Hauton C, Hühnerbach V, Le Bas T, Wolff GA (2011) A picture on the wall: innovative mapping reveals cold-water coral refuge in submarine Canyon. *PLoS ONE* 6(12):e28755. doi:[10.1371/journal.pone.0028755](https://doi.org/10.1371/journal.pone.0028755)
- James NP, Bourque P-A (1992) Reefs and mounds. In: Walker RG, James NP (eds) *Facies Models, response to sea level change*. Geological Association of Canada, Geotext (1), pp 323–347
- James NP, Clarke JDA (eds) (1997) Cool-water carbonates. SEPM Special Publication 56, Tulsa, OK, pp 1–20
- Jones CG, Lawton JH, Shachak M (1994) Organisms as ecosystem engineers. *Oikos* 69:373–386

- Kamenos NA, Hoey TB, Nienow P, Fallick AE, Clavere T (2012) Reconstructing greenland ice sheet runoff using coralline algae. *Geology* 40(12):1095–1098
- Kano A, Ferdelman TG, Williams T, Henriet JP, Ishikawa T, Kawagoe N, Takashima, C, Kakizaki Y, Abe K, Sakai S, Browning E, Li X, The IODP Expedition 307 Scientists (2007) Age constraints on the origin and growth history of a deep-water coral mound in the northeast Atlantic drilled during integrated ocean drilling program expedition 307. *Geology* 35(11): 1051–1054
- Kenyon NH, Akhmetzhanov AM, Wheeler AJ, Van Weering TCE, De Haas H, Ivanov MK (2003) Giant carbonate mud mounds in the southern Rockall Trough. *Mar Geol* 195:5–30
- Klement KW (1967) Practical classification of reefs and banks, bioherms and biostromes. *Am Assoc Pet Geol Bull* 51:167–168
- Kružić P (2013) Bioconstructions in the Mediterranean: present and future. In: Goffredo S, Dubinsky Z (eds) *The Mediterranean Sea: its history and present challenges*, Springer, Berlin, pp 435–447
- Laborel J (1961) Le concrétionnement algal ‘Coralligène’ et son importance géomorphologique en Méditerranée. *Recueils Trav Stat Mar Endoume* 23:37–60
- Laborel J (1987) Marine biogenic constructions in the Mediterranean. a review. *Sci Rep Port-Cros Natl Park* 13:97–126
- Laubier L (1966) Le coralligène des Albères. *Monographie biocénotique. Annales Institut Océanographique*, Paris, 43(2):137–316
- Le Guilloux E, Olu K, Bourillet JF, Savoye B, Iglesias FP, Sibuet M (2009) First observations of deep-sea coral reefs along the Angola margin. *Deep-Sea Res II* 56:2394–2403
- Lindberg B (2004) Cold-water coral reefs on the norwegian shelf—acoustic signature, geological, geomorphological and environmental setting. Ph.D. thesis. Department of Geology, University of Tromsø
- Lindberg B, Berndt C, Mienert J (2007) The Fugløy Reef at 70°N; acoustic signature, geologic, geomorphologic and oceanographic setting. *Int J Earth Sci* 96–1, Special volume: carbonate mounds on the NW European margin: a window into earth history
- Lo Iacono C, Gracia, E, Ranero C, Emelianov M, Huvenne V, Bartolome R, Booth-Rea G, Prades J, MELCOR Cruise Party (2014a) The West Melilla cold water coral mounds, Eastern Alboran Sea: morphological characterization and environmental context. *Deep-Sea Res II* 99:316–326
- Lo Iacono C, Huvenne VAI, Gonzalez LV, Vertino A, Van Rooij D, Gràcia E, Ranero CR, the GATEWAYS Cruise Party (2016) Living reefs and CWC mounds in the Alboran Sea (Western Mediterranean). Holocene evolution and present-day conditions. 6th ISDSC, 11–16 September, Boston, USA
- Lo Iacono C, Savini A, Huvenne V, Gràcia E, 2018. Habitat mapping of cold-water corals in the Mediterranean Sea. In: Orejas C, Jimenez C (eds) *Past, present and future: Mediterranean cold-water corals*. Springer, Berlin
- Lo Iacono C, Victorero Gonzalez L, Huvenne VAI, Van Roji D, Gràcia E, Ranero C, The GATEWAYS Cruise Party (2014b) Morphology and shallow stratigraphy of the West Melilla and Cabliers CWC Mounds (Alboran Sea). Preliminary insights from the GATEWAYS MD194 Cruise. Second Deep-Water Circulation Congress, Ghent (Belgium), Sept 2014
- Lopes D, Hajdu D (2014) Carnivorous sponges from deep-sea coral mounds in the Campos Basin (SW Atlantic), with the description of six new species (Cladophorididae, Poecilosclerida, Demospongidae). *Mar Biol Res* 10(4):329–356
- Lowenstam HA (1950) Niagaran reefs of the Great Lakes area. *J Geol* 58:431–487
- Lowenstam HA (1981) Minerals formed by organisms. *Science* 211:1126–1131
- Lunden JJ, Georgian SE, Cordes EE (2013) Aragonite saturation states at cold-water coral reefs structured by Lophelia pertusa in the northern Gulf of Mexico. *Limnol Oceanogr* 58:354–362
- Marion F (1883) *Esquisse d'une topographie zoologique du Golfe de Marseille*. Annales Muséum Histoire Naturelle Marseille 1(1):1–108
- Martin CS, Giannoulaki M, De Leo F, Scardi M, Salomidi M, Knitweiss L, Pace ML, Garofalo G, Grristina M, Ballesteros E, Bavestrello G, Belluscio A, Cebrian E, Gerakaris V, Pertent G,

- Pergent-Martini C, Schembri PJ, Terribile K, Rizzo L, Ben Souissi J, Bonacorsi M, Guarneri G, Krzelj M, Macic V, Punzo E, Valavanis V, Fraschetti S (2014) Coralligenous and maerl habitats: predictive modelling to identify their spatial distributions across the Mediterranean Sea. *Sci Rep* 4:5073. doi:[10.1038/srep05073](https://doi.org/10.1038/srep05073)
- Martorelli E, Petroni G, Chiocci FL, Party Pantelleria Scientific (2011) Contourites offshore Pantelleria Island (Sicily Channel, Mediterranean Sea): depositional, erosional and biogenic elements. *Geo-Mar Lett* 31:481–493
- Masson DG, Bett BJ, Billett DSM, Jacobs CL, Wheeler AJ, Wynn RB (2003) The origin of deep-water, coral-topped mounds in the northern Rockall Trough, Northeast Atlantic. *Mar Geol* 194:159–180
- Mazzini A, Akhmetzhanov A, Monteys X, Ivanov M (2012) The Porcupine Bank Canyon coral mounds: oceanographic and topographic steering of deep-water carbonate mound development and associated phosphatic deposition. *Geo-Mar Lett* 32(3):205–225
- Messing CG, Neumann AC, Lang JC (1990) Biozonation of deep-water lithoherms and associated hardgrounds in the northeastern Straits of Florida. *Palaeos* 5:15–33
- Mienis F, De Stigter HC, White M, Duineveld G, De Haas H, Van Weering TCE (2007) Hydrodynamic controls on cold-water coral growth and carbonate-mound development at the SW and SE Rockall Trough Margin, NE Atlantic Ocean. *Deep Sea Res Part I* 54(9):1655–1674
- Mienis F, Duineveld GCA, Davies AJ, Lavaleye MMS, Ross SW, Seim H, Bane J, Van Haren H, Bergman MJN, De Haas H, Brooke S, Van Weering TCE (2014) Cold-water coral growth under extreme environmental conditions, the Cape Lookout area, NW Atlantic. *Biogeosciences* 11:2543–2560
- Mohn C, Rengstorf A, White M, Duineveld G, Mienis F, Soetaert K, Grehan A (2014) Linking benthic hydrodynamics and cold-water coral occurrences: a high-resolution model study at three cold-water coral provinces in the NE Atlantic. *Prog Oceanogr* 122:92–104
- Montaggioni LF, Braithwaite CJR (2009) Quaternary coral reef systems. History, development processes and controlling factors. *Developments in marine geology* 5, Elsevier, 550 pp
- Montagna P, McCulloch M, Taviani M, Mazzoli C, Vendrell B (2006) Phosphorus in cold-water corals as a proxy for seawater nutrient chemistry. *Science* 312(5781):1788–1791
- Monty CLV (1995) The rise and nature of carbonate mud-mounds: an introductory actualistic approach. In: Monty CLV, Bosence DWJ, Bridges PH, Pratt BR (eds) *Carbonate mud-mounds: their origin and evolution*. IAS Special Publication 23, p 11–48
- Moreno Navas J, Miller PL, Henry LA, Hennige SJ, Roberts JM, (2014) Ecohydrodynamics of cold-water coral reefs: a case study of the mingulay reef complex (Western Scotland). *PLoS-ONE* 9–5
- Morganti C, Cocito S, Sgorbini S (2001) Contribution of biocostructor to coralligenous assemblages exposed to sediment deposition. *Biol Mar Mediterr* 8:283–286
- Murray RJ, Murray F, Anagnostou E, Hennige S, Gori A, Henry L-A, Fox A, Kamenos N, Foster GL (2016) Cold-water corals in an era of rapid global change: are these the deep ocean's most vulnerable ecosystems? In: Goffredo S, Dubinsky Z (eds) *The cnidaria, past, present and future*, Part VIII, pp 593–606
- Nalin R, Basso D, Massari F (2006) Pleistocene coralline algal build-ups (coralligène de plateau) and associated bioclastic deposits in the sedimentary cover of Cutro marine terrace (Calabria, Southern Italy) In: Pedley HM, Carannante G (eds) *Coolwater carbonates: depositional systems and palaeoenvironmental control*. London Geological Society Special Publications 255, pp 11–22
- Naumann MS, Orejas C, Ferrier-Pagès C (2014) Species-specific physiological response by the cold-water corals *Lophelia pertusa* and *Madrepora oculata* to variations within their natural temperature range. *Deep-Sea Res II* 99:36–41
- Navone A, Bianchi CN, Orrù P, Ulzega A (1992) Saggio di cartografia geomorfologica e bionomica nel parco marino di Tavolara – Capo Coda Cavallo (Sardegna Nord-orientale). *Oebalia* (suppl XVII):469–478
- Naylor LA (2005) The contribution of biogeomorphology to the emerging field of geobiology. *Pal Pal* 219(1–2):35–51

- Nelson CS, Freiwald A, Titschack J, List S (2001) Lithostratigraphy and sequence architecture of temperate mixed siliciclastic-carbonate facies in a new Plio-Pleistocene section at Plimiri, Rhodes Island (Greece). *Occas Rep* 25:1–50 (Department of Earth Sciences, University of Waikato)
- Neumann AC, Kofoed JW, Keller GH (1977) Lithoherms in the Straits of Florida. *Geology* 5(1): 4–10
- Novosel M, Olujic G, Cocito S, Pozar-Domac A (2004) Submarine freshwater springs in the Adriatic Sea: a unique habitat for the nryozoan *Pentapora fascialis*. In: Moyano HI, Cancino JM, WyseJackson PN (eds) *Bryozoan studies*, A.A. Balkema Publisher, Lisse
- Orejas C, Gori A, Lo Iacono C, Puig P, Gili JM (2009) Distribution of the deep corals *Madrepora oculata*, *Lophelia pertusa*, *Dendrophyllia cornigera*, and quantification of anthropogenic impact in the Cap de Creus Canyon (North Western Mediterranean). *MEPS—Marine Ecology Progress Series* 397, pp 37–51
- OSPAR Commission (2008) Descriptions of habitats on the OSPAR list of threatened and/or declining species and habitats. Reference number 2008–7
- Paoli C, Montefalcone M, Morri C, Vassallo P, Bianchi CN (2016) Ecosystem functions and services of the marine animal forests. In: Rossi S, Bramanti L, Gori A, Saco del Valle CO (eds) *Marine animal forests the ecology of benthic biodiversity hotspots*, Springer, Switzerland, ISBN: 978-3-319-17001-5
- Pedley HM, Carannante G (2006) Cool-water carbonates: depositional systems and palaeoenvironmental controls. Geological Society London Special Publications, vol 255
- Pérès JM (1982) Structure and dynamics of assemblages in the benthal. *Mar Ecol* 5(1):119–185. In: Kinne O (ed) *Marine ecology: a comprehensive, integrated treatise on life in oceans and coastal waters: 5. Ocean management*, vol 1, pp 119–185
- Pérès JM, Picard J (1951) Note sur les fonds coralligènes de la région de Marseille. *Archives de zoologie expérimentale et générale* 88:24–38
- Pérès JM, Picard J (1964) Nouveau manuel de bionomie benthique de la Mer Méditerranée. Rec Tr St Mar Endoume 31(47):1–137
- Raddatz J et al (2011) Paleoenvironmental reconstruction of Challenger Mound initiation in the Porcupine Seabight, NE Atlantic. *Mar Geol* 282:79–90
- Rasser MW (2000) Coralline red algal limestones of the late Eocene alpine Foreland Basin in upper Austria: component analysis, facies and paleoecology. *Facies* 42(1):59–92. doi:[10.1007/BF02562567](https://doi.org/10.1007/BF02562567)
- Rasser MW, Piller WE (2004) Crustose algal frameworks from the Eocene Alpine Foreland. *Pal Pal* 206:21–39
- Relini G (Ed) (2009) *Marine bioconstructions—nature's architectural seascapes*. Italian habitats 22. Italian Ministry of the Environment and Territorial Protection, Friuli Museum of Natural History, Comune di Udine, 87 p
- Remia A, Taviani M (2005) Shallow-buried Pleistocene Madrepora-dominated coral mounds on a muddy continental slope, Tuscan Archipelago, NE Tyrrhenian Sea. *Facies* 50:419–425
- Riding R (2002) Structure and composition of organic reefs and carbonate mud mounds: concepts and categories. *Earth Sci Rev* 58:163–231
- Ries JB (2006) Aragonite production in calcite seas: effect of seawater Mg/Ca ratio on the calcification and growth of the calcareous alga *Penicillus capitatus*. *Paleobiology* 31(3): 445–458
- Robert K, Jones D, Tyler P, Van Rooij D, Huvenne V (2015) Finding the hotspots within a biodiversity hotspot: fine-scale biological predictions within a submarine canyon using high-resolution acoustic mapping techniques. *Mar Ecol* 36:1256–1276
- Robert K, Jones D, Roberts M, Huvenne V (2016) Improving predictive mapping of deep-water habitats: considering multiple model outputs and ensemble techniques. *Deep Sea Res Part I Oceanogr Res Pap* 80–89
- Roberts JM, Brown CJ, Long D, Bates CR (2005) Acoustic mapping using a multibeam echosounder reveals cold-water coral reefs and surrounding habitats. *Coral Reefs* 24:654–669

- Roberts JM, Wheeler AJ, Freiwald A (2006) Reefs of the deep: the biology and geology of cold-water coral ecosystems. *Science* 312:543–547
- Roberts JM, Wheeler AJ, Freiwald A, Cairns S (2009) Cold-water corals: the biology and geology of deep-sea coral habitats. Cambridge University Press, Cambridge, United Kingdom
- Rodolfo-Metalpa R, Martin S, Ferrier-Pagès C, Gattuso JP (2010) Response of the temperate coral *Cladocora caespitosa* to mid- and long-term exposure to pCO₂ and temperature levels projected for the year 2100 AD. *Biogeosciences* 7:289–300
- Rodríguez-Martínez M (2011) Mud mounds. In: Encyclopedia of geobiology, pp667–675
- Rogers AD (1999) The Biology of (L 1758) and other deep-water reef-forming corals and impacts from human activities. *Int Rev Hydrobiol* 84(4):315–406
- Rogers AD, Baco A, Griffi H, Hart T, Hall-Spencer JM (2007) Corals on seamounts. In: Pitcher TJ, Morato T, Hart PJB, Clark MR, Haggan N, Santos RS (eds) Seamounts: ecology, fisheries & conservation, Wiley-Blackwell, pp 141–169
- Rokoengen K, Østmo SR (1985) Shallow geology off Fedje western Norway. IKU report. 24.1459/01/85
- Ross SW, Quattrini AM (2007) The fish fauna associated with deep coral banks off the southeastern United States. *Deep Sea Res Part I* 54–6:975–1007
- Ross RE, Howell KL (2012) Use of predictive habitat modelling to assess the distribution and extent of the current protection of ‘listed’ deep-sea habitats. *Divers Distrib* 19:433–445
- Rosso A, Sanfilippo R (2009). The contribution of bryozoans and serpuloideans to coralligenous concretions from SE Sicily. In: UNEP-MAP-RAC/SPA, Proceedings of the first symposium on the coralligenous and other calcareous bio-concretions of the Mediterranean Sea, Tabarka, 15–16 Jan 2009, pp 123–128
- Salomidi M, Katsanevakis S, Borja Á, Braeckman U, Damalas D, Galparsoro I, Mifsud R, Mirto S, Pascual M, Pipitone C, Rabaut M, Todorova V, Vassilopoulou V, Vega Fernández T (2012) Assessment of goods and services, vulnerability, and conservation status of European seabed biotopes: a stepping stone towards ecosystem-based marine spatial management. *Mediterranean Mar Sci* 13(1):49–88
- Sarà M (1971) Un biotopo da proteggere: il coralligeno pugliese. *Atti I Simp Naz Conserv Nat* 1–25:145–151
- Sartoretto S (1994) Structure et dynamique d'un nouveau type de bioconstruction à *Mesophyllum lichenoides* (Ellis) Lemoine (Corallinales, Rhodophyta). *Comptes Rendus de l'Académie des Sciences de Paris, Sciences de la Vie* 317:156–160
- Sartoretto S, Verlaque M, Laborel J (1996) Age of settlement and accumulation rate of submarine “coralligène” (-10 to -60 m) of the north Western Mediterranean Sea; relation to Holocene rise in sea level. *Mar Geol* 130:317–331
- Savini A, Marchese F, Verdicchio G, Vertino A (2016) Submarine slide topography and the distribution of vulnerable marine ecosystems: a case study in the Ionian Sea (Eastern Mediterranean). In: Lamarche G, et al (eds) Submarine mass movements and their consequences, advances in natural and technological hazards research, vol 41. Springer, Dordrecht, pp 163–170
- Savini A, Vertino A, Marchese F, Beuck L, Freiwald A, Roberts JM (2014) Mapping cold-water coral habitats at different scales within the Northern Ionian Sea (Central Mediterranean): an assessment of coral coverage and associated vulnerability. *PloS ONE* 9(1):e87108
- Somoza L, Ercilla G, Urgorri V, León L, Medialdea T, Paredes M, Gonzalez FJ, Nombelae MA (2014) Detection and mapping of cold-water coral mounds and living *Lophelia* reefs in the Galicia Bank, Atlantic NW Iberia margin. *Mar Geol* 349:73–90
- Squires DF (1964) Fossil coral thickets in Wairarapa, New Zealand. *J Palaeontology* 38:904–915
- Stewart HA, Davies JS, Guinan J, Howell KL (2014) The dangeard and explorer canyons, South Western approaches UK: geology, sedimentology and newly discovered cold-water coral mini-mounds. *Deep-Sea Res II* 104:230–244
- Stone RP (2006) Coral habitat in the Aleutian Islands of Alaska: depth distribution, fine-scale species associations, and fisheries interactions. *Coral Reefs* 25(2):229–238

- Thiem O, Ravagnan E, Fosså JH, Berntsen J (2006) Food supply mechanisms for cold-water corals along a continental shelf edge. *J Mar Syst* 60:207–219
- Thierens M, Browning E, Pirlet H, Loutre MF, Dorschel B, Huvenne VAI, Titschack J, Colin C, Fouquet A, Wheeler AJ (2013) Cold-water coral carbonate mounds as unique palaeo-archives: the plio-pleistocene challenger mound record (NE Atlantic). *Quatern Sci Rev* 73:14–30
- Titschack J, Nelson CS, Beck T, Freiwald A, Radtke U (2008) Sedimentary evolution of a late pleistocene temperate red algal reef (Coralligène) on Rhodes, Greece: correlation with global sea-level fluctuations. *Sedimentology* 55:1747–1776
- Tittensor DP, Baco AR, Brewin PE, Clark MR, Consalvey M, Hall-Spencer J, Rowden AA, Schlacher T, Stocks KI, Rogers AD (2009) Predicting global habitat suitability for stony corals on seamounts. *J Biogeogr* 36:1111–1128
- Toomey DF, Finks RM (1969) Middle Ordovician (Chazyan) mounds, southern Quebec, Canada: a summary report. New York State Geological Association, 41st annual meeting, Guidebook to field excursions. Plattsburgh, New York, pp 121–134
- Tracey DM, Rowden AA, Mackay KA, Compton T (2011) Habitat-forming cold-water corals show affinity for seamounts in the New Zealand region. *Mar Ecol Prog Ser* 430:1–22
- Tribollet A, Godinot C, Atkinson M, Langdon C (2009) Effects of elevated pCO₂ on dissolution of coral carbonates by microbial euendoliths. *Global Biogeochem Cycles* 23:3
- Tribot A-S, Mouquet N, Villéger S, Raymond M, Hoff F, Boissery P, Holon F, Deter J (2016) Taxonomic and functional diversity increase the aesthetic value of coralligenous reefs. *Sci Rep* 6:34229. doi:10.1038/srep34229
- UNEP-MAP (2011) Convention for the protection of the marine environment and the coastal region of the mediterranean and its protocols. MAP Special Publications http://195.97.36.231/dbases/MAPpublications/BCP_Eng.pdf. Accessed 24 July 2015. Monitoring deep Mediterranean rhodolith beds. Available from: https://www.researchgate.net/publication/287760121_Monitoring_deep_Mediterranean_rhodolith_beds. Accessed Jan 11 2017
- UNEP-MAP-RAC/SPA (2008) Action plan for the conservation of the coralligenous and other calcareous bio-concretions in the Mediterranean Sea. Ed. RAC/SPA Tunis, 21 pp
- UNEP-MAP-RAC/SPA (2010) The Mediterranean Sea Biodiversity: state of the ecosystems, pressures, impacts and future priorities. In: Bazairi H, Ben Haj S, Boero F, Cebrian D, De Juan S, Limam A, Lleonart J, Torchia G, Rais C (eds) RAC/SPA, Tunis, pp 100
- Van Oevelen D, Duineveld GCA, Lavaleye MSS, Mienis F, Soetaert K, Heipa CHR (2009) The cold-water coral community as a hot spot for carbon cycling on continental margins: a food-web analysis from Rockall Bank (northeast Atlantic). *Limnol Oceanogr* 54(6):1829–1844
- Van Rooij D, De Mol B, Huvenne V, Ivanov M, Henriet JP (2003) Seismic evidence of current-controlled sedimentation in the Belgica mound province, upper Porcupine slope, southwest of Ireland. *Mar Geol* 195:31–53
- Van Rooij D, Huvenne VAI, Blamart D, Henriet JP, Wheeler A, De Haas H (2009) The Enya mounds: a lost mound-drift competition. *Int J Earth Sci (Geol Rundsch)* 98:849–863
- Van Rooij D, Blamart D, De Mol L, Mienis F, Pirlet H, Wehrmann LM, Barbieri R, Maignien L, Templer SP, De Haas H, Hebbeln D, Frank N, Larmagnat S, Stadnitskaia A, Stivaletta N, Van Weering T, Zhang Y, Hamoumi N, Cnudde V, Duyck P, Henriet JP (2011) Cold-water coral mounds on the Pen Duick Escarpment, Gulf of Cadiz: the microsystems project approach. *Mar Geol* 282:102–117
- Van Weering TCE, De Haas H, De Stigter HC, Lykke-Andersen H, Kouvaev I (2003) Structure and development of giant carbonate mounds at the SW and SE Rockall Trough margins, NE Atlantic Ocean. *Mar Geol* 198:67–81
- Victorero L, Blamart D, Pons-Branchu E, Mavrogordato MN, Huvenne VAI (2016) Reconstruction of the formation history of the Darwin Mounds, N Rockall Trough: how the dynamics of a sandy contourite affected cold-water coral growth. *Mar Geol* 378:186–195
- Virgilio M, Airoldi L, Abbiati M (2006) Spatial and temporal variations of assemblages in a Mediterranean coralligenous reef and relationships with surface orientation. *Coral Reefs* 25:265–272

- Watling L, Norse EA (1997) Disturbance of the seabed by mobile fishing gear: a comparison to forest clearcutting. *Conserv Biol* 12–6:1180–1197
- Wienberg C, Beuck L, Heidkamp S, Hebbeln D, Freiwald A, Pfannkuche O, Monteys X (2008) Franken Mound-facies and biocoenosis mapping of a newly-discovered ‘carbonate mound’ at the West Rockall Bank, NE-Atlantic. *Facies* 54:1–24
- Wild C, Wehrmann LM, Mayr C, Schöttner SI, Allers E, Lundälv T (2009) Microbial degradation of cold-water coral-derived organic matter: potential implication for organic C cycling in the water column above Tisler Reef. *Aquat Biol* 7:71–80
- Wilson JL (1975) Carbonate facies in geologic history. Springer, New York 471 pp
- Wilson JB (1979) ‘Patch’ development of the deep-water coral *Lophelia pertusa* (L.) on Rockall Bank. *J Mar Biol Assoc UK* 59:165–177
- Wilson MFJ, O’Connell B, Brown C, Guinan JC, Grehan AJ (2007) Multiscale terrain analysis of multibeam bathymetry data for habitat mapping on the continental slope. *Mar Geodesy* 30:3–35
- Wissak M, Schönberg CHL, Form A, Freiwald A (2014) Sponge bioerosion accelerated by ocean acidification across species and latitudes? *Helgol Mar Res* 201468:385
- Wood RA (1999) Reef evolution. Oxford University Press, UK, 414 pp
- Woodroffe CD, Webster JM (2015) Coral reefs and sea-level change. *Mar Geol* 352:248–267
- Zibrowius H (1980) Les Scléractiniaires de la Méditerranée et de l’Atlantique nordoriental. Mémoires de l’Institut Océanographique vol. 11. Mémoires de l’Institut Océanographique, Monaco

Part III

Applied Submarine Geomorphology

Applied Geomorphology and Geohazard Assessment for Deepwater Development

Roger Moore, Geoff Davis and Oliver Dabson

Abstract Development of offshore hydrocarbon resources has in recent decades advanced into frontier deepwater regions around the world posing significant technical challenges for the design and installation of oil and gas wells and facilities. Development sites are typically remote and inaccessible and little is known about the seabed geomorphology and ground conditions to be encountered. Potential geohazards are at a larger scale than found onshore and include deep canyons and terrain highs, landslides and turbidity flows, faults, salt diapirism, gas/fluid expulsion, sedimentary bedforms and adverse soil conditions. Triggering events may include seismicity, volcanism, deep ocean currents and construction activity. Early acquisition and calibration of field-wide Autonomous Underwater Vehicle (AUV) high-resolution data is essential to ensure that development plans are not exposed to avoidable geohazard risks. A key element of the approach is the application of integrated geophysical, geomorphological and geotechnical methods that make best use of high-resolution data. This paper presents an illustrated approach for applied geomorphology and geohazard assessment for deepwater development that has been adopted by leading offshore oil and gas companies. Experience from major projects around the world demonstrates considerable value in the avoidance and de-risking of geohazards through comprehensive geomorphological assessment.

Keywords Subsea · Geomorphology · Geohazards · Risk · Development

R. Moore (✉) · G. Davis
CH2M, Lyndon House, 62 Hagley Road, Edgbaston Birmingham, B16 8PE, UK
e-mail: roger.moore@ch2m.com

R. Moore
Professor of Applied Geomorphology, University of Sussex, Falmer, Brighton BN1 9RH, UK

O. Dabson
CH2M, Elms House, 43 Brook Green, London W6 7EF, UK

1 Introduction

This paper illustrates how an understanding of subsea geomorphology and ground conditions can inform geohazard risk assessments of proposed oil and gas development sites. Characterisation of subsea geomorphology features is an important first step in this process.

Assessment of subsea geomorphology, geohazards and ground conditions is an integral part of risk assessment for offshore oil and gas projects. However, there are no established industry standards or methods for the assessment of geohazards and high-resolution geophysical data to support development and engineering. Prior and Hooper (1999) provide a good review of past achievements and future directions for engineering geomorphology mapping of the seafloor and Hampton and Lee (1996) provide similar for submarine landslides research. Locat (2001) and Locat and Lee (2002) provide a geomorphological and geotechnical perspective of seafloor instability and submarine landslides along ocean margins. There has been an emerging literature of regional-scale case studies and assessments of submarine landslides and canyons as a result of the capture and release of high resolution bathymetry and seismic data for research e.g. McAdoo et al. (2000), Huhnerbach and Masson (2004), Masson et al. (2002, 2006), Ten Brink et al. (2006), Gee et al. (2007), Cauchon-Voyer et al. (2008) and Twichell et al. (2009).

In addition to the increasingly broad literature surrounding the subject, technological improvements to deepwater surveying methods have produced high-resolution datasets of the sea floor that come close to the best terrestrial datasets. This facilitates comparison between subaerial and subsea geomorphology to produce analogues, and build a greater appreciation of the nature of seabed geohazards. An illustration of subsea geohazards that are likely to be of concern to any proposed deepwater development is presented in Fig. 1.

2 Approach

An integrated approach to the systematic mapping of seafloor geomorphology (Hough et al. 2011) is fundamental to underpinning qualitative and/or quantitative geohazard risk assessment for development and engineering proposals. Such risk assessments benefit significantly from the availability of development-wide high-resolution (engineering-quality) geophysical data that enables detailed interpretation, analysis and understanding of seafloor geomorphology, features, processes and ground conditions.

The integrated approach followed by the authors is presented in Fig. 2, and would typically involve the following tasks:

- (a) Comprehensive geological, geomorphological and geotechnical desk studies of the development area.

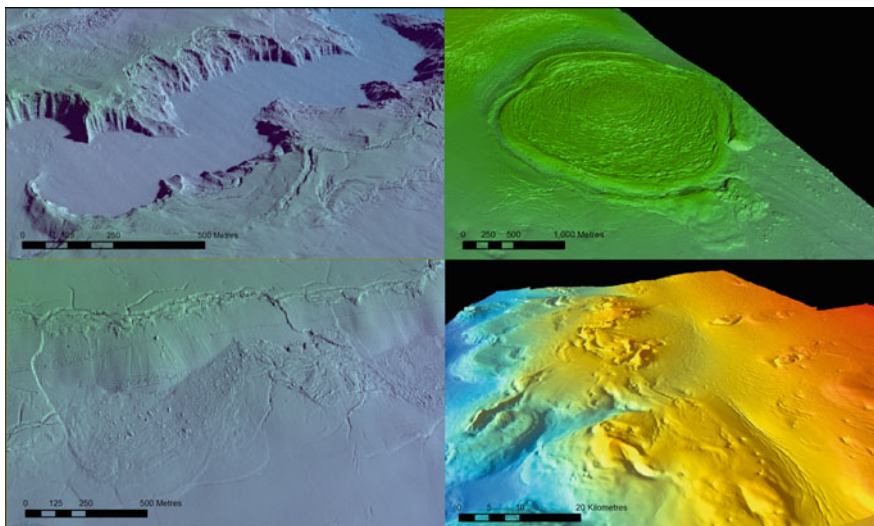


Fig. 1 Examples of subsea geohazards of concern to deepwater development. *Top left* deep canyons, subject to turbidity flows and unstable flanks; *Top right* mud volcanoes subject to fluid expulsion, rim collapse and mud flows; *Lower left* landslides and associated tension cracks, run-out and compression lobes; *Lower right* salt diapirs and sag basins producing topographic hard grounds and complex bedforms. Images courtesy of BP

- (b) Integrated geomorphological mapping of the seabed across the development-area and interpretation of shallow (i.e. less than 1 km below mudline) geohazard features through integration of bathymetry and seismic data.
- (c) Development of geohazard conceptual ground models.
- (d) Preparation of a geohazard register, screening and assessment of geohazards of significance to development proposals.
- (e) Optimisation of seismic surveys and geotechnical data acquisition to support development planning, engineering design and site-specific geohazard investigations and mitigation.
- (f) Guidance and communication on geohazards and ground conditions to wells and facilities engineers during project appraisal, design and construction stages.

A key element of the approach is the integrated seismic-geomorphological mapping of the seabed (Fig. 3). This provides a means of integrating data on seabed geomorphology interpreted from bathymetry, with sub-seabed geological data interpreted from seismic data, to give a three-dimensional understanding of geohazard processes (Posamentier 2000). The mapping approach developed for the

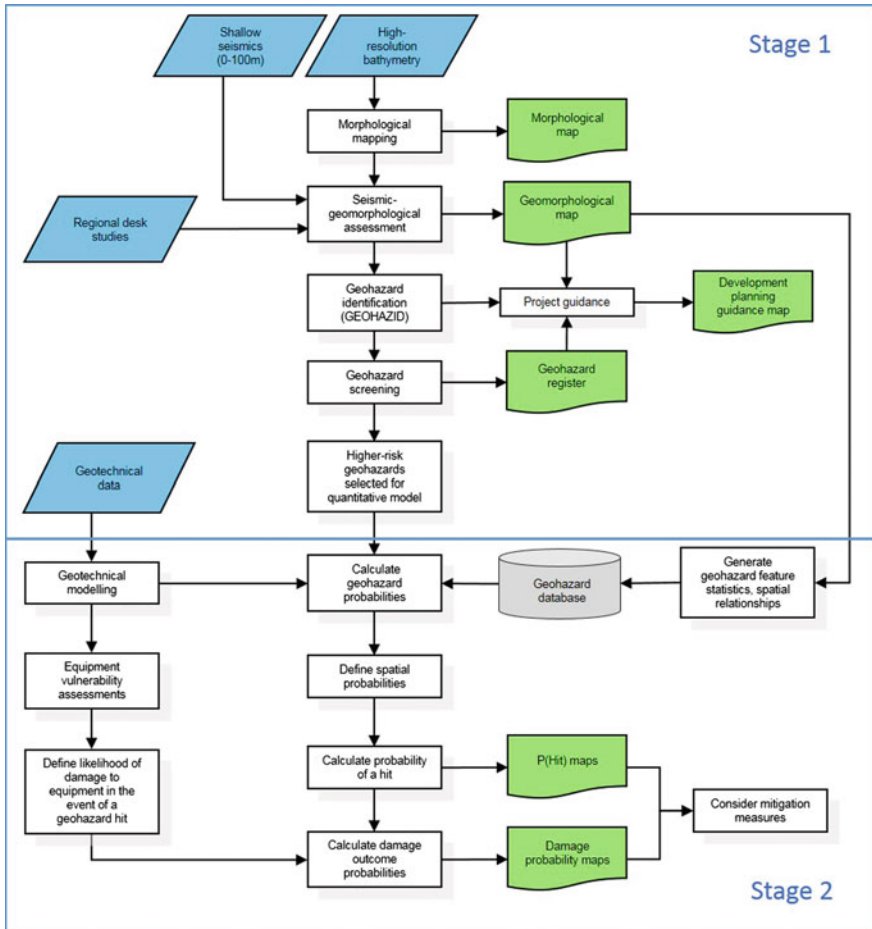


Fig. 2 Integrated approach for definition of subsea geohazards combining geomorphological mapping and probabilistic geohazard modelling. The application of geomorphology in stage 1 assessments is the main focus of this paper. In practice, the approach is often undertaken several times in a series of iterations

seafloor follows the principles of detailed morphological mapping reported by Savigear (1965), Brunsden and Jones (1972) and Cooke and Doornkamp (1990), and has been developed to incorporate a conceptual understanding of geohazard magnitude and frequency. Since the availability of high-resolution sea floor images, with continuous coverage over large areas, investigations into sea floor processes using geomorphological mapping have been undertaken through large collaborative projects, e.g. STRATA-FORM (Nittrouer and Kravitz 1996) and COSTA-Canada

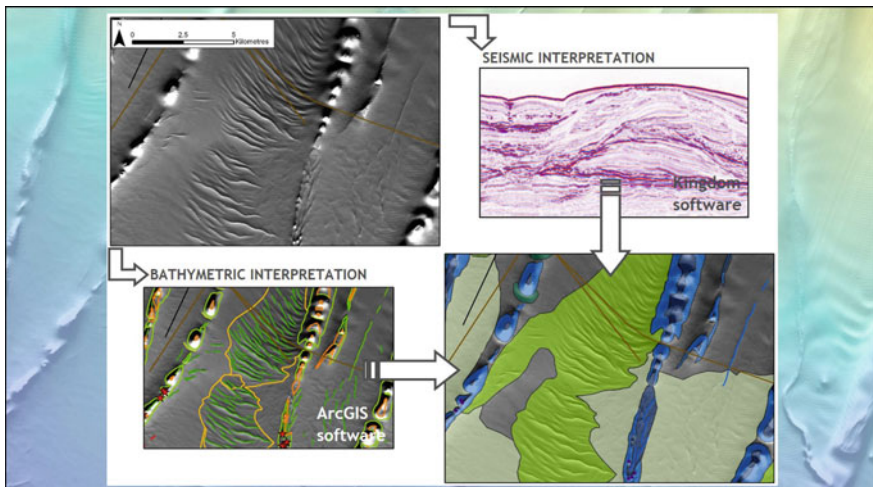


Fig. 3 Integrated seismic-geomorphology interpretation stages. *Top left* seabed relief from MBES bathymetry; *top right* 2D high resolution seismic imaging of sub-surface seabed; *lower left* morphological mapping of seabed features and stress forms; *lower right* interpretation of seabed features, geohazards and soils. Images courtesy of Tullow

(Cauchon-Voyer et al. 2008); large regional studies e.g. across the US continental slope (McAdoo et al. 2000; Twichell et al. 2009); off the coast of northwest Africa (Masson et al. 2006); the western Canary Islands (Masson et al. 2002) and for site-specific studies e.g. northwest Borneo (Gee et al. 2007).

The approach expands on regional terrain assessment style mapping (e.g. Bryn et al. 2005) and more detailed feature mapping (e.g. Moore et al. 2007; Micallef et al. 2009) often undertaken for offshore geohazard studies. The morphological map provides a record of the seabed form and features which are not necessarily portrayed by bathymetry or contours. The morphological map provides an important spatial context (framework) of existing seabed forms and potential processes, and how these may interact with development proposals. This spatial framework is used to underpin interpretation and derivative maps including definition of terrain units, geomorphology, geohazards, soil conditions and development planning guidance. The integrated seismic-geomorphological approach provides a ground model framework for subsequent work and specifications to evaluate the magnitude and frequency of potential geohazard events for quantitative risk analysis.

The integrated approach is very similar to the practice of establishing geological models for land-based engineering projects, in which the complete geological history of the site is used to predict the performance of the ground in response to engineering work and to identify the likely presence of geohazards (Brunsden 2002).

3 Datasets

Sites can typically cover up to 1000 km² and the reliability of geohazard assessments depends on the availability, quality and extent of the geophysical and geotechnical data across the area. 3D exploration-quality data is typically available early on in the project and provides a good dataset for the initial assessment and screening of geohazards. High-resolution engineering-quality data is generally not available early on in projects but is used to resolve features and ground conditions in the shallow section (i.e. less than 15 m below mudline) and may include ultra-high resolution (UHR), and autonomous underwater vehicle (AUV) surveys including multibeam echosounder (MBES), side scan sonar (SSS) and shallow seismic reflection (CHIRP) data.

Table 1 summarises the typical resolution and penetration of the geophysical datasets acquired by ocean survey vessels and AUVs for geohazard and ground condition assessments. For example MBES collected by AUV attains a 3 m resolution through acquisition of 0.5 m ping spacing with a distance of approximately 2 m between individual beams. These are followed by optimised phases of geophysical, geotechnical, met-ocean and environmental site investigations to calibrate the geophysical data and to provide dating of geohazard features, geotechnical soil parameters and other information for engineering design.

Table 1 also illustrates the relationship between resolution and penetration depth for geophysical datasets. The highest resolution CHIRP dataset can only resolve the structure of a comparatively shallow section of sediments, while 3D seismic data penetrate to depths of many kilometres but provide poorer resolution of sediment thickness and stratigraphy (more information can be found in chapter “[Reflection and Refraction Seismic Methods](#)” of this book).

Other sources of data, such as exploration and development well drilling reports, environmental baseline surveys (still or video footage with limited grab sampling of seabed materials) using Remote Operated Vehicles (ROV) and ocean current monitoring, can be incorporated into the geohazard assessment.

Table 1 Summary of geophysical data types, resolution and penetration

Geophysical data types	Resolution (m)		Penetration (m below seabed)
	Horizontal	Vertical	
3D seismic	12.5	10	5000
2D UHR	12.5	3	750
AUV CHIRP	0.5	0.25	80
AUV multibeam echosounder	3	0.5 relative 2 absolute	n/a
AUV side scan sonar	0.2	3	n/a

4 Morphology Mapping and Geomorphology Assessment

The systematic mapping of morphological features observed in seafloor imagery provides a factual dataset for geomorphological interpretation and provides freedom for derivative maps to be superimposed on the same mapped features. The key objective of morphological mapping is to characterise the form of the seafloor (i.e. scarp slope, smooth convex slope, ridge, etc.) and should avoid interpretation of the feature which should be conducted as a separate task. A bespoke set of slope morphology lines and symbols are used for mapping based on published standards to represent sharp breaks and smooth changes in slope, conical and linear depressions, ridges and areas of variable seabed texture (e.g. Cooke and Doornkamp 1990). Where necessary, new symbols are developed to fit the specific requirements of the seabed environment (e.g. Moore et al. 2007; Hough et al. 2011). Systematic mapping of all features is undertaken at a consistent scale appropriate for the project. Typically a scale of 1:5000 is used; however, larger scales may be needed to map in details of complex landforms, and also smaller scales may be used to better understand the broader context of the site.

Following morphological mapping, geomorphological interpretation of seafloor features and processes is conducted using all the available baseline image layers and seabed morphology factual data. The interpretation uses classified shading and linework to indicate the distribution and types of existing features and potential processes, which may include for example major terrain features (e.g. plateau, canyons), mass movement features (e.g. pre-existing landslides, tension and compression features, slabs and runout), sediment scour and deposition features (channels, flutes, bedforms, moats) and fluid expulsion features (mud volcanoes, pockmarks). Interpretation of seabed features revealed on bathymetry datasets must be integrated with interpretation of sub-surface geophysical data to ensure consistency and quality of interpretation.

The value of morphological mapping and geomorphological interpretation was demonstrated in explaining the Storegga landslide system, offshore Norway (Fig. 4). The ‘Ormen Lange Project’ was set up in 1999, with the goal of securing a safe gas production development in the headscarp of the Storegga landslide. A large volume of high resolution swath bathymetry and seismic data was acquired and an integrated programme of studies carried out to investigate the potential geohazards of significance to the development (Solheim et al. 2005). Morphological mapping and seismic-geomorphology interpretation was key to unravelling the complex features observed at seabed and in the shallow subsurface (Bryn et al. 2005). Micallef et al. (2009) subsequently carried out a detailed geomorphometry study of the north-eastern Storegga landslide scar.

Storegga is one of the largest submarine landslides discovered (Bugge 1983). The landslide occurred about c. 8200 cal. years BP and caused a tsunami wave that had a major impact on the coastal regions of the north Atlantic (Bondevik et al. 2003). The general morphology reveals several dominant features at seabed including headwalls/scars, various landslide types, stress forms, and deposition

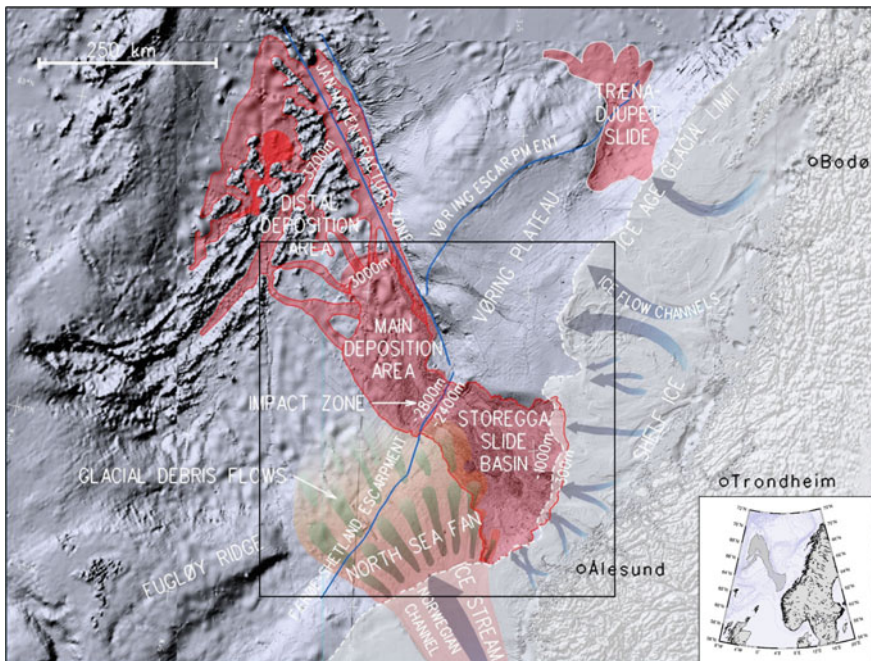


Fig. 4 Geomorphological setting of the massive Storegga landslide offshore Norway that occurred c. 8200 cal. years BP. Deposition occurred as debris flow deposits around the impact zone and main deposition area, and from turbidity currents in the distal, deep sea region. Figure 5 inset. Courtesy Forsberg et al. (2002)

areas (Figs. 4 and 5). The rear scarp is 320 km across whilst the landslide narrows to 60 km between the North Sea Fan and Voring Plateau (Fig. 4). Lower headwalls and scarps (Figs. 5 and 6) indicate the landslide is multi-level with a strong stratigraphic control on the landslide development.

Various landslide types are apparent at seabed (Fig. 6). Spreading failures are the most common morphological feature observed particularly towards the upper headwall. They appear as parallel ridges and troughs, between 200 and 800 m across, and are formed by extensional displacement of the sediments above a weak layer.

Debris slides are characterised by parallel sides and a blunt head (Fig. 6). Pull-apart windows and larger exposed areas of the failure surface are associated with debris slides, but also occur where spreading failure has initiated rapid translational down slope sliding.

The mid-slope hummocky terrain (Fig. 6) is interpreted to be deposited from debris flows as lobes. The sediments do not appear to be completely disaggregated but may have flowed as more or less solid rafts of disturbed material. The north flank of the slide scar (Fig. 5) has features mapped as debris flows which include multiple source areas that coalesce into flow tracks scoured by the passage of debris.

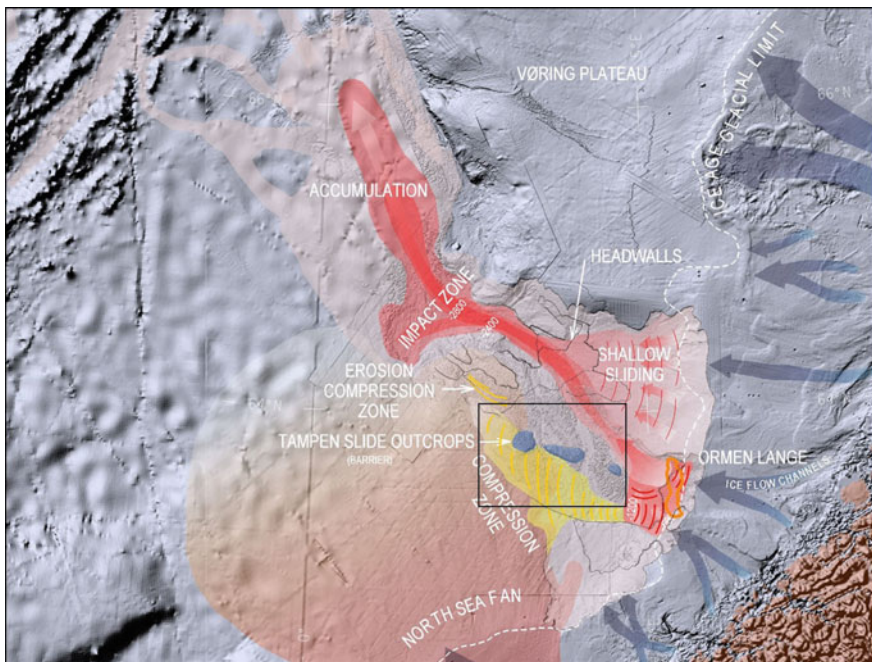


Fig. 5 The geomorphology of the main features and sequence of events was built up from morphological mapping of seabed features and integrated with subsurface seismic interpretation and dating of sediments. Formation of the compression zone is due to the impact of large slide blocks displaced from the Storegga headwall. Debris slides continued down into the impact zone and the main accumulation zone further northwest. Figure 6 inset. Courtesy Forsberg et al. (2002)

Three remnants of the Tampen slide, a megaslides from about ~ 100 krys BP (Riis et al. 2005; Bryn et al. 2005) are interpreted to be exposed in the central slide scar (Figs. 5, 6 and 7); the megaslides blocks and headwalls were deeply buried by subsequent sedimentation. The Tampen slide blocks appear to form hard points or barriers in the central part of the Storegga Landslide; compression ridges formed to the west and a shear zone that crosses the westernmost remnant (Figs. 6 and 7) indicates that little movement of the Tampen landslide occurred. They appear to have played an important role in the Storegga landslide development.

There are shear zones between debris flow lobes and spreading failures, and between landslide sediments and the undisturbed sediments along the landslide perimeter. Shear zones between different landslide masses can be identified by breaks in the ridges/troughs and the chevron patterns (Fig. 7). These breaks are often also associated with lineations parallel to the flow direction of the landslide masses.

A striking feature of the morphology of the Storegga landslide is the pronounced channels that flow from the headscarp across the entire width of the landslide complex Figs. 5, 6 and 7. They are almost 200 km long and cut across the landslide

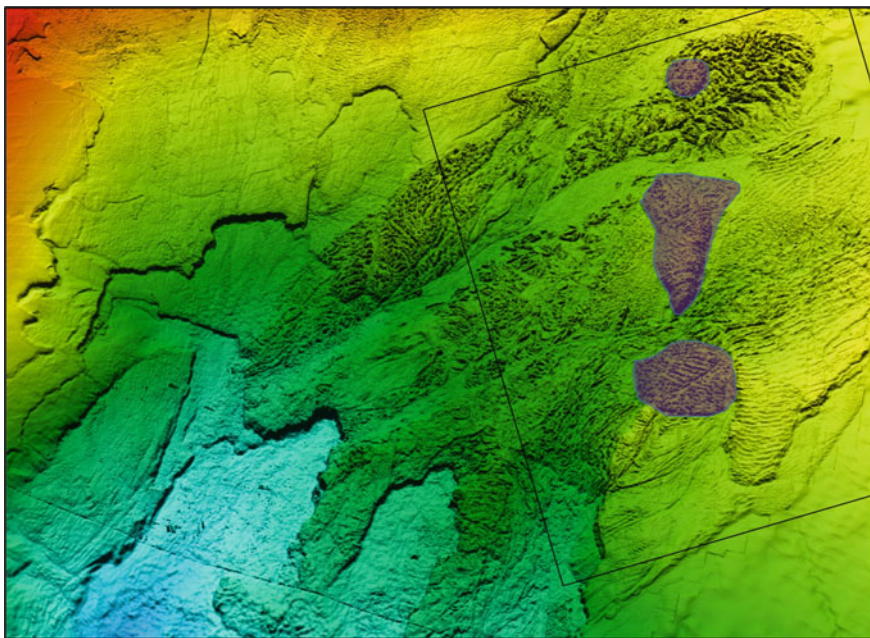


Fig. 6 Perspective view of the Storegga landslide scar central area revealing a complex pattern of morphological features, surface forms, legacy events and processes. Tampen remnants are highlighted. Figure 7 inset. Image courtesy Peter Bryn, Statoil (formerly Norsk-Hydro)

deposits of previous large scale events and shape many of the remnant deposits into flow bedforms. They cut through the remnants of the Tampen landslide and other old landslide deposits. There are indications that the channels have cut back into the compression ridges and other older landslide deposits.

Morphological classifications show that spreading failures, debris slides and debris flows were the main landslides mechanisms of the Storegga landslide. Spatial relationships and the rules of superposition show that shallow failures in the uppermost layers of the upper slope sediments occurred first. These indicate that initial failure occurred on the lower to mid slope and retrogressed more rapidly in the upper sediments than the deep failures. Furthermore, as retrogression proceeded up slope, the landslide bifurcated, developing separate branches. The main tsunami-generating sliding most likely occurred when retrogression reached the upper slope where thick sediment accumulations were mobilised. The compression zone was formed from the impulse produced by the thick upper slope sediments as they displaced down slope. The southeast part of the landslide scar was the last branch to fail and produced the flow channels that originate between the barriers formed by the Tampen remnants. The near horizontal and over-consolidated (glacially loaded) sediments of the shelf eventually arrested the landslide development.

Morphological mapping of the Storegga landslide features was key to characterising geohazards in detail and was fully integrated with geophysical and

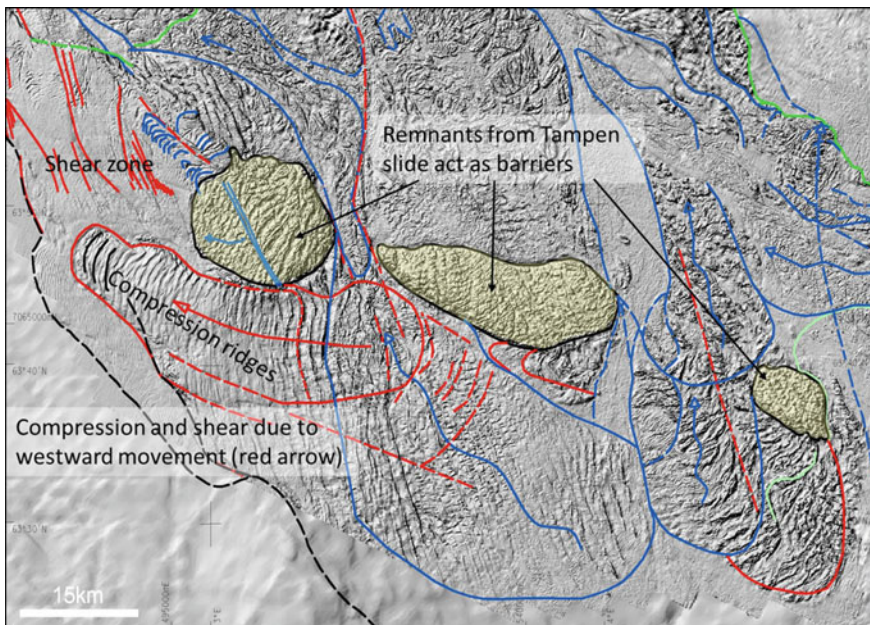


Fig. 7 The seabed morphology was mapped in detail using high-resolution bathymetry and seismic data, revealing a variety of landslide systems, features and failure modes. Blue lines signify debris flow systems, green lines debris slide systems, and red lines Tampen landslide stress forms. Figure 6 for location. Courtesy Forsberg et al. (2002), interpretation by Brunsden and Moore

geomechanical interpretations of the sub-seabed to inform planning and risk assessment of the Ormen Lange development.

5 Geohazard Assessment

There are many geohazards that could lead to an adverse impact on development. Technology advancements in high-resolution surveying, imaging and seismic profiling of the deep ocean seabed is revealing features in ever increasing detail that nowadays allows characterization of geohazards on a par with terrestrial analogues. However, with over 70% of the planet covered by deep oceans many areas remain to be surveyed and characterised at this level of detail, and for these areas, potential geohazards will be a significant risk to any proposed development. Building a global database of experience and examples of subsea geomorphology and geohazards has potential value for early screening of development proposals, noting that some are unlikely to have significant implications to development over engineering timescales. Based on the authors' experience of a number of deep water

development projects for oil and gas clients in recent decades, Table 2 provides a summary of typical geohazards of concern and their implications to development. Geohazard assessment is described further in this section whilst the implications to development is considered further in Sect. 6.

Geohazards may be grouped into three categories:

1. **Geohazard features:** static conditions that exist due to previous depositional or post-depositional processes or events. These include geological features, steep slopes, very weak or very strong soils and irregular seabed topographies. Geohazards in this category do not involve any contemporary processes taking place.
2. **Reactivation of geohazard features:** present-day dynamic processes and potential reactivation of pre-existing geological features, either by natural or man-made triggers, for example submarine landslides reactivated by an earthquake.
3. **Potential (first-time) geohazards:** processes or events which could occur for the first time at a particular location due to natural or man-made triggers, such as a new submarine landslide.

Geohazards in the first category exist on the seabed at present (see Fig. 1), whilst those in the second and third categories are potential geohazards which could occur at some time in the future during the life of the development. Some geological features may fall under more than one category.

A typical sequence of work will begin with a comprehensive desk study based on pre-existing data or published reports covering the area of interest (Fig. 2). The work will include a regional geological, geomorphological and geotechnical assessment of the development area to provide important context to the regional setting and its past and future evolution. The desk study is followed by a high-level screening of the more significant potential geohazards that may exist within or affect the proposed development area. These first two stages enable informed decisions to be made on the scope of data acquisition needed to support project appraisal and design, and the appropriate scale of seabed mapping and sampling. Detailed interpretation of these data is then performed which may involve completion of multidisciplinary assessments as required by the project, such as fault and seismic hazard analysis, pockmark hazard analysis, slope stability analysis, salt diapir analysis, probabilistic geohazard analysis. This information allows the development of a series of seismic-stratigraphy, geohazard ground models and soil models. The interpretation of existing and potential geohazard processes should be documented in the project risk register and development planning guidance provided to the project and engineering teams (Fig. 2 and Sect. 6).

The level of detail of an assessment should be proportional to the degree of the anticipated hazard and risk, with a high risk setting requiring a higher level of investigation. It requires a systematic search for geohazards using appropriate data to catalogue geohazard features, ground conditions and seabed processes. Based on a sound understanding of the controls of past natural geohazards and processes, the

likelihood of future processes and events can be estimated (e.g. Locat and Lee 2002; Jeanjean et al. 2005). In order to undertake a full quantitative geohazard risk assessment, it is necessary to understand the vulnerability of development and subsea facilities to these geohazard processes (Evans et al. 2007). Such an approach has developed significantly in the last decade, allowing geohazard risk mitigation strategies to be implemented in practice (Jeanjean et al. 2005; Kvalstad 2007; Moore et al. 2007).

Illustrated examples of a selection of potential geohazards is provided in Figs. 8, 9 and 10. The significance of such geohazards will be unique to every site and the specific development layout and proposals which will change many times throughout the planning stage. The severity of geohazards for the examples given ranges from low to high without mitigation.

Localised instability of the seabed will be a function of the site-specific and time-dependent conditions promoting or resisting slope failure and should be properly investigated at an appropriate scale. For each mapped geohazard, guidance is presented that characterises the form and potential geohazard processes, and the potential implications for facilities and field layout (Figs. 8, 9 and 10). Where the seabed has undergone recent slope failure or successive failure in the past there may be a relatively high probability of failure of these sites in the future due to the presence of weakened soils and conditions promoting slope failure. In situations where the seabed shows no signs of prior slope failure or evidence of recent instability, these areas are more likely to have a lower probability of failure under present natural conditions.

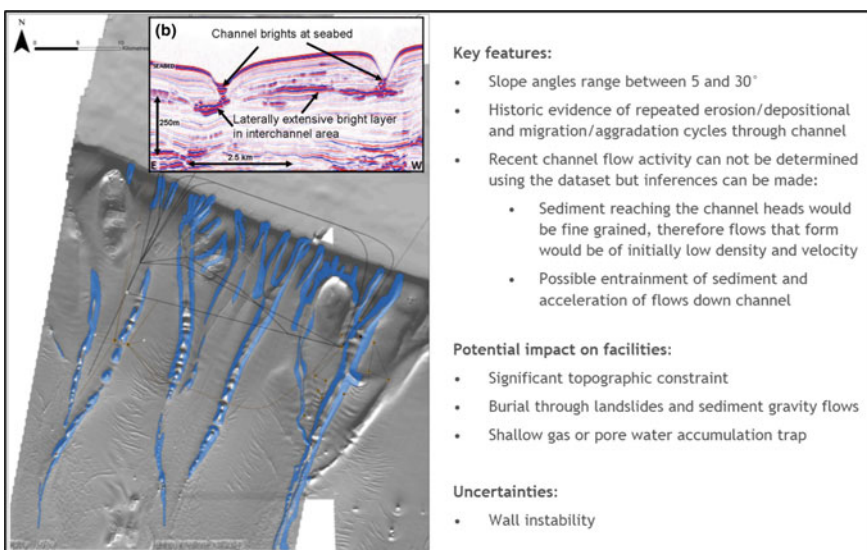


Fig. 8 Example geohazard assessment for canyon walls. *Courtesy Tullow*

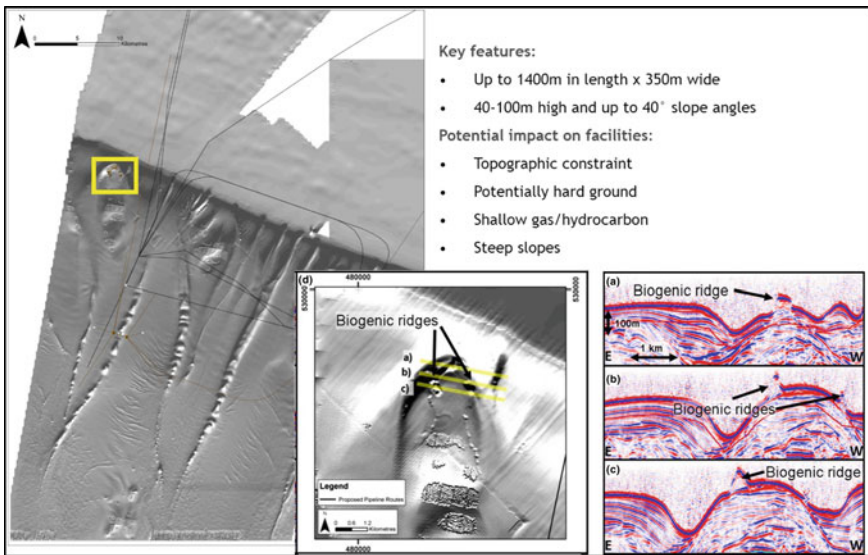


Fig. 9 Example geohazard assessment for biogenic ridges. *Courtesy Tullow*

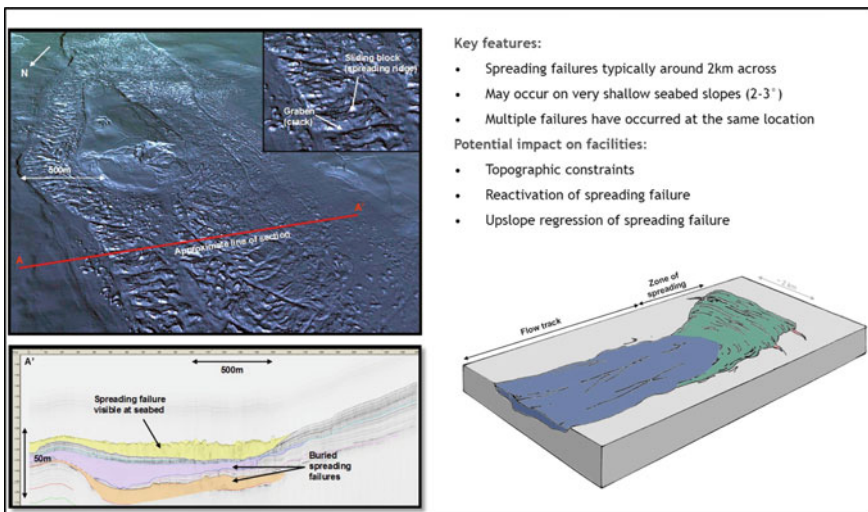


Fig. 10 Example geohazard assessment for landslides. *Courtesy BP*

Using the fully-integrated seismic datasets, geomorphology maps and geotechnical knowledge, conceptual ground models can be developed as an effective means of communicating geohazards and the risk associated with them (Fig. 2). Ground models can provide an illustrative description of the nature of geohazard features,

materials, mechanisms and potential processes for the given development sites (Figs. 8, 9 and 10). They can also be produced at a range of scales (development-wide to local) for specific geohazard features (e.g. landslides) to illustrate sediment variability and soil characteristics, and to illustrate key structural features and environmental conditions. For example, a series of landslide type models can be produced to understand more fully their magnitude, frequency, susceptibility and causes. These models are used to support engineering design including supporting data and information, technical guidance and quality assurance.

Hence, in a reasonably straightforward way, geohazards can adequately be identified through the mapping stages, and communicated to developers in the form of development planning guidance maps and illustrations (Figs. 2, 8, 9 and 10).

6 Implications for Development

A developer's perspective in dealing with offshore geohazards is given by Jeanjean et al. (2005) and Evans et al. (2007). A key objective of the multidisciplinary geohazard assessment approach is to identify potential geomorphological hazards and then to quantify the frequency and magnitude of geohazard events that could impact a future subsea development over its design lifetime. The integrated ground model, provides the spatial and temporal framework for identifying geohazards and quantifying their potential impacts.

An outline of the approach is shown in Fig. 2. Integrated seismic-geomorphological mapping, informed by desk studies, is used to generate interpretive geomorphological maps and geohazard registers, which may then be used to prepare recommendations for development planning. An outline of common subsea geohazards and their typical implications for development is given in Table 2. In practice, the approach is often undertaken in a series of iterations, with early geomorphological assessments identifying potentially significant geohazard risks, including possible 'showstoppers', and informing preliminary development layouts and specifications for further data acquisition.

The principal method of mitigation for most types of geohazard is to avoid the hazard wherever possible. Hence, the planning guidance maps may be looked upon as 'geohazard avoidance maps' for field planning purposes. Guidance on safe 'stand-off' or 'buffer' distances from the most significant geohazards is provided in the risk registers and guidance maps.

In some instances, the desire to avoid geohazards is outweighed by the fundamental requirements of development. For example, it may not be possible to route all pipelines away from every possible geohazard location. In these instances, the geomorphological assessments underpin more detailed geomechanical modelling and risk assessments, which may include calculating the probabilities of geohazard event taking place during the life of the development and the possible consequences of such events if they were to occur. In other instances geomorphological

Table 2 Summary of common subsea geohazards and their typical implications for development

Geohazard feature or process	Description of geohazard	Typical implications for subsea developments
Biogenic mounds	Formed from the activity of biological communities around carbonates seeps. Mounds may represent a topographic obstruction as well, as well as a potential source of corrosive chemicals and an environmental constraint	Chemical attack on engineering materials. Considered to be a routine engineering issue, taken into account during design
Channel avulsion	The diversion of an existing submarine channel with the formation of a new channel	Possible scour and potential for slope movement causing damage or burial of wells and facilities
Debris field reactivation	Failure of existing landside debris field	Possible flowline-spanning issues in undulating terrain Potential for slope movement causing damage or burial of wells and facilities
Deep-seated failure of steep scarps/plateau margins	Deep failure of scarp or plateau margins, as opposed to relatively shallow scarp face failure	Installation difficulties associate with steep slopes Potential for slope movement causing damage or burial of wells and facilities
Downslope creep of shallow cover sediments	Slow, cumulative downslope movement of soil in the shallow section	Small movements are not generally expected to cause significant damage to equipment or facilities
Fault displacement causing cracks and graben at seabed	Creep displacement due to consolidation settlement or progressive fault movement. Episodic rapid movement along faults	Creep displacement not generally expected to cause significant damage to equipment or facilities over engineering timescales. Rapid episodic movement may cause damage to flowlines
Formation of new mud volcano	Formation of a new mud volcano	Large-scale disturbance to subsea infrastructure
Gas hydrate dissociation	Transformation of hydrate to water and methane, causing soil disturbance	Possible flowline-spanning issues in undulating terrain Potential for slope movement causing damage or burial of wells and facilities
Extremely large landsliding	Occurrence of new extremely large landslide on a regional scale	Large-scale disturbance/damage to subsea infrastructure

(continued)

Table 2 (continued)

Geohazard feature or process	Description of geohazard	Typical implications for subsea developments
Pockmarks and fluid expulsion depressions	Depressions formed by expulsion of small quantities of liquid or gas, which may or may not still be active	A topographic constraint. Local instability of side slopes. Chemical attack on engineering materials
Debris flow runout	Low viscosity runout, sourced from an landslide failure upslope	Potential for impact causing damage or burial of wells and facilities
Salt diapirism	Salt diapirs form bathymetric highs and sharp changes in relief of hundreds of metres and surrounded by moats tens of metres deep	A topographic constraint. Instability of diaper flanks. Possible flowline-spanning and facilities installation issues. Highly variable soil conditions, salt intrusion and hard grounds may prevent penetration of suction caissons
Scarp face failure	Landslide which affects the full or partial height of exposed scarp faces	Installation difficulties associated with the steep scarp slopes Possible flowline-spanning issues. Potential for slope movement causing damage or burial of wells and facilities
Seismic shaking	Ground shaking due to earthquakes	Usually considered a routine engineering issue, taken into account in design
First-time slab slide	Formation of slab slide morphology on previously unfailed seabed	Potential for slope movement causing damage or burial of wells and facilities
Reactivation of existing slab slide	Collapse of pre-existing slab slide morphology, e.g. failure of scarp headwall or lateral scarp	Installation difficulties associated with steep slopes Possible flowline-spanning issues in undulating terrain Potential for slope movement causing damage or burial of wells and facilities
Spreading failure	Formation of retrogressive spreading zone greater by toe release of previously unfailed seabed, with subsequent flow runout downslope of spreading zone	Installation difficulties associated with steep slopes Possible flowline-spanning issues in undulating terrain Potential for slope movement causing damage or burial of wells and facilities
Steeply sloping seabed, abrupt changes in slope	Steep slopes at increased risk of landsliding	Topographic constraints usually considered a routine engineering issue, taken into account in design

(continued)

Table 2 (continued)

Geohazard feature or process	Description of geohazard	Typical implications for subsea developments
Tophole drilling hazards	Flows of shallow gas, shallow water flow and related shallow drilling hazards	Considered a routine engineering issue, taken into account in design
Tsunami	Water waves generated either by a large on-site landslide or by an off-site earthquake	Potential for damage to shallow water and shoreline installations. Not usually an issue in deep water
Turbidity currents	Sediment-laden flows at seabed	Impact of sediment-laden flows on equipment, scour
Variations in soil geotechnical characteristics, such as strength and permeability		Considered a routine engineering issue, taken into account in design

assessment may demonstrate that the geohazard risk in certain areas is less than previously thought and thereby allow development to proceed.

The significance of a particular geohazard impact on a particular component, such as an oil well, will depend upon its capacity to withstand the associated loads and stresses. Standard design of wells and facilities will have an inherent capacity to resist geohazard-related loads from relatively minor geohazard events such as small landslides, and hence not all geohazard events will be damaging. Geomorphological data, such as the size distribution of landslides, may be used to estimate geohazard loading on equipment using standard soil and fluid mechanics principles and models, which when compared with the structural capacity of the seabed equipment in question (e.g. Parker et al. 2009), may be used to estimate the overall probability of damage during the life of the development. Probability of a hit or probability of damage taking account of equipment vulnerability may be presented as a layer on the development planning guidance maps (Fig. 2).

In some situations, even if a particular geohazard scenario is credible event over the life of the development, the probability of the event causing damage may be relatively low and hence the associated risk may be acceptable to the developer. Should the level of risk not be acceptable, then options may be available for special geohazard-resistant design or mitigation measures to be taken to achieve an increased level of engineering reliability. Such measures may include the provision of stronger equipment components, anchoring of structures to help to resist movement, burial of pipelines or the provision of emergency shut-off valves for use in the event of a failure. For larger geohazard events, however, there will be a threshold beyond which geohazard-resistant engineering design or protection is neither technically possible nor cost-effective.

7 Conclusions

Geomorphological assessments of the seabed, based upon high resolution bathymetry and shallow seismic data, are of critical importance in the planning and design of subsea oil and gas developments. The value of a comprehensive geomorphological assessment for deepwater projects is obvious and can be summarised:

- Geomorphology is key to unravelling the past history of deepwater regions providing the setting and context for development sites and proposals.
- Geomorphological definition of features/systems provides a necessary spatial and temporal framework for derivative studies, soil maps, risk assessment, etc.
- Preliminary geomorphology assessment and geohazard screening may reveal potentially significant geohazard risks that require early investment in appropriate studies and investigations to support development planning and design.
- The geomorphology of sites is used to develop the rationale and optimisation of acquisition of high-resolution geophysical and geotechnical investigations to inform detailed evaluation and modelling of geohazard risks.
- Morphological mapping of features is key to characterising geohazards in detail and combined with geophysical and geomechanical interpretation of the sub-seabed ensures a holistic and robust evaluation of the implications to development.
- Geomorphology forms the basis of conceptual ground models which in turn may be used to estimate the risk to subsea equipment from features and processes on the seabed, and to assist in determining optimal equipment layouts which avoid the areas of greatest risk. Geomorphological data also provides the basis for the geohazard-resistant design of equipment.
- Geomorphological assessments are often carried out in a series of iterations, in which the understanding of geohazards is increased and the risk to the project reduced at each step aligned to the project schedule and funding strategy.

Geomorphology assessment is therefore key to guiding development layout and design to avoid or accommodate geohazards over the life of the project thereby ensuring safe, sustainable and economic development of deepwater oil and gas infrastructure and operations.

Acknowledgements The authors are grateful to colleagues in BP, Statoil (formerly Norsk-Hydro), IntecSea, Royal Dutch Shell (formerly BG Group), Tullow, CH2M (formerly Halcrow Group Ltd) D'Appolonia, NGI and Fugro for their collaboration in developing the subsea geomorphological mapping and geohazard assessment approach presented herein. The authors are particularly grateful to Prof. Denys Brunsden who has been an integral part of the development of the approach and mentor of the CH2M geohazard assessment team over several decades.

References

- Bondevik S, Mangerud J, Dawson S, Dawson A, Lohne Ø (2003) Record-breaking height for 8000-year old tsunami in the North Atlantic. *EOS Trans Am Geophys Union* 84(31):289–293
- Brunsdon D (2002) The fifth glossop lecture. Geomorphological roulette for engineers and planners: some insights into an old game. *Q J Eng GeolHydrogeol* 35:101–142
- Brunsdon D, Jones DKC (1972) The morphology of degraded landslide slopes in South West Dorset. *Q J Eng GeolHydrogeol* 5:205–222
- Bryn P, Berg K, Forsberg CF, Solheim A, Kvalstad TJ (2005) Explaining the Storegga Slide. *Mar Pet Geol* 22:11–19
- Bugge T (1983) Submarine slides on the Norwegian continental margin with special emphasis on the Storegga Slide. IKU Report 110:1–152
- Cauchon-Voyer G, Locat J, St-Onge G (2008) Late-Quaternary morpho-sedimentology and submarine mass movements of the Betsiamites area, Lower St. Lawrence Estuary, Quebec, Canada. *Mar Geol* 251:233–252
- Cooke RU, Doornkamp JC (1990) *Geomorphology in environmental management*. Clarendon Press, Oxford
- Evans TG, Moore R, Usher N (2007) Management of geotechnical and geohazard risks in the West Nile Delta. In: 6th international conference, Offshore Site investigation and geotechnics: confronting new challenges and sharing knowledge, London
- Forsberg CF, Berg K, Brunsden D, Moore R (2002) Morphological studies of the Storegga Slide. Summary and technical report: 37-00-NH-G15-00098, Norsk Hydro. In: Gee MJR, Uy HS, Warren J, Morley CK, Lambiase JJ (eds) (2007) The Brunei slide: a giant submarine landslide on the North West Borneo Margin revealed by 3D seismic data. *Mar Geol* 246:9–23
- Gee MJR, Uy HS, Warren J, Morley CK, Lambiase JJ (2007) The Brunei slide: a giant submarine landslide on the North West Borneo Margin revealed by 3D seismic data. *Mar Geol* 246 (1):9–23
- Hampton MA, Lee HJ (1996) Submarine landslides. *Rev Geophys* 34(1):33–59
- Hough G, Green J, Fish P, Mills A, Moore R (2011) A geomorphological mapping approach for the assessment of seabed geohazards and risk. *Mar Geophys Res* 32(1–2):151–162
- Huhnerbach V, Masson DG (2004) Landslides in the North Atlantic and its adjacent seas: an analysis of their morphology, setting and behaviour. *Mar Geol* 213(2004):343–362
- Jeanjean P, Liedtke E, Clukey EC, Hampson K, Evans TG (2005) An operator's perspective on offshore risk assessment and geotechnical design in geohazard-prone areas. In: Gourvenec, Cassidy (eds) *Frontiers in offshore geotechnic: ISFOG 2005*
- Kvalstad TJ (2007) What is the current “Best Practice” in offshore geohazard investigations? A state-of-the -art review. In: Offshore technology conference, Houston, Texas
- Locat J (2001) Instabilities along ocean margins: a geomorphological and geotechnical perspective. *Mar Pet Geol* 18:503–512
- Locat J, Lee HJ (2002) Submarine landslides: advances and challenges. *Can Geotech J* 39(1):193–212
- Masson DG, Watts AB, Gee MJR, Urgeles R, Mitchell NC, Le Bas TP, Canals M (2002) Slope failures on the flanks of western Canary Islands. *Earth Sci Rev* 57:1–35
- Masson DG, Harbitz CB, Wynn RB, Pedersen G, Løvholt F (2006) Submarine landslides: processes, triggers and hazard prediction. *Philos Trans Roy Soc A* 364:2009–2039
- McAdoo BG, Pratson LF, Orange DL (2000) Submarine landslide geomorphology, US continental slope. *Mar Geol* 169:103–136
- Micallef A, Masson DG, Berndt C, Stow DAV (2009) Development and mass movement processes of the north-eastern Storegga Slide. *Quatern Sci Rev* 28:433–448
- Moore R, Usher N, Evans TG (2007) Integrated multidisciplinary assessment of West Nile Delta geohazards. In: 6th international conference, offshore site investigation and geotechnics: confronting new challenges and sharing knowledge, London. Society of Underwater Technology, paper SUT-OSIG-07-033

- Nittrouer CA, Kravitz JH (1996) STRATAFORM: a program to study the creation and interpretation of sedimentary strata on continental margins. *Oceanography* 9:146–152
- Parker E et al (2009) Geohazard risk assessment—vulnerability of subsea structures to geohazards—some risk implications. Prof. Offshore Technology Conf., Houston, TX, Paper OTC20090
- Posamentier HW (2000) Seismic stratigraphy into the next millennium; a focus on 3D seismic data. In: American association of petroleum geologists annual conference, New Orleans, LA, 16–19 Apr, A118
- Prior DB, Hooper JR (1999) Sea floor engineering geomorphology: recent achievements and future directions. *Geomorphology* 31:411–439
- Riis F, Berg K, Cartwright JA, Eidvin T, Hansch K (2005) Formation of large crater-like evacuation structures in ooze sediments in the Norwegian Sea. Possible implications for the development of the Storegga Slide. *Mar Pet Geol* 22:257–273
- Savigear RAG (1965) A technique of morphological mapping. *Ann Assoc Am Geogr* 53:514–538
- Solheim A, Bryn P, Sejrup HP, Mienert J, Berg K (2005) Ormen Lange—an integrated study for the safe development of a deep-water gas field within the Storegga Slide Complex, NE Atlantic continental Margin; executive summary. *Mar Pet Geol* 22:1–9
- Ten Brink US, Geist EL, Andrews BD (2006) Size distribution of submarine landslides and its implications to tsunami hazard in Puerto Rico. *Geophys Res Lett* 33(L11307):1–4
- Twichell DC, Chaytor JD, Ten Brink US, Buczkowski B (2009) Morphology of late Quaternary submarine landslides along the U.S. Atlantic continental margin. *Mar Geol* 264(2009):4–15
- M.J.R. Gee, H.S. Uy, J. Warren, C.K. Morley, J.J. Lambiase, (2007) The Brunei slide: A giant submarine landslide on the North West Borneo Margin revealed by 3D seismic data. *Marine Geology* 246 (1):9-23

Seabed Mining

Anne Peukert, Sven Petersen, Jens Greinert and François Charlot

Abstract Seafloor morphology plays a key role in submarine mineral exploration as precious minerals are associated with specific geomorphological settings. Mn-nodules occur in abyssal plains, seafloor massive sulphides are strongly connected to volcanic areas and sand, gravel and other marine minable aggregates are deposited in coastal environments. For resource assessments and exploitation, a detailed knowledge of the seafloor morphology is essential to evaluate areas of terrain that cannot be mined due to technical limitations, and to estimate abundance, extent and thickness of the deposits. The most important method used is multibeam mapping, from which bathymetric and backscatter data are derived. These are often linked to side scan sonar surveys and sub-bottom profiling. Optical video and photo data provide additional information about substrate type and ecology, and help improve and adapt exploration and exploitation plans and technology. For the three most important marine mineral types—sand and gravel, Mn-nodules and seafloor massive sulphides—exploration and exploitation methods are described and the environmental impacts associated with mining these resources are discussed.

1 Introduction

A steady population growth, increasing metal demand and lower grades of mineral deposits mined on land have fostered an interest in the economic potential of marine mineral resources. While mining of some commodities has already been carried out for many years in the shallow marine environment, others—especially in the deep sea—are still in the state of exploration.

A. Peukert (✉) · S. Petersen · J. Greinert
GEOMAR Helmholtz-Center for Ocean Research, Kiel, Germany
e-mail: apeukert@geomar.de

F. Charlot
Global Sea Mineral Resources NV, Kingston, Jamaica

1.1 Marine Mineral Deposits

The seabed is already an important source of commodities for humankind. Sand and gravel used for construction purposes or beach restoration as well as oil and gas have been mined from the sea for decades. Additionally, placer deposits of diamonds have been extracted off the coast of South Africa and Namibia for a long time, in addition to deposits of tin, titanium, and gold along the coasts of Africa, Asia, and Australia (Cronan 1992; Rona 2003, 2008). These placer deposits are accumulations of minerals with a high density and chemical resistance to weathering, which form along beaches by gravity settling due to wave or current movement. Marine phosphorite deposits may potentially be used to extract phosphate for fertilizers (Rona 2003). Such deposits can be found on the continental shelf in tropical upwelling regions, where cold deep water is rising to the surface (Föllmi 1996, Murton 2000). Dissolved phosphate in the low temperature waters precipitates along the upper slopes of continental margins and on the continental shelf. The continental shelf itself is underlain by bedrocks that are submerged and covered by sediments. Since these bedrocks host a variety of mineral deposit types that are currently being mined onshore, but close to the coast lines, the interest in shelf areas may increase even further if extensions of onshore mines can be traced into the shallow ocean (Hannington et al. 2017).

Raw materials are, however, not confined to shallow waters. Potential deep-sea mineral resources include manganese nodules, cobalt-rich manganese crusts and seafloor massive sulphides (Rona 2008; Hein et al. 2013; Petersen et al. 2016). Manganese nodules occur on the sediment-covered abyssal plains at depths of about 4000–6500 m. They are mineral concretions made up largely of manganese and iron oxides and oxyhydroxides. These form around a hard nucleus and incorporate economically interesting metals, such as copper, cobalt, and nickel, together with potentially valuable metals such as lithium, molybdenum, titanium, and rare earth elements (REE) from the sediment and seawater. Cobalt-rich ferromanganese crusts form on the sediment-free flanks of volcanic seamounts, ridges, and plateaus and are composed of manganese oxides and iron oxyhydroxides that precipitate directly from seawater. They are usually several cm thick, with the thickest and most metal-rich crusts forming in depths between 800 and 2500 m (Hein et al. 2013). The elements of interest are similar to those in manganese nodules.

Seafloor massive sulphides (SMS) are another deep sea mineral resource, associated with volcanically active areas along divergent plate boundaries. These deposits form at or below the seabed as a consequence of the interaction of seawater with a heat source in the sub-seafloor. Hot fluids leach economically interesting metals such as copper, zinc, gold and silver from the ambient rocks and transport them to the seafloor where they precipitate as metal sulphides forming SMS deposits. Their composition is highly variable as a consequence of variations in source rock composition, water depth, and input of magmatic volatiles (Hannington et al. 2005).

Marine mineral resources fall under two different legal regimes depending on their location: they either occur within the legal boundaries of national jurisdiction of a coastal state or occur in areas beyond national jurisdictions. In the latter case exploration and exploitation are managed by the International Seabed Authority (ISA) that was established in Kingston (Jamaica) in 1994 based on the United Nations Convention on the Law of the Sea (UNCLOS).

1.2 General Exploration Methods for Resource and Environmental Impact Assessment

Hydro-acoustic mapping of the seafloor with multibeam echosounder (MBES) and side scan sonar (SSS) systems are the most important tools for the exploration of submarine mineral resources. These methods provide a quick overview of the bathymetric and substrate properties of the area of interest. Both are very important for evaluating the possible minable terrain and to estimate resource potentials. After mapping with hull-mounted MBES systems, which provide information about major terrain structures, areas of interest will be mapped in detail using deep/close to the seafloor operating platforms. This is especially important for deep sea resources, where the resolution of hull-mounted systems provides only a resolution of several tens to a hundred of metres, not enough for a detailed assessment. In contrast hydro-acoustic mapping (MBES, SSS) with autonomous underwater vehicles (AUVs) operating at several tens to a few metres altitude (depending on mission and terrain variability) provides a detailed insight in small scale terrain structures with few metres or even less than a metre resolution. Backscatter (BS) data, photos or video data, recorded by either AUV's, ROV's or towed camera systems, as well as specific sampling platforms are used for ground truthing, substrate characterisation. Sub-bottom profiling reveals valuable information about sediment thickness and underlying structures, which can be important for resource evaluation of some deposits. Apart from resource assessments, the same methods are used to study mining-related environmental impacts; this needs to be part of any exploration action undertaken under the jurisdiction of the ISA [ISBA/19/LTC/8]. Habitat mapping, which forms the basis for environmental impact assessments (EIA), requires information about bathymetry and substrate characteristics on various scales. Video and photo data, as well as biological sampling, reveal the respective benthic and epi-benthic fauna and community structures, which are only poorly studied, particularly in the deep sea. As benthos and ecosystem services of the top sediment layers are essential to local and regional biogeochemical processes and ecosystems, the consequences of habitat destruction through seabed mining need to be properly evaluated.

In the following sub-chapters, the exploration, exploitation and monitoring methods for environmental impact assessments are described in more detail for sand and gravel, Mn-nodules and SMS deposits.

2 Resource Description

2.1 Sand and Gravel

Sand and gravel deposits are terms used to describe marine aggregate deposits based on grain sizes and performance, rather than the mineralogical components (Padan 1983). The size thresholds defining the nomenclature varies between countries, but scientifically, sand defines grain sizes between 0.63 and 2 mm in diameter, and larger grains are classified as gravel (Collins 2010). These deposits occur on the continental shelf at or close to the seabed surface and as relicts from river and coastal bank deposits. These were formed under low sea level conditions during the last glacial period, when rivers extended onto large parts of the continental shelf, filling their river-beds with eroded continental runoff material. Modern deposits are a product of present hydrodynamic and sedimentary particle reworking and are therefore strongly related to coastal sediment budgets and dynamics (Collins 2010). The composition can be very variable depending on their formation history. Relict deposits mainly consist of land derived particles, while modern sand and gravel bodies also contain a considerable amount of shell fragments, which influences the resource quality (Collins 2010).

2.2 Mn Nodules

Ferromanganese Nodules are widely abundant in global oceans and occur mostly at the sediment surface (Fig. 1) or in near-surface sediment layers. They are concretions of Mn-oxides and Fe-hydroxides that precipitated around some kind of a nucleus, such as rock fragments, shark teeth, shells or fragments of micro-nodules.

Besides their name-giving main components, the nodules also contain trace metals adsorbed within the oxy-hydroxides, which make them of interest to the mining industry. Two major formation types can be distinguished: hydrogenetic nodules that form by precipitation from the ambient seawater, and diagenetic nodules, which grow by precipitation from the sediment pore water. Most of the nodules are mixed-types rather than grown from only one of the end member formation types (Hein and Koschinsky 2013). Depending on the formation type and geographic occurrence, the growth rate varies, which influences the metal enrichment within the concretions. The formation itself is affected by the metal supply, the seafloor morphology that influences the depositional environment (bottom current strength and sediment composition), as well as by bioturbation (Hein and Koschinsky 2013). Only in some places of the world's oceans the nodule grade, according to size and content of the most precious metals (Cu, Co, Ni, REE's), is high enough for a possible mining. These places lie in sediment-covered abyssal plains at water depths between 4000 and 6500 m. Here the sedimentation rate is very low ($<1 \text{ cm/ky}^{-1}$), which allows slow nodule growth rates (only 1–20 mm/Ma) in a semi-liquid surface layer with sufficient pore

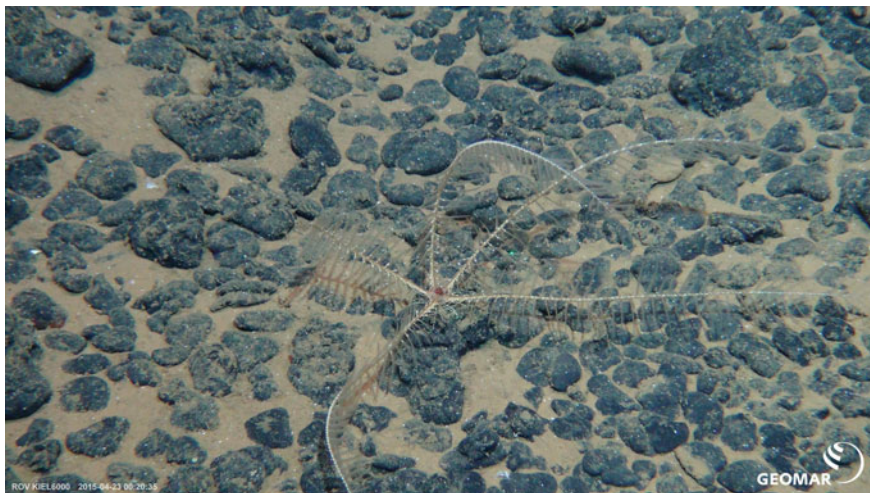


Fig. 1 Mn-Nodules covering the sediment surface within the CCZ and organism associated with the nodules as hard substrate habitat (ROV Kiel 6000, GEOMAR)

water for the diagenetic growth. The bottom waters are also well-oxygenated enabling the formation of oxy-hydroxides (Petersen et al. 2016). Areas of young oceanic crust (<10 Ma), high sedimentation rates and a local morphology of >300 m relief are generally not suitable as a possible exploration area (Petersen et al. 2016). The largest high-grade Mn-nodule occurrences are known to be in the Central Indian Ocean Basin, the Peru Basin and in the Clarion-Clipperton Zone (CCZ) in the equatorial Pacific between Hawaii and Mexico. Here, a 4.2 million km² area is managed by the ISA, with several countries having shown a commercial interest for decades and where mining could become reality in the near-future.

2.3 Seafloor Massive Sulphides (SMS)

Metal-rich hydrothermal deposits form as a consequence of seawater circulating through the oceanic crust in volcanically active areas. Cold ocean water penetrates through cracks into the sub-surface where it is heated by a heat source, commonly magma. The hot fluids leach metals and sulphur from the surrounding rocks within the crust and finally ascend back to the seafloor, where a part of the dissolved metals precipitate as a reaction with the cold seawater, forming the characteristic chimneys (black smokers) or mounds on the seafloor (Fig. 2; Hannington et al. 2005). Some portion of the fluid is expelled into the overlying water column, forming hydrothermal plumes that are commonly used to search for active deposits (Petersen et al. 2016, Baker et al. 2016). Active black smoker systems have been discovered at all plate boundaries as in spreading centres of Mid Ocean Ridges

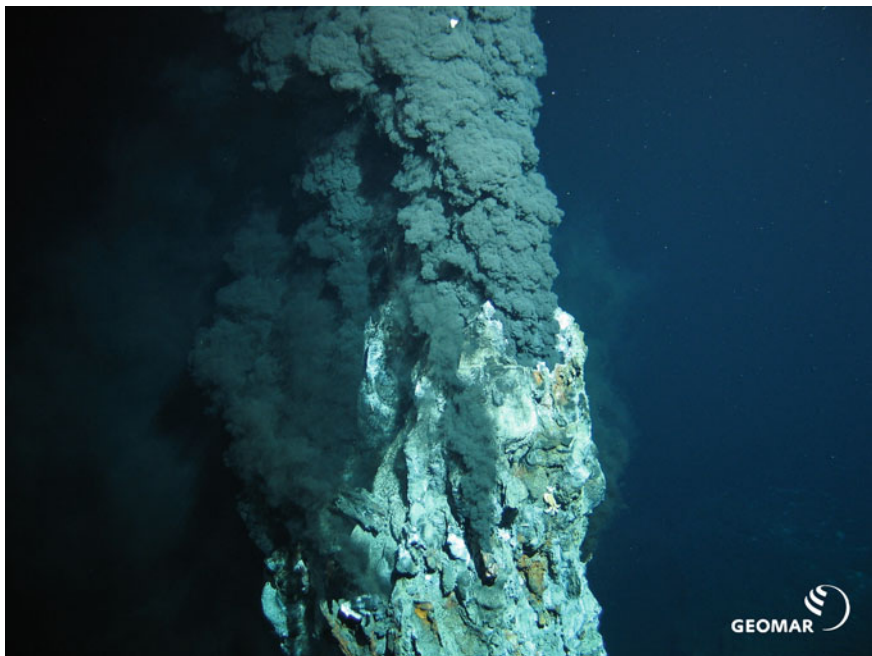


Fig. 2 Active black smoker chimney at the Mid-Atlantic Ridge. *Photo ROV Kiel 6000, GEOMAR*

(MOR), along active submarine volcanic arcs and in back-arc basins. Only very few deposits are known to occur in association with intraplate volcanoes. The greatest economic potential of the deposits can be expected in water depths between 1000 and 5000 m (Petersen et al. 2016).

3 Exploration Methods

3.1 Sand and Gravel

For exploring the horizontal and vertical extent and surficial character of sand and gravel deposits, MBES and SSS systems are employed and BS data play an important role. Based on these data, deposits of the required grain size are identified based on sampling, local knowledge about the sediment geology, as well as Angular Response Analysis (ARA). ARA uses the characteristic BS strength variations with incidence angle for different substrate types and frequencies. By comparison with model results, the substrate type can be evaluated. Highly detailed bathymetric information in correlation with sub-bottom profile data is used to identify deposits in the sub-seafloor; structures such as paleo-channels or

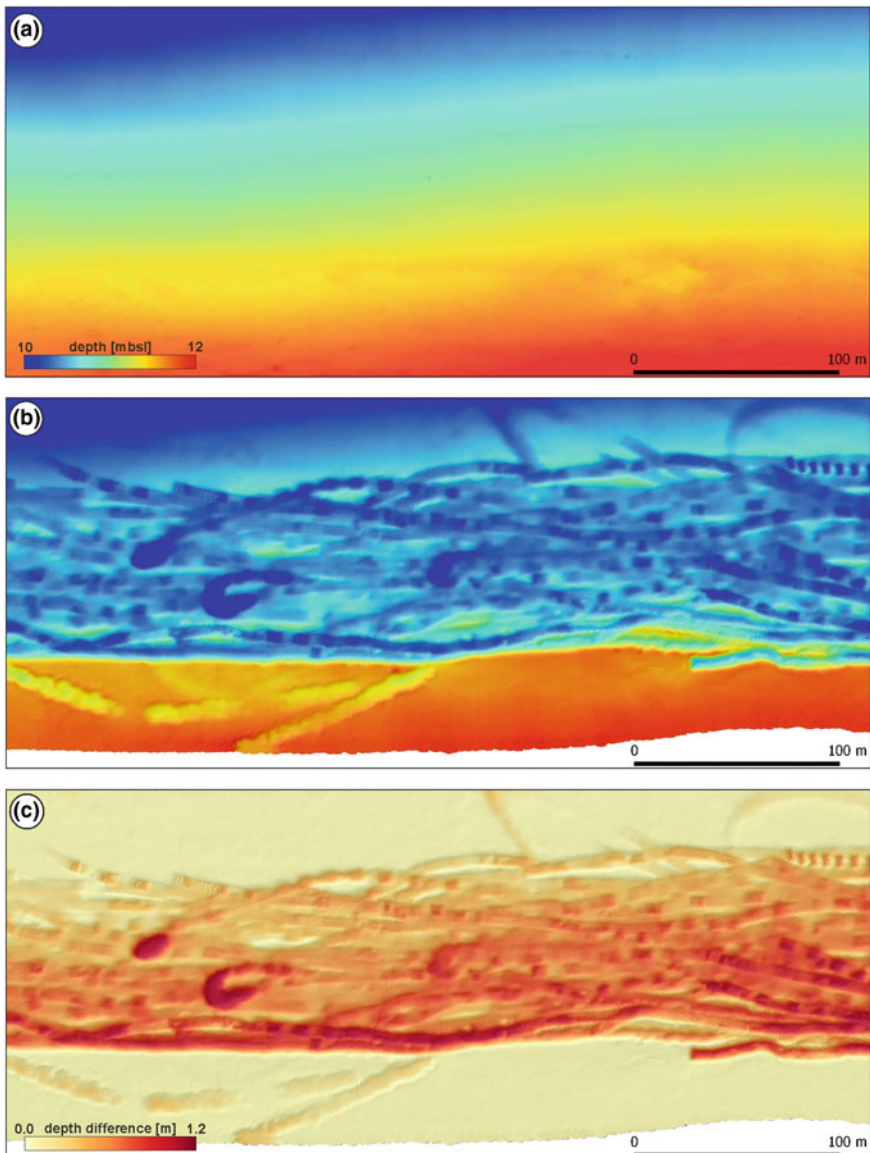


Fig. 3 **a** Detailed bathymetry before and **b** after mining; the dredge tracks are clearly visible. **c** Difference between before and after dredging, furrows are up to 1.2 m deep. *Source* DEME-Dredging environmental and marine engineering

paleo-river beds, which are most probably filled with the material of interest, are targeted. Detailed sediment sampling, coring and drilling finally provide validation of the acoustic mapping results and reveal the resource quality. Detailed MBES data

from the extraction area before and after the mining (Fig. 3) are an important basis to evaluate the extraction process efficiency, amount of sediment removed and the related potential impact on the local hydrography/current regime and ecology.

3.2 *Mn-Nodules*

Besides bio-geochemical factors and oceanographic parameters, the seafloor morphology is a key parameter in evaluating Mn-nodule resources in the deep sea. Satellite-derived bathymetric data even with a low resolution of 1–3.7 km (ETOPO2 or GEBCO30 data) allow the identification of abyssal plains in relation to seamounts, ridges, or troughs located in the admired water depths. One of these abyssal plains lies in the Peru Basin where the abundance and grade of occurring Mn-nodules were considered as economically valuable and which has been studied in detail since the 70s (Von Stackelberg 2000). In 1989, the seafloor of an area called “DISCOL Experimental Area” was disturbed by a plough harrow and has been revisited since then several times in order to study the ecological recovery from this disturbance and thus gain knowledge with respect to deep sea mining EIAs (Thiel 2001; www.discol.de). The following example is from the DISCOL area (Greinert 2015), located approximately 500 miles west off the Peruvian coast. MBES mapping with the hull-mounted system of RV SONNE (EM122; 0.5° by 1° beam angle, 18 kHz) reveals the bathymetry of the area with a resolution of 50 m (Fig. 4a, b); the relief of this ‘abyssal plain’ shows depth variations of 300 m.

The different bathymetric settings (seamounts, ridges, basins, plains) influenced sediment depositional settings that also cause variability in Mn-nodule abundances and compositions. Backscatter data recorded with ship-based MBES systems (Fig. 5a, b) allow the identification of higher/lower Mn-nodule abundances (Rühlemann et al. 2011). Areas of higher Mn-nodule abundance are typically associated with higher BS values because the existence of ‘many’ hard and irregularly shaped bodies on the seafloor increase the scattering potential in comparison to no-nodule areas (all this needs to consider the slope/incidence angle of the respective hydro acoustic beam). The results need validation by direct sampling (e.g. box coring) but in general enable the evaluation and segmentation of potentially low and high Mn-nodule abundance on large scale in a relatively short time.

Recent studies show that a more detailed knowledge of the local terrain is important for a realistic resource assessment that also needs to consider the minable terrain (Madureira et al. 2016; <10° slope, Fig. 6) determined by the technical limitations of the crawler capabilities. For planning mining operations, ship-based bathymetry is not sufficient. Over the last decade MBES systems have been reduced in size so that they can now routinely be used on remotely operated vehicles (ROVs) and on autonomous underwater vehicles (AUVs) providing bathymetric data with a resolution down to a few decimetres, depending on the altitude at which these instruments are deployed (Caress et al. 2012; Yoshikawa et al. 2012; Clague et al. 2014). The AUV-based bathymetry presented was typically acquired at 80–50 m

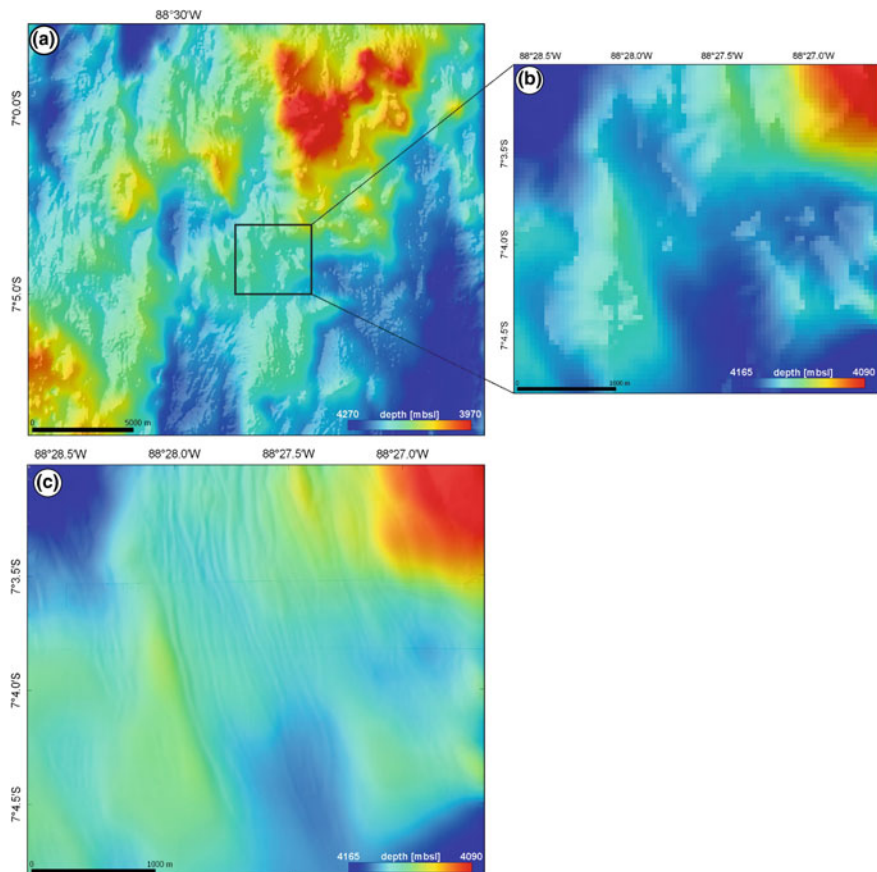


Fig. 4 **a** Ship-based bathymetric map revealing the morphology with a horizontal resolution of 50 m. Black square marks the AUV-mapped central DISCOL area. **b** Extract from the ship-based bathymetry showing the AUV-mapped area with the 50 m cell size resolution. **c** AUV-obtained bathymetry with a horizontal resolution of 2 m revealing small-scaled structures that were not resolved in the ship-based bathymetric map

above the seafloor, delivering data of about 2 m horizontal and decimetre vertical resolution, from which smaller-scaled in-homogeneities, also in habitat distribution, can be derived (Fig. 4c). Terrain analysis clearly shows flat areas suitable for mining (Fig. 6) and correlating AUV- or ROV-obtained photo data reveal variabilities in Mn-nodule coverage within several metres to tens of metres distance, clearly linked to bathymetric changes.

AUV-obtained BS and SSS data provide an equally detailed insight into the local substrate properties with a resolution of up to 1 m (SSS). With this mapping method, nodule-free patches or substrate types that could be challenging for the mining gear (e.g. talus block fields) can be identified. These small-scale changes in

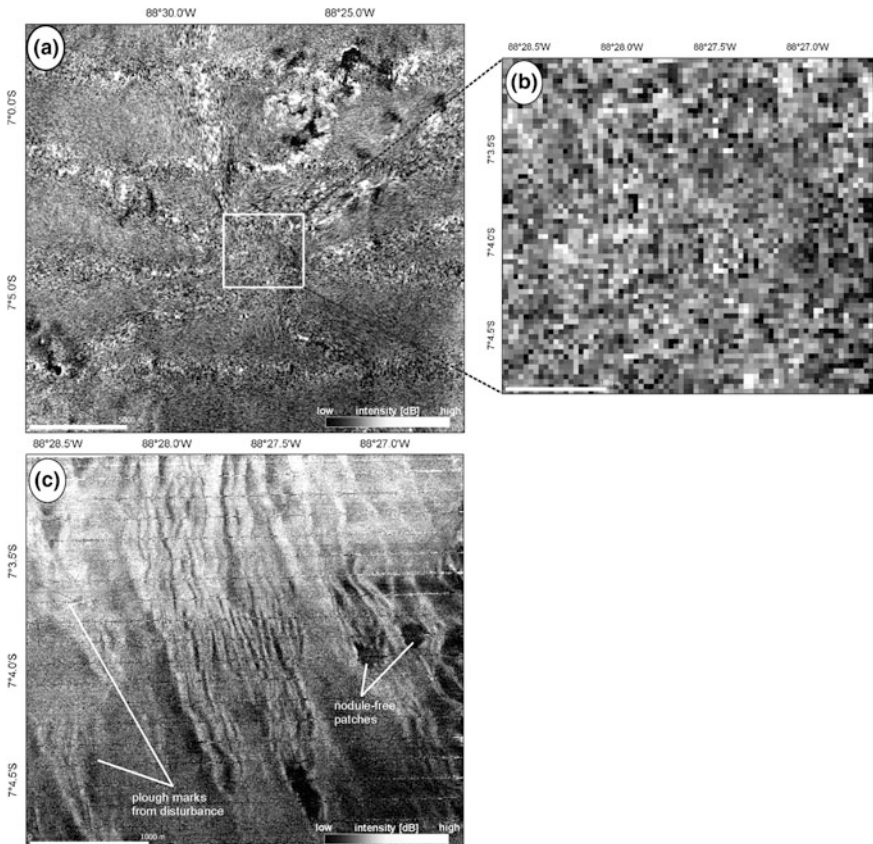


Fig. 5 **a** BS data from hull-mounted MBES system; resolution 50 m. Bright to dark grey scales indicate high to low BS signal strength. **White square** marks the AUV-mapped central DISCOL area. **b** Extract from the ship-obtained BS data showing the AUV-mapped area in a low resolution. **c** AUV-obtained BS data with a horizontal resolution of 2 m revealing small-scaled structures and nodule-free areas (very low BS signal strength) that were not resolved in the ship-based BS map

Mn-nodule abundance can be visualised in the BS data of Fig. 5c where nodule-free patches stand out as very low BS areas. In a seafloor classification effort different statistical values of BS measurements falling in a larger grid cell (here 6 m) can be used in an un-supervised approach to improve knowledge about small-scale seafloor/habitat changes (Fig. 7). At the same time these results lead to a better understanding of driving processes in nodule formation, in particular in combination with additional sub-bottom profile data, specific direct sampling and optical investigations.

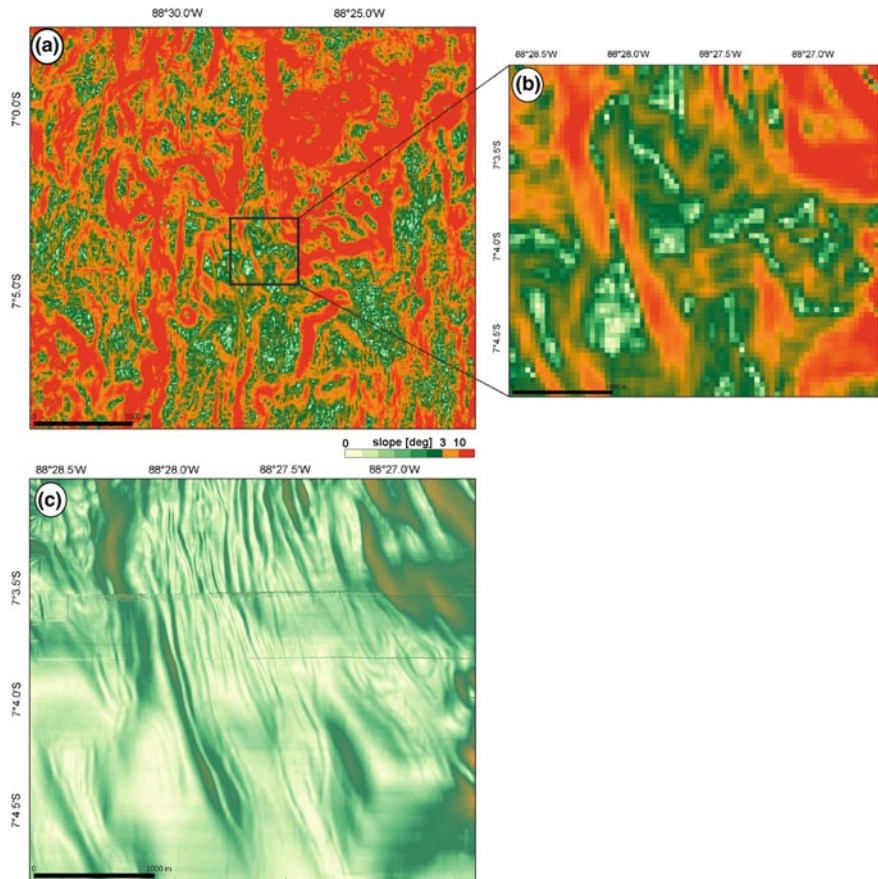


Fig. 6 **a** Slope calculated from the ship-obtained bathymetric data. **b** Extract of the AUV-mapped area with the ship-based bathymetry resolution. **c** Slope map of the central DISCOL area derived from AUV-obtained bathymetric data. *Green* and *orange* areas are suitable for mining (color figure online)

3.3 Seafloor Massive Sulphides

For the prospection for SMS occurrence, global satellite-derived topographic data can be used to define regions of interest, e.g. the location of the spreading axis in areas where no other data are available. The small size of the resource targets—tens to a few hundreds of metres for individual deposits—implies the need to obtain higher resolution data. Even ship-based bathymetric data (Fig. 8) will not identify individual occurrences, but will allow defining target areas more precisely due to detectable indications of e.g. faulting and recent volcanic activity. The capability of acquiring high resolution AUV-based data has profound impacts, not only on our ability to detect SMS, but also on assessing the resource potential. In a recent

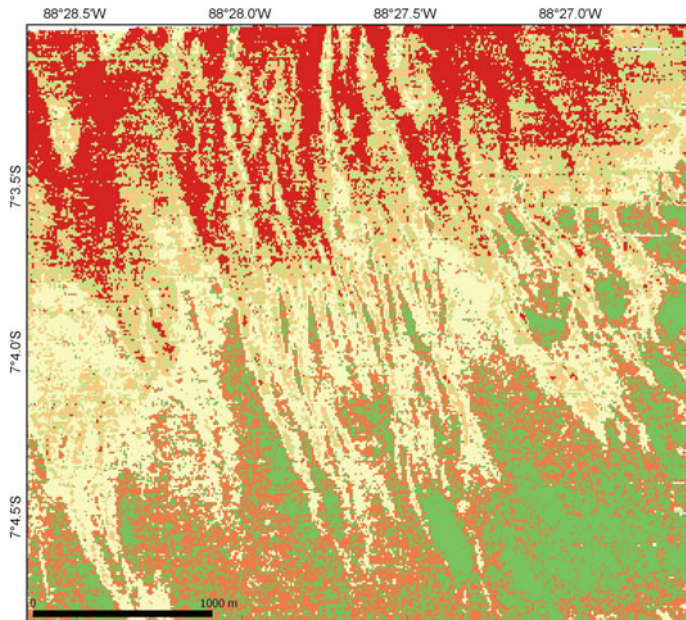


Fig. 7 Unsupervised classified map based on statistics of AUV-obtained BS data (mean, mode, min, max; ISODATA algorithm in SAGA-system for automated geoscientific analyses) for identifying areas of different Mn-nodule coverage

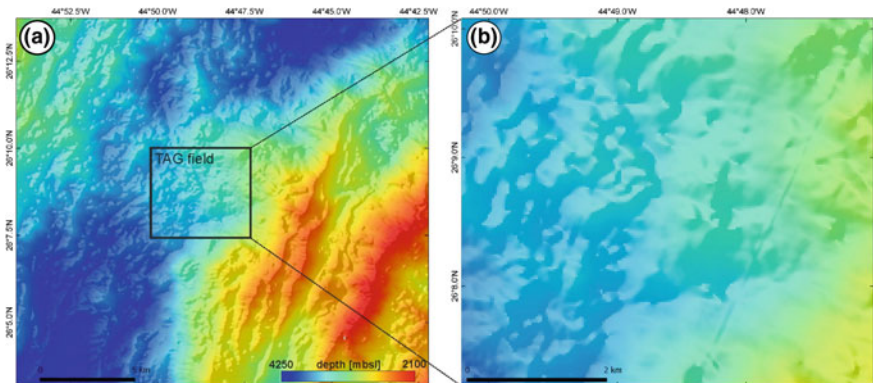


Fig. 8 **a** Ship-obtained bathymetry of a section of the Mid-Atlantic Ridge with the TAG vent field located on the hanging wall of an active detachment fault. **b** Zoomed-in view of TAG field (ship-based bathymetry; Resolution: 30 m)

two-week long survey at the Endeavour Segment in the Northeast Pacific Ocean, AUV-based bathymetry quadrupled the number of identified hydrothermal chimneys and mounds (Jamieson et al. 2014), although this vent site has seen well over

one hundred submersible and ROV dives over the past 30 years and is considered one of the best studied vent fields in the oceans.

Such high-resolution hydro-acoustic surveys overcome another shortfall of SMS exploration. So far prospecting technologies have mainly been developed for the search of actively venting sites that can easily be traced through physical and chemical anomalies in the water column as temperature, concentration variations in Mn or Fe, redox potential (Eh), and particle concentration. These plume surveys have been a primary tool for the exploration of SMS systems, but they only identify active, and therefore mostly young and thus small mineral occurrences. Economically more interesting deposits are inactive and have gone through their entire life cycle (Hannington et al. 2005). It has been recognised that these deposits are not only much larger than active deposits, but that they and can often be identified based on their shape, aspect ratio, or slope (Fig. 9) derived from high-resolution bathymetric surveys. The combination with other geophysical parameters such as magnetic or self-potential-sensor data recorded during the same survey, may be used to further distinguish volcanic mounds from hydrothermal occurrences.

A first resource assessment can be made by estimating the thickness of such mound-style occurrence by comparison with the surrounding seafloor and estimates of bulk sulphide density derived from previous studies (Jamieson et al. 2014). However, former sampling has revealed that such deposits can be very variable in terms of internal composition, which makes sampling and drilling a necessity for a proper resource assessment. Detailed AUV-based MBES mapping (Fig. 9) allows the identification of SMS deposits and distinction of mounds, based on their slopes and shape (Jamieson et al. 2014). For the identification of old and possibly larger deposits that are unfortunately sediment covered, new exploration methods still need to be developed (Petersen et al. 2016).

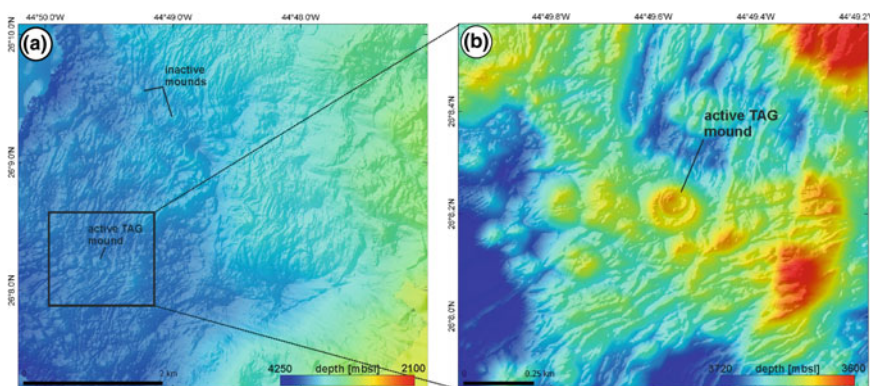


Fig. 9 **a** AUV-obtained bathymetry of the TAG field (resolution: 2 m) revealing the active TAG mound and inactive mounds. **b** Zoomed-in view showing the active TAG mound and the surroundings in more detail

Current exploration models assume that large extinct SMS occurrences can be found in a strip of up to few tens of kilometres away from the mid-ocean ridge. Further away from the ridge axis, the coverage by sediments or lava may become too thick for exploitation and/or the sulphuric minerals are ‘destroyed’ by dissolution from oxidized seawater. Still, the potential to find extinct sulphide deposits far from the ridge axis adds an additional vast seafloor area for future exploration.

In general, AUV-based high-resolution surveys, as needed for deep sea resource exploration, will need to cover large areas of the seafloor. It is unlikely that this can be done with single AUV surveys, and fleets of AUVs working together will be operated in the future, as time is an additional factor in exploration and each contractor to the International Seabed Authority has to explore 10,000 km² within the 15-year runtime of the contract, during which 50% of the area has to be returned to ISA after eight years. Deep sea exploration needs to be fast and cost-effective and therefore acoustic mapping of the seafloor will be the method of choice for decades to come.

4 Exploitation Methods

4.1 Sand and Gravel

Sand and gravel deposits commonly get extracted by static or trailer suction dredging, where the material is hydraulically sucked into the dredging vessel by pumps through a large pipe system (Fig. 10). During static suction, dredging the material is extracted punctually, creating up to 25 m deep and 200 m wide extraction craters (Collins 2010). This method allows the exploitation of deeper located and thick deposits as is typically done for diamonds (e.g. offshore Africa). For the trailer suction method, the vessel slowly moves, dragging the suction pipe over the seafloor, which creates extraction furrows up to a few metres deep (Fig. 3b, c). This method is used for the exploitation of thinner surficial deposits as sand and gravel. Although a wide area will be affected, the environmental impact is believed to be lower than the deep pit structures created by static suction dredging. Besides these two most common dredging methods, numerous other concepts are available for special circumstances (Cruickshank and Hess 1978).

Depending on the application, the material is screened at the vessel and immediately discharged onto a barge, to the shore through a pipeline system or back into the water column (Padan 1983) when not matching the required size or properties, to minimise the amount of unwanted material. The material is removed from the vessel onshore by different kinds of machinery. For beach nourishment, hydraulic discharge functions are also available on the vessel.



Fig. 10 Antigoon Trailing Suction Hopper Dredger from the DEME group, which can reach a maximum dredging depth of 45 m. The diameter of the suction pipe is 1200 mm. Image kindly provided by DEME—Dredging environmental and marine engineering

4.2 Mn Nodules

For several years, different methods for Mn-nodule extraction have been discussed. Early considerations in the 1970s included the use of an “air lift dredge” (a system consisting of a collector head, which is connected with a suction system pumping the material to the surface) and a “Continuous Line Bucket System” (consisting of a cable loop, where buckets are mounted in 25–50 m intervals; this cable loop lowers the buckets, skims them over the bottom where they get filled with Mn-nodules and finally rises the filled buckets back up to the sea surface) (Pearson 1975). The methods considered nowadays comprise a mining technique consisting of 3 sub-systems (Fig. 11). At the sea surface there is the mining vessel, from which the mining operation on the seafloor can be controlled and from which the lift pipe system (riser pipe) will be suspended. The actual mining will be done by crawler(s) which move over the seafloor and extract the nodules hydraulically or mechanically, depending on the mining concept (Oebius et al. 2001). According to a German concept developed by Aker Wirth GmbH, the crawler is approximately 17 m wide and 15 m long (Kuhn et al. 2011) and will move with approximately 1 m/s, removing the upper 10–20 cm of sediment. The collectors, which are still under development, need to extract 5–8 thousand tons of nodules per day for an

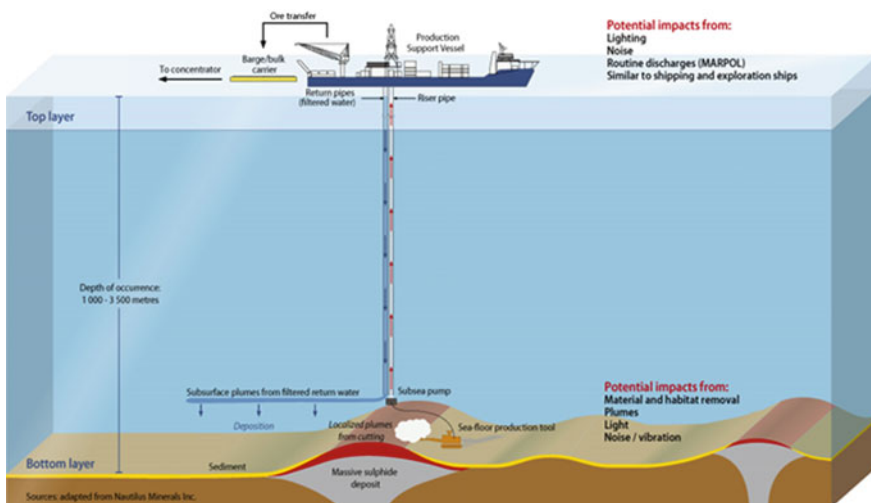


Fig. 11 Simplified scheme for the Mn-nodule mining system and the associated environmental impacts of the different system sections. The nodules will be collected and crushed by crawlers and the material will be transported through the Riser pipe to the production support vessel. The waist material from on-board processing will be discharged through a return pipe. Source GRID Arendal: http://www.grida.no/graphicslib/detail/example-of-a-sea-floor-manganese-nodule-mining-system-and-related-sources-of-potential-environmental-impact_f38d)

economically valuable mining operation while keeping the environmental harm to a minimum (Madureira et al. 2016). After the separation of sediment and nodules within the crawler, the crushed nodules are transported through the lift pipe system to the surface platform, where the material might be further processed and transported to the shore.

4.3 Seafloor Massive Sulphides

Since SMS deposits can be several tens of metres thick and the terrain they occur in is very rugged, the mining technology needs to be able to move not only in a difficult terrain but also needs to include cutting devices for fragmenting the SMS deposit rocks (Liu et al. 2016). The crushed material may be collected and transported through the riser system to the surface support vessel to be pre-processed and transported to the shore. The leading technology is orientated on mining technology deployed in land mines. Seafloor mining machines will be equipped with some kind of cutter head, similar to gear used for cutting through rock while coal mining (Ishiguro et al. 2013; Liu et al. 2016). In most scenarios a collector machine is added to collect the fragmented rocks, similar to a Mn-nodule ‘harvester’. The fragments will be pumped into the crawler, possibly transferred into a buffer

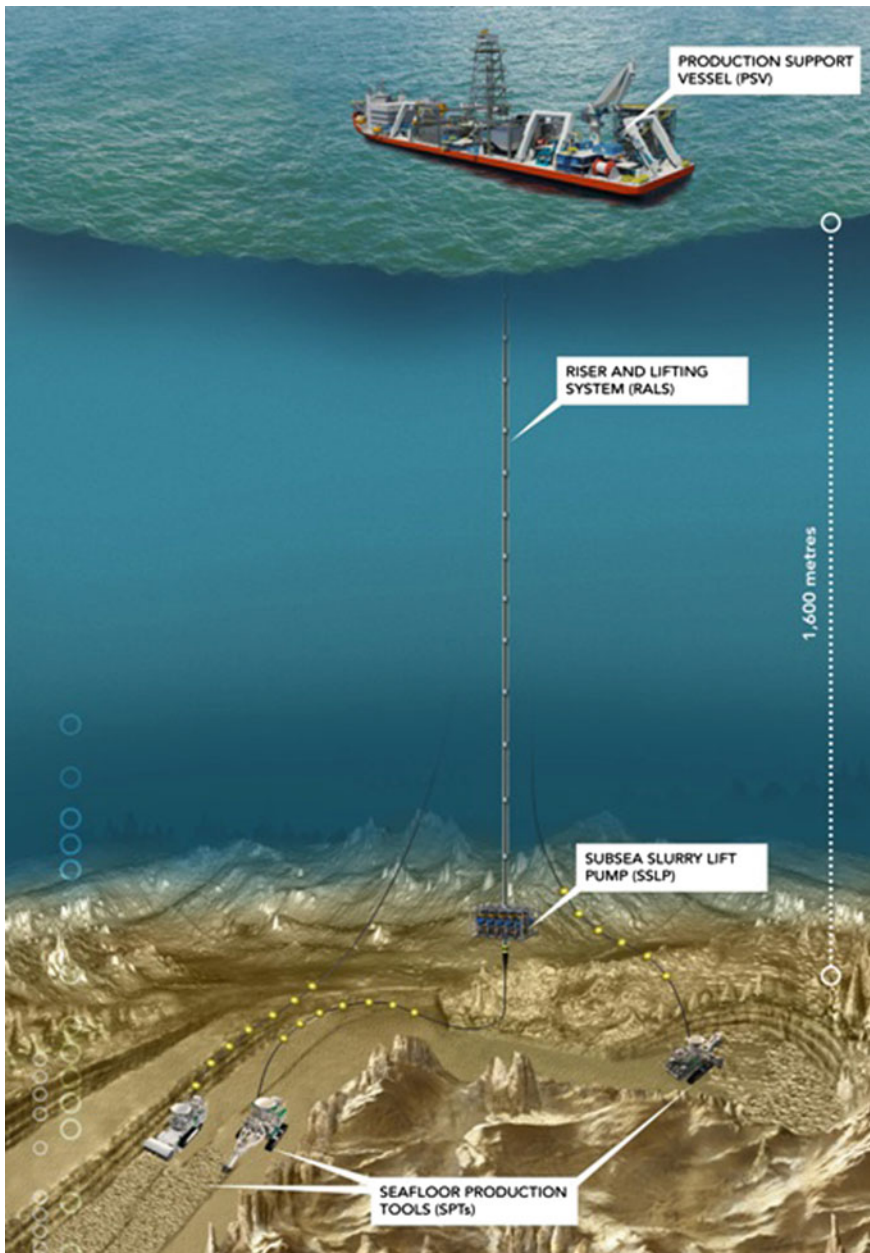


Fig. 12 Mining concept of nautilus minerals for SMS exploitation. Three kinds of seafloor production tools will be deployed: The Auxiliary Cutter will be used to flatten the rough seafloor. The bulk cutter will then be moving along the created flat benches extracting material from the deposits. The extracted material will then be collected by a collecting machine, which also transfers the slurry to the Riser and Lifting System. *Source* Nautilus Minerals

system, and then through the riser to the support vessel. According to the concept of Nautilus Minerals three different kinds of seafloor production tools will be deployed (Fig. 12): The Auxiliary Cutter (AC) will flatten the rough terrain and create benches to move on for the following tools. The Bulk Cutter (BC) will cut material from the deposits moving on the flat terraces created by the AC. Finally, the extracted material will be collected and transferred to the Riser and Lifting System by the collecting machine (CM, www.nautilusminerals.com). Other mining systems try to include the fragmentation and collection within one vehicle (Ishiguro et al. 2013). Alternatively large-scale grab systems may be used but further developments of mining systems based on currently ongoing tests will determine the most efficient exploitation technology for SMS deposits.

5 Monitoring Exploitation and Environmental Impact

5.1 Sand and Gravel

The environmental impact from sand and gravel extraction includes physical and biological effects, most prominently the complete destruction and removal of the seafloor surface, the creation of sediment plumes with unnatural turbidity as well as more or less pronounced impacts on the local current regimes and wave patterns. Due to the coastal proximity of the deposits, this impacts will eventually affect the coastal environment (Cruickshank and Hess 1978). The recovery of the excavation site is likely to take several decades in some areas. To avoid increased coastal erosion, prediction models are run prior to any exploitation activity—based on water depth, distance to the shore, depth and distribution of the resource, mobility of the seabed as well as oceanographic parameters—to secure coastal integrity (Collins 2010). Consequently, the evaluation of these data needs to be included in the exploration phase.

Unavoidable ecological impacts during sand and gravel mining include changes in fauna/flora diversity, density and community structures, particularly of benthic organisms due to the physical effects (Collins 2010). Substrate removal and changes in the local current regime considerably alter the habitat properties of the benthic communities. Increased turbidity can affect filter feeding sessile fauna by either clogging/hampering their filter capacity or burial by the re-settling sediment plume even at larger distance from the actual mining site. The final impact assessment of dredging on organisms needs to be based on a reliable knowledge of the local community and stress factors the organisms are naturally exposed to, such as tide-storm-caused enhanced sediment load. Ecosystems and fauna communities accustomed to such natural variabilities will likely be less affected by the dredging activities (Collins 2010). Studies of benthic community structures with direct sampling, visual observations and hydro-acoustic mapping (MBES, SSS) are needed for an accurate habitat mapping which is of great importance for the sand and gravel mining-related EIAs.

5.2 Mn Nodules

The extraction of the Mn-nodules from the seafloor will come with a clear risk for the benthic ecosystem. On one hand the removal of substrate will cause habitat loss for sessile fauna depending on the nodules as hard substrate (Fig. 1; Vanreusel et al. 2016) and for organisms living in the uppermost fluffy sediment layer. Both nodules and the top 10–20 cm will be removed and either be transported to the surface support vessel (Mn-nodules with as little sediment as possible) or to a large extent re-sedimented on the seafloor. In addition, the movement of the crawler itself will create a sediment plume that will be distributed uncontrollably over larger areas with the consequence that the re-deposition of the suspended sediment buries sessile organisms and clogs filter feeders even outside the actual mining area resulting in an increased mortality (Markussen 1994; Sharma 2011). Large amounts of suspended and re-depositing sediment are very unusual for the deep sea low sedimentation environment and could also cause bio-geochemical disequilibria impacting the local environment (Shirayama and Fukushima 1997; Kotlinski and Stoyanova 1998; Sharma 2001). Estimating the size and distribution pattern of the re-settled sediment cloud is therefore of specific interest for correctly assessing the extent of the area which would be ecologically influenced/harmed by the mining activity.

The evaluation of the mining-related environmental impact needs a precise knowledge of the benthic habitat distribution on different scales. While ship-based MBES data points at large scale habitat changes on kilometre-scale, small-scaled habitats on metre to even sub-metre scale are important to identify. These can only be efficiently mapped by a combination of AUV/ROV-based MBES data, SSS and backscatter analyses providing information about substrate types, linked to visual observations and their expert annotation/evaluation.

Studies undertaken in 2015 in the CCZ and the DISCOL area show that the re-sedimentation of bottom near sediment plumes are affected by the local morphology even on sub-metre vertical scale changes. Such an approach could effectively monitor the impacted area after mining activities. With AUV-obtained SSS (resolution 1 m) and BS data (resolution 2 m) the tracks left behind can be monitored and used to better document the change of the seafloor ecosystem (Fig. 5c). A total recovery of the Mn-nodule ecosystem as it existed before the mining will not be possible as the Mn-nodules, being an important micro-habitat in the abyss, have been removed. Thus the primary goal is to mitigate the impact as much as possible and allow for similar or new ecosystem services fulfilling habitats to establish in the shortest time possible.

Besides the seafloor generated sediment plume, the waste material from the processing at the mining support vessel will be discharged back into the water column. Discussions are still ongoing at which depth these tailings should be finally released, considering technical, economic and ecologic aspects. Any chemical leaching from pre-processing steps should be avoided, as this might add an unnecessary toxicity component.

5.3 Seafloor Massive Sulphides

Hydrothermal vent fields are characterised by high biomass and low diversity, whereas inactive deposit sites are colonised by fauna also typically associated with hard substrate seamount communities (Boschen et al. 2013). The microbial communities of inactive occurrences will, however, be very specialised due to the presence of sulphides as a substrate. Like any other mining activity, SMS mining comes along with the removal of habitat substrate, reducing edifices and altering the texture of the substrate (Baker and Beaudoin 2013). Mining active vent sites would change the distribution of venting sites for tens to hundreds of metres, directly affecting sessile benthic fauna. However, due to the general small size of the deposit and the high temperature/low pH very close to the vent sites, targeted mining of active vent sites is rather unlikely.

The mining of the SMS deposits will expose fresh sulphide mineral surfaces, from crushed down material and the freshly exposed rock surfaces, to oxygen rich bottom water that cause the sulphides to be oxidised. Acid generation during this process is likely small (Bilenger et al. 2016), but a significant increase of toxic metals in the bottom water (e.g. Cu, Zn) will happen on short time scales (<day) possibly reaching lethal concentrations in the near field and cause accumulative effects further away on a longer run. This impact will vary from one deposit to another based on the differences in the geochemical inventory of the deposits (Hannington et al. 2005) but can be considered essential, as the spatial impact of SMS mining will be much smaller compared to Mn-nodule and sand and gravel extraction. As for these other two resources, hydro-acoustic mapping techniques paired with visual studies and direct sampling are the tools for evaluating the immediate and long-term impact of SMS mining.

References

- Baker E, Beaudoin Y (2013) Deep Sea Minerals: sea floor massive sulphides, a physical, biological, environmental, and technical review, SPC
- Baker ET, Resing JA, Haymon RM et al (2016) How many vent fields? New estimates of vent field populations on ocean ridges from precise mapping of hydrothermal discharge locations. *Earth Planet Sci Lett* 449:186–196
- Bilenger LD, Romano GY, McKibben MA (2016) Kinetics of sulfide mineral oxidation in seawater: implications for acid generation during in situ mining of seafloor hydrothermal vent deposits. *Appl Geochem* 75:20–31
- Boschen RE, Rowden AA, Clark MR et al (2013) Mining of deep-sea seafloor massive sulphides: a review of the deposits, their benthic communities, impacts from mining, regulatory frameworks and management strategies. *Ocean Coast Manag* 84:54–67
- Caress DW, Clague DA, Paduan JB et al (2012) Repeat bathymetric surveys at 1-metre resolution of lava flows erupted at axial seamount in April 2011. *Nat Geosci* 5:483–488
- Clague DA, Dreyer BM, Paduan JB et al (2014) Eruptive and tectonic history of the Endeavour Segment, Juan de Fuca Ridge, based on AUV mapping data and lava flow ages. *Geochem Geophys Geosyst* 15:3364–3391

- Collins M (2010) Offshore sand and gravel mining. *Mar Policy Econ A Deriv Encycl Ocean Sci* 265
- Cronan DS (1992) Marine minerals in exclusive economic zones. Springer, p 209
- Cruickshank M, Hess H (1978) Marine sand and gravel mining. Government Printing Office, Washington
- Föllmi B (1996) The phosphorus cycle, phosphogenesis and marine phosphate-rich deposits. *Earth Sci Rev* 40:55–124
- Greinert J (2015) RV SONNE Fahrbericht/Cruise Report SO242-1: JPI OCEANS Ecological Aspects of Deep-Sea Mining, DISCOL Revisited, Guayaquil-Guayaquil (Ecuador), 28 Aug–25 Sept 2015
- Hannington MD, de Ronde CD, Petersen S, (2005) Sea-floor tectonics and submarine hydrothermal systems. *Econ Geol 100th Anniv Vol* 111–141
- Hannington M, Petersen S, Krätschell A (2017) Subsea mining moves closer to shore. *Nature Geosci* 1–2
- Hein JR, Koschinsky, A (2013) Deep-ocean ferromanganese crusts and nodules. In: Holland HD, Tuerkian, KK (eds) *Treatise on geochemistry* (2nd edn) 11, Elsevier, pp 273–291
- Hein JR, Mizell K, Koschinsky A, Conrad TA (2013) Deep-ocean mineral deposits as a source of critical metals for high- and green-technology applications: comparison with land-based resources. *Ore Geol Rev* 51:1–14 <http://dx.doi.org/10.1016/j.oregeorev.2012.12.001>
- Ishiguro S, Yamauchi Y, Odaka H et al (2013) Development of mining element engineering test machine for operating in seafloor hydrothermal deposits. *Mitsubishi Heavy Ind Tech Rev* 50(2):21
- Jamieson JW, Claude DA, Hannington MD (2014) Hydrothermal sulfide accumulation along the Endeavour Segment, Juan de Fuca Ridge. *Earth Planet Sci Lett* 395:136–148
- Kotlinski R, Stoyanova V (1998) Physical, chemical, and geological changes of marine environment caused by the benthic impact experiment at the 10 M BIE Site. In: 8th International offshore and polar engineering conference, international society of offshore and polar engineers
- Kuhn T, Rühlemann C, Wiedicke-Hombach M et al (2011) Tiefseeförderung von Manganknollen. Schiff und Hafen 5:78–83
- Liu S, Hu J, Zhang R et al (2016) Development of mining technology and equipment for seafloor massive sulfide deposits. *Chin J Mech Eng* 29(5):863–870
- Madureira P, Brekke H, Cherkashov G et al (2016) Exploration of polymetallic nodules in the area: reporting practices, data management and transparency. *Marine Policy* 70:101–107
- Markussen JM (1994) Deep seabed mining and the environment: consequences, perceptions, and regulations. Citeseer 31–39
- Murton B (2000) A global review of non-living resources on the extended continental shelf. *Rev Bras de Geofi* 18(3). doi:[10.1590/S0102-261X2000000300007](https://doi.org/10.1590/S0102-261X2000000300007)
- Oebius HU, Becker HJ, Rolinski S et al (2001) Parametrization and evaluation of marine environmental impacts produced by Deep-Sea manganese nodule mining. *Deep Sea Res Part II* 48(17–18):3453–3467
- Padan J (1983) Offshore sand and gravel mining. In: Offshore technology conference
- Pearson JS (1975) Ocean floor mining. England Noyes Data Corporation, London
- Petersen S, Krätschell A, Augustin N et al (2016) News from the seabed—geological characteristics and resource potential of deep-sea mineral resources. *Mar Policy* 70:175–187
- Rona PA (2003) Resources of the sea floor. *Science* 299:673–674
- Rona PA (2008) The changing vision of marine minerals. *Ore Geol Rev* 33:618–666
- Rühlemann C, Kuhn T, Kasten S et al (2011) Current status of manganese nodule exploration in the German license area. In: 9th ISOPE ocean mining symposium, international society of offshore and polar engineers
- Sharma R (2001) Indian Deep-Sea environment experiment (INDEX): an appraisal. *Deep Sea Res Part II* 48(16):3295–3307
- Sharma R (2011) Deep-sea mining: Economic, technical, technological, and environmental considerations for sustainable development. *Mar Technol Soc J* 45(5):28–41

- Shirayama Y, Fukushima T (1997) Responses of a meiobenthos community to rapid sedimentation. In: Proceedings of the international symposium on environmental studies for Deep-Sea Mining
- Thiel H (2001) Use and protection of the deep sea—an introduction. *Deep-Sea Res II* 48:3427–3432
- Vanreusel A, Hilario A, Ribeiro PA et al (2016) Threatened by mining, polymetallic nodules are required to preserve abyssal epifauna. *Sci Rep* 6:26808
- Von Stackelberg U (2000) Manganese Nodules in the Peru Basin. In: Handbook of marine mineral deposits. CRC Press, Cronan DS, pp 197–238
- Yoshikawa S, Okino K, Asada M (2012) Geomorphological variations at hydrothermal sites in the southern Mariana Trough: relationship between hydrothermal activity and topographic characteristics. *Mar Geol* 303–306:172–182

Fishing Activities

Ferdinand K.J. Oberle, Pere Puig and Jacobo Martín

Abstract Unlike the major anthropogenic changes that terrestrial and coastal habitats underwent during the last centuries such as deforestation, river engineering, agricultural practices or urbanism, those occurring underwater are veiled from our eyes and have continued nearly unnoticed. Only recent advances in remote sensing and deep marine sampling technologies have revealed the extent and magnitude of the anthropogenic impacts to the seafloor. In particular, bottom trawling, a fishing technique consisting of dragging a net and fishing gear over the seafloor to capture bottom-dwelling living resources has gained attention among the scientific community, policy makers and the general public due to its destructive effects on the seabed. Trawling gear produces acute impacts on biota and the physical substratum of the seafloor by disrupting the sediment column structure, overturning boulders, resuspending sediments and imprinting deep scars on muddy bottoms. Also, the repetitive passage of trawling gear over the same areas creates long-lasting, cumulative impacts that modify the cohesiveness and texture of sediments. It can be asserted nowadays that due to its recurrence, mobility and wide geographical extent, industrial trawling has become a major force driving seafloor change and affecting not only its physical integrity on short spatial scales but also imprinting measurable modifications to the geomorphology of entire continental margins.

F.K.J. Oberle (✉)

US Geological Survey—Pacific Coastal and Marine Science Center,
2885 Mission Street, Santa Cruz, CA 95060, USA
e-mail: foberle@usgs.gov

P. Puig

Institut de Ciències del Mar (ICM-CSIC), Passeig Marítim de la Barceloneta,
37-49, 08003 Barcelona, Spain
e-mail: ppuig@icm.csic.es

J. Martín

Laboratorio de Oceanografía y Procesos Hidrosedimentarios,
Centro Austral de Investigaciones Científicas (CADIC-CONICET),
Bernardo Houssay 200, V9410CAB Ushuaia, Tierra del Fuego, Argentina
e-mail: jmartin@cadic-conicet.gob.ar

1 Introduction

In the analyses of anthropogenic factors affecting the seabed and geomorphology of continental shelves and slopes, bottom trawling has been shown to be a very important factor to consider (Barnes and Thomas 2005; Halpern et al. 2008; Martín et al. 2014b; Oberle et al. 2016a; Puig et al. 2012). In fact, Benn et al. (2010) and Eastwood et al. (2007) have concluded that by comparison to other offshore human activities that also impact the seafloor, such as waste discharge and dumping, mining, cable installation or warfare, the contribution of bottom trawling to the disturbance of the seafloor is notably higher than all other anthropogenic stressors combined.

The widespread and intensive use of towed bottom-fishing gears on the continental shelves and slopes of the world has generated much debate about its sustainability, and several studies have highlighted the direct and indirect impacts of this activity over the ecosystems and living resources (Jones 1992; Thrush et al. 1995; Watling and Norse 1998; Freese et al. 1999; Thrush and Dayton 2002). Reviews of the impacts by bottom trawling and dredging on the benthic habitats and on the seafloor also exist in the scientific literature (Rester 2000; Johnson et al. 2002; Martín et al. 2014b; O'Neill and Ivanović 2016). This chapter summarizes the impacts of fishing activities on the sediments and seabed structure, with a particular emphasis on the consequences of this human practice on the morphology of submarine landforms.

The direct physical effects of dragging bottom trawling gear over the seafloor includes not only the scraping and plowing of the seafloor, but also the resuspension of sediment with an associated significant increase in near-bottom turbidity (e.g., Dellapenna et al. 2006; Durrieu de Madron et al. 2005; Jones 1992; Martín et al. 2014c; O'Neill and Summerbell 2011; Palanques et al. 2001, 2014; Pilskaln et al. 1998). Furthermore, these effects can cause alterations in surface sediment properties and sedimentary budgets (e.g., Martín et al. 2008, 2014a; Oberle et al. 2016a; Puig et al. 2015), ultimately leading to a potentially dramatic modification of the submarine geomorphology, both at small and large spatial scales (e.g., de Groot 1984; DeAlteris et al. 1999; Friedlander et al. 1999; Puig et al. 2012; Roberts et al. 2006).

For a complete evaluation of the impact of bottom trawling on submarine geomorphology the history of bottom trawling (see Sect. 1.1) and its present spatial distribution and frequency (Sect. 2.1) have to be considered. The geomorphological impact of bottom trawling can be subdivided into the detrital impacts to the water column (Sect. 2.2), the lithological (Sect. 2.3) and geochemical seabed changes (Sect. 2.4), the chemical changes in the water column (Sect. 2.5), the effects on biota (Sect. 2.6), and finally, the cumulative effects of these subdivisions recorded by the changes in soft sediment seascapes (Sect. 2.7) and impacts to reefs and other biogenic seascapes (Sect. 2.8).

1.1 A Brief History

Throughout the history and prehistory of mankind, fishing techniques have evolved from simple hunter-gatherer schemes to a present-day fishing industry of such a power and size that it has pushed many fishing stocks to the border of commercial extinction (Pauly et al. 2002). Detailed information on bottom fishing methods and equipment can be found in e.g. von Brandt (2005), Sainsbury (1996) or Smolowitz (1998). Ways of harvesting fish at the coasts and the open sea vary widely, and a number of them are designed to target species living on or close to the bottom and hence have the potential to disturb the seafloor. Among these techniques, caging, gillnetting and some types of near-bottom long-lining can be quoted as fishing devices in contact with the bottom but not exerting substantial damage to the physical substratum or only during deployment/retrieval operations, when the nets and anchoring systems can be briefly dragged along the bottom. On the other hand, fishing gear included within the broad term “bottom trawling” consist of heavy devices which are actively dragged along the seafloor for a sustained period of time, thus exerting a significant disturbance on the seabed.

While industrial bottom trawling has dominated globally since the 1960s (Watson et al. 2006), a significantly more rudimentary form of bottom trawling (Fig. 1) has been around since the 14th century. The earliest known report on bottom trawling was an environmental complaint to King Edward III in 1376:

[...] and that the great and long iron of the wondyrechaun [bottom trawl] runs so heavily and hardly over the ground when fishing that it destroys the flowers of the land below water there [...] The fishermen take such quantity of small fish [...] [causing] a great damage of the commons of the realm and the destruction of the fisheries. (Roberts 2007)

Bottom trawling does not only have a long tradition in European waters. It was also recognized in 1704 during the Edo era in Japan as a common fishing method. A slightly different approach was developed where the “Utase Ami” “trawled bottom net” was deployed from a sideways sailing boat (Nakamura and Ourakami 1900) (Fig. 1).

Considering the fact that an argument about the impacts of bottom trawling on benthic organisms was raised over 600 years ago, it is surprising how little is yet known about the cumulative effects on the seafloor. Watling et al. (2014) showed that only approximately 250 original research papers exist in total, with almost all of them addressing the effects on biota and very few (10–20%) concerning themselves with the many aspects of seabed sediment alteration or geomorphic change.

In the mid 19th century the Industrial Revolution in Northern Europe brought about a quantum leap for fishing industries that quickly spread all over the world. The development of the steam engine allowed fishing vessels to have a much larger range offshore than ever before. As a result, bottom trawling was no longer limited to close-shore activities (<100 m depth) but could now extend across the entire shelf. With the inception of the diesel engine in the 20th century the cruising range was further advanced into deeper waters, and by the 1980s bottom trawling was

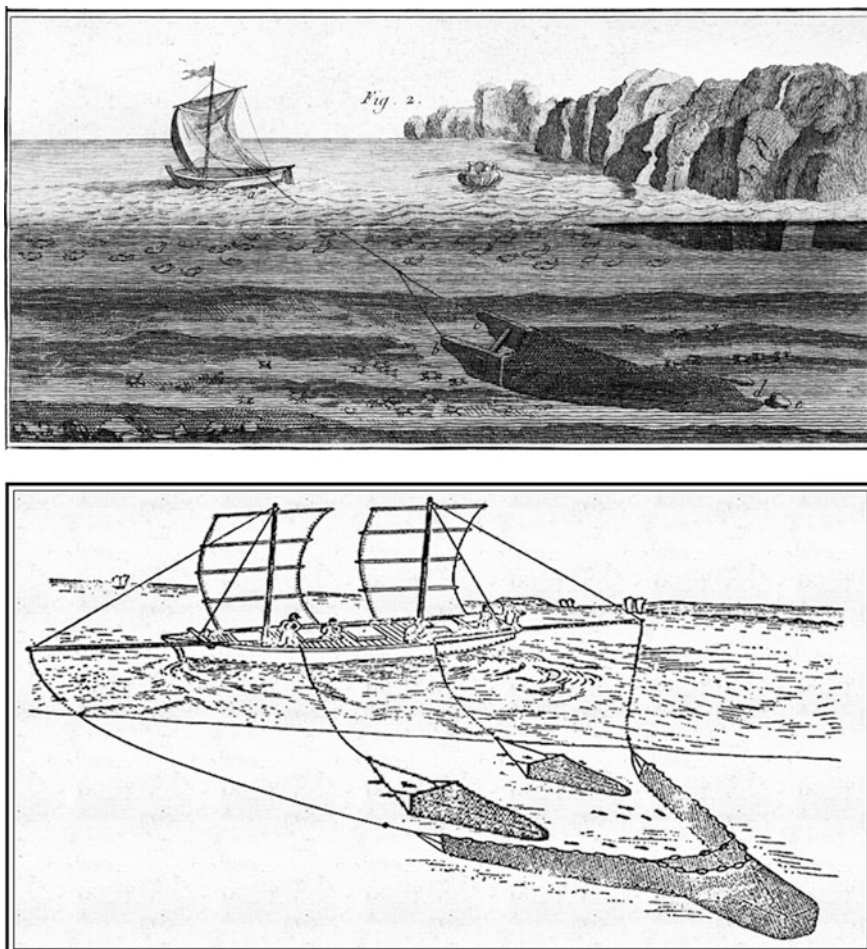


Fig. 1 Upper Entry in French encyclopaedia from 1771 (Diderot and D'Alembert 1771). Lower Japanese “Utase Ami” have been in use almost unchanged for the last 300 years (Jonsson 1967; Tadashino 2016)

becoming a global, nearly depth-unlimited endeavour (Martín et al. 2014b). Currently, the race for deep-sea trawling is expanding each year, with bottom trawling occurring far beyond 1000 m depth (Morato et al. 2006; Williams et al. 2011).

In this chapter bottom trawling refers only to fishing gear that has been categorized as either otter trawls, beam trawls, demersal seines or dredges (Fig. 2). O’Neill and Summerbell (2016) have shown that the individual gear components designed to spread the fishing gear (otter doors, sweeps and seine ropes), maintain contact with the seabed (otter doors, beamtrawl shoes, groundgear etc.), protect the gear from the seabed (groundgear and seine ropes), and ensure the gear fishes

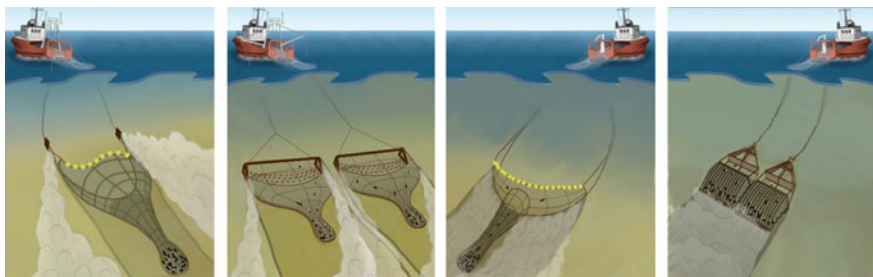


Fig. 2 Bottom trawling types (*left to right*): Otter board trawl, beam trawl, demersal seine trawl and scallop dredges, respectively. In general, ground gear (ground ropes, sweeps and net) penetrates less deep into the seabed but causes wider disturbance than trawling doors and sleds

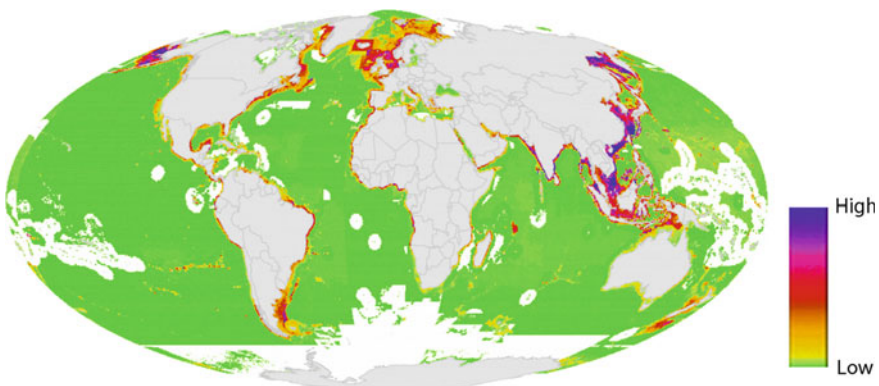


Fig. 3 Global distribution and relative intensity of ground penetrating fishing activities (modified from Halpern et al. 2008; Oberle et al. 2016a; Puig et al. 2012)

efficiently (tickler chains, dredge teeth etc.), have seabed altering effects of varying magnitude. Valdemarsen et al. (2007) and Martín et al. (2014b) give detailed overviews of the different gear types, their ability to disturb the submarine terrain.

Today, bottom trawling is a worldwide and common fishing technique that accounts for approximately 23% of all commercially sold fish (FAO 2009), with most fish being harvested on the continental shelf (Watson et al. 2006). The most recent calculation of the total global bottom trawled area is 22.36 million km² (Halpern et al. 2008) with 13.67 million km² occurring on the soft sediments of the shelf (Oberle et al. 2016a), 4.40 million km² on the slope (Puig et al. 2012) and roughly 4.29 million km² in areas deeper than the slope (Fig. 3). However, all of these calculations may have an unknown error associated with them as they are at least partially derived from the catch rate (Mt) per area (km²). More advanced ways to calculate the spatial distribution of bottom trawling efforts have recently been developed using vessel mounted GPS tracking systems.

2 Results

2.1 Spatial Distribution and Frequency of Bottom Trawling Efforts

Essential to the evaluation of the impact of bottom trawling on submarine geomorphology is the knowledge of its spatial distribution and frequency. When evaluating bottom trawling-induced changes to the natural environment, the frequency with which impacts to the seabed occur must be known for the accurate interpretation of environmental data. An accurate evaluation of the number of times the seabed is impacted is a meaningful indicator of the environmental pressure on benthic diversity and biomass (Queirós et al. 2006; Thrush and Dayton 2002) as well as the backbone of any evaluation of sediment resuspension and geomorphic change. Following the EU Marine Strategy Framework Directive (European Parliament 2008), a number of studies have attempted to quantify the frequency with which the seafloor is trawled through the use of a GPS-based Vessel Monitoring System (VMS) (Eastwood et al. 2007; Stelzenmuller et al. 2008; Gerritsen et al. 2013). Fishing intensity was deducted in previous studies by one of two methods: point summation or track interpolation. Point summation is based on summing the swept areas associated with each VMS point in a defined cell. Point summation can be flawed because the estimate of fishing intensity is based on the number of records within a geographic cell (Diesing et al. 2013; Lambert et al. 2011; Murawski et al. 2005; Piet and Hintzen 2012; Piet and Quirijns 2009; Gerritsen et al. 2013). The cell size is variable and arbitrary, thus making smaller grid cells more likely to be free of trawling activity than larger cells. Also, the area-percentile of an affected cell cannot be accurately deducted, making larger cells more likely to be less affected than smaller cells. Track interpolation, on the other hand, reconstructs vessel tracks between data points. Although track interpolation can be imperfect with VMS points because the data reporting frequency of 2-h results exhibit potentially high deviation from the real vessel track (Skaar et al. 2011; Lambert et al. 2012), the recently developed and globally used Automatic Identification System (AIS) records GPS points every 6 s, thereby allowing for accurate determination of the vessel track using straight line interpolation (Oberle et al. 2016a).

Regional studies that were based on point summation methods or log books have yielded estimates of the frequency with which seabed impact occurs. To name a few examples, the total fished seafloor is disturbed at least once per year on the New England shelf (Pilskaln et al. 1998), three times per year in the Gulf of Mexico, roughly every 2 years for all Alaskan fishing areas (Bering Sea, Aleutian Islands and Gulf of Alaska), every three years for the California shelf and slope, and roughly every four years for the fishing areas off of the Oregon and Washington coasts (NRC 2002). Similarly, the frequency of disturbance is roughly once per year for the fished seafloor of the United Kingdom (Foden et al. 2010), and roughly more than 4 times per year for large areas of the continental shelf of the Bay of

Biscay (Mengual et al. 2016). An exemplary, in-depth study of the footprint of bottom trawling carried out by the government of New Zealand shows that most fishing areas off New Zealand are impacted at least once per year (Black and Tilney 2015). Oberle et al. (2016a) have shown that for the NW Iberian shelf a mean trawling frequency of about 6 times per year occurs over the AIS covered area. It is important to keep in mind that these are average bottom trawling frequencies over large areas, and closer analysis of the statistical data shows that many subareas, for example, of the Gulf of Mexico, were swept more than 70 times per year, or not at all (NRC 2002). Similarly, while some areas off the Cumbrian coast in the UK were trawled more than 20 times per year (Hinz et al. 2009) or even up to 84 times per year on the NW Iberian shelf (Oberle et al. 2016a), many such areas experienced bottom trawling impacts of less than once per year (ICES 2015). In the Mediterranean Sea most of the trawl fleets operate at short distance from the coast and need to return to harbours every day, and therefore, their mobility patterns are recursive, visiting the same areas periodically, in occasions on a daily basis (Puig et al. 2012).

Although AIS data have been widely available, this interpolation approach has only very recently been applied to determine bottom trawling effort (Oberle et al. 2016a, b; de Souza et al. 2016). Today profound developments in the real-time analysis of AIS data are making fast advances on a global scale to identify fishing locations and efforts (Witkin et al. 2016). While the leading public database for fishing effort analysis (<http://globalfishingwatch.org>) does not yet involve the differentiation of fishing gear types, plans are in place to make these differentiations available to the public in the near future (personal communication with Oceana, (<http://oceana.org>) 2016). When examining regional or global spatial distributions of fishing activities it is important to keep in mind that the relative stress on the seafloor from bottom trawling may not just depend on the gear type and the frequency of trawling alone, but also on how naturally disturbed an ecosystem is. For example, high disturbance ecosystems (i.e. coastal areas subject to the recurrent influence of tidal currents or storm waves) should be more resilient to high-frequency or high-intensity bottom trawling activities than low disturbance ecosystems (i.e. most deep-sea environments).

2.2 *Bottom Trawling Affected Sediment Transport*

Together with the natural transport mechanisms (e.g., currents and waves), bottom trawling has been shown to cause measurable resuspension and sediment transport alterations. The scale of the sediment advection effect of bottom trawling can be seen from space in satellite images that show large sediment plumes trailing behind bottom trawlers (Fig. 4).

An early study by Churchill (1989) produced a theoretical model for different sediment types that defines the sediment resuspension rate on the towing speed and depth and width of the bottom trawling door track of the fishing gear. The author

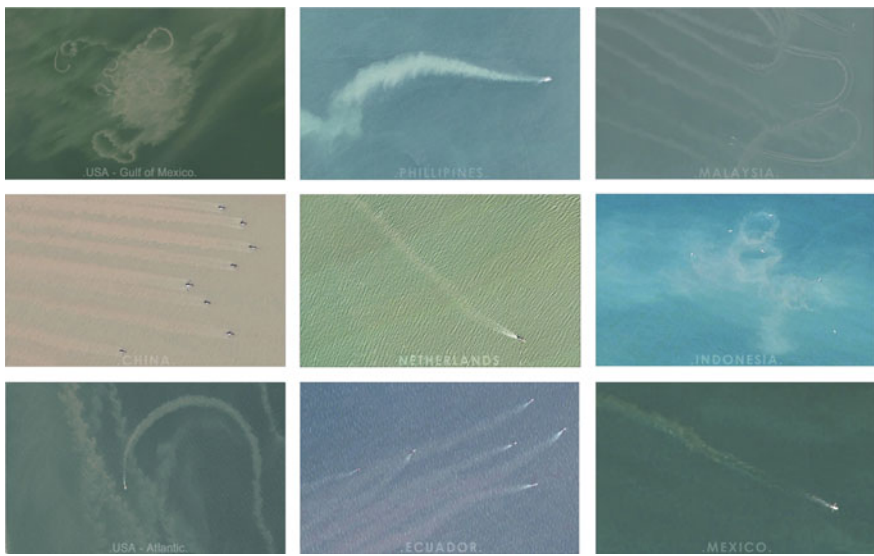


Fig. 4 Satellite bottom trawling imagery from eight countries. Sediment plumes in the wake of bottom trawlers can be seen at the ocean surface in water depths ranging from 2 to 68 m (photo courtesy USDA and Skytruth 2008)

concluded that enormous amounts of *more than 100 kg of resuspended material per second per ship* could be produced and that bottom trawling induced sediment resuspension could be a primary source of suspended sediment over the outer shelf of New England. However, measuring the combined off-shelf or off-slope sediment transport for wave-, current- and bottom trawling-induced resuspension is difficult because each shelf has its own wave climate, current regime, seabed sediment cover and bottom trawling frequency. Determining these factors for an entire fishing region requires the integration of numerous studies, including many that require in situ measurements on the seabed. In general, the most important component of accurately calculating suspended sediment transport is that the net current has to be integrated over time (to account for factors such as tidal movement). There are very few studies (Churchill 1989; Ferré et al. 2008; Oberle et al. 2016a; Mengual et al. 2016) which have attempted to do this and produced source-to-sink sediment budgets that include bottom trawling-induced transport. For the Gulf of Lion, a modelling study by Ferré et al. (2008) concluded that bottom trawling-induced resuspension causes one-third of the total off-shelf export of suspended sediment. Mengual et al. (2016) recently calculated that in the Bay of Biscay bottom trawling can be the prime source of sediment resuspension during the main fishing season but only makes up a small fraction compared to annual storm induced resuspension. Calculations for the NW Iberian shelf by Oberle et al. (2016a) suggest that over long time scales bottom trawling can have a six-fold increase in off-shelf sediment transport over natural processes. Similar predictions, where bottom trawling

exceeded wave induced sediment resuspension, were determined for the Gulf of Maine (Pilskaln et al. 1998), the partly enclosed Kattegat Sea (Floderus and Pihl 1990), and the Ebro shelf (Palanques et al. 2014). Other studies including Dellapenna et al. (2006) in Galveston Bay, Dounas (2006), Dounas et al. (2007) in Heraklion Bay, and Durrieu de Madron et al. (2005) in the Gulf of Lion, have attempted to compare the effect of natural and anthropogenic sediment resuspension without calculating off-shelf or off-slope transport budgets. Palanques et al. (2001) discovered that the effect of bottom trawling in the Barcelona inner shelf was mainly localized around the trawling tracks due to a very low net transport resultant of the local currents.

O'Neill and Summerbell produced the most recent studies that precisely quantified the resuspended mass of seabed sediment from fine sand to coarse silt, indicating that bottom trawling-induced sediment resuspension was largely dependent on sediment size and hydrodynamic drag (O'Neill and Summerbell 2011, 2016; O'Neill et al. 2013). One of the most important findings of these studies, that stands in stark contrast to previous assumptions, is that the weight of the fishing gear does not influence the amount of sediment put into the water column (O'Neill and Summerbell 2016). Utilizing the existing erosion rate estimates available in the literature (Churchill 1989; Durrieu de Madron et al. 2005; Dellapenna et al. 2006; Dounas et al. 2007; O'Neill and Summerbell 2011), Oberle et al. (2016a) have recently proposed a general formulation of trawling-induced resuspension rates as a function of the seabed composition (i.e. grain size-specific substrate type, average silt and clay content) (Fig. 5). Combining this calculation with global soft-sediment distribution data on all continental shelves and worldwide bottom trawling intensity estimates, Oberle et al. (2016a) showed that bottom trawling-induced resuspended sediment mass amounts to $21.87 \text{ Gt year}^{-1}$, approximately the same as the sediment mass supplied to the continental shelves through the world's rivers. It is important to remember, however, that the accuracy of this approach depends on the precise measurements of sediment put into the water column in the wake of different gear, and would therefore greatly benefit from further refining studies. Ideally this would be done as a legal requirement by the manufacturers of the fishing gear, similar to requirements for carbon dioxide emissions studies in the automobile industry.

A common conclusion of all relevant studies was that bottom trawling had a measurable impact on sediment resuspension compared to natural forces and that these effects were likely more profound in deeper environments below the wave base. Martín et al. (2014b) and Diesing et al. (2013) conclude that artificial perturbations on the sea floor leave more acute and long-lasting imprints with increasing water depth because water depth and the natural level of physical disturbance upon the seabed are inversely related.

Multiple studies have shown that sediment resuspended by bottom trawling is incorporated in the bottom nepheloid layer and transported across and along the shelf, potentially resulting in sediment transport efficiencies that are nine times higher than during periods without trawling (i.e., during the closed season) (Pilskaln et al. 1998; Palanques et al. 2014). These accounts also may help give

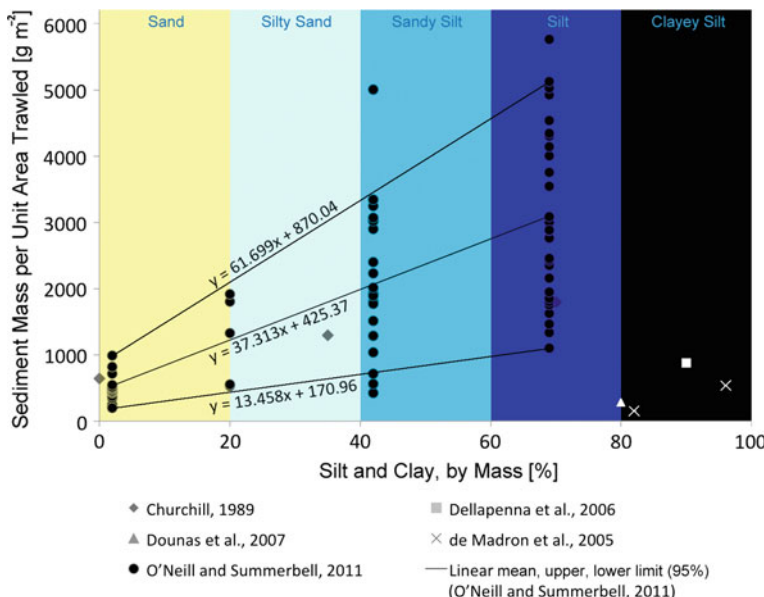


Fig. 5 Resuspended sediment per unit trawled area with respect to grain size-specific substrate type and average percent silt and clay content. Linear functions are fitted to the sand to silt data. The excursion of the clayey silt data (white symbols) is attributed to the greater cohesive forces

credit to numerous reports where the shifting of the so-called mud-line (outer limit of highly turbid waters in estuaries and coastal areas) progressively offshore was associated with bottom trawling (Caddy 1973; Black and Parry 1999). In general, many studies have seen shifts in sediment grain size distribution as the larger grain sizes drop out of resuspension significantly faster than smaller grain sizes. As sediments are resuspended by trawling gears and under certain conditions exported to other (generally deeper) locations, the next questions to pose is where do the advected particles resettle and if this artificial redistribution of sediments can define erosion and net deposition areas distinguishable above natural baselines. Very little literature exists on this particular subject.

A dramatic case of trawling-induced relocation of sediments takes place when trawling is carried out along steep gradients such as those found in submarine canyon flanks. Studies conducted in La Fonera (or Palamós) Canyon (NW Mediterranean) documented that part of the resuspended sediments are transported by downslope-flowing sediment-laden flows (Palanques et al. 2006; Martín et al. 2014c; Puig et al. 2012). Such trawling-induced sediment gravity flows reached maximum downslope velocities of up to 38 cm s^{-1} and concentrations of more than 200 mg/l near the bottom (5 m above). Instantaneous sediment fluxes up to $34 \text{ g m}^2 \text{s}^{-1}$ were calculated and the sediment transport integrated in the first 50 m above the bottom yielded a minimum of 5.4×10^3 metrical tons of sediment exported from the fishing ground in the 136 days of the experimental deployment. These

resuspended particles are subsequently accumulated along the canyon axis down to 1700 m water depth, and have generated an anthropogenic depocenter with recent accumulation rates $\sim 2.4 \text{ cm year}^{-1}$, one order of magnitude higher than the natural (i.e., pre-1970s) rates, before the rapid industrialization of the local trawling fleet (Martín et al. 2008; Puig et al. 2015). No submarine canyon in the world has been studied as intensively as La Fonera Canyon for the effects of bottom fishing gear, but given that canyons are often targeted by fisheries, it is likely that similar and other impacts have occurred and are occurring in other canyons elsewhere in the world. In Whittard Canyon (NE Atlantic), unusual peaks in nepheloid layers with much higher concentrations of suspended particulate matter than normal have been observed, and with the use of VMS data those could be also linked to trawling activity (Wilson et al. 2015).

2.3 *Lithological Effects of Bottom Trawling*

Although a pioneering study by Schwinghamer et al. (1996) using sediment acoustic methods indicated that bottom trawling decreased the complexity of the seabed sediment and a small experimental study by Mayer et al. (1991) exhibited how bottom trawling can cause sediment mixing, there are very few studies that specifically address the lithological alterations from bottom trawling. Underwater photography has documented that bottom trawling leaves significant trawling marks in all substrates, from mud to rock (Fig. 6). The fact that the structure of the seabed (e.g., porosity, grain size, water content) not only strongly influences the benthic community structure (Ellingsen 2002) but also many fish species (Auster et al. 1997) underlines the necessity of better understanding bottom trawling-induced lithological seabed changes.

Although it has been widely recognized that bottom trawling can leave behind durable seabed trawl marks (Friedlander et al. 1999), the depth of the trawling impact to the seabed is a matter of debate. Some reviews have concluded that bottom trawling on soft sediments (mud–sand) is limited to the top centimeters (Lokkeborg 2005) or can reach up to 30 cm (Linnane et al. 2000; Oberle et al. 2016b) while others (Andersson and Jonsson 2003) have reported trawl marks as deep as 1 m. Early reviews have suggested that on sandy bottoms, the bottom trawling tracks are short-lived, whereas on mud bottoms, the tracks are deeper and last longer (DeAlteris et al. 2000). However, this is a broad oversimplification that does not take into account differences in natural sediment dynamics. A more in-depth analysis of the relative persistence of trawl marks (Johnson et al. 2002) indicated that on both muddy and sandy bottoms, trawl marks can still be identified one year later (Schwinghamer et al. 1998; Tuck et al. 1998). The few existing studies that have investigated the modified sedimentary structure and texture of the seabed have classified their results as either “trawled” or “untrawled” (e.g., Bhagirathan et al. 2010; Brown et al. 2005; Dellapenna et al. 2006; Hixon and Tissot 2007; Palanques et al. 2014; Simpson and Watling 2006). A commonly



Fig. 6 Underwater photography of bottom trawling effects. *Upper row* Trawling doors and a fishing net ploughing the seabed and resuspending sediment. *Middle row (left to right)* Trawling marks in mud, sandy and gravel, coralline, and bedrock substrate. *Lower row (left to right)* Gently undulating, wavy, jagged, and deeply incised (0.5 m deep) seabed surfaces. Photo courtesy from *upper left to lower right*: Main and Sangster (1981), Crown (1989), Montaigne and Skerry (2007), Vinson (2013), Ocean Network Canada (2012), Fossa (2013), Horn (2005), Waller (2013), Jørgensen (2013), NIWA (2010), CRG (2012), Hopkins (2004)

observed effect of trawling is the sorting of sediment grains as they are repeatedly resuspended and the lighter fractions being more easily advected with water currents, while heavier particles tend to settle back more quickly. However, studies focusing on bottom trawling-induced changes to sediment texture have returned conflicting results, ranging from no effects (Bhagirathan et al. 2010; Dellapenna et al. 2006; Oberle et al. 2016b) to major winnowing effects (Ferré et al. 2008; Oberle et al. 2016b; Palanques et al. 2001, 2014) sometimes reported as a bed armouring process (Martín et al. 2014a). Bottom-trawling effects on the porosity of sediments have also shown inconsistent results with some studies reporting no changes (e.g., Percival 2004; Simpson and Watling 2006) and others reporting a significant compaction of trawled sediments (e.g., Pusceddu et al. 2014; Schwinghamer et al. 1998). One of the largest challenges in the assessment of bottom trawling-induced lithological changes to the seabed stems from the fact that sufficiently large control sites under similar hydrographic and geologic conditions are becoming increasingly rare on the shelf (Halpern et al. 2008; Watson et al. 2006), thus making comparisons to natural states progressively more difficult.

Martín et al. (2014a) analyzed ^{210}Pb in sediment cores collected at trawled and untrawled sites along the flanks of La Fonera Canyon. At the untrawled sites, excess ^{210}Pb inventories were relatively high and the vertical profiles exhibited a three-layered vertical profile characteristic of depositional systems, including a 5–10 cm topmost bioturbated layer of very low density, a region of exponential ^{210}Pb decay and increasing dry bulk densities with depth and a deep layer of constant (supported) ^{210}Pb concentration. In contrast, at most trawled sites, ^{210}Pb inventories, surface concentrations and vertical profiles showed evidence of erosion or thorough mixing. The topmost sediments poorest in excess ^{210}Pb were also very dense and compacted, as the uncovering of long-buried, old sediments. Martin et al. (2014a) concluded that the trawled flanks of La Fonera Canyon are denuded of recent sediments by the frequent sediment flows triggered by trawling gear.

Going beyond a classification of “trawled” or “untrawled” a recent study on bottom trawling-induced lithological change has documented a range of seabed

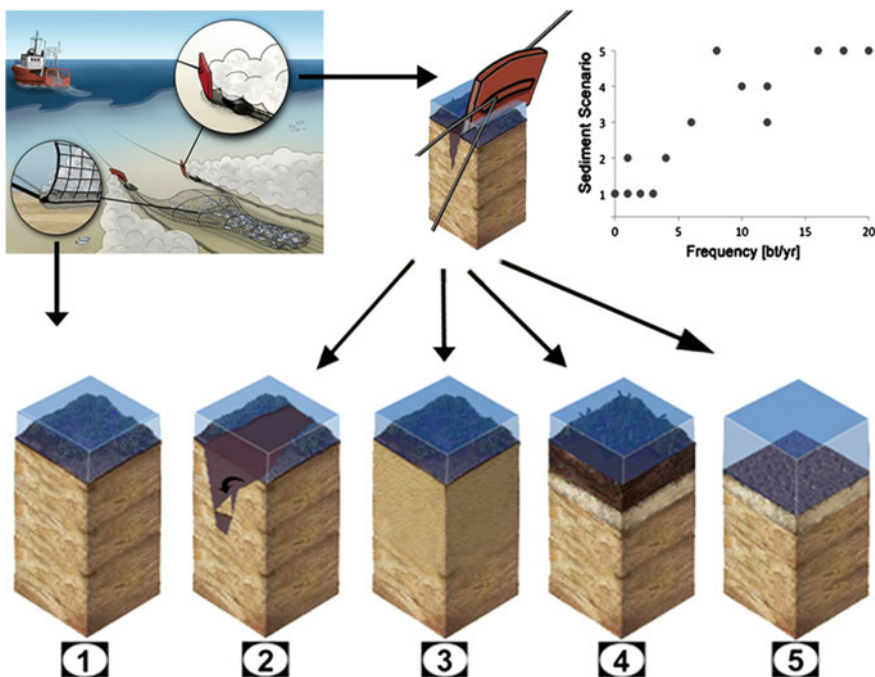


Fig. 7 Five conceptual scenarios describing the potential effects of bottom trawling on the seabed sediment structure: (1) minimal effect; (2) groove with sediment overturning and elevated sidewalls; (3) complete mixing; (4) material re-sorting and layering; (5) grain size dependent material winnowing with mud extraction. *Upper right* 7 Bottom trawling induced seabed sediment disturbance scenarios (1–5) related to bottom trawling frequency (modified from Oberle et al. 2016b)

alterations and has classified them in accordance with how often the seabed was disturbed by bottom trawlers (Fig. 7). The study found that each lithological state or scenario is strongly dependent on the bottom trawling frequency in combination with natural bottom current conditions. Most described scenarios include significant seabed disturbances and are thus likely to have a profound environmental impact on seabed geochemistry, benthic organisms and, indirectly, higher trophic levels (Oberle et al. 2016b).

Scenario 1: No sediment mixing, very low sediment alteration.

Only the surficial mud is marginally resuspended but settles immediately on-site without significant transport or sorting. Sand and gravel may be physically moved minimally in a horizontal direction but are not mixed vertically. There are negligible stratigraphic environmental consequences, probably owing only to the impact of the trawling net, sweeplines and other relatively light components of the trawling gear but not to heavy elements such as trawling doors or tickler chains.

Scenario 2: Sediment overturning, minor mixing but without sediment depletion, medium sediment alteration.

Bottom trawling causes ploughing of sediments that can potentially lead to overturning of coherent sediment packages associated with relatively minor overall sediment mixing. Resuspension and component re-partitioning are quantitatively minor. Consequently, the physical properties might remain largely unchanged while the natural succession is largely destroyed. Sessile organisms can be affected and dissolved matter can be injected into the water column.

Scenario 3: Full sediment mixing but without material depletion, medium to high sediment alteration.

Bottom trawling leads to a full disturbance and mixing of the sub-bottom sediments, but resuspension and material re-grading are quantitatively minor. Consequently, the physical properties might remain largely unchanged while the natural succession is completely destroyed. Sessile organisms should be affected and dissolved matter injected into the water column.

Scenario 4: Full sediment mixing and on-site resettling of fines leading to secondary layering, high sediment alteration.

The sediment is fully mixed, the coarse particles remain at the seafloor but large portions of the fine fraction are brought into suspension. Due to rapid re-settling of the suspended material and calm hydrodynamic conditions, the succession shows no gross material depletion but a secondary fining-upward gradation. The surface composition is thus altered toward a more fine-grained habitat and dissolved matter is injected into the water column.

Scenario 5: Full sediment mixing and resuspension of fines with grain size selective lateral export, very high sediment alteration.

Bottom trawling causes vertical disturbance of the stratigraphic succession. The mud fraction is intensively re-suspended and transported away by the prevailing bottom current regime. A long-term enrichment in coarse-grained seabed surfaces is the consequence, thus changing the ecological habitat drastically. Dissolved matter is completely released into the water column.

2.4 *Geochemical Effects of Bottom Trawling to the Seabed Sediment*

Essential ecosystem functions in soft-sediment environments rely on biogeochemical processes associated with remineralization of organic substrates and the recycling of nutrients (Olsgard et al. 2008). These biochemical processes are an essential factor for the three dimensional structures built and inhabited by benthic organisms and consequently also an influential aspect of the geomorphology of the seabed. The primary bottom trawling-induced geochemical changes of seabed sediment come from the alteration of oxygen content (Collie et al. 2000) and macrobenthic irrigation activity (Trimmer et al. 2005). The quantity and quality of available organic matter are recognized to be major factors affecting benthic ecosystems (Olsgard et al. 2008). A recent summary on the limited existing research on seabed carbon alterations (Martín et al. 2014b) indicates that there are large discrepancies between studies resulting in both decreases (e.g., Bhagirathan et al. 2010) and increases (e.g., Palanques et al. 2014) of organic carbon. Regardless of these discrepancies, it is likely that the long-term result of chronic sediment mixing by bottom trawling causes a reduction in organic carbon because remineralization efficiency is highest when sediments go through alternating cycles of aerobic and anaerobic conditions (Hulthe et al. 1998). Furthermore, soft-sediment seafloor habitats maintain microbially and benthically mediated denitrification, a critical ecosystem function that helps buffer against eutrophication. Other studies (Olsgard et al. 2008) indicate that the effect of bottom-trawling nitrogen cycling depends on which species is more effected by bottom trawling. Although bioturbators that bulldoze through the sediment cause a nitrogen reduction in sediment, benthic organisms that irrigate burrows increase nitrogen content. Consequently, it remains unclear whether the seabed acts as a nitrogen sink or source unless relative species abundance and activity are known. Several studies indicated that the direction of nitrate and phosphate fluxes changed from moving into untrawled seabed sediments to emitting out of them (ICES 1992; Percival 2004). While little is known about the specific effects of bottom trawling on nitrate, phosphate, and silicate sediment cycling, macrofaunal abundance appears to be a major determining factor (Aller 1982; Hooper et al. 2005; Olsgard et al. 2008). Another important aspect of bottom trawling-induced chemical changes in seabed sediments was identified as increased ^{210}Pb (lead) content in trawled sediments, which was attributed to the compacting effect of bottom trawling (Pusceddu et al. 2014). This is a potentially important factor not commonly considered in ^{210}Pb geochronology on the shelf.

2.5 *Geochemical Effects of Bottom Trawling to the Water Column*

Although the subject of trawling-induced changes in the water column remains largely unexplored territory, a few studies suggest that bottom trawling can both

resuspend and bury biologically recyclable organic material, changing the flow of nutrients and carbon through the food web (Mayer et al. 1991) and thereby alter geomorphological landscapes. Pilskaln et al. (1998) suggested that half of the nutrient quantities in the water column on most continental shelves typically come from a steady influx of organic material decaying in the sediment. Olsgard et al. (2008) suggests that the trawling-induced nutrient flux changes from chronic and widespread seabed disturbance are potentially large enough to significantly interfere with global nutrient cycles. Consequently, it is generally thought that the resuspension of sediments by bottom trawling causes a large pulse of nutrients and micronutrients into the water column, similar to the observed sediment resuspending effect of large storms. Fanning et al. (1982), for example, reported that within a storm's track, in waters depths of 70 m, 1 mm of remobilized sediment was able to triple the nutrient levels in the photic zone. Similarly, Duplisea et al. (2001) calculated that a single trawler passage of approximately 0.27 km² to a depth of ca. 6 cm, can increase nutrient levels up to 30 times on average over the ambient undisturbed sediment nutrient flux. However, in general, there are very few studies that have directly measured the potential of bottom trawling to alter nutrient budgets in the water column (Durrieu de Madron et al. 2005; Dounas 2006; Dounas et al. 2007). The mechanical resuspension of sediments causes sediment plumes up to 10 m above the seabed (Churchill 1989; Durrieu de Madron et al. 2005; O'Neill and Summerbell 2011; O'Neill et al. 2013), which prolongs the exposure of sedimentary organic matter to oxic conditions. Dounas et al. (2007) found that this ultimately accelerates the mineralization process and increases nitrogen availability, leading to greater amounts of phytoplankton production if these advected nutrients can reach the photic zone. It remains to be determined whether this could shift the balance of higher trophic levels. Bottom trawling activity has also been correlated to hypoxia at mid-slope depth, which in turn was associated with a reshaping of the benthic megafauna community structure (De Leo et al. 2016). Multiple large-scale reviews (NRC 2002; ICES 2006) have noted that there is a great need for further studies that properly examine the effects of nutrient remobilization. Finally, it has also been shown that bottom trawling can reactivate bioavailable industrial contaminants from the seabed by advecting them into the water column and spreading them with the prevailing currents (Bradshaw et al. 2012). Large-scale closures of bottom trawling activities over entire shelves have, in the past, been sanctioned to avoid the spread of contaminants. This is most regularly seen after large oil spills, where heavy oil settles on the seabed. Examples of such closures include the NW Iberian shelf in 2002 after the *Prestige* oil spill (Punzón et al. 2009) and the W Florida and Louisiana shelf after the Deep Water Horizon Oil spill (NOAA 2010).

2.6 Effects of Bottom Trawling on Biota

The widespread disturbance of seabed sediments by bottom trawling has been recognized to have significant impacts to the benthic biota and their communities

living on the shelf. Benthic organisms can have a large impact on the sediment transport processes on the shelf by resuspending sediments (Cadée 2001), altering seabed roughness (Huettel and Gust 1992), and creating internal seabed structures and secretions that can stabilize sediments (Jumars and Nowell 1984). Two previously published meta-studies by Kaiser and Clarke (2006) and Collie et al. (2000), as well as three agency meta-studies by Lokkeborg (2005), Hopkins (2004) and Linnane et al. (2000), make clear that the state of knowledge is still rudimentary. There has been a strong push to develop highly generalized conclusions to show that bottom trawling causes an overall reduction in biodiversity, a decrease in species characterized by low reproduction rates, changes in relative abundance, larger effects on surface-living species more than burrowing species, increases in species characterized by high reproduction rates, increases in scavenger populations, and a drop in geographic range. Martín et al. (2014b) have summarized this evolution of marine biogenic seascapes under chronic trawling pressure by two major steps, namely, a natural state and a switch to a mixed seabed sediment structure with a lower abundance of sessile organisms, resembling changes from a former forest into a ploughed crop field (Puig et al. 2012).

However, other meta-analyses of the existing literature (approximately 110 original research studies) (Hilborn et al. 2014; Hughes et al. 2014) indicate that the effects on biota may not be as straightforward as previously thought. For example, there are a number of studies on the shelf that show an increase in benthic species abundance (De Biasi 2004; Prantoni et al. 2013) after mechanical seabed disturbance. Along the slope, however, more conclusive findings have shown that chronic bottom trawling of the soft sediment of seabed has led to an 80% reduction in meiofauna abundance and 50% lower biodiversity compared to similar areas where no trawling occurs. The negative effects of trawling are also evident in the decrease in the number of species of nematodes (the dominant component of the meiofauna at these depths), which decreases by 25% (Pusceddu et al. 2014).

Although a knowledge base on the direct effects of bottom trawling on higher trophic levels, such as fish or crabs (e.g., Pitcher et al. 2007; Thurstan et al. 2010), and to some degree also on benthic communities (e.g., Kaiser and Clarke 2006; Collie et al. 2000), has been established, the sediment resuspension effects and with it geomorphological impact on higher trophic levels remain largely unknown (Fig. 8).

Studies addressing bottom trawling-induced changes in benthic communities on higher trophic levels, such as in fish populations, have found that although most species abundances are negatively impacted from trawling (Pitcher et al. 2007), some species benefit from bottom trawling by feeding on unburied infauna or carrion (killed benthos) (Hiddink et al. 2008). However, little data exists to support the causality of such claims other than, for example, the filming of higher densities of scavenging crabs and predatory fish that gather in the tracks left behind by dredges (Caddy 1973). Other effects on higher trophic levels that are directly linked to the resuspension of sediments may include the smothering of sponges (DFO et al. 2013) and corals (Rogers 1999) or the stress indicated by elevated hormonal levels produced in some fish from higher levels of turbidity (Humborstad et al. 2006). The indirect consequences to higher trophic levels include the reduction in

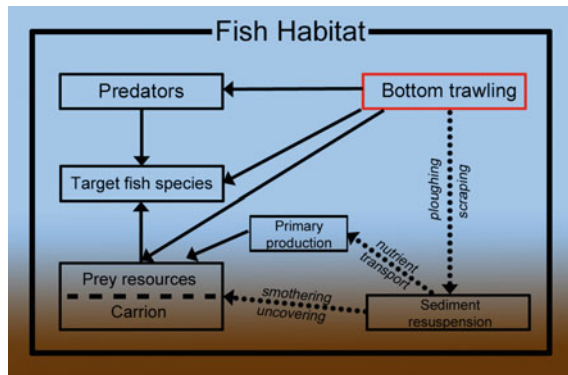


Fig. 8 Largely known and unknown effects of bottom trawling on fish habitat. Known effects that potentially alter fish production are indicated with *solid arrows*. Largely unknown are the effects of sediment resuspension, indicated by *dotted arrows* (modified from Hilborn et al. 2014)

photosynthetic organisms due to lower light availability after trawling-induced sediment resuspension (Caddy 2000; Johnson et al. 2002) or, conversely, the increase in primary producers due to the advection of nutrients from the seabed (Dounas et al. 2007). The resuspension of contaminated sediments by bottom trawlers may also cause filter feeding mussels to increase toxin accumulation to levels at which they become unfit for human consumption (Bradshaw et al. 2012).

Lokkeborg (2005) raised an important question, asking why in most studies documenting a change in species abundance or diversity, species spatial variability was rarely taken into account. One of the largest problems in the analysis of the effects of bottom trawling on biota comes from the simple fact that control sites large enough to reflect the temporal and spatial variability of natural states have become increasingly rare, making it difficult to assess anthropogenic change (Pauly et al. 2002; Halpern et al. 2008; Snelgrove et al. 2014).

In a meta-analysis of the existing literature Lokkeborg (2005) confirmed this problem showing that a third of all studies lack appropriate replicate controls. Consequently, when effects to benthic communities are not detected, it still cannot be concluded that there is no impact from bottom trawling. Despite these concerns, on a very basic level, it can be universally concluded that the impact of chronic bottom trawling changes the functional composition of benthic invertebrate communities (Tillin et al. 2006).

2.7 Bottom Trawling-Induced Changes to Soft Sediment Seascapes

Early recognition of the physical effects of bottom trawling influencing natural sediment transport came from the recognition that the seabed surface roughness was

being altered (Schwinghamer et al. 1996; Tuck et al. 1998). The result of bottom trawling on surface roughness is the smoothing of low-relief topographic features (ripples and mounds) that are interspersed with higher relief track marks caused by the ploughing of trawl doors (Kaiser et al. 2002). Chronic bottom trawling occurs predominantly on sedimentary shelf and slope areas where most of the shallow-infaunal organisms have their habitat (NRC 2002; Thrush and Dayton 2002; Barnes and Thomas 2005; Malik and Mayer 2007). These largely soft sediment seascapes hold some of the ocean's highest benthic biodiversity and thus have a significant function as a cradle of life to higher trophic levels (Gray et al. 1997; Snelgrove 1999; Thrush et al. 2001; Snelgrove et al. 2014).

On short spatial and temporal scales, bottom trawling can leave a variety of different traces on the seafloor depending on the fishing gear and substrate. Furrows and berms created by the trawl doors are the most conspicuous physical impacts from otter trawls (Fig. 9). On most continental shelves and slopes of the world, a dense tapestry of overlapped otter trawl marks are the most evident morphological feature observed by multi-beam, side scan or underwater video surveys (Schwinghamer et al. 1998; DeAlteris et al. 1999; Friedlander et al. 1999; Humborstad et al. 2004; Smith et al. 2007; Palanques et al. 2014; Oberle et al. 2016a). Although less common, trawl marks are also recorded by acoustic or video surveys well below 1000 m depth (Fosså et al. 2002; Freiwald and Roberts 2005;

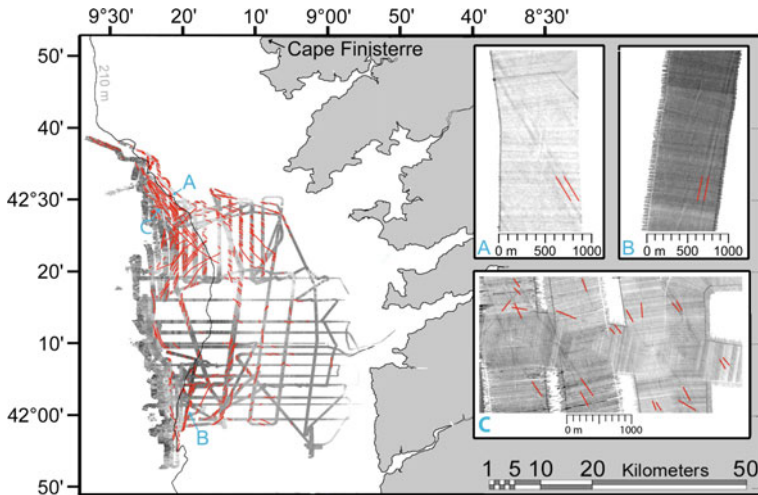


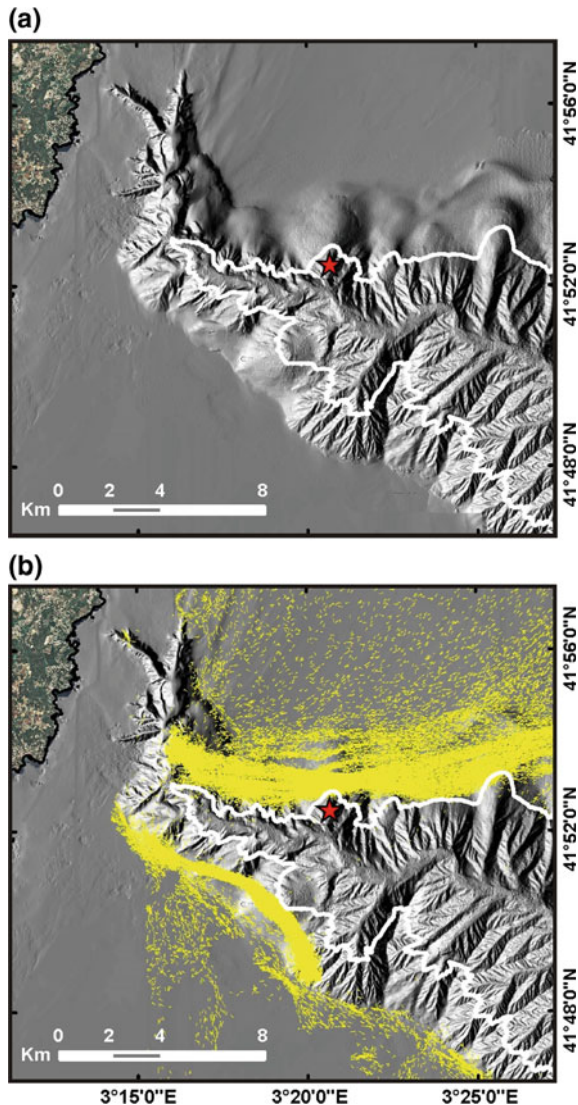
Fig. 9 Spatial distribution of trawl marks as recorded with high-resolution echosounder multibeam equipment during May 2011. The highest density of recorded track marks was found along the shelf edge. Only few track marks could be detected in areas above the 5-year maximum storm wave base, which extends to approximately 150 m water depth (modified from Oberle et al. 2014a, b)

Baco et al. 2010; Clark et al. 2010). The sheer strength with which trawl doors plow the seabed was described by Freese et al. (1999), who showed that within their study area on the Alaskan shelf roughly a quarter of all boulders larger than 75 cm in diameter had been moved by bottom trawlers.

In general the most commonly reported morphological finding is a homogenization of the small-scale relief caused by the dragging of sweeplines and ground gear that is then crisscrossed by deeper otter board tracks. Dredges have been reported to level or flatten seafloor features and leave deep trenches. Industrial scallops drive <30 cm long rake fingers through the seabed, leaving behind a rougher seafloor due to the uncovering of boulders and gravel embedded within the fines (Caddy 1973). As previously mentioned, on short-temporal scales, the most conspicuous physical impact by beam trawlers and dredges is a flattening of bottom features such as ripples and irregular topography (Thrush et al. 1995; Currie and Parry 1996; Kaiser and Spencer 1996). Substrate microtopography such as bioturbation mounds and polychaete tubes are also shown to be eliminated in the tracks of beam trawls and scallop dredges (Currie and Parry 1996; Hall-Spencer 1999). These microtopographies have previously been shown to exert control over spatial heterogeneity because they strongly influence sediment grain size, sorting, and organic richness (Buatois and Mángano 2011). The longevity of the seafloor-altering effects is determined by its frequency of disturbance, sediment type and natural disturbances (tidal current, wave actions and biological activities), and has been shown to last from a few hours to years (Lokkeborg 2005; Kaiser et al. 2006; Pitcher et al. 2009; Foden et al. 2010; Grieve et al. 2014). Collie et al. (1997) found recovery from scallop dredging in shallow gravel sediment to take 5–10 years. However, in general data are too scarce and also often not recorded at microtopographic or benthic habitat level to allow a clear relationship between persistence of trawl marks and bottom type/natural disturbance to be made (Lokkeborg 2005).

On longer temporal scales, the net or long-term effect of repeated trawling or dredging over the same spots is almost always a general flattening and homogenization of the seafloor relief. This was already discovered in the 1970s, when scientists observed that bottom trawling had dramatically changed the overall topography of sheltered bays in Corsica (de Groot 1984). Similarly, large scale sand waves (~15 m height) on the New England shelf were reported to be leveled by bottom trawlers and dredges within a two year time frame (Bennett 1998). Along La Fonera submarine canyon flanks, Puig et al. (2012) documented that the erosion, caused by repeated sediment resuspension and sediment plowing from trawling gear over several decades, transformed a dendritic network of tributaries with up to 5 orders of bifurcation into a smoothed seafloor relief (Fig. 10). These authors concluded that during the last decades, following the industrialization of fishing fleets, bottom trawling has become an important driver of deep seascape evolution, producing comparable effects on the deep seafloor to those generated by agricultural ploughing on emerged land.

Fig. 10 Shaded relief image from a 15 m resolution bathymetric grid of La Fonera submarine canyon showing gullied and smoothed seafloor regions, the latter at depths shallower than 800 m (white contour) especially on the northern flank but also in parts of the southern flank (a). Bottom trawling vessels VMS data (small yellow arrows) from 2007 to 2010 show a clear spatial correlation between the trawled and smoothed regions (b). The red star indicates the positions of the oceanographic mooring that recorded daily trawling-induced sediment gravity flows (adapted from Puig et al. 2012)



2.8 Bottom Trawling-Induced Changes to Reefs and Other Biogenic Seascapes

The highly diversified ecosystem of most biogenic seascapes such as sea-grass meadows, kelp forests, sponge fields, and coral reefs consists of comparatively few dominant sessile species that make up their three-dimensional architectural frame (Wilkinson 2008). Bottom trawling preferentially removes these biogenic structures as well as any other erect, sessile, large, long-living macro- and megafauna (Reise

1982; Smith et al. 2000; Jennings et al. 2001; de Juan et al. 2007). While bottom trawling activities are increasingly restricted from kelp forests and sea-grass areas, coral reefs continue to be threatened by bottom trawling activities worldwide (Barnes and Thomas 2005). When a bottom trawl is dragged along the seafloor, it breaks coral reefs and destroys a habitat that could potentially require centuries to recover, if it does at all (Rogers 1999). Collie et al. (1997) demonstrated that biogenic reefs showed no signs of recovery after >4 years. Particularly vulnerable to these activities are the slow growing cold water corals that have only recently been found on seamounts and along the continental slope throughout the global ocean (Fosså 2013; Freiwald and Roberts 2005). Hall-Spencer et al. (2002) and Mortensen et al. (2001) have reported trawling induced plowing of coral reefs that are dated to ~4000 and ~8600 years BP respectively. Given the longevity of these reefs the widely publicized comparison of bottom trawling to forest clearcutting (Watling and Norse 1998) is not entirely adequate as forests can potentially regrow at a rate of anywhere between a few centimeters to meters per year (ADF 2016) while cold water corals typically grow only a few millimeters per year (Pitcher et al. 2007). An assessment of the current global state of coral reefs suggests that 19% of the original area of coral reefs have been lost; 15% are seriously threatened with loss within the next 10–20 years; and 20% are under threat of loss in 20–40 years (Wilkinson 2008). While there are many other factors contributing to the vulnerable condition of coral reefs (Bruno and Valdivia 2016) (e.g. climate change, acidification), bottom trawling has repeatedly been mentioned as a major stressor contributing to their declining coverage (Wilkinson 2008).

3 Conclusion and Outlook

3.1 *Adding the Effects of Bottom Trawling to the Geological Framework*

Erosion or deposition in one part of the submarine system leads to sediment-storage modifications within an adjacent segment (e.g. from shelf to slope to abyssal plain). The processes controlling this interplay between erosion and deposition within a source-to-sink system are highly complex. The traditional view (e.g., Chiocci and Chivas 2014; Nittrouer et al. 2007) has been that sedimentary systems on the shelf, slope, and abyssal plains are driven by interactions between endogenous (e.g., geodynamic) and exogenous (e.g., climate-related) processes on different geological time scales. However, while the sediment nature and seafloor physiology are largely controlled by the interplay between plate tectonic processes, sea-level changes, the position and load of sediment sources, and the hydrodynamic processes operating on the continental margin, the effect from human impacts on the seafloor—not from recent climate change or alterations in terrestrial sediment runoff but by direct physical impacts to the sediments on the shelf and slope from bottom trawling—has

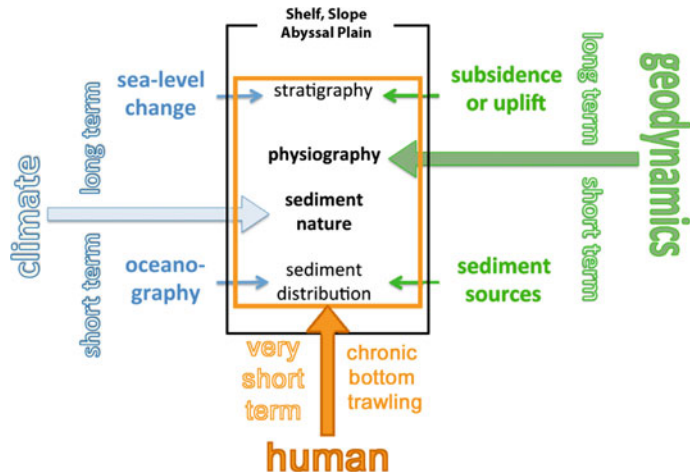


Fig. 11 Factors that control the shelf, slope and abyssal plain character over both long and short geological timescales. A largely unknown factor influencing these interactions comes from very recent human activity, namely bottom trawling (modified from Chiocci and Chivas 2014)

only recently been shown to play a significant role. Although the natural mechanisms that cause sediment resuspension and transport have controlled the sediment distribution and geomorphology in the submarine realm over billions of years (Eriksson et al. 1998), today, the physical resuspension and alteration of seabed sediment is a combination of both natural and anthropogenic processes (Fig. 11).

3.2 Outlook

Although significant advances have been made in the understanding of bottom trawling-induced morphological change through the analysis of sediment resuspension and lithological seabed alteration, many aspects of the effects of bottom trawling remain unexplored or barely studied. For example, in the absence of obvious sedimentological or biotic disturbance signals, bottom trawling effects often go unnoticed, especially in sediment core based studies, because resuspension and settling after bottom trawling often produce their own natural-looking lithology, chemistry, and benthic community structure.

In this context, a systematic assessment of the major biogeochemical signals in the seabed that are affected by different intensities of bottom trawling is desperately needed. With respect to different trawling intensities, it can be expected that each grain size class (clay to gravel) may have different bottom trawling-induced threshold values where seabed sediments change their chemical state, for example, from anoxic to oxic or vice versa. With this in mind, it is important to develop further geochemical proxies that could be easily and rapidly employed to determine

the impact-depth of a bottom trawling-affected seabed. At larger spatial scales, swath bathymetric surveys revealing seafloor smoothing surfaces and backscatter anomalies should be contrasted with AIS and/or VMS density maps to establish causative relationships of seafloor morphological changes that could be attributable to fishing activities.

Furthermore, the number of publications that have assessed bottom trawling-induced sediment mass per unit of trawled area in the wake of bottom trawlers is very limited. The systematic quantification of resuspended mass of different grain sizes and from different bottom-trawling gears is an urgent next step that is needed to refine. With respect to cohesive sediments, little is known about their disaggregation and flocculation behavior after bottom trawling-induced sediment resuspension. However, this is most likely very important for the accurate assessment of settling rates and sediment fluxes of clay particles and their resulting seabed geomorphologies.

Other topics more indirectly related to geomorphic change, such as nutrient advection on continental shelves, the shelf being the area where most of the world's phytoplankton is produced, must also be addressed. Bottom trawling occurs primarily on continental shelves and induces nutrient advection that may result in phytoplankton production. To this day, only one study has attempted to demonstrate the direct link between bottom trawling and phytoplankton production (Dounas et al. 2007). The necessity of studying the link between bottom trawling and primary production is further underlined when considering the very high global amount of bottom trawling-induced resuspended sediment ($\sim 22\text{GT}$) (Oberle et al. 2016a) that can potentially cause a global bottom trawling-induced fertilization effect, leading to yet further unknown climate feedback loops.

The consequences of bottom trawling-induced changes to primary production are also likely to affect changes in higher trophic levels by altering the amounts of food to both fish and benthic fauna and flora and consequently must also play a role for physical habitats. Although such interactions are difficult to determine, they must always begin with an assessment of the primary effects of bottom trawling on the water column, seabed, and geomorphology. Because bottom trawling is continuously expanding on many shelves around the world, the study of its unknown effects is an increasingly pressing issue and a difficult task, as adequate control sites are becoming progressively rare.

References

- ADF (2016) The Arbor Day Foundation Tree Database. Arbor Day Foundation, Lincoln, NE, USA
Aller RC (1982) The effects of macrobenthos on chemical properties of marine sediments and overlying water. In: McCall PL, Tevesz MJS (eds) Animal sediment relations. Springer Science, pp 53–102
Andersson K, Jonsson P (2003) En ROV-undersökning av trålspår i södra Östersjön. J R Swedish Agric For Acad 142:39–42

- Auster PJ, Malatesta RJ, Donaldson CLS (1997) Distributional responses to small-scale habitat variability by early juvenile silver hake, *Merluccius bilinearis*. Environ Biol Fishes 50:195–200. doi:[10.1023/A:1007305628035](https://doi.org/10.1023/A:1007305628035)
- Baco AR, Rowden AA, Levin LA et al (2010) Initial characterization of cold seep faunal communities on the New Zealand Hikurangi margin. Mar Geol 272:251–259. doi:[10.1016/j.margeo.2009.06.015](https://doi.org/10.1016/j.margeo.2009.06.015)
- Barnes PW, Thomas JP (2005) Benthic habitats and effects of fishing. American Fisheries Society symposium
- Benn AR, Weaver PP, Billet DSM et al (2010) Human activities on the deep seafloor in the North East Atlantic: an assessment of spatial extent. PLoS ONE 5:e12730. doi:[10.1371/journal.pone.0012730](https://doi.org/10.1371/journal.pone.0012730)
- Bennett F (1998) Effect of fishing gear on the sea floor of New England changes to the sea floor in the Chatham area. In: Dorsey EM, Pederson J (eds) Effect of fishing gear on the sea floor of New England. Conservation Law Foundation, Boston, pp 115–116
- Bhagirathan U, Meenakumari B, Jayalakshmy KV et al (2010) Impact of bottom trawling on sediment characteristics—a study along inshore waters off Veraval coast, India. Environ Monit Assess 160:355–369. doi:[10.1007/s10661-008-0700-0](https://doi.org/10.1007/s10661-008-0700-0)
- Black KP, Parry GD (1999) Entrainment, dispersal, and settlement of scallop dredge sediment plumes: field measurements and numerical modelling. Can J Fish Aquat Sci 56:2271–2281. doi:[10.1139/f99-159](https://doi.org/10.1139/f99-159)
- Black J, Tilney R (2015) Monitoring New Zealand's trawl footprint for deepwater fisheries: 1989–90 to 2010–11. New Zeal Aquat Environ Biodivers Rep 142:1–56
- Bradshaw C, Tjensvoll I, Sköld M et al (2012) Bottom trawling resuspends sediment and releases bioavailable contaminants in a polluted fjord. Environ Pollut 170:232–241. doi:[10.1016/j.envpol.2012.06.019](https://doi.org/10.1016/j.envpol.2012.06.019)
- Brown EJ, Finney B, Domisse M, Hills S (2005) Effects of commercial otter trawling on the physical environment of the southeastern Bering Sea. Cont Shelf Res 25:1281–1301. doi:[10.1016/j.csr.2004.12.005](https://doi.org/10.1016/j.csr.2004.12.005)
- Bruno JF, Valdivia A (2016) Coral reef degradation is not correlated with local human population density. Sci Rep 6:29778. doi:[10.1038/srep29778](https://doi.org/10.1038/srep29778)
- Buatois LA, Mángano MG (2011) Ichnology: organism-substrate interactions in space and time. Cambridge University Press, Cambridge
- Caddy JF (1973) Underwater observations on tracks of dredges and trawls and some effects of dredging on a scallop ground. J Fish Res Board Canada 30:173–180. doi:[10.1139/f73-032](https://doi.org/10.1139/f73-032)
- Caddy JF (2000) Marine catchment basin effects versus impacts of fisheries on semi-enclosed seas. ICES J Mar Sci 57:628–640. doi:[10.1006/jmsc.2000.0739](https://doi.org/10.1006/jmsc.2000.0739)
- Cadée GC (2001) Sediment dynamics by bioturbating organisms. In: Ecological comparisons of sedimentary shores. Springer, Berlin, pp 127–148
- Chiocci FL, Chivas AR (eds) (2014) Continental shelves of the world: their evolution during the Last Glacio-Eustatic Cycle. Geological Society, London
- Churchill J (1989) The effect of commercial trawling on sediment resuspension and transport over the Middle Atlantic Bight continental shelf. Cont Shelf Res 9:841–864
- Clark MR, Rowden AA, Schlacher T et al (2010) The ecology of seamounts: structure, function, and human impacts. Ann Rev Mar Sci 2:253–278. doi:[10.1146/annurev-marine-120308-081109](https://doi.org/10.1146/annurev-marine-120308-081109)
- Collie J, Escanero G, Valentine P (1997) Effects of bottom fishing on the benthic megafauna of Georges Bank. Mar Ecol Prog Ser 155:159–172. doi:[10.3354/meps155159](https://doi.org/10.3354/meps155159)
- Collie JS, Hall SJ, Kaiser MJ, Poiner IR (2000) A quantitative analysis of fishing impacts shelf-sea benthos. J Anim Ecol 69:785–798. doi:[10.1046/j.1365-2656.2000.00434.x](https://doi.org/10.1046/j.1365-2656.2000.00434.x)
- CRG (2012) Fish trawling reshapes deep-sea canyons. CRG marine geosciences, University of Barcelona. In: Nat News. <http://www.nature.com/news/fish-trawling-reshapes-deep-sea-canyons-1.11356>
- Crown (1989) Trawl door trials in the Moray Firth—Marine Laboratory and Sea Fish Industry, Aberdeen

- Currie DR, Parry GD (1996) Effects of scallop dredging on a soft sediment community: a large-scale experimental study. *Mar Ecol Prog Ser* 134:131–150. doi:[10.3354/meps134131](https://doi.org/10.3354/meps134131)
- De Biasi AM (2004) Impact of experimental trawling on the benthic assemblage along the Tuscany coast (north Tyrrhenian Sea, Italy). *ICES J Mar Sci* 61:1260–1266. doi:[10.1016/j.icesjms.2004.07.024](https://doi.org/10.1016/j.icesjms.2004.07.024)
- de Groot SJ (1984) The impact of bottom trawling on benthic fauna of the North Sea. *Ocean Manag* 9:177–190. doi:[10.1016/0302-184X\(84\)90002-7](https://doi.org/10.1016/0302-184X(84)90002-7)
- de Juan D, Thrush SF, Demestre M (2007) Functional changes as indicators of trawling disturbance on a benthic community located in a fishing ground (NW Mediterranean Sea). *Mar Ecol Prog Ser* 334:117–129
- De Leo FC, Gauthier M, Nephin J et al (2016) Bottom trawling and oxygen minimum zone influences on continental slope benthic community structure off Vancouver Island (NE Pacific). *Deep Sea Res Part II Top Stud Oceanogr* 1:1–30. doi:[10.1016/j.dsro.2016.11.014](https://doi.org/10.1016/j.dsro.2016.11.014)
- de Souza EN, Boerder K, Matwin S, Worm B (2016) Improving fishing pattern detection from satellite AIS using data mining and machine learning. *PLoS ONE* 11:e0158248. doi:[10.1371/journal.pone.0158248](https://doi.org/10.1371/journal.pone.0158248)
- DeAlteris J, Skrobe L, Lipsky C (1999) The significance of seabed disturbance by mobile fishing gear relative to natural processes: a case study in Narragansett Bay, Rhode Island. In: Fish habitats: essential fish habitat and rehabilitation, pp 224–237
- DeAlteris JT, Skrobe LG, Castro KM (2000) Effects of mobile bottom fishing gear on biodiversity and habitat in offshore New England waters. *Northeast Nat* 7:379. doi:[10.2307/3858519](https://doi.org/10.2307/3858519)
- Dellapenna TM, Allison MA, Gill GA et al (2006) The impact of shrimp trawling and associated sediment resuspension in mud dominated, shallow estuaries. *Estuar Coast Shelf Sci* 69:519–530. doi:[10.1016/j.ecss.2006.04.024](https://doi.org/10.1016/j.ecss.2006.04.024)
- DFO, Centre for Science Advice, Fisheries and Ocean Canada (2013) Identification and evaluation of biological effects and impacts of sediment to sponge communities in Hecate Strait. *Can Sci Advis Secr Sci Advis Rep* 1–11
- Diderot D, D'Alembert J (1771) “Pêches – Pêches de mer, pêches de rivière – Fabrique des filets [Planches I-XXVII],” *Encyclopédie ou Dictionnaire raisonné des sciences, des arts et des métiers*, 8th edn, Paris
- Diesing M, Stephens D, Aldridge J (2013) A proposed method for assessing the extent of the seabed significantly affected by demersal fishing in the Greater North Sea. *ICES J Mar Sci* 70:1085–1096. doi:[10.1093/icesjms/fst066](https://doi.org/10.1093/icesjms/fst066)
- Dounas CG (2006) A new apparatus for the direct measurement of the effects of otter trawling on benthic nutrient releases. *J Exp Mar Bio Ecol* 339:251–259. doi:[10.1016/j.jembe.2006.07.022](https://doi.org/10.1016/j.jembe.2006.07.022)
- Dounas C, Davies I, Triantafyllou G et al (2007) Large-scale impacts of bottom trawling on shelf primary productivity. *Cont Shelf Res* 27:2198–2210. doi:[10.1016/j.csr.2007.05.006](https://doi.org/10.1016/j.csr.2007.05.006)
- Duplisea DE, Jennings S, Malcolm SJ et al (2001) Modelling potential impacts of bottom trawl fisheries on soft sediment biogeochemistry in the North Sea. *Geochim Trans* 2:112. doi:[10.1186/1467-4866-2-112](https://doi.org/10.1186/1467-4866-2-112)
- Durrieu de Madron X, Ferré B, Le Corre G et al (2005) Trawling-induced resuspension and dispersal of muddy sediments and dissolved elements in the Gulf of Lion (NW Mediterranean). *Cont Shelf Res* 25:2387–2409. doi:[10.1016/j.csr.2005.08.002](https://doi.org/10.1016/j.csr.2005.08.002)
- Eastwood PD, Mills CM, Aldridge JN et al (2007) Human activities in UK offshore waters: an assessment of direct, physical pressure on the seabed. *ICES J Mar Sci* 64:453–463. doi:[10.1093/icesjms/fsm001](https://doi.org/10.1093/icesjms/fsm001)
- Ellingsen KE (2002) Soft-sediment benthic biodiversity on the continental shelf in relation to environmental variability. *Mar Ecol Prog Ser* 232:15–27. doi:[10.3354/meps232015](https://doi.org/10.3354/meps232015)
- Eriksson PG, Condie KC, Tirsgaard H, Mueller WU, Altermann W, Miall AD, Aspler LB, Catuneanu O, Chiarenzelli JR (1998) Precambrian clastic sedimentation systems. *Sediment Geol* 120(1–4):5–53
- European Parliament (2008) Directive 2008/56/EC of the European Parliament and of the Council of 17 June 2008 establishing a framework for community action in the field of marine environmental policy (Marine Strategy Framework Directive). *Off J Eur Union* 1–22

- Fanning KA, Carder KL, Betzer PR (1982) Sediment resuspension by coastal waters: a potential mechanism for nutrient re-cycling on the ocean's margins. Deep Sea Res Part A Oceanogr Res Pap 29:953–965. doi:[10.1016/0198-0149\(82\)90020-6](https://doi.org/10.1016/0198-0149(82)90020-6)
- FAO (2009) The state of world fisheries and aquaculture
- Ferré B, Durrieu de Madron X, Estournel C et al (2008) Impact of natural (waves and currents) and anthropogenic (trawl) resuspension on the export of particulate matter to the open ocean. Application to the Gulf of Lion (NW Mediterranean). Cont Shelf Res 28:2071–2091. doi:[10.1016/j.csr.2008.02.002](https://doi.org/10.1016/j.csr.2008.02.002)
- Floderus S, Pihl L (1990) Resuspension in the Kattegat: impact of variation in wind climate and fishery. Estuar Coast Shelf Sci 31:487–498. doi:[10.1016/0272-7714\(90\)90039-T](https://doi.org/10.1016/0272-7714(90)90039-T)
- Foden J, Rogers SI, Jones AP (2010) Recovery of UK seabed habitats from benthic fishing and aggregate extraction—towards a cumulative impact assessment. Marine Ecol Progress Ser 411:259–270. doi:[10.3354/meps08662](https://doi.org/10.3354/meps08662)
- Fosså JH (2013) Fishery impact—bottom trawling in Norwegian waters. In: Webpage Inst Mar Res. http://www.imr.no/coral/fishery_impact.php
- Fosså JH, Mortensen PB, Furevik DM (2002) Hydrobiologia 471:1–12. doi:[10.1023/A:1016504430684](https://doi.org/10.1023/A:1016504430684)
- Freese L, Auster P, Heifetz J, Wing B (1999) Effects of trawling on seafloor habitat and associated invertebrate taxa in the Gulf of Alaska. Mar Ecol Prog Ser 182:119–126
- Freiwald A, Roberts JM (2005) Cold-water corals and ecosystems. Springer, Berlin
- Friedlander A, Boehlert G, Field M et al (1999) Sidescan-sonar mapping of benthic trawl marks on the shelf and slope off Eureka, California. Fish Bull 786–801
- Gerritsen HD, Minto C, Lordan C (2013) How much of the seabed is impacted by mobile fishing gear? Absolute estimates from Vessel Monitoring System (VMS) point data. ICES J Mar Sci 70:523–531. doi:[10.1093/icesjms/fst017](https://doi.org/10.1093/icesjms/fst017)
- Gray J, Poore G, Ugland K (1997) Coastal and deep-sea benthic diversities compared. Mar Ecol Prog Ser 159:97–103
- Grieve C, Brady D, Polet H (2014) Review of habitat dependent impacts of mobile and static fishing gears that interact with the sea bed. Mar Steward Counc Sci Ser 2:18–88
- Hall-Spencer J (1999) The impact of Rapido trawling for scallops, *Pecten jacobaeus*(L.), on the benthos of the Gulf of Venice. ICES J Mar Sci 56:111–124. doi:[10.1006/jmsc.1998.0424](https://doi.org/10.1006/jmsc.1998.0424)
- Hall-Spencer J, Allain V, Fosså JH (2002) Trawling damage to Northeast Atlantic ancient coral reefs. Proc R Soc London B Biol Sci 269:507–511. doi:[10.1098/rspb.2001.1910](https://doi.org/10.1098/rspb.2001.1910)
- Halpern BS, Walbridge S, Selkoe KA et al (2008) A global map of human impact on marine ecosystems. Science 319:948–952. doi:[10.1126/science.1149345](https://doi.org/10.1126/science.1149345)
- Hiddink JG, Rijnsdorp AD, Piet G (2008) Can bottom trawling disturbance increase food production for a commercial fish species? Can J Fish Aquat Sci 65:1393–1401. doi:[10.1139/F08-064](https://doi.org/10.1139/F08-064)
- Hilborn R, Jennings S, Rijnsdorp A et al (2014) Trawling: finding common ground on the scientific knowledge regarding best practices. Report of the third meeting of the Trawling Best Practices Study Committee. <https://trawlingpractices.files.wordpress.com/2012/10/third-meeting-report.pdf>
- Hinz H, Prieto V, Kaiser MJ (2009) Trawl disturbance on benthic communities: chronic effects and experimental predictions. Ecol Appl 19:761–773
- Hixon MA, Tissot BN (2007) Comparison of trawled vs untrawled mud seafloor assemblages of fishes and macroinvertebrates at Coquille Bank, Oregon. J Exp Mar Bio Ecol 344:23–34. doi:[10.1016/j.jembe.2006.12.026](https://doi.org/10.1016/j.jembe.2006.12.026)
- Hooper DU, Chapin FS, Ewel JJ et al (2005) Effects of biodiversity on ecosystem functioning: a consensus of current knowledge. Ecol Monogr 75:3–35. doi:[10.1890/04-0922](https://doi.org/10.1890/04-0922)
- Hopkins CCE (2004) The dangers of bottom trawling in the Baltic Sea. A report for Coalition Clean Baltic. Aqua Mar Advis 1:1–14
- Horn L (2005) National Undersea Research Center—After bottom trawling photo. In: National Undersea Research Center. <http://www.terrานature.org/OculinaRubble.htm>

- Huettel M, Gust G (1992) Impact of bioroughness on interfacial solute exchange in permeable sediments. Mar Ecol Prog Ser 89:253–267. doi:[10.3354/meps089253](https://doi.org/10.3354/meps089253)
- Hughes KM, Kaiser MJ, Jennings S et al (2014) Investigating the effects of mobile bottom fishing on benthic biota: a systematic review protocol. Environ Evid 3:23. doi:[10.1186/2047-2382-3-23](https://doi.org/10.1186/2047-2382-3-23)
- Hulthe G, Hulth S, Hall POJ (1998) Effect of oxygen on degradation rate of refractory and labile organic matter in continental margin sediments. Geochim Cosmochim Acta 62:1319–1328. doi:[10.1016/S0016-7037\(98\)00044-1](https://doi.org/10.1016/S0016-7037(98)00044-1)
- Humborstad OB, Nøttestad L, Løkkeborg S, Rapp HT (2004) RoxAnn bottom classification system, sidescan sonar and video-sledge: spatial resolution and their use in assessing trawling impacts. ICES J Mar Sci 61:53–63. doi:[10.1016/j.icesjms.2003.10.001](https://doi.org/10.1016/j.icesjms.2003.10.001)
- Humborstad OB, Jørgensen T, Grotmol S (2006) Exposure of cod *Gadus morhua* to resuspended sediment: an experimental study of the impact of bottom trawling. Mar Ecol Prog Ser 309:247–254. doi:[10.3354/meps309247](https://doi.org/10.3354/meps309247)
- ICES (1992) Report by the International Council for the Exploration of the Sea on ecosystem effects of fishing activities. ICES C 11:1–144
- ICES (2006) International Council for the Exploration of the Sea (ICES): report of the Working Group on Ecosystem Effects of Fishing Activities. ACE 05:1–179
- ICES (2015) Report of the Working Group on Spatial Fisheries Data (WGSFD), Copenhagen, Denmark
- Jennings S, Dinmore TA, Duplisea DE, Warr KJ, Lancaster JE (2001) Trawling disturbance can modify benthic production processes. J Anim Ecol 70(3):459–475
- Johnson K, Stevenson D, Reid R et al (2002) A review of national and international literature on the effects of fishing on benthic habitats. NOAA Tech Memo 57:1–72
- Jones JB (1992) Environmental impact of trawling on the seabed: a review. N Z J Mar Freshw Res 26:59–67
- Jonsson HK (1967) Proceedings of the world scientific conference on the biology and culture of shrimps and prawns. FAO Fish Rep 57:77–587
- Jørgensen L (2013) Barents Sea South East—mother nature's pantry. In: Mareano—Collect Mar Knowl. http://mareano.no/en/news/news_2013/barents_sea_south_east_mother_natures_pantry
- Jumars PA., Nowell ARM (1984) Effects of benthos on sediment transport: difficulties with functional grouping. Cont Shelf Res 3:115–130. doi:[10.1016/0278-4343\(84\)90002-5](https://doi.org/10.1016/0278-4343(84)90002-5)
- Kaiser MJ, Spencer BE (1996) The effects of beam-trawl disturbance on infaunal communities in different habitats. J Anim Ecol 65:348. doi:[10.2307/5881](https://doi.org/10.2307/5881)
- Kaiser MJ, Clarke KR, Hinz H et al (2006) Global analysis of response and recovery of benthic biota to fishing. Mar Ecol Prog Ser 311:1–14. doi:[10.3354/meps311001](https://doi.org/10.3354/meps311001)
- Kaiser MJ, Collie JS, Hall SJ, Jennings S, Poiner IR (2002) Modification of marine habitats by trawling activities: prognosis and solutions. Fish Fish 3(2):114–136
- Lambert G, Jennings S, Kaiser M et al (2011) Quantification and prediction of the impact of fishing on epifaunal communities. Mar Ecol Prog Ser 430:71–86. doi:[10.3354/meps09112](https://doi.org/10.3354/meps09112)
- Lambert GI, Jennings S, Hiddink JG et al (2012) Implications of using alternative methods of vessel monitoring system (VMS) data analysis to describe fishing activities and impacts. ICES J Mar Sci 69:682–693. doi:[10.1093/icesjms/fss018](https://doi.org/10.1093/icesjms/fss018)
- Linnane A, Ball B, Munday B et al (2000) A review of potential techniques to reduce the impact of demersal trawls. Irish Fish Investig 7:1–32
- Løkkeborg S (2005) Impacts of trawling and scallop dredging on benthic habitats and communities. FAO Fish Tech Pap 472:1–58
- Main J, Sangster G (1981) A study of the sand clouds produced by trawl boards and their possible effect on fish capture. Scottish Fish Res Rep Dep Agric Fish Scotland, Mar Lab Aberdeen 20:1–20
- Malik M, Mayer L (2007) Investigation of seabed fishing impacts on benthic structure using multi-beam sonar, sidescan sonar, and video. ICES J Mar Sci 1998:1053–1065

- Martín J, Puig P, Palanques A et al (2008) Effect of commercial trawling on the deep sedimentation in a Mediterranean submarine canyon. *Mar Geol* 252:150–155. doi:[10.1016/j.margeo.2008.03.012](https://doi.org/10.1016/j.margeo.2008.03.012)
- Martín J, Puig P, Masqué P et al (2014a) Impact of bottom trawling on deep-sea sediment properties along the flanks of a submarine canyon. *PLoS ONE* 9:e104536. doi:[10.1371/journal.pone.0104536](https://doi.org/10.1371/journal.pone.0104536)
- Martín J, Puig P, Palanques A, Giampartone A (2014b) Commercial bottom trawling as a driver of sediment dynamics and deep seascape evolution in the Anthropocene. *Anthropocene* 7:1–15. doi:[10.1016/j.ancene.2015.01.002](https://doi.org/10.1016/j.ancene.2015.01.002)
- Martín J, Puig P, Palanques A, Ribó M (2014c) Trawling-induced daily sediment resuspension in the flank of a Mediterranean submarine canyon. *Deep Res Part II Top Stud Oceanogr* 104:174–183. doi:[10.1016/j.dsr2.2013.05.036](https://doi.org/10.1016/j.dsr2.2013.05.036)
- Mayer LM, Schick DF, Findlay RH, Rice DL (1991) Effects of commercial dragging on sedimentary organic matter. *Mar Environ Res* 31:249–261. doi:[10.1016/0141-1136\(91\)90015-Z](https://doi.org/10.1016/0141-1136(91)90015-Z)
- Mengual B, Cayocca F, Le Hir P et al (2016) Influence of bottom trawling on sediment resuspension in the “Grande-Vasière” area (Bay of Biscay, France). *Ocean Dyn* 66:1181–1207. doi:[10.1007/s10236-016-0974-7](https://doi.org/10.1007/s10236-016-0974-7)
- Montaigne F, Skerry B (2007) Das Drama im Meer. In: Natl Geogr Mag. <http://www.nationalgeographic.de/reportagen/das-drama-im-meer>
- Morato T, Watson R, Pitcher TJ, Pauly D (2006) Fishing down the deep. *Fish Fish* 7:24–34. doi:[10.1111/j.1467-2979.2006.00205.x](https://doi.org/10.1111/j.1467-2979.2006.00205.x)
- Mortensen PB, Hovland T, Fosså JH, Furevik DM (2001) Distribution, abundance and size of *Lophelia pertusa* coral reefs in mid-Norway in relation to seabed characteristics. *J Mar Biol Assoc UK* 81:581–597. doi:[10.1017/S002531540100426X](https://doi.org/10.1017/S002531540100426X)
- Murawski S, Wigley S, Fogarty M et al (2005) Effort distribution and catch patterns adjacent to temperate MPAs. *ICES J Mar Sci* 1167:1150–1167. doi:[10.1016/j.icesjms.2005.04.005](https://doi.org/10.1016/j.icesjms.2005.04.005)
- Nakamura E, Ourakami T (1900) Histoire de l’ industrie de la pêche maritime et fluviale ou Japon. (Translated from the Japanese into French). Bureau des produits maritimes et fluviaux du ministère d’agriculture et commerce, Tokyo
- Nittrouer CA, Austin JA, Field ME et al (2007) Continental margin sedimentation: from sediment transport to sequence stratigraphy. Blackwell, Oxford, UK
- NIWA (2010) The Ocean survey 20/20. In: New Zealand Gov Initiat. <http://www.os2020.org.nz/>
- NOAA (2010) Fishery closure boundary as of 6 pm Eastern Time 21 June 2010 due to the Deepwater Horizon oil spill, extending from Atchafalaya Bay, Louisiana to Panama City, Florida. In: Natl Ocean Atmos Adm News. <http://www.noaa.gov/deepwaterhorizon/>
- NRC (2002) (National Research Council) Effects of trawling and dredging on seafloor habitat. National Academies Press, Washington, DC
- O'Neill FG, Ivanović A (2016) The physical impact of towed demersal fishing gears on soft sediments. *ICES J Mar Sci J du Cons* 73:i5–i14. doi:[10.1093/icesjms/fsv125](https://doi.org/10.1093/icesjms/fsv125)
- O'Neill FG, Summerbell K (2011) The mobilisation of sediment by demersal otter trawls. *Mar Pollut Bull* 62:1088–1097. doi:[10.1016/j.marpolbul.2011.01.038](https://doi.org/10.1016/j.marpolbul.2011.01.038)
- O'Neill FG, Summerbell KJ (2016) The hydrodynamic drag and the mobilisation of sediment into the water column of towed fishing gear components. *J Mar Syst* 164:76–84. doi:[10.1016/j.jmarsys.2016.08.008](https://doi.org/10.1016/j.jmarsys.2016.08.008)
- O'Neill FG, Simmons SM, Parsons DR et al (2013) Monitoring the generation and evolution of the sediment plume behind towed fishing gears using a multibeam echosounder. *ICES J Mar Sci* 70:892–903. doi:[10.1093/icesjms/fst051](https://doi.org/10.1093/icesjms/fst051)
- Oberle Fkj, Hanebuth TJJ, Baasch B, Schwenk T (2014a) Volumetric budget calculation of sediment and carbon storage and export for a late Holocene mid-shelf mudbelt system (NW Iberia). *Cont Shelf Res* 76:12–24. doi:[10.1016/j.csr.2013.12.012](https://doi.org/10.1016/j.csr.2013.12.012)
- Oberle Fkj, Storlazzi CD, Hanebuth TJJ (2014b) Wave-driven sediment mobilization on a storm-controlled continental shelf (Northwest Iberia). *J Mar Syst* 139:362–372. doi:[10.1016/j.jmarsys.2014.07.018](https://doi.org/10.1016/j.jmarsys.2014.07.018)

- Oberle FKJ, Storlazzi CD, Hanebuth TJ (2016a) What a drag: quantifying the global impact of chronic bottom trawling on continental shelf sediment. *J Mar Syst* 159:109–119. doi:[10.1016/j.jmarsys.2015.12.007](https://doi.org/10.1016/j.jmarsys.2015.12.007)
- Oberle FKJ, Swarzenski PW, Reddy CM et al (2016b) Deciphering the lithological consequences of bottom trawling to sedimentary habitats on the shelf. *J Mar Syst* 159:120–131. doi:[10.1016/j.jmarsys.2015.12.008](https://doi.org/10.1016/j.jmarsys.2015.12.008)
- Ocean Networks Canada (2012) Digital fishers: new mission. In: Ocean Networks Canada. <http://www.oceanetworks.ca/digital-fishers-new-mission>
- Olsgard F, Schaanning MT, Widdicombe S et al (2008) Effects of bottom trawling on ecosystem functioning. *J Exp Mar Bio Ecol* 366:123–133. doi:[10.1016/j.jembe.2008.07.036](https://doi.org/10.1016/j.jembe.2008.07.036)
- Palanques A, Guillén J, Puig P (2001) Impact of bottom trawling on water turbidity and muddy sediment of an untrawled continental shelf. *Limnol Oceanogr* 46:1100–1110
- Palanques A, Martín J, Puig P et al (2006) Evidence of sediment gravity flows induced by trawling in the Palamós (Fonera) submarine canyon (northwestern Mediterranean). *Deep Sea Res Part I Oceanogr Res Pap* 53:201–214. doi:[10.1016/j.dsr.2005.10.003](https://doi.org/10.1016/j.dsr.2005.10.003)
- Palanques A, Puig P, Guillén J et al (2014) Effects of bottom trawling on the Ebro continental shelf sedimentary system (NW Mediterranean). *Cont Shelf Res* 72:83–98. doi:[10.1016/j.csr.2013.10.008](https://doi.org/10.1016/j.csr.2013.10.008)
- Pauly D, Christensen V, Guénette S et al (2002) Towards sustainability in world fisheries. *Nature* 418:689–695. doi:[10.1038/nature01017](https://doi.org/10.1038/nature01017)
- Percival P (2004) Impacts of trawl fisheries on marine benthic biogeochemistry. PhD thesis, University of Newcastle
- Piet GJ, Hintzen NT (2012) Indicators of fishing pressure and seafloor integrity. *ICES J Mar Sci* 69:1850–1858. doi:[10.1093/icesjms/fss162](https://doi.org/10.1093/icesjms/fss162)
- Piet GJ, Quirijns FJ (2009) The importance of scale for fishing impact estimations. *Can J Fish Aquat Sci* 66:829–835. doi:[10.1139/F09-042](https://doi.org/10.1139/F09-042)
- Pilskaln C, Churchill J, Mayer L (1998) Resuspension of sediment by bottom trawling in the Gulf of Maine and potential geochemical consequences. *Conserv Biol* 12:1223–1229
- Pitcher TJ, Hart PJB, Clark MR, Santos RS (2007) Seamounts: ecology, fisheries & conservation. Blackwell, Amsterdam
- Pitcher CR, Burridge CY, Wassenberg TJ et al (2009) A large scale BACI experiment to test the effects of prawn trawling on seabed biota in a closed area of the Great Barrier Reef Marine Park, Australia. *Fish Res* 99:168–183. doi:[10.1016/j.fishres.2009.05.017](https://doi.org/10.1016/j.fishres.2009.05.017)
- Prantoni A, Lana P, Sandrini-Neto L et al (2013) An experimental evaluation of the short-term effects of trawling on infaunal assemblages of the coast off southern Brazil. *J Mar Biol Assoc U K* 93:495–502. doi:[10.1017/S002531541200029X](https://doi.org/10.1017/S002531541200029X)
- Puig P, Canals M, Company JB et al (2012) Ploughing the deep sea floor. *Nature* 489:286–289. doi:[10.1038/nature11410](https://doi.org/10.1038/nature11410)
- Puig P, Martín J, Masqué P, Palanques A (2015) Increasing sediment accumulation rates in La Fonera (Palamós) submarine canyon axis and their relationship with bottom trawling activities. *Geophys Res Lett* 42:8106–8113. doi:[10.1002/2015GL065052](https://doi.org/10.1002/2015GL065052)
- Punzón A, Trujillo V, Castro J et al (2009) Closed area management taken after the “Prestige” oil spill: effects on industrial fisheries. *Mar Biodivers Rec*. doi:[10.1017/S1755267209000517](https://doi.org/10.1017/S1755267209000517)
- Pusceddu A, Bianchelli S, Martín J et al (2014) Chronic and intensive bottom trawling impairs deep-sea biodiversity and ecosystem functioning. *Proc Natl Acad Sci U S A* 111:1–6. doi:[10.1073/pnas.1405454111](https://doi.org/10.1073/pnas.1405454111)
- Queirós AM, Hiddink JG, Kaiser MJ, Hinz H (2006) Effects of chronic bottom trawling disturbance on benthic biomass, production and size spectra in different habitats. *J Exp Mar Biol Ecol* 335(1):91–103
- Reise K (1982) Long-term changes in the macrobenthic invertebrate fauna of the Wadden Sea: are polychaetes about to take over? *Neth J Sea Res* 16:29–36
- Rester JK (2000) Annotated bibliography of fishing impacts on habitat. *Gulf States Mar Fish Comm* 178
- Roberts C (2007) The unnatural history of the sea. Island Press

- Roberts JM, Wheeler AJ, Freiwald A (2006) Reefs of the deep: the biology and geology of cold-water coral ecosystems. *Science* 312(5773):543–547
- Rogers AD (1999) The biology of *Lophelia pertusa* (Linnaeus 1758) and other deep-water reef-forming corals and impacts from human activities. *Int Rev Hydrobiol* 84:315–406. doi:[10.1002/iroh.199900032](https://doi.org/10.1002/iroh.199900032)
- Sainsbury JC (1996) Commercial fishing methods: an introduction to vessels and gears, 3rd edn. Fishing News Books, Oxford, UK
- Schwinghamer P, Guigné JY, Siu WC (1996) Quantifying the impact of trawling on benthic habitat structure using high resolution acoustics and chaos theory. *Can J Fish Aquat Sci* 296:288–296
- Schwinghamer P, Gordon DC, Rowell TW et al (1998) Effects of experimental otter trawling on surficial sediment properties of a sandy-bottom ecosystem on the Grand Banks of Newfoundland. *Conserv Biol* 12:1215–1222. doi:[10.1046/j.1523-1739.1998.0120061215.x](https://doi.org/10.1046/j.1523-1739.1998.0120061215.x)
- Simpson A, Watling L (2006) An investigation of the cumulative impacts of shrimp trawling on mud-bottom fishing grounds in the Gulf of Maine: effects on habitat and macrofaunal community structure. *ICES J Mar Sci* 63:1616–1630. doi:[10.1016/j.icesjms.2006.07.008](https://doi.org/10.1016/j.icesjms.2006.07.008)
- Skaar KL, Jorgensen T, Ulvestad BKH, Engas A (2011) Accuracy of VMS data from Norwegian demersal stern trawlers for estimating trawled areas in the Barents Sea. *ICES J Mar Sci* 68:1615–1620. doi:[10.1093/icesjms/fsr091](https://doi.org/10.1093/icesjms/fsr091)
- Smith C (2000) Impact of otter trawling on an eastern Mediterranean commercial trawl fishing ground. *ICES J Mar Sci* 57(5):1340–1351
- Smith CJ, Banks AC, Papadopoulou K-N (2007) Improving the quantitative estimation of trawling impacts from sidescan-sonar and underwater-video imagery. *ICES J Mar Sci* 64:1692–1701. doi:[10.1093/icesjms/fsm165](https://doi.org/10.1093/icesjms/fsm165)
- Smolowitz R (1998) Bottom tending gear used in New England. In: Dorsey EM, Pederson J (eds) Effects of fishing gear on the sea floor of New England. Conservation Law Foundation, Boston, MA
- Snelgrove PVR (1999) Getting to the bottom of marine biodiversity: sedimentary habitats. *Bioscience* 49:129–138. doi:[10.2307/1313538](https://doi.org/10.2307/1313538)
- Snelgrove PVR, Thrush SF, Wall DH, Norkko A (2014) Real world biodiversity-ecosystem functioning: a seafloor perspective. *Trends Ecol Evol* 29:398–405. doi:[10.1016/j.tree.2014.05.002](https://doi.org/10.1016/j.tree.2014.05.002)
- Stelzenmuller V, Rogers SI, Mills CM (2008) Spatio-temporal patterns of fishing pressure on UK marine landscapes, and their implications for spatial planning and management. *ICES J Mar Sci* 65:1081–1091. doi:[10.1093/icesjms/fsn073](https://doi.org/10.1093/icesjms/fsn073)
- Todashino K (2016) 日本漁具・漁法図説 (translation: Japanese Fishing Gear). Seizando-Shoten Publishing, Tokyo
- Thrush SF, Dayton PK (2002) Disturbance to marine benthic habitats by trawling and dredging: implications for marine biodiversity. *Annu Rev Ecol Syst* 33:449–473. doi:[10.1146/annurev.ecolsys.33.010802.150515](https://doi.org/10.1146/annurev.ecolsys.33.010802.150515)
- Thrush SF, Hewitt JE, Cummings VJ, Dayton PK (1995) The impact of habitat disturbance by scallop dredging on marine benthic communities: what can be predicted from the results of experiments? *Mar Ecol Prog Ser* 129:141–150
- Thrush S, Hewitt J, Funnell G, Cummings V (2001) Fishing disturbance and marine biodiversity: role of habitat structure in simple soft-sediment systems. *Mar Ecol Prog Ser* 221:255–264
- Thurstan RH, Brockington S, Roberts CM (2010) The effects of 118 years of industrial fishing on UK bottom trawl fisheries. *Nat Commun* 1:15. doi:[10.1038/ncomms1013](https://doi.org/10.1038/ncomms1013)
- Tillin HM, Hiddink JG, Jennings S, Kaiser MJ (2006) Chronic bottom trawling alters the functional composition of benthic invertebrate communities on a sea-basin scale. *Mar Ecol Prog Ser* 318:31–45. doi:[10.3354/meps318031](https://doi.org/10.3354/meps318031)
- Trimmer M, Petersen J, Sivyer D (2005) Impact of long-term benthic trawl disturbance on sediment sorting and biogeochemistry in the southern North Sea. *Mar Ecol Prog Ser* 298:79–94

- Tuck ID, Hall SJ, Robertson MR et al (1998) Effects of physical trawling disturbance in a previously unfished sheltered Scottish sea loch. *Mar Ecol Prog Ser* 162:227–242. doi:[10.3354/meps162227](https://doi.org/10.3354/meps162227)
- USDA Farm Service Agency via Google Earth and SkyTruth (2008) Impacts of fishing: sediment plumes from bottom trawling. In: Satel Image Compil. <https://www.flickr.com/photos/skytruthsets/72157613362420565/>
- Valdemarsen JW, Jorgensen T, Engas A (2007) Options to mitigate bottom habitat impact of dragged gears. *FAO Fish Tech Pap* 506:1–43
- Vinson M (2013) Film of USGS fish trawling in Lake Superior. <https://www.youtube.com/watch?v=CqW43SKJefI>
- von Brandt (2005) Fish catching methods of the world, 4th edn. Wiley-Blackwell, London, UK
- Waller R (2013) Ideas and insight from explorers. In: *Natl Geogr Mag*. <http://voices.nationalgeographic.com/2013/06/24/clear-cutting-the-seafloor/>
- Watling L, Norse EA (1998) Disturbance of the seabed by mobile fishing gear: a comparison to forest clearcutting. *Conserv Biol* 12:1180–1197. doi:[10.1046/j.1523-1739.1998.0120061180.x](https://doi.org/10.1046/j.1523-1739.1998.0120061180.x)
- Watling L, Hoofd M, Boulanger M et al (2014) The bottom line on bottom trawling: How much more science do we need? ICES symposium effects of fishing on benthic fauna, habitat and ecosystem function, pp 2–3
- Watson R, Revenga C, Kura Y (2006) Fishing gear associated with global marine catches. *Fish Res* 79:103–111. doi:[10.1016/j.fishres.2006.01.013](https://doi.org/10.1016/j.fishres.2006.01.013)
- Wilkinson C (2008) Status of coral reefs of the world: 2008. Global Coral Reef Monitoring Network and Reef and Rainforest Research Centre, Townsville, Australia
- Williams A, Althaus F, Mike F et al (2011) Bottom fishery impact assessment. *Aust Rep South Pacific Reg Fish Manag Organ* 1–86
- Wilson AM, Kiriakoulakis K, Raine R, Gerritsen HD, Blackbird S, Allcock AL, White M (2015) Anthropogenic influence on sediment transport in the Whittard Canyon, NE Atlantic. *Mar Pollut Bull* 101(1):320–329
- Witkin T, Reyer A, Savitz J (2016) Global fishing watch reveals a fisheries management success in the Phoenix Islands. *Ocean Rep* 1–20

National Programmes: Geomorphological Mapping at Multiple Scales for Multiple Purposes

Terje Thorsnes, Lilja R. Bjarnadóttir, Alexandra Jarna,
Nicole Baeten, Gill Scott, Janine Guinan, Xavier Monteys,
Dayton Dove, Sophie Green, Joana Gafeira and Alan Stevenson

Abstract A better understanding of marine geomorphology is a common goal for seabed mapping programmes, with various mapping approaches, methodologies and challenges associated with systematically describing geomorphological features. To address these issues, and highlight the overall value of geomorphological mapping, a group of representatives from the seabed mapping programmes of the geological surveys of Norway, Ireland and the United Kingdom have formed a partnership to share their knowledge, expertise and technologies. Here we describe

MIM partnership: MAREANO-INFOMAR-MAREMAP.

The original version of this chapter was revised: For detailed information please see Erratum. The erratum to this chapter is available at https://doi.org/10.1007/978-3-319-57852-1_28

T. Thorsnes · L.R. Bjarnadóttir · A. Jarna · N. Baeten
MAREANO, Geological Survey of Norway, Trondheim, Norway
e-mail: Terje.Thorsnes@NGU.NO

L.R. Bjarnadóttir
e-mail: Lilja.Bjarnadottir@NGU.NO

A. Jarna
e-mail: Alexandra.Jarna@NGU.NO

N. Baeten
e-mail: nicole.baeten@ngu.no

G. Scott · J. Guinan (✉) · X. Monteys
INFOMAR Programme, Department of Communications,
Climate Action and Environment, Geological Survey of Ireland,
Haddington Road, Dublin D04 K7X4, Ireland
e-mail: Janine.Guinan@gsi.ie

G. Scott
e-mail: Gill.Scott@gmail.com

X. Monteys
e-mail: Xavier.Monteys@gsi.ie

the first year of collaboration by outlining the background to and motivation for the groups' national seabed mapping programmes, and presenting several case studies as well as tests to potentially adopt a harmonised classification scheme.

1 Introduction

In December 2015, representatives from the seabed mapping programmes of Norway, Ireland and the UK (MAREANO, INFOMAR and MAREMAP respectively) formed a partnership (MIM) to cooperate on advancing best practice for geological seabed mapping by sharing experiences, knowledge, expertise and technology. One of the key areas identified for collaboration concerned the challenges inherent in geomorphological mapping. In addition to sharing expertise and developing effective mapping approaches, it was agreed that the group would work towards a harmonised geomorphological classification scheme. In this chapter we report on the results of MIM's first year of collaboration by (i) describing the background and motivations of national programmes to characterise seabed geomorphology, (ii) introducing and discussing the developing classification system, and (iii) presenting several case studies from Norway, Ireland, and the UK to demonstrate the various advantages, challenges and overall value of geomorphological mapping of the seabed.

While the three survey programmes in the MIM group differ in terms of history, formation and governance, all are charged with geological mapping of their respective sovereign seabed areas to meet the needs of a variety of end-users and stakeholders, often at multiple scales. Norway and Ireland lay claim to the largest (2.1 million km²) and second-largest (850,000 km²) seabed areas in Europe respectively, yet neither had an established seabed survey programme until late last century, coincident with the widespread availability of high-resolution multibeam echosounder system (MBES) seabed mapping technology. In the 1990s and the beginning of the twenty-first century, several proposals for an extensive seabed mapping programme were presented to the Norwegian Government, but it was not

D. Dove · S. Green · J. Gafeira · A. Stevenson
MAREMAP, British Geological Survey, The Lyell Centre,
Research Avenue South, Edinburgh EH14 4AP, UK
e-mail: dayt@bgs.ac.uk

S. Green
e-mail: soph@bgs.ac.uk

J. Gafeira
e-mail: jdlg@bgs.ac.uk

A. Stevenson
e-mail: agst@bgs.ac.uk

until development of the first plan for integrated ocean management that the pressing need for greater knowledge of the benthic environment was recognised, leading directly to the establishment of the MAREANO programme in 2005 (<http://www.mareano.no>). Meanwhile, the Irish Government contracted a commercial company in 1996, to survey the continental margins to the west of Ireland as part of a submission to the United Nations Convention on the Law of the Sea, which set the criteria for determining the extent of a nation's sovereignty, and which required accurate and verifiable mapping. Subsequently, in early 1999, a proposal was put to the Irish Government outlining the importance of a national seabed survey to manage and identify the opportunities presented by Ireland's extensive seabed territory. The decision was made to first focus on surveying those waters deeper than 200 m resulting in the establishment of the Irish National Seabed Survey. In 2006, the deep-water programme was succeeded by an inshore programme that was renamed as INFOMAR (Integrated Mapping for the Sustainable Development of Ireland's Marine Resource; <http://www.infomar.ie>).

In contrast to Ireland and Norway, there was a broad understanding of the seabed geology in the UK prior to the widespread availability of MBES data. Between the late 1970s and early 1990s, mainly driven by the need to support the developing offshore oil and gas industry, the British Geological Survey (BGS) undertook a regional, reconnaissance sampling and geophysical survey programme. The broad-scale information provided by this programme brought significant scientific, commercial, and policy value but the need for more detailed information and research on which to base commercial and policy decisions has ensured regular MBES-based mapping of the UK seabed over the last circa 15 years. Recently, other marine organisations in the UK have increasingly shared their MBES data. These new 'open data' policies and data-sharing agreements resulted in the establishment of the UK Marine Environmental Mapping Programme (MAREMAP) in 2010 which pools and integrates the resources and expertise of a number of marine science organisations across the UK (<http://www.maremap.ac.uk>).

While the three surveys in the MIM group conduct similar mapping activities, their main motivations are variable. For example, both Norway and the UK have significant offshore oil and gas and other maritime industries (e.g. aquaculture, offshore renewables). As a consequence, the MAREANO programme caters particularly to the requirement for new knowledge about the seabed in relation to integrated management plans for the North Sea, Norwegian Sea and Barents Sea, with a special emphasis on ecosystems and habitat/biotope mapping. Similarly, MAREMAP responds to the regular requirement for detailed and accurate mapping of the seabed to serve multiple purposes (research, commercial, conservation, and policy), but this impetus is greater now than ever before as increasing development of the seabed has paralleled the growing awareness of valuing the marine ecosystem, and the need to establish Marine Protected Areas (MPAs).

Ireland's maritime economy, however, is far less developed than its neighbours, so the primary motivation for the INFOMAR programme is the need to underpin opportunities for marine economic growth, the 'Blue Economy', by providing data, products

(e.g. databases, charts, physical habitat maps) and services (marine decision support tools) to support marine spatial planning (MSP) and infrastructural development.

Notwithstanding these differences, all three survey programmes have in common that they are directed to carry out mapping activities which support a diversity of end-uses including MSP, MPAs, identification of landslide hazards, habitat-mapping, fisheries and numerous other commercial, policy and research interests. In addition, European projects such as MESH (Development of a framework for Mapping European Seabed Habitats), MESH-Atlantic, GeoSeas and EMODnet-Geology (European Marine Observation and Data Network; <http://www.emodnet-geology.eu>) have spurred mapping efforts and allowed participation in the development of agreed international standards for production of socio-economically important maps.

2 Geomorphological Mapping—Approaches and Challenges

Geomorphological mapping provides a fundamental and effective means to characterise the seabed, an important interface between the geological substrate and the water column where a range of biological, chemical, and hydrodynamic phenomena are dependent on both the morphological and geological character of the seabed. While information on seabed morphology/geomorphology is useful for a wide range of end-uses (e.g. habitat mapping, engineering, fisheries etc.) and therefore a priority for seabed surveys, production of such maps has not always been straightforward.

Until recently, geomorphological mapping in the UK has been data-limited, in terms of high-resolution MBES bathymetry, and complicated by the large number of organisations who acquire and hold such data. It is estimated that only c.30% of the UK's seabed has been mapped by MBES in contrast to the extensive BGS repositories of ground-truthing and other seabed information. Increased availability of MBES data, however, is enabling UK scientists to better distinguish the genetic origin of seabed features and, with datasets covering sufficiently extensive areas, allows feature assemblages to be understood in the context of broader environmental systems. This progress has been facilitated by the formation of MAREMAP and aforementioned data-sharing and coordination efforts. Conversely, the Irish survey has prioritised the collection and processing of bathymetric data, having mapped over 85% of its seabed. Geomorphological and other secondary mapping has been an auxiliary activity; finite resources meant that such work was carried out piecemeal and was usually project-driven. Furthermore, a paucity of ground-truthing has been an issue for Ireland due to the prioritisation of MBES data collection. However, an increase in, and optimisation of ground-truthing campaigns is a priority for INFOMAR going forward.

The Norwegian survey has also collected extensive MBES datasets and though only c. 10% of the seabed area has been surveyed to date, this is a significant achievement considering the size of the Norwegian marine area and the relatively recent establishment of the survey programme. MAREANO routinely collects both video-line and seabed sampling data and produces a wide range of interpretive mapping including maps delineating the distribution of larger physiographic regions (landscape types) and smaller geomorphic features (landforms). Landscape-type mapping is conducted in a semi-automatic manner using GIS-tools (Elvenes et al. 2013), while detailed geomorphological mapping has, hitherto, been produced for the most part by manual digitisation based on expert interpretation. This is particularly labour- and cost-intensive as the occurrence of many seabed features (e.g. biogenic mounds, iceberg ploughmarks) can number in the thousands for some areas of the Norwegian continental shelf. MAREANO has now started exploring automated methods as described in the case study below.

In general, production of interpretive, geomorphological mapping from data collected for bathymetric purposes presents a number of challenges, common to most mapping organisations. Collection of sufficient and appropriate ground-truthing is particularly problematic as marine territories are vast and the cost of seabed sampling is very high. However, optimisation of sampling strategies is being explored by another working group within the MIM partnership and is not discussed here.

More fundamentally, bathymetric data can vary in terms of quality and resolution e.g. MBES data acquired for hydrographic charting purposes versus regional-scale bathymetric compilations. The ubiquity of artefacts in bathymetric data can make delineation of features in the processed output problematic, particularly when using semi-automated techniques. Artefacts may result from increases in the signal-to-noise ratio caused by changes in MBES settings or poor weather or sea conditions. Perhaps surprisingly, it is also worth noting that data acquired to meet International Hydrographic Office (IHO) bathymetric standards may not always be best-suited for geomorphological mapping; this is discussed further in the INFOMAR case study below.

Another issue for mapping programmes is that maps may need to cover areas with substantial changes in water depth. This results in significant variability in the resolution of the underlying data due to the increase in size of the MBES footprint with depth and the concomitant decrease in data density. While resolutions of the order of metres are possible for the shelf (<200 m depth), this is reduced to the order of tens of metres, at best, in 4000 m water depths (ship borne MBES). This significantly impacts on the minimum size of detectable features. Resolvability issues are further compounded by the fact that the MBES frequencies required for deeper waters also result in a reduction in the accuracy of depth measurements.

While more data are welcomed, increasing data volumes requires that traditional, expert manual interpretation be supplemented with more time-efficient and, potentially, more accurate semi-automated approaches (e.g. image-based and statistical methods). These approaches can reduce mapping subjectivity and bias, but

manual interpretation is still frequently used to sense-check semi-automated outputs and characterise natural complexity and detail that may have gone undetected.

Finally, a key challenge for national mapping programmes is the need to produce map products for diverse users, at multiple scales as is discussed in the MAREMAP case studies below. With marine spatial planners, developers and researchers requiring more accurate and up-to-date geological information at multiple scales, there is a need to develop consistent mapping and geomorphological classification approaches. Based on work carried out by BGS, development of such a scheme has been one of the key activities of the MIM group.

3 Seabed Geomorphological Classification

The science of seabed geomorphological mapping is developing rapidly, but as this publication also demonstrates, the field is now well established, with its own, very active sub-disciplines. To an extent, these sub-disciplines have developed independently of one-another with researchers deriving from different scientific backgrounds. While this is advantageous for understanding the variable environmental processes recorded at the seabed, it also results in scientists using different terminology and relying on inconsistent classification criteria. Despite the relative youth of the modern field, i.e. common usage of high-resolution MBES bathymetry (1990s-present), it is perhaps surprising that there have not been (as far as we are aware) more concerted efforts to develop more integrated and coherent mapping approaches. Marine scientists have after all been interpreting the nature of the seabed for as long as they have been surveying it (e.g. Thompson 1874). The first half of the twentieth century saw the development and use of single-beam echo sounders (SBES), and it was the accumulation of these data that enabled the compilation and production of the first global-scale depiction of the seabed (Heezen and Tharp 1977). This work was particularly important because it demonstrated that through presenting and characterising the variation in seabed morphology, scientists could extract further scientific value, in this case significantly contributing to the plate tectonic revolution.

The field continued to progress through the application of side-scan sonars (SSS) (e.g. Belderson et al. 1972), MBES for bedform and regional-scale studies (Clarke et al. 1996), satellite altimetry for continental and global-scale studies (Smith and Sandwell 1997), and most recently with AUVs (Wynn et al. 2014), as well as LiDAR (Finkl et al. 2005) and satellite-derived imagery for coastal environments. While typically based on good science and observation, these mapping efforts commonly employ inconsistent mapping principles without reference to geomorphological standards, since very few exist. This has merit in advancing our understanding of the seabed, but neglects the value of implementing robust classification criteria to ensure accurate seabed characterisation and, perhaps more importantly, to enable comparison and integration between different geographic regions, data types, and mapping scientists. Such classification resources are more common in terrestrial

(e.g. Nanson and Croke 1992) and planetary geomorphology (Barlow et al. 2000), as well as within benthic habitat mapping (e.g. Greene et al. 1999).

The scientific community has of course not entirely ignored the value of applying standards in submarine geomorphology. A notable early example was the publication by Ashley (1990) in which marine bed forms were compared with fluvial analogues and classified. There are also standardised International Hydrographic Organisation (IHO) feature lists (IHO and IOC 2013), but importantly these lists are limited when it comes to diversity of features, and do not organise features in a structure that is relevant to their origin or morphology. The field of benthic habitat mapping itself has provided probably the greatest impetus to develop standardised ways of describing the seabed in the recent years. While this has largely focussed on hard substrates and seabed sediment character, there has been increasing recognition of the importance of seabed geomorphology in understanding the distribution of benthos (e.g. Harris et al. 2011). It is perhaps global-scale studies, however, which prove most instructive for progressing our characterisation of submarine geomorphology in more complex systems at finer scales. Because of the availability of continuous, albeit lower-resolution, bathymetric models, scientists have been able to adopt more systematic approaches in characterising the seabed, to examine for example the global distribution of seamounts (e.g. Hillier and Watts 2007), or more widely to assess global seabed geomorphology (Harris et al. 2014).

It is this systematic approach that is applied and advanced here to develop the means to describe the geomorphology of the seabed (metres—100s kilometres scale features) in an accurate, robust, and consistent way. This is particularly useful for mapping organisations, and requires a flexible new classification system that is applicable to multiple and diverse environments. The approach should be both sufficiently detailed and interpretive to be informative, but not so detailed that features are over-interpreted or mired in disputed designations or definitions.

In this context, and in response to the increasing requirement for seabed characterisation for multiple purposes and at multiple scales, the BGS developed a two-part Seabed Geomorphology classification system ('Morphology' and 'Geomorphology') to facilitate this work. Feedback on the evolving classification system from expert groups (e.g. submarine glacial geomorphology) demonstrated that other programmes (e.g. MAREANO and INFOMAR) and marine data networks (e.g. EMODnet) across Europe were also directing attention to geomorphology. As a result of this shared interest, one of the first activities of the MIM partnership has been to provisionally adopt the BGS approach and, through testing and revision, collaboratively improve the classification system (Dove et al. 2016). Version 1 of this classification is presented in Fig. 1.

A central objective of the classification system is to communicate useful and specific geological information while also providing an objective physical description of the seabed. Early attempts to include both elements in a single, logically-consistent classification proved either excessively complicated or overly prescriptive, broadly resulting from the non-unique relationship between morphology and feature origin. The solution was to employ two independent

Two-part geomorphological classification system

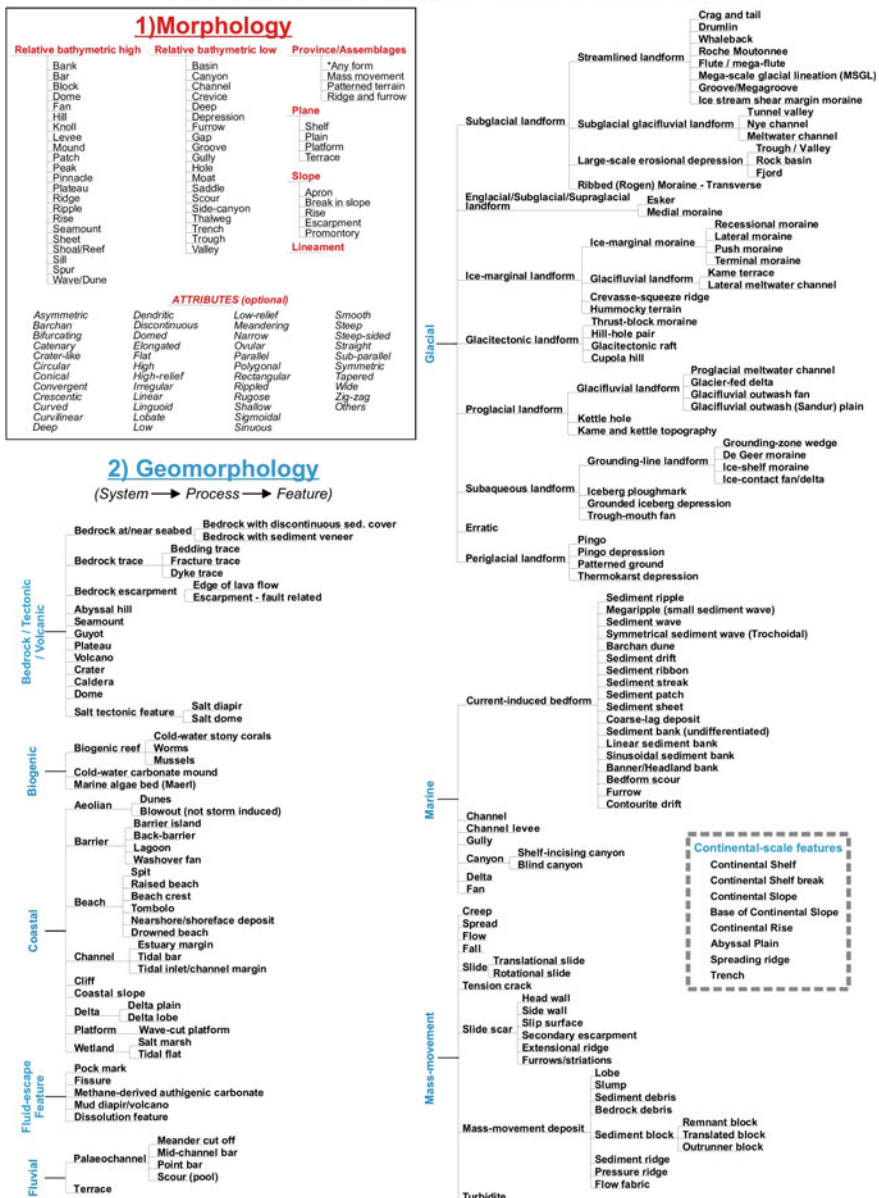


Fig. 1 Version 1 of the two-part seabed geomorphology classification system. System incorporates two independent classification trees: morphology and geomorphology

hierarchical classification trees, ‘Morphology’ and ‘Geomorphology’. ‘Morphology’ features are those characterised by their physical attributes (e.g. shape, size, texture) and ‘Geomorphology’ features are those defined by their process origin and/or the principal environment in which they were formed; e.g. ‘Biogenic’ features are formed primarily by biological processes and ‘Glacial’ features are formed in a glacial environment. Simply put, ‘Morphology’ provides the fundamental, objective description of the feature(s) whereas ‘Geomorphology’ provides an interpretation of the feature(s). Employing this two-step approach is robust as well as flexible because it allows the mapper to separate physical observations and descriptions from their informed interpretations, in effect better future-proofing their work. This is particularly relevant in the marine environment where mapping is heavily dependent on remotely-sensed data, due to the relative paucity of ground-truthing data.

Morphological forms are organised into two broad groups: “Relative bathymetric high” or “Relative bathymetric low”, together with several other features that do not fit into the ‘high’ or ‘low’ categories (i.e. plane, slope, and lineament features as well as provinces/assemblages of features). Further morphological attributes (e.g. ‘sinuous’) may also be appended to feature designations to assign greater detail. The geomorphological classification tree presently incorporates 8 environmental systems/themes: Biogenic, Coastal, Fluid-escape, Fluvial, Glacial, Marine, Mass-movement, and Bedrock-Tectonic-Volcanic, with the intention to eventually incorporate ‘Anthropogenic’ (Fig. 1).

To demonstrate how the two independent classification trees might be used to map a single feature, we give the example of a ‘Sediment wave’ below:

- (1) Morphology: ‘Bathymetric high’ >> ‘Wave/Dune’ >> ‘Curvilinear wave/dune’
- (2) Geomorphology: ‘Marine’ >> ‘Current-induced bedform’ >> ‘Sediment wave’.

A feature may be designated at any hierarchical level, ensuring that it is mapped at a level of precision consistent with the intrinsic nature of the feature, the data quality and confidence of interpretation. A set of bespoke GIS tools, modified from those originally developed by BGS for terrestrial mapping (SIGMA—<http://www.bgs.ac.uk/research/sigma/home.html>) are also being developed to implement the new classification system. These tools will enable more efficient mapping as well as provide a means to incorporate further quantitative (e.g. height, maximum slope) and qualitative (e.g. active vs. moribund, free-text comments) attributes, again adding to the flexibility of the approach.

The classification system provides a logical and consistent framework on which to base seabed geomorphological characterisation. Although a primary objective of the MIM partnership is to develop and collate good-practice mapping techniques and methodologies (e.g. automated numerical and imaged-based protocols vs. expert interpretation), it is intended that this classification system can function independently, and is applicable regardless of the mapping methodology that is used.

4 Case Studies

4.1 MAREANO, Norway—Automated Identification of Biogenic Reefs on the Norwegian Shelf

Coral reefs occur abundantly on the Mid-Norwegian shelf, particularly between 200 and 400 m depth along the continental shelf break and on morainic ridges (Fosså et al. 2002). Some coral reefs are elongated. Looking downstream, these have living ‘head’ colonies, which face the current, followed by a transition zone of recently-dead *Lophelia* colonies and gorgonians, blocks of dead *Lophelia* colonies with *Paragorgia arborea* and *P. resedaeformis* and a reef tail consisting of *Lophelia* rubble (Buhl-Mortensen et al. 2010). These elongated reefs form ridges composed mainly of biogenic material, ranging from mud through gravel to blocks. Circular reefs known as ‘mounds’ are similarly composed. Based on available ground-truthing, only a limited number of confirmed occurrences of live corals have been associated with the structures, though the sediments are clearly biogenic with a high proportion of coral-derived debris. This has called for a nomenclature based on sediment composition and geomorphology, rather than the presence of living corals; the non-living parts of these reefs are classified as ‘bioclastic sediments’ and are mapped out as a separate geological unit. Morphologically, both mounds and ridges are classified as ‘biogenic reefs’.

Maps of bioclastic sediments have received special attention, as these usually form the major parts of reefs, and can be identified using remote sensing (MBES bathymetry and backscatter) with limited visual and/or physical ground-truthing. Knowing the exact location of coral reefs is of major interest for integrated ocean management, because it forms the basis for legislative measures in order to protect the reefs. Since the 1990s, the official coral database managed by the Institute of Marine Research has been based mainly on visual observations of coral reefs using a remotely-operated vehicle or towed video platforms.

Mapping based on MBES data, gridded at 5 m and covering an area of 175,000 km² on the Norwegian shelf, reveals in excess of 100,000 mound and ridge structures, likely representing mounds and ridges composed of bioclastic sediments, which may or may not include living corals, normally found on the steepest slopes facing the current. Until now, mapping of biogenic mounds and ridges has involved delineating polygons containing one large structure or many small structures, based on expert interpretation and using manual digitisation (Bellec et al. 2014).

Scientists at MAREANO are now developing an alternative, automated mapping method based on a combination of MBES bathymetry and backscatter, processed and analysed using the object-based image analysis tool eCognition (version 9.2). Several test areas representing different geological settings have been trialled. In this case study, we present an area north of Skjoldryggen in water depths of 280–400 m (Fig. 2) for which ground-truthing includes 6 video lines, with a total length of nearly 3000 m, and 6 grab samples.

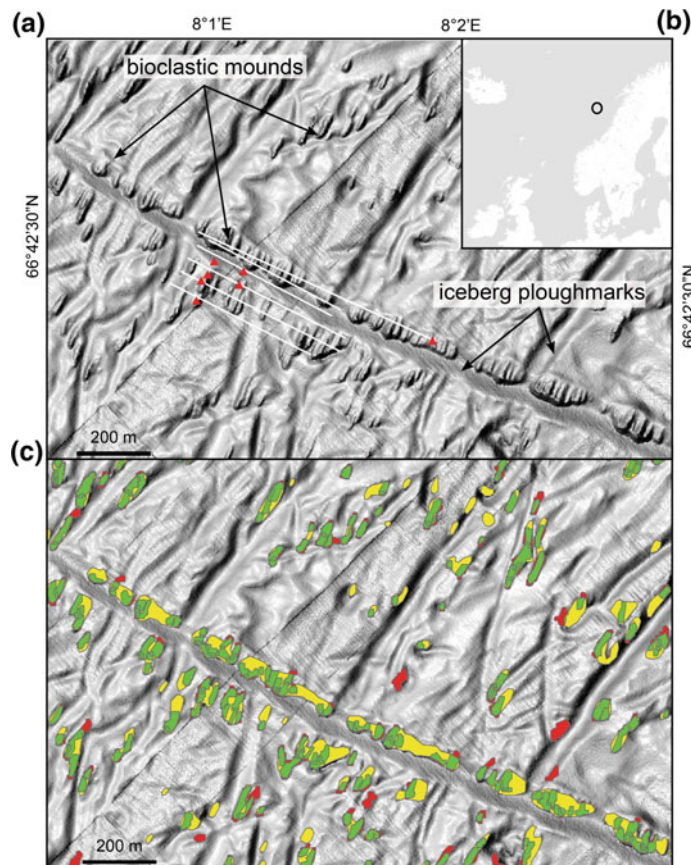


Fig. 2 **a** Overview of the study area. Water depth 295–305 m. Grayscale shaded relief image, 2 m grid, sun lightning from 315°, white lines indicate video lines, red triangles show grab samples. **b** Index map showing location of the study area. **c** Composite image comparing manual interpretation (MI) and eCognition classification (EC) of bioclastic mounds. Green intersection of MI and EC. Yellow mounds classified by MI, but not by EC. Red mounds classified by EC, but not verified by MI

In the study area, biogenic reefs represented by numerous mounds and NNE-SSW trending ridges with bioclastic sediments occur (Fig. 2a), typically up to 70 m long, 20–30 m wide and 10 m high. They occur particularly along the SSW-facing margins of iceberg ploughmarks, which are up to c. 100 m wide, up to c. 10 m deep and extend for several kilometres. The non-biogenic sediments are dominated by gravelly sand with cobbles and boulders. The ridges are thought to reflect development of coral reefs responding to the local hydrographic regime with a prevailing NNE current.

For automated delineation of the ridges, the workflow was as follows:

1. Terrain derivatives such as Bathymetric Position Index (BPI), curvature and slope were calculated from 5 m resolution MBES bathymetry using ArcMap and QGIS.
2. The terrain derivatives were imported to eCognition to form the basis of an image segmentation using an eCognition algorithm (Multiresolution segmentation with a scale parameter of 5 and compactness of 0.1).
3. A rule-based classification of the segmented objects of interest (mounds and ridges with bioclastic sediments) was then performed. In the case study, the criteria used were that BPI values (based a 5×5 and 20×20 windows) should be positive, mean slope should exceed 5° , standard deviation of slope should exceed 2.3° , standard deviation of curvature should exceed 12° m^{-1} and mean curvature should exceed 28° m^{-1} .
4. The classified data were exported to an ArcGIS polygon shapefile where a buffer of 3 m was added. This format ensures that the mound outlines can be integrated with other datasets in a desktop GIS environment or used as basis for WMS map services.
5. Finally intersect and union analyses were performed in ArcGIS to assess the performance of the classification against manual interpretation.

Preliminary results show that the classification using eCognition has a high, though not complete, overlap with ground-truthing (video, grabs) and expert-based manual interpretation (Fig. 2c). 98% of the predicted polygons intersect with the manually mapped polygons, while 2% of the predicted polygons are false. In terms of area, the predicted polygons make up 49% of the area of manually interpreted polygons. This means that the current parameters give a conservative prediction with very few classified polygons not verified by manual interpretation, but also that the current algorithm is not sufficiently sensitive to detect the more diffuse objects that can be identified by expert interpretation. Future work will include refining the choice of layers for segmentation, refining the rule sets for classification, and developing ways of representing confidence in the classified objects.

Delineation of individual reefs with bioclastic sediments has, until now, been too time consuming and thus beyond the capacity of the interpreters and the MAREANO budget. However, based on this trial, we now conclude that development of semi-automated methods will allow us to delineate individual reefs with high precision while expending far less time than for expert manual interpretation.

4.2 INFOMAR, Ireland—Reprocessing of Bathymetric Data for Geomorphological Mapping

The link between habitat heterogeneity, particularly morphological complexity and species diversity, has been well-established (e.g. Jumars 1976; Levin and Sibuet 2012). Seafloor habitat features, such as mounds and seamounts, are often given

special legislative protection to ensure they can continue to perform important eco-system services, for example by acting as nursery grounds for commercial fish species. However, deep-water features are, in general, significantly underrepresented in Marine Protected Areas (MPAs; Macmillan-Lawler et al. 2013). This underrepresentation may be even more pronounced than their analysis suggests as smaller and lower-relief features are usually poorly resolved for deeper waters, meaning that potentially important habitats may be missed (Robert et al. 2014). To support good policy decisions concerning deep and, indeed, all seabed areas seabed surveys must strive to produce the best maps possible from the data collected.

The first phase of the Irish seabed mapping programme focussed on deep-waters (>200 m) and revealed much morphological variety in the extensive ($>0.5 \times 10^6$ km 2) seabed area surveyed. Details and bathymetric imagery were published in an Atlas (Dorschel et al. 2010) but the production of interpretive mapping such as geomorphology from the data is a relatively recent endeavour (Sacchetti et al. 2012; Thébaudeau et al. 2015).

All INFOMAR bathymetric data are processed to IHO standards. However, there are some significant differences between data that are sufficient for hydrographic purposes and data that are optimal for geomorphological mapping, one of the most significant being the acceptable level of noise and artefacts. To deal with these, geomorphologists often apply smoothing algorithms before further analysis, which can obscure those features at the artefact scale. Furthermore, bathymetric processing for hydrographic purposes has a number of implications for geomorphological mapping that it is important to be aware of. For example, hydrographic mapping aims to preserve the most shoal soundings to identify navigational hazards. While this is important in shallower waters, the same principles are often applied in deeper settings. Hydrographers will also try to preserve data density whereas, from a morphological perspective, preservation of underlying shape is more important. Additionally, hydrographers are not overly concerned with line-to-line artefacts as long as the depth differences are within the IHO specifications. Geomorphologists, however, prefer to minimise these artefacts even though this may call for a compromise on data density.

In the period since the Irish deep-water mapping programme was completed, data processing technology, particularly data visualisation, has advanced apace making detailed processing more practicable. Given these advances and the need to produce interpretive mapping, INFOMAR is currently exploring reprocessing of deep-water data specifically for this purpose.

To test the benefits of reprocessing, a pilot study area from the head of the Whittard Canyon was chosen (see Fig. 3). The area lies in 200–400 m water depth and is notable for large bedforms. Smaller bedforms are perceptible but, in the original images, are made indistinct by line artefacts of a similar size.

Reprocessing the data to reduce or remove artefacts involved several steps, including careful analysis and reapplication of the most appropriate sound-velocity profile calibrations, together with further manual correction for refraction effects. Subtle ship's roll effects were corrected and careful manual cleaning of the data was performed in accordance with the geomorphological principles outlined above.

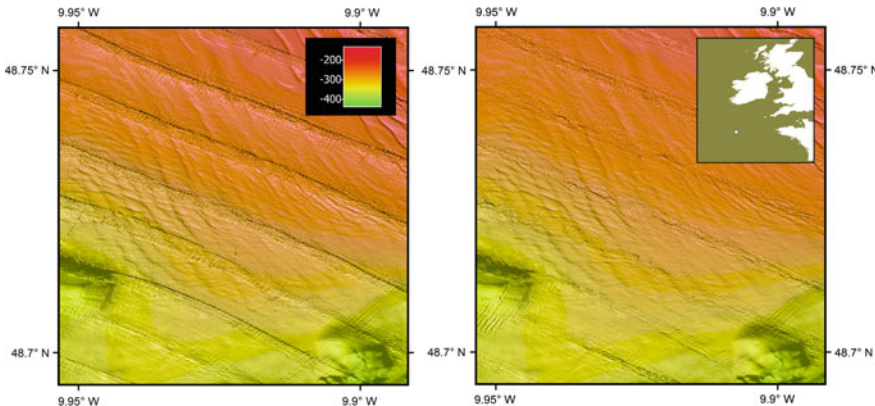


Fig. 3 Comparison of bedform area at the head of the Whittard Canyon located on the continental margin southwest of Ireland **a** before reprocessing of bathymetry for geomorphological mapping, where line-to-line and other artefacts partially obscure the bedforms which are of a similar scale **b** after reprocessing for geomorphological mapping where artefacts have been minimised and the bedforms better captured. Figures are shown in UTM29N and image settings chosen to exaggerate artefacts

Artefacts in the resulting image were found to be significantly reduced, making it possible to better identify the relatively smaller bedforms (Fig. 3).

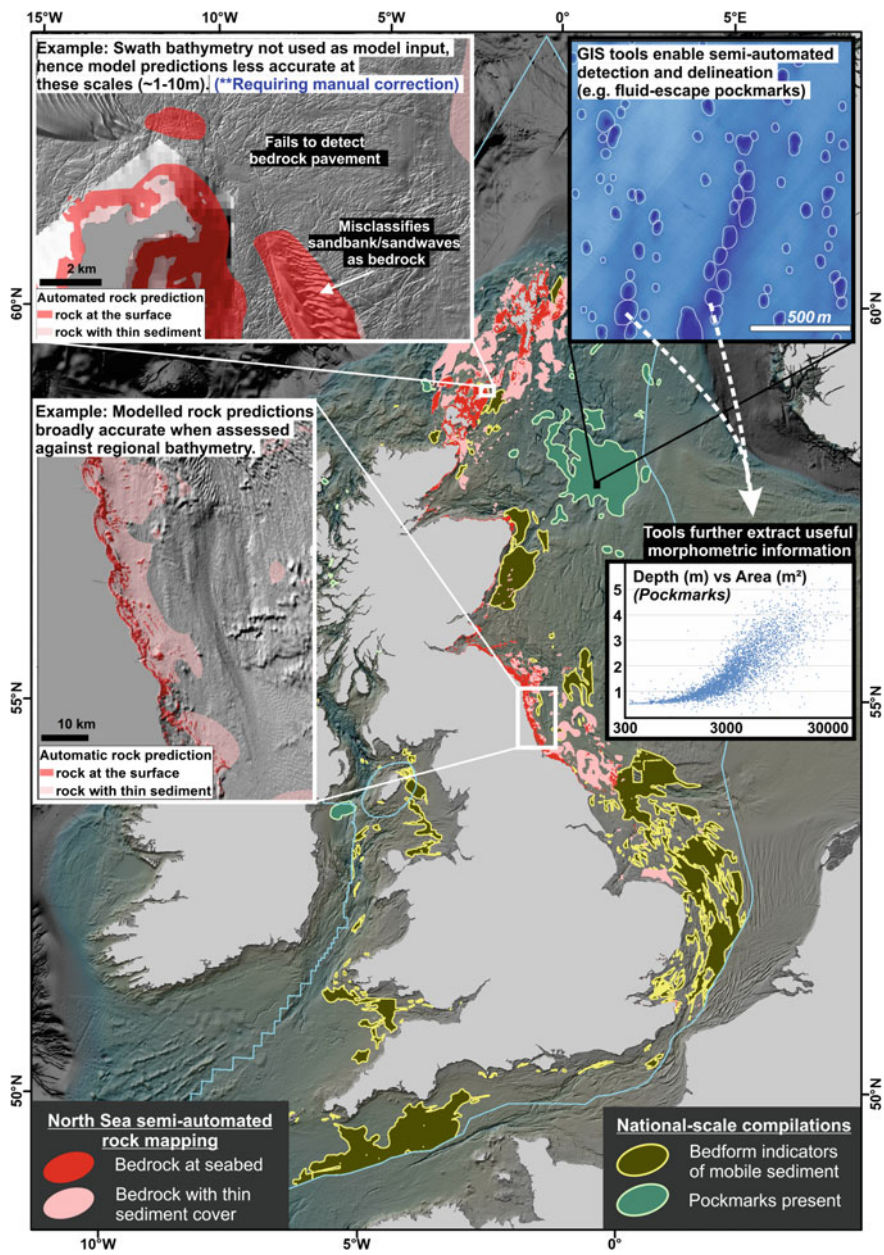
Finally, it should always be borne in mind that submarine geomorphology, even when produced by automated methods, is an interpretation. Confidence in this interpretation is partly a function of the quality and quantity of bathymetric readings. Currently, most geomorphological analysis is carried out using bathymetric grids of a particular resolution, often assumed to indicate the minimum size of feature detectable. However, a more accurate assessment can be made by considering three factors: data density (i.e. the number of bathymetric readings per grid cell); beam footprint, which increases in size from both shallower to deeper waters and with increasing swath angle, giving an incremental reduction in the ability to resolve smaller features; and vertical accuracy, which is primarily a function of the frequency of the MBES system. INFOMAR is currently exploring this kind of confidence information in addition to the development of quality control indices that could, in the future, be included in the map metadata to better support geomorphological and other interpretations made using INFOMAR bathymetric data.

4.3 MAREMAP, UK—Addressing Multiple End-Users at Multiple-scales

Here we present three examples of geomorphological mapping illustrating how MAREMAP addresses multiple end-uses at multiple scales for the UK offshore.

These examples describe different methodologies utilising variable data types (in terms of age and resolution) but employing a consistent, ‘fit-for-purpose’ mapping approach. We describe (a) a semi-automated seabed mapping tool that utilises high-resolution bathymetry data to identify and delineate features according to pre-determined criteria and extracts useful quantitative information (e.g. depth, orientation) relevant to the origin and potential activity of seabed features; (b) how existing data and information have been compiled and re-analysed to produce national-scale geomorphological map layers to underpin engineering constraint mapping for seabed development; (c) a mapping approach that combines semi-automated spatial prediction using multiple data-types with manual quality checks to predict the distribution of rock at seabed.

- (a) **Semi-automated seabed feature detection and characterisation.** Many distinct seabed features occur in vast and densely distributed numbers. Pockmarks (fluid-escape depressions) are one such example and in some areas of the North Sea more than 30% of the seabed is characterised by this type of morphology (Gafeira et al. 2012) (Fig. 4). Because manual mapping of these features is both time-consuming and subjective, BGS scientists developed a suite of semi-automated ArcGIS-based tools to more accurately and efficiently recognise, spatially delineate and morphologically describe seabed features. The tools also generate and store a range of morphometric attributes to an associated geodatabase. With more than 4500 pockmarks mapped on the UK continental shelf, these morphometric data have enabled unprecedented statistical characterisation of the features. Combined with geological and oceanographic information such analysis is greatly enhancing the understanding of their development, important for both geohazard assessment and potential climate change impact.
- (b) **National-scale compilation and constraint mapping.** National-scale geomorphological characterisation is required in the UK for both spatial planning and management purposes. One recent project with the Crown Estate (owner and/or effective ‘landlord’ of UK seabed) aimed to understand how the seabed and shallow sub-seabed geology (e.g. Quaternary thickness) constrains the design, installation, and operation of seabed infrastructure. For the geomorphological mapping component the approach was two-fold: compile and harmonise existing regional maps, and utilise the most recent bathymetric data to review and manually update the boundaries. These geological ‘factor maps’ (Fig. 4) were then combined with bathymetrically-derived morphological attributes (e.g. rugosity) to provide constraint parameters for specific seabed engineering activities using a rules-based scoring approach.
- (c) **Semi-automated regional mapping of rock outcrop.** The presence of hard-substrate is known to influence the distribution and character of benthic habitats and is, therefore, important to a range of groups with a stake in the seabed environment. Two regional studies (English Channel and Celtic Sea, North Sea) were recently conducted in collaboration with the Centre for Environment, Fisheries and Aquaculture Science and the Joint Nature



◀Fig. 4 Examples of geomorphological mapping at national, regional, and local scales within the UK offshore. National-scale compilations include areas of pockmarks and mobile sediment bedforms. Regional, semi-automated bedrock mapping in the North Sea is also presented, (*left side insets*) depicting instances where automated predictions worked well, and where expert interpretation was required to correct inaccurate model predictions. Feature-scale characterisation of pockmarks also demonstrates the advantages of semi-automated mapping (*right side insets*) revealing how useful morphometric information may be extracted from objectively delineated features

Conservancy Council (JNCC) to delineate rock outcrops for accurate, robust and repeatable mapping using a two-step approach (Diesing et al. 2015; Downie et al. 2016). The first phase involved the development and application of a random forest ensemble model in which predictor variables included broad-scale bathymetry, bathymetric derivatives, hydrodynamic forcings, and a number of pre-existing map layers indicative of seabed properties (e.g. mobile sediment indicators). The model was trained and the most significant variables were retained to make probability predictions for the presence of rock at seabed.

The outputs were then reviewed in a GIS environment where knowledge-based enhancements were made in accordance with the character of the local/regional geological environment, and with reference to high-resolution MBES data sets and supporting information such as seabed sediment samples and maps, and industry reports (Fig. 4). Importantly, this step also identified incorrect predictions from the automated process, for example, the misclassification of sandbanks as bedrock due to their elevation/slope (Fig. 4 inset) and, conversely, failure to identify bedrock pavement due to lack of morphological variability. All modifications were documented through metadata, providing a feedback loop to the modelling phase to facilitate improved performance in future efforts.

References

- Ashley GM (1990) Classification of large-scale subaqueous bedforms: a new look at an old problem. *J Sediment Petrol* 60:160–172
- Barlow NG, Boyce JM, Costard FM et al (2000) Standardizing the nomenclature of Martian impact crater ejecta morphologies. *J Geophys Res* 105(E11):26733–26738
- Belderson RH, Kenyon NH, Stride AH et al (1972) Sonographs of the sea floor. A picture atlas, Elsevier, Holland
- Bellec V, Thorsnes T, Bøe R et al (2014) Mapping of bioclastic sediments—data, methods and confidence. *NGU Rep* 2014:006
- Buhl-Mortensen L, Vanreusel A, Gooday AJ et al (2010) Biological structures as a source of habitat heterogeneity and biodiversity on the deep ocean margins. *Mar Ecol* 31:21–50
- Diesing M, Green SL, Stephens D et al (2015) Semi-automated mapping of rock in the English Channel and Celtic Sea. JNCC Report No. 569
- Dorschel B, Wheeler AJ, Monteys X et al (2010) Atlas of the deep-water seabed. Springer Science & Business Media, Ireland

- Dove D, Bradwell T, Carter G et al (2016) Seabed geomorphology: a two-part classification system. BGS open report OR/16/001
- Downie AL, Dove D, Westhead RK et al (2016) Semi-automated mapping of rock in the North Sea. JNCC Report No. 592
- Elvenes S (2013) Landscape mapping in MAREANO. NGU Report 2013.035
- Finkl CW, Benedet L, Andrews JL (2005) Interpretation of seabed geomorphology based on spatial analysis of high-density airborne laser bathymetry. *J Coastal Res* 21:501–514
- Fosså JH, Mortensen PB, Furevik DM (2002) The deep-water coral *Lophelia pertusa* in Norwegian waters: distribution and fishery impacts. *Hydrobiologia* 471:1–12
- Gafeira J, Long D, Diaz-Doce D (2012) Semi-automated characterisation of seabed pockmarks in the central North Sea. *Near Surf Geophys* 10(4):303–314
- Greene HG, Yoklavich MM, Starr RM et al (1999) A classification scheme for deep seafloor habitats. *Oceanol Acta* 22(6):663–678
- Harris PT, Baker EK (eds) (2011) Seafloor geomorphology as benthic habitat: GeoHab atlas of seafloor geomorphic features and benthic habitats. Elsevier
- Harris PT, Macmillan-Lawler M, Rupp J et al (2014) Geomorphology of the oceans. *Mar Geol* 352:4–24
- Heezen BC, Tharp M (1977) World ocean floor panorama, New York. In full color, painted by H. Berann, Mercator Projection, scale 1:23,230,300, 1168 × 1930 mm
- Hillier JK, Watts AB (2007) Global distribution of seamounts from ship-track bathymetry data. *Geophys Res Lett* 34:L113304
- Hughes Clarke JE, Mayer LA, Wells DE (1996) Shallow-water imaging multibeam sonars: a new tool for investigating seafloor processes in the coastal zone and on the continental shelf. *Mar Geophys Res* 18(6):607–629
- International Hydrographic Organization and Intergovernmental Oceanographic Commission (2013) Standardization of undersea feature name: guidelines, proposal form, terminology, Edition 4.1.0. IHO–IOC Publication B-6
- Jumars PA (1976) Deep-sea species diversity: does it have a characteristic scale. *J Mar Res* 34(2):217–246
- Levin LA, Sibuet M (2012) Understanding continental margin biodiversity: a new imperative. *Ann Rev Mar Sci* 4:79–112
- Macmillan-Lawler M, Harris PT, Baker E et al (2013) What's in and what's not: using the new global seafloor geomorphic map to examine the representativeness of global marine protected areas. In: International marine protected areas congress (IMPAC3), Marseille, France, 21–27 Oct 2013
- Nanson GC, Croke JC (1992) A genetic classification of floodplains. *Geomorphology* 4(6): 459–486
- Robert K, Jones DO, Huvenne VA (2014) Megafaunal distribution and biodiversity in a heterogeneous landscape: the iceberg scoured Rockall Bank, NE Atlantic. *Mar Ecol Prog Ser* 501:67–88
- Sacchetti F, Benetti S, Georgioupolou A et al (2012) Deep-water geomorphology of the glaciated Irish margin from high-resolution marine geophysical data. *Mar Geol* 291:113–131
- Smith WHF, Sandwell DT (1997) Global sea floor topography from satellite altimetry and ship depth soundings. *Science* 277(5334):1956–1962
- Thébaudeau B, Monteys X, McCarron S et al (2015) Seabed geomorphology of the porcupine bank, West of Ireland. *J Maps* 12(5):1–12
- Thomson CW (1874) An account of the general results of the dredging cruises of H.M.S.S. ‘Porcupine’ and ‘Lightning’ during the summers of 1868, 1869, and 1870, Under the Scientific Direction of Dr. Carpenter, J. Gwyn Jeffreys, and Dr. Wyville Thomson
- Wynn RB, Huvenne VAI, Le Bas TP et al (2014) Autonomous underwater vehicles (AUVs): Their past, present and future contributions to the advancement of marine geoscience. *Mar Geol* 352:451–468

Part IV

Conclusion

Conclusion

Aaron Micallef, Sebastian Krastel and Alessandra Savini

The chapters in this book have emphasised the central role played by advances made in seafloor data acquisition, processing and interpretation methodologies in the improved understanding of submarine landforms and processes. We would like to conclude this book by considering three key challenges and opportunities related to such advances that are shared by all fields of submarine geomorphic research:

- i. **Big data at multiple spatio-temporal scales:** Submarine geomorphology is undergoing a transformation from a data-poor to data-rich field of research. The volume of seafloor data is increasing at a fast pace, due to the implementation of seabed mapping programmes worldwide and the wider availability of a diverse range of seafloor surveying instruments. The increased automation of marine surveying, on the other hand, has reduced overall survey costs and resulted in data sets with high spatial and temporal resolutions. We identify at least two challenges associated with these recent technological advances:

A. Micallef (✉)

Marine Geology and Seafloor Surveying, Department of Geosciences,
University of Malta, Msida MSD 2080, Malta
e-mail: aaron.micallef@um.edu.mt

S. Krastel

Institute of Geosciences, Christian-Albrechts-Universität zu Kiel,
Otto-Hahn-Platz 1, 24118 Kiel, Germany

A. Savini

Department of Earth and Environmental Sciences, Universita' degli Studi
di Milano Bicocca, Piazza della Scienza 4, 20126 Milan, Italy

- There is an urgent need for the development and use of appropriate statistical and computational techniques to analyse large data sets to reveal meaningful geomorphic patterns, trends and associations in a relatively short period of time. As explained in the Chapter “[Quantitative Analyses of Morphological Data](#)”, submarine geomorphology has already been shifting towards a more quantitative analytical approach that exploits the full potential of seafloor data sets in a rapid, objective and consistent manner. A more standardised, automated landform mapping methodology based on an internationally-agreed nomenclature and symbology is especially required.
 - Due to the increasing availability of fine-scale spatial and temporal data, submarine geomorphology is being drawn towards a mechanistic and reductionist approach of enquiry. It is not yet clear, however, how small-scale processes can be used to explain events at larger spatio-temporal scales because landscapes are systems characterised by a hierarchy of forms and complex relationships. There will therefore be the need to develop robust strategies to link the large spatial/temporal scales of traditional seafloor data sets, with the fine spatial/temporal scales of new and future seafloor data sets. These strategies are likely to involve approaches already used in subaerial geomorphology (e.g. fractal scaling, kriging, and non-linear dynamics).
- ii. **Direct observation:** The aspect where submarine geomorphology clearly lags behind subaerial geomorphology is the direct observation and monitoring of geomorphic processes. The hardest parameter to quantify in submarine geomorphic models is process rate. In the past few years, there has been a drive towards temporal monitoring of changes in seafloor form and processes using seafloor observatories—stand-alone, cable, and moored - equipped with multiple sensors (e.g. EMSO, NEMO, CORK), as well as geodetic instruments, tiltmeters, and repeat surveys. If properly integrated with remote sensing and numerical models, such field measurements are likely to play a central role in submarine geomorphology in the next decade.
- iii. **Interaction with subaerial geomorphologists:** Due its longer history, subaerial geomorphology has matured into a scientific discipline based on a solid theoretical and methodological framework. Submarine geomorphologists, on the other hand, tend to have a better grasp of the internal structure of landforms, their history and their controls. The exchange of ideas and experiences between subaerial and submarine geomorphologists is unquestionably beneficial for the development of both fields of research, and will be a main goal of the Submarine Geomorphology working group of the International Association of Geomorphologists in the years to come.

Erratum to: Submarine Geomorphology

Aaron Micallef, Sebastian Krastel and Alessandra Savini

Erratum to:

A. Micallef et al. (eds.), *Submarine Geomorphology*, Springer Geology, <https://doi.org/10.1007/978-3-319-57852-1>

The original version of the book was inadvertently published with the following errors, which have been now corrected:

In Chapter “Oceanic Trenches”, the overlapped Fig. 5 has been corrected.

In Chapter “Cold-Water Carbonate Bioconstructions” the reference “Guinan et al. (2000)” has been changed to read as “Guinan et al. (2009)” in the reference list and citation, which is a belated correction.

In Chapter “National Programmes: Geomorphological Mapping at Multiple Scales for Multiple Purposes”, Figs. 1, 3 and 4 have been replaced correctly.

The erratum book has been updated with the changes.

The updated original online version of this book can be found at
<https://doi.org/10.1007/978-3-319-57852-1>